NORTHWESTERN UNIVERSITY

Light-Driven Carbene Catalysis for the Synthesis of Carbonyl Compounds

A DISSERTATION

SUBMITTED TO THE GRADUATE SCHOOL
IN PARTIAL FULFILLMENT OF THE REQUIREMENTS

for the degree

DOCTOR OF PHILOSOPHY

Chemistry

By

Anna V. Bay

EVANSTON, ILLINOIS

September 2022

ABSTRACT

The construction of new C–C bonds remains a central facet of organic chemistry due to its critical role in the synthesis of pharmaceutical compounds and organic materials. Mild and selective methodologies are often required for efficient formation of these bonds in natural product total synthesis, medicinal chemistry campaigns, and more. *N*-heterocyclic carbenes (NHCs) have emerged as unique Lewis basic catalysts that mediate a range of transformations through umpolung (polarity reversal) reactivity. While the utility of two-electron NHC reactivity has continued to expand, the inability of NHC-derived operators to engage sp^3 electrophiles limits their scope, thus highlighting the opportunity for single-electron NHC reactivity. The research described herein focuses on the development of methods at the interface of NHC catalysis and photocatalysis, leveraging the redox properties of each to construct key C–C bonds. Photoredox-catalyzed expansions on these processes are also described.

Thesis Advisor: Professor Karl A. Scheidt

ACKNOWLEDGMENTS

The day is here. It has been a long and challenging road – one filled with hard work, countless hours at my hood, effective brainstorming sessions, some venting sessions, what felt like never-ending struggles, many laughs, and, perhaps most importantly, the making of lifelong mentors, friends, and family. This journey requires an army of people, and I could not have made it to where I am today alone. I am grateful and indebted to so many individuals, and I will do my best to thank each of you below.

Many talented individuals have advised me over the past decade. While an unofficial advisor, I must first thank Professor Nicholas Shaw. I would be getting my Doctor of Medicine instead of my Doctor of Philosophy if you had not taught me chemistry at the College of Wooster, and, for that, I am extremely thankful. You are an incredible professor, and you made general chemistry and organic chemistry fun classes (how you managed that is beyond me). Your support and teachings during the first two years of my undergraduate studies served as the basis for my Ph.D. I owe so much to Professor Emily Pentzer. My laboratory skills grew tremendously during my time in your lab during the NSF REU at Case Western Reserve University. I was and still am inspired by you, an incredibly strong female scientist in a male-dominated field. You showed me that I can do whatever I want to do, even if the majority of those around me do not look like me. I quite literally would not be here today if you had not introduced me to Karl and his research. "I think you would really enjoy working in Uncle Karl's lab at Northwestern." You called it from the very start. I must thank Dr. Michael Peterson. My time working in your lab for my senior thesis taught me how to do independent research and the importance of mentoring the next generation of scientists. The Ugi reaction was a fun project to work on for a year. I enjoyed my time in your lab

and learned the ins and outs of what it means to be a chemist from you. Thank you for your constant support and advice over the years.

Professor Karl Scheidt, my most recent advisor, deserves a paragraph of his own. Karl, you took a chance on me: at the time, a young scientist with a lot to learn, coming from a small, liberal arts school in Ohio. Working in your lab the summer after my junior year of college was an unforgettable experience. You opened my eyes to how incredible (and complex) organic chemistry can be, and then you welcomed me back into your lab in 2018 as a graduate student. You have a brilliant mind for organic chemistry, named reactions, bond disconnections, and so much more. Learning from a scholar like you has been a blessing. I can say with certainty that you have been the perfect advisor for me. You push me to ask and then answer the hard questions. You teach me something new every time we talk, whether it be chemistry, history, a movie reference, how to cook a steak; the list goes on and on. You have supported me from the start. It has truly been a pleasure working in your lab, and, while a big part of me is sad to go, I know that you have prepared me to excel in the world of Big Pharma and to combat any challenges with which I am faced in the future. I will always be open to collaboration with you and this lab, so please keep in touch. Thank you for everything.

To my committee members, Professor Regan Thomson and Professor Rick Silverman, thank you for all of your support and feedback over the past few years. I learned so much from each of you while taking your classes during my first year, and I have continued to learn more from you both in the years that followed. Your advice has always been greatly appreciated. Professor Paul Cheong, Gisela González-Montiel, and Abdikani Farah, thank you for showing me

what an excellent collaboration looks like. You are phenomenal computational chemists, and I wish you all the best.

A lot of respect and appreciation is owed to the students who came before me. Mark Maskeri, the king of computers and random knowledge. Having you as an office mate kept life interesting. I learned more about making chocolate than I would like to admit from you. Let me know once you make a phone application for ChemDraw. Rick Betori, you showed me what hard work looks like and inspired me to think more deeply about my chemistry. Thank you for answering all my questions during my first year. Your food choices were arguably blander and more boring than mine, which is saying something, and your taste in music was questionable at best, but I am so glad we were office mates during our overlap in the group. Alison Bayly, the whisperer (or screamer?) of all news and gossip in the Department and the lab. You were a blast to be around, and your kindness and happiness were always uplifting. Keep being you. Eric Miller, your knowledge of total synthesis, named reactions, and mechanisms has always been admirable. Our unspoken agreement to not talk in the morning was peculiar and funny and helped me stay focused on the work that needed to be done. I learned a lot from you. And lastly, Keegan Kitzpatrick (kidding, Fitzpatrick), the other half of the A-team. You taught me how to approach methodology problems, how to purify compounds more efficiently, and so much more. You are the definition of an honest and kind person, and I hope the Scheidt lab can be blessed with more people like you in the future.

I also need to thank all the postdoctoral fellows that have been in the lab throughout my time here. 할아버지 (hal-abeoji) Seunghwan Byun, thank you for teaching me Korean on our hood sashes. 나는 호박을 진짜 좋아해. I will miss our daily laughs. You are going to be so successful

at whatever you choose to do in the future. Keep in touch! PQP, one of the kindest humans I have ever met. You are such a nice person and a talented chemist. I am excited to read your future Science paper someday. Pengzhi Wang, it was great to see you expand on some of the single-electron NHC chemistry. You will be a great professor or industrial chemist wherever you end up. Nao Tanaka, I am entrusting you with my favorite instrument in the laboratory – the GCMS. Take care of it please! Stay safe during any thunderstorms you encounter in your future. Grant Frost and Stephen Laws, the two of you worked in the same hood at different times and both taught me an incredible amount about chemistry and reaction setup. Stephen, you showed me how to keep a hood clean and still work productively, and Grant, you have one of the most contagious laughs I have ever heard. Paige Monsen and Ann Fernandez, thank you for your fashion advice before presentations. The two of you have made the lab a happier place. While not a postdoctoral fellow, Purav Vagadia, you know such much about chemistry, and you have an extraordinary future in business. Your positive attitude impacts us all.

And then there are the incredible graduate students who have been in the group throughout my time here. We have been through thick and thin together. Joshua Zhu (lab Josh), I'm not crying.. yet. From train buddies, to carpooling every once and a while, to going to Starbucks when we are having a rough day, you have been my closest friend in the lab. Thank you for teaching me so much chemistry, allowing me to ask any and all questions ("Hi, Josh." "Hi, Anna."), and being the rock of this lab. You are so incredibly smart, and I cannot wait to see what all you accomplish – your future is bright! Let's be coworkers again soon please. Ada Kwong and Meghan Orr, where would I be without the two of you? We have truly been through it all together. I am so grateful that I became friends with the two of you during the pandemic. Ada, I will miss our Starbucks trips

and will be lost without your technology tips. You are going to kill it in California. Meghan, I am excited to see what all you do in the future. You are truly gifted and will cure a disease one day. Dalton Kim, your extensive knowledge of organic chemistry and Chicago restaurants is impressive. You have been so helpful in the lab and have taught me a lot about reaction setup and distillations. I am sure your future is filled with lots of good food and success.

The younger graduate students and undergraduates in the lab also deserve immense gratitude. Mike Rourke, your love of organic chemistry and original passion for lab work is astonishing. Your abundance of random and wild stories never ceases to make everyone laugh and keep us all entertained. I cannot wait to read your sulfur carbene paper soon. Cullen Schull and Yunchan Nam, I am so happy that the two of you joined this lab. It has been so great getting to know each of you, and I know that you both will be successful in your futures. Cullen, keep up the good work and excellent work ethic – you are going to crush graduate school. Yunchan, you are so kind and extraordinarily brilliant, and I look forward to reading your future JACS papers. Emmie Farnam, you are the MVP of all undergraduates in this lab. Your ability to run reactions efficiently and independently is so natural and very impressive. You are going to be an amazing doctor in the future, and, if you change your mind, Emelia Farnam, Ph.D. sounds pretty good. Anthony Tam, Mr. Goldwater, your kindness and desire to help is admirable. You're going to be a stellar scientist someday. To all of the other undergraduates, keep working hard and your successes will follow. Your futures are full of potential.

To all the future students, for what it is worth, my advice to you is this: treat graduate school like a job. Respect the boss, respect your peers, be professional, and, of course, work hard. Communication really is key in graduate school. Talk to your PI about your goals, ask what you

need to do to accomplish them, and appreciate the constructive feedback. Stay positive, even when you get negative results. Be creative and think outside the box when you are presented with a problem. Safety *always* comes first in the lab, so do not take unnecessary shortcuts; respect the chemicals and the chemistry, and always be prepared. Keep your bench and hood clean and organized. Get involved in the Chemistry Department and science community outside of the lab by joining a student group (I am partial to RSSI). Stay focused, but remember to have fun. Graduate school is what you make it, so make it a good time and accomplish all that you set out to do.

My friends and family are core to my success. Allison Sheehan. People in my lab know you as "Toog," naturally. We are childhood best friends living in the same city after graduating from college - what a blessing you are in my life. I am forever thankful to have you as one of my best friends. Thank you for always pushing me to get out and enjoy life when sometimes I got too "in the zone" during graduate school. I cannot wait to see what adventures we go on together. Leah McCormick, you are a shining example of living life to the fullest, and I hope to go explore parts of the world with you in the future. Rachel Molé, having another science friend who I can talk to about anything and everything is incredible. You are an amazing person, your happiness is infectious, and I always have a good time when we are together. Keeping being you. To all of my other friends, Taryn Szalay, Khue Hoang, and so many more, I am lucky to have you all in my life. Josh Davies (brother Josh), the second favorite child, thank you for always keeping me on my feet. Your light-hearted advice for what I should say during presentations or interviews always has me laughing hysterically. I enjoy our morning conversations and venting sessions each week, and I am so grateful to have you as my big brother. Your support over the past few years has been so greatly appreciated.

My grandparents have been a saving grace during my graduate school experience. I owe each of you the biggest of big hugs. Grandpa Pat, our weekly conversations during my first two years of graduate school never ceased to make me smile. I wish you could be here today to see the end, but I know you are smiling from up above. I love you and miss you immensely. Grandpa Jim, I always enjoy talking to you about life and hearing stories about your childhood. It would be amazing to go back and see you run hurdles. You are such a fighter, and I hope to help beat the fight against cancer someday for you. Grandma Gay, your style is impeccable, and your decorating skills are always spot on. Grandpa Glenn, I always get excited when you pick up the phone. You are such a good person, and your wisdom is unmatched.

Dad. Really, I should have thanked you first. Remember the summer after my freshman year of college? You spent two weeks teaching me organic chemistry in the dining room at home so I would be prepared for the ~elusive~ sophomore Organic Chemistry I and II classes at the College of Wooster. But, I had to save the best people for last, so here you are, and here I am, following in your footsteps by earning my Ph.D. in (Organic) Chemistry! While we will always debate whether organic chemistry is better than organometallic chemistry (obviously, organic chemistry is *the* best, just kidding.. kind of), our conversations over the past few years have been a true highlight. Your perspective continues to force me to think outside the box, and your advice cannot be beaten. I would not be where I am today without you, and, of course, without mom. Mom, thank you for being my awesome mom. Remember the molecule game we played together when I was a kid (I really should have thanked you first)? Our daily conversations have kept me inspired and focused, and I apologize for all the times our conversations were hijacked by a

chemistry topic. Your ability to bring unwavering happiness and joy into my life is without a doubt a real superpower. I love you and Dad so much and wouldn't be here without you both.

Last, but certainly not least, I must thank my incredible husband, Michael Bay. MB, you deserve an award for all the support that you have given me. You have been my rock. I vividly remember calculating how much time would be saved if you drove me up to Evanston instead of me taking the redline in the morning: if you drove me, I would get an extra thirty minutes of lab work done every day, which would translate to completing my Ph.D. in two-to-three months less time than if I had taken public transportation to work. And here we are, three years and ten months later ☺. You encouraged me to work hard each and every day, including Saturdays and Sundays, even it meant that you would be home alone. You read my papers and watched my presentations, even though organic chemistry can feel like a foreign language sometimes. You helped me work through some very difficult situations and hardships, and you supported me every single day with your love, your encouragement, and your commitment. From the very bottom of my heart, thank you, and I love you.

LIST OF ABBREVIATIONS

3 Å MS	3 ångström molecular sieves
AcOH	acetic acid
Ar	aryl
Ac	acetyl
Az	azolium
Boc	*tert*-butyloxycarbonyl
Bu	butyl
Bz	benzoyl
δ	chemical shift (parts per million)
DBU	1,8-diazabicyclo[5.4.0]undec-7-ene
DCE	1,2-dichloroethane
DCM	dichloromethane
DFT	density functional theory
DIPEA	diisopropylethylamine
DMAP	4-(dimethylamino)pyridine
DMP	Dess-Martin periodane
DMSO	dimethylsulfoxide
dr	diastereomeric ratio
DTBM	di-*tert*-butyl-4-methoxy-phenyl
ee	enantiomeric excess
equiv	equivalents

er	enantiomeric ratio
EI	electron impact
ESI	electrospray ionization mass spectrometry
EtOAc	ethyl acetate
GC	gas chromatography
GCMS	gas chromatography mass spectrometry
HAT	hydrogen-atom transfer
HOMO	highest occupied molecular orbital
HPLC	high-performance liquid chromatography
HRMS	high-resolution mass spectrometry
HWE	Horner-Wadsworth-Emmons
IMes	2,4,6-trimethylphenylimidazole
IPA	isopropanol
IR	infrared
J	coupling constant
KRED	ketoreductase
KO*t*Bu	potassium *tert*-butoxide
LA	Lewis acid
LiHMDS	lithium hexamethyldisilazane
LDA	lithium diisopropylamide
LRMS	low-resolution mass spectroscopy
LUMO	lowest unoccupied molecular orbital

Me	methyl
MeOH	methanol
Mes	2,4,6-trimethylphenyl
mg	milligram
MnO_2	manganese(IV) oxide
NAD+	nicotinamide adenine dinucleotide
NHC	*N*-heterocyclic carbene
NMR	nuclear magnetic resonance
ORTEP	Oak Ridge thermal ellipsoid plot
PC	photocatalyst
Ph	phenyl
R_f	response factor
rt	room temperature
SCE	saturated calomel electrode
SDS	solvent delivery system
SET	single-electron transfer
TEA	triethylamine
TEMPO	(2,2,6,6-tetramethylpiperidin-1-yl)oxyl
TEP	Tolman electronic parameter
THF	tetrahydrofuran
TIPS	triisopropylsilyl
TLC	thin layer chromatography

TMS	trimethylsilyl
p-TsOH	*para*-toluenesulfonic acid
UV	ultraviolet

For my family

In loving memory of Patricia H. Smith

TABLE OF CONTENTS

LIST OF FIGURES

LIST OF SCHEMES

LIST OF TABLES

CHAPTER 1: SINGLE-ELECTRON CARBENE CATALYSIS

Portions of this chapter appear in the following publication:

Bay, A. V.; Scheidt, K. A. Single-electron carbene catalysis in redox processes. *Trends Chem.* **2022**, *4*, 277–290.

1.1 An Overview of Catalysis

At a simple level, a chemical reaction is the combination of two or more elements or compounds to make a chemically distinct product. The Arrhenius equation states that a reaction proceeds when reactants, A and B, collide in an appropriate orientation and with sufficient energy to overcome the energy barrier that exists between the reactants and the product (**Figure 1-1**).[1] Among other factors, this activation energy barrier ($\Delta G^{\ddagger}$) dictates the outcome of a chemical reaction; if it is overcome, the reaction proceeds to form product. However, there is not sufficient energy to overcome the activation energy barrier, then the product will not be formed.[2-3]

Catalysts are chemical species that accelerate reactions by mediating an alternative, energetically favorable pathway from reactants to products.[4] A catalytic cycle is often initiated by interaction of the catalyst with one or both reactants. This interaction lowers the overall energy of the system, and the subsequent reaction step between the starting materials, A and B, can proceed

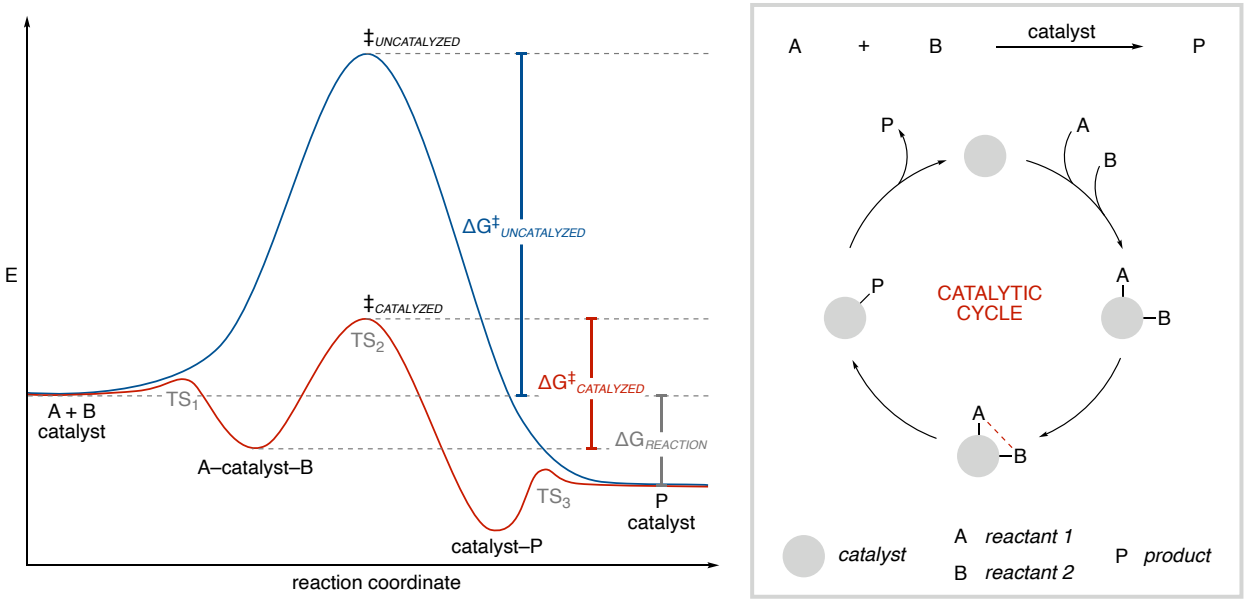

Figure 1-1. Reaction coordinate diagram of an uncatalyzed reaction (blue) and a catalyzed reaction (red), and a general catalytic cycle.

while bound to the catalyst. The activation energy associated with this rate-limiting bond formation step ($\Delta G^{\ddagger}_{CATALYZED}$) is significantly smaller compared to that of the corresponding uncatalyzed reaction ($\Delta G^{\ddagger}_{UNCATALYZED}$, **Figure 1-1**).[5] Once the activation energy barrier is overcome, the product and the catalyst dissociate to afford the desired product and regenerate the catalyst, which is free to interact with additional molecules of A and B.

Catalysts have become an integral component of synthetic chemistry due to their ability to enable chemical reactions that otherwise may not be possible. First termed "catalytic power" by Jöns Jakob Berzelius in 1835, the field of catalysis dates back to 1552 when Valerius Cordus employed sulfuric acid to catalyze the conversion of ethanol into diethyl ether for treatment of bacterial and viral infections.[6-7] Since its initial discovery, the field of catalysis has grown rapidly and has branched into three primary subdisciplines: heterogeneous, homogeneous, and biological catalysis (**Figure 1-2**). Heterogeneous catalysis refers to methods in which the catalyst and the reactants and products are in different phases (e.g., a solid catalyzes a reaction between reagents in solution or in the gaseous phase). In homogeneous catalysis, the catalyst and reactants are in the same phase (e.g., in solution).[8-9] Often considered its own class, biological catalysis refers to methods that employ biological sources, such as enzymes, to enhance the rate of reactions.[10]

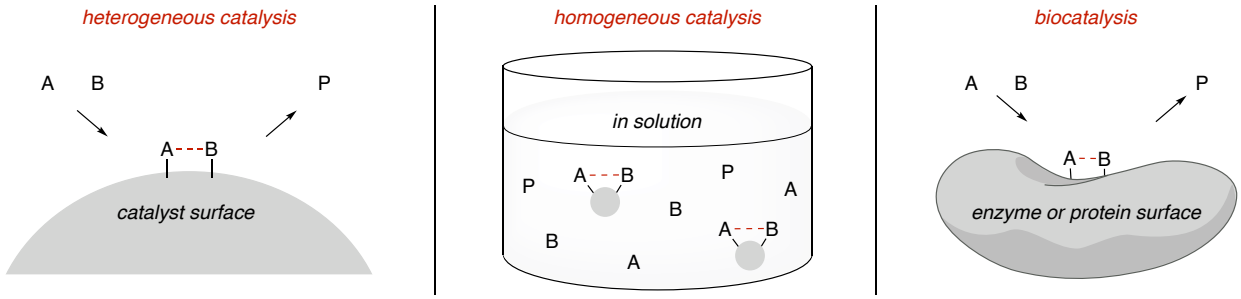

Figure 1-2. The three primary subdisciplines of catalysis.

Today, each subdiscipline has been studied extensively and has been applied to enable a broad spectrum of chemical transformations.

1.2 Introduction to *N*-Heterocyclic Carbenes

N-Heterocyclic carbenes (NHCs) are unique, highly reactive chemical species that are represented in all three subdisciplines of catalysis (vide supra). Due to their distinct steric and electronic properties, NHCs are commonly employed as ligands in transition metal catalysis, an important facet of heterogeneous and homogeneous catalysis (see section 1.3).[11] While less common, solid-supported NHC-metal complexes (e.g., on polymers, silica, nanoparticles, etc.) have been developed for use in various cross coupling reactions, hydrogenations, and more.[12-13] NHCs frequently function as organocatalysts as well, spurring the evolution of umpolung (polarity reversal) reactivity in recent decades (see section 1.4).[14] These reactive species also play an integral role in sustaining life in many organisms, as the heterocyclic motifs serve as cofactors in numerous biocatalytic processes and can thus be found in the active site of various proteins.[15]

1.2.1 Properties

The ability of NHCs to serve as versatile ligands and powerful catalysts stems from their exceptional tunability and unique properties. The term "NHC" broadly refers to heterocyclic species that feature a carbene carbon (C2) and at least one nitrogen atom within a ring system.[16] These cyclic species have a singlet ground state electronic configuration with an unoccupied *p*-orbital contributing to the lowest unoccupied molecular orbital (LUMO) and a formally sp^2-hybridized lone pair at the C2 carbon contributing to the highest occupied molecular orbital (HOMO). The adjacent nitrogen and heteroatom (i.e., *N*, *S*, or *O*) are σ-electron-withdrawing and

π-electron-donating, thus providing inductive stabilization by decreasing the energy of the occupied σ-orbital while offering mesomeric stabilization through donation of electron density into the unoccupied *p*-orbital (**Figure 1-3**). The cyclic configuration of NHCs further contributes towards stabilization of the singlet state by enforcing a bent conformation, thus providing the carbene carbon with more sp^2-like character.

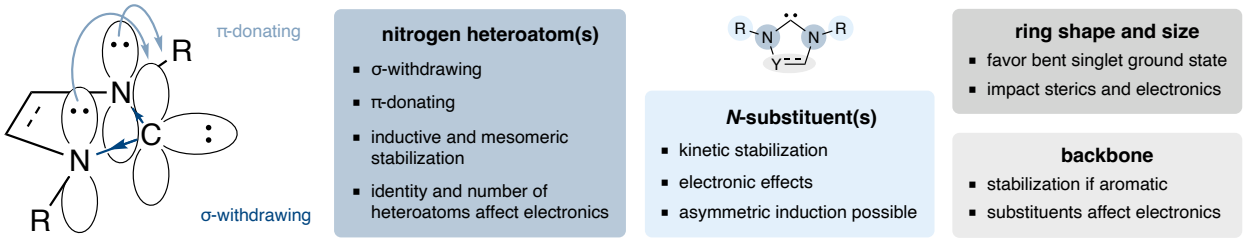

Figure 1-3. Structural features and properties of NHCs.

Within the broad definition of NHCs exist several classes, typically distinguished by their degree of heteroatom stabilization (**Figure 1-4**).[17] The number and identity of the heteroatoms significantly affects the electronics of the carbene (e.g., those derived from heteroaromatic compounds often feature increased stabilization due to their partial aromaticity) and are key factors in differentiating NHC classes. NHCs containing two adjacent nitrogen atoms are derived from the root "imidazole," and inclusion of a third nitrogen atom in the backbone of the heterocycle describes the class of triazoles. Carbenes containing one adjacent nitrogen atom and an adjacent sulfur or oxygen atom are described as thiazoles and oxazoles, respectively. While less common, NHCs that feature an adjacent carbon atom stem from the root pyrrole, and those with both an adjacent carbon atom as well as a nitrogen atom in the backbone of the heterocycle are best described as mesoionic or abnormal carbenes.[18] Perhaps the least commonly used group of NHCs are *N,N*-diamido carbenes, which have diagnostic carbonyl groups on the backbone.[19]

NHCs can be further classified by their backbone and *N*-substitution, which significantly affect the properties of the free carbene (**Figure 1-4**).[20] Impacting the electronics of the system, the backbone of an NHC can contain saturation or unsaturation, ring fusion, or substitution.[21] For example, an aromatic backbone provides an increased degree of electronic stabilization due to increased delocalization.[22] Similarly, the *N*-substituent(s) offer kinetic stabilization from steric bulk as well as an electronic influence.[23] The ability to dynamically alter the *N*-substitution has also allowed for the development of chiral NHCs that have the potential for asymmetric induction.[24-25]

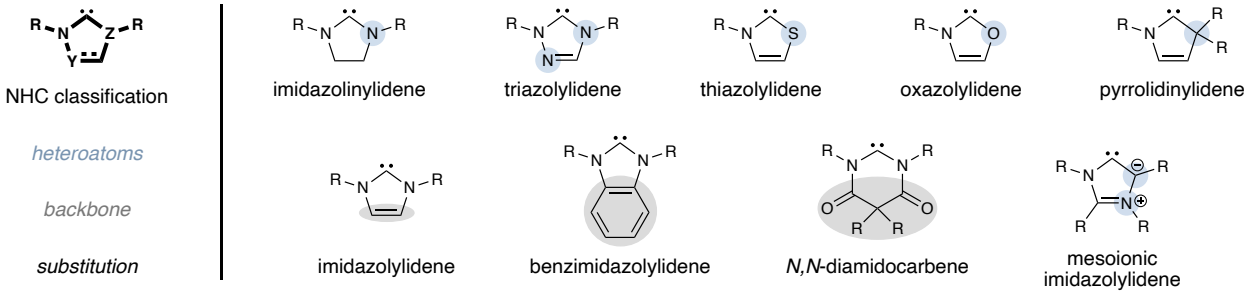

Figure 1-4. Common NHC classes.

Due to the relative ease of preparation, libraries of structurally diverse analogues have been developed to date.[14] The free NHC is most commonly afforded by deprotonation of the corresponding cationic heterocyclic azolium salt for which synthetic routes have been established for centuries.[26] The modular synthetic sequences employed to access these NHC precursors have enabled the ability to precisely tune the steric and electronic parameters (as measured by the buried volume and Tolman electronic parameter, respectively) through alteration of the backbone, *N*-substitution, ring size, and more.[27-30]

1.2.2 The Origins of N-Heterocyclic Carbenes in Synthesis

These reactive species have their origins in an essential catalytic cycle in many living organisms: the synthesis of acetyl coenzyme A (acetyl-CoA). In this vital process, thiamine pyrophosphate acts as a coenzyme for the oxidative decarboxylation of pyruvic acid. The formation of a redox-active enamine enables single-electron transfers (SET) to various acceptors, including lipoamides, flavin adenine dinucleotide, and ferredoxin.[31-32] Acylation of coenzyme-A occurs following two consecutive single-electron oxidations of this enamine intermediate by the acceptor (e.g., ferredoxin), synthesizing acetyl-coenzyme A (acetyl-CoA) and regenerating thiamine pyrophosphate (**Scheme 1-1**).

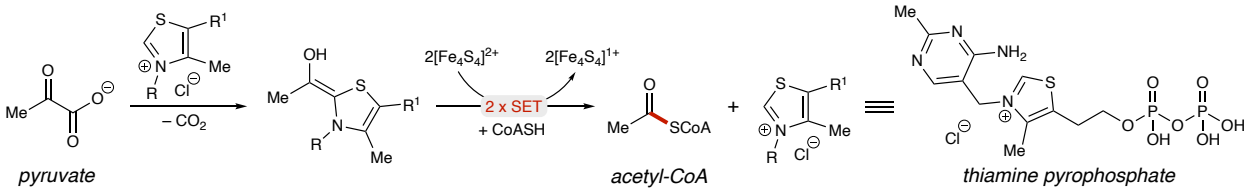

Scheme 1-1. Oxidative decarboxylation of pyruvate via thiamine pyrophosphate catalysis.

Motivated by these natural processes, chemists have developed NHCs as versatile ligands and catalysts to forge a variety of C–X (X = N, O, etc.) and C–C bonds (**Figure 1-5**). Their properties have enabled their use as ligands for some of the most well-known transition metal catalysts developed to date. Moreover, the Lewis basicity of NHCs positions them to be powerful organocatalysts; these reactions are often initiated by carbene addition into a carbonyl, and subsequent proton transfer affords the Breslow intermediate,[33-35] a species that is nucleophilic at a previously electrophilic carbonyl carbon. This unique reversal in polarity enables carbonyl carbons (via the Breslow intermediate intermediate) or traditionally electrophilic β-carbons (via the homoenolate intermediate) to react with various sp^2 electrophiles (**Figure 1-5**).

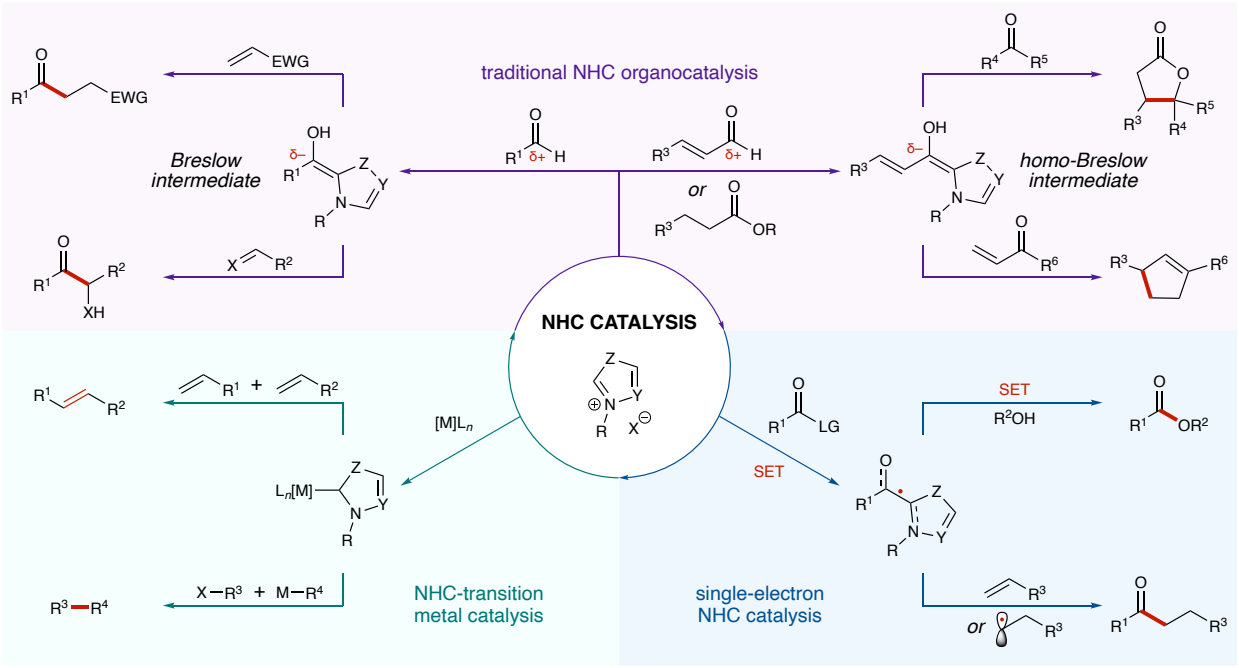

Figure 1-5. Overview of NHC catalysis in synthesis.

1.3 Carbenes as Ligands in Transition Metal Catalysis

The majority of applications of NHCs in synthesis feature their use as ligands in coordination chemistry. Dating back to 1968 when Wanzlick and Öfele independently synthesized NHC-mercury(II) and chromium(0) species, respectively, the use of NHCs as ligands for transition metals stems from their inherent σ-donor capabilities.[36-37] The formal sp^2-hybridized lone pair of the free carbene species is available for donation into a transition metal's σ-accepting orbital. Moreover, π-donation from the carbene *p*-orbital as well as π-back-bonding into the carbene *p*-orbital contribute to the excellent metal-ligand binding **(Figure 1-6)**.[38-39] Studied by numerous groups and reviewed by many, the strong σ-donating and relatively weak π-accepting properties of these carbene species facilitate enhanced coordination to transition metals.[40-41]

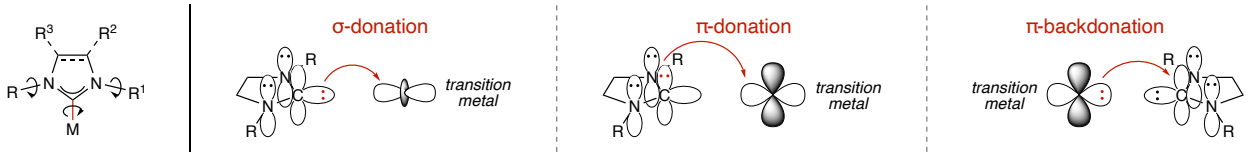

Figure 1-6. Electronic properties of NHCs as ligands in transition metal catalysis.

Analysis of NHCs as transition metal ligands frequently results in comparison to the coordination characteristics of phosphine ligands, a ubiquitous class of auxiliary ligands in transition-metal coordination chemistry.[42] General comparison of their Tolman electronic parameters (TEP) suggests that NHCs often exhibit more electron-donating capabilities than their respective phosphine counterparts; this increased σ-donation results in thermodynamically stronger metal-ligand bonding, as demonstrated by the shortened bond lengths and greater bond dissociation energies compared to phosphine ligands (excluding interference that may be caused by steric hindrance).[27,43] Similarly, most classes of NHCs take on a fan- or umbrella-like conformation, with the *N*-substituents pointed towards the metal center, thus increasing the overall steric demands imposed by NHC ligands in comparison to phosphine ligands.[44] Coupled with the relative synthetic ease and tunability of NHCs, these steric and electronic properties have enabled carbene species to parallel phosphine ligands as one of the primary ligand classes in organometallic chemistry.

A vast array of transformations has been catalyzed by metals featuring NHC ligands, likely due to the low rate of catalyst decomposition that results from strong metal-ligand binding. The enhanced catalytic activity of these species has enabled their use in staple reactions such as iridium- and ruthenium-catalyzed hydrogenation and hydrogen transfer reactions,[45] rhodium and platinum-catalyzed hydrosilylations,[46] and gold-catalyzed activation of alkenes.[47] Perhaps the most well-known class of catalytic reactions involving carbene ligands are palladium-catalyzed

cross-coupling reactions and ruthenium-catalyzed olefin metathesis.[48] Grubbs' second-generation olefin metathesis catalyst (SIMes-Ru(II)) is commonly employed for its low catalyst loading, high reactivity, and broad range of suitable substrates (**Scheme 1-2**). The success of this catalyst and similar scaffolds in metathesis reactions was acknowledged in 2005 when Professors Robert Grubbs, Yves Chauvin, and Richard Schrock were awarded the Nobel Prize for chemistry.[49]

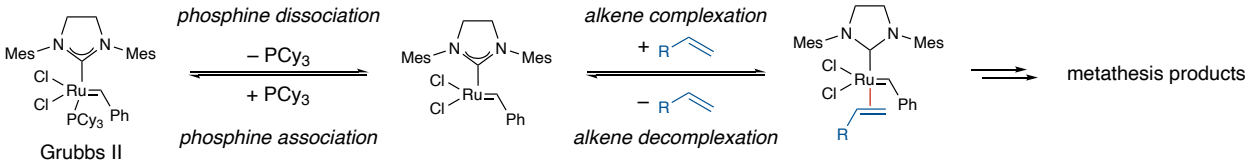

Scheme 1-2. Grubbs' second-generation olefin metathesis catalyst.

1.4 Carbenes as Organocatalysts

NHCs have also taken a role as powerful organocatalysts, complementing their use as ligands in transition metal catalysis. Dating back to 1832, the compelling concept of polarity reversal in synthetic chemistry was first demonstrated by Wöhler and Liebig in their report of a cyanide-catalyzed benzoin reaction.[50] At the onset of the next century, Lapworth proposed the mechanism for the condensation reaction in 1903.[51] Ukai and coworkers later illustrated that thiazolium salts catalyze the benzoin reaction in 1943. Shortly thereafter, Mizuhara and coworkers demonstrated that furoin and acetoin can be generated from furfural and pyruvate, respectively, using the thiamine cofactor under alkaline reaction conditions. [35,52-54] In addition to the early work involving cyanide catalysis, these seminal reports employing NHCs sparked the genesis of umpolung catalysis.

1.4.1 Early Work

Significant efforts were made by numerous groups to understand the mechanism involved in NHC catalyzed umpolung reactivity. In 1958, Breslow proposed that in situ deprotonation of a thiazolium salt afforded the free carbene active catalyst species.[33] Nucleophilic attack of the amphiphilic NHC on the electrophilic aldehyde occurs, and a subsequent proton transfer yields a species known today as the Breslow intermediate. This enamine-like Breslow intermediate is nucleophilic at C1, the formerly electrophilic carbonyl carbon, due to π-donation from the carbene heteroatoms. The acyl anion equivalent then reacts with an electrophile, and a final proton transfer yields a tetrahedral intermediate that can collapse to afford the desired product and regenerate the NHC catalyst (**Scheme 1-3**). This proposed mechanism explains the reversal in polarity that was previously observed in thiazolium-catalyzed reactions and has been adopted as the dominant mechanism for a large portion of NHC reactivity. Nearly four decades after Ukai disclosed the first NHC-catalyzed benzoin reaction, Bertrand and coworkers disclosed evidence that carbenes are the catalytically active species in these reactions through their synthesis of a stable phosphinocarbene.[55] In addition to the isolation and characterization of a free carbene in 1991 by Arduengo, the mechanistic studies by Bertrand revealed that free carbenes are stable and robust.[56] These unique species have since been employed as organocatalysts to accomplish a plethora of transformations.[16,57]

The benzoin condensation is one of the most well-studied NHC-catalyzed reaction to date. This staple reaction yields α-hydroxy ketones via condensation between two molecules of aldehyde, where one functions as an acyl anion equivalent and the other acts as a carbonyl electrophile. The benzoin reaction was first accomplished on a synthetically useful scale in 1976

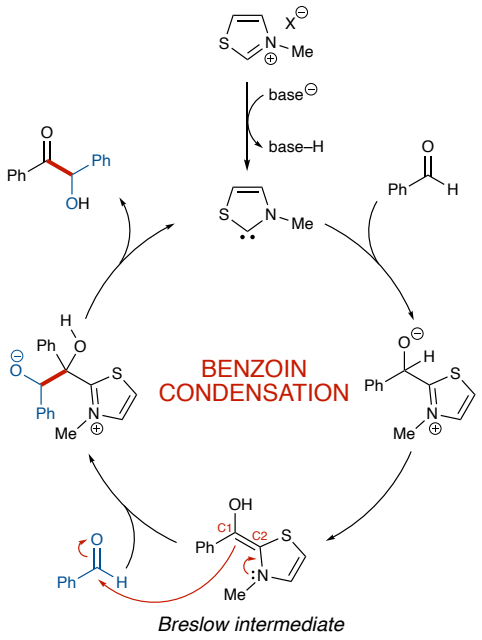

Scheme 1-3. Breslow's proposed mechanism for the NHC-catalyzed benzoin condensation.

by Stetter and was subsequently studied by many in the decades that followed.[58] Nonetheless, conditions to afford product in high yield and with high selectivity were not disclosed until 2002 by Enders and coworkers.[59] Since these initial reports, homo-benzoin (i.e., the coupling of two identical aldehydes), cross-benzoin (i.e., the reaction of two different aldehydes), aza-benzoin (i.e., the condensation between an imine and an aldehyde), and intramolecular benzoin condensations have been developed and further studied at length, making the benzoin reaction a pillar of NHC organocatalysis (**Scheme 1-4**).[60-61]

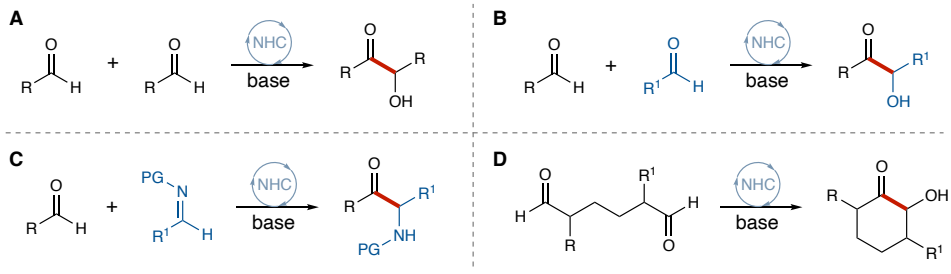

Scheme 1-4. General schemes for the **A)** homo-benzoin reaction, **B)** cross-benzoin reaction, **C)** aza-benzoin reaction, and **D)** intramolecular benzoin reaction.

Another key class of NHC-catalyzed reactions was established in 1976 when Stetter revealed that the Breslow intermediate can undergo 1,4-additions to α,β-unsaturated compounds (**Scheme 1-5**).[62] The same transformation was achieved by Stetter and Schreckenberg three years prior when they disclosed cyanide-catalyzed conjugate additions of aldehydes to α,β-unsaturated carbonylic esters, ketones, and nitriles.[63] Now termed the Stetter reaction, this umpolung reactivity allows access to 1,4-dicarbonyl compounds, the synthesis of which is non-trivial using traditional approaches.[64] This reaction features irreversible addition of the nucleophilic Breslow intermediate to a Michael acceptor, and a subsequent proton transfer and regeneration of the free carbene yields the desired product.

Notably, with the Breslow intermediate as the reactive species, the Stetter reaction is known to suffer from undesired benzoin reactivity. The efficiency of these reactions is therefore dependent on the aldehyde and the catalyst, as the benzoin condensation is a reversible process. To circumvent undesired reactivity, intramolecular Stetter reactions can be performed, as first demonstrated merely a few years following Stetter's initial report in 1979 in the total synthesis of hirsutic acid C.[65] The development of intramolecular Stetter reactions has thus been the focus of significant efforts by numerous research groups, including those of Ciganek, Enders, Rovis, and Harmada, allowing access to a variety of 5- and 6-membered functionalized heterocycles.[66-72] First demonstrated by our group, the use of acylsilanes as aldehyde surrogates has also been a successful tactic for achieving the desired reactivity.[73-75] Since the discovery and development of the Stetter reaction and the benzoin condensation, the field of NHC catalysis has continued to expand, allowing access to wide range of achiral and chiral products.

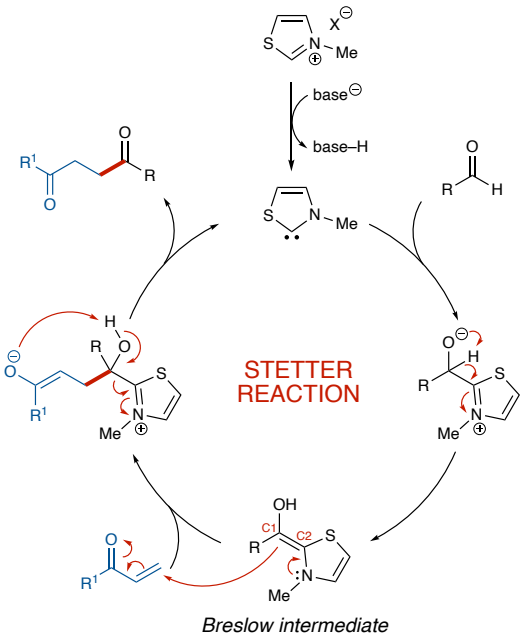

Scheme 1-5. Proposed mechanism for the Stetter reaction.

1.4.2 Asymmetric Catalysis

The modular synthesis of azolium salts has enabled the development of numerous chiral carbene classes, which have been exploited to achieve an array of asymmetric syntheses. A chiral thiazolium precatalyst was first employed in 1966 by Sheehan and Hunneman to access the desired benzoin product in 22% enantiomeric excess (**Scheme 1-6**).[76] While low, the selectivity achieved was one of the first examples of asymmetric organocatalysis and paved the way for the development of enantioselective NHC catalysis. Studies suggest that the low selectivity achieved

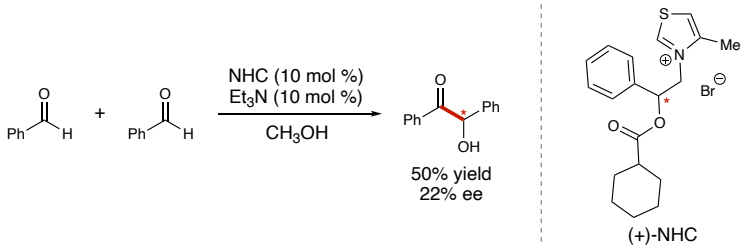

Scheme 1-6. The first enantioselective NHC-catalyzed reaction.[76]

early on with thiazolium precatalysts can be attributed to the free rotation around the chiral center.[77-78]

The emergence of bicyclic triazolidene carbenes by Leeper as well as triazolidene carbenes by Enders and Teles improved the enantioselectivities for the benzoin reaction.[59,79-81] Enders was able to access the first Stetter products in high enantiomeric excess (74%) in his chiral triazolidene-catalyzed synthesis of chromanones (**Scheme 1-7**).[67] Significant development of chiral NHC catalysts by the groups of Rovis, Bode, and other groups over the past two decades has led to improved enantioselectivities in these reactions and an array of additional NHC-catalyzed reactions.[25,82-83]

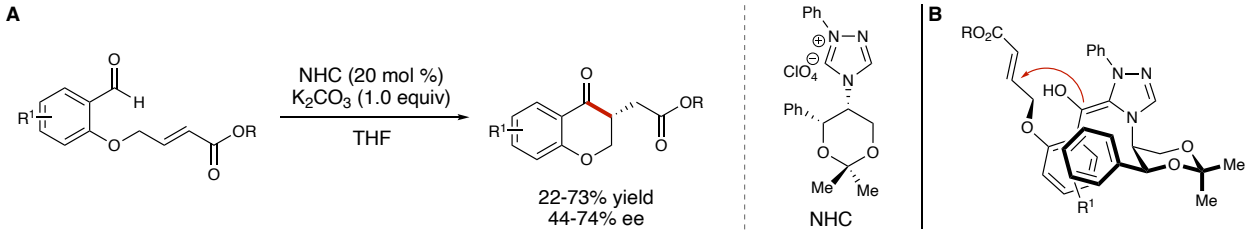

Scheme 1-7. A) The first enantioselective Stetter reaction by Enders, and **B)** a model explaining the facial selectivity.[67]

1.4.3 Cooperative Catalysis

To increase the efficiency and utility of NHCs in synthesis, the exploration of multi-catalyst manifolds has also been developed. Cooperative catalysis refers to systems wherein two catalysts independently activate distinct substrates to generate a single product with exceptional efficiency and selectively.[84] NHC catalysis has been cooperatively combined with numerous other modes of catalysis, including catalysis of Lewis acids, Brønsted acids, Brønsted bases, hydrogen bond donors, transition metals, and more.[85] For example, Scheidt and coworkers disclosed the first report of NHC/Lewis acid cooperative catalysis in 2010 using a carbene and a titanium(II) species

to access substituted cyclopentenes (**Scheme 1-8**).[86] Trans products were primarily observed without the Lewis acid cocatalyst, but the addition of catalytic titanium led to a reversal of diastereoselectivity, yielding the cis isomer. Computational analysis by Domingo suggested that the cocatalysts align the Breslow intermediate and the electrophile for cis-selective C–C bond formation.[87-88] Cooperative NHC catalysis involving Lewis acids and other catalytic modes has continued to grow, resulting in methods to access unique chemical scaffolds in high selectivity and with superior efficiency.[85]

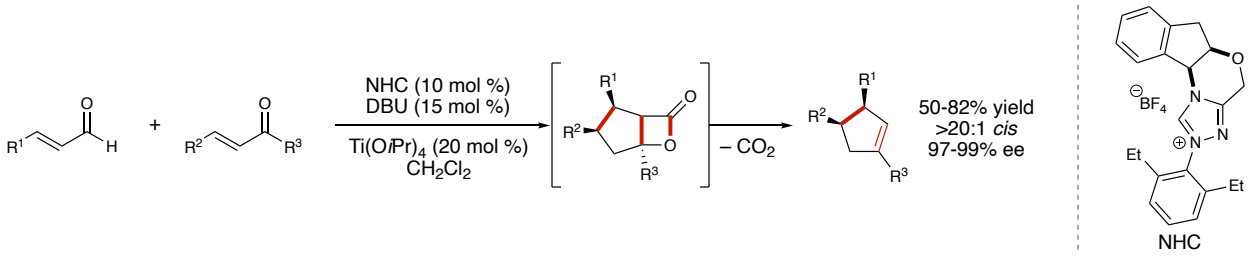

Scheme 1-8. A carbene- and Lewis acid-catalyzed synthesis of trisubstituted cyclopentenes.[86]

1.5 Overview of Single-electron NHC Operators

While NHC reactivity continues to expand, the dearth of NHC-derived operators to engage sp^3-hybridized electrophiles limits their scope, thus highlighting the potential opportunity for single-electron NHC species. NHC-derived radical species have gradually gained increasing attention in recent decades, primarily due to the strong reducing capabilities of the Breslow intermediate disclosed by the Fukuzumi group in the late 1990s.[89-92,93] These synthetic operators can be generated via single-electron oxidation or single-electron reduction. In the oxidation pathway, NHC addition into an aldehyde generates a Breslow intermediate, which can reduce a radical acceptor to generate a key NHC-derived ketyl radical species (**I**$^{\bullet}$; **Scheme 1-9**). Mechanistic and computational studies suggest that this process occurs via SET from the electron-rich Breslow

enolate to the acceptor molecule,[94] and a recent report by Martin and Tomás-Mendivil revealed that a wide range of NHCs can generate strong reducing agents ($E_{1/2} > -1.7$ V vs. saturated calomel electrode (SCE)).[95] Alternatively, this radical species can be accessed via single-electron reduction of the electron-deficient acyl azolium intermediate, which is generated by a two-electron oxidation of the Breslow intermediate or by NHC addition into an activated carbonyl system (e.g., acyl imidazole, acyl fluoride, activated esters, etc.). With modest reduction potentials ($E_{1/2} \sim -0.8$ V vs. SCE),[95] acyl azoliums can undergo single-electron reduction from a wide range of photocatalysts or other reducing species.

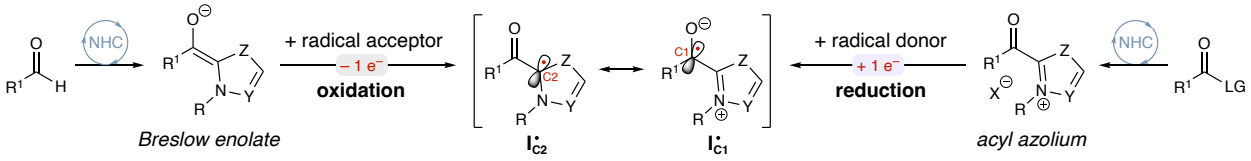

Scheme 1-9. Generation of single-electron NHC species via single-electron oxidation or reduction.

The unique properties of **I•** have gained increasing attention in recent years.[96] Due in part to delocalization into the carbene, these captodative radicals offer increased stability compared to traditional acyl radicals, allowing for selective radical cross-coupling with transient partners.[90] Mechanistic studies performed by Bertrand, Martin, and others suggest that the spin density is distributed primarily between C1, C2, O, and the carbene heteroatoms, with more radical character at C2 than C1 in most cases (**Scheme 1-9**).[94,97] The majority of mechanisms in the literature depict the radical centered on C1 (**I•$_{C1}$**), as this carbon is involved in the desired bond-formation. It is important to note that additional reactivity modes (e.g., coupling with **I•$_{C2}$**) may also occur as a result of the radical distribution.[97] Moreover, various studies suggest that the steric and electronic properties of the NHC influence the reactivity and persistency of the corresponding radical

species.[97-98] As a result, modulation of these parameters has enabled expansion of substrate scopes, further showcasing the potential advantages of these radical species in synthesis **(Figure 1-7)**.

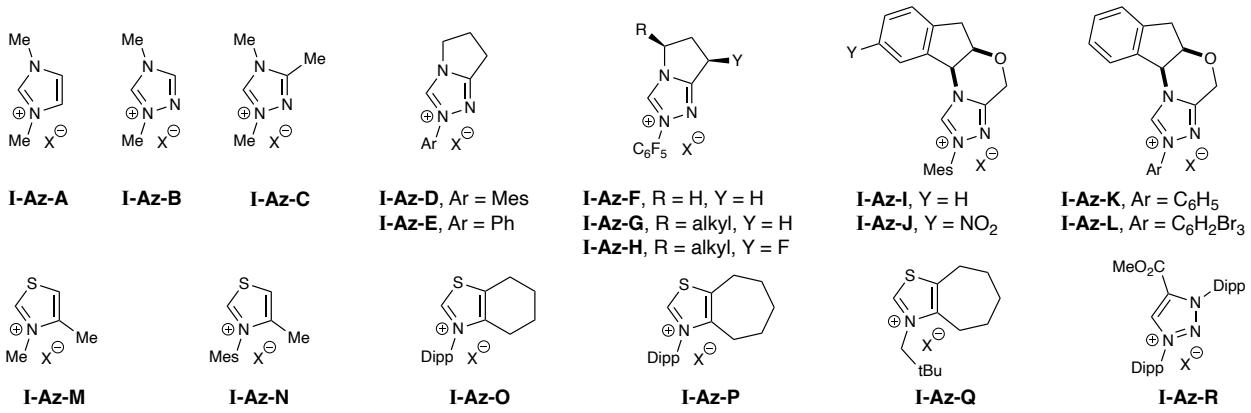

Figure 1-7. Common NHC precursors used in single-electron NHC catalysis.

1.6 Oxidative Generation of Radical Carbene Operators

1.6.1 Early Radical NHC Organocatalysis

Early work from our group and Studer's group showcased the potential for radical carbene operators in NHC-catalyzed mild oxidations of allylic alcohols and aldehydes to esters.[34,54,99-100] In these processes, two consecutive single-electron oxidations of the Breslow intermediate afford the acyl azolium intermediate, and displacement of the NHC by an alcohol forges the desired C–O bond (**Scheme 1-10)**. Boydston, Studer, and others then removed the need for stoichiometric oxidants in their independent reports featuring anodic oxidation, ruthenium redox, and more, respectively.[101-104] While significant improvements in NHC-catalyzed processes were made in the decade that followed, these strategies largely have been confined to the formation of C–X bonds (X = O, N, etc.).

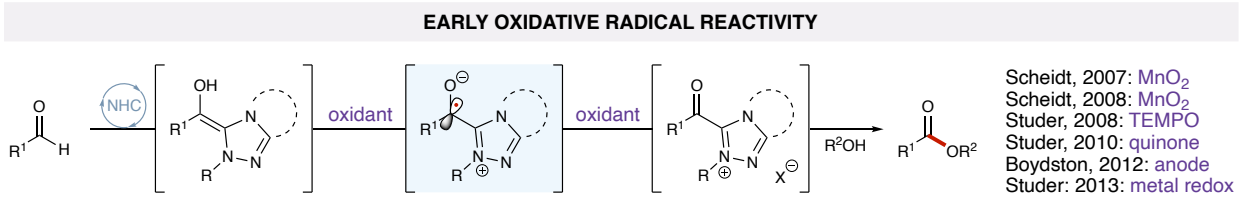

Scheme 1-10. Early oxidative esterification strategies

1.6.2 Indirect Radical Reactivity

The construction of C–C bonds via a single-electron manifold with NHC catalysis was first accomplished by the groups of Chi, Rovis, and Ye, who independently reported the single-electron reduction of nitro-compounds by the Breslow intermediate. In 2014, Chi and coworkers disclosed a β,β-coupling reaction of nitroalkenes initiated by SET between a nitroalkene and the Breslow intermediate (**Scheme 1-11**).[105] The generation of the Breslow intermediate radical cation occurs concurrently with reduction of the nitroalkene to the radical anion, which then undergoes a 1,4-addition to a second equivalent of nitroalkene. Two SET oxidation events of **I**• generate the corresponding acyl azolium. Protonation of the nitroalkane-derived radical anion and NHC turnover by methanol produces the homo-coupled nitroalkane and ester products. Chi's group has since developed various coupling and cascade reactions, including the coupling of nitrobenzyl bromides with activated ketones or imines.[106-108] This initial work by Chi demonstrated the ability of the Breslow intermediate to act as an electron donor while not participating in the final desired bond formation step (**Scheme 1-11**). Although NHCs have also been employed as catalytic single-electron reductants, hydrogen-atom transfer (HAT) reagents, and more,[109-113] the majority of recent progress in the field of single-electron carbene catalysis features oxidation of the Breslow intermediate to persistent **I**•.

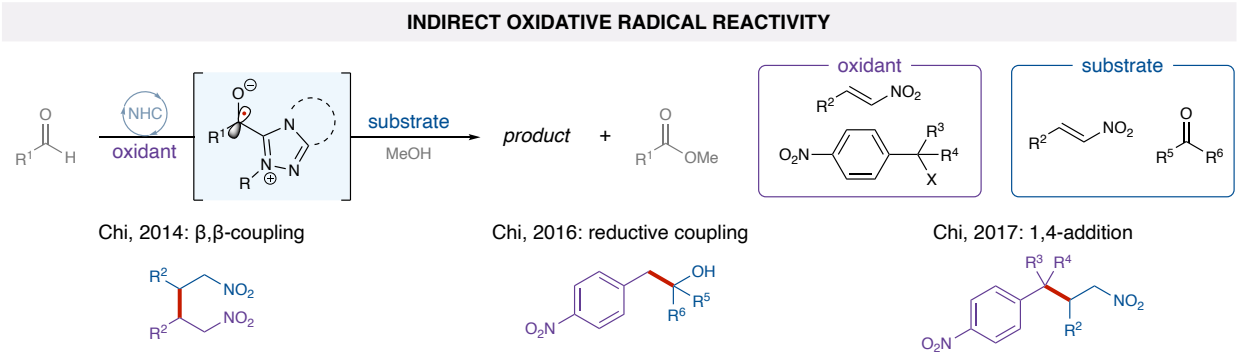

Scheme 1-11. Transient oxidative NHC radical processes.

1.6.2.1 Homoenolate Functionalization

In late 2014 and 2015, Rovis and Chi independently developed enantioselective β-hydroxylation reactions of enals with nitro compounds using chiral **I-Az-G** or **I-Az-I**, respectively.[114-115] These reports revealed that single-electron oxidation of the NHC homoenolate intermediate produces a radical intermediate featuring significant radical character at the β-carbon (**Scheme 1-12**). Following in situ formation, the homoenolate was proposed to undergo a single-electron oxidation derived radical anion yields an NHC-bound alkoxide intermediate, affording the enantioenriched β-hydroxylated ester following trapping with methanol. This transformation was recently rendered enantioselective via a chiral nitrobenzene with achiral **I-Az-E** by Chi and coworkers.[116]

In the development of their β-hydroxylation protocol (vide supra), Rovis and coworkers observed cyclopentanone formation when non-nucleophilic solvents were employed. Optimization of this process led to an enantioselective homocoupling to yield 3,4-disubstituted cyclopentanones (**Scheme 1-12**).[117] Following addition of the homoenolate radical cation into a second equivalent of homoenolate, single-electron oxidation by the nitrobenzene radical anion affords a dimer

intermediate. A cyclopentanone acyl azolium species is then accessed via intramolecular cyclization, and subsequent hydrolysis and decarboxylation affords the desired product.

Cross-coupling of the homoenolate and an enolate is also possible and was first realized by Ye in 2017 and was later extended to the construction of contiguous tetrasubstituted stereocenters.[118-119] In their [3+2] annulation of dioxindole and enals, spirocyclic oxindole-γ-lactones were isolated with high-to-excellent diastereo- and enantioselectivities (**Scheme 1-12**). While various plausible two-electron pathways can lead to the products, TEMPO-trapping and EPR experiments suggested a radical-based mechanism. Nitrobenzene was used as an oxidant to afford the homoenolate radical, and HAT to the resulting nitrobenzene radical anion provides the dioxindole enolate radical. Based on their mechanistic studies, the key bond-forming step is the cross-coupling of the homoenolate radical and enolate radical. Protonation gives the acyl azolium and lactonization yields the spirocyclic oxindole-γ-lactone and turns over the NHC.

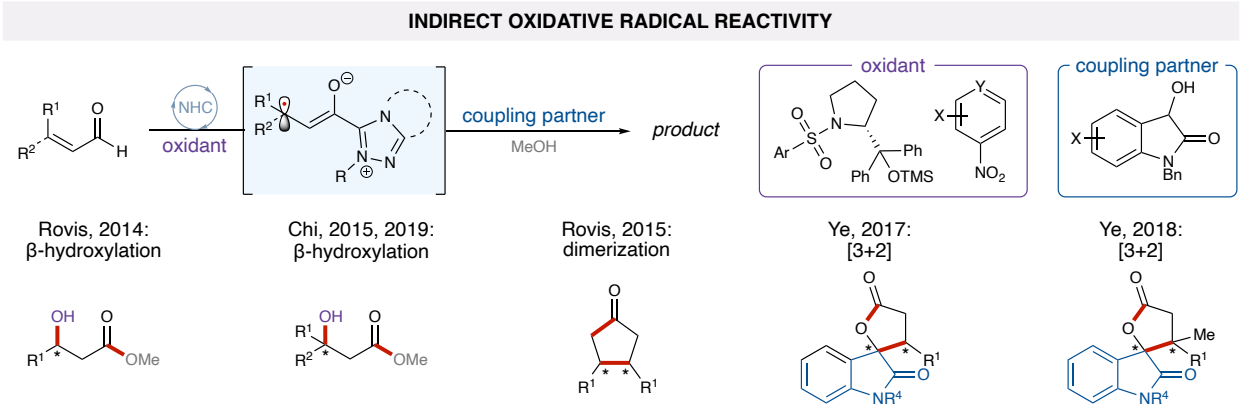

Scheme 1-12. β-functionalization strategies via radical homoenolate reactivity.

1.6.2.2 Extended Systems: γ- and ε-Functionalization

The distributed radical character afforded by conjugation in unsaturated Breslow intermediates can be further extended for remote functionalization. Sun and coworkers disclosed

an NHC-catalyzed γ-dihalomethylenation process using carbon tetrabromide and bromotrichloromethane as SET oxidants to access radicals derived from dienolates (**Scheme 1-13**).[120] Although the mechanism is unclear, it is proposed to feature elimination of a pre-placed leaving group to convert the Breslow intermediate into its dienolate form. Following SET, radical-radical coupling between a trihalomethyl radical and the extended γ-radical dienolate or radical addition to the γ-position of the dienolate yields a γ-substituted α,β-unsaturated acyl azolium. NHC turnover by an alcohol and elimination of HBr yields the desired product. This work also included one of the first examples of combined NHC and photoredox catalysis[121,122] wherein γ-dichloromethylenation using carbon tetrachloride as the terminal oxidant afforded the desired product in moderate yield.

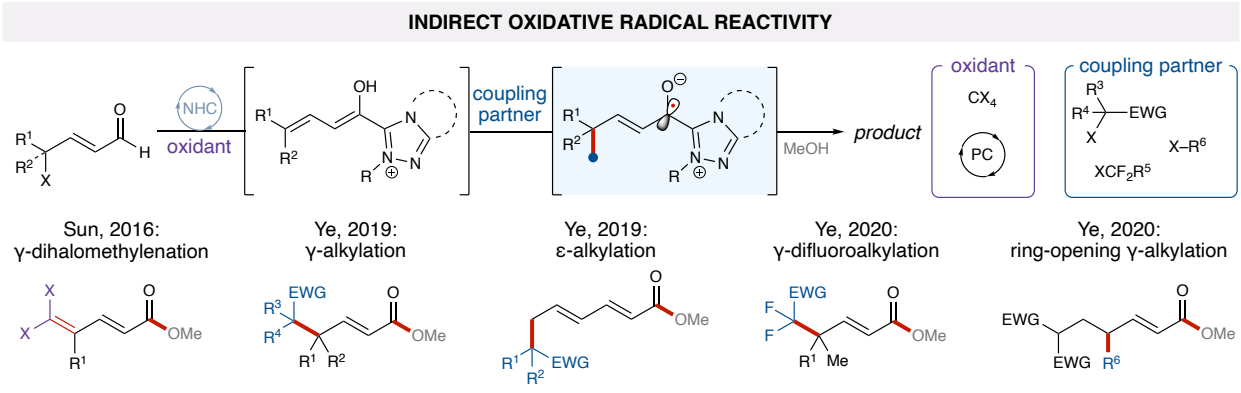

Scheme 1-13. γ-Functionalization and ε-functionalization approaches.

The combination of NHC and photoredox catalysis was fully realized for the construction of C–C bonds by Ye and coworkers in 2019 with their reaction of alkyl halides and NHC-derived enals to give γ-substituted-α,β-unsaturated esters.[123] They extended this work to the ε-functionalization of strategically placed γ-vinyl-substituted α,β- and δ,ε-unsaturated aldehydes (**Scheme 1-13**). Based on mechanistic studies, they suggested that the excited photocatalyst

reduces an alkyl halide, and the resulting alkyl radical undergoes γ-addition to the Breslow dienolate or ε-addition to the Breslow trienolate. Single-electron oxidation of the resulting radical followed by displacement of the NHC by methanol yields the γ- or ε-alkylated product, respectively. The same group disclosed protocols for the photoredox and NHC-catalyzed synthesis of γ-difluoroalkyl-α,β-unsaturated esters from bromodifluoroacetates or iodoperfluoroalkanes as well as the ring-opening of cyclopropane enals to give similar γ-substituted ester products (**Scheme 1-13**).[124-125]

1.6.2.3 Radical Relay Processes

A four-component reaction was recently developed by Chen and Huang to provide β-tertiary-γ-quaternary esters and amides (**Scheme 1-14**).[126] Using Togni I as a trifluoromethyl radical source, an olefin was employed to convert the electrophilic trifluoromethyl radical into a nucleophilic alkyl radical, thus increasing the rate of radical-radical coupling with the homoenolate β-radical. Final displacement of the NHC by an alcohol or amine affords the desired ester or amide product, respectively.

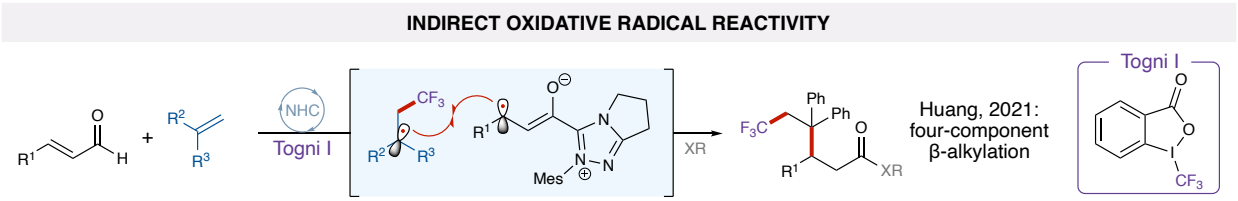

Scheme 1-14. Indirect radical relay reactivity.

1.6.3 Direct Carbene Radical Reactivity

It was not until early 2019 that oxidatively generated **I**• was directly coupled with carbon-based radicals. In a key report by Ohmiya and coworkers, the persistent radical effect was harnessed to achieve an **I-Az-P**-catalyzed decarboxylative coupling of aryl aldehydes with alkyl

radicals derived from redox-active esters (**Scheme 1-15**).[127] The authors suggest that the Breslow enolate reduces the redox-active ester to afford **I**• and an alkyl radical. Direct radical-radical coupling afforded a range of aryl ketones and functionalized bioactive molecules.

Since this initial report, a variety of transformations employing direct radical carbene operator reactivity have been developed. A similar protocol using Katritzky pyridinium salts in place of redox-active esters was disclosed by the Hong group in 2020 (**Scheme 1-15**).[128] Both of these reactions were initially limited to the use of aryl aldehydes. In 2020, however, Ohmiya and Nagao redesigned the thiazolium NHC, changing the *N*-aryl substitution (**I-Az-P**) to *N*-neopentyl (**I-Az-Q**).[98] This difference in *N*-substitution enabled aliphatic aldehydes to be used in oxidative Breslow intermediate-derived radical processes.[98] Based on the substrate, both NHCs have since been used to effect new transformations via similar mechanisms. Ohmiya and coworkers later employed both NHCs in the synthesis of β-ketocarbonyl compounds from aldehydes and α-bromoesters or α-bromoamides.[129] Similarly, Liu and Shu reported a photocatalyzed amide synthesis featuring a reductive quenching cycle wherein the excited organophotocatalyst performs a single-electron oxidation of the Breslow intermediate followed by single-electron reduction of an imine (**Scheme 1-15**).[130]

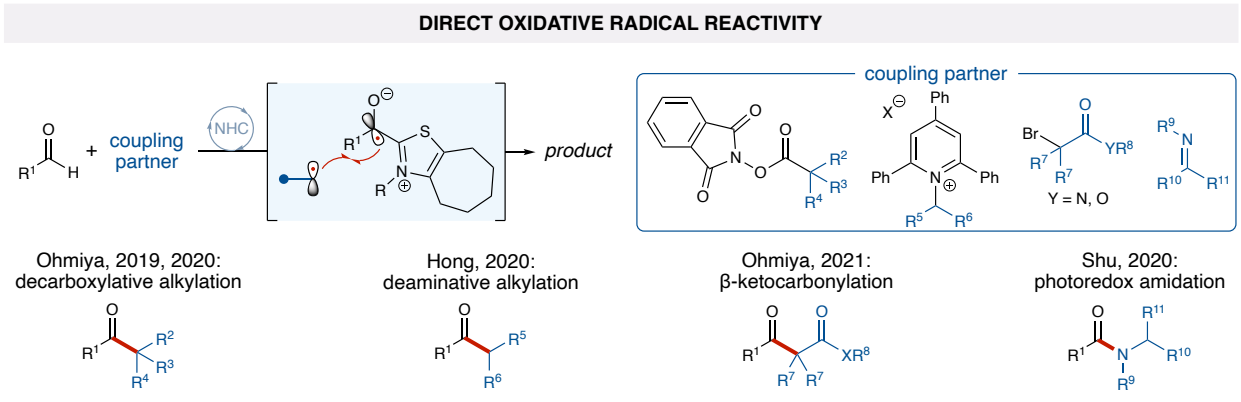

Scheme 1-15. Radical–radical coupling reactions featuring direct oxidative radical reactivity.

1.6.3.1 Radical Relay Processes

Building on this reactivity, the groups of Ohmiya and Hong independently reported alkyl radical cascade reactions that require reaction rates of various competing reactions to be properly matched to achieve the desired reactivity (**Scheme 1-16**). In an elegant report, Ohmiya and coworkers added a conjugate acceptor to their standard reaction conditions to generate a more stabilized radical via initial alkyl radical addition into the alkene.[131] Coupling with **I•** afforded the functionalized ketone. Ohmiya followed up with a similar protocol using tertiary α-bromo esters instead of redox-active esters to yield δ-keto esters.[132] In the same report as their direct Katritzky salt coupling, Hong and coworkers modified their reaction conditions to achieve a three-component radical cascade reaction.[128]

Using simple aryl iodides as aryl radical precursors, Ohmiya and coworkers recently and disclosed a protocol for the arylacylation of styrenes as well as the C(sp^3)–H acylation of secondary amides (**Scheme 1-16**).[133] They suggest that aryl radical generation occurs catalytically through a thermodynamically unfavorable SET event with the Breslow enolate (E_{ox} = –0.97 V vs. SCE; aryl iodide, E_{red} = –2.24 V vs. SCE). Backed by baseline DFT calculations, this pathway is hypothesized to be kinetically feasible due to the small reorganization energy of the Breslow intermediate coupled with the fast mesolytic cleavage of the C(sp^2)–I bond. Unlike the arylacylation radical relay strategy that features the same mechanism as previous reports, their strategy for the α-amino C(sp^3)–H acylation of secondary aryl amides employs the generated aryl radical as an intramolecular HAT reagent. Intramolecular 1,5-HAT likely affords an α-amino C(sp^3)-centered radical that directly couples with **I•** to give a range of acylated secondary amides.

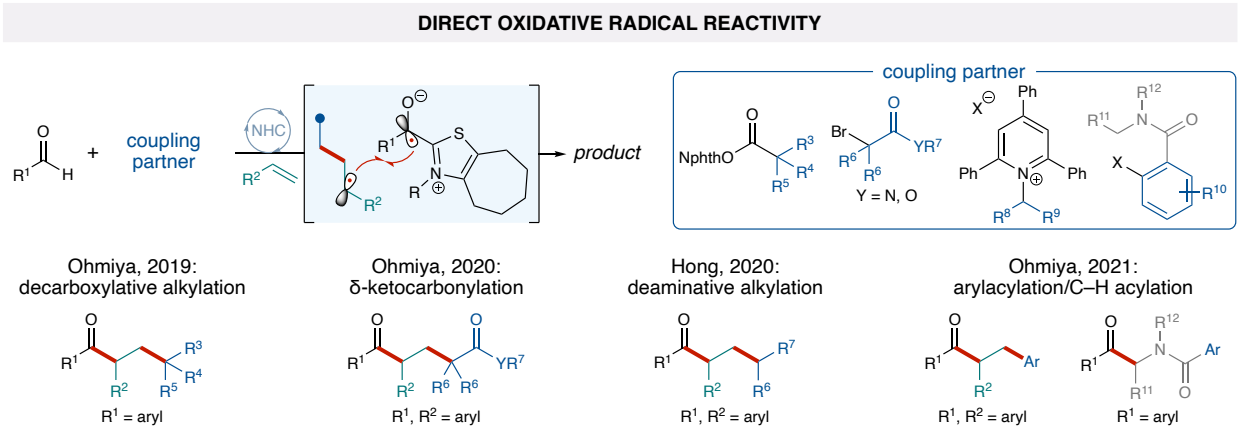

Scheme 1-16. Direct oxidative radical relay reactivity with alkyl radicals.

A variety of transformations involving the ring-opening of cyclic oximes and eventual coupling to **I**• were recently reported (**Scheme 1-17**). In early 2021, an NHC and magnesium co-catalyzed acylcyanoalkylation of alkenes using cycloalkanone oxime esters was reported by Du and coworkers.[134,135] In this process, thermally controlled SET from the Breslow enolate generates an open-shell *N*-centered radical and β-scission provides the corresponding translocated transient cyanoalkyl radical, which is captured by an olefin. The resultant radical couples with **I**• to yield multifunctionalized nitrile-containing ketones, including motifs important in the development of

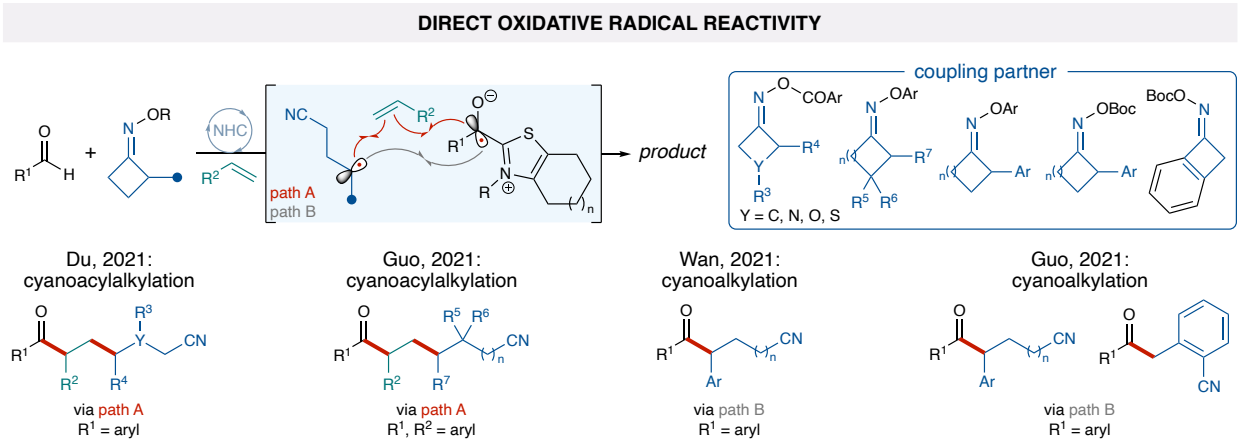

Scheme 1-17. Radical relay reactions with oxime-derived radicals.

proteolysis targeting chimeras (PROTACs). At the same time, Guo described a 1,2-cyanoalkylacylation of alkenes using readily available cyclobutanone oxime ethers as the source of cyanoalkyl radicals.[136] Shortly thereafter, a ring-opening coupling between cyclopentanone oxime ethers or esters and **I**• was independently disclosed by the groups of Wan and Guo, respectively.[137-138]

This three-component radical relay paradigm has also been extended to the acylhalogenation of alkenes by the groups of Li, Wang, Wu, and Ohmiya (**Scheme 1-18**).[139-142] Various three-component trifluoromethylation reactions employed either Togni I or perfluoroalkylbromides as the fluoroalkyl radical source. Ohmiya and coworkers recently disclosed a trichloromethylation acylation of alkenes using carbon tetrachloride as a transient trichloromethyl radical source.[142] Featuring mechanisms similar to the original work by Ohmiya and Hong, these reactions afforded a variety of β-functionalized aryl ketones.

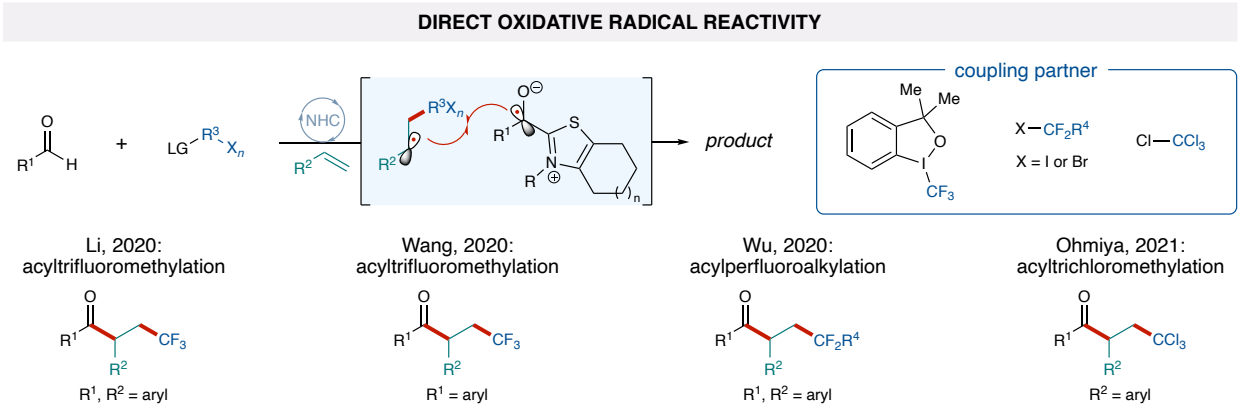

Scheme 1-18. Haloalkyl radicals in radical relay processes.

Photoredox catalysis and carbene catalysis were merged again by the Shu group in their strategy for the vinylation of aldehydes with alkenes (**Scheme 1-19A**).[143] Following mechanistic studies, the authors suggest a complex mechanism featuring two distinct photoredox cycles. The

reaction is initiated by interaction of an excited photocatalyst with phenylsulfinate to generate a phenylsulfonyl radical, which promptly adds into an alkene to yield a carbon-centered radical. Regeneration of the ground state photocatalyst occurs by single-electron oxidation of a quinone-derived oxidant to the corresponding radical anion. Coupling of these two radical species yields a substituted quinone-derived intermediate, which is reduced in a second photoredox cycle following generation of **I•** by single-electron oxidation of the Breslow intermediate. Coupling of the resulting radical with **I•** yields a β-phenylsulfonyl-substituted ketone, and consecutive elimination of phenylsulfonate provides the vinyl ketone product.

The majority of oxidative NHC-catalyzed three-component radical relay processes developed to date feature a radical NHC operator derived from an aryl aldehyde and a thiazolium-based NHC. Recently, however, Yan and coworkers developed mesoinic **I-Az-R** for the arylacylation of alkenes (**Scheme 1-19B**).[144] While the mechanism for initial radical generation is unclear,[145] the authors suggest that addition of a transient aryl radical into an alkene followed by radical-radical coupling with **I•** affords a variety of β-arylated aryl ketones. This reactivity was extended to intramolecular annulation and cascade acylations for the construction of more complex motifs.

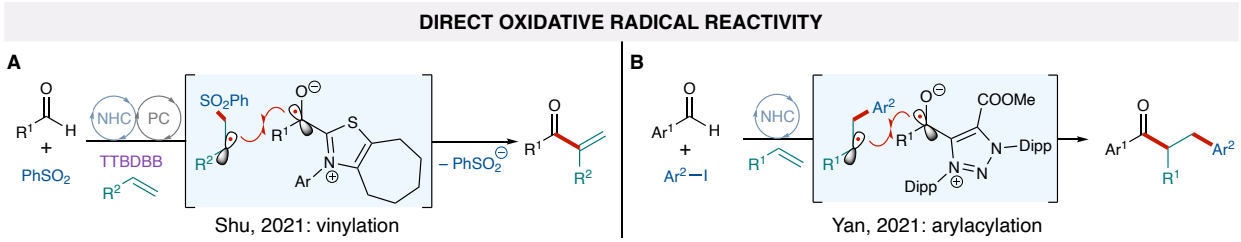

Scheme 1-19. A) Radical relay via photoredox catalysis, and **B)** radical relay using a mesoionic carbene.

1.7 Reductive Generation of Radical Carbene Species

While oxidatively generated radical carbene processes have seen significant recent development, accessing I• via single-electron reduction is less explored. In contrast to the oxidative pathway, the majority of reductive processes begin with displacement of a leaving group by an NHC to form an acyl azolium species. Subsequent excitation or single-electron reduction of this electron-deficient intermediate affords a diradical or **I•**, respectively, thus enabling a variety of transformations in recent years.

1.7.1 Indirect Reactivity

To date, limited remote or indirect functionalization strategies using reductively generated **I•** have been developed. In 2020, Hopkinson reported an NHC-catalyzed photoenolization/Diels-Alder reaction wherein ultraviolet A (UVA) irradiation of an acyl azolium generates substituted chromanones (**Scheme 1-20**).[146] In a mechanism supported by time-dependent DFT calculations and mechanistic studies, an acyl azolium undergoes direct excitation and intersystem crossing to generate a triplet diradical species. 1,5-HAT from the *o*-benzylic position to the carbonyl oxygen radical is suggested to afford the triplet dienol biradical. Subsequent rotation of the aryl group and relaxation gives rise to a ground state hydroxy-*o*-quinodimethane species. A final cycloaddition

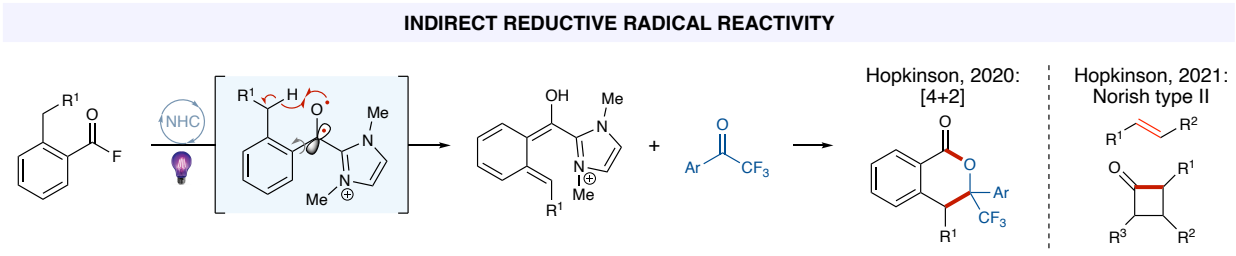

Scheme 1-20. Indirect reductive radical carbene reactivity.

reaction with a trifluoromethyl aryl ketone followed by NHC ejection provides the chromanone product. Recent work by Hopkinson described Norrish type II reactions of acyl azoliums via a similar mechanism.[147]

1.7.2 Direct Reactivity

Our group reported the first examples of radical-radical coupling for C–C bond formation via single-electron reduction of an acyl azolium.[148-149] In collaboration with the Mrksich laboratory, we employed a high-throughput photocapture method for the discovery of a single-electron reductive coupling process involving an isolated acyl azolium and a Hantzsch ester as precursors to the radical coupling partners (**Scheme 1-21**).[148] This reaction discovery platform enabled the efficient evaluation of nearly 2,000 reactions and revealed that the acyl benzimidazolium salt outperformed other isolated acyl azoliums screened. The desired ketone product was isolated in 70% yield, thus highlighting the potential utility of reductively generated **I**˙. Our group later extended the synthetic utility of preformed acyl azolium species in radical carbene processes to the construction of C–C bonds for the synthesis of esters (**Scheme 1-21**).[150] Reduction by a photocatalyst enabled preformed azolium esters to be employed as stabilized alkoxycarbonyl radical surrogates. Radical-radical coupling with an array of potassium trifluoroborate-derived alkyl and benzyl radicals afforded substituted ester products.

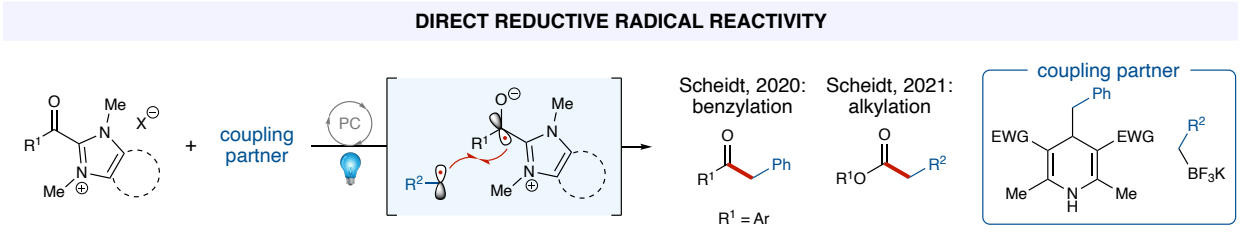

Scheme 1-21. Direct cross-coupling of reductively generated preformed acyl azolium-derived radicals.

As the first report of reductive radical carbene catalysis, we disclosed a combined NHC/photoredox-catalyzed process for the formation of ketones from activated carboxylic acids and Hantzsch esters (**Scheme 1-22**; see Chapter 2).[149] Activation of carboxylic acids with carbonyldiimidazole enabled facile generation of a variety of acyl imidazoles, and catalytic NHC allowed for the in situ construction of the corresponding acyl azolium. Mechanistic studies suggested that the photocatalyst undergoes a reductive quenching cycle wherein single-electron oxidation of the Hantzsch ester affords the respective benzyl or alkyl radical partner. Reduction of the acyl azolium by the reduced photocatalyst furnishes $\mathbf{I}^{\bullet}$, and subsequent radical-radical coupling followed by ejection of the NHC catalyst yields the desired ketone products. Notably, this work disclosed the first examples of reductively generated aliphatic radical carbene operators, albeit in diminished yields. The utility of this reaction was highlighted in the direct late-stage functionalization of pharmaceutically relevant compounds, and moderate enantioselectivity at the α-carbon was achieved using chiral **I-Az-K**.

Subsequent reports by our group and others have demonstrated the crucial role that NHC structure plays on reactivity. Computational and experimental data detailed in our recent work suggests that reactivity is governed by radical stability, distribution ($\mathbf{I}^{\bullet}_{C1}$ vs. $\mathbf{I}^{\bullet}_{C2}$), and accessibility; as such, we found that employing sterically encumbering **I-Az-D** in place of **I-Az-B** as the NHC precursor increased the efficacy of this protocol in the construction of aliphatic and α-amino ketones (**Scheme 1-22**; see Chapter 3).[97] Utilizing **I-Az-O**, Chi's group disclosed a photocatalyst-free coupling of an acyl azolium with Hantzsch ester-derived radicals (**Scheme 1-22**).[151] Mechanistic studies suggest that the excited state of the acyl azolium intermediate, accessed via direct photoexcitation with visible light, acts as a single-electron oxidant ($E_{1/2}$ estimated to be +1.9

V vs SCE).[151] Moreover, Ohmiya and coworkers recently developed an alkylation strategy using **I-Az-D** to catalyze a light-driven alkylation of acyl imidazoles with alkylborates.[152]

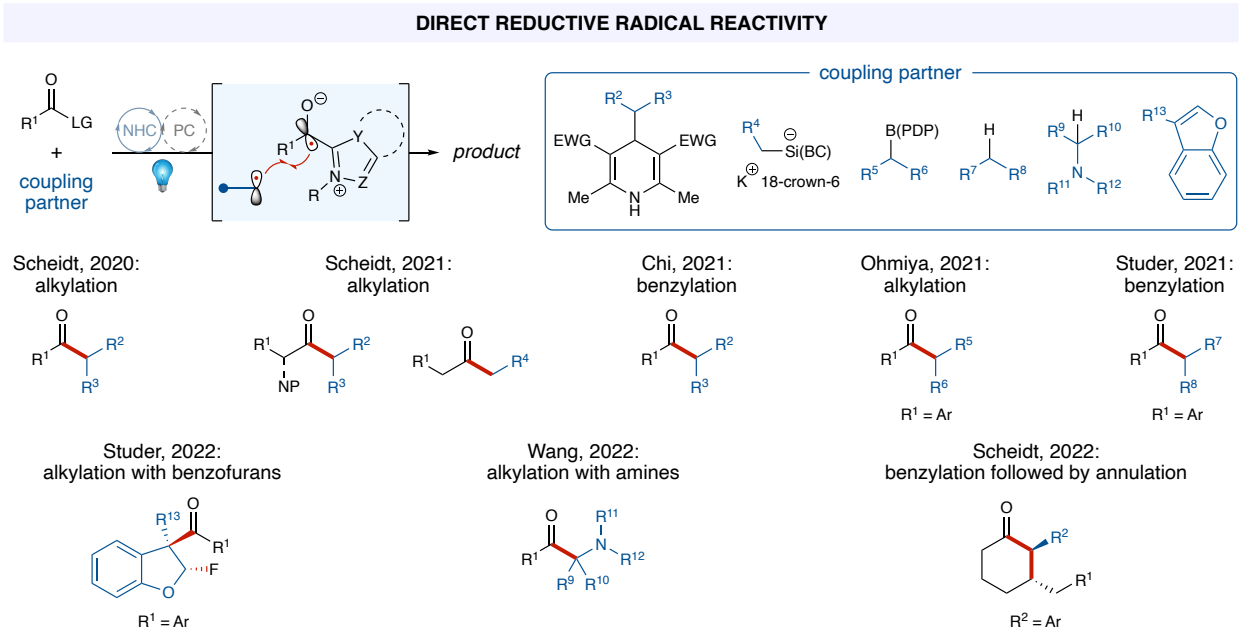

Scheme 1-22. Direct reductive radical–radical coupling processes using catalytic NHC.

In an example from the Studer group, a direct acylation of benzylic C–H bonds was accomplished using an organophotocatalyst and visible light to afford benzylic ketones from acyl fluorides and ethyl anisole derivates (**Scheme 1-22**).[153] The authors propose that reductive quenching of the photocatalyst by the electron-rich arene leads to formation of the arene radical cation. Deprotonation of the radical cation generates a benzylic radical, which then couples with reductively generated **I**$^{\bullet}$ to afford the desired benzyl ketone products following NHC ejection. Featuring a similar mechanism, Studer later accomplished the fluoroaroylation of benzofurans.[154] Reductively generated **I**$^{\bullet}$ undergoes radical-radical coupling with a radical cation species that is accessed from single-electron oxidation of benzofuran. The resulting oxocarbenium intermediate is relieved by nucleophilic addition of fluoride (from the acyl fluoride starting material), and NHC

fragmentation yields the fluoroaroylated benzofuran product. Wang and coworkers then employed *N*-alkyl anilines as radical precursors to synthesize α-amino ketones.[155] In a mechanistically similar process, single-electron oxidation of the aniline affords a radical cation that is deprotonated to give the radical coupling partner.

Recently, our lab reported a tandem photocatalyzed annulation for the synthesis of substituted cycloalkanones (**Scheme 1-22**; see Chapter 4).[156] Using Hantzsch esters as the oxidatively generated radical precursor, δ,ε-unsaturated ketones are formed in situ from the corresponding acyl imidazole via radical-radical coupling between a Hantzsch ester-derived benzylic radical and **I•**. Unlike other single-electron carbene processes, the formed ketone is merely an intermediate in this reaction. Base and photocatalyst are used in a second and distinct photoredox cycle to generate an α-radical, and an intramolecular 6-exo-trig cyclization yields the desired cyclohexanone product.

1.7.2.1 Radical Relay Processes

Reductively generated radical carbene species have also been employed in radical relay processes, further diversifying the scope of possible transformations. Studer reported an NHC/photoredox catalyzed three-component reaction to construct trifluoromethylated ketones, complementing the oxidative pathway disclosed by Li and others.[139,157] In this process, Langlois reagent was used as the oxidatively generated radical precursor, and aroyl fluorides were employed as the acyl azolium precursor (**Scheme 1-23**). Similarly, Ohmiya and coworkers expanded the scope of their alkylborate coupling process (vide supra) to the alkylacylation of activated alkenes through a radical-relay process.[152] Our group later reported the synthesis of γ-aryloxyketones using aryloxymethyl potassium trifluoroborate salts as the alkyl radical precursor.[158]

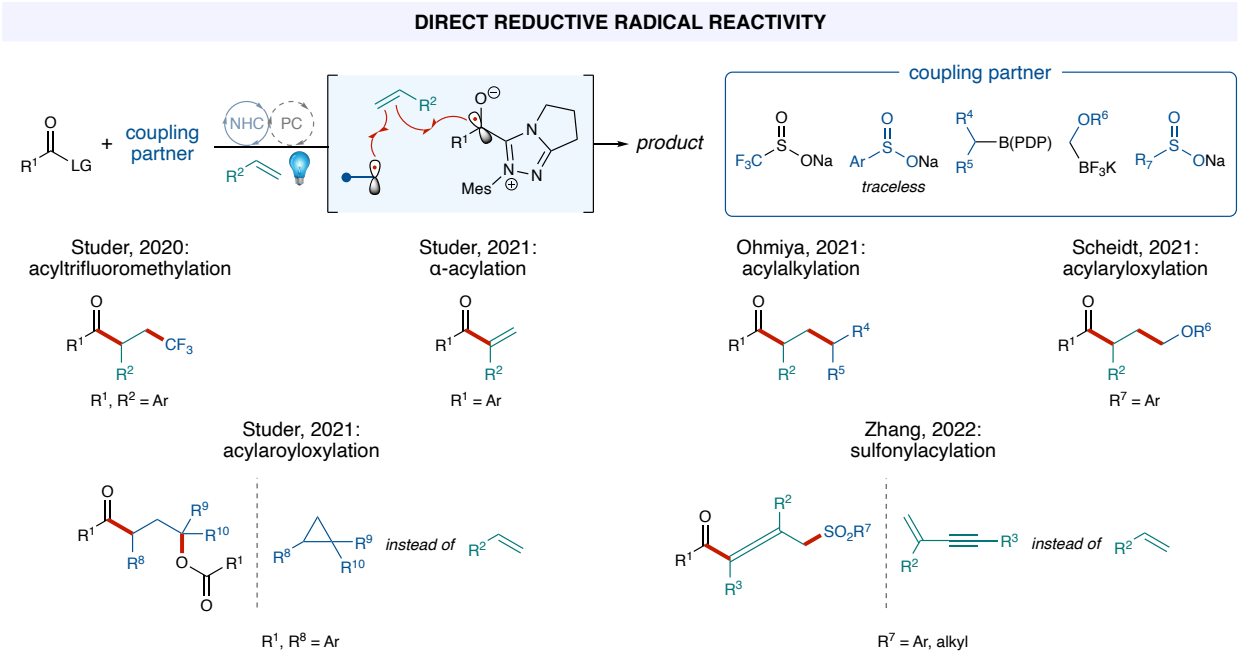

Scheme 1-23. Radical relay processes featuring reductively generated radical carbene species.

Studer extended their protocol further to the direct α-acylation of alkenes via an NHC, sulfinate, and photoredox cooperative catalytic system that proceeds through a radical addition/coupling/elimination sequence.[159] This process features single-electron oxidation of an aryl sulfinate by the excited photocatalyst to yield an aryl sulfonyl radical. Radical addition into the alkene provides an alkyl radical, which then couples with **I'** to yield α-substituted vinyl ketones. The same group recently reported a ring-opening of aryl cyclopropanes that allowed access to 1-aroyloxylated-2-acylated alkanes.[160] In a unique mechanism, the authors suggest that the acyl fluoride starting material reacts with cesium carbonate to afford a bisacyl carbonate intermediate in situ. Subsequent reaction with the NHC catalyst yields the acyl azolium intermediate, a benzoate anion, and carbon dioxide. Single-electron oxidation of the cyclopropane by an organophotocatalyst generates an aryl cyclopropane radical cation, which undergoes ring opening

by the nucleophilic benzoate, and the resulting benzylic radical couples with reductively generated **I•** to yield the desired product (**Scheme 1-23**).

Inspired by these reports, Zhang and coworkers developed an NHC/photoredox-catalyzed 1,4-sulfonylacylation of 1,3-enynes for the synthesis of tetrasubstituted allenyl ketones (**Scheme 1-23**).[161] They propose an oxidative quenching cycle wherein generation of **I•** is followed by single-electron oxidation of the aryl sulfinate. Using 1,3-enynes in place of an activated alkene, the resulting aryl sulfonyl radical adds to the olefin to deliver a propargyl radical that is in resonance with a trisubstituted allenyl radical. It is suggested that the latter species undergoes radical-radical coupling with **I•** to yield the final allenyl ketone product.

1.8 Outlook

While NHCs have a broad spectrum of uses, their application in single-electron processes has significantly expanded their utility in synthesis in recent years. Their redox properties enable generation of **I•** via single-electron oxidation of the Breslow intermediate or single-electron reduction of the acyl azolium. The ability to access these radical species catalytically from easily accessible starting materials (e.g., aldehydes, acyl imidazoles, acyl fluorides, etc.) and couple them with reductively or oxidatively generated radical partners further highlights the advantages of this growing field.

Despite the advances that have been made, significant challenges remain for the field of radical carbene catalysis. For example, enhanced stereocontrol has yet to be achieved in radical processes using chiral NHCs. Similarly, radical relay processes employing trifluoromethyl radicals and aryl radicals have been developed, yet methods that enable the direct coupling of these radicals with **I•** have not been accomplished. While numerous radical precursors have been successful in

these radical coupling processes, the field would greatly benefit from the development of new approaches that employ feedstock chemicals that do not require prefunctionalization as radical precursors. The expansion of this work into new chemical space and application of these protocols in the construction of complex molecules is eagerly anticipated in years to come. Future contributions might seek to address these challenges and ultimately realize the full potential of single-electron NHC species in synthesis.

CHAPTER 2: LIGHT-DRIVEN CARBENE CATALYSIS FOR THE SYNTHESIS OF ARYL KETONES

Portions of this chapter appear in the following publications:

Bay, A. V.; Fitzpatrick, K. P.; Betori, R. C.; Scheidt, K. A. Combined Photoredox and Carbene Catalysis for the Synthesis of Ketones from Carboxylic Acids. *Angew. Chem. Int. Ed.* **2020**, *59*, 9143–9148.

Bay, A. V.; Fitzpatrick, K. P.; González-Montiel, G. A.; Farah, A. O.; Cheong, P. H.-Y.; Scheidt, K. A. Light-Driven Carbene Catalysis for the Synthesis of Aliphatic and a-Amino Ketones. *Angew. Chem. Int. Ed.* **2021**, *60*, 17925–17931.

2.1 Open-Shell Radical Reactivity

The concept of a radical was first described in 1789 by Antoine-Laurent Lavoisier in his *Traité élémentaire de chimie*, a piece of writing proclaimed to be the first chemistry textbook written.[162] As described by Lavoisier, a radical was a single element or combination of elements in oxygen-containing acids that cannot be broken down further.[163] Over the decades and centuries that followed, the meaning of the term has evolved. In 1900, Moses Gomberg reported the first isolated free radical species in his synthesis of a stable triphenylmethyl radical by mixing chlorotriphenylmethane with silver, mercury, or zinc in benzene.[164] After significant investigation, he stated:

"The experimental evidence… forces me to the conclusion that we have to deal here with a free radical, tri-phenylmethyl, $(C_6H_5)_3C^{\bullet}$. On this assumption alone do the results… become intelligible and receive an adequate explanation. The action of zinc results, as it seems to me, in the mere abstraction of the halogen, leaving the free radical,

$$(C_6H_5)_3CCl + Zn(0) = (C_6H_5)_3C^{\bullet} + ZnCl$$

The radical so formed is apparently stable, for it can be kept both in solution and in the dry crystalline state for weeks. The radical refuses to unite with another one of its kind, and thus forms a distinct exception to all similar reactions… This work will be continued and I wish to reserve the field for myself."[164]

Open-shell species are molecular structures with one or more unpaired electrons. As a result of their incomplete valency, the majority of radicals are thermodynamically and kinetically unstable.[165] Once produced, these species will often react quickly with surrounding molecules or solvent. Radicals participate in many covalent bonding processes, the most common of which includes coupling to form dimers, hydrogen abstraction, recombination, or disproportionation.[166]

2.1.1 Stability vs. Reactivity: Persistent, Transient, and Unstable Radicals

In 1976, Griller and Ingold sought to classify radical species by their reactivity.[167] Prior to

their report, carbon-centered radicals were deemed stable if they were derived from a compound wherein the C–H bond strength was less than that of the C–H bond strength in an alkane (~105 kcal/mol).[168] This lack of precision allowed the term "stable" to fluctuate in meaning between different groups and throughout many decades, introducing unnecessary ambiguity. Therefore, it was proposed that radical species be classified by their relative reactivity: a radical can be persistent or transient in nature and can be stable, stabilized, or destabilized. A transient radical, such as a methyl radical, decays rapidly by reaction with another equivalent of itself (i.e., $H_3C^{\bullet}$ + $^{\bullet}CH_3 \rightarrow C_2H_6$) or by reaction with the surrounding solvent. A radical is persistent if its lifetime is significantly greater than that of methyl under the same conditions (**Figure 2-1**).[167] The persistence of a radical is influenced by its environment and can be represented quantitatively by the rate of radical decay under certain experimental conditions; radical persistency thus refers to kinetic stability. Describing the thermodynamic stability of a radical, however, a stable radical species refers only to that which is so unreactive under ambient conditions that it can be handled and stored in a similar manner to standard organic reagents. Therefore, it can be stated that all stable radicals are persistent, but not all persistent radicals are stable. These classifications, as defined by Griller and Ingold, were adopted by the rest of the chemical community and are still in use today.[169-170]

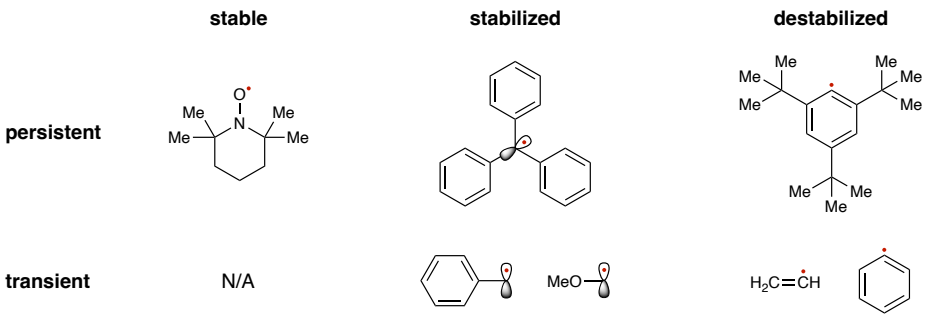

Figure 2-1. Examples of radical species as classified by relative persistence and stability.

While few truly stable radicals exist, radical species can be described by their relative stability, which is often dependent on the species' substituents. The stability of radicals can be modulated by tuning the steric environment around the electron (**Figure 2-2A**).[171] Kinetic stabilization can be afforded to organic radicals through steric protection with bulky substituents, which can prevent or slow the interaction of organic radicals with other species in solution. One of the most studied radical species to date, 2,2,6,6-tetramethylpiperidinyloxyl (**II-1**, TEMPO), has four methyl groups that generate steric hindrance to shield the radical and prevent self-reaction (**Figure 2-2B**, left structure).[172] Similarly, the increased stability of the triphenylmethyl (**II-2**, trityl) radical is in part due to the steric protection afforded by the three phenyl rings (**Figure 2-2B**, right structure).[164,173]

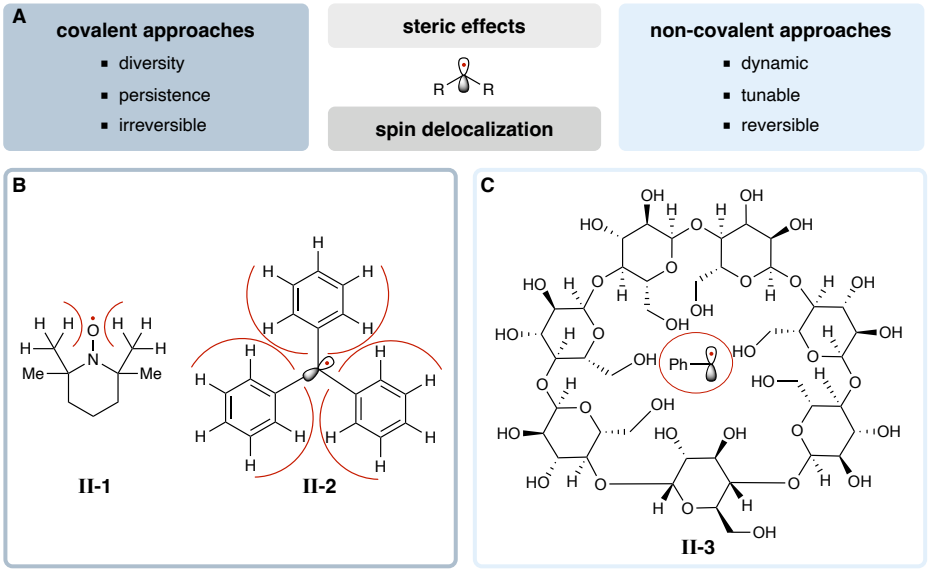

Figure 2-2. A) Approaches for tuning radical stability. **B)** Examples of steric stabilization in radical species, including TEMPO (left) and the trityl radical (right). **C)** Cyclodextrin-stabilized benzyl radical.

Radical stability can also be altered by refining electron delocalization through the inclusion of conjugation, polar substituents, and heteroatoms (**Figure 2-2A**). The radical spin

density can be distributed across multiple atoms in conjugated systems, often decreasing the overall reactivity of the radical species. For example, the spin density is delocalized in the α-positions of the phenalenyl radical (**II-4**), thus improving the stability of the radical species (**Figure 2-3**).[174] The charge distribution can also be tuned through inductive effects afforded by the inclusion of electron-withdrawing and electron-donating groups. Electron-withdrawing groups can limit the electron transfer between radical species, while electron-donating groups can help stabilize organic radicals through contribution of electron density to the half-filled orbital.[175] Similarly, the inclusion of anionic functional groups stabilizes radical cation species, and addition of cationic functional groups helps to stabilize radical anion species (e.g., a positively charged imidazolium substituent stabilizes a radical anion).[176-178]

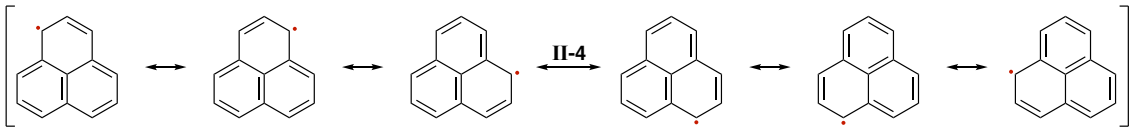

Figure 2-3. Delocalization of spin density in the phenalenyl radical (**II-4**).

Apart from covalent means of tuning the activity of organic radicals, several non-covalent approaches have been established (**Figure 2-2A**). Although they feature similar strategies, such as steric protection and delocalization of spin densities, non-covalent approaches are more dynamic in nature. For example, host-guest chemistry, such as the stabilization of benzyl radicals by cyclodextrin (**II-3**), can prevent radical species from undesired self-reactions (**Figure 2-2C**).[179] Thermodynamic stabilization can also be achieved via π-π interactions, electrostatic interactions, hydrogen bonds, and coordination bonds (i.e., dative bonds).[180-183] The numerous non-covalent strategies that have been developed enable the activity of organic radicals to be tuned dynamically and reversibly, offering a distinct advantage compared to more traditional covalent approaches.

General trends have thus been established for radical stability based on these principles. The more electron donation offered by surrounding substituents, the more stable the radical species. For example, a methyl radical is extremely unstable, while a tertiary radical is more stable in comparison (**Figure 2-4**). Similarly, spin delocalization through resonance increases radical stability significantly. As a result, benzylic radicals and allylic radicals are more stable than a standard alkyl radical species.

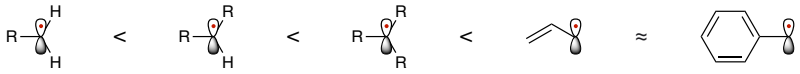

Figure 2-4. General trends for radical reactivity and stability. Radical reactivity increases from left to right.

2.1.2 Principles Governing Radical Reactivity

The stability of radical species has a significant impact on their reactivity. Traditional radical chain reactions exhibit three distinct steps: initiation, propagation, and termination.[184-185] These reactive species are often produced in an initiation step from uncharged, closed-shell precursors through homolytic bond dissociation (**Figure 2-5**). Homolysis describes the process wherein a covalent bond is broken and the electrons that were previously shared are equally distributed to the disconnected atoms.[186] The energy barrier involved in homolytic cleavage is high (e.g., bond dissociation energies often range from 80-120 kcal/mol).[187] The energy required to promote homolytic bond cleavage is most frequently supplied in the form of heat, UV irradiation, or a catalyst. Once a radical species is formed, it can react with closed-shell molecules to form new free radicals (**Figure 2-5**).[185] Known as propagation, this step often involves hydrogen atom abstraction or addition of the free radical to unsaturated bonds. After one or numerous propagation events, termination can occur when two radical species react to form a closed-shell adduct (**Figure**

2-5). While thermodynamically downhill, the low concentration of radical species at a given time results in a decreased probability of collision and termination.[188]

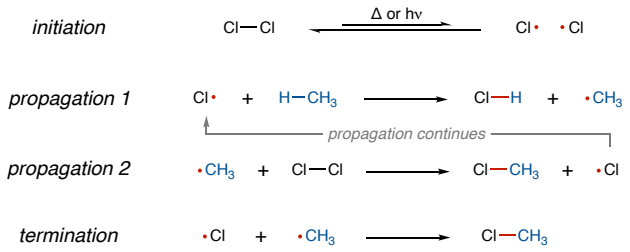

Figure 2-5. Elementary steps of a standard radical chain reaction.

While radical chain reactivity is still common, chemists have focused significant effort on the development of methods that reduce or eliminate radical propagation and instead rely on selective radical termination.[189-190] However, achieving selective cross-coupling between two radicals is non-trivial due to the highly reactive nature of open-shell species. Despite the challenges that exist, there has been a renaissance of radical chemistry in recent decades due in part to a kinetic phenomenon referred to as the persistent radical effect.[191-193] This guiding principle refers to the efficient and selective radical cross-coupling that will dominate if distinct radical species 1) have sufficiently different lifetimes and 2) are generated at equal rates (**Scheme 2-1**).[170]

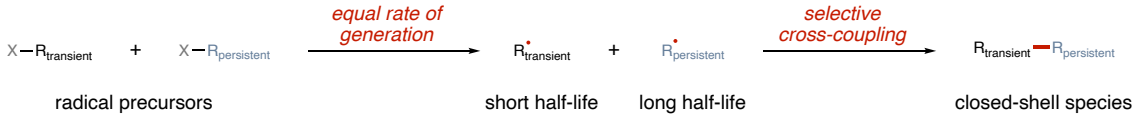

Scheme 2-1. Selective cross-coupling between a transient and persistent radical species.

To harness the persistent radical effect, the two radical species of interest must have distinct properties.[193] The propensity of radical species to react with another equivalent of itself, a reaction known as homocoupling, is largely dictated by its stability. The rate constant of a stabilized

radical's self-reaction is zero, while persistent radicals are merely reluctant to undergo homocoupling. As a result, the half-life of a persistent radical can span from seconds to years. On the contrary, transient radical species have half-lives of less than a millisecond (10^{-3} seconds).[194] As persistent and transient radicals feature significantly different half-lives and self-reaction rate constants, selective cross-coupling can be achieved (**Scheme 2-1**).[195] The reaction between these two classes of species is highly efficient, with rate constants that are diffusion- or near-diffusion-controlled (approximately 10^9 M^{-1} s^{-1}).[193] Due to the increased propensity of transient radicals to engage in homocoupling, the concentration of a persistent radical increases over time with respect to the concentration of a transient radical (**Figure 2-6**). First alluded to by Bachmann and coworkers in 1936, it is the inherent difference in relative stability, and therefore difference in relative concentration, between transient and persistent radicals that results in a highly selective cross-coupling reaction so long as they are generated at equal rates.[195]

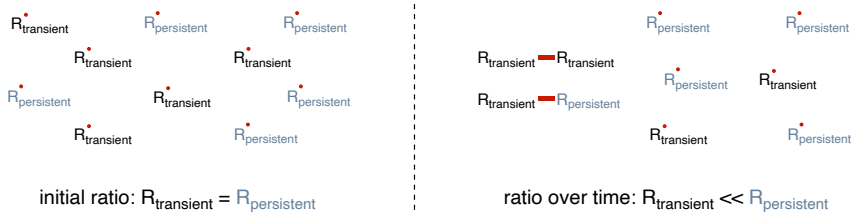

Figure 2-6. Ratio of transient radicals and persistent radicals over time.

2.2 Introduction to Photoredox Catalysis

The generation of radical species is of great interest due to their utility in synthesis, materials, and more. In 1908, Giacomo Ciamician revolutionized chemical synthesis when he proclaimed that there is an "agent of the highest importance… which deserves to be studied in detail, and this is light…," recognizing light as a reagent in synthesis that would eventually allow

access to radical species.[196-197] Photochemistry is a subfield within chemistry that studies light as a renewable, abundant, non-toxic, and inexpensive reagent to drive chemical reactivity.[198] Despite the vast benefits of light-driven reactivity, the utility of light as a reagent in synthesis is largely hampered by the inability of common organic molecules to absorb the most abundant wavelengths of visible light. As such, early attempts to apply photochemistry to organic synthesis often employed high intensity ultraviolet (UV) light.[199] While use of UV light has enabled the discovery of new reactivity, these processes often suffer from chemoselectivity issues.[200] Undesired reactivity can occur when using UV light because a broad array of organic compounds absorb the high intensity photons. Use of a catalyst that absorbs visible light and facilitates redox processes with selected substrates thus offers an exciting opportunity in organic synthesis (**Figure 2-7**).

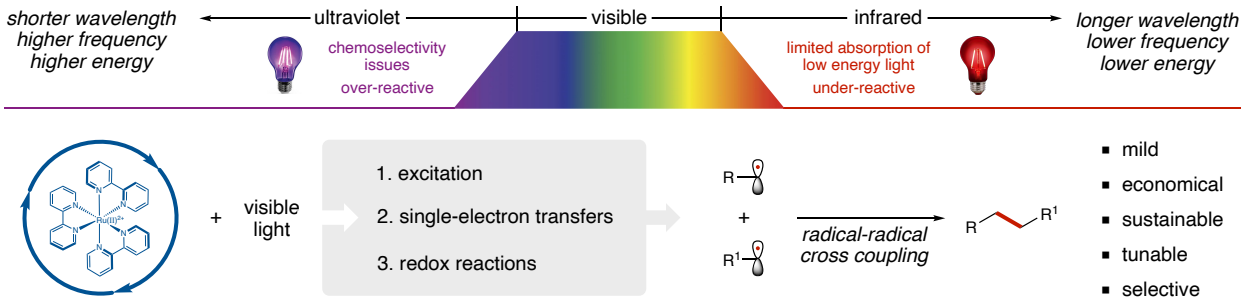

Figure 2-7. Visible-light photoredox catalysis in organic synthesis.

2.2.1 Principles of Photoredox Catalysis

Photocatalysts are chromophores that can enable chemical reactions that would not otherwise be thermodynamically viable by harnessing the powerful redox activity that is accessed in their excited state. These species are often highly conjugated, which enables the absorption of lower energy light compared to that which can be absorbed by most organic compounds.[201] While each photocatalytic system has unique properties, the general photophysical concepts are standard

across photocatalysts. Generally, a photocatalytic process is initiated by absorption of a photon. Absorption of light produces an electronically excited molecule via excitation of an electron from the singlet ground state (S_0) to a singlet excited state (S_n; **Figure 2-8**).[202] The energy gap that exists between the zeroth vibrational states of the electronic ground and excited states is known as the excited state energy ($E_{0,0}$). A range of singlet excited states with different vibrational energies can be accessed based on the energy of the electromagnetic radiation (i.e., wavelength). As a result, high energy light is often required to excite the most powerful photocatalysts, which tend to have larger excited state energies.[202] Access to the excited state of photocatalysts with a high $E_{0,0}$ is thus frequently accompanied by loss in chemoselectivity, as a large array of molecules in solution may also absorb the high energy light. Choice of photocatalyst and light is thus important and can dictate the outcome of photochemical reactions. Within a matter of picoseconds

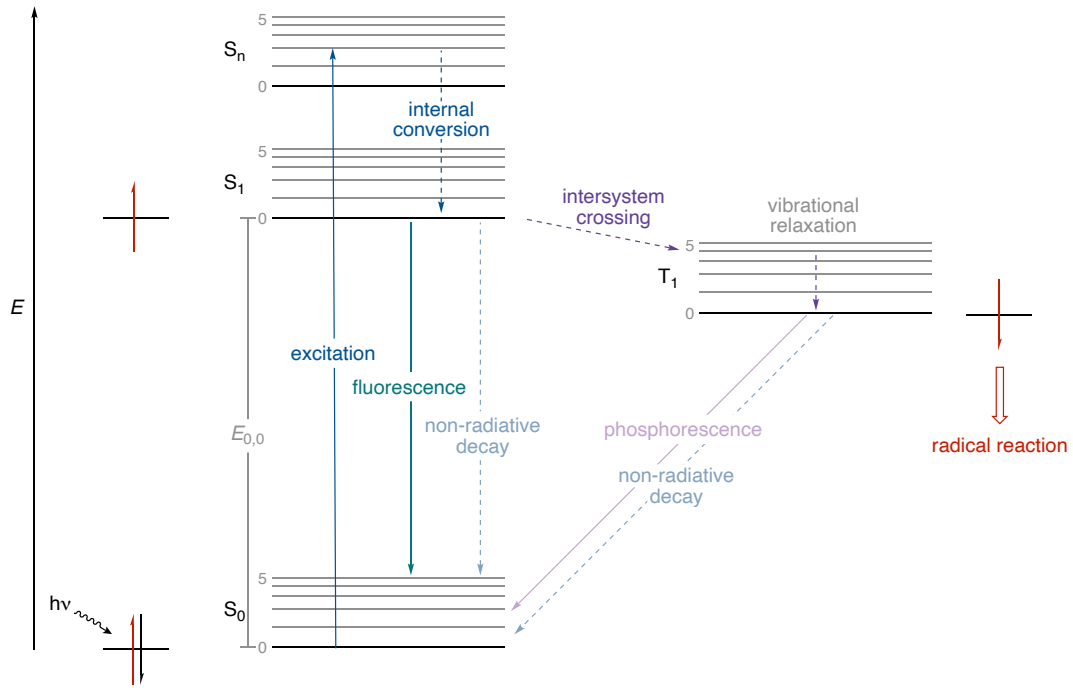

Figure 2-8. Jablonski diagram showing the processes involved in single-electron excitation (solid arrow = radiative process; dashed arrow = non-radiative process).

following initial excitation, all higher lying excited states relax to the first singlet excited state (S_1) via vibrational relaxation and internal conversion.[202]

The fate of the first singlet excited state is dependent on both radiative and nonradiative pathways.[201] Radiative decay occurs when S_1 transitions to lower energy states via emission of light in a process known as fluorescence ($S_1 \rightarrow S_0$; **Figure 2-8**). The transition to lower energy states can also occur by internal conversion (IC; $S_1 \rightarrow S_0$), wherein the excited electron decays non-radiatively back to the ground state without a change in molecular spin state. Alternatively, intersystem crossing (ISC) can occur to give rise to a triplet state (T_1) via a spin-forbidden process ($S_1 \rightarrow T_1$; **Figure 2-8**).[203] Triplet states often have longer lifetimes (nanoseconds to milliseconds), as relaxation of an electron in the triplet state ($T_1 \rightarrow S_0$) is also a spin-forbidden process. The ground state can be accessed via numerous pathways from the triplet state, including radiative decay, which results in phosphorescence, and nonradiative pathways, which are dominant under standard conditions. Alternatively, a photocatalyst in the triplet excited state can engage in energy transfer or electron transfer in a bimolecular reaction due to its long lifetime..[204] Among other factors, the outcome of photoredox catalyzed reaction relies on photoinduced electron transfer (PET), which refers to the overall process of excitation and electron transfer between the excited state molecule (i.e., the photocatalyst) and a ground state molecule (i.e., the substrate).[205]

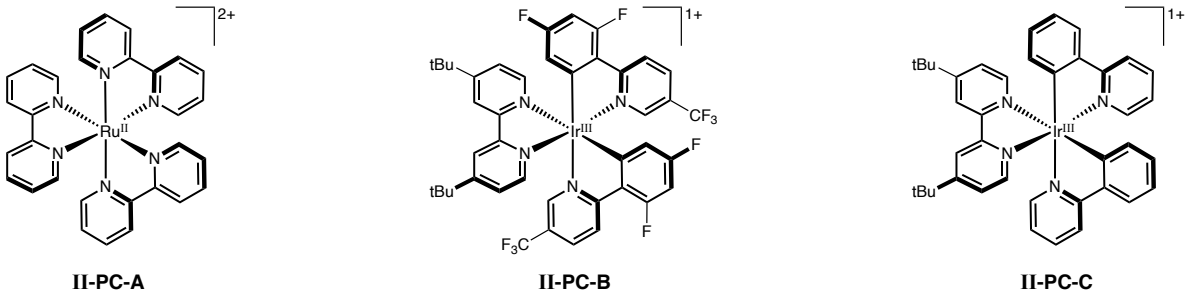

II-PC-A **II-PC-B** **II-PC-C**

Figure 2-9. Heavy metal photocatalysts commonly employed in photoredox catalysis.

A large portion of photocatalysts in use today are derived from transition metals such as ruthenium (Ru), iridium (Ir), and more (**Figure 2-9**). For example, tris(2,2′-bipyridyl)ruthenium(II) chloride (**II-PC-A**, $Ru(bpy)_3Cl_2$) is one of the most used photocatalysts to date due to its broad redox potentials.[206] To engage in PET, this metal-based photocatalyst absorbs a photon into a mixed charge transfer band. Upon absorption of light, an electron in one of the photocatalyst's metal-centered t_{2g} orbitals (S_0) is excited into a ligand-centered π^*_{bpy} orbital (S_1) in a process known as metal-to-ligand charge transfer (MLCT; **Figure 2-10**).[207] Although the resulting species initially exists in the singlet excited state (i.e., $[Ru^{III}(bpy)_2(bpy^{\bullet-})]^{2+*}$), the transition metal in the complex facilitates rapid intersystem crossing (ISC, tens to hundreds of fs) to generate the corresponding triplet mixed charge transfer state (T_1; **Figure 2-10**).[202] The resulting species features two singly occupied molecular orbitals (SOMOs), with one unpaired electron in

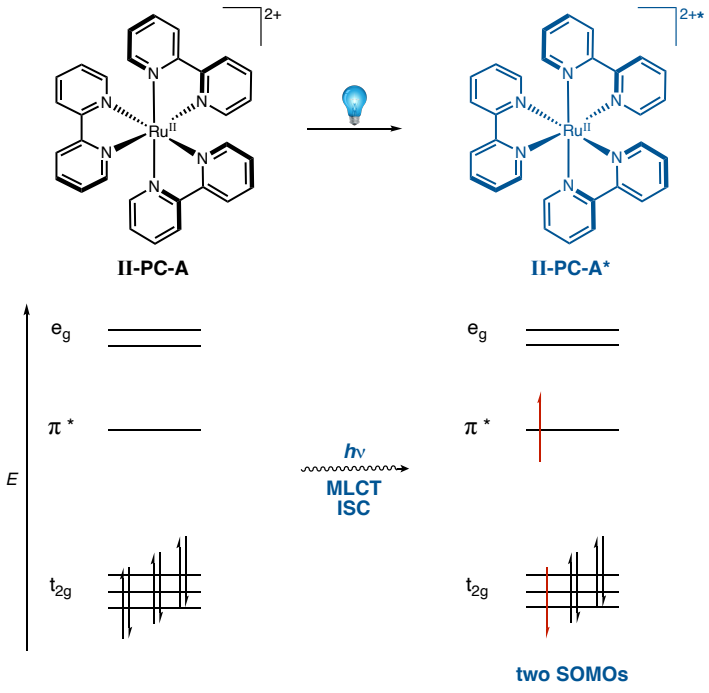

Figure 2-10. Excitation of an electron in heavy metal-derived photocatalyst **II-PC-A**.

S_0 (t_{2g}) and another in T_1 (π^*). The lone electron in the excited triplet state can relax radiatively back to the ground state in the form of phosphorescence or can interact with a substrate.[202]

2.2.2 Generation of Open-Shell Intermediates

Chemists have harnessed the unique redox properties of photocatalysts to access an array of products via single-electron oxidations or reductions (**Figure 2-11**). From either the excited singlet state (S_1) or, more commonly, the longer-lived triplet excited state (T_1), photocatalysts

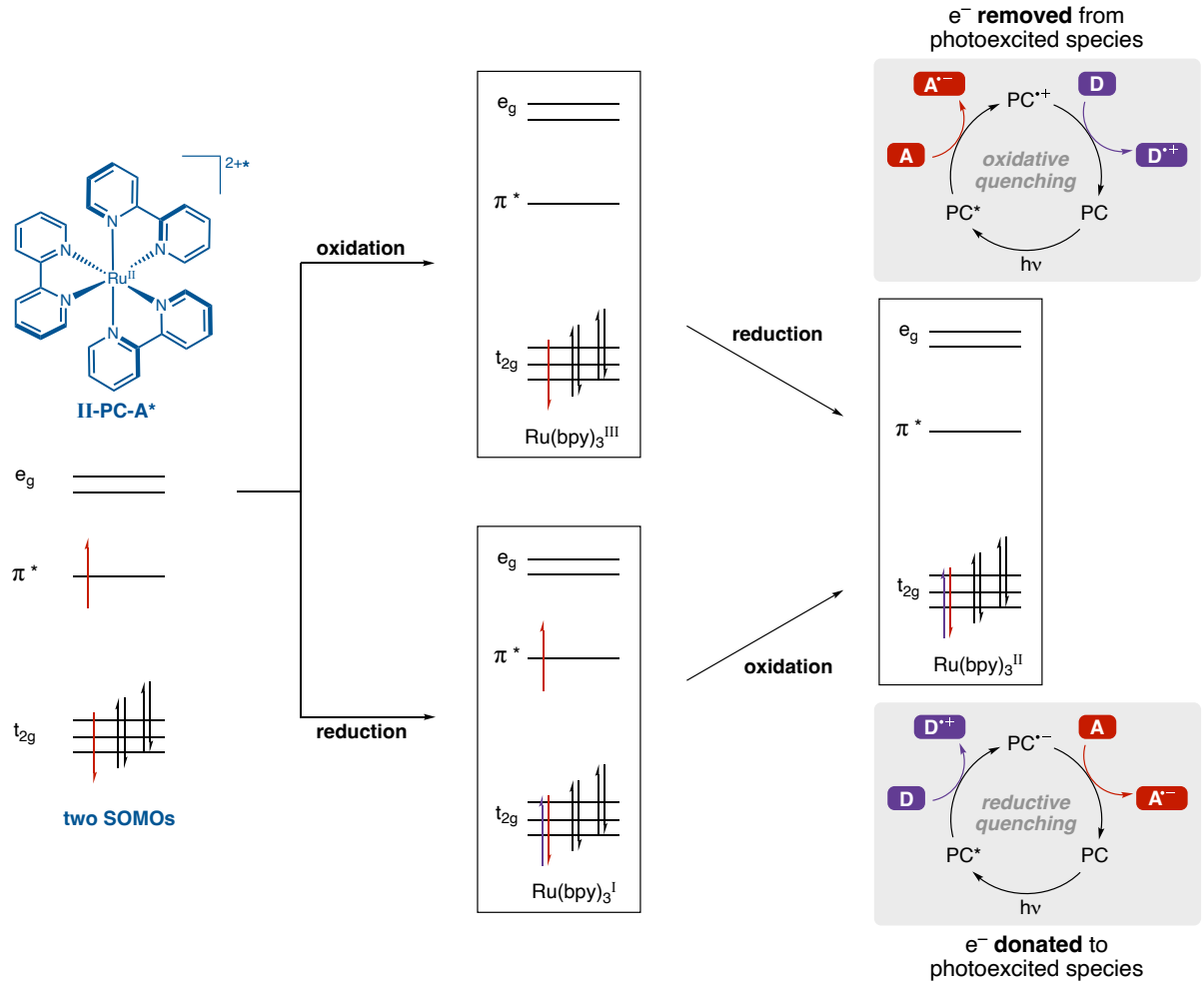

Figure 2-11. Oxidative (top) and reductive (bottom) quenching cycles of a photocatalyst following initial excitation to form two singly occupied molecular orbitals.

engage in a one-electron transfer process with another molecule in solution (i.e., the substrate).[208] Traditionally, photoredox reactions are classified by the mechanism by which the substrate and photocatalyst interact. The excited photocatalyst acts as a reductant in an oxidative quenching mechanism, wherein one electron is transferred from the photocatalyst to an acceptor molecule. The oxidized photocatalyst subsequently accepts one electron from a donor molecule, reducing the photocatalyst and returning it the ground state (**Figure 2-11**, top pathway).[208] Alternatively, an excited photocatalyst can act as a oxidant in a reductive quenching mechanism. Following excitation, the photocatalyst can accept one electron from a donor molecule by performing a single-electron oxidation. The reduced photocatalyst then reduces an acceptor molecule, returning the photocatalyst back to the ground state (**Figure 2-11**, bottom pathway).[208] The mechanism by which photoinduced electron transfers occur is governed by the thermodynamic properties of the substrates of interest relative to the photocatalyst.

Photoredox reactions can also be classified by the net redox outcome (**Figure 2-12**). Redox neutral reactions refer to those in which substrates undergo both a single-electron oxidation and reduction, thus closing the catalytic cycle without the need for an additive.[209] Differentiating

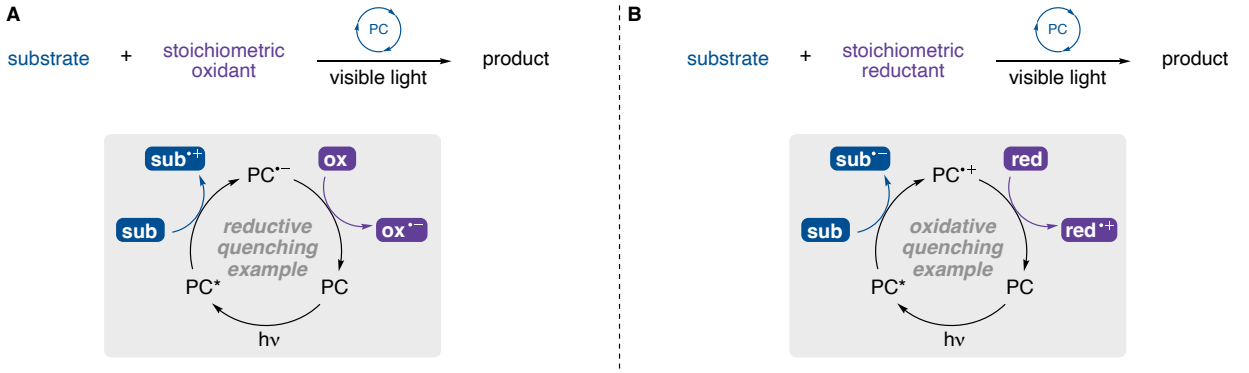

Figure 2-12. General schematic and example of a catalytic cycle for **A)** net oxidative reactions and **B)** net reductive reactions.

photoredox reactions from traditional redox reactions, chemists can perform both oxidative and reductive processes simultaneously in one pot. Conversely, a net oxidative mechanism describes a reaction in which the substrate of interest undergoes an oxidation by the photocatalyst. An external stoichiometric oxidant (e.g., O_2, air, etc.) is thus required to bring the reduced photocatalyst back to the ground state, turning it over for use in subsequent cycles (**Figure 2-12A**).[210] Net reductive processes are also possible, wherein a photocatalyst reduces the substrate of interest and thus requires a stoichiometric reductant (e.g., iPr_2NEt) for catalyst turnover (**Figure 2-12B**).[210] With three possible net redox outcomes as well as multiple mechanisms for photocatalyst quenching, photoredox catalysis offers a versatile and tunable platform for redox reactivity.

2.2.3 Origins of Photoredox Catalysis

Photoredox catalysis dates back to 1978 when Kellogg and coworkers reported increased rates of a hydride transfer reaction using neon fluorescent lamps and a ruthenium photocatalyst ($Ru(bpy)_3Cl_2$; **Scheme 2-2**).[211] Using *N*-methyl 1,4-dihydropyridines (**II-5**) as a terminal reductant, alkanes and thioethers were accessed by reduction of the corresponding sulfonium ions. Following reports of similar reactivity,[212-213] Cano-Yelo and Deronzier disclosed the first net oxidative photoredox catalyzed reaction to access aldehydes from carbinols using aryldiazoniums as the terminal oxidant.[214] Around the same time, they reported the first redox-neutral photoredox catalyzed reaction, disclosing a photo-initiated method to synthesize phenanthrenes via the Pschorr reaction.[215] Instrumental reports by Fukuzumi, Oda, and others continued to shine a light on photoredox catalysis over the decades that followed.[216-221]

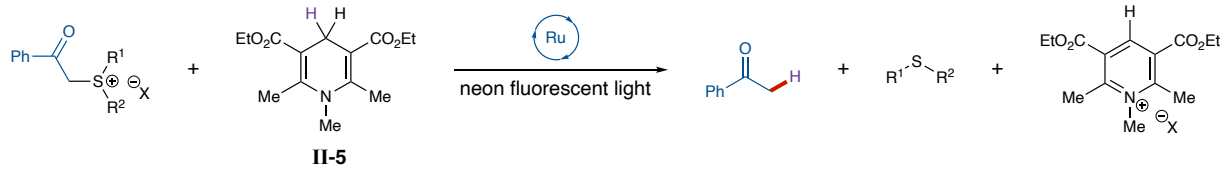

Scheme 2-2. The first published report of a photocatalytic reaction by Kellogg and coworkers.[211]

Scattered reports employing visible light-mediated photoredox catalysis in organic chemistry continued to appear over the following few decades. However, the field exploded following three seminal reports that were published within a mere twelve-month period. In 2008, MacMillan and Nicewicz merged organocatalysis and photoredox catalysis in their development of a method for the direct asymmetric α-alkylation of aldehydes.[222] Previously, MacMillan and coworkers had discovered that use of a superstoichiometric oxidant, ceric ammonium nitrate (CAN), enables single-electron oxidation of an enamine species.[223] The resulting 3-π-electron radical cation features a singly occupied molecular orbital that can react with numerous π-rich nucleophiles. While an important discovery, the scope of reaction partners was limited to alkenes, and MacMillan sought to address this limitation. With visible light-absorbing ruthenium-derived bipyridyl catalysts gaining momentum in solar cell research at the time, MacMillan and Nicewicz hypothesized that photoredox catalysis using low energy visible light in place of UV light would allow for generation of a radical from an alkyl halide (**Scheme 2-3**).[222]

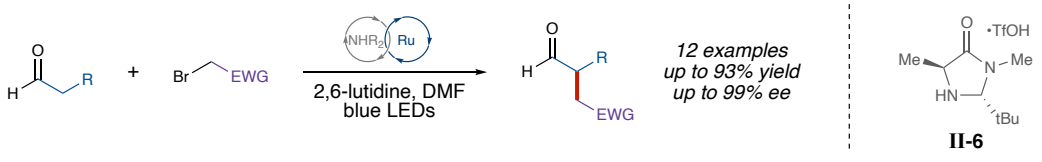

Scheme 2-3. Combined enamine and photoredox catalysis for the α-functionalization of aldehydes developed by MacMillan and Nicewicz.[222]

Enamine and photoredox combined catalysis were successfully merged using amine **II-6** and ruthenium-derived **II-PC-A** to expand the scope of the asymmetric α-alkylation process beyond π-rich electrophiles (**Scheme 2-3**).[222] It was hypothesized that an electron-deficient alkyl radical would undergo radical addition to an electron-rich enamine that is accessed by condensation of amine catalyst **II-6** with an aldehyde substrate.[224] A sacrificial quantity of this enamine species would initially undergo single-electron oxidation by the excited photocatalyst to initiate the photoredox cycle, and single-electron reduction of an alkyl bromide (for phenacyl bromide, $E_{1/2}$ = –0.49 V vs SCE) by the oxidized photocatalyst (for $Ru(bpy)_3^+$, $E_{1/2}$ = –1.33 V vs SCE) would yield a reactive alkyl radical while bringing the photocatalyst back to its ground state.[216,225-226] The authors proposed that radical addition to the enamine occurs, and the resulting radical species undergoes single-electron oxidation by an excited photocatalyst to afford an iminium intermediate. The amine catalyst **II-6** is then regenerated by hydrolysis of the iminium, affording the desired enantioenriched α-functionalized aldehyde product. The reduced photocatalyst reduces another equivalent of alkyl halide, turning over the photocatalyst and producing an alkyl radical ready to engage with another equivalent of the enamine species.

Yoon and coworkers disclosed a photoredox-catalyzed [2+2] cycloaddition of dienones in a manuscript that was published online on the exact same day that MacMillan's work (vide supra) first appeared online (**Scheme 2-4**).[227] Krische previously disclosed that single-electron reduction of an enone by catalytic cobalt or copper leads to [2+2] cyclization products.[228-230] Inspired by this report, Yoon hypothesized that ruthenium photocatalyst **II-PC-A** can act as a photoreductant to achieve the same cycloaddition process. Using sunlight (afforded by a GE sunlamp) to excite the photocatalyst and superstoichiometric amine to act as an external reductant, they were able to

access 13 cyclized products in good-to-excellent yields. The authors propose that this reaction proceeds through a reductive quenching mechanism, wherein the excited photocatalyst oxidizes the sacrificial amine reductant (i.e., iPr_2NEt). The reduced photocatalyst then engages in single-electron reduction of a lithium-activated enone species to generate a β-radical, thus initiating the [2+2] cycloaddition cascade while returning the photocatalyst to the ground state.

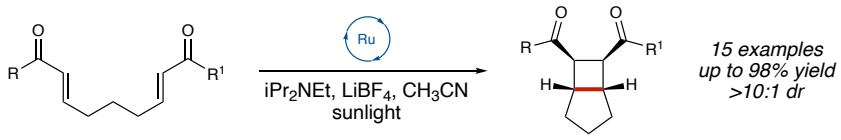

Scheme 2-4. Photoredox-catalyzed [2+2] cycloaddition reported by Yoon and coworkers.[227]

A few months following the reports by MacMillan and Yoon, a photoredox-catalyzed method for the dehalogenation of bromopyrroloindolines and esters was disclosed by Stephenson and coworkers as an alternative to traditional tin-mediated dehalogenation processes (**Scheme 2-5**).[231] In a reductive quenching mechanism similar to that reported by Yoon, an external reductant is required for photocatalyst turnover. Using a 1,4-dihydropyridine (i.e., Hantzsch ester) or an amine and an acid to serve as a both an external reductant and a hydrogen atom source, they propose that ruthenium photocatalyst **II-PC-A** reductively dehalogenates an alkyl halide. The resulting radical species then abstracts a hydrogen atom from the hydrogen atom source to yield the desired dehalogenated product in up to 99% yield.

Scheme 2-5. Photoredox-catalyzed dehalogenation reaction by Stephenson and coworkers.[231]

These three seminal reports demonstrated the power of photoredox catalysis, sparking the bold resurgence of visible light-mediated single-electron chemistry.[210] The field expanded exponentially in the years that followed and is continuing to grow today. Using light as a natural source of energy, redox-mediated processes can proceed under relatively mild reaction conditions, negating the need for toxic and harsh reagents. Photoredox catalysis has thus been employed by many for the synthesis of C–C and C–X (X = N, O, etc.) bonds and has allowed access to a vast array of chemical scaffolds under mild reaction conditions.[210,232-233]

2.3 Combined Photoredox and Carbene Catalysis

2.3.1 Significance of Ketones

There is an ongoing need for mild synthetic methods with broad functional group tolerance for the construction of C–C and C–X (X = O, N, S, etc.) bonds in natural products, pharmaceutical compounds, and organic materials. In particular, the formation of carbonyl-containing scaffolds remains a priority due to their synthetic utility and high prevalence in medicinally active compounds.[234-241] Carbonyl-containing functional groups make up approximately 35% of the most common functional groups in bioactive compounds.[242] Ketones, among other carbonyl motifs, are featured in numerous bioactive compounds (e.g., **II-7** to **II-10**, **Figure 2-13**).[243-246] Ketones can

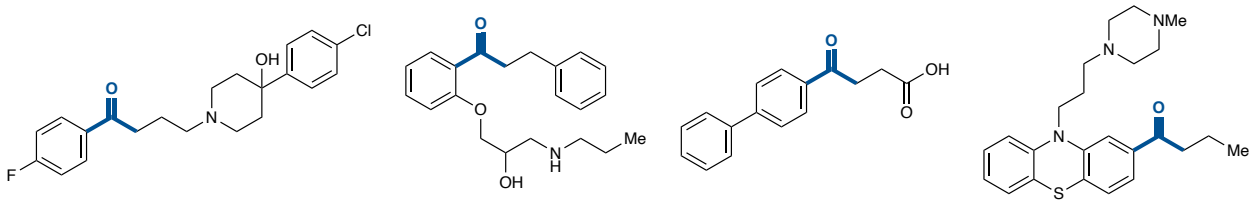

II-7
haloperidol

II-8
propafenone

II-9
fenbufen

II-10
butaperazine

Figure 2-13. Selected examples of FDA approved drugs featuring a ketone functional group.

act as a hydrogen bond acceptor and can participate in dipole-dipole interactions, properties which may enable the functional group to participate in critical interactions within a drug binding pocket.

Ketones are versatile synthetic groups that can undergo a multitude of chemical transformations, making them a staple functional group in many synthetic sequences (**Figure 2-14**).[185] For example, ketones can undergo reductions to the corresponding alcohol or alkane, or they can be oxidized to the corresponding carboxylic acids. Due to the polarized nature of carbonyl groups, ketones are also electrophilic at the carbonyl carbon and are thus targets for an array of nucleophilic addition reactions, offering routes to access alcohols, cyanohydrins, acetals, and more. Imines and enamines can be synthesized from a ketone via nucleophilic addition of the corresponding amine, and alkenes can be made via addition of phosphonium ylides in the Wittig or Horner-Wadsworth-Emmons reactions.[247-248] In addition to reactions that occur at the carbonyl carbon, functionalization of the adjacent α-carbon is also possible using well-established enolate chemistry, and α,β-unsaturated ketones can undergo 1,2- and 1,4-additions using more remote functionalization strategies. The broad landscape of reactivity inherent to ketones highlights their broad utility in synthesis.

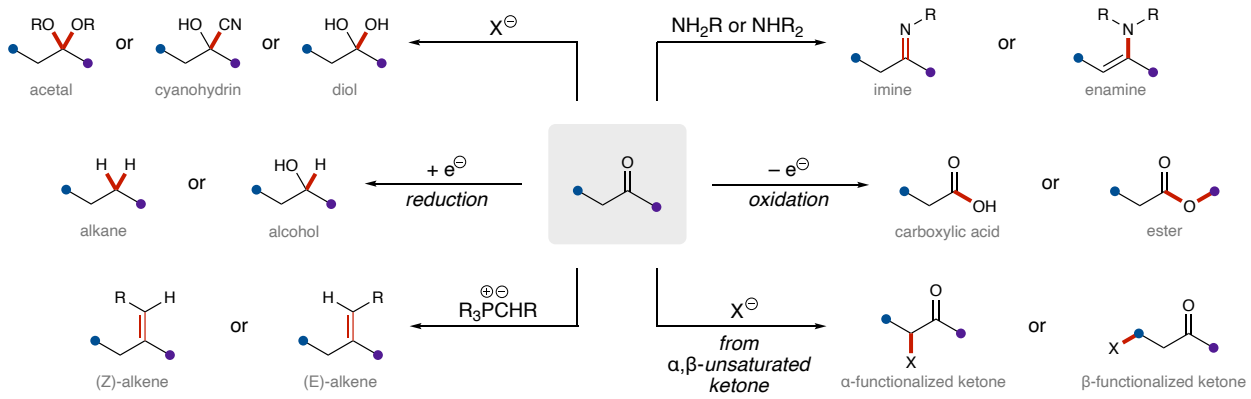

Figure 2-14. Selected reactions of ketones.

2.3.2 Traditional Methods for the Synthesis of Ketones

Living organisms, including the human species, are highly dependent on ketones for energy. Ketones are naturally produced through the breakdown of ketogenic amino acids and fatty acids in a biochemical process called ketogenesis (**Scheme 2-6**). In humans, the production of ketones occurs mainly in the mitochondria of liver cells, where different enzymes, such as thiolase, β-hydroxy-β-methylglutaryl-CoA (HMG-CoA, **II-13**) synthase, and HMG-CoA lyase, catalyze the synthesis of acetoacetate (**II-14**), acetone (**II-15**), and D-β-hydroxybutyrate (**II-16**) from acetyl-CoA (**II-11**). These ketones are further metabolized, eventually leading to the energy required to sustain life.

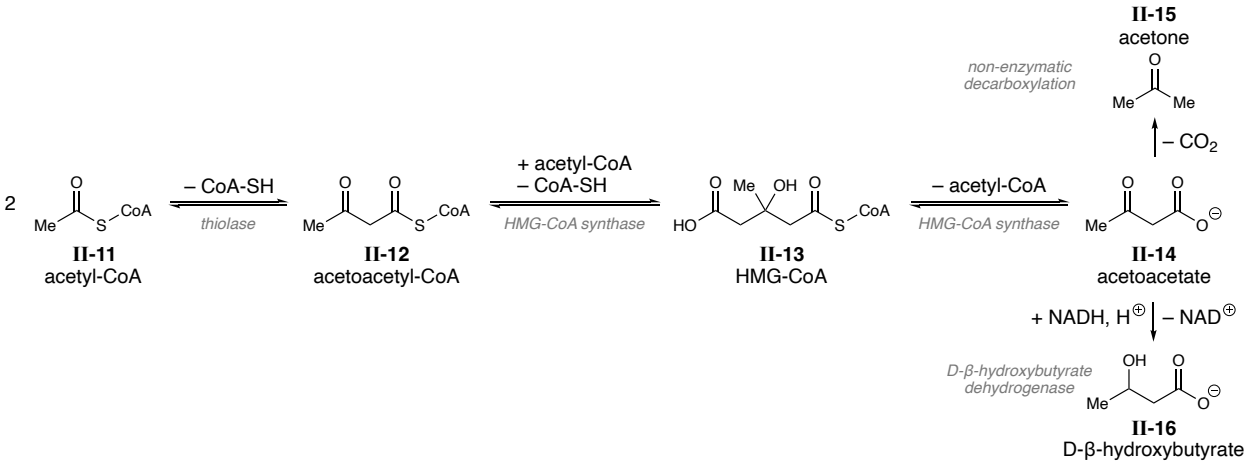

Scheme 2-6. Ketogenesis pathway for the generation of ketone bodies.

While many living organisms naturally synthesize ketones through ketogenesis or photosynthesis, the synthesis and subsequent functionalization of ketones have been ongoing for all of modern organic chemistry.[249-255] Apart from numerous oxidations, the majority of approaches to make this functional group rely on efficient formation of one of the C–C bonds. For example, the Grignard reaction can access ketones or alcohols from acyl electrophiles using

organometallic reagents (**Scheme 2-7**).[256-261] Developed by Victor Grignard in 1900, this reaction employs organomagnesium halide species (RMgX, where X is usually Cl or Br) to promote addition of the R-group to an electrophile.[256] A secondary alcohol can be accessed using an aldehyde as the electrophile, and use of a Weinreb amide as the electrophilic source affords a ketone product (via the Weinreb–Nahm reaction using Grignard reagents; **Scheme 2-7**).[257]

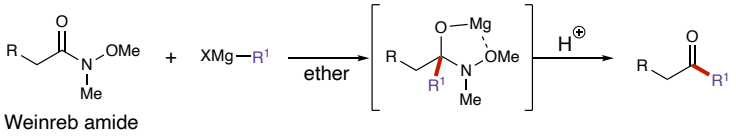

Scheme 2-7. General scheme for addition of a Grignard reagent into a Weinreb amide.

The development of additional two-electron methods to access ketones from acyl electrophiles dates back to the 19th century. A well-known reaction for aryl ketone formation is the Friedel-Crafts acylation, which reacts an acyl chloride or anhydride with an arene using Lewis acids or strong protic acids **(Scheme 2-8)**.[262-263] Notably, stoichiometric acid is required for substrate activation, thus facilitating the electrophilic aromatic substitution reaction. Transition-metal-catalyzed cross-coupling reactions, such as the Fukuyama coupling (which uses $PdCl_2(PPh_3)_2$ as a catalyst), can also be employed to forge the C–C bond of ketone motifs.[264-266] Although their utility in synthetic chemistry is undisputed, these protocols are limited in some cases by low regioselectivity, poor functional group tolerance, and generation of corrosive waste.

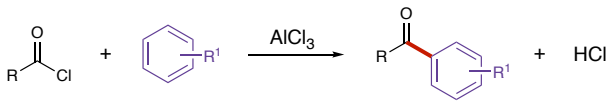

Scheme 2-8. Friedel-Crafts acylation reaction for the synthesis of aryl ketones.

2.3.3 Brief Overview of Radical Carbene Catalysis

Umpolung (polarity reversal) reactivity offers a distinct alternative to standard two-electron chemistry for the synthesis of ketones as well as other C–C and C–X bonds that would not otherwise be possible (**Scheme 2-9**).[267-269] In recent decades, *N*-heterocyclic carbenes (NHCs) have transformed the field of umpolung chemistry and emerged as a versatile tool for the catalytic generation of acyl anion synthons, enolates, and homoenolates.[16,57,85,270-275] However, the scope of NHC-catalyzed transformations was limited by the inability to engage sp^3 electrophiles until the merger of single-electron chemistry with carbene catalysis (see Chapter 1).

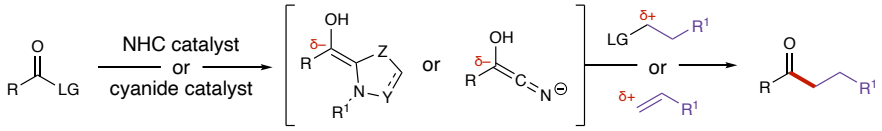

Scheme 2-9. Umpolung reactivity for the synthesis of ketones using NHC catalysis or cyanide catalysis.

The recent renaissance of single-electron chemistry via photoredox catalysis and electrocatalysis has further enabled bond connections that were previously inaccessible using traditional pathways. While radical chemistry is well-established, the revival of photocatalysis and electrosynthesis has accelerated modern synthetic chemistry.[210,232,276-283] These advances have furnished numerous strategies for the synthesis of ketones.[284-288] For example, photoredox/nickel dual catalysis has gained attention for its ability to synthesize ketone moieties via cross-coupling between nucleophilic acyl radicals and other radical species (e.g., aryl radicals from aryl halides).[289-290] In this combined catalytic protocol developed by MacMillan and coworkers, Ni(I) is employed to turn over the photocatalyst following a photocatalyzed single-electron reduction of a keto acid to yield an acyl radical (**Scheme 2-10**). The oxidized Ni catalyst is hypothesized to

engage with an aryl iodide via oxidative addition, and the acyl radical is subsequently trapped by the electrophilic metal complex. Finally, reductive elimination yields the final ketone product.[290] These advances in radical chemistry have provided new modes of reactivity, and the merging of single-electron chemistry with umpolung reactivity has facilitated even more opportunities.

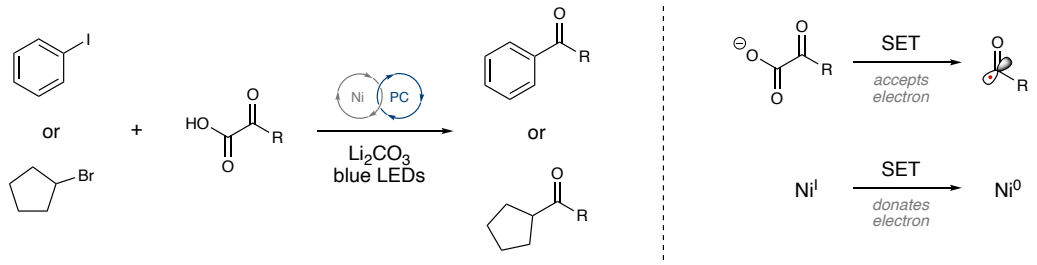

Scheme 2-10. Combined photoredox and nickel catalysis for the synthesis of ketones.

NHC-derived radical reactivity dates back to the early 2000s.[32,100,114-115,291-292] Early work from our group showcased a mild oxidation of allylic alcohols[34] and aldehydes[99] to esters using an NHC and MnO_2 (**Scheme 2-11**). Oxidation of the Breslow intermediate with stoichiometric MnO_2 was employed to access an acyl azolium intermediate, and subsequent displacement by an alcohol afforded the desired C–O bond. Shortly thereafter, Studer and coworkers developed an NHC-catalyzed oxidation of aldehydes to esters mediated by TEMPO (**Scheme 2-11**).[100] To broaden the scope of substrates, Studer followed up in 2010 with a report featuring 3,3',5,5'-tetra-*tert*-butyldiphenoquinone as the stoichiometric oxidant in place of TEMPO (**Scheme 2-11**).[54] While these NHC-catalyzed radical functionalizations have set the precedent for a variety of other transformations,[293-294] the use of toxic and wasteful stoichiometric oxidants has limited their overall utility in synthesis.[295]

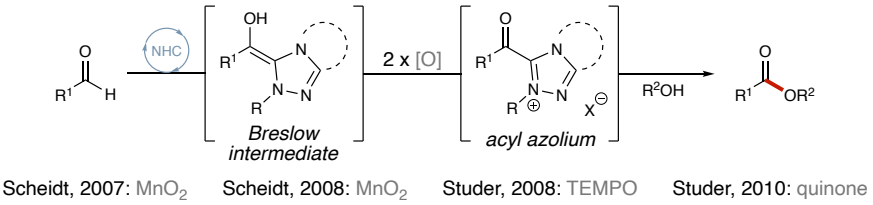

Scheme 2-11. Early oxidative esterification protocols using stoichiometric oxidants.

To circumvent the need for stoichiometric oxidants, Boydston developed a direct NHC-catalyzed anodic oxidation of aldehydes for the formation of esters in 2012 (Scheme 1B).[101] Similarly, Studer employed air as the terminal oxidant in a cooperative NHC- and metal redox esterification of aldehydes (**Scheme 2-12**).[102] While significant improvements in NHC-catalyzed processes have been made over the past decade, the majority of these strategies are confined to the formation of C–X bonds (X = O, N, etc.).

Scheme 2-12. Oxidative esterification approaches using catalytic oxidants.

Various research groups, including ours, have thus become interested in developing single-electron transfer methods to extend the chemistry involving Breslow intermediates or acyl azolium species to the formation of C-C bonds. In 2019, Ohmiya reported an NHC-catalyzed decarboxylative alkylation of aldehydes using *N*-(acyloxy)-phthalimide derivatives (**II-18**) to afford ketones with quaternary α-centers (**Scheme 2-13**).[127] In this process, single-electron transfer (SET) to redox-active ester occurs from the deprotonated Breslow intermediate ($E_{1/2} \approx -0.95$ V vs. SCE) to generate an acyl azolium radical (**II-I**$^{\bullet}$) and an alkyl radical.[90,296-298] Subsequent radical-radical coupling affords the desired ketone following loss of the NHC. Following this initial report,

similar modes of oxidative reactivity have been developed for the synthesis of ketones (see Chapter 1).[131,299]

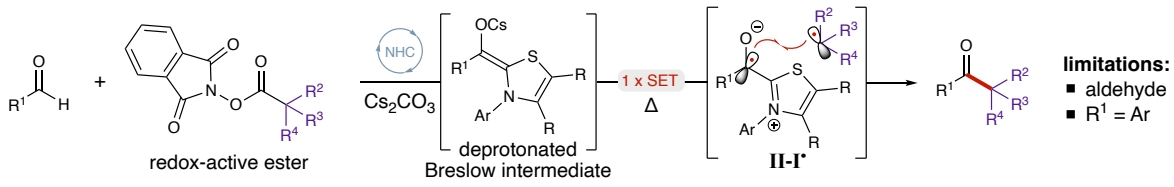

Scheme 2-13. Decarboxylative alkylation strategy for the synthesis of ketones developed by Ohmiya and coworkers.

In line with our experience in oxidations of the Breslow intermediate and our growing interest in photoredox catalysis,[300-302] we envisioned an opportunity for the development of novel reactivity at the interface of NHC catalysis and photochemistry. Our work in the field of cooperative NHC catalysis in addition to the contributions by other groups[85] has resulted in a variety of new transformations featuring the combination of NHCs with Lewis acids,[303-308] Brønsted acids,[309] and transition metals.[310-311] Similar tenets of cooperative catalysis have recently been exploited in photoredox chemistry, where the combination of organocatalysts,[312-313] Lewis acids,[314] Brønsted acids,[315-316] and transition metals[317-319] has enabled the expedient construction of synthetically tractable molecules. A limited number of reports explore the combination of NHC catalysis with photoredox catalysis.[121,124,146] As such, we aimed to further bridge the existing gap between the fields of NHC catalysis and photocatalysis by leveraging their unique redox properties. We envisioned a system wherein combined NHC and photoredox catalysis would allow access to acyl azolium radical **II-I•** via single-electron reduction, and radical-radical coupling with an oxidatively generated alkyl radical would afford a diverse array of ketone products (**Scheme 2-14**).

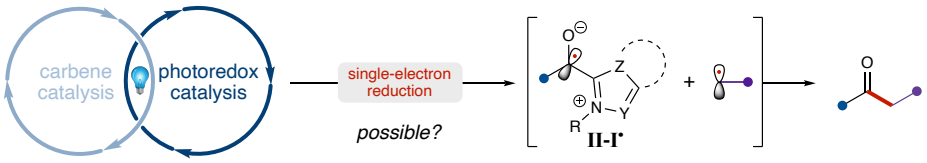

Scheme 2-14. Combined NHC and photoredox catalysis for the synthesis of ketones.

2.3.4 Hypothesis: Combined Catalysis for Ketone Construction

We hypothesized that in situ activation of carboxylic acid **II-17** (e.g., with carbonyldiimidazole to make acyl imidazole **II-18**) followed by NHC addition would afford an acyl azolium, a species which has been used extensively in NHC-redox acylations for the preparation of esters, amides, and carboxylic acids (**Scheme 2-15**).[16,320] Single-electron reduction of the resulting species would provide an acyl azolium radical **II-I•** that, when coupled with an alkyl radical derived from an oxidatively generated radical precursor (e.g., Hantzsch ester **II-19**, etc. vide infra), would furnish synthetically valuable ketones **II-20**. Traditional methods for accessing acyl radicals, which are functionally equivalent to achiral **II-I•**, involve the use of aldehydes,[321-323] α-keto acids,[324-326] and others,[327] many of which suffer from significant drawbacks (i.e. toxicity, instability, superstoichiometric additive requirements, etc.). Additionally, carboxylic acids have recently gained attention for their ability to generate acyl radicals via a decarboxylation-carbonylation strategy[328] or pre-functionalization with an activating agent (e.g. dimethyldicarbonate,[329-333] alkyl phosphine,[254,334-335] etc.[336]). However, carboxylic acid-derived acyl radicals have primarily been employed in Giese-type additions to activated alkenes.[327] Limited reports describe the coupling of an acyl radical with an alkyl radical,[337] thus presenting an opportunity to explore and develop new reactivity. As a complementary approach to recent

advancements in acyl radical chemistry, this work showcases the coupling of an alkyl radical with an "acyl radical surrogate" accessed from readily available carboxylic acids.

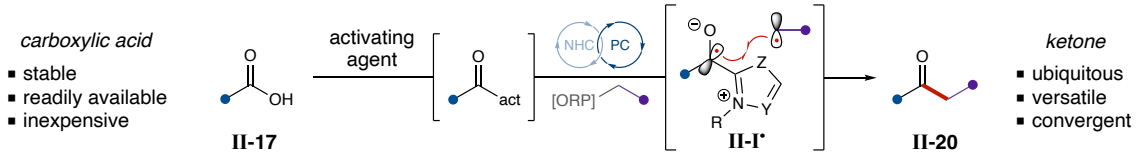

Scheme 2-15. Hypothesis for the synthesis of ketones from carboxylic acids using combined NHC and photoredox catalysis.

2.4 Reaction Discovery

2.4.1 Redox Properties of Acyl Azoliums

In the late 1990s, Fukuzumi reported the reducing capabilities of Breslow-type intermediates, setting the ground for the single-electron NHC catalysis that emerged years later.[296-297] While this initial report was instrumental in providing a broad understanding of the redox properties inherent to NHC-derived species, a recent report by Martin and coworkers expanded upon these studies to provide a more detailed and thorough analysis.[95] It was discovered that the initial reducing capabilities reported by Fukuzumi were affected by the base additive used at the time, and Breslow enolates derived from thiazolylidenes are in fact stronger reducing agents than previously believed. The newly adjusted reducing capabilities of Breslow intermediates (between –1.30 to –1.45 V vs SCE) accounts for many of the reported single-electron transfer processes that employ reductively generated radical precursors (e.g., redox active esters; see Chapter 1). Based on these studies, Breslow enolates are highly reducing species capable of engaging in various SET processes, thereby reducing a substrate while undergoing a single-electron oxidation (where $E_{ox} \approx$ +1.37 V vs SCE) to give radical NHC species **II-I•**.

Contrary to Breslow enolates, acyl azoliums have been demonstrated to afford **II-I**• by single-electron reduction. Adjusted redox values for these species were again provided in the extensive study performed by Martin and coworkers (vide supra).[95] With reduction potentials between –0.8 to –1.3 V vs SCE, we hypothesized that acyl azolium species might be capable of engaging with a photocatalyst in a photoredox cycle. A broad array of photocatalysts have been developed to date, and we expected that the electron transfer might be feasible using a photocatalyst featuring redox potentials within the necessary range.

2.4.2 Oxidatively Generated Radical Precursors

It was anticipated that reduction of the acyl azolium would be coupled to the oxidation of an oxidatively generated radical precursor in a net neutral photoredox cycle. A landscape of alkyl radical sources have been developed over the past few decades for use in redox processes.[338] Many distinct oxidatively generated radical precursors are now employed in photoredox reactions, the most synthetically tractable of which include 1,4-dihydropyridines (Hantzsch esters, **II-19**) alkyl silanes (**II-21**),[339-340] bis-catecholato silicates (**II-22**),[341] potassium trifluoroborate salts[342] (**11-23**, **Figure 2-15**).

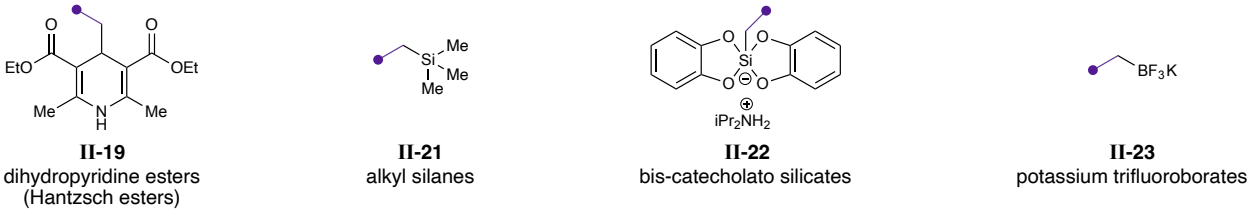

II-19 dihydropyridine esters (Hantzsch esters) | **II-21** alkyl silanes | **II-22** bis-catecholato silicates | **II-23** potassium trifluoroborates

Figure 2-15. Common oxidatively generated radical precursors.

Many alkyl radical precursors are designed to enable facile cleavage of a C–Y bond, where Y is often a metalloid (e.g., boron, silicon, etc.), due to the difference in bond dissociation energies.

While use of alkyl silanes **II-21** as radical precursors is less common, bis-catecholato silicates **II-22** have been employed in numerous photoredox reactions to access alkyl radicals. The hypervalent silicon derivative was first synthesized by Frye in 1964 and was introduced as a versatile oxidatively generated radical precursor by Fensterbank in 2015.[341,343] Silicates are bench-stable and easily accessible radical sources that feature low oxidation potentials (E_{ox} = +0.34 to +0.89 V vs SCE, depending on the alkyl group), thus enabling their use under a broad range of photocatalytic conditions.[341] Similarly, potassium trifluoroborates **II-23** have gained traction for use as alkyl radical precursors.[344] First employed as alkyl sources in transition metal catalysis, these atom economic salts can be oxidized between +0.75 to +1.10 V vs SCE.[344-347]

Another class of radical precursors includes those which undergo C–C homolytic bond cleavage to generate the radical species. Arthur Hantzsch first synthesized 1,4-dihydropyridines (now referred to as Hantzsch esters) in 1881.[348] Inspired by nicotinamine adenine dinucleotide (NADH) coenzyme, these esters were originally developed as a hydride source and were later employed as hydrogen radical sources using light and transition metal catalysis.[349-350] Hantzsch esters **II-19** were finally developed and popularized as efficient and mild alkyl radical sources by Molander in 2016.[319] These dihydropyridine-derived species are easily prepared from the corresponding aldehyde and generate inert byproducts.[351-353] Moreover, Hantzsch esters are slightly active in the absence of photocatalyst due to their strong absorbing characteristics afforded by their extensive conjugation. To facilitate even more efficient generation of alkyl radicals from Hantzsch esters (E_{ox} = +1.05 V vs SCE), a variety of photocatalysts can be employed using photoredox catalysis.[319]

2.4.3 High-throughput Experimentation

Our initial search for the desired reactivity was guided by our semi-high-throughput experimentation (HTE) platform, which allowed for numerous reaction components to be screened in parallel (**Figure 2-16**).[354-356] Initial HTE screening was performed using preformed phenyl benzimidazolium salt **II-24** instead of catalytic NHC, as a simplified system composed of only one catalytic cycle (i.e., photocatalytic cycle vs photocatalytic cycle and NHC catalytic cycle) was expected to provide initial trends in reactivity. Five photocatalysts with redox potentials spanning a broad range, four solvents featuring various polarities, and four oxidatively generated radical

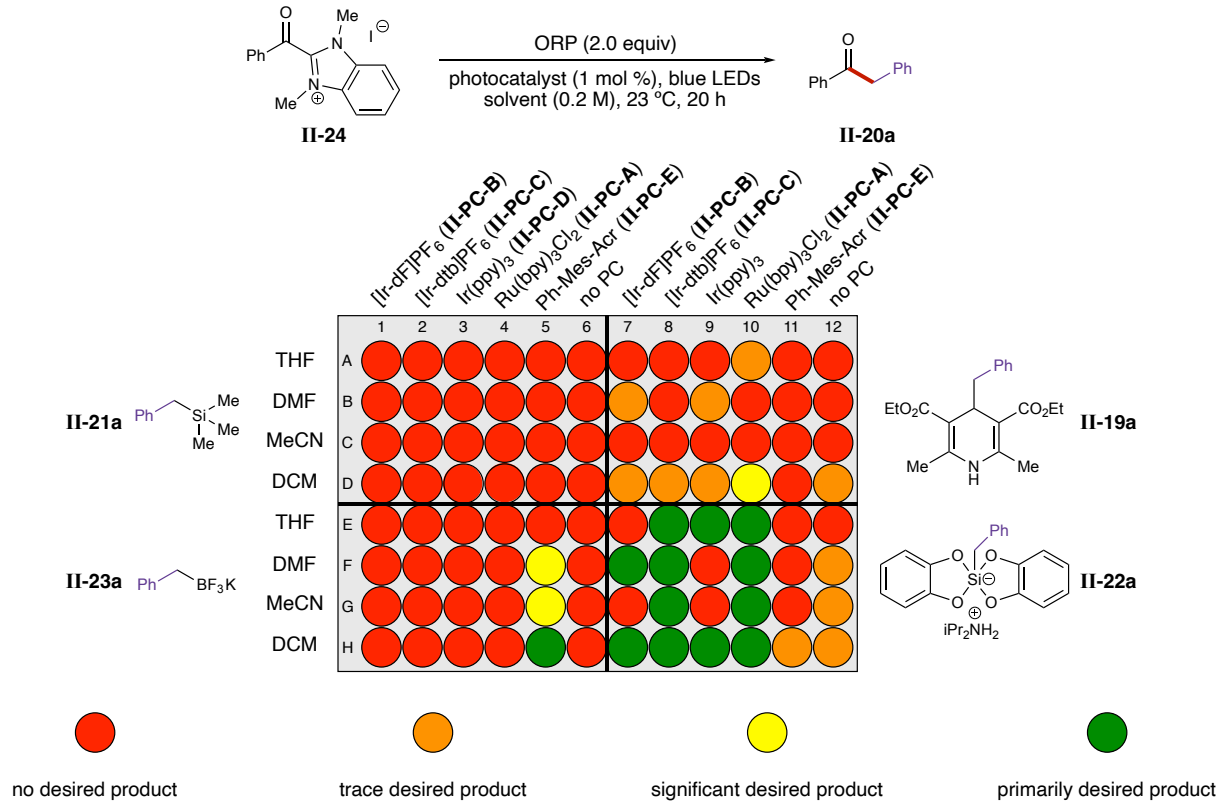

Figure 2-16. HTE results for the reaction of an isolated acyl benzimidazolium with various oxidatively generated radical precursors (ORPs). Results for this plate were measured qualitatively using UPLC-MS. [Ir-dF]PF_6 = [Ir(dF[CF_3]ppy)$_2$(dtbpy)]PF_6 (**II-PC-B**).

precursors were screened, and the efficiency of each set of conditions was analyzed qualitatively using ultra-performance liquid chromatography mass spectrometry (UPLC-MS; **Figure 2-16**). While a few sets of conditions using potassium trifluoroborate **II-23a** or Hantzsch ester **II-19a** afforded the desired product, it was quickly determined that bis-catecholato silicate **II-22a** was the optimal radical precursor for the reaction employing the preformed acyl benzimidazolium **II-24**.

The reaction between bis-catecholato silicate **II-22a** and the preformed acyl benzimidazolium **II-24** was investigated further. Control reactions revealed that ruthenium photocatalyst **II-PC-A** was not required to synthesize the desired product; however, no reaction occurred in the absence of light, suggesting the potential formation of an electron donor-acceptor (EDA) complex (**Figure 2-17A**). EDA complexes are systems in which a molecular aggregation is formed between an electron acceptor substrate and an electron donor substrate, and this complex

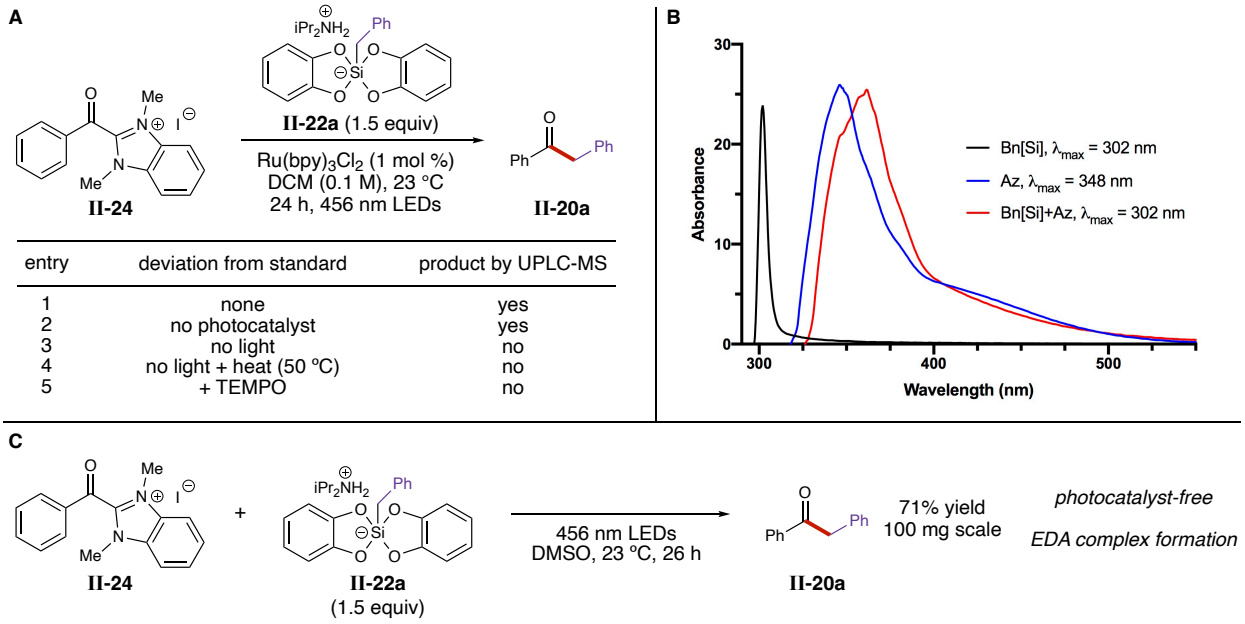

Figure 2-17. A) Control reactions as mechanistic studies. **B)** UV-visible spectrophotometry studies indicate EDA complex formation. **C)** Scaled up reaction between the isolated phenyl benzimidazolium and benzyl silicate.

absorbs light, triggering a single-electron transfer event.[357] UV-visible spectrophotometry studies were thus performed, measuring the absorbance of each reaction component separately and as a mixture (**Figure 2-17B**). A significant red shift (of nearly 50 nm) was observed for the sample containing both the acyl azolium salt and the silicate, signifying formation of an EDA complex. Following additional optimization of the reaction conditions, the desired product **II-20a** was isolated in 71% yield, thus confirming that acyl azolium radical **I**• can be successfully coupled with an oxidatively generated radical precursor (**Figure 2-17C**). While this reaction has potential for further exploration, the general trends in reactivity were used to explore whether this reaction can be performed using catalytic NHC.

A plate was executed to verify formation of an acyl azolium species (**II-I**) in situ from the corresponding acyl imidazole (**II-18a**, **Figure 2-18**). Using methanol as a nucleophile, azoliums,

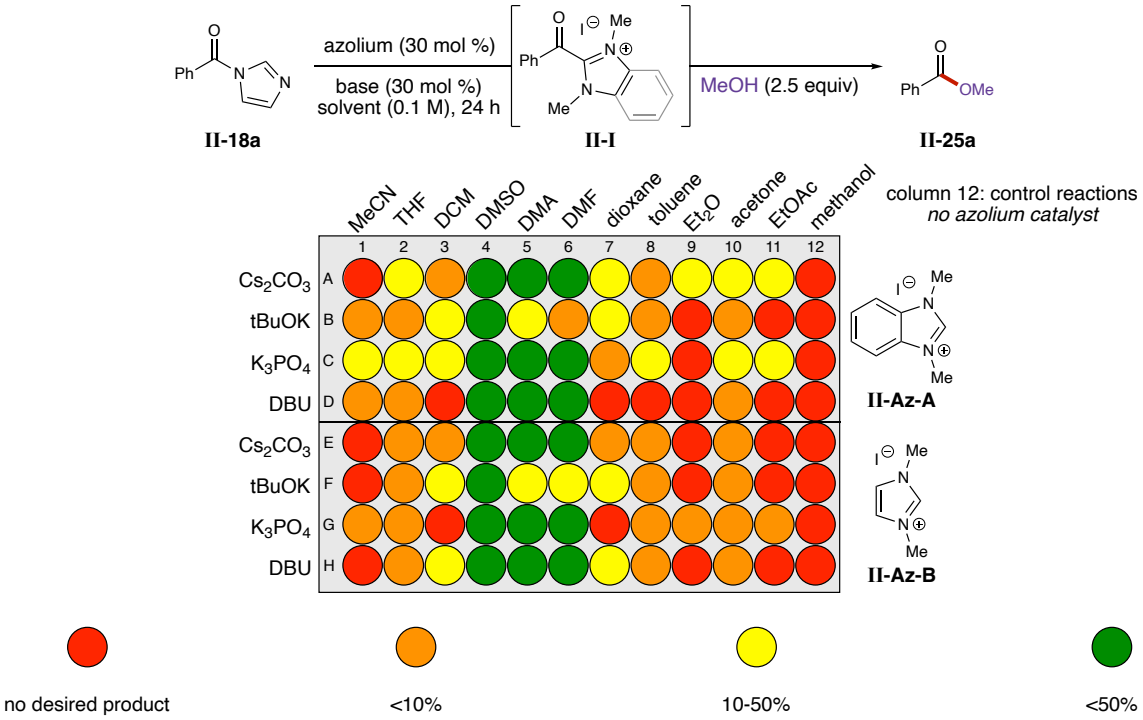

Figure 2-18. HTE results de-risking the catalytic system. Results for this plate were measured quantitatively using GCMS.

bases, and solvents were screened. The desired ester **II-25a** was observed in most of the reaction wells, and no ester product was identified in the absence of NHC, thus confirming formation of the acyl azolium. A variety of activated carboxylic acids were synthesized for use in additional HTE experiments, including perfluorophenyl esters and acyl imidazoles. Following addition of catalytic NHC, these activated carboxylic acid species were expected to yield the desired acyl azolium in situ.

Different 96-well plates were designed and carried out in search of conditions for a combined carbene and photoredox catalyzed synthesis of ketones from carboxylic acids (**Figure 2-19**). Initial screening ensued using acyl imidazoles **II-18**, activated esters **II-26**, or acyl chlorides **II-27** as the acyl azolium precursor in combination with silanes **II-21**, bis-catecholato silicates **II-22**, BF_3K salts **II-23**, or Hantzsch esters **II-19** as the oxidatively generated radical precursor. Each 96-well plate screened a variety of photocatalysts, bases, NHC precursors, and solvents.

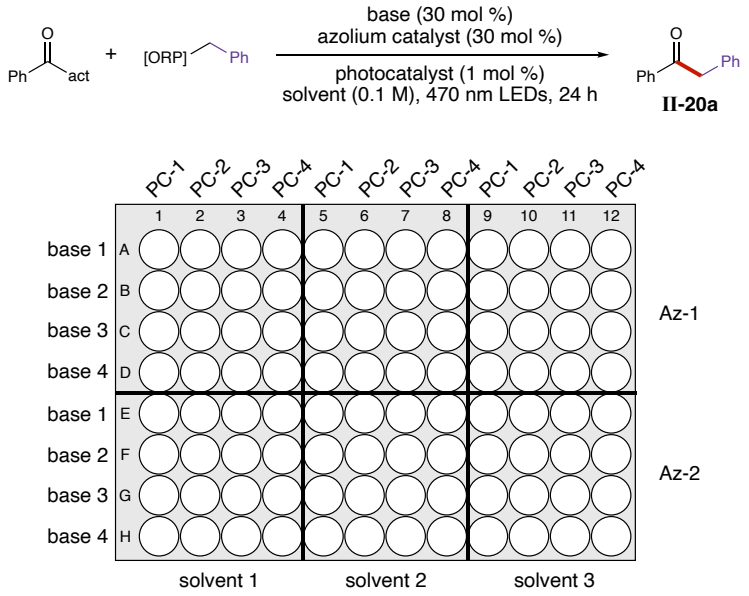

Figure 2-19. General plate setup for HTE screening in search of conditions for a combined catalytic reaction. Act = activating group; ORP = oxidatively generated radical precursor; PC = photocatalyst; Az = azolium.

2.4.4 Trends in Reactivity

HTE enabled facile screening of over 900 unique reaction conditions and rapid identification of the most optimal reaction components for this transformation (**Figure 2-20**). While limited reactivity was achieved with silane **II-21a** and BF_3K **II-23a**, conversion to product was observed using silicate **II-22a** and Hantzsch ester **II-19a**, with the latter radical precursor being the most efficient alkyl radical source. Only trace product was observed using acid chloride **II-27a** as the activated carboxylic acid starting material, and acyl imidazole **II-18a** significantly outperformed perfluorophenyl ester **II-26a**. Moreover, the reaction was most efficient in polar solvents, with cesium-derived bases, and with triazolium NHC precursors. Analysis of these reactivity trends was followed by reaction optimization using phenyl acyl imidazole (**II-18a**) and benzyl Hantzsch ester (Bn-HE, **II-19a**; $E_{1/2}$ = +1.00 V vs SCE)[358] as radical coupling partners, iridium-based **II-PC-B** as the photocatalyst, dimethytriazolium iodide (**II-Az-C**) as the NHC precursor, and cesium carbonate as the base in tetrahydrofuran (THF; **Table 2-1**).

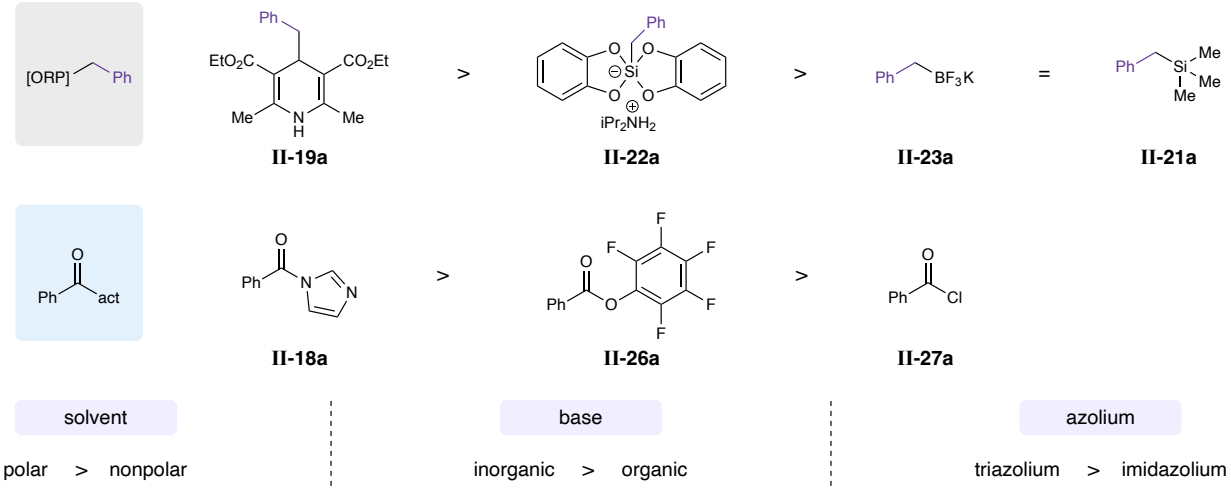

Figure 2-20. General trends in reactivity from analysis of HTE screening.

2.6 Optimization of Reaction Conditions

A brief survey of photocatalysts, azolium catalysts, bases, and solvents allowed for identification of optimal reaction conditions. Due to its broad potential range ($E_{1/2}$ Ir^{III*}/Ir^{II} to $E_{1/2}$ Ir^{III}/Ir^{II} = +1.21 to –1.37 V vs SCE),[359] iridium catalyst **II-PC-B** was found to be the best photocatalyst. The use of strongly reducing catalysts (**II-PC-D**: $E_{1/2}$ Ir^{III*}/Ir^{II} to $E_{1/2}$ Ir^{III}/Ir^{II} = +0.31 to –2.10 V vs SCE)[360] or strongly oxidizing catalysts (**II-PC-E**: $E_{1/2}$ PC^{*}/PC^{-} to $E_{1/2}$ PC/PC^{-} = +2.17 to –0.50 V vs SCE)[361-362] resulted in lower yields, presumably because the photocatalysts were unable to perform both redox events efficiently (**Table 2-1**, entries 1-3). Easily accessible

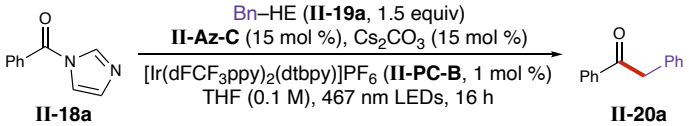

entry	deviation from standard	GCMS yield (%)
1	none	63
2	**II-PC-D** instead of **II-PC-B**	11
3	**II-PC-E** instead of **II-PC-B**	0
4	**II-Az-A** instead of **II-Az-C**	14
5	**II-Az-B** instead of **II-Az-C**	0
6	**II-Az-D** instead of **II-Az-C**	0
7	**II-Az-E** instead of **II-Az-C**	11
8	CsOAc instead of Cs_2CO_3	38
9	K_2CO_3 instead of Cs_2CO_3	8
10	Li_2CO_3 instead of Cs_2CO_3	0
11	MeCN instead of THF	72
12	DCM instead of THF	41
13	DMF instead of THF	65

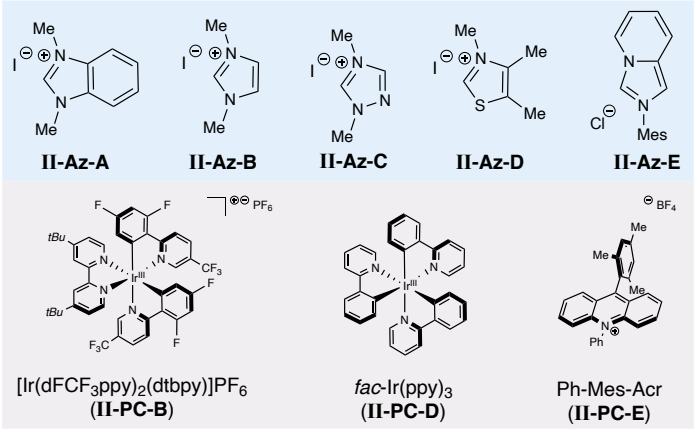

Table 2-1. Optimization of reaction conditions.

organophotocatalyst 2,4,5,6-tetra(9H-carbazol-9-yl)isophthalonitrile (4CzIPN) afforded **II-20a** in slightly diminished yield compared to **II-PC-1**, offering a cost-effective alternative (see Chapter 2.11.3). Examination of different NHC precursors revealed **II-Az-C** to be the only azolium catalyst to efficiently afford the desired ketone via the phenyl acyl azolium intermediate ($E_{1/2}$ = –1.29 V vs SCE), with all other NHC precursors having at least a three-fold decrease in reactivity (**Table 2-1**, entries 4-7). Only cesium bases allowed for significant conversion to product, with cesium carbonate being the most suitable base; all other bases screened showed less than a 10% GC yield (**Table 2-1**, entries 8-10). Finally, a brief solvent screen revealed acetonitrile (MeCN) to be the best solvent, providing a ten percent increase in yield compared to THF (**Table 2-1**, entries 11-13).

The standard reaction conditions were independently implemented to investigate the sensitivity of the reaction conditions (**Figure 2-21**). These studied revealed little-to-no sensitivity to the stir rate (i.e., 0% change from standard conditions with a low stir rate (SR)). When the light

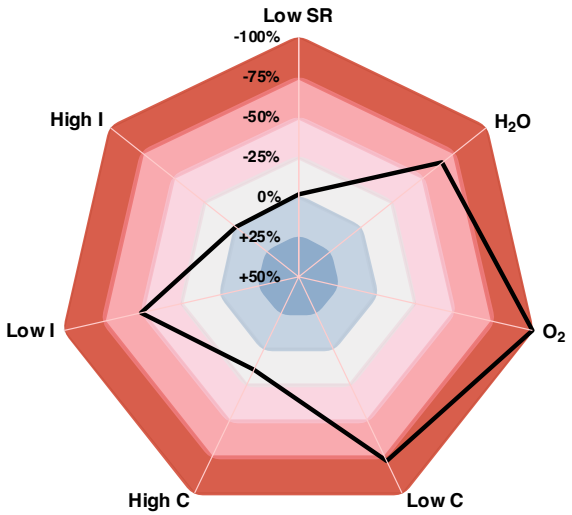

Figure 2-21. Analysis of reaction sensitivity. Sensitivity is analyzed as a percent change in yield from standard conditions (-50% = half reaction efficiency, 0% = standard reaction efficiency, +50% = double reaction efficiency). SR = stir rate, C = concentration, I = intensity.

intensity or reaction concentration was lowered significantly (e.g., 0.05 M instead of 0.10 M), the reaction efficiency decreased. Similarly, high sensitivity to water and oxygen was observed, which was expected given the impact that high water and oxygen content often has in redox reactions (**Figure 2-21**). Based on these studies, this reaction should be reproducible using other laboratory setups if the standard reaction conditions are used and exposure to atmosphere is limited.

Isolation of the desired product was non-trivial due to coelution with the Hantzsch ester pyridine byproduct **II-28**. Various reports in the literature describe the difficulties encountered with removal of **II-28**: the byproduct is known to streak significantly on column chromatography, and other methods of removal (e.g., aqueous workup) have proven unsuccessful. Numerous strategies were employed to remove **II-28** prior to chromatography (**Table 2-2**). Stirring with hydroxide at room temperature successfully removed the byproduct; however, significant decomposition of the desired ketone product **II-20a** was observed. Additional workup conditions included stirring with copper sulfate ($CuSO_4$) or copper chloride ($CuCl_2$), as copper is known to coordinate to pyridine, and it was hypothesized that Cu–pyridine complexation may transfer the byproduct to the aqueous layer. Similarly, a mild acid-base workup was attempted to remove **II-28** through protonation of the nitrogen atom. Unfortunately, these aqueous workup conditions were unsuccessful at removing the undesired byproduct from solution.

Additional purification techniques were required to remove Hantzsch pyridine **II-28**. Column chromatography was attempted using a wide array of solvent combinations with various additives, but coelution still occurred in most cases. It was found that careful column chromatography with non-polar eluent (a slow gradient from 100% hexanes up to 5-10% ethyl acetate in hexanes) enabled separation of **II-28** from the desired ketone. Alternatively, the

byproduct could be removed using preparative high-performance liquid chromatography (HPLC) if coelution occurred using standard chromatography. Further studies on the removal of **II-28** can be found in Chapter 4.3.1).

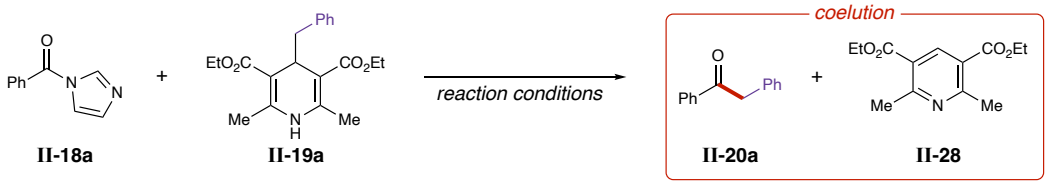

entry	purification conditions	removal of **II-28**	decomposition of **II-20a**
1	stir with $LiOH{\cdot}H_2O$ in THF:H_2O (2:1)	yes	yes
2	stir with KOH in EtOH	yes	yes
3	aqueous $CuSO_4$ workup	no	no
4	aqueous $CuCl_2$ workup	no	no
5	mild acid-base workup	no	no

Table 2-2. Conditions attempted for the removal of Hantzsch pyridine **II-28**.

2.7 Substrate Scope

2.7.1 Acyl Imidazole Variation

With these optimized reaction conditions, the scope of acyl imidazoles **II-18** amenable to alkylation was surveyed (**Table 2-3**). A variety of electron-withdrawing and electron-donating substituents were tolerated on aryl acyl imidazoles. Methyl-substituted aryl ketones (**II-20b-c**) were isolated in good-to-high yields, and halogenated aryl acyl imidazoles afforded the desired ketones (**II-20d-f**) in good yields. Of note, alkylation of ester-substituted acyl imidazole to afford **II-20g** occurred in good yield, showing tolerance to functional groups that traditional methods for ketone formation (e.g., Grignard reaction) may affect.

The conversion of heteroaromatic substrates, such as 4-pyridinyl acyl imidazole and indole acyl imidazole, to the respective ketones (**II-20h-i**) was accomplished in good yields. Products containing pi systems (**II-20j-k**) as well as sterically encumbering substituents (**II-20l**) were also

synthesized using this method. Notably, the reaction with aliphatic substrates was achieved in modest yields (**II-20m-p**). Potentially due to the instability of aliphatic azolium radicals, methods featuring similar modes of NHC-mediated reactivity that have been developed to date have been unsuccessful when applied to aliphatic substrates.[127,131] Efforts to improve the yield of reactions using aliphatic acyl imidazoles are discussed in detail in Chapter 3.

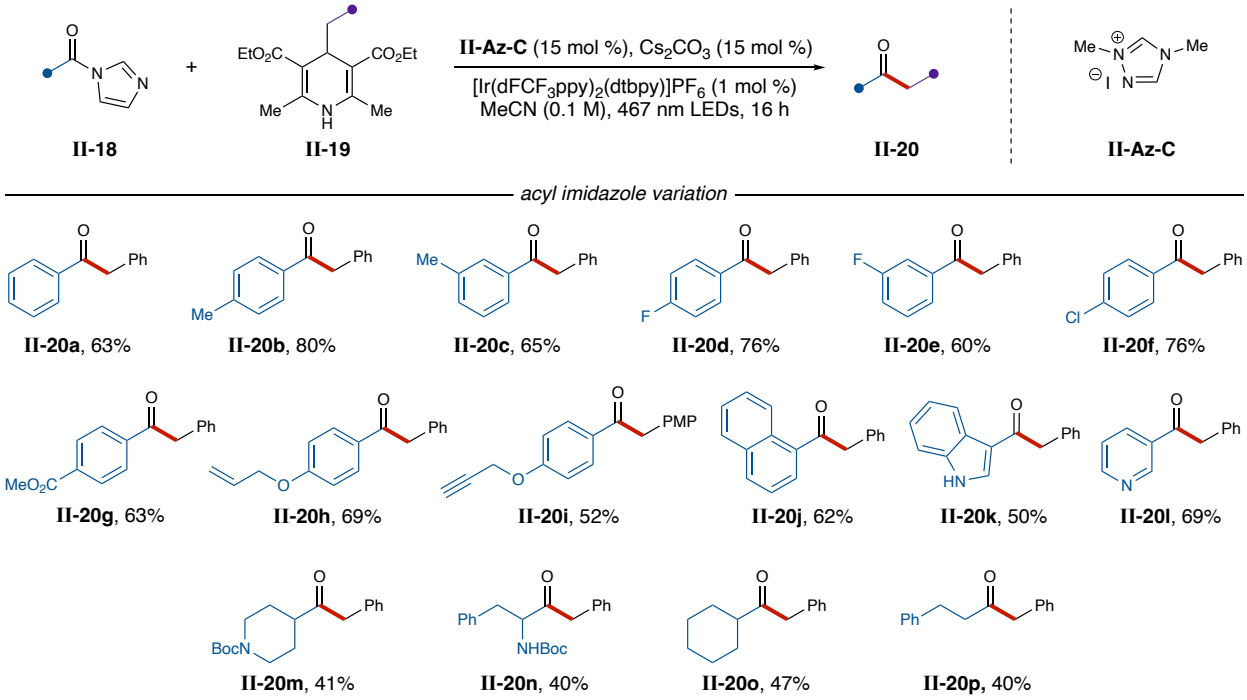

Table 2-3. Acyl imidazole variation in the substrate scope for the synthesis of ketones from carboxylic acids using combined NHC and photoredox catalysis.

2.7.2 Hantzsch Ester Variation

A variety of Hantzsch esters were also successfully employed for the conversion of phenyl acyl imidazole (**II-18a**) to an array of ketones (**Table 2-4**). Substituted benzyl Hantzsch esters bearing electron-withdrawing and electron-donating groups, including halogenated and methoxy substituents, were tolerant of the reaction conditions (**II-20q-t**). Moreover, cyclohexyl Hantzsch

ester productively served as an alkyl radical precursor, suggesting that the use of non-benzylic alkyl radicals for the formation of aliphatic ketones is possible (**II-20u**). Various Meyer nitrile[363] derivatives were also examined as alkyl radical precursors and allowed for the synthesis of ketones containing α-tertiary (**II-20v-w**) and α-quaternary centers (**II-20x-y**).

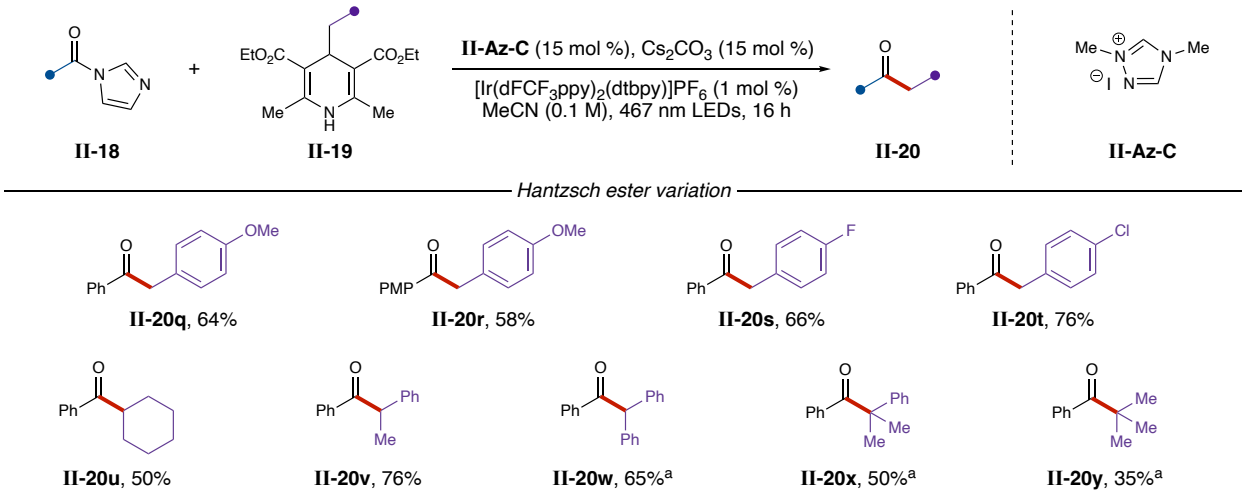

Table 2-4. Hantzsch ester variation in the substrate scope. [a] The corresponding Meyer nitrile was employed in place of the Hantzsch ester.

2.7.3 Late-stage Functionalization of Pharmaceutical Compounds

To demonstrate the ease and practicality of this method, the standard reaction to make deoxybenzoin (**II-20a**) was performed starting from benzoic acid (**Table 2-5**). In situ generation of phenyl acyl imidazole (**II-19a**) using carbonyldiimidazole (CDI) was confirmed by gas chromatography-mass spectrometry (GC-MS) and subsequent subjection to the reaction conditions furnished **II-20a** in 65% yield (compared to 63% when starting from isolated **II-19a**). To further evaluate the utility of this transformation, the reaction conditions were then employed for the late-stage functionalization (LSF) of various pharmaceutical compounds. As a critical component of many medicinal chemistry campaigns or total syntheses, LSF allows for the

incorporation of important functional groups in the final steps of a synthesis, thus creating the need for efficient methodologies.[364] When the in situ reaction conditions were applied to the LSF of telmisartan, a carboxylic acid-containing drug used for the treatment of hypertension,[365] the desired ketone product (**II-20z**) was isolated in 91% yield. This direct, one-step alkylation was applied to various other pharmaceutical compounds to afford ketone products (**II-20aa-ab**) in moderate-to-good yields (**Table 2-5**).

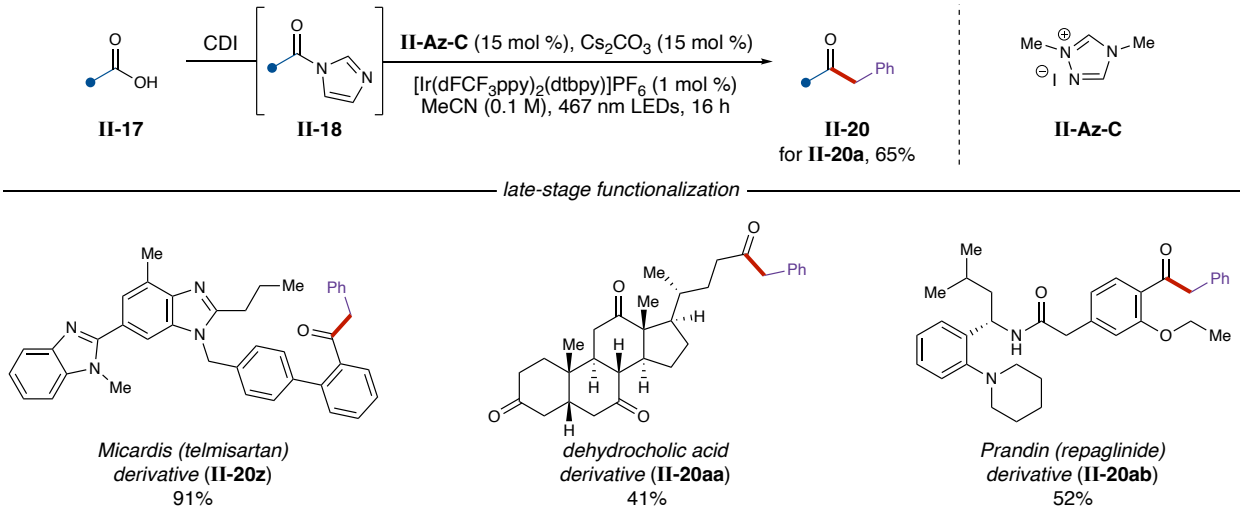

Table 2-5. Late-stage functionalization of bioactive compounds.

Ketone products, such as **II-20**, can undergo an array of transformations, making them a key functional group in organic synthesis. The utility of this reaction was demonstrated through a selective reduction of **II-20a** using a ketoreductase (KRED; **Scheme 2-16**). KREDs are enzymes that enable the enantioselective conversion of prochiral ketones to the corresponding alcohols.[366] Nine of the 19 KREDs that were screened completely converted pure **II-20a** to **II-29a**. Analysis of the enantiomeric ratios (er) revealed that four distinct KREDs (P1-B02, P1-B05, P1-B10, and P1-B12) performed the reduction in high enantiocontrol, affording the desired alcohol in > 99:1

er. The efficiency with which this reduction occurred offers a potential opportunity for additional exploration of a one-pot procedure for the enantioselective synthesis of secondary alcohols from carboxylic acids in the future.

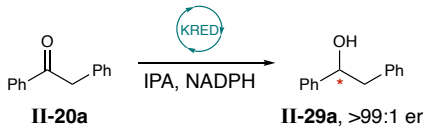

Scheme 2-16. Enantioselective reduction of **II-20a** to **II-29a** using a ketoreductase (KRED). Codex KRED-P1-B10 and Codex KRED-P1-12 gave **II-29a** in >99:1 er with complete conversion from **II-20a**.

2.8 Preliminary Investigations using a Chiral NHC

The successful formation of product **II-20v** presented an opportunity to explore controlling enantioselectivity using chiral NHCs. A variety of chiral NHCs were screened to investigate the enantioselective synthesis of ketones using the combined NHC and photoredox method. Modest enantioselectivity was observed using **II-Az-G** instead of **II-Az-C**, and further improvement in the selectivity was achieved by decreasing the temperature of the reaction (**Table 2-6**). To the best of

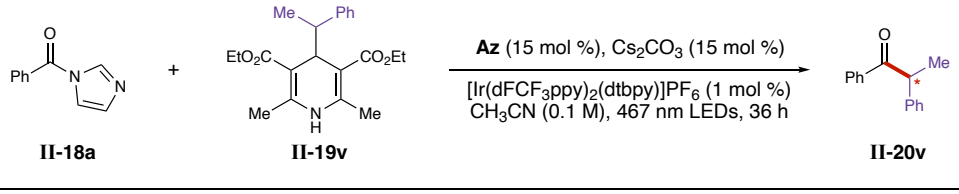

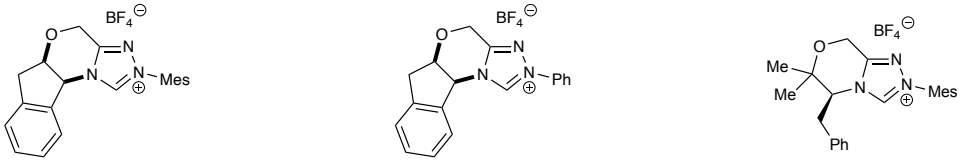

temperature (°C)	II-Az-F	II-Az-G	II-Az-H
35	51:49	60:40	44:56
5	52:48	66:34	-
– 20	-	-	-

Table 2-6. Screen of chiral NHCs for initial investigations into an enantioselective reaction.

our knowledge, this preliminary result demonstrates a novel enantioselective acyl-like radical-radical coupling for the formation of ketones bearing an α-stereogenic center, thus differentiating this work from other acyl radical processes.[323,327,337,367-368]

2.9 Mechanism for the Synthesis of Aryl Ketones

2.9.1 Mechanistic Studies

Control reactions were performed to probe the mechanism of this reaction. As previously noted (vide supra), acyl imidazole **II-18a** is converted to product **II-20a** in 63% yield under the standard reaction conditions. No product was observed in the absence of photocatalyst or light, suggesting that a photoredox-catalyzed process occurs. Similarly, the reaction does not proceed without NHC or base, indicating an NHC-catalyzed reaction (**Figure 2-22**).

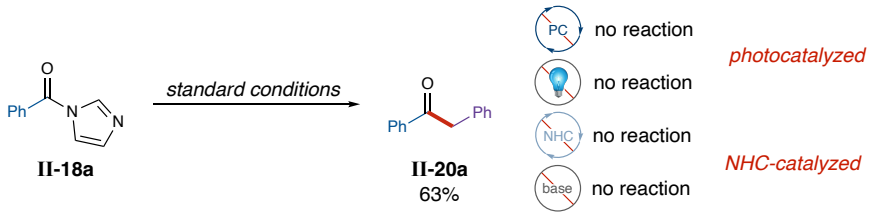

Figure 2-22. Control reactions to probe the mechanism.

TEMPO-trapping studies were performed to further probe the mechanism. As expected, the reaction did not proceed under standard conditions using TEMPO as a radical trap. Only the TEMPO-benzyl mass adduct was observed by ultra-performance liquid chromatography-mass spectrometry (UPLC-MS), thus confirming a radical mechanism and suggesting that the Hantzsch ester is oxidized prior to reduction of the acyl azolium (**Scheme 2-17**). Moreover, the potentials of **II-PC-B** ($E_{1/2}$ Ir^{III*}/Ir^{IV} - $E_{1/2}$ Ir^{IV}/Ir^{III} = –0.89 - 1.69 V vs SCE) do not support reduction of the acyl

azolium prior to oxidation of the Hantzsch ester, as the reduction potential of the acyl azolium is outside the range of the photocatalyst. It is also reasonable to assert that Hantzsch ester oxidation occurs first due to the limited amount of acyl azolium present at a given time relative to superstoichiometric Hantzsch ester. The TEMPO-acyl adduct **II-31** was observed when the reaction was run in the absence of Hantzsch ester, suggesting that single-electron reduction of acyl azolium **II-I** occurs to form **II-I**$^{\bullet}$ and providing additional evidence for a reductive quenching cycle (**Scheme 2-17**).

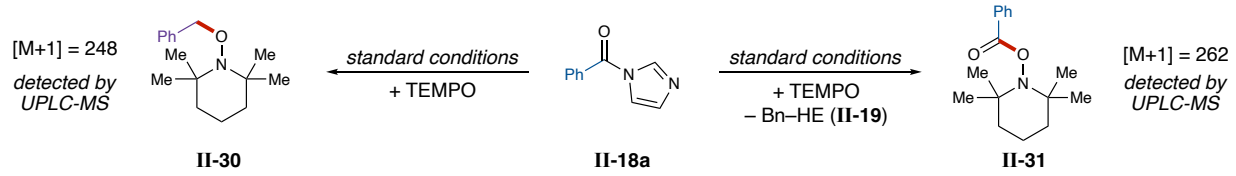

Scheme 2-17. TEMPO-trapping studies performed to probe the mechanism.

2.9.2 Original Proposed Mechanism

A detailed reaction mechanism featuring two catalytic cycles can be proposed based on the results of the mechanistic studies. In situ activation of benzoic acid with carbonyldiimidazole (CDI) affords acyl imidazole **II-18**. The free carbene, generated via deprotonation by cesium carbonate, undergoes nucleophilic addition to **II-18** to give the acyl triazolium **II-I**. Following photoexcitation of the iridium photocatalyst **II-PC-B** (to access Ir^{III}*), the proposed reductive quenching photoredox cycle involves initial oxidation of Hantzsch ester **II-19** to the radical cation by the photoexcited photocatalyst. Fragmentation of the Hantzsch ester radical cation **II-19**$^{+\bullet}$ affords the benzyl radical coupling partner, and single-electron reduction of the acyl triazolium provides azolium radical **II-I**$^{\bullet}$ while regenerating the ground-state photocatalyst (Ir^{III}). Loss of the NHC and radical-radical combination affords the desired ketone (**II-20**; **Figure 2-23**). The recent

mechanistic studies of Breslow intermediates and acyl azoliums reported by Bertrand and Martin suggest that definitive evidence of radical intermediates in thermal NHC-catalyzed processes does not exist.[94] In contrast, this NHC-mediated reaction is conducted under photochemical conditions. Moreover, the observed enantioselectivity (vide supra) provides additional evidence that an NHC-bound radical species is most likely involved in this process. Further investigation of the mechanism can be found in Chapter 3.

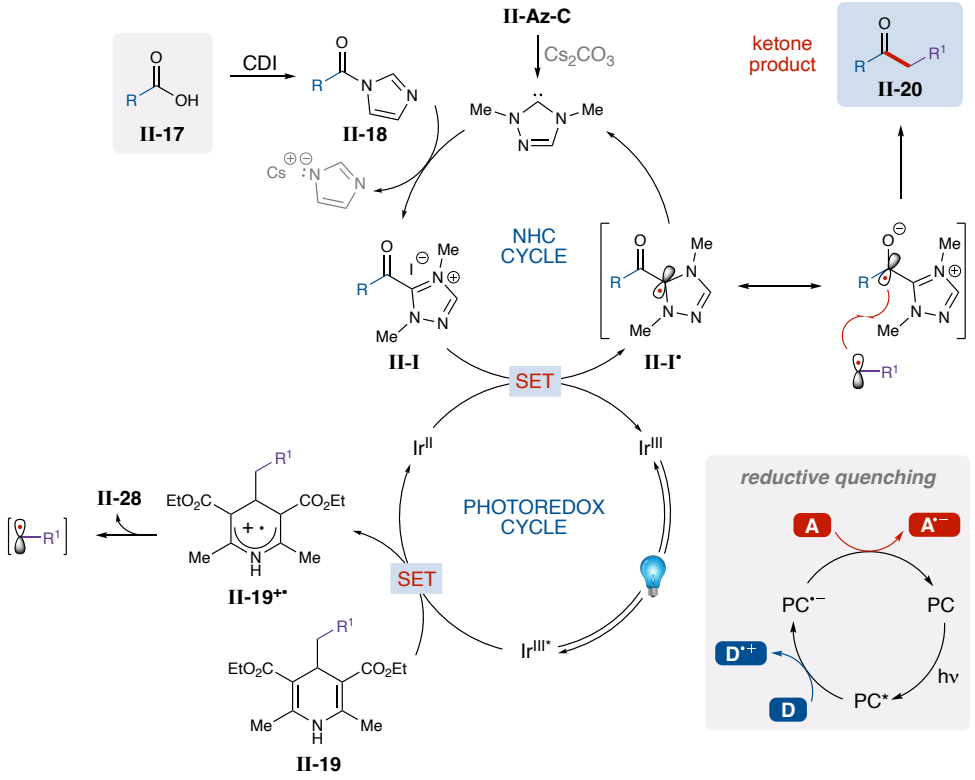

Figure 2-23. Proposed mechanism for the synthesis of ketones from carboxylic acids using combined NHC and photoredox catalysis.

2.10 Conclusion

In summary, a reductive single-electron alkylation of acyl azoliums to form ketones from carboxylic acids was developed. Activation of readily available carboxylic acids with CDI

followed by addition of the NHC catalyst produces the acyl azolium intermediate in situ. This combined NHC-photoredox catalysis enables a one-electron reduction of the acyl azolium, and subsequent radical-radical combination allows for the facile construction of a C–C bond to furnish a ketone. The utility of this method in synthesis was showcased in the direct, one-step late-stage functionalization of pharmaceutical compounds. Importantly, preliminary results using a chiral NHC demonstrated that enantioselectivity is possible using this process, thus highlighting the potential advantage of using acyl azolium radicals in acyl radical transformations.

2.11 Experimental Protocols and Analyses

2.11.1 General Information

All reactions were carried out under an argon or nitrogen atmosphere in oven-dried glassware with magnetic stirring. All solvents were purified by passing through a bed of activated alumina, dried over 3Å molecular sieves, and then degassed using the freeze-pump-thaw method (3-4 cycles). Purification of reaction products was carried out by flash chromatography on Biotage Isolera 4 systems with Ultra-grade silica cartridges or by preparative HPLC. Reverse phase preparative HPLC was performed on a Gilson preparative HPLC with the following conditions: Phenomenex Kinetex C18 50 x 30 mm (short column) or 150 x 21 mm (long column). Gradients ranged from of 5-98 % acetonitrile:water with 0.1 % formic acid over 5 or 25 min, respectively, followed by 1 min at 98 % acetonitrile. The flow rate was 50 mL/min for the short column and 20 mL/min for the long column. Silicycle SiliaFlash P60 silica gel 60 (230-400 mesh) was used for column chromatography. Analytical thin layer chromatography was performed on EM Reagent 0.25 mm silica gel 60-F plates. Visualization was accomplished with UV light.

^{1}H NMR spectra were recorded on AVANCE III 500 MHz w/ direct cryoprobe (500 MHz) spectrometer and are reported in ppm using solvent as an internal standard ($CDCl_3$ at 7.26 ppm). Data are reported as (ap = apparent, s = singlet, d = doublet, t = triplet, q = quartet, m = multiplet, b = broad; coupling constant(s) in Hz; integration.) Proton-decoupled ^{13}C NMR spectra were recorded on an AVANCE III 500 MHz w/ direct cryoprobe (125 MHz) spectrometer and are reported in ppm using solvent as an internal standard ($CDCl_3$ at 77.16 ppm). Reactions were monitored by LCMS or GCMS using a WATERS Acquity-H UPLC-MS with a single quad detector (ESI) or an Agilent 7890 gas chromatograph equipped with a 5975C single quadrupole EI-MS, respectively. High-resolution mass spectrometry (HRMS) was obtained using an Agilent 6201 MSLC-TOF (ESI). All photocatalytic reactions were carried out in a SynLED Parallel Photoreactor (465-470 nm) purchased from Sigma-Aldrich. Enantioselectivity measurements were made on an Agilent 1290 Infinity SFC using Chiralpak IA-3, IB-3, IC-3, ID-3, IG-3 chiral stationary phases. Electrochemical measurements were recorded on a NuVant EZstat Pro using platinum working, platinum counter, and Ag/Ag^{+} pseudoreference electrodes in a 0.04 M solution in MeCN with 0.1M $N(Bu)_4PF_6$ electrolyte. Voltages are reported relative to SCE based on an internal ferrocene standard. $[Ir(dF(CF_3)ppy)_2(dtbpy)]PF_6$ (**II-PC-B**) was purchased from Strem Chemicals and used as received or synthesized according to the literature procedure.[369] No discrepancies were observed using synthesized or commercially available **II-PC-B**.

2.11.2 General Synthetic Procedures

2.11.2.1 General Procedure for the synthesis of acyl imidazoles

II-17 **II-18**

Scheme 2-18. Synthesis of acyl imidazoles from carboxylic acids.

Acyl imidazoles **II-18a-p** were prepared based on the method of Lee and Scheidt:[370] The appropriate acid **II-17** (10 mmol, 1.0 equiv) was dissolved in dry dichloromethane (0.3 M), and CDI (carbonyldiimidazole, 15 mmol, 1.5 equiv) was added slowly (caution, exothermic). The resulting mixture was stirred for 12 h at room temperature. Upon completion, the solution was transferred to a separatory funnel and washed with deionized water (2 x 25 mL), and then the organic layer was dried over $MgSO_4$. Concentration under reduced pressure afforded the acyl imidazole, which was used in the following reaction without further purification.

All alkyl radical precursors (Hantzsch esters and Meyer nitriles) were synthesized according to the established literature procedure and matched the reported spectral data.[285,371-372]

2.11.2.2 General Procedure 1 for the alkylation of acyl azoliums using Hantzsch esters

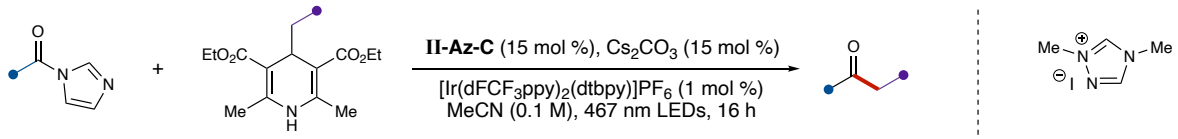

II-18 **II-19** (1.5 equiv) **II-20** **II-Az-C**

Scheme 2-19. Combined NHC and photoredox-catalyzed synthesis of ketones.

All reactions were set up inside a glovebox under N_2 atmosphere. To an oven-dried 2-dram vial containing a stir bar was added the respective Hantzsch ester **II-19** (1.5 equiv, 0.38 mmol),

respective acyl imidazole **II-18** (1.0 equiv, 0.25 mmol), iridium-derived **II-PC-B** (2.50 μmol, 1 mol %), dimethyltriazolium iodide NHC precursor **II-Az-C** (8.8 mg, 0.15 equiv, 38 μmol), and cesium carbonate (12 mg, 0.15 equiv, 38 μmol). Acetonitrile (2.5 mL, 0.1M) was added, and the reaction was capped and taken out of the glovebox. Parafilm was wrapped around the cap to prevent air from entering and the vial was stirred in a SynLED Parallel Photoreactor (467 nm blue LEDs) with monitoring by GCMS or UPLC-MS. When complete consumption of the acyl imidazole was observed (typically 4-16 h), the reactions were concentrated under reduced pressure and then purified by column chromatography or preparative HPLC.

2.11.2.3 General Procedure 2 for the alkylation of acyl azoliums using Meyer nitriles:

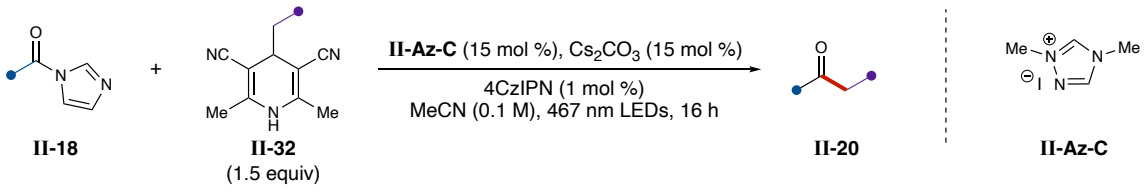

Scheme 2-20. Synthesis of ketones using Meyer nitriles in place of Hantzsch esters.

All reactions were set up inside a glovebox under a nitrogen atmosphere. To an oven-dried 2-dram vial containing a stir bar was added the respective Meyer nitrile **II-32** (1.5 equiv, 0.38 mmol), appropriate acyl imidazole **II-18** (1.0 equiv, 0.25 mmol), 4-CzIPN (0.01 equiv, 1 mol %), dimethyltriazolium iodide NHC precursor **II-Az-C** (8.8 mg, 0.15 equiv, 38 μmol), and cesium carbonate (12 mg, 0.15 equiv, 38 μmol). Acetonitrile (2.5 mL, 0.1M) was added to the vial, and the reaction was capped and taken out of the glovebox. Parafilm was wrapped around the cap to prevent air from entering and the vial was in a SynLED Parallel Photoreactor (467 nm blue LEDs) with monitoring by GCMS or LCMS. When complete consumption of the acyl imidazole was

observed (typically 4-16 h), the reactions were concentrated under reduced pressure and then purified by column chromatography.

2.11.2.4 General Procedure 3 for the one-pot in situ activation of carboxylic acids

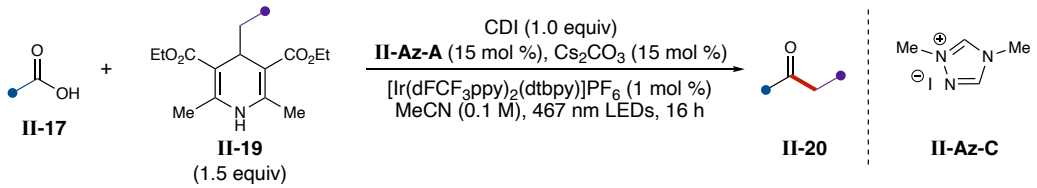

Scheme 2-21. One-pot reaction for the synthesis of ketones from carboxylic acids.

All reactions were set up inside a glovebox under nitrogen atmosphere. To an oven-dried 2-dram vial containing a stir bar were added CDI (1.0 equiv., 0.25 mmol) and the appropriate carboxylic acid **II-17** (1.0 equiv., 0.25 mmol). The solids were dissolved in acetonitrile (2.5 mL, 0.1 M) and the reaction was allowed to stir in the glovebox at room temperature for 2 h or until the solution became homogenous. **Note**: If the reaction did not become homogenous, 0.400 mL of DMF was added to the vial to help solubilize the carboxylic acid, and the reaction was allowed to stir for another 4 h. At this time, to a separate vial containing a stirbar was added the respective Hantzsch ester **II-19** (1.5 equiv., 0.38 mmol), **II-PC-B** (0.01 equiv., 1 mol %), and dimethyltriazolium iodide NHC precursor (**II-Az-C**, 8.8 mg, 0.15 equiv., 38 μmol). The vial containing the in situ generated acyl imidazole **II-18** was added to the vial containing the solids, followed by the addition of cesium carbonate (12 mg, 0.15 equiv., 38 μmol). The vial was capped and taken out of the glovebox. Parafilm was wrapped around the cap to prevent air from entering and the vial was stirred in a SynLED Parallel Photoreactor (467 nm blue LEDs). The reaction was allowed to stir for 24 h unless otherwise noted. Following completion, the reactions were concentrated under reduced pressure and then purified by column chromatography.

2.11.3 Optimization of Reaction Conditions

The reaction was optimized according to General Procedure 1 for the alkylation of acyl azoliums using acyl imidazole **II-18a** and Hantzsch ester **II-19a** as the radical coupling partner precursors. Reactions were monitored by GCMS.

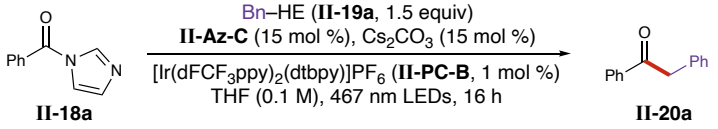

entry	deviation from standard	GCMS yield (%)
1	none	63
2	**II-PC-D** instead of **II-PC-B**	11
3	**II-PC-E** instead of **II-PC-B**	0
4	**II-PC-F** instead of **II-PC-B**	42
5	**II-Az-A** instead of **II-Az-C**	14
6	**II-Az-B** instead of **II-Az-C**	0
7	**II-Az-D** instead of **II-Az-C**	0
8	**II-Az-E** instead of **II-Az-C**	11
9	**II-Az-I** instead of **II-Az-C**	0
10	**II-Az-J** instead of **II-Az-C**	0
11	CsOAc instead of Cs_2CO_3	38
12	K_2CO_3 instead of Cs_2CO_3	8
13	Li_2CO_3 instead of Cs_2CO_3	0
14	+ LiCl	0
15	+ $Mg(OTf)_2$	26
16	+ 4 angstrom molecular sieves	12
17	MeCN instead of THF	72
18	DCM instead of THF	41
19	DMF instead of THF	65

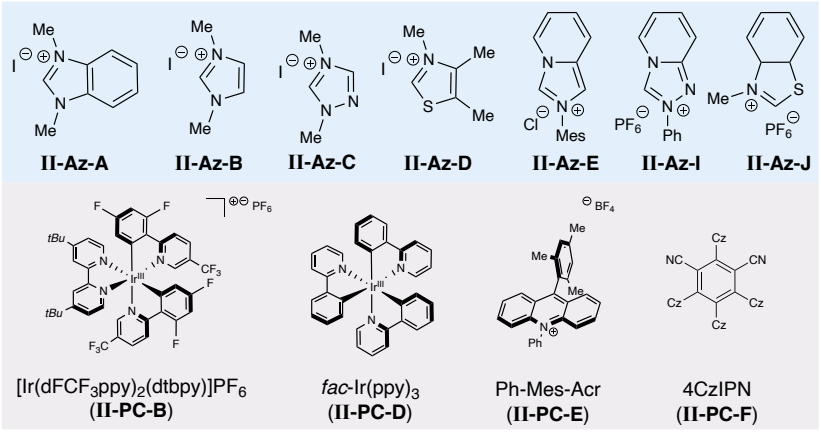

Table 2-7. Complete optimization table. [a] GCMS yield based on calibration curve using 1,3,5-trimethoxybenzene as internal standard. [b] Reactions performed at a 0.10 mmol scale.

2.11.4 Control Experiments

Control experiments were set up according to General Procedure 1 for the alkylation of acyl azoliums using the respective acyl imidazole and Hantzsch ester.

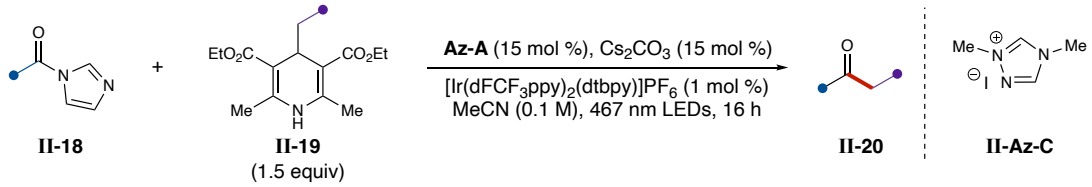

entry	deviation from standard	GC yield (%)[a,b]
1	none	63
2	no base	0
3	no azolium	0
4	no photocatalyst	0
5	no light	0

Table 2-8. Control reactions as mechanistic studies. [a] GCMS yield based on calibration curve using 1,3,5-trimethoxybenzene as internal standard. [b] Reactions performed at a 0.10 mmol scale.

2.11.5 Cyclic Voltammetry Graphs

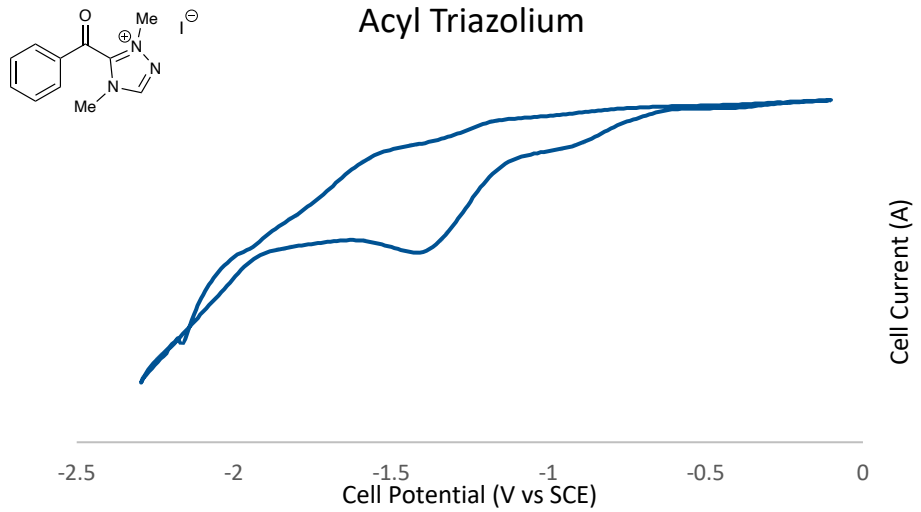

Figure 2-24. Cyclic voltammogram of the acyl azolium intermediate. Note: acyl azolium intermediate was made in situ from the corresponding acyl imidazole and Cs_2CO_3.

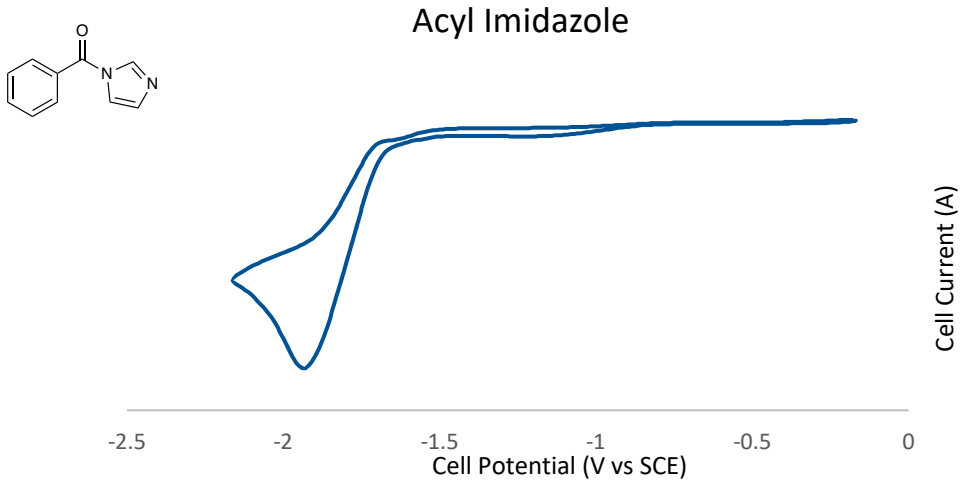

Figure 2-25. Cyclic voltammogram of the acyl imidazole.

2.11.6 Enantioselective Variant SFC traces

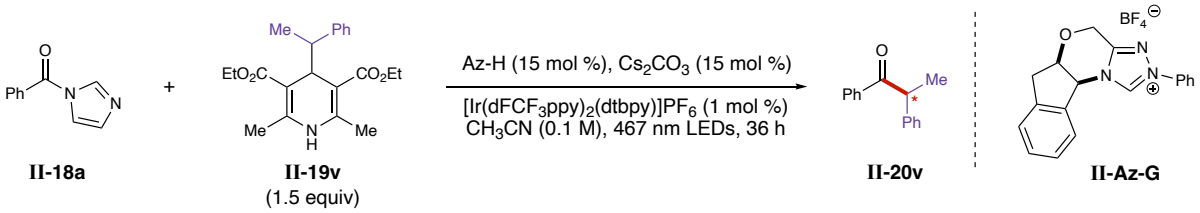

entry	temperature	enantiomeric ratio
1	35 °C	60:40
2	5 °C	66:34
3	–20 °C	-

Table 2-9. Enantiomeric ratios as a function of temperature using chiral **II-Az-G**.

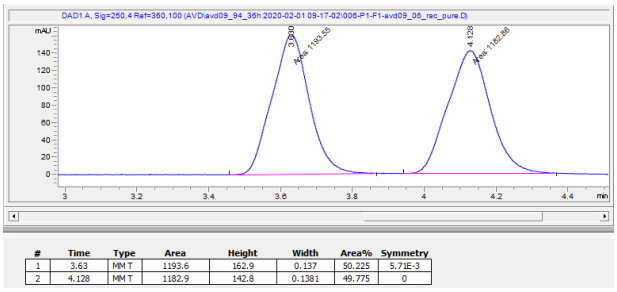

Figure 2-26. SFC trace using achiral **II-Az-A**.

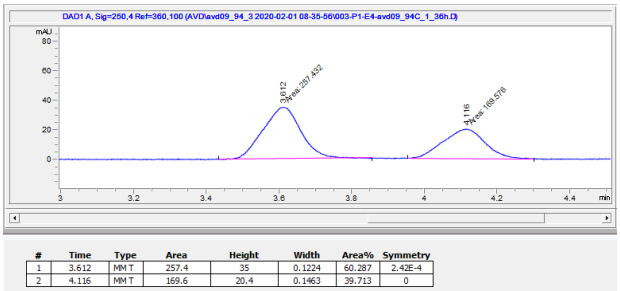

#	Time	Type	Area	Height	Width	Area%	Symmetry
1	3.612	MM T	257.4	35	0.1224	60.287	2.42E-4
2	4.116	MM T	169.6	20.4	0.1463	39.713	0

Figure 2-27. SFC trace using chiral **II-Az-G** at 35 ºC (entry 1, **Table 2-9**).

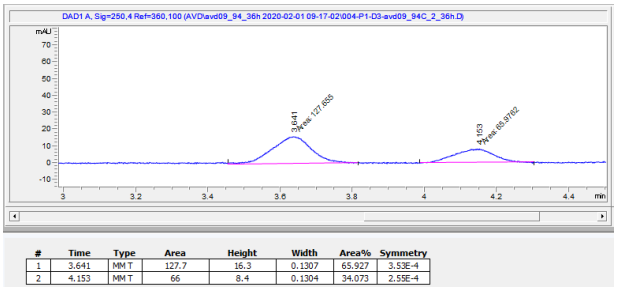

#	Time	Type	Area	Height	Width	Area%	Symmetry
1	3.641	MM T	127.7	16.3	0.1307	65.927	3.53E-4
2	4.153	MM T	66	8.4	0.1304	34.073	2.55E-4

Figure 2-28. SFC trace using chiral **II-Az-G** at 5 ºC (entry 2, **Table 2-9**).

2.11.7 Tabulated Data

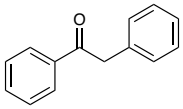

1,2-diphenylethan-1-one (**II-20a**). Prepared according to General Procedure 1 for the alkylation of acyl azoliums using the respective acyl imidazole (43 mg, 1.0 equiv) and Hantzsch ester. **II-PC-B** was used as the photocatalyst. The reaction mixture was purified by column chromatography (wet loaded with toluene, 5-15% ethyl acetate/hexanes) to yield the desired product as a white solid (63%). Can also be prepared with general procedure **(3)** using benzoic acid to afford the desired material (31 mg, 65%). Product is a known substrate and matched the literature data.[373]

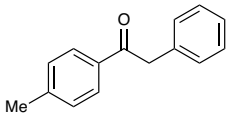

2-phenyl-1-(*p*-tolyl)ethan-1-one (**II-20b**). Prepared according to General Procedure 1 for the alkylation of acyl azoliums using the respective acyl imidazole (46.5 mg, 1.0 equiv) and Hantzsch ester. **II-PC-B** was used as the photocatalyst. The reaction mixture was purified by column chromatography (wet loaded with toluene, 2-20% ethyl acetate/hexanes) to yield the product as a white solid (42 mg, 80%). Product is a known substrate and matched the literature data.[373]

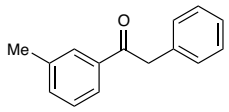

2-phenyl-1-(*m*-tolyl)ethan-1-one (**II-20c**). Prepared according to General Procedure 1 for the alkylation of acyl azoliums using the respective acyl imidazole (46.5 mg, 1.0 equiv) and Hantzsch ester. **II-PC-B** was used as the photocatalyst. The reaction mixture was purified by column chromatography (0-5% ethyl acetate/hexanes) to yield the product as an off-white solid (34 mg, 65%). Product is a known substrate and matched the literature data.[374]

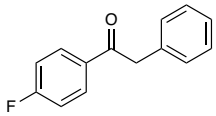

1-(4-fluorophenyl)-2-phenylethan-1-one (**II-20d**). Prepared according to General Procedure 1 for the alkylation of acyl azoliums using the respective acyl imidazole (47.5 mg, 1.0 equiv) and Hantzsch ester. **II-PC-B** was used as the photocatalyst. The reaction mixture was purified by

column chromatography (wet loaded with toluene, 2-20% ethyl acetate/hexanes) to yield the product as a white solid (41 mg, 76%). Product is a known substrate and matched the literature data.[373]

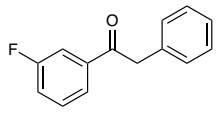

1-(3-fluorophenyl)-2-phenylethan-1-one (**II-20e**). Prepared according to General Procedure 1 for the alkylation of acyl azoliums using the respective acyl imidazole (48 mg, 1.0 equiv) and Hantzsch ester. **II-PC-B** was used as the photocatalyst. The reaction mixture was purified by column chromatography (dry loaded with silica, 2-20% ethyl acetate/hexanes) to yield the desired product as a white solid (32 mg, 60%). Product is a known substrate and matched the literature data.[375]

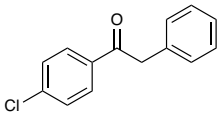

1-(4-chlorophenyl)-2-phenylethan-1-one (**II-20f**). Prepared according to General Procedure 1 for the alkylation of acyl azoliums using the respective acyl imidazole (51.6 mg, 1.0 equiv) and Hantzsch ester. **II-PC-B** was used as the photocatalyst. The reaction mixture was purified by column chromatography (wet loaded with toluene, 2-20% ethyl acetate/hexanes) to yield the product as a white solid (57.7 mg, 76%). Product is a known substrate and matched the literature data.[376]

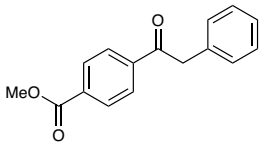

methyl 4-(2-phenylacetyl)benzoate (**II-20g**). Prepared according to General Procedure 1 for the alkylation of acyl azoliums using the respective acyl imidazole (57.6 mg, 1.0 equiv) and Hantzsch ester. **II-PC-B** was used as the photocatalyst. The reaction mixture was purified by preparative HPLC (long column, 20-90% MeCN/H_2O) to yield the desired product as an off-white solid (40.2 mg, 63%). Product is a known substrate and matched the literature data.[377]

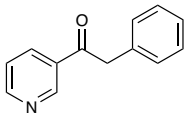

2-phenyl-1-(pyridin-3-yl)ethan-1-one (**II-20h**). Prepared according to General Procedure 1 for the alkylation of acyl azoliums using the respective acyl imidazole (43.0 mg, 1.0 equiv) and Hantzsch ester. **II-PC-B** was used as the photocatalyst. The reaction mixture was purified by preparative HPLC (short column, 10-90% MeCN/H_2O) to yield the desired product (34.0 mg, 69%). Product is a known substrate and matched the literature data.[378]

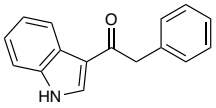

1-(1*H*-indol-3-yl)-2-phenylethan-1-one (**II-20i**). Prepared according to General Procedure 1 for the alkylation of acyl azoliums using the respective acyl imidazole (53 mg, 1.0 equiv) and Hantzsch ester. **II-PC-B** was used as the photocatalyst. The reaction mixture was purified by

column chromatography (wet loaded with toluene, 20-60% ethyl acetate/hexanes) to yield the desired product as a white solid (29.5 mg, 50%). Analytical data for **II-20i**: ^{1}H NMR (500 MHz, DMSO-d_6) δ 11.99 (s, 1H), 8.52 (d, J = 3.0 Hz, 1H), 8.22 – 8.11 (m, 1H), 7.46 (dt, J = 8.1, 1.0 Hz, 1H), 7.37 – 7.33 (m, 2H), 7.32 – 7.27 (m, 2H), 7.23 – 7.14 (m, 3H), 4.15 (s, 2H). ^{13}C NMR (126 MHz, DMSO-d_6) δ 192.6, 136.7, 136.5, 134.6, 129.3, 128.2, 126.1, 125.5, 122.8, 121.7, 121.3, 116.0, 112.1, 45.7. HRMS (ESI/TOF) m/z: $[M+Na]^+$ Calcd. for $C_{16}H_{13}NONa$ 258.0895; Found 258.0895. IR has been reported for this compound.[379]

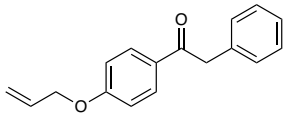

1-(4-(allyloxy)phenyl)-2-phenylethan-1-one (**II-20j**). Prepared according to General Procedure 1 for the alkylation of acyl azoliums using the respective acyl imidazole (57 mg, 1.0 equiv) and Hantzsch ester. **II-PC-B** was used as the photocatalyst. The reaction mixture was purified by column chromatography (dry loaded with silica, 2-20% ethyl acetate/hexanes) to yield the desired product as a white solid (39.7 mg, 69%). Analytical data for **II-20j**: Note NMR contains a mixture of tautomers. ^{1}H NMR (500 MHz, Chloroform-d) Ketone form: δ 8.03 – 7.96 (m, 2H), 7.32 (dd, J = 8.1, 6.8 Hz, 2H), 7.29 – 7.22 (m, 3H), 6.97 – 6.90 (m, 2H), 6.04 (ddt, J = 17.3, 10.5, 5.3 Hz, 1H), 5.47 – 5.29 (m, 2H), 4.59 (dt, J = 5.3, 1.5 Hz, 2H), 4.23 (s, 2H). Enol form: δ 9.89 (s, 0.04 H), 7.84 (m, 0.12 H), 7.02 (m, 0.12 H), 4.63 (m, 0.08 H). ^{13}C NMR (126 MHz, Chloroform-d) δ 196.3, 162.6, 135.0, 132.5, 131.0, 129.8, 129.5, 128.7, 126.9, 118.4, 114., 69.02, 45.3. HRMS (ESI/TOF) m/z: $[M+H]^+$ Calcd. for $C_{17}H_{17}O_2$ 253.1228; Found 253.1223. FTIR (ATR) cm^{-1}: 3098, 3061, 3034, 2901, 1680.

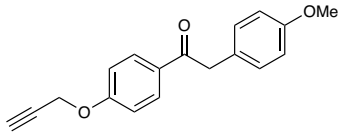

2-(4-methoxyphenyl)-1-(4-(prop-2-yn-1-yloxy)phenyl)ethan-1-one (**II-20k**). Prepared according to General Procedure 1 for the alkylation of acyl azoliums using the respective acyl imidazole (53 mg, 1.0 equiv) and Hantzsch ester. **II-PC-B** was used as the photocatalyst. The reaction mixture was purified by column chromatography (dry loaded with silica, 2-10% ethyl acetate/hexanes) to yield the desired product as a white solid (34 mg, 52%). Analytical data for **II-20k**: ^{1}H NMR (500 MHz, Chloroform-*d*) δ 8.05 – 7.96 (m, 2H), 7.23 – 7.15 (m, 2H), 7.05 – 6.98 (m, 2H), 6.91 – 6.83 (m, 2H), 4.75 (d, *J* = 2.4 Hz, 2H), 4.17 (s, 2H), 3.78 (s, 3H), 2.55 (t, *J* = 2.4 Hz, 1H). ^{13}C NMR (126 MHz, Chloroform-*d*) δ 196.7, 161.5, 158.7, 131.0, 130.6, 127.0, 114.8, 114.3, 77.9, 76.4, 56.0, 55.4, 44.6. HRMS (ESI/TOF) m/z: $[M+H]^+$ Calcd. for $C_{18}H_{17}O_3$ 281.1177; Found 281.1175. FTIR (ATR) cm^{-1}: 3305, 3263, 2994, 1684.

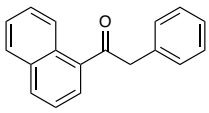

1-(naphthalen-2-yl)-2-phenylethan-1-one (**3l**). Prepared according to General Procedure 1 for the alkylation of acyl azoliums using the respective acyl imidazole (55.6 mg, 1.0 equiv) and Hantzsch ester. **II-PC-B** was used as the photocatalyst. The reaction mixture was purified by column chromatography (wet loaded with toluene, 2-20% ethyl acetate/hexanes) to yield the desired product as a white solid (38 mg, 62%). Product is a known substrate and matched the literature data.[373]

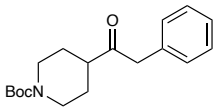

tert-butyl 4-(2-phenylacetyl)piperidine-1-carboxylate (**II-20m**). Prepared according to General Procedure 1 for the alkylation of acyl azoliums using the respective acyl imidazole (69.8 mg, 1.0 equiv) and Hantzsch ester. **II-PC-B** was used as the photocatalyst. The reaction mixture was purified by column chromatography (wet loaded with toluene, 2-20% ethyl acetate/hexanes) to yield the desired product as a clear oil (31 mg, 41%). Analytical data for **II-20m**: ^{1}H NMR (500 MHz, Chloroform-*d*) δ 7.38 – 7.29 (m, 2H), 7.30 – 7.26 (m, 1H), 7.19 (dd, *J* = 7.2, 1.7 Hz, 2H), 4.11 (m, 2H), 3.75 (s, 2H), 2.74 (t, *J* = 12.7 Hz, 2H), 2.59 (tq, *J* = 11.4, 3.8 Hz, 1H), 1.74 (m, 2H), 1.55 (dtd, *J* = 13.4, 11.7, 4.3 Hz, 2H), 1.44 (s, 9H). ^{13}C NMR (126 MHz, Chloroform-*d*) δ 209.5, 154.7, 134.0, 129.5, 128.8, 127.2, 79.7, 48.0, 47.9, 28.5, 27.7. HRMS (ESI/TOF) m/z: $[M+Na]^+$ Calcd. for $C_{18}H_{25}NO_3Na$ 326.1732; Found 326.1732. FTIR (ATR) cm^{-1}: 3006, 2977, 2929, 1680.

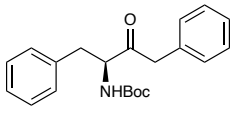

tert-butyl (*S*)-(3-oxo-1,4-diphenylbutan-2-yl)carbamate (**II-20n**). Prepared according to General Procedure 1 for the alkylation of acyl azoliums using the respective acyl imidazole (78.8 mg, 1.0 equiv) and Hantzsch ester. **II-PC-B** was used as the photocatalyst. The reaction mixture was purified by preparative HPLC (short column, 30-95% MeCN/H_2O) to yield the product as an off-white solid (34 mg, 40%). Analytical data for **II-20n**: ^{1}H NMR (500 MHz, Chloroform-*d*) δ 7.38 – 7.22 (m, 6H), 7.11 (dd, *J* = 16.5, 7.3 Hz, 4H), 5.10 (d, *J* = 7.8 Hz, 1H), 4.63 (q, *J* = 7.0 Hz, 1H), 3.77 – 3.58 (m, 2H), 3.00 (qd, *J* = 13.8, 6.7 Hz, 2H), 1.41 (s, 9H). ^{13}C NMR (126 MHz,

Chloroform-*d*) δ 206.7, 155.2, 136.3, 133.2, 129.7, 129.0, 128.84, 128.7, 127.2, 127.1, 80.1, 59.6, 48.0, 37.9, 28.4. HRMS (ESI/TOF) m/z: $[M+Na]^+$ Calcd. for $C_{21}H_{25}NO_3Na$ 362.1732; Found 362.1730. FTIR (ATR) cm^{-1}: 3379, 3029, 2978, 1723, 1681.

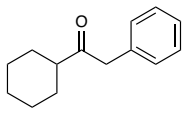

1-cyclohexyl-2-phenylethan-1-one (**II-20o**). Prepared according to General Procedure 1 for the alkylation of acyl azoliums using the respective acyl imidazole (46.6 mg, 1.0 equiv) and Hantzsch ester. **II-PC-B** was used as the photocatalyst. The reaction mixture was purified by column chromatography (wet loaded with toluene, 0-10% ethyl acetate/hexanes) to yield the desired product as a clear oil (24 mg, 47%). Product is a known substrate and matched the literature data.[380]

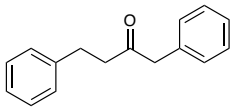

1,4-diphenylbutan-2-one (**II-20p**). Prepared according to General Procedure 1 for the alkylation of acyl azoliums using the respective acyl imidazole (50 mg, 1.0 equiv) and Hantzsch ester. **II-PC-B** was used as the photocatalyst. The reaction mixture was purified by preparative HPLC (short column, 30-95% MeCN/H_2O) to yield the product as a clear oil (23 mg, 41%). Product is a known substrate and matched the literature data.[381]

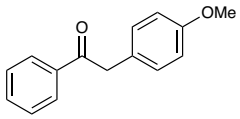

2-(4-methoxyphenyl)-1-phenylethan-1-one (**II-20q**). Prepared according to General Procedure 1 for the alkylation of acyl azoliums using the respective acyl imidazole (43.0 mg, 1.0 equiv) and Hantzsch ester. **II-PC-B** was used as the photocatalyst. The reaction mixture was purified by column chromatography (dry loaded with silica, 0-10% ethyl acetate/hexanes) to yield the desired product as a white solid (36 mg, 64%). Product is a known substrate and matched the literature data.[382]

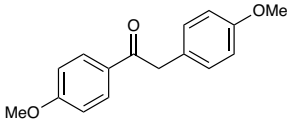

1,2-bis(4-methoxyphenyl)ethan-1-one (**II-20r**). Prepared according to General Procedure 1 for the alkylation of acyl azoliums using the respective acyl imidazole (51 mg, 1.0 equiv) and Hantzsch ester. **II-PC-B** was used as the photocatalyst. The reaction mixture was purified by column chromatography (dry loaded with silica, 2-10% ethyl acetate/hexanes) to yield the desired product as a white solid (37 mg, 58%). Product is a known substrate and matched literature data.[382]

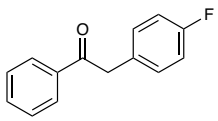

2-(4-fluorophenyl)-1-phenylethan-1-one (**II-20s**). Prepared according to General Procedure 1 for the alkylation of acyl azoliums using the respective acyl imidazole (43 mg, 1.0 equiv) and

Hantzsch ester. **II-PC-B** was used as the photocatalyst. The reaction mixture was purified by column chromatography (dry loaded with silica, 2-20% ethyl acetate/hexanes) to yield the desired product as a white solid (65 mg, 66%). Product is a known substrate and matched the literature data.[383]

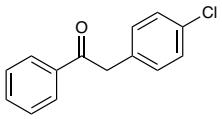

2-(4-chlorophenyl)-1-phenylethan-1-one (**II-20t**). Prepared according to General Procedure 1 for the alkylation of acyl azoliums using the respective acyl imidazole 43 mg, 1.0 equiv) and Hantzsch ester. **II-PC-B** was used as the photocatalyst. The reaction mixture was purified by column chromatography (dry loaded with silica, 0-10% ethyl acetate/hexanes) to yield the desired product as a white solid (44 mg, 76%). Product is a known substrate and matched the literature data.[384]

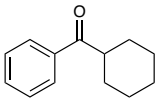

cyclohexyl(phenyl)methanone (**II-20u**). Prepared according to General Procedure 1 for the alkylation of acyl azoliums using the respective acyl imidazole (43 mg, 1.0 equiv) and Hantzsch ester. **II-PC-B** was used as the photocatalyst. The reaction mixture was purified by column chromatography (wet loaded with toluene, 2-20% ethyl acetate/hexanes) to yield the desired product (24 mg, 50%). Product is a known substrate and matched the literature data.[385]

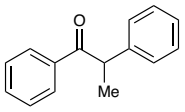

1,2-diphenylpropan-1-one (**II-20v**). Prepared according to General Procedure 1 for the alkylation of acyl azoliums using the respective acyl imidazole (43 mg, 1.0 equiv) and Hantzsch ester. **II-PC-B** was used as the photocatalyst. The reaction mixture was purified by column chromatography (dry loaded with silica, 2-20% ethyl acetate/hexanes) to yield the desired product as a clear oil (40 mg, 76%). Product is a known substrate and matched the literature data.[386] **II-Az-G** was used for the enantioselective variant of this reaction (see below). For entry 2, the SynLED photoreactor was placed inside a cold room registering 5 °C. Enantiomeric ratio was measured by chiral phase SFC (Chiralpak IG-3, 5% MeOH/CO2, flow rate = 2.5 mL/min, 250 nm, Rt (major) = 3.6 min, Rt (minor) = 4.1 min; Entry 1 er: 60:40, Entry 2 er: 66:34.

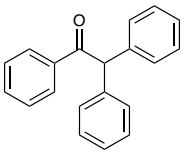

1,2,2-triphenylethan-1-one (**II-20w**). Prepared according to General Procedure 2 for the alkylation of acyl azoliums using the respective acyl imidazole (43 mg, 1.0 equiv) and Meyer nitrile. 4-CzIPN **II-PC-F** was used as the photocatalyst. The reaction mixture was purified by column chromatography (wet loaded with toluene, 0-20% ethyl acetate/hexanes) to yield the desired product as a white solid (44 mg, 50%). Product is a known substrate and matched the literature data.[378]

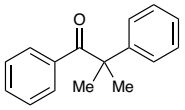

2-methyl-1,2-diphenylpropan-1-one (**II-20x**). Prepared according to General Procedure 2 for the alkylation of acyl azoliums using the respective acyl imidazole (43 mg, 1.0 equiv) and Meyer nitrile. **II-PC-F** was used as the photocatalyst. The reaction mixture was purified by column chromatography (wet loaded with toluene, 0-20% ethyl acetate/hexanes) to yield the desired product as a clear oil (28 mg, 50%). Product is a known substrate and matched the literature data.[387]

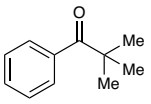

2,2-dimethyl-1-phenylpropan-1-one (**II-20y**). Prepared according to General Procedure 2 for the alkylation of acyl azoliums using the respective acyl imidazole (43 mg, 1.0 equiv) and Meyer nitrile. Note: **II-PC-B** was used as the photocatalyst for this reaction. The reaction mixture was purified by column chromatography (dry loaded with silica, 2-10% ethyl acetate/hexanes) to yield the desired product as a clear oil (14 mg, 35%). Product is a known substrate and matched the literature data.[387]

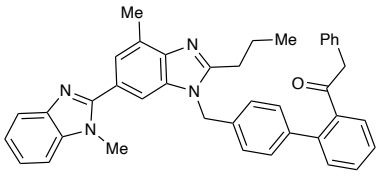

1-(4'-((1,7'-dimethyl-2'-propyl-1*H*,3'*H*-[2,5'-bibenzo[*d*]imidazol]-3'-yl)methyl)-[1,1'-biphenyl]-2-yl)-2-phenylethan-1-one (**II-20z**). Prepared according to General Procedure 3 for the alkylation of

acyl azoliums (*in situ* activation) using telmisartan (51.5 mg, 1.0 equiv) and the respective Hantzsch ester. **II-PC-B** was used as the photocatalyst. The reaction mixture was purified by column chromatography (wet loaded with toluene, 60-100% ethyl acetate/hexanes) to yield the desired product as an off-white solid (54 mg, 91%). Analytical data for **II-20z**: ^{1}H NMR (500 MHz, Chloroform-*d*) δ 7.81 – 7.76 (m, 1H), 7.51 (d, *J* = 1.6 Hz, 1H), 7.46 (td, *J* = 7.5, 1.5 Hz, 1H), 7.44 – 7.40 (m, 2H), 7.38 – 7.24 (m, 7H), 7.15 – 7.06 (m, 5H), 6.85 – 6.80 (m, 2H), 5.45 (s, 2H), 3.73 (s, 3H), 3.55 (s, 2H), 2.98 – 2.87 (m, 2H), 2.78 (s, 3H), 1.87 (dt, *J* = 15.3, 7.5 Hz, 2H), 1.03 (t, *J* = 7.3 Hz, 3H). ^{13}C NMR (126 MHz, Chloroform-*d*) δ 204.4, 156.5, 154.7, 143.3, 142.9, 140.5, 140.3, 139.3, 136.7, 135.8, 135.2, 133.9, 130.8, 130.3, 129.7, 129.6, 129.5, 128.4, 128.23, 127.7, 126.9, 126.7, 124.1, 124.0, 122.6, 122.4, 119.6, 109.7, 108.9, 49.6, 47.0, 31.9, 29.9, 22.0, 17.0, 14.2. HRMS (ESI/TOF) m/z: $[M+H]^+$ Calcd. for $C_{40}H_{37}N_4O$ 589.2967; Found 589.2965. FTIR (ATR) cm^{-1}: 3062, 3028, 2964, 2931, 1692.

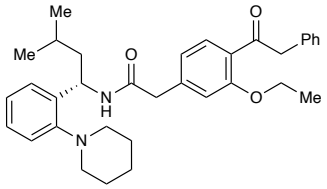

(*S*)-2-(3-ethoxy-4-(2-phenylacetyl)phenyl)-*N*-(3-methyl-1-(2-(piperidin-1-yl)phenyl)butyl)acetamide (**II-20aa**). Prepared according to General Procedure 3 for the alkylation of acyl azoliums (in situ activation) using repaglinide (45.3 mg, 1.0 equiv) and the respective Hantzsch ester. **II-PC-B** was used as the photocatalyst. The reaction mixture was purified by column chromatography (wet loaded with toluene, 0-40% ethyl acetate/hexanes) to yield the desired product as a white solid (27.1 mg, 52%). Analytical data for **II-20aa**: ^{1}H NMR (500 MHz,

Chloroform-*d*) δ 7.60 (d, *J* = 7.8 Hz, 1H), 7.32 – 7.15 (m, 7H), 7.08 – 7.01 (m, 2H), 6.84 – 6.77 (m, 2H), 6.72 (d, *J* = 8.1 Hz, 1H), 5.35 (td, *J* = 8.7, 6.6 Hz, 1H), 4.30 (s, 2H), 4.11 – 3.95 (m, 2H), 3.50 (s, 2H), 2.91 (s, 2H), 2.59 (t, *J* = 10.2 Hz, 2H), 1.74 – 1.64 (m, 2H), 1.64 – 1.46 (m, 6H), 1.46 – 1.37 (m, 4H), 0.90 (d, *J* = 6.6 Hz, 6H). ^{13}C NMR (126 MHz, Chloroform-*d*) δ 199.8, 168.9, 158.3, 152.7, 141.5, 138.8, 135.4, 131.4, 129.8, 128.5, 128.1, 127.9, 127.2, 126.7, 125.2, 123.0, 121.5, 113.1, 64.3, 50.2, 50.1, 46.8, 44.3, 26.9, 25.5, 24.3, 22.9, 22.7, 14.9. HRMS (ESI/TOF) m/z: $[M+H]^+$ Calcd. for $C_{34}H_{43}N_2O_3$ 527.3273; Found 527.3273. FTIR (ATR) cm^{-1}: 3300 (br), 3029, 2980, 2955, 2876, 1676, 1640.

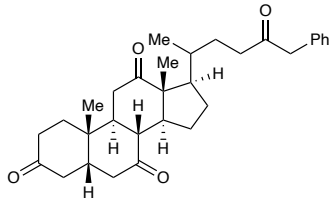

(5*S*,8*R*,9*S*,10*S*,13*R*,14*S*,17*R*)-10,13-dimethyl-17-(5-oxo-6-phenylhexan-2-yl)dodecahydro-3*H*-cyclopenta[*a*]phenanthrene-3,7,12(2*H*,4*H*)-trione (**II-20ab**). Prepared according to General Procedure 3 for the alkylation of acyl azoliums (in situ activation) using dehydrocholic acid (40.3 mg, 1.0 equiv) and the respective Hantzsch ester. **II-PC-B** was used as the photocatalyst. The reaction mixture was purified by column chromatography (wet loaded with toluene, 20-80% ethyl acetate/hexanes) to yield the desired product as a white solid (19 mg, 40%). Analytical data for **II-20ab**: ^{1}H NMR (500 MHz, Chloroform-*d*) δ 7.32 (dd, *J* = 8.1, 6.7 Hz, 2H), 7.28 – 7.23 (m, 1H), 7.22 – 7.18 (m, 2H), 3.68 (s, 2H), 2.99 – 2.77 (m, 3H), 2.52 (ddd, *J* = 17.0, 9.2, 5.1 Hz, 1H), 2.42 (ddd, *J* = 16.7, 8.7, 6.7 Hz, 1H), 2.36 – 2.18 (m, 6H), 2.17 – 2.08 (m, 2H), 2.05 – 1.91 (m, 4H), 1.87 – 1.74 (m, 2H), 1.61 (td, *J* = 14.3, 5.0 Hz, 1H), 1.39 (s, 3H), 1.35 – 1.26 (m, 2H), 1.25 – 1.17

(m, 2H), 1.03 (s, 3H), 0.76 (d, J = 6.6 Hz, 3H). ^{13}C NMR (126 MHz, Chloroform-*d*) δ 212.0, 209.0, 208.74, 208.69, 134.3, 129.4, 128.7, 127.0, 56.9, 51.7, 50.3, 49.0, 46.9, 45.6, 45.5, 45.0, 42.8, 39.0, 38.6, 36.5, 36.0, 35.3, 35.3, 29.2, 27.5, 25.1, 21.9, 18.7, 11.9. HRMS (ESI/TOF) m/z: $[M+Na]^+$ Calcd. for $C_{31}H_4O_4Na$ 499.2824; Found 499.2824 FTIR (ATR) cm^{-1}: 3028, 2991, 2967, 1721, 1705, 1691.

CHAPTER 3: SYNTHESIS OF ALIPHATIC KETONES VIA COMBINED CARBENE AND PHOTOREDOX CATALYSIS

Portions of this chapter appear in the following publications:

Bay, A. V.; Fitzpatrick, K. P.; González-Montiel, G. A.; Farah, A. O.; Cheong, P. H.-Y.; Scheidt, K. A. Light-Driven Carbene Catalysis for the Synthesis of Aliphatic and α-Amino Ketones. *Angew. Chem. Int. Ed.* **2021**, *60*, 17925–17931.

3.1 Early Limitations of Carbene Catalysis

The carbonyl group is inherently electrophilic at the carbonyl carbon atom due to the electron-withdrawing nature of the oxygen atom. However, umpolung approaches have been developed to reverse the polarity of carbonyl groups, thus expanding the reactivity of these compounds significantly.[388] For example, addition of an *N*-heterocyclic carbene (NHC) to an aldehyde forms an acyl anion equivalent known as the Breslow intermediate by formally reversing the polarity of the carbonyl carbon.[268]

NHCs have a broad landscape of organocatalytic reactivity (**Scheme 3-1**; see Chapter 1).[268] Nucleophilic addition of the Breslow intermediate into an activated alkene affords a ketone in the Stetter reaction, and α-hydroxy or α-amino ketones can be accessed by reaction of the Breslow intermediate with aldehydes or imines, respectively, in benzoin condensation reaction.[58,62] These organocatalysts are also known to add into extended systems (i.e., α,β-unsaturated aldehydes or aliphatic esters to form homoenolate equivalents, which can react with ketones in a [3 + 2] cycloaddition or can add into Michael acceptors in a decarboxylative cycloaddition process.[389-391]

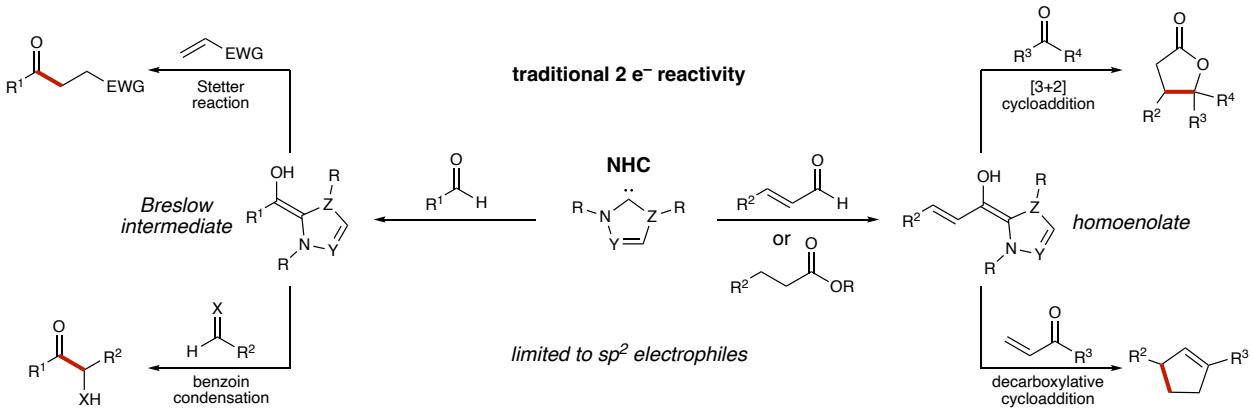

Scheme 3-1. Overview of traditional NHC-catalyzed reactivity.

While NHC catalysis has enabled access to a range of products, this two-electron reactivity is limited to sp^2 electrophiles, highlighting the potential opportunity for single-electron NHC catalysis. For example, two consecutive single-electron oxidations of the Breslow intermediate afford an electron-deficient acyl azolium, a process which has been employed for the synthesis of esters from aldehydes (see Chapters 1.6.1 and 2.3.3).[34,99-100,392] Inspired by these reports and the rise in radical chemistry in recent decades, there has been significant effort by chemists to expand the scope of reaction partners beyond π-containing electrophiles for the synthesis of synthetically valuable ketones (**Scheme 3-2**).

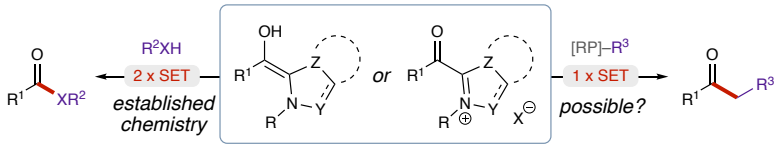

Scheme 3-2. Single-electron transfers in NHC catalysis for the synthesis of C–X (X = N, O, S, etc.) and C–C bonds.

3.1.1 Significance of Aliphatic Ketones

Ketones are a primary class of organic molecules. The broad versatility of ketones (e.g., functionalization to access alcohols, amines, etc.; see Chapter 2.3.1) highlights their utility in synthesis. In particular, aliphatic ketones are recognized as valuable synthetic precursors and targets due to their ability to engage in enolate chemistry. Moreover, aliphatic ketones can be found in numerous natural products and bioactive compounds, including prasugrel (**III-1**), a blood thinner often used prior to heart procedures, and methadone (**III-2**), a medication employed for pain prevention that is also approved to treat drug addiction.[393-394] Synthetic routes to access aliphatic ketones are thus of high importance due to both their utility in organic synthesis and their prevalence in medicinally relevant compounds.

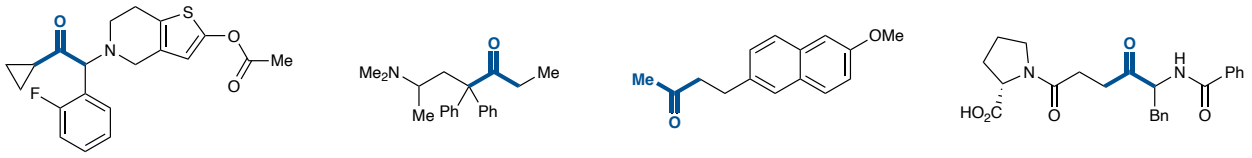

Figure 3-1. Selected examples of aliphatic ketones in pharmaceutically relevant compounds.

3.1.2 Initial Limitations of Radical Carbene Catalysis

There has been a marked increase in single-electron NHC-catalyzed methods for the construction of C–C bonds reported in recent years in part due to the importance of ketones in synthesis.[395-399] Various groups across the globe hypothesized that radical acyl azolium species **III-I•** could undergo radical-radical coupling with an array of coupling partners to increase the utility of NHCs in synthesis.[127,131,148-149] The highly reducing Breslow intermediate could be accessed from an aldehyde and could reduce an acceptor substrate, undergoing a single-electron oxidation to access **III-I•**.[127] Alternatively, an activated carboxylic acid could be employed as a precursor for the acyl azolium, which could undergo single-electron reduction by a donor molecule to yield key radical intermediate **III-I•**.[149]

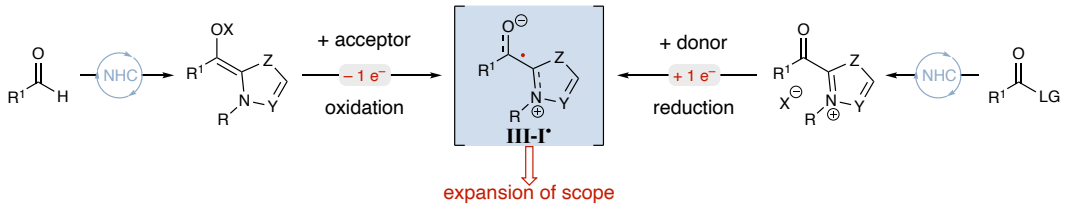

Scheme 3-3. Routes to access **III-I•** via single-electron oxidation (left) and single-electron reduction (right). *The reader is referred to Chapter 1 for a thorough review of these processes.*

In 2019, Ohmiya and coworkers described the coupling of a persistent Breslow intermediate-derived radical with a transient alkyl radical (see Chapters 1.6.3 and 2.3.3).[127] This pioneering example of thermal single-electron NHC catalysis paved the pathway for the

development of similar protocols by the groups of Li,[139] Wang,[140] and Hong,[128] among others.[131,141] While instrumental in sparking interest in the field of radical carbene catalysis, the initial work by Ohmiya and coworkers was limited in scope. In particular, the reaction was unsuccessful when applied for the synthesis of aliphatic ketones, perhaps due to the relative instability of **III-I•** when R^1 is alkyl compared to that when R^1 is aryl.

Concurrent with this work, light-driven carbene methods by our group,[148,400] Hopkinson,[401-402] Studer,[153,157,159] and others demonstrated complementary reactivity to established two-electron carbene catalysis.[123,151,157] In 2020, Hopkinson and coworkers reported a light-activated, NHC-catalyzed Diels-Alder reaction to construct isochromanone derivatives.[401] Our group reported the first single-electron reduction of an acyl azolium (**III-I**) for the formation of ketones from carboxylic acids (see Chapter 2.3.4-2.11.7).[400] Radical-radical coupling of a Hantzsch ester-derived alkyl radical with acyl azolium radical **III-I•** was achieved via a reductive quenching cycle. Notably, this protocol allowed for the synthesis of aliphatic ketones, but the yields were significantly diminished in comparison to aryl ketones (**Scheme 3-4**). While this work highlights the utility of reductively generated single-electron NHC operators, the scope was primarily limited to aryl substrates, such as deoxybenzoin (**III-7a**).

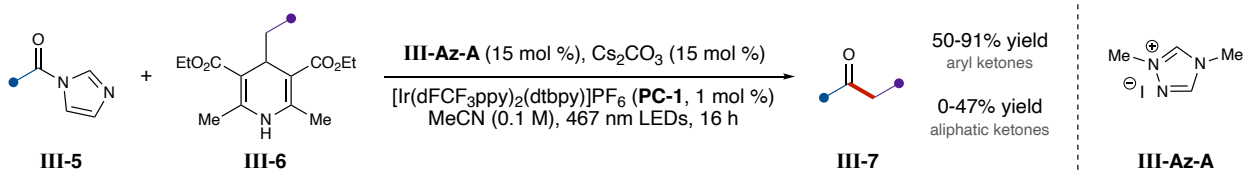

Scheme 3-4. NHC and photoredox-catalyzed synthesis of ketones.[400]

Additional reaction conditions for our combined catalysis approach were screened in attempt to improve the yield with aliphatic substrates. The addition of a Lewis acid was expected to lower the reduction potential of the corresponding aliphatic acyl azolium, which would increase

the efficiency with which **III-I•** is generated. Unfortunately, Lewis acids were found to decrease the yield of **III-7b** compared to the standard reaction conditions (entries 2-5, **Table 3-1**). Given that the redox potential of aliphatic acyl azolium species is likely different from that of aryl acyl azolium species, a variety of photocatalysts were also explored. The use of organophotocatalyst 4CzIPN afforded **III-7b** in the same yield as the standard iridium-derived photocatalyst, but none of the screened photocatalysts increased the yield (entries 6-9, **Table 3-1**). Bases were screened as well, but the reaction yield did not improve in comparison to the standard reaction conditions (entries 10-13, **Table 3-1**).

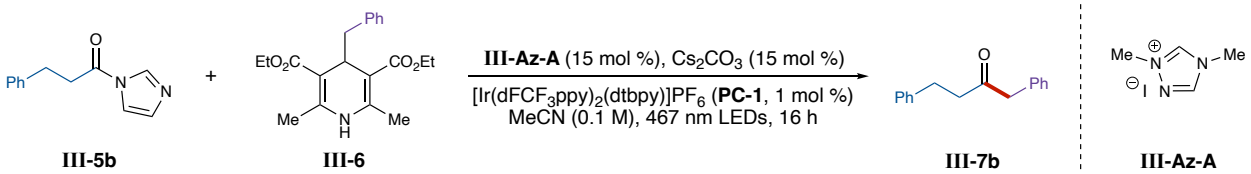

III-5b + III-6 → III-7b; III-Az-A

entry	deviation from standard	GCMS yield (%)
1	none	40
2	+ $Sc(OTf)_3$	23
3	+ $Cu(OTf)_2$	25
4	+ $Mg(OTf)_2$	31
5	+ $Zn(OAc)_2$	5
6	*fac*-$Ir(ppy)_3$ instead of **PC-1**	0
7	4CzIPN instead of **PC-1**	40
8	Ph-Mes-Acr instead of **PC-1**	0
9	$Ru(bpy)_3$ instead of **PC-1**	0
10	KOAc instead of Cs_2CO_3	0
11	Na_2CO_3 instead of Cs_2CO_3	0
12	NaOAc instead of Cs_2CO_3	0
13	K_2CO_2 instead of Cs_2CO_3	16

Table 3-1. Screen of reaction conditions for the synthesis of aliphatic ketones using combined NHC and photoredox catalysis.

The inability to synthesize aliphatic ketones was a widespread limitation in the majority of initial reports on radical NHC processes. Protocols that were able to successfully access aliphatic ketones were only able to do so with low efficiency. There existed a significant opportunity to solve this problem that was widespread across field of radical carbene catalysis. As a result, we

hypothesized that we could solve this pervasive issue using a combination of computational and experimental approaches to study the reaction mechanism.

3.2 Radical Distribution

Bertrand and Martin disclosed a detailed study on the key radical intermediates in oxidative NHC processes in 2019.[403] Contrary to many mechanistic proposals in the literature, their studies suggest that these oxidative pathways proceed through single-electron transfer (SET) from the corresponding electron-rich enolate of the Breslow intermediate or through proton-coupled electron transfer (PCET) from the enol. They concluded that the relevant radical intermediates in these reactions have radical spin density concentrated primarily on the carbene carbon (C2, 40%) and not on the carbonyl carbon (C1, 10%; **Figure 3-2**).[403] While these results do not directly translate to our system due to substantial differences in radical generation (i.e., thermal vs. photochemical), their work provoked important mechanistic questions regarding the nature of single-electron NHC species.

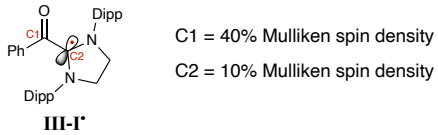

III-I•

Figure 3-2. Mulliken spin densities of **III-I•** derived from diisopropylphenyl-substituted imidazolium reported by Martin and coworkers. Dipp = diisopropylphenyl.[403]

Based on Bertrand's report, our previous results,[400] and a key report from Ohmiya,[98] we hypothesized that both electronic and steric alterations to the NHC could impact radical distribution and stability, thus *imparting control over reactivity*. To explore this possibility, we collaborated with Cheong Research Group at Oregon State University and performed density functional theory investigations with PBE[404-405]/6-31G*[406] & LANL2DZ[407] (for Cs) level of theory

and SMD solvation corrections[408] in acetonitrile as implemented in Gaussian 16. Acyl azoliums derived from benzoic acid and hydrocinnamic acid were chosen as the model substrates to study the reactivity of aryl and aliphatic systems, respectively (**Figure 3-3**, acyl imidazole starting materials **III-5a** and **III-5b**, respectively). To analyze the steric and electronic impact of the NHC, our previously optimized NHC precursor (**III-Az-A**) and mesityl-substituted pyrrolotriazolium (**III-Az-B**) were the primary focus of this study.

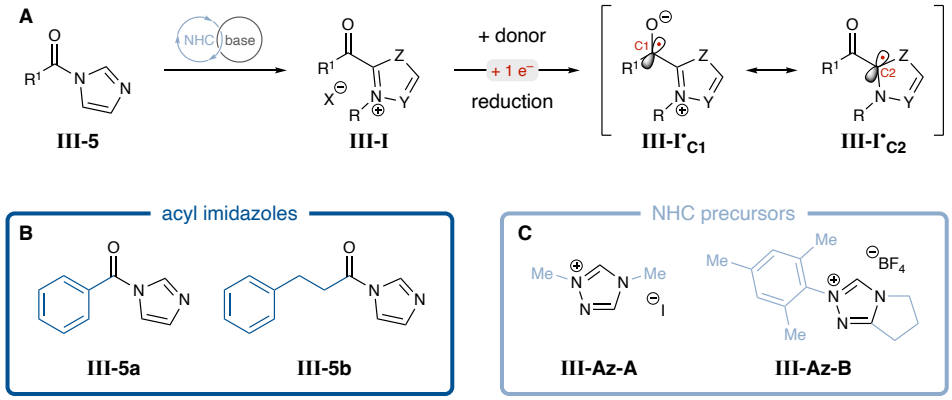

Figure 3-3. A) Single-electron reduction of an in situ-formed acyl azolium (**III-I**) to access radical acyl azolium **III-I•**. **B)** Acyl imidazoles **III-5a** and **III-5b** used to study the aryl and aliphatic systems, respectively. **C)** NHC precursors **III-Az-A** and **III-Az-B** that feature different steric and electronic properties.

3.2.1 Spin Density Distribution

It is often assumed that the radical spin density population is concentrated on C1 (i.e., the key radical intermediate is **III-I•$_{C1}$**) and, as a result, selective radical-radical coupling occurs at the carbonyl carbon.[395-399] An initial spin density analysis of the optimized aliphatic and aryl acyl azolium radical structures **III-I•** with **III-Az-A** or **III-Az-B** revealed significant radical character on C1, C2, and the carbonyl oxygen atom, with the majority of spin density distributed between C1 and C2 (**Figure 2-4**). Mulliken spin densities, which describe the electron density of molecular systems based on the wave function, were also calculated for each acyl azolium radical system,

revealing more Mulliken spin density on C2 compared to C1 for all **III-I•** analyzed.[409] These results agree with the conclusions by Martin and coworkers and suggest that the mechanism for radical-radical coupling may be more complex than originally anticipated.

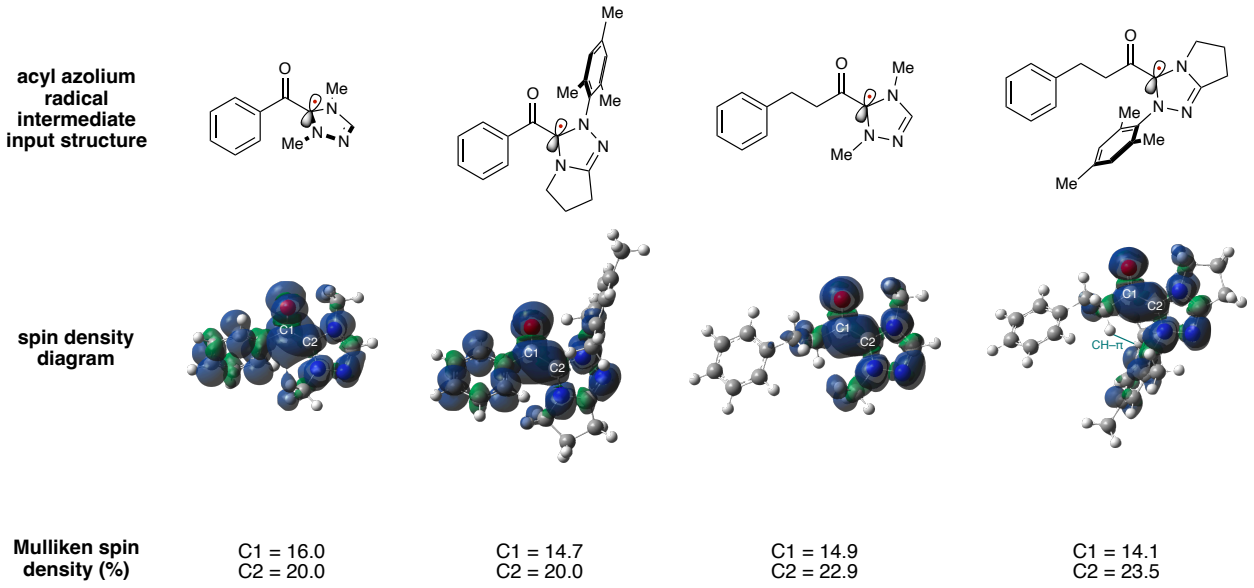

Figure 3-4. Radical acyl azolium intermediates (**III-I•**), the corresponding spin density diagram, and the Mulliken spin densities of the carbonyl carbon atom (C1) and the carbene carbon atom (C2).

3.2.2 Possible Mechanistic Pathways

Given this distribution in the radical spin population, two potential intermediates may be formed: one with the radical localized on C1 (**III-I•$_{C1}$**) and the other with spin density concentrated on C2 (**III-I•$_{C2}$**). We can then envision at least two operative radical-radical coupling pathways: 1) coupling at C1 or 2) coupling at C2 (**Figure 3-5**). The radical coupling partner can couple at the carbonyl carbon (C1) via a direct route to access tetrahedral intermediate **III-II$_{C1}$**, which will collapse to give the ketone product and the free carbene. Alternatively, radical-radical coupling at the carbene carbon via an indirect route may afford a C2-coupled intermediate **III-II$_{C2}$**, which could undergo a potential 1,2-shift to yield the same tetrahedral intermediate (**III-II$_{C1}$**) that will

collapse to give the free NHC and the ketone product. It is also plausible that the C2-coupled intermediate could not react, thus consuming the NHC and halting the reaction progress altogether or could engage in undesired off-cycle reactivity. These alternative reaction pathways offer potential explanations for the low yields observed using aliphatic acyl imidazoles (e.g., **III-5b** to make the corresponding **III-7b**).

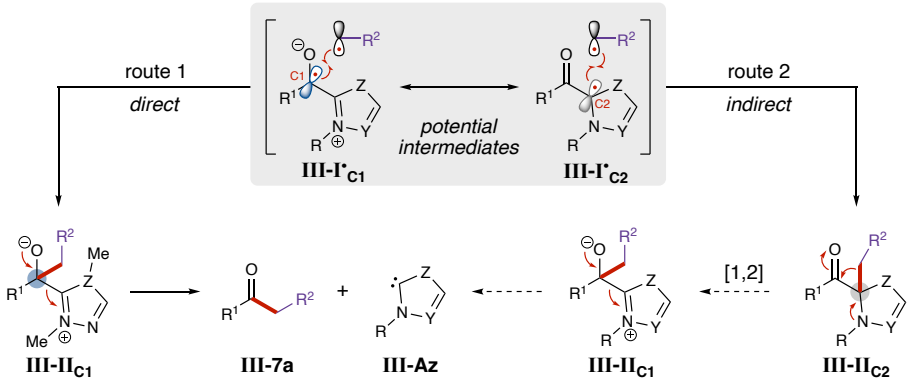

Figure 3-5. Possible mechanistic pathways for the radical-radical coupling event.

The viability of these alternative mechanistic pathways was investigated experimentally. Hydrocinnamyl acyl imidazole **III-5b** and benzyl Hantzsch ester **III-6a** were reacted under the previously determined standard conditions, using stoichiometric NHC precursor **III-Az-A** and base in place of the standard catalytic quantities (**Table 3-2**). Product **III-7b** was observed by UPLC-MS in addition to a variety of mass adducts that shed light on the reaction mechanism. Distinct peaks indicative of C1-coupled intermediate **III-II$_{C1}$** and C2-coupled intermediate **III-II$_{C2}$** were identified in the crude mixture. While separation and isolation of the corresponding compounds was unsuccessful, the presence of two peaks with a mass-to-charge (m/z) ratio of 322 suggests that the two mechanistic pathways (i.e., the direct route and the indirect route, as

designated in **Figure 3-5**) may be operative under the standard reaction conditions using **III-Az-A** as the NHC precursor.

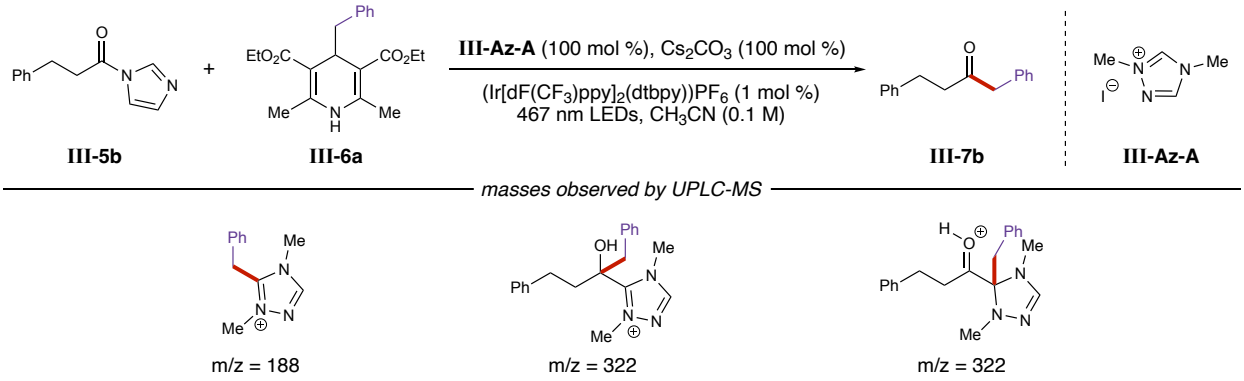

Table 3-2. Mass adducts observed by UPLC-MS using stoichiometric **III-Az-A**.

3.3 Hypothesis for the Synthesis of Aliphatic Ketones

These initial results suggest two pathways may be viable under the standard reaction conditions, but important mechanistic details remain unanswered. Given the difference in yields using aryl acyl imidazole **III-5a** and aliphatic acyl imidazole **III-5b**, we aimed to determine the effect that acyl imidazole substitution has on the reaction outcome. Moreover, we hypothesized that modulation of the NHC steric and electronic parameters may enable selective and improved reactivity by 1) altering the stability of **III-I˙** and 2) impacting the steric environment at undesired C2.

3.3.3 Radical Stability via Analysis of Isodesmic Reactions

A model system was developed to better understand the thermodynamic stability of the radical at C1 versus C2. An isodesmic reaction is one in which the number of each type of formal bond is retained; it describes hypothetical or actual bond separation processes.[410] This type of computational analysis can provide insight into the thermodynamic properties of molecules or

reaction systems by breaking specific bonds. For example, the isodesmic reaction for **III-I˙** can be written by breaking the bond between C1 and C2, and the stability of the radical on C1 and C2 can be analyzed (**Scheme 3-5**).

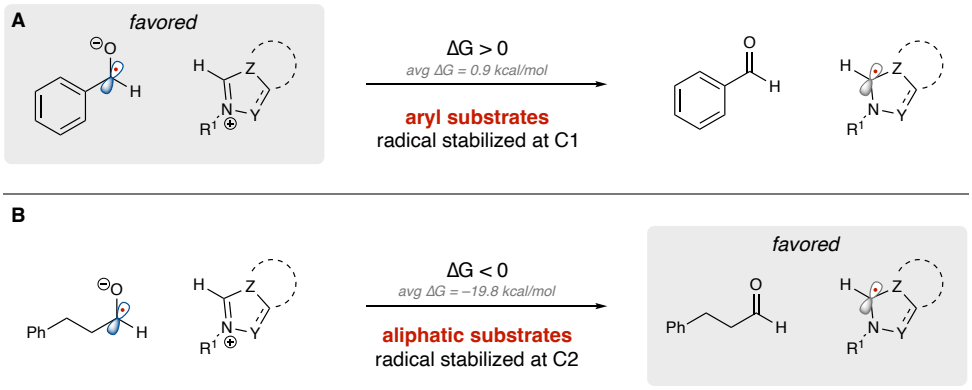

Scheme 3-5. The isodesmic reactions of **A)** phenyl acyl azoliums and **B)** hydrocinnamyl acyl azoliums.

Calculations of the isodesmic reactions of **III-I˙** were performed to gain insight into the impact that the substrate has on reactivity. Acyl azoliums derived from aryl **III-5a** and aliphatic **III-5b** with an array of different NHCs were studied (**Scheme 3-5**; see Chapter 3.10.5 for additional details). Analysis of the isodesmic reactions revealed that the radical is favored at the carbonyl carbon, C1, for aryl substrates, with an average Gibbs free energy of +0.9 kcal/mol. The stability of the radical at C1 for aryl substrates is likely due to the conjugative stability afforded by the aromatic ring system. On the contrary, examination of the isodesmic reactions reveals that the radical is favored at the carbene carbon, C2, for aliphatic substrates, likely due to the lack of substrate conjugation. Comparison between the two substrate classes offers potential insight into the difference in reactivity between aromatic and aliphatic substrates. Direct coupling at C1 may dominate for aryl substrates while indirect C2-coupling may be favored for aliphatic substrates. Given this data, I hypothesized that modulation of the NHC steric and electronic parameters may

enable direct coupling at desired C1 for aliphatic substrates by impacting selectivity between the two carbon centers.

3.4 Conformation of an Acyl Azolium Radical Species

Given that electronic changes were unlikely to inhibit C2-coupling, we investigated whether NHC steric parameters may be tuned to favor productive coupling at C1. When we juxtaposed the acyl azolium radicals **III-I•** derived from **III-Az-A** and **III-Az-B**, different conformations were observed for the aliphatic radical intermediate (**Figure 3-6**). Due to both the torsional flexibility of the aliphatic substrate and the orthogonality of the mesityl group, **III-Az-B** rotates 180º with respect to the carbonyl to form a stabilizing CH-π interaction (1.5 kcal/mol more stable), potentially leading to efficacy of **III-Az-B** over **III-Az-A** (**Figure 3-6**). Moreover, this interaction further rigidifies the conformation and enforces the steric encumbrance imposed by the mesityl ring, likely contributing to favorable coupling at kinetically accessible C1 (**Figure 3-6B**).[411]

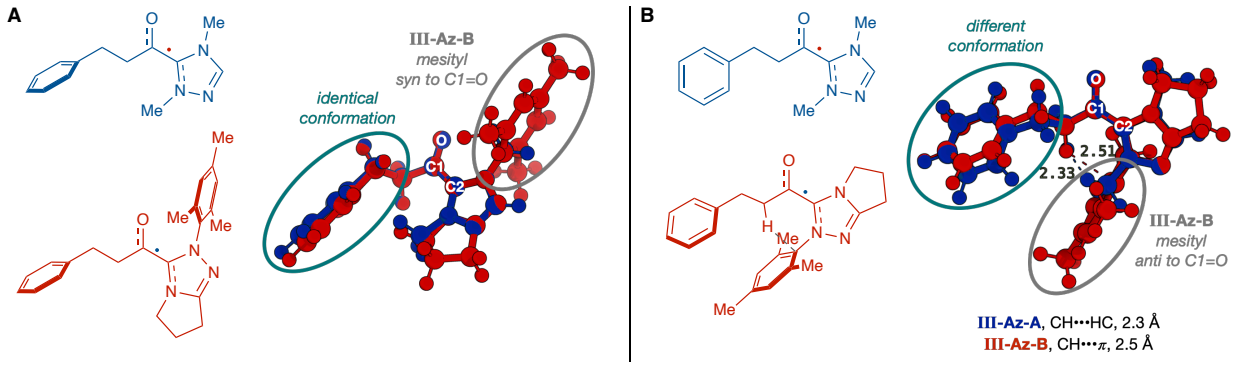

Figure 3-6. Conformational analysis of **III-I•** derived from **III-Az-A** (blue) and **III-Az-B** (red) in an orientation where the mesityl ring of **III-Az-B** is **A)** syn to the carbonyl or **B)** anti to the carbonyl.

3.4.1 NHC Steric and Electronic Effects on Reactivity

NHCs with different electronic and steric parameters were examined under the standard reaction conditions to probe the impact of NHC structure on radical reactivity. NHC structure was found to have less impact on reactivity for aryl acyl azolium radicals, likely due to the conjugative stability imparted by the aryl ring on the radical at C1. However, for aliphatic substrates, reactivity was anticipated to be more NHC-dependent due to the increased radical stability at C2. Analysis of three NHC scaffolds allows trends in reactivity to be identified (**Figure 3-7**). Comparison of **III-Az-C** with fluorinated **III-Az-D** suggests that electron withdrawing NHCs may stabilize the radical at C2 even further, contributing to a decrease in yield when using **III-Az-D**. A significant steric impact can be observed by comparison of **III-Az-B** to sterically smaller **III-Az-C**. This analysis shows that both the NHC steric and electronic components significantly affect reactivity, with an increase in steric hinderance resulting in a 51% increase in NMR yield.

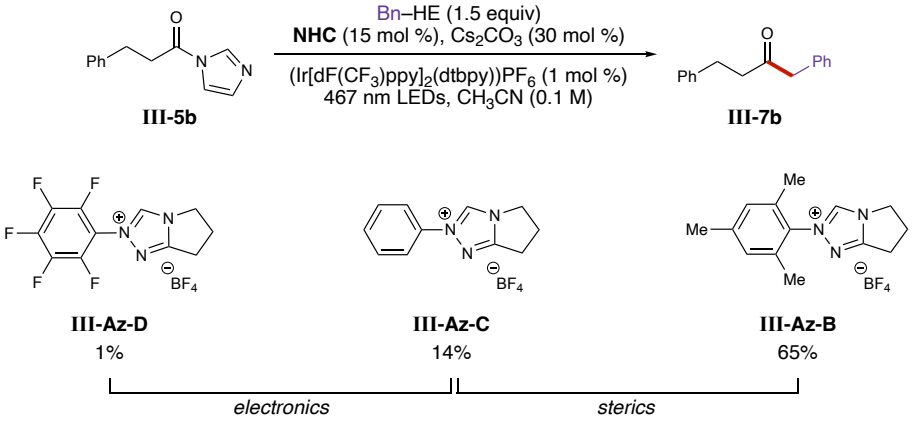

Figure 3-7. Analysis of the electronic and steric impacts of the NHC precursor. Yields shown are NMR yields obtained using 1,3,5-trimethoxybenzene as an internal standard.

3.4.2 Site Accessibility and Selectivity

These computational and experimental results suggest that the NHC steric and electronic parameters may impact reactivity significantly. Given the increase in yield observed using more

sterically hindering NHCs, both C1 and C2 of **III-I˙** derived from previously optimized **III-Az-A** may be accessible for radical-radical coupling, resulting in little-to-no selectivity (**Figure 3-8**). As mentioned previously, radical-radical coupling at the C2-carbon center may result in undesired off cycle reactivity, offering a potential explanation for the decreased yields using **III-Az-A**. On the contrary, C1 is more accessible than hindered C2 using sterically bulky **III-Az-B**, and the steric hindrance imposed by the mesityl ring may enable a more selective reaction.

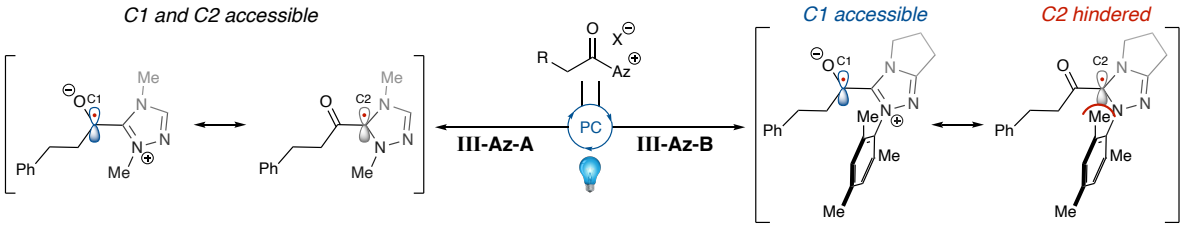

Figure 3-8. Steric impact on accessibility of C1 and C2.

The reaction using aliphatic acyl imidazole **III-5b** was performed using **III-Az-A** and **III-Az-B** to investigate the selectivity of each reaction. The two reactions were monitored by GCMS, and the components of each crude reaction were analyzed after 16 hours. The reaction did not go to completion using **III-Az-A**, and a variety of off-cycle side products can be observed in the chromatogram (**Figure 3-9**). On the contrary, a clean reaction profile with complete consumption of starting material can be observed using **III-Az-B**. Comparison of these two chromatograms suggests that the reaction is selective using **III-Az-B** as the NHC precursor. This analysis supports the hypothesis that the diminished yield using **III-Az-A** as the NHC precursor may be due to the lack of selectivity for the radical-radical coupling between the oxidatively generated radical partner and the C1- and C2-carbon centers.

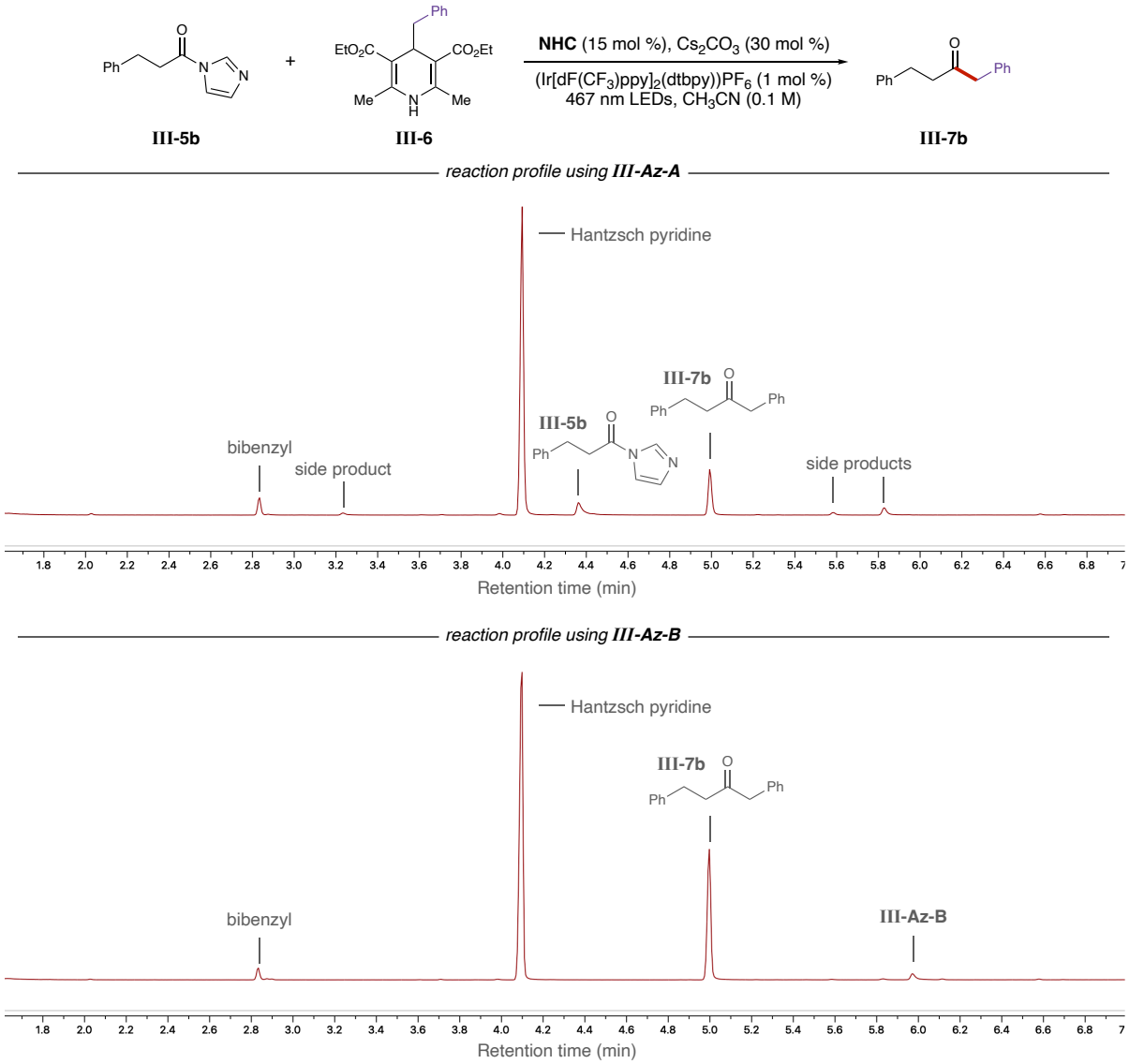

Figure 3-9. GCMS traces of the standard reaction with aliphatic acyl imidazoles using **III-Az-A** (top) and **III-Az-B** (bottom).

3.5 Updated Mechanistic Understanding for Radical Carbene Reactivity

3.5.1 Proposed Mechanism

We propose a combined NHC and photocatalytic mechanism (**Figure 3-10**). Operating through a reductive quenching photocatalytic cycle, the radical coupling partner is accessed via a

single-electron oxidation event with the excited photocatalyst. Subsequent single-electron reduction of the acyl azolium (**III-I**, ΔG = 7.6 kcal/mol) furnishes an open-shell acyl azolium radical species (**III-I•**, ΔG = 16.1 kcal/mol) with the radical distributed between C1 and C2. The radical coupling partner then approaches **III-I•** to give **III-II$_{C1}$** and **III-II$_{C2}$** through a three-membered transition state (**TS-3**, $\Delta G^{\ddagger}$ = 21.1 kcal/mol). Finally, the release of the NHC catalyst (**TS-4**, $\Delta G^{\ddagger}$ = 13.4 kcal/mol) affords the observed ketone product **III-7b** (ΔG = –16.3 kcal/mol).

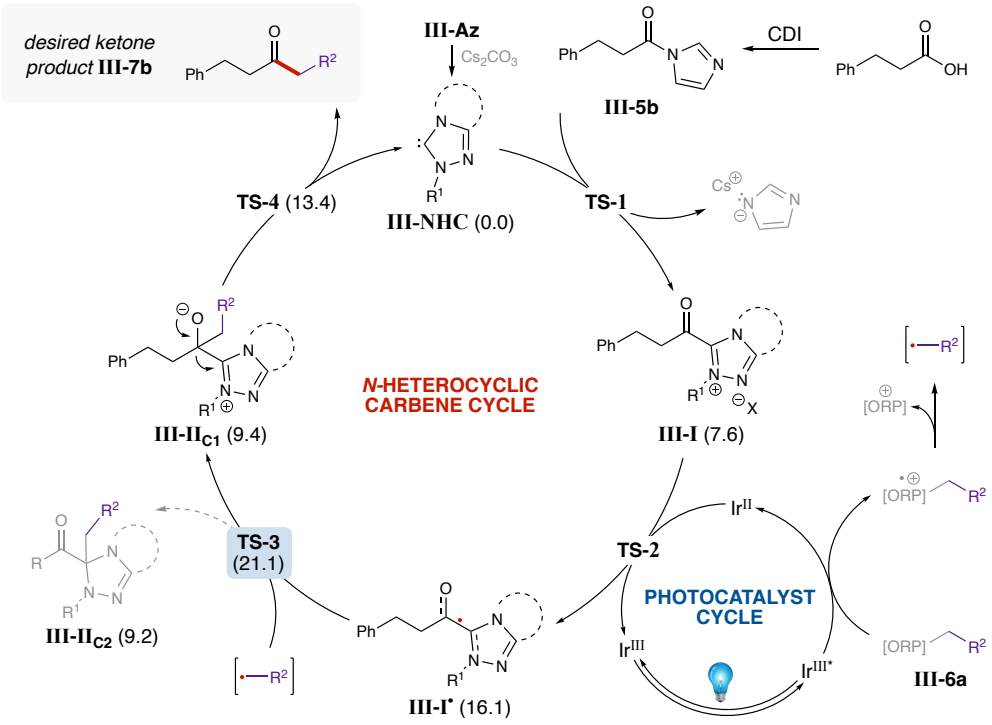

Figure 3-10. Updated mechanism for the NHC and photoredox-catalyzed synthesis of ketones from carboxylic acids.

3.5.2 In-depth Analysis of the Key Transition State

Whether coupling occurs at desired C1 or undesired C2 is dictated by **TS-3**, which was identified with a variety of different NHC structures including our previously optimized NHC precursor (**III-Az-A**) and sterically hindering **III-Az-B**. As mentioned previously, the intermediate

will likely collapse to afford the ketone product if coupling occurs at C1. Undesired C2 coupling may also occur, and this intermediate may engage in off cycle reactivity. Importantly, analysis of the optimized transition state structures shows the key CH-π interaction that makes the transition state 1.5 kcal/mol more stable with mesityl-substituted **III-Az-B** compared to methyl-substituted **III-Az-A**. This interaction also rigidifies the system and is likely to enforce the steric encumbrance imposed by the NHC.

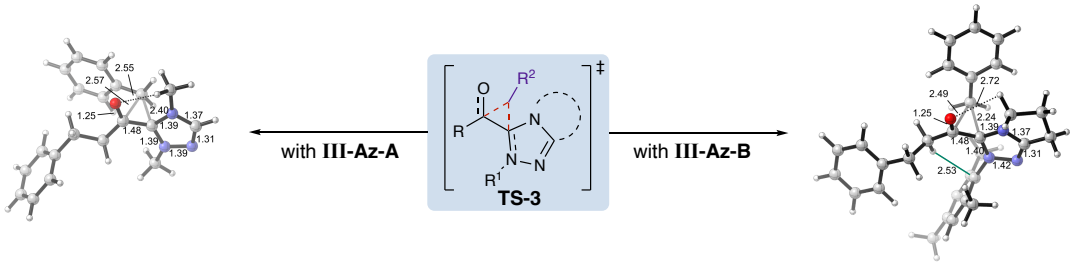

Figure 3-11. Three-membered transition state with bonds forming between the incoming radical partner, C1, and C2, and the optimized structures identified by computational analysis of the transition state.

The energies surrounding the three-membered transition state were investigated to gain insight into the radical-radical coupling. Our collaborators calculated potential energy surfaces (PES) to further rationalize which carbon, C1 or C2**,** is most likely to participate in radical-radical coupling; this data allows for visualization of the energy landscape surrounding the transition state. Formation of the transition state with the dimethyl triazolium-derived acyl azolium and the incoming benzyl radical occurs. This **III-Az-A**-derived PES revealed downhill energy paths leading to both C1- and C2-coupling products, suggesting a non-selective reaction wherein considerable **III-II$_{C2}$** is formed (**Figure 3-12**). For **III-Az-B**, the energy topography visually appears different and clearly favors coupling at C1. In contrast to the PES for **III-Az-A**, an uphill barrier exists on the path to undesired C2, which translates to a preference of 2.3 kcal/mol for C1

over C2, in line with the hypothesis that the mesityl group of **III-Az-B** may hinder coupling at the C2 center (**Figure 3-12**). These observations suggest a *greater likelihood* for efficient C1-coupling over inefficient and unproductive C2-coupling using **III-Az-B** as the NHC precursor (**III-II$_{C1}$** and **III-II$_{C2}$**, $\Delta G = 9.4$ and 9.2 kcal/mol, respectively).

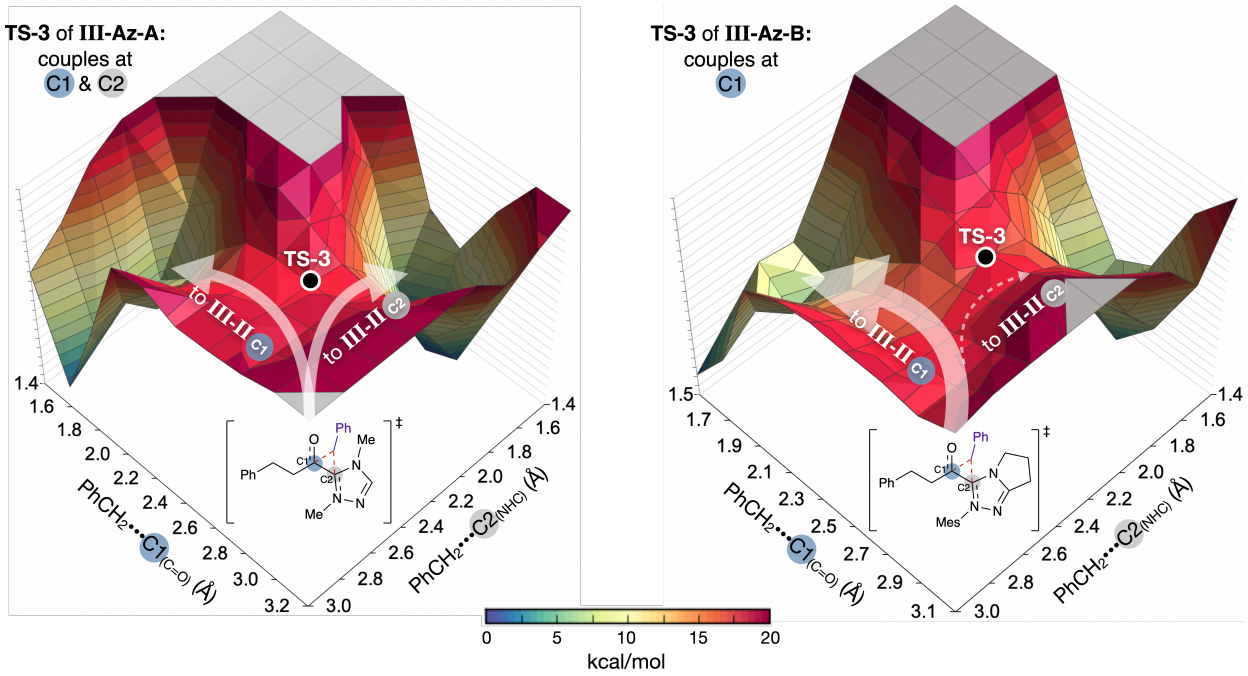

Figure 3-12. Potential energy surfaces for the transition state from acyl azolium radicals **III-I•** derived from **III-Az-A** (left) and **III-Az-B** (right).

3.6 Substrate Scope for the Synthesis of Aliphatic Ketones

This proposed mechanism thus directed experimental efforts wherein benzylation of **5b** was performed using **III-Az-B** as the NHC precursor. To our delight, the reaction not only proceeded to completion, but the desired aliphatic ketone **7b** was isolated in 72% yield, a 32% increase compared to the reaction using **III-Az-A**. Given this result, the scope of aliphatic acyl imidazoles amenable to benzylation was investigated using **III-Az-B** as the NHC precursor (**Table 3-3**).

3.6.1 Acyl Imidazole Scope

Additional substituted hydrocinnamic acyl imidazoles were tolerated to provide the respective ketones in good yields (**III-7c,d**, **Table 3-3**). The reaction proceeded smoothly with nitrogen- and ether-containing substrates, affording the respective ketone products (**III-7e,f,i**) in good-to-excellent yields. Of note is the successful isolation of unsaturated **III-7h**, an alkene-containing product that offers a functional group handle for further diversification (albeit low-yielding due to radical addition into the alkene). The reaction with cyclopropane acyl imidazoles afforded their respective ketone products (**III-7j,k**) in good yields, an unexpected result that provides additional mechanistic insight into the nature of **III-I**•. The distribution of radical character between C1 and C2 likely offers more radical stability than that of traditional acyl radicals, which have demonstrated radical clock-like reactivity, thus illustrating a significant advantage of NHC-based radical chemistry.[170,412] The chemoselectivity of this process was demonstrated in the isolation of ester-containing **III-7l**, illustrating a bond construction that suffers from functional group incompatibility using conventional methods of ketone formation (e.g.,

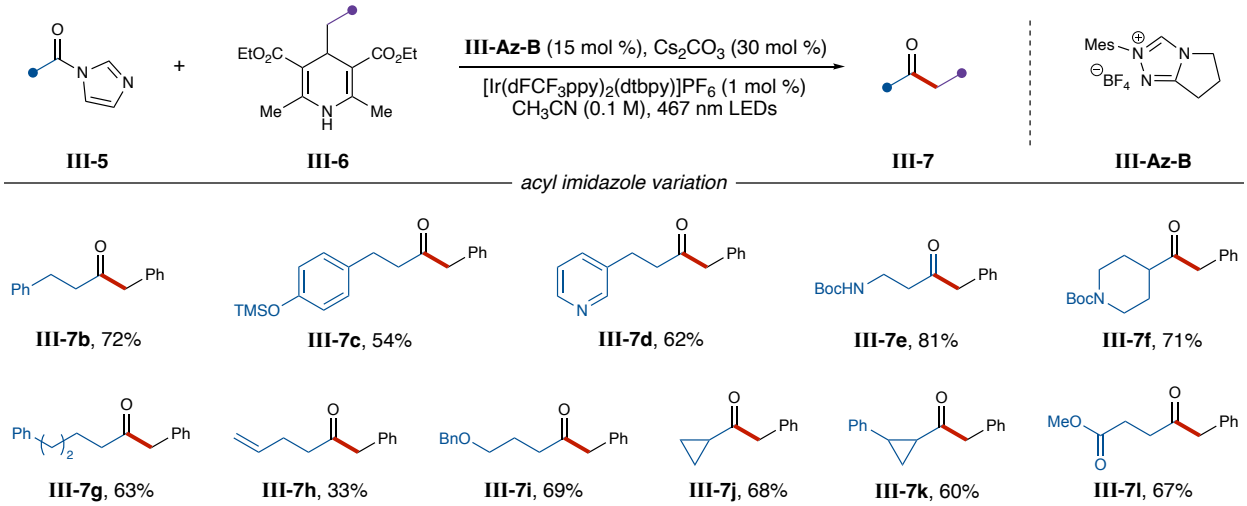

Table 3-3. Acyl imidazole variation using Hantzsch esters.

Grignard reaction, see SI). In general, use of **III-Az-B** instead of **III-Az-A** with aliphatic acyl imidazoles resulted in significant increases in yield (e.g., 32% increase for **III-7b** and 64% increase for **III-7e**) and enabled inclusion of a variety of substrates that demonstrated little-to-no reactivity using **III-Az-A** (e.g., **III-7h** and **III-7l**).

The reaction with other radical coupling partners was also studied to further increase the practicality and overall utility of this method.[413-414] In addition to their ease of preparation, bis-catecholato silicates are bench stable and offer excellent substrate diversity. Minor modification of the reaction conditions enabled reactivity to be achieved using bis-catecholato silicates as an alternative radical precursor (**III-8**), affording selected ketone products in comparable yields to those using Hantzsch esters (**Table 3-4**). In addition to tolerating different radical precursors as coupling partners, it was also determined that an organophotocatalyst (3DPAFIPN) could be substituted for the iridium-based photocatalyst, providing a more cost-effective variant for alkylation.

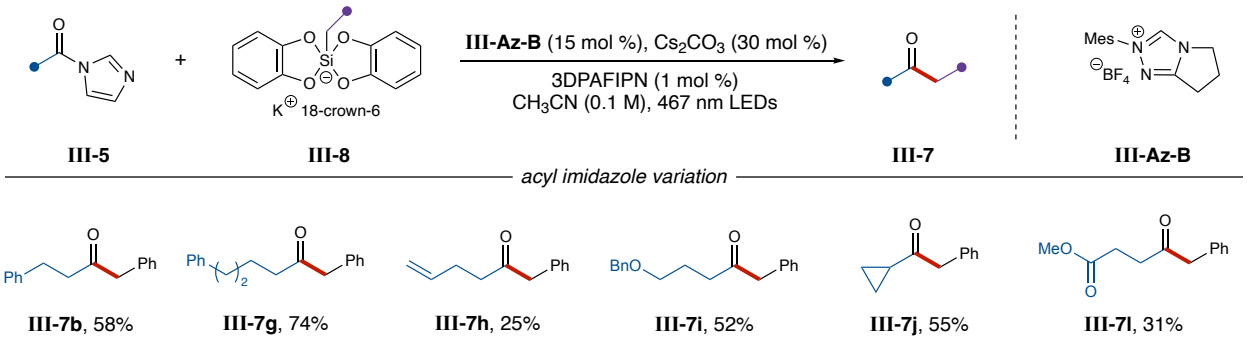

Table 3-4. Benzylation of acyl azoliums using alkyl silicate **III-8** as the oxidatively generated radical precursor.

3.6.2 Scope of Oxidatively Generated Radical Precursors

A survey of Hantzsch esters (**III-6**), bis-catecholatosilicates (**III-8**), and Meyer nitriles (**III-9**) enabled addition of various functional groups while demonstrating the array of coupling

partners viable in this reaction (**Table 3-5**). Benzyl Hantzsch esters containing electron-withdrawing and electron-donating groups afforded ketones (**III-7m-p**) in good yields. Carbazole-containing **III-7r** was isolated in high yield, offering a potential method to tag molecular probes for fluorescence studies.[415-417] The reaction proceeded smoothly with sterically congested radical precursors (**III-7q,s**) as well as primary, secondary, and tertiary alkyl radicals (**III-7t-v**).

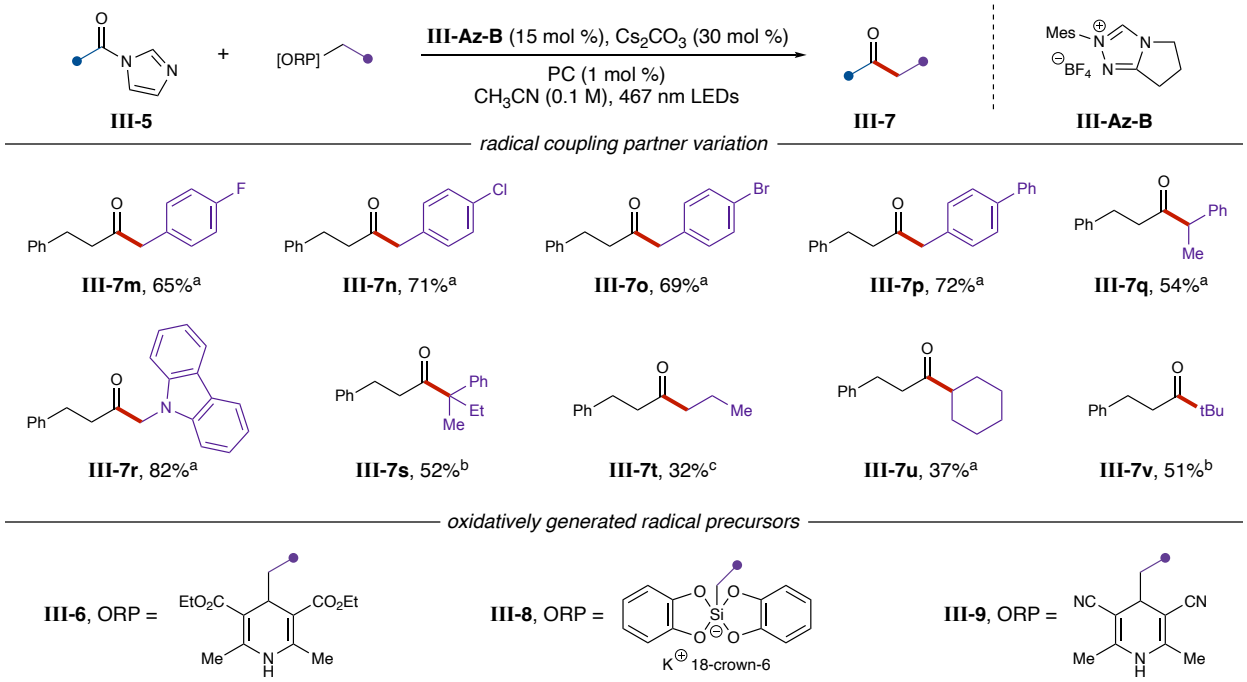

Table 3-5. Substrate scope with variation of the radical partner. [a] Reaction used **III-6** as the ORP and [Ir(dF[CF_3]ppy)$_2$(dtbpy)]PF_6 as the photocatalyst. [b] Reaction used **III-9** as the ORP and 4CzIPN as the photocatalyst. [c] Reaction used **III-8** as the ORP and 3DPAFIPN as the photocatalyst.

3.6.3 Late-stage Functionalization of Bioactive Compounds

The direct functionalization of amino acids was achieved via in situ activation with carbonyldiimidazole (CDI). Various amino acids, including alkyl amino acids (e.g., *N*-Boc-L-valine), aromatic amino acids (e.g., *N*-Boc-L-tryptophan), and others were suitable for direct benzylation to afford α-amino ketones **III-7w-ac** in good-to-excellent yields (**Table 3-5**). Even

under the slightly basic conditions of this reaction, α-amino ketone **III-7x** was prepared directly from *N*-Boc-L-valine with moderate stereoretention (87:13 er), suggesting that alkylation of chiral carboxylic acids is possible without complete erosion of stereochemistry.

Lastly, the late-stage functionalization of bioactive compounds was accomplished using the same one-step protocol (**Table 3-6**). The benzylation of a dipeptide was successful (**III-7ad**), suggesting that this methodology may be suitable for converting short peptides into their ketone counterparts with additional optimization. Naproxen, an anti-inflammatory drug used to treat bone disorders, was directly benzylated to afford the corresponding ketone (**III-7ae**) in excellent yield. The late-stage functionalization of heterobicyclic D-biotin, a vitamin essential to metabolism, was also achieved to give **III-7af** in moderate yield, further highlighting the synthetic utility of this process.

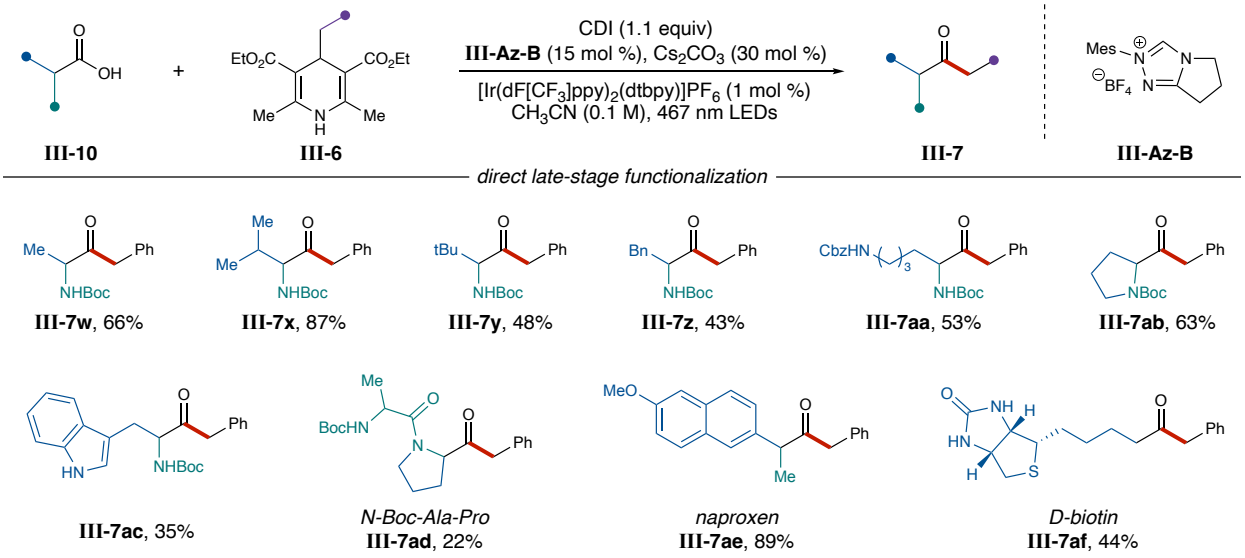

Table 3-6. Substrate scope for the direct late-stage functionalization of bioactive compounds starting from the corresponding carboxylic acids.

3.7 Conclusion and Outlook

We addressed a common limitation of single-electron NHC processes, revealing mechanistic insights that may be applied to this catalysis platform to further advance the field, expand substrate scopes, and increase the overall utility of NHCs in synthesis (**Figure 3-13**). The tunability of these single-electron operators was highlighted in a combined NHC-catalyzed and photoredox protocol to synthesize aliphatic ketones from activated carboxylic acids. Modulation of steric and electronic parameters of the NHC enabled increased yields of up to 65% compared to our previous results. In addition to significantly expanding the scope of this reaction, amino acids were directly functionalized to afford the corresponding α-amino ketones using a one-pot procedure, and the utility of this method was showcased in the late-state tailoring of bioactive compounds.

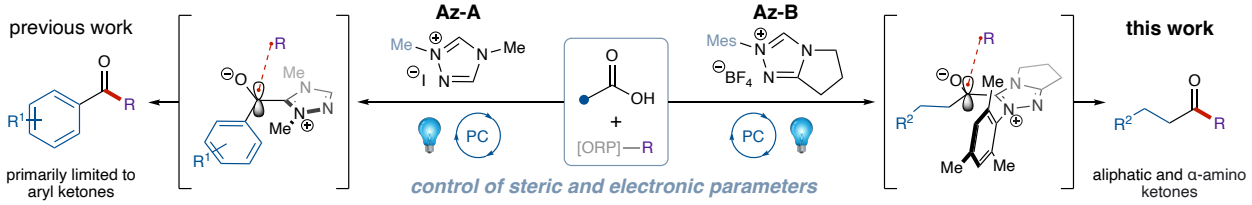

Figure 3-13. Progress made towards expanding the scope of radical carbene catalysis via control of the steric and electronic parameters of the NHC precursor.

3.9 Experimental Synthesis Protocols and Analyses

3.9.1 General Information

All reactions were carried out under an argon or nitrogen atmosphere in oven-dried glassware with magnetic stirring. All solvents were purified by passing through a bed of activated alumina, dried over 3Å molecular sieves, and then degassed using freeze-pump-thaw method (3-4 cycles). Purification of reaction products was carried out by flash chromatography on Biotage

Isolera 4 systems with Ultra-grade silica cartridges. Analytical thin layer chromatography was performed on EM Reagent 0.25 mm silica gel 60-F plates. Visualization was accomplished with UV light or ceric ammonium molybdate stain followed by heating.

^{1}H NMR spectra were recorded on AVANCE III 500 MHz w/ direct cryoprobe (500 MHz) spectrometer and are reported in ppm using solvent as an internal standard ($CDCl_3$ at 7.26 ppm). Data are reported as (ap = apparent, s = singlet, d = doublet, t = apparent triplet, q = quartet, m = multiplet, b = broad; coupling constant(s) in Hz; integration.) Proton-decoupled ^{13}C NMR spectra were recorded on an AVANCE III 500 MHz w/ direct cryoprobe (126 MHz) spectrometer and are reported in ppm using solvent as an internal standard ($CDCl_3$ at 77.16 ppm). Mass spectra were obtained on a WATERS Acquity-H UPLC-MS with a single quad detector (ESI) or an Agilent 7890 gas chromatograph equipped with a 5975C single quadrupole EI-MS. High-resolution mass spectrometry (HRMS) was obtained using an Agilent 6201 MSLC-TOF (ESI) or Bruker IMPACT II (ESI). Enantioselective measurements were made on an Agilent 1290 Infinity SFC using Chiralpak IA-3, IB-3, IC-3, ID-3, IG-3 chiral stationary phases. All photocatalytic reactions were carried out in a SynLED Parallel Photoreactor (465-470 nm) purchased from Sigma-Aldrich. $[Ir(dF(CF_3)ppy)_2(dtbpy)]PF_6$was purchased from Strem Chemicals and used without purification, or synthesized according to the literature procedure.[369] 3DPAFIPN and 4CzIPN were prepared according to the literature procedure.[418] **III-Az-B**, **III-Az-C**, and **III-Az-D** were prepared based on a known literature procedure.[419]

3.9.1 General Synthetic Procedures

3.9.1.1 General Procedure for the Synthesis of Acyl Imidazoles:

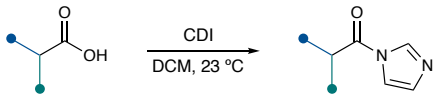

III-10 **III-5**

Scheme 3-6. Synthesis of acyl imidazoles from carboxylic acids.

The starting acyl imidazoles **III-5** were prepared based on the method of Lee and Scheidt: The appropriate acid **III-10** (10 mmol, 1.0 equiv) was dissolved in dry dichloromethane (0.3 M), and CDI (carbonyldiimidazole, 15 mmol, 1.5 equiv) was added slowly. The resulting mixture was stirred for 1-12 h at ambient temperature. Upon completion, the resulting solution was transferred to a separatory funnel and washed with deionized water (2 x 25 mL), and the organic layer was dried over $MgSO_4$. Concentration under reduced pressure afforded the acyl imidazole product **III-5**, which was used in the following reaction without further purification.

All alkyl radical precursors **III-6**, **III-8**, and **III-9** were synthesized according to the established literature procedure and matched the reported spectral data.[285,371-372,414,420-421]

3.9.1.2 General Procedure 1 for the Alkylation of Acyl Azoliums using Hantzsch Esters:

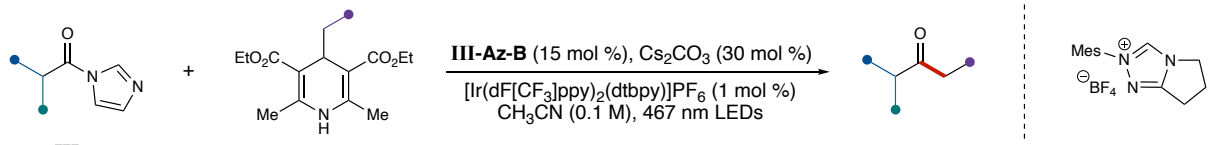

III-5 **III-6** **III-7** **III-Az-B**

Scheme 3-7. Combined NHC and photoredox-catalyzed synthesis of aliphatic ketones using **III-Az-B.**

All reactions were set up inside a glovebox under N_2 atm. To an oven-dried 2-dram vial containing a stirbar was added the respective Hantzsch ester **III-6** (1.5 equiv, 0.38 mmol), respective acyl imidazole **III-5** (1.0 equiv, 0.25 mmol), [Ir(dF[CF_3]ppy)$_2$(dtbpy)]PF_6 (0.01 equiv, 1 mol %), *N*-mesityl-substituted pyrrolotriazolium NHC precursor (**III-Az-B**, 11.8 mg, 0.15 equiv, 38 µmol), and cesium carbonate (24.4 mg, 0.30 equiv, 75 µmol). Acetonitrile (2.5 mL, 0.1 M) was added, and the reaction was capped and removed from the glovebox. Parafilm was wrapped around the cap to prevent air from entering, and the vial was stirred in a SynLED Parallel Photoreactor (467 nm blue LEDs). The reactions were monitored by GCMS or LCMS. When complete consumption of the acyl imidazole was observed (typically 4-16 h), the reactions were concentrated under reduced pressure and then purified by column chromatography on silica gel.

3.9.1.3 General Procedure 2 for the Alkylation of Acyl Azoliums using Meyer Nitriles:

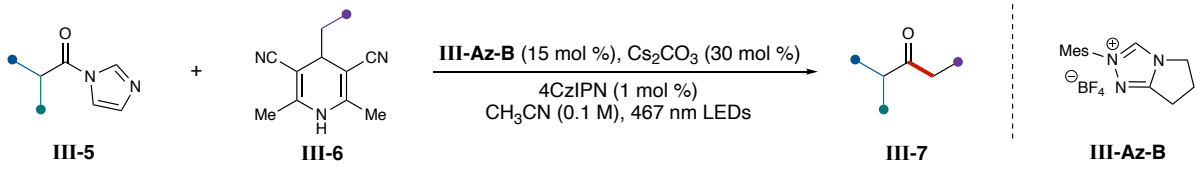

Scheme 3-8. Synthesis of aliphatic ketones using Meyer nitriles in place of Hantzsch esters.

All reactions were set up inside a glovebox under N_2 atm. To an oven-dried 2-dram vial containing a stirbar was added the respective Meyer nitrile (1.5 equiv, 0.38 mmol), appropriate acyl imidazole (1.0 equiv, 0.25 mmol), 4CzIPN (0.01 equiv, 1 mol %), *N*-mesityl-substituted pyrrolotriazolium NHC precursor (Az-B, 11.8 mg, 0.15 equiv, 38 µmol), and cesium carbonate (24.4 mg, 0.30 equiv, 75 µmol). Acetonitrile (2.5 mL, 0.1M) was added, and the reaction was capped and taken out of the glovebox. Parafilm was wrapped around the cap to prevent air from entering, and the vial was stirred in a SynLED Parallel Photoreactor (467 nm blue LEDs). The

reactions were monitored by GCMS or LCMS. When complete consumption of the acyl imidazole was observed (typically 4-16 h), the reactions were concentrated under reduced pressure and then purified by column chromatography.

3.9.1.4 General Procedure 3 for the Alkylation of Acyl Azoliums using Bis-catecholato Silicates:

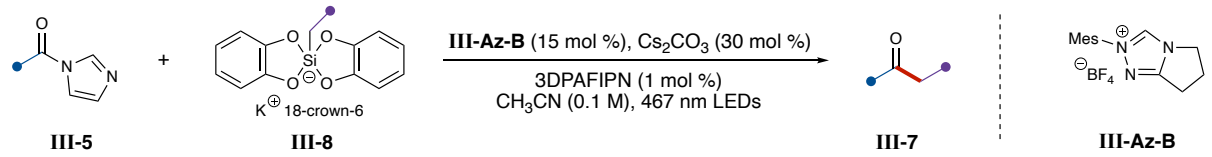

Scheme 3-9. Synthesis of aliphatic ketones using bis-catecholato silicates in place of Hantzsch esters.

All reactions were set up inside a glovebox under N_2 atm. To an oven-dried 2-dram vial containing a stirbar was added the respective silicate (2.0 equiv, 0.50 mmol), appropriate acyl imidazole (1.0 equiv, 0.25 mmol), 3DPAFIPN (0.01 equiv, 1 mol %), *N*-mesityl-substituted pyrrolotriazolium NHC precursor (11.8 mg, 0.15 equiv, 38 µmol), and cesium carbonate (12 mg, 0.15 equiv, 38 µmol) unless otherwise stated. Acetonitrile (2.5 mL, 0.1M) was added, and the reaction was capped and taken out of the glovebox. Parafilm was wrapped around the cap to prevent air from entering, and the vial was stirred in a SynLED Parallel Photoreactor (467 nm blue LEDs). The reactions were monitored by GCMS. When complete consumption of the acyl imidazole was observed (typically 16-32 h), the reactions were concentrated under reduced pressure and then purified by column chromatography.

3.9.1.5 General Procedure 4 for the Direct Alkylation of Carboxylic Acids:

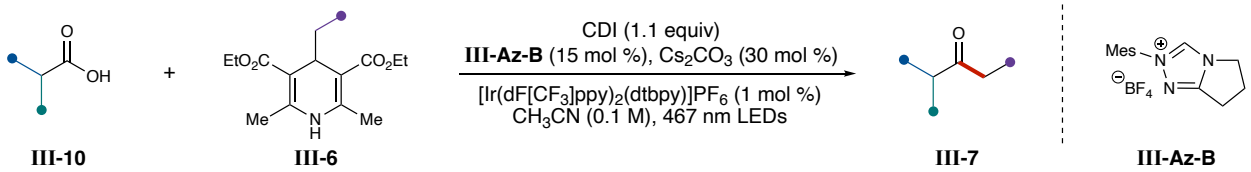

III-10 **III-6** **III-7** **III-Az-B**

Scheme 3-10. One-pot synthesis of aliphatic ketones directly from carboxylic acids.

All reactions were set up inside a glovebox under N_2 atm. To an oven-dried 2-dram vial containing a stirbar was added CDI (1.0 equiv, 0.25 mmol), the appropriate amino acid or carboxylic acid (1.0 equiv, 0.25 mmol), the respective benzyl Hantzsch ester (2.0 equiv, 0.50 mmol), PC-1 (0.01 equiv, 1.0 mol %), cesium carbonate (24.4 mg, 0.30 equiv, 75 µmol), and *N*-mesityl-substituted pyrrolotriazolium NHC precursor (11.8 mg, 0.15 equiv, 38 µmol). The solids were dissolved in acetonitrile (2.5 mL, 0.1 M). The vial was capped and taken out of the glovebox. Parafilm was wrapped around the cap to prevent air from entering, and the vial was stirred in a SynLED Parallel Photoreactor (467 nm blue LEDs). The reactions were allowed to stir for 24 h unless otherwise noted. Following completion, the reactions were concentrated under reduced pressure and then purified by column chromatography.

3.9.2 Optimization of Reaction Conditions with Oxidatively Generated Radical Precursors

The reaction was optimized according to General Procedures 1-3 for the alkylation of acyl azoliums from acyl imidazoles **III-5b** and the corresponding oxidatively generated radical precursor. Reactions using benzyl silicates **III-8a** and **III-8b** were performed by Keegan Fitzpatrick. Reactions were monitored by GCMS. GCMS yields are based on a calibration curve using 1,3,5-trimethoxybenzene as the internal standard, and the corresponding reactions were

performed at a 0.1 mmol scale. Reactions with isolated yields were performed at a 0.25 mmol scale.

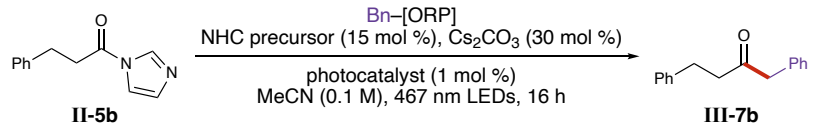

entry	NHC precursor	ORP	photocatalyst	yield (%)
1	Az-B	**III-6a** (2.0 equiv)	Ir-dF	72 (isolated)
2	Az-B	**III-8a** (1.5 equiv)	Ir-dF	40 (GC)
3	Az-B	**III-8b** (1.5 equiv)	Ir-dF	trace (GC)
4	Az-B	**III-11a** (1.5 equiv)	Ir-dF	16 (GC)
5	Az-B	**III-8a** (2.0 equiv)	Ir-dF	60 (isolated)
6	Az-C	**III-8a** (2.0 equiv)	Ir-dF	9 (GC)
7	Az-D	**III-8a** (2.0 equiv)	Ir-dF	3 (GC)
8	Az-B	**III-8a** (2.0 equiv)	3DPAFIPN	58 (isolated)
9	Az-B	**III-8a** (2.0 equiv)	4CzIPN	39 (GC)

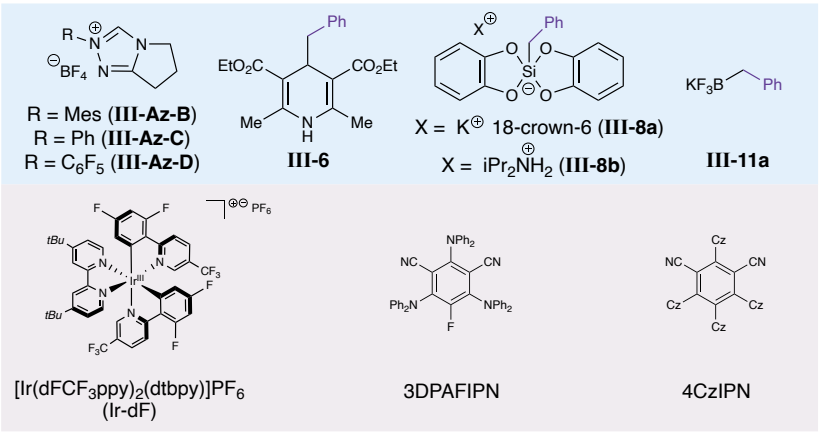

Table 3-7. Optimization of reaction conditions with a screen of oxidatively generated radical precursors.

3.9.3 NHC Screens

3.9.3.1 NHC Screen for Aryl Systems using Phenyl Acyl Imidazole

These yields were determined by NMR using a stock solution of 1,3,5-trimethoxybenzene in $CDCl_3$ (0.33 equiv of 1,3,5-trimethoxybenzene compared to 1.0 equiv of starting acyl imidazole) which was added to the crude reaction material after concentration. For consistency and comparison to the azolium screen for the aliphatic system, this screen as performed using 30 mol

% Cs_2CO_3 (differing from the 15 mol % in the optimized reaction conditions for aryl substrates),[10] which may account for the lower NMR yields compared to isolated yields.

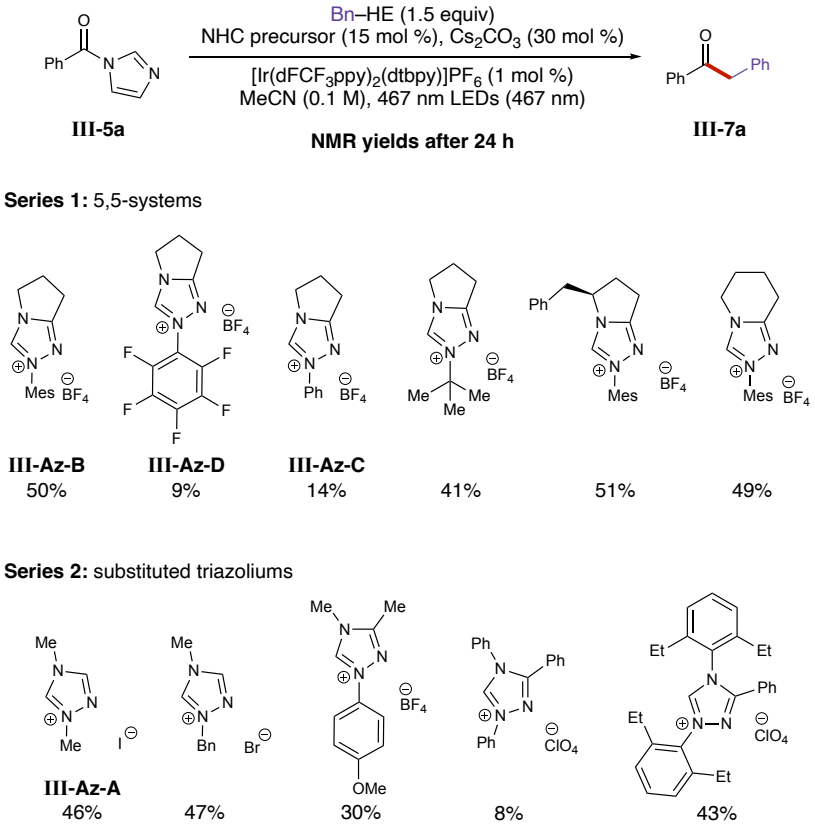

Table 3-8. Screen of NHC precursors for the model reaction of aryl substrates.

3.9.3.2 NHC Screen for Aliphatic Systems using Hydrocinnamyl Acyl Imidazole

The reaction yields were determined by NMR using a stock solution of 1,3,5-trimethoxybenzene in CDCl3 (0.33 equiv of 1,3,5-trimethoxybenzene compared to 1.0 equiv of starting acyl imidazole) which was added to the crude reaction material after concentration. This may account for a slightly lower yield compared to the isolated yield for **III-Az-B**.

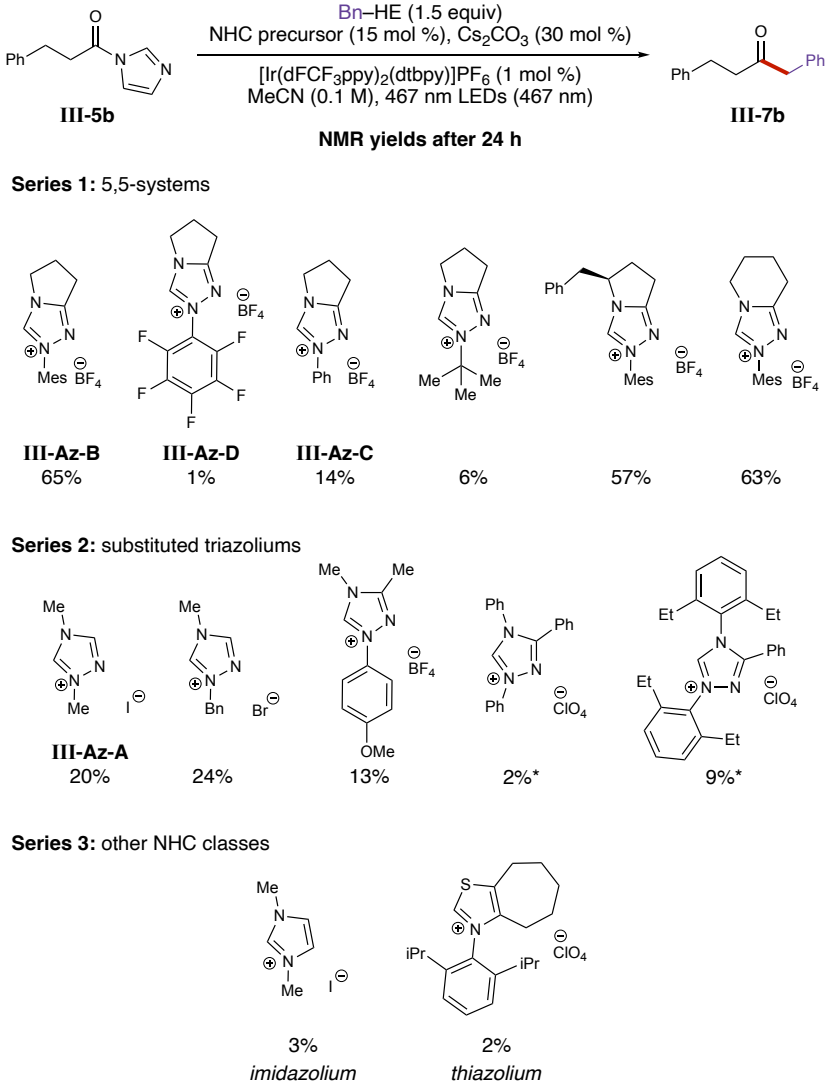

Table 3-9. Screen of NHC precursors for the model reaction of aliphatic substrates. *The presence of multiple highly stabilizing groups was found to decrease yield.

3.9.4 Control Experiments

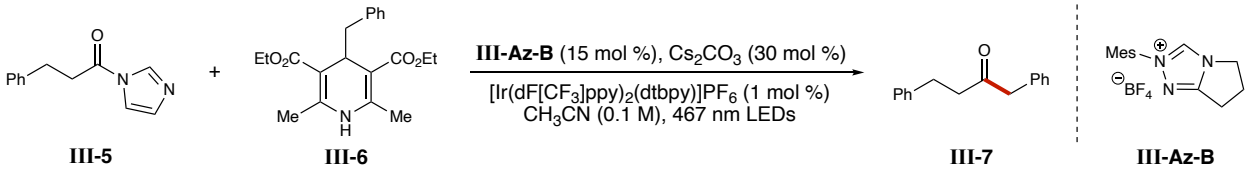

III-5 III-6 III-7 III-Az-B

entry	deviation from standard	yield (%)
1	none	72
2	no base	0
3	no azolium	0
4	no base + no azolium	0
5	no photocatalyst	0
6	no light	0

Table 3-10. Control experiments demonstrating that the reaction is NHC and photoredox catalyzed.

Note: The same control experiments were run with the benzyl silicates **III-8a**, and some product formation was observed when entries 2-4 were applied. However, the majority of the reaction was unreacted starting material (after 16 h). While further experiments are ongoing to understand these results, the most efficient and highest yielding conditions for the benzyl silicates were observed with the NHC-catalyzed conditions as established in Table S-1.

3.9.5 Chemoselectivity Experiment

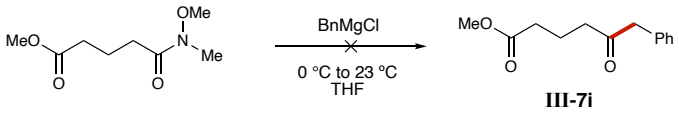

III-7i

Scheme 3-11. Benzylation of a Weinreb amide to make **III-7i**.

The chemoselectivity of the alkylation strategy described herein demonstrates another notable benefit of this reactivity platform. For example, benzylation of a 1,4-dicarbonyl acyl imidazole yielded ester-containing **III-7i** in good yield, demonstrating a bond construction that

suffers from functional group incompatibility using conventional methods of ketone formation (e.g. Grignard reaction, see above reaction scheme). When the corresponding Weinreb amide was reacted with benzylmagnesium chloride, the desired product was either not produced or was produced in small quantities (using 1 or 5 equivalents of BnMgCl, respectively). Moreover, when the desired product was produced, multiple isolation attempts proved unsuccessful due to the abundance of over-alkylated side products (e.g. products from double- and triple-benzylation). On the contrary, when the corresponding acyl imidazole was subjected to our combined catalytic protocol, no over-alkylation was observed, thus demonstrating excellent functional group compatibility.

3.9.5.1 Procedure for benzylation of Weinreb amide:

To a stirred solution of weinreb amide (1.0 equiv) at 0 °C in THF, was slowly added benzyl magnesium chloride (2 M in THF, 1.0 or 5.0 equiv) and the resulting mixture was reacted for 20 hours at ambient temperature under N_2 atm. The reaction mixture was cooled, diluted with aqueous HCl (2 M), and extracted with diethyl ether. The organic layer was dried over Na_2SO_4, filtered, and concentrated to yield a mixture of products that were unable to be isolated.

3.9.6 SFC Traces

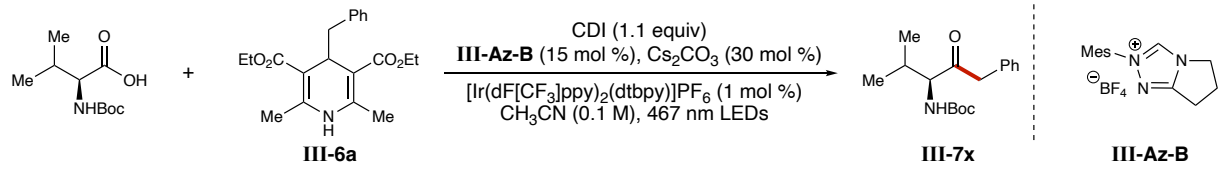

Scheme 3-12. Synthesis of **III-7x** from the corresponding amino acid.

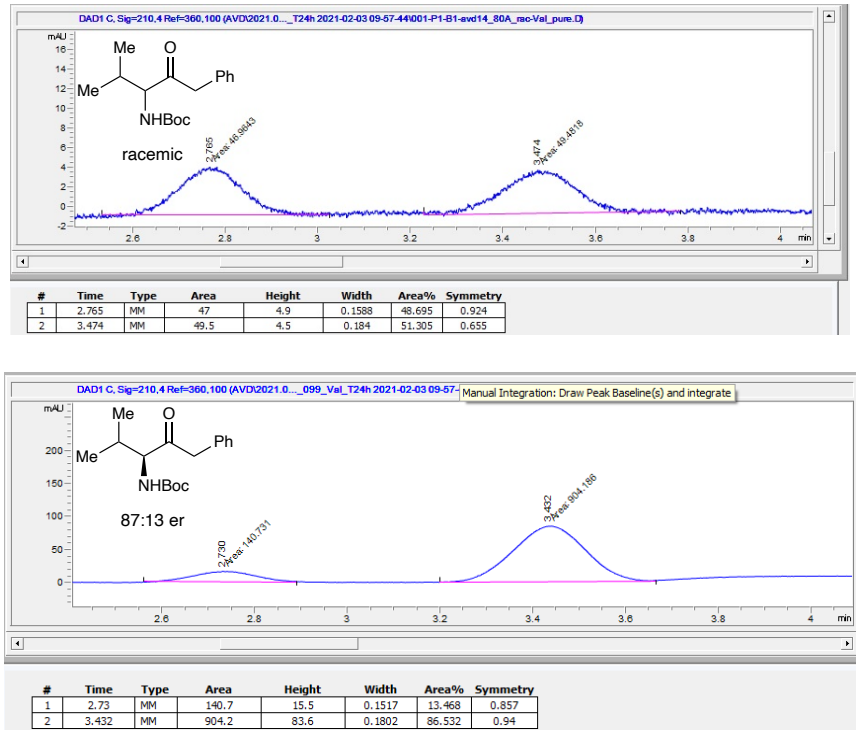

#	Time	Type	Area	Height	Width	Area%	Symmetry
1	2.765	MM	47	4.9	0.1588	48.695	0.924
2	3.474	MM	49.5	4.5	0.184	51.305	0.655

#	Time	Type	Area	Height	Width	Area%	Symmetry
1	2.73	MM	140.7	15.5	0.1517	13.468	0.857
2	3.432	MM	904.2	83.6	0.1802	86.532	0.94

Figure 1-14. SFC traces showing that moderate retention of stereochemistry occurs using this process.

3.9.10 Tabulated Data

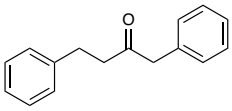

1,4-diphenylbutan-2-one (**III-7b**). Prepared according to General Procedure 1 for the alkylation of acyl azoliums using the respective acyl imidazole (50 mg, 1.0 equiv) and benzyl Hantzsch ester. The reaction mixture was purified by column chromatography (0-10% ethyl acetate/hexanes) to yield the desired product as a clear oil (72%). Can also be prepared with General Procedure 3 to afford the desired material (56 mg, 58%). Product is a known compound and matches reported literature data.[400]

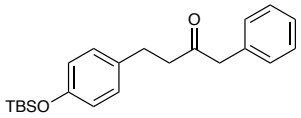

4-(4-((*tert*-butyldimethylsilyl)oxy)phenyl)-1-phenylbutan-2-one (**III-7c**). Prepared according to General Procedure 1 for the alkylation of acyl azoliums using the respective acyl imidazole (82 mg, 1.0 equiv) and benzyl Hantzsch ester. The reaction mixture was purified by column chromatography (0-10% ethyl acetate/hexanes) to yield the product as a white solid (48 mg, 54%). Analytical data for **III-7c**: ^{1}H NMR (500 MHz, $CDCl_3$) δ 7.37 – 7.28 (m, 2H), 7.29 – 7.25 (m, 1H), 7.20 – 7.10 (m, 2H), 6.97 (d, J = 8.1 Hz, 2H), 6.78 – 6.66 (m, 2H), 3.65 (s, 2H), 2.80 (t, J = 7.7 Hz, 2H), 2.76 – 2.69 (m, 2H), 0.97 (d, J = 1.1 Hz, 9H), 0.17 (d, J = 1.1 Hz, 6H). ^{13}C NMR (126 MHz, $CDCl_3$) δ 207.8, 154.0, 134.3, 133.7, 129.6, 129.3, 128.9, 127.2, 120.1, 50.6, 43.9, 29.2, 25.8, 18.3, -4.3. FTIR (diamond, anvil, solid) cm^{-1}: 3060, 3031, 2952, 2930, 2896, 2858, 1706, 1608. HRMS (ESI): Mass calcd for $C_{22}H_{31}O_2Si^+$ $[M+H]^+$: 355.2088; found 355.2071.

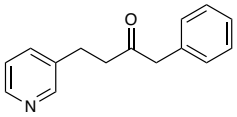

1-phenyl-4-(pyridin-3-yl)butan-2-one (**III-7d**). Prepared according to the General Procedure 1 for the alkylation of acyl azoliums using the respective acyl imidazole and benzyl Hantzsch ester. The reaction mixture was purified by column chromatography (2-50% ethyl acetate/hexanes) to yield the product as a yellow oil (62%). Analytical data for **III-7d**: ^{1}H NMR (500 MHz, $CDCl_3$) δ 8.53 (s, 2H), 7.62 – 7.52 (m, 1H), 7.45 – 7.33 (m, 3H), 7.32 – 7.22 (m, 3H), 3.77 (s, 2H), 2.97 (t, J = 7.1 Hz, 2H), 2.88 (t, J = 7.4 Hz, 2H). FTIR (diamond, anvil, oil) cm^{-1}: 3076, 3056, 2984, 2934, 1714, 1657. HRMS (ESI): Mass calcd for $C_{15}H_{16}NO^+$ $[M+H]^+$: 226.1226; found 226.1226.

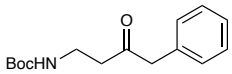

tert-butyl (3-oxo-4-phenylbutyl)carbamate (**III-7e**). Prepared according to General Procedure 1 for the alkylation of acyl azoliums using the respective acyl imidazole and benzyl Hantzsch ester. The reaction mixture was purified by column chromatography (2-20% ethyl acetate/hexanes) to yield the product as a clear oil (81%). Analytical data for **III-7e**: ^{1}H NMR (500 MHz, $CDCl_3$) δ 7.38 – 7.31 (m, 2H), 7.30 – 7.25 (m, 1H), 7.19 (dd, *J* = 7.2, 1.6 Hz, 2H), 4.95 (s, 1H), 3.69 (s, 2H), 3.32 (q, *J* = 5.9 Hz, 2H), 2.68 (t, *J* = 5.7 Hz, 2H), 1.40 (s, 9H). ^{13}C NMR (126 MHz, $CDCl_3$) δ 207.9, 155.9, 133.8, 129.4, 129.4, 128.8, 127.2, 79.3, 50.3, 41.9, 35.2, 28.4. FTIR (diamond, anvil, oil) cm^{-1}: 3364 (broad), 3061, 3029, 2979, 2932, 1702, 1602. HRMS (ESI): Mass calcd for $C_{15}H_{21}NO_3Na^+$ $[M+Na]^+$: 286.1414; found 286.1412.

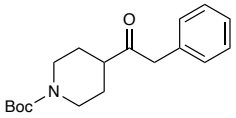

tert-butyl 4-(2-phenylacetyl)piperidine-1-carboxylate (**III-7f**). Prepared according to General Procedure 1 for the alkylation of acyl azoliums using the respective acyl imidazole and benzyl Hantzsch ester. The reaction mixture was purified column chromatography (2-20% ethyl acetate/hexanes) to yield the desired product a clear oil (71%). Product is a known compound and matches reported literature data.[400]

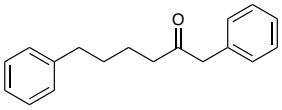

1,6-diphenylhexan-2-one (**III-7g**). Prepared according to General Procedure 1 for the alkylation of acyl azoliums using the respective acyl imidazole (57 mg, 1.0 equiv) and benzyl Hantzsch ester. The reaction mixture was purified by column chromatography (0-10% ethyl acetate/hexanes) to yield the product as a clear oil (63%). Can also be prepared with general procedure **(3)** to afford the desired material (63 mg, 74%). Analytical data for **III-7g**: ^{1}H NMR (500 MHz, $CDCl_3$) δ 7.38 – 7.30 (m, 2H), 7.30 – 7.23 (m, 3H), 7.22 – 7.10 (m, 5H), 3.66 (s, 2H), 2.57 (t, *J* = 7.2 Hz, 2H), 2.46 (t, *J* = 6.8 Hz, 2H), 1.67 – 1.49 (m, 4H). ^{13}C NMR (126 MHz, $CDCl_3$) δ 208.4, 142.3, 134.5, 129.5, 128.9, 128.5, 128.4, 127.1, 125.9, 50.3, 41.9, 35.8, 30.9, 23.5. FTIR (diamond, anvil, oil) cm^{-1}: 3061, 3026, 2932, 2858, 1705, 1602. HRMS (ESI): Mass calcd for $C_{18}H_{20}ONa^{+}$ $[M+Na]^{+}$: 275.1406; found 275.1407.

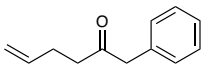

1-phenylhex-5-en-2-one (**III-7h**). Prepared according to General Procedure 1 for the alkylation of acyl azoliums using the respective acyl imidazole (38 mg, 1.0 equiv) and benzyl Hantzsch ester. The reaction mixture was purified by column chromatography (0-10% ethyl acetate/hexanes) to yield the desired product as a clear oil (14.5 mg, 33%). Can also be prepared with general procedure **(3)** to afford the desired material (11 mg, 25%). Product is a known compound and matches reported literature data.[422]

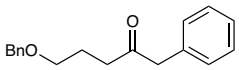

5-(benzyloxy)-1-phenylpentan-2-one (**III-7i**). Prepared according to General Procedure 1 for the alkylation of acyl azoliums using the respective acyl imidazole (61 mg, 1.0 equiv) and benzyl Hantzsch ester. The reaction mixture was purified by column chromatography (0-10% ethyl acetate/hexanes) to yield the desired product as a clear oil (46 mg, 69%). Can also be prepared with general procedure **(3)** to afford the desired material (35 mg, 52%). Product is a known compound and matches reported literature data.[253]

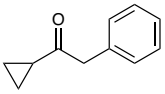

1-cyclopropyl-2-phenylethan-1-one (**III-7j**). Prepared according to General Procedure 1 for the alkylation of acyl azoliums using the respective acyl imidazole (34 mg, 1.0 equiv) and benzyl Hantzsch ester. The reaction mixture was purified by column chromatography (0-10% ethyl acetate/hexanes) to yield the desired product as a clear oil (68%). Can also be prepared with general procedure **(3)** to afford the desired material (22 mg, 55%). Product is a known compound and matches reported literature data.[423]

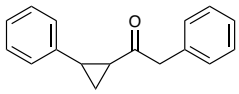

2-phenyl-1-(2-phenylcyclopropyl)ethan-1-one (**III-7k**). Prepared according to General Procedure 1 for the alkylation of acyl azoliums using the respective acyl imidazole (53 mg, 1.0 equiv) and benzyl Hantzsch ester. The reaction mixture was purified by column chromatography (0-10% ethyl

acetate/hexanes) to yield the desired product as a clear oil (35.5 mg, 60%). Analytical data for **III-7k**: ^{1}H NMR (500 MHz, $CDCl_3$) δ 7.37 – 7.31 (m, 2H), 7.30 – 7.16 (m, 6H), 7.02 – 6.97 (m, 2H), 3.87 (s, 2H), 2.51 (ddd, *J* = 9.1, 6.6, 4.0 Hz, 1H), 2.22 (ddd, *J* = 8.0, 5.3, 4.0 Hz, 1H), 1.68 (ddd, *J* = 9.2, 5.2, 4.2 Hz, 1H), 1.34 (ddd, *J* = 8.1, 6.6, 4.2 Hz, 1H). ^{13}C NMR (126 MHz, $CDCl_3$) δ 206.5, 140.3, 134.3, 129.7, 128.9, 128.6, 127.1, 126.7, 126.4, 51.1, 31.9, 29.8, 19.2. FTIR (diamond, anvil, oil) cm^{-1}: 3030, 2980, 2971, 2888, 1691. HRMS (ESI): Mass calcd for $C_{17}H_{17}O^+$ $[M+H]^+$: 237.1274; found 237.1273.

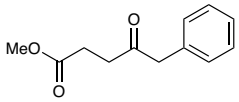

methyl 4-oxo-5-phenylpentanoate (**III-7l**). Prepared according to General Procedure 1 for the alkylation of acyl azoliums using the respective acyl imidazole (46 mg, 1.0 equiv) and benzyl Hantzsch ester. The reaction mixture was purified by column chromatography (0-10% ethyl acetate/hexanes) to yield the desired product as a clear oil (67%). Can also be prepared with general procedure **(3)** to afford the desired material (16 mg, 31%). Product is a known compound and matches reported literature data.[424]

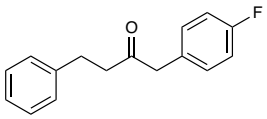

1-(4-fluorophenyl)-4-phenylbutan-2-one (**III-7m**). Prepared according to General Procedure 1 for the alkylation of acyl azoliums using the respective acyl imidazole (50 mg, 1.0 equiv) and benzyl Hantzsch ester. The reaction mixture was purified by column chromatography (2-20% ethyl

acetate/hexanes) to yield the desired product as a pale yellow oil (39.5 mg, 65%). Analytical data for **III-7m**: ^{1}H NMR (500 MHz, $CDCl_3$) δ 7.57 – 7.49 (m, 2H), 7.48 – 7.43 (m, 1H), 7.43 – 7.34 (m, 4H), 7.32 – 7.21 (m, 2H), 3.90 (s, 2H), 3.15 (t, *J* = 7.5 Hz, 2H), 3.04 (dd, *J* = 7.9, 6.7 Hz, 2H). ^{13}C NMR (126 MHz, $CDCl_3$) δ 207.3, 163.08, 161.13, 140.9, 131.1, 131.0, 129.9, 129.8, 128.6, 128.5, 126.3, 115.8, 115.6, 49.5, 43.7, 29.9. FTIR (diamond, anvil, oil) cm^{-1}: 3062, 3028, 2980, 2929, 1711, 1602. HRMS (ESI): Mass calcd for $C_{16}H_{15}FNaO^+$ $[M+Na]^+$: 265.0999; found 265.0999.

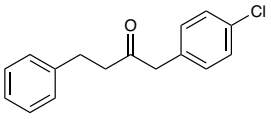

1-(4-chlorophenyl)-4-phenylbutan-2-on*e* (**III-7n**). Prepared according to General Procedure 1 for the alkylation of acyl azoliums using the respective acyl imidazole (50 mg, 1.0 equiv) and benzyl Hantzsch ester. The reaction mixture was purified by column chromatography (2-20% ethyl acetate/hexanes) to yield the desired product as a white solid (46 mg, 71%). Analytical data for **III-7n**: ^{1}H NMR (500 MHz, $CDCl_3$) δ 7.30 – 7.23 (m, 4H), 7.22 – 7.16 (m, 1H), 7.15 – 7.11 (m, 2H), 7.09 – 7.05 (m, 2H), 3.63 (s, 2H), 2.88 (t, *J* = 7.5 Hz, 2H), 2.82 – 2.71 (m, 2H). ^{13}C NMR (126 MHz, $CDCl_3$) δ 206.9, 140.9, 133.2, 132.6, 130.9, 128.9, 128.7, 128.5, 126.3, 49.6, 43.8, 29.9. FTIR (diamond, anvil, solid) cm^{-1}: 3068, 3028, 2896, 1706. HRMS (ESI): Mass calcd for $C_{16}H_{15}ClNaO^+$ $[M+Na]^+$: 281.0704; found 281.0704.

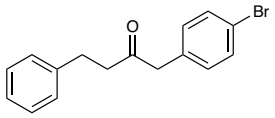

1-(4-bromophenyl)-4-phenylbutan-2-one (**III-7o**). Prepared according to General Procedure 1 for the alkylation of acyl azoliums using the respective acyl imidazole (50 mg, 1.0 equiv) and benzyl Hantzsch ester. The reaction mixture was purified by column chromatography (2-20% ethyl acetate/hexanes) to yield the product as a white solid (52 mg, 69%). Analytical data for **III-7o**: ^{1}H NMR (500 MHz, $CDCl_3$) δ 7.50 – 7.38 (m, 2H), 7.32 – 7.23 (m, 2H), 7.23 – 7.16 (m, 1H), 7.16 – 7.09 (m, 2H), 7.07 – 6.98 (m, 2H), 3.61 (s, 2H), 2.88 (t, J = 7.5 Hz, 2H), 2.83 – 2.72 (m, 2H). ^{13}C NMR (126 MHz, $CDCl_3$) δ 206.8, 140.9, 133.1, 131.9, 131.3, 128.7, 128.5, 126.3, 121.2, 49.7, 43.8, 29.9. FTIR (diamond, anvil, solid) cm^{-1}: 3028, 2933, 2897, 1706. HRMS (ESI): Mass calcd for $C_{16}H_{15}BrNaO^{+}$ $[M+Na]^{+}$: 325.0198; found 325.0196.

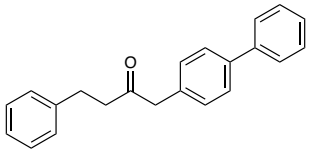

1-([1,1'-biphenyl]-4-yl)-4-phenylbutan-2-one (**III-7p**). Prepared according to General Procedure 1 for the alkylation of acyl azoliums using the respective acyl imidazole (50 mg, 1.0 equiv) and benzyl Hantzsch ester. The reaction mixture was purified by column chromatography (0-10% ethyl acetate/hexanes) to yield the desired product as a white solid (72%). Analytical data for **III-7p**: ^{1}H NMR (500 MHz, $CDCl_3$) δ 7.64 – 7.53 (m, 4H), 7.46 (dd, J = 8.4, 6.9 Hz, 2H), 7.40 – 7.34 (m, 1H), 7.31 – 7.14 (m, 7H), 3.72 (s, 2H), 2.96 – 2.88 (m, 2H), 2.87 – 2.80 (m, 2H). ^{13}C NMR (126 MHz, $CDCl_3$) δ 207.5, 141.0, 140.9, 140.1, 133.2, 129.9, 128.9, 128.6, 128.5, 127.6, 127.4, 127.2,

126.2, 50.1, 43.7, 29.9. FTIR (diamond, anvil, solid) cm^{-1}: 3062, 3031, 2941, 2891, 1703. HRMS (ESI): Mass calcd for $C_{22}H_{20}NaO^+$ $[M+Na]^+$: 323.1406; found 323.1406.

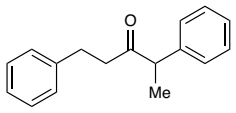

1,4-diphenylpentan-3-one (**III-7q**). Prepared according to General Procedure 1 for the alkylation of acyl azoliums using the respective acyl imidazole (50 mg, 1.0 equiv) and benzyl Hantzsch ester. The reaction mixture was purified by column chromatography (2-20% ethyl acetate/hexanes) to yield the product as a clear oil (32 mg, 54%). Product is a known compound and matches reported literature data.[425]

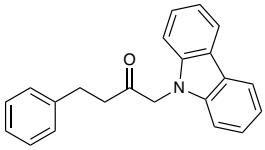

1-(9*H*-carbazol-9-yl)-4-phenylbutan-2-one (**III-7r**). Prepared according to General Procedure 1 for the alkylation of acyl azoliums using the respective acyl imidazole (50 mg, 1.0 equiv) and benzyl Hantzsch ester. The reaction mixture was purified by column chromatography (0-10% ethyl acetate/hexanes) to yield the desired product as a white solid (82%). Analytical data for **III-7r**: ^1H NMR (500 MHz, $CDCl_3$) δ 8.20 (d, J = 7.8 Hz, 2H), 7.54 (ddd, J = 8.3, 7.1, 1.2 Hz, 2H), 7.45 – 7.22 (m, 7H), 7.11 (dd, J = 6.9, 1.9 Hz, 2H), 4.97 (s, 2H), 2.94 (t, J = 7.4 Hz, 2H), 2.70 (t, J = 7.4 Hz, 2H). ^{13}C NMR (126 MHz, $CDCl_3$) δ 206.3, 140.5, 140.4, 128.7, 128.5, 126.4, 126.3, 123.4, 120.7, 119.9, 108.3, 52.9, 40.7, 29.5. FTIR (diamond, anvil, solid) cm^{-1}: 3051, 3024, 2954, 2907, 2894, 1718. HRMS (ESI): Mass calcd for $C_{22}H_{19}NONa^+$ $[M+Na]^+$: 336.1359; found 336.1358.

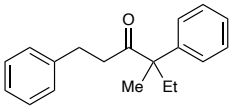

4-methyl-1,4-diphenylhexan-3-one (**III-7s**). Prepared according to General Procedure 1 for the alkylation of acyl azoliums using the respective acyl imidazole (50 mg, 1.0 equiv) and benzyl Hantzsch ester. The reaction mixture was purified by column chromatography (2-20% ethyl acetate/hexanes) to yield the desired product as a clear oil (52%). Analytical data for **III-7s**: ^{1}H NMR (500 MHz, $CDCl_3$) δ 7.44 – 7.37 (m, 2H), 7.37 – 7.28 (m, 3H), 7.28 – 7.22 (m, 3H), 7.13 (dd, *J* = 7.0, 1.8 Hz, 2H), 2.96 – 2.82 (m, 2H), 2.60 (m, 2H), 2.15 – 2.01 (m, 2H), 1.52 (s, 3H), 0.83 (t, *J* = 7.4 Hz, 3H). ^{13}C NMR (126 MHz, $CDCl_3$) δ 212.1, 142.9, 141.4, 128.8, 128.5, 128.4, 126.9, 126.6, 126.0, 56.1, 39.8, 30.6, 30.0, 20.9, 8.8. FTIR (diamond, anvil, oil) cm^{-1}: 3085, 3060, 2969, 2935, 1703. HRMS (ESI): Mass calcd for $C_{19}H_{22}ONa^{+}$ $[M+Na]^{+}$: 289.1563; found 289.1560.

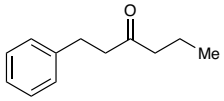

1-phenylhexan-3-one (**III-7t**). Prepared according to General Procedure 3 for the alkylation of acyl azoliums *with slight modifications* using the respective acyl imidazole (50 mg, 1.0 equiv), benzyl silicate (738 mg, 5.0 equiv), and 5 mol % of the photocatalyst. The reaction mixture was purified by column chromatography (0-10% ethyl acetate/hexanes) to yield the desired product as a clear oil (14 mg, 32%). Product is a known compound and matches reported literature data.[426]

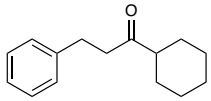

1-cyclohexyl-3-phenylpropan-1-one (**III-7u**). Prepared according to General Procedure 1 for the alkylation of acyl azoliums using the respective acyl imidazole (50 mg, 1.0 equiv) and benzyl Hantzsch ester. The reaction mixture was purified by column chromatography (2-20% ethyl acetate/hexanes) to yield the desired product as a clear oil (37%). Product is a known compound and matches reported literature data.[427]

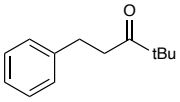

4,4-dimethyl-1-phenylpentan-3-one (**III-7v**). Prepared according to General Procedure 1 for the alkylation of acyl azoliums using the respective acyl imidazole (50 mg, 1.0 equiv) and Hantzsch ester. The reaction mixture was purified by column chromatography (2-20% ethyl acetate/hexanes) to yield the desired product as a clear oil (51%). Product is a known compound and matches reported literature data.[428]

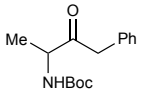

tert-butyl (3-oxo-4-phenylbutan-2-yl)carbamate (**III-7w**). Prepared according to General Procedure 4 for the alkylation of acyl azoliums (in situ activation) using the respective amino acid (47 mg, 1.0 equiv) and benzyl Hantzsch ester. The reaction mixture was purified by column chromatography (0-5% MeOH/DCM) to yield the desired product as a white solid (43 mg, 66%). Product is a known compound and matches reported literature data.[429]

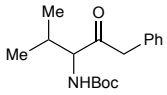

tert-butyl (4-methyl-2-oxo-1-phenylpentan-3-yl)carbamate (**III-7x**). Prepared according to General Procedure 4 for the alkylation of acyl azoliums (in situ activation) using the respective amino acid (54 mg, 1.0 equiv) and benzyl Hantzsch ester. The reaction mixture was purified by column chromatography (0-10% ethyl acetate/hexanes) to yield the desired product as a white solid (63 mg, 87%). Product is a known compound and matches reported literature data.[430]

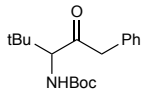

tert-butyl (4,4-dimethyl-2-oxo-1-phenylpentan-3-yl)carbamate (**III-7y**). Prepared according to General Procedure 4 for the alkylation of acyl azoliums (in situ activation) using the respective amino acid (76.4 mg, 1.0 equiv) and benzyl Hantzsch ester. The reaction mixture was purified by column chromatography (0-40% ethyl acetate/hexanes) to yield the desired product as a white solid (48 mg, 48%). Analytical data for **III-7y**: ^{1}H NMR (500 MHz, Chloroform-*d*) δ 7.39 (t, *J* = 7.3 Hz, 2H), 7.32 (t, *J* = 7.3 Hz, 1H), 7.29 – 7.22 (m, 2H), 5.18 (d, *J* = 9.5 Hz, 1H), 4.37 (d, *J* = 9.5 Hz, 1H), 4.02 – 3.85 (m, 2H), 1.49 (s, 9H), 1.07 (s, 9H). ^{13}C NMR (126 MHz, Chloroform-*d*) δ 208.2, 155.7, 133.4, 129.8, 128.7, 127.2, 79.9, 65.2, 50.9, 34.9, 28.4, 26.8. FTIR (diamond, anvil, solid) cm^{-1}: 3370, 3299, 2973, 2943, 2907, 1728, 1698. HRMS (ESI): Mass calcd for $C_{18}H_{27}NO_3Na^+$ $[M+Na]^+$: 328.1883; found 328.1883.

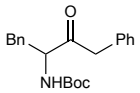

tert-butyl (3-oxo-1,4-diphenylbutan-2-yl)carbamate (**III-7z**). Prepared according to General Procedure 4 for the alkylation of acyl azoliums (in situ activation) using the respective amino acid (66 mg, 1.0 equiv) and benzyl Hantzsch ester. The reaction mixture was purified by column chromatography (0-10% ethyl acetate/hexanes) to yield the desired product as a white solid (36 mg, 43%). Product is a known compound and matches reported literature data.[430]

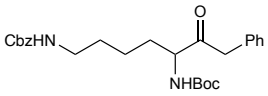

benzyl *tert*-butyl (6-oxo-7-phenylheptane-1,5-diyl)dicarbamate (**III-7aa**). Prepared according to General Procedure 4 for the alkylation of acyl azoliums (in situ activation) using the respective amino acid (95 mg, 1.0 equiv) and benzyl Hantzsch ester. The reaction mixture was purified by column chromatography (0-40% ethyl acetate/hexanes) to yield the desired product as a light yellow solid (60.5 mg, 53%). Analytical data for **III-7aa**: ^{1}H NMR (500 MHz, $CDCl_3$) δ 7.30 – 7.15 (m, 8H), 7.11 (dd, *J* = 7.0, 1.7 Hz, 2H), 5.12 (d, *J* = 7.7 Hz, 1H), 5.00 (s, 2H), 4.68 (s, 1H), 4.38 – 4.24 (m, 1H), 3.76 – 3.64 (m, 2H), 3.05 (m, 2H), 1.81 – 1.62 (m, 1H), 1.33 (m, 14H). ^{13}C NMR (126 MHz, $CDCl_3$) δ 206.9, 156.6, 155.7, 136.7, 133.4, 129.7, 128.9, 128.7, 128.3, 128.3, 127.4, 80.1, 66.8, 58.7, 46.9, 40.6, 31.2, 28.5, 28.0, 22.2. FTIR (diamond, anvil, oil) cm^{-1}: 3333, 3063, 3031, 2979, 2933, 1756, 1693. HRMS (ESI): Mass calcd for $C_{26}H_{34}N_2O_5Na^+$ $[M+Na]^+$: 477.2360; found 477.2360.

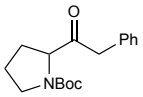

tert-butyl 2-(2-phenylacetyl)pyrrolidine-1-carboxylate (**III-7ab**). Prepared according to General Procedure 4 for the alkylation of acyl azoliums (in situ activation) using the respective amino acid and benzyl Hantzsch ester. The reaction mixture was purified by column chromatography (0-50% ethyl acetate/hexanes) to yield the desired product as a white solid (63%). Product is a known compound and matches reported literature data.[431] Product is a mixture of rotamers.

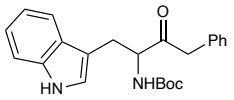

tert-butyl (1-(1*H*-indol-3-yl)-3-oxo-4-phenylbutan-2-yl)carbamate (**III-7ac**). Prepared according to General Procedure 4 for the alkylation of acyl azoliums (in situ activation) using the respective amino acid (76 mg, 1.0 equiv) and benzyl Hantzsch ester. The reaction mixture was purified by column chromatography (0-30% ethyl acetate/hexanes) to yield the desired product as an off-white solid (28 mg, 35%). Analytical data for **III-7ac**: ^{1}H NMR (500 MHz, $CDCl_3$) δ 8.09 (s, 1H), 7.58 (d, J = 7.9 Hz, 1H), 7.36 (d, J = 8.1 Hz, 1H), 7.32 – 7.17 (m, 5H), 7.13 (t, J = 7.5 Hz, 1H), 7.02 (d, J = 7.3 Hz, 2H), 6.93 (d, J = 2.4 Hz, 1H), 5.20 (d, J = 7.5 Hz, 1H), 4.75 (q, J = 6.8 Hz, 1H), 3.75 – 3.56 (m, 2H), 3.30 – 3.13 (m, 2H), 1.43 (s, 9H). ^{13}C NMR (126 MHz, $CDCl_3$) δ 207.4, 155.5, 136.3, 133.4, 129.8, 128.7, 127.6, 127.2, 122.8, 122.5, 119.9, 119.1, 111.4, 110.5, 80.0, 59.2, 47.9, 28.5, 27.8. FTIR (diamond, avil, solid) cm^{-1}: 3346 (br), 3027, 2974, 2928, 1717, 1686. LRMS (EI): Product reacts via McLafferty rearrangement during analysis, mass calcd for $C_{19}H_{19}N_2O_3^+$ [M-tBu+H]$^+$: 323.1390; found 323.26.

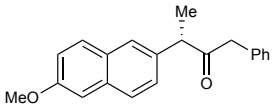

(*S*)-3-(6-methoxynaphthalen-2-yl)-1-phenylbutan-2-one (**III-7ad**). Prepared according to General Procedure 4 for the alkylation of acyl azoliums (in situ activation) using naproxen and the respective benzyl Hantzsch ester. The reaction mixture was purified by column chromatography (0-20% ethyl acetate/hexanes) to yield the desired product as a clear oil (89%). Product is a known compound and matches reported literature data.[432]

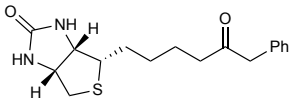

(3a*S*,4*S*,6a*R*)-4-(5-oxo-6-phenylhexyl)tetrahydro-1*H*-thieno[3,4-*d*]imidazol-2(3*H*)-one (**III-7ae**). Prepared according to General Procedure 4 for the alkylation of acyl azoliums (in situ activation) using biotin and the respective benzyl Hantzsch ester. The reaction mixture was purified by column chromatography (0-10% MeOH/DCM) to yield the desired product as an off-white solid (44%). Analytical data for **III-7ae**: ^{1}H NMR (500 MHz, $CDCl_3$) δ 7.35 – 7.30 (m, 2H), 7.28 – 7.26 (m, 1H), 7.22 – 7.17 (m, 2H), 5.59 (d, *J* = 4.3 Hz, 1H), 5.32 (s, 1H), 4.48 (ddt, *J* = 7.6, 5.0, 1.2 Hz, 1H), 4.27 (ddd, *J* = 7.9, 4.6, 1.5 Hz, 1H), 3.67 (s, 2H), 3.11 (ddd, *J* = 8.4, 6.5, 4.6 Hz, 1H), 2.89 (dd, *J* = 12.9, 5.0 Hz, 1H), 2.71 (d, *J* = 12.8 Hz, 1H), 2.47 (t, *J* = 7.3 Hz, 2H), 1.66 – 1.54 (m, 4H), 1.39 – 1.30 (m, 2H). ^{13}C NMR (126 MHz, $CDCl_3$) δ 208.5, 163.7, 134.4, 129.6, 128.9, 127.2 62.1, 60.3, 55.4, 50.3, 41.6, 40.7, 28.5, 28.4, 23.6. FTIR (diamond, anvil, solid) cm^{-1}: 3232 (broad), 3085, 3062, 2927, 2860, 1688, 1666, 1648. HRMS (ESI): Mass calcd for $C_{17}H_{22}N_2O_2SNa^+$ $[M+Na]^+$: 341.1294; found 341.1294.

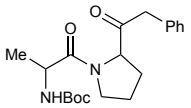

tert-butyl (1-oxo-1-(2-(2-phenylacetyl)pyrrolidin-1-yl)propan-2-yl)carbamate (**III-7af**). Prepared according to General Procedure 4 for the alkylation of acyl azoliums (in situ activation) using the respective dipeptide and benzyl Hantzsch ester. The reaction mixture was purified by column chromatography (5-40% ethyl acetate/hexanes) to yield the desired product as a clear oil (22%). Analytical data for **III-7af**: ^{1}H NMR (500 MHz, $CDCl_3$) δ 7.36 – 7.27 (m, 3H), 7.22 (d, *J* = 7.5 Hz, 2H), 5.31 (d, *J* = 9.0 Hz, 1H), 4.68 (t, *J* = 6.6 Hz, 1H), 4.47 (t, *J* = 7.5 Hz, 1H), 3.89 – 3.79 (m, 2H), 3.71 (d, *J* = 9.2 Hz, 1H), 3.58 – 3.50 (m, 1H), 1.95 (qd, *J* = 17.1, 14.5, 8.0 Hz, 3H), 1.74 (q, *J* = 8.1, 7.0 Hz, 1H), 1.43 (s, 9H), 1.34 (d, *J* = 6.8 Hz, 3H), 1.26 (s, 1H). ^{13}C NMR (126 MHz, $CDCl_3$) δ 206.1, 171.7, 155.4, 133.6, 129.8, 128.8, 127.3, 79.7, 64.2, 47.9, 47.8, 47.2, 29.8, 28.5, 25.3, 18.5. FTIR (diamond, anvil, oil) cm^{-1}: 3636, 2980, 2971, 2884, 1721, 1709. HRMS (ESI): Mass calcd for $C_{20}H_{28}N_2O_4Na^+$ $[M+Na]^+$: 383.1941; found 383.1941.

3.10 Computational Protocols and Analyses

3.10.1 Software Packages (with Authors)

Gaussian 16, Revision A.03

M. J. Frisch, G. W. Trucks, H. B. Schlegel, G. E. Scuseria, M. A. Robb, J. R. Cheeseman, G. Scalmani, V. Barone, G. A. Petersson, H. Nakatsuji, X. Li, M. Caricato, A. V. Marenich, J. Bloino, B. G. Janesko, R. Gomperts, B. Mennucci, H. P. Hratchian, J. V. Ortiz, A. F. Izmaylov, J. L. Sonnenberg, D. Williams-Young, F. Ding, F. Lipparini, F. Egidi, J. Goings, B. Peng, A. Petrone,

T. Henderson, D. Ranasinghe, V. G. Zakrzewski, J. Gao, N. Rega, G. Zheng, W. Liang, M. Hada, M. Ehara, K. Toyota, R. Fukuda, J. Hasegawa, M. Ishida, T. Nakajima, Y. Honda, O. Kitao, H. Nakai, T. Vreven, K. Throssell, J. A. Montgomery, Jr., J. E. Peralta, F. Ogliaro, M. J. Bearpark, J. J. Heyd, E. N. Brothers, K. N. Kudin, V. N. Staroverov, T. A. Keith, R. Kobayashi, J. Normand, K. Raghavachari, A. P. Rendell, J. C. Burant, S. S. Iyengar, J. Tomasi, M. Cossi, J. M. Millam, M. Klene, C. Adamo, R. Cammi, J. W. Ochterski, R. L. Martin, K. Morokuma, O. Farkas, J. B. Foresman, and D. J. Fox, *Gaussian, Inc.*, Wallingford CT, **2016**.

CYLview

CYLview, 1.0b; Legault, C. Y., Université de Sherbrooke, 2009 (http://www.cylview.org)

GaussView, Version 6.0.16

Roy Dennington, Todd A. Keith, and John M. Millam, Semichem Inc., Shawnee Mission, KS, 2016.

PyMOL, Version 2.1

The PyMOL Molecular Graphics System, Version 2.1.1 Schrödinger, LLC, New York, NY, 2018

Schrodinger Macromodel

Schrödinger Release 2019-4: MacroModel, Schrödinger, LLC, New York, NY, 2019.

3.10.2 General Information

All computations were performed using Density Functional Theory (DFT) as implemented in the Gaussian 16 software package. All reactants, intermediates, transition structures, and products were optimized using PBE/6-31G* level of theory with LANL2DZ basis set and effective core potential for Cs and SMD solvation corrections in acetonitrile. All stationary points were

verified by frequency analyses, and all transition structures were checked with intrinsic reaction coordinate (IRC) computations. Furthermore, key stationary points were evaluated with restricted and unrestricted geometry optimizations and stability tests to verify that the most relevant and stable electronic configurations were being considered. Conformational search was performed using Schrodinger Macromodel software package. All reported energy values are free energies in kcal/mol, and all distances are in Ångströms (Å). Figures of structures were rendered in GaussView, CYLview, or PyMOL software.

3.10.3 Acyl Azolium Radical Structures

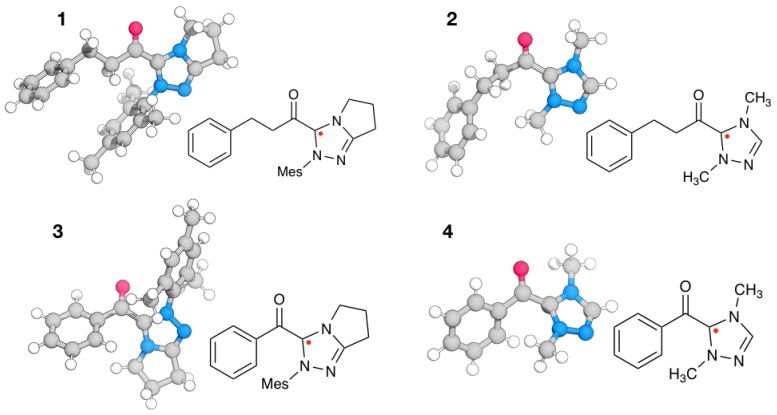

Figure 3-15. Rendered PyMOL images of lowest energy structures of aliphatic and aryl acyl azolium radicals with NHC precursors **III-Az-A** and **III-Az-B**.

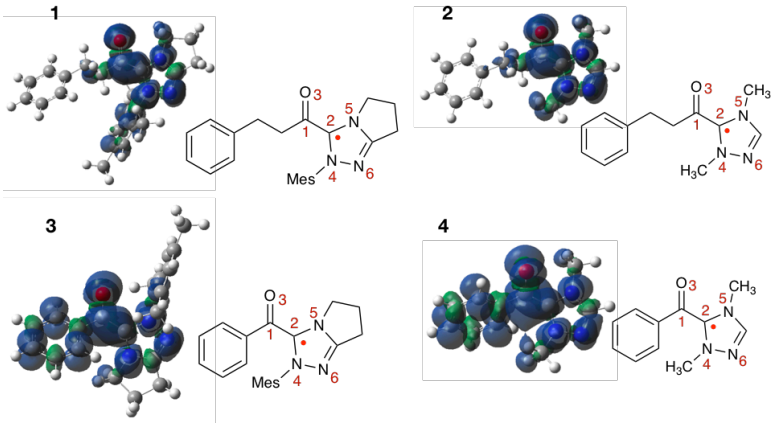

Figure 3-16. Computed radical spin densities of lowest energy structures of aliphatic and aryl acyl azolium radicals with NHCs **III-Az-A** and **III-Az-B**. The radical distributed over C1 and C2 atoms.

X	1	2	3	4
% Spin Densities[a]				
on C_1	14.1	14.9	14.7	16.0
on C_2	23.5	22.9	20.0	20.0
on C_1+C_2	37.6	37.8	34.7	36.0
on O_3	27.5	28.7	29.8	30.0
on N_4	16.5	16.5	14.6	12.3
on N_5	8.8	10.5	6.7	7.5
on N_6	6.4	4.5	4.7	3.3
on N[b]	31.8	31.5	26.0	23.1

[a]Mulliken spin densities. [b]Sum of spin density on all nitrogen atoms.

Table 3-11. Mulliken spin densities of acyl azolium radicals 1-4.

3.10.4 ESP map and CHELPG charges

Rendered images of computed electrostatic potential map (left) and CHELPG charges (right) for acyl azolium radicals. A summarized table can be found following the figures.

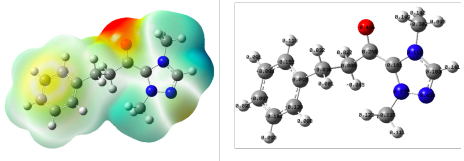

Figure 3-17. Aliphatic acyl azolium radical with **III-Az-A**.

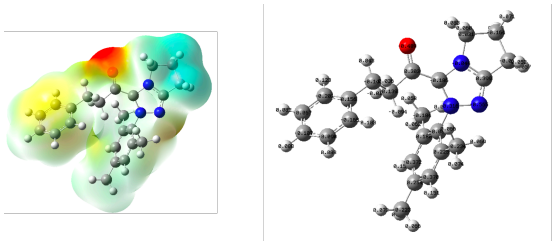

Figure 3-18. Aliphatic acyl azolium radical with **III-Az-B**.

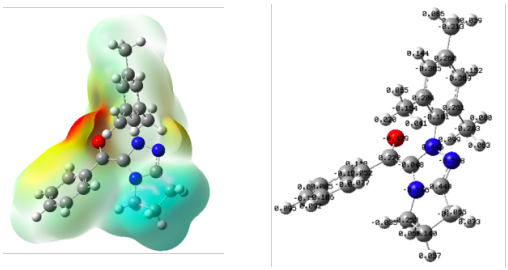

Figure 3-19. Aryl acyl azolium radical with **III-Az-B**.

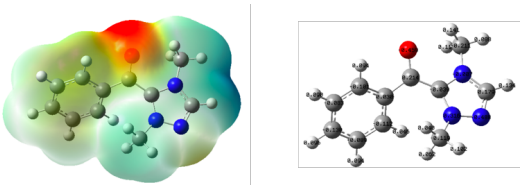

Figure 3-20. Aryl acyl azolium radical with **III-Az-A**.

acyl azolium radical	carbonyl carbon (C1)	carbonyl carbon (C2)
1	0.266	-0.161
2	0.303	-0.186
3	0.222	-0.048
4	0.214	-0.039

Table 3-12. Computed CHELPG charges of acyl azolium radicals.

3.10.5 Radical stability model

Computed isodesmic reactions to determine the radical stability of acyl-radical in comparison to the corresponding acyl azolium radicals. When R = hydrocinnamyl, the NHC radicals are substantially lower in energy than when R = phenyl, suggesting that the radical is better stabilized on the azolium compared to the acyl radical for the aliphatic system.

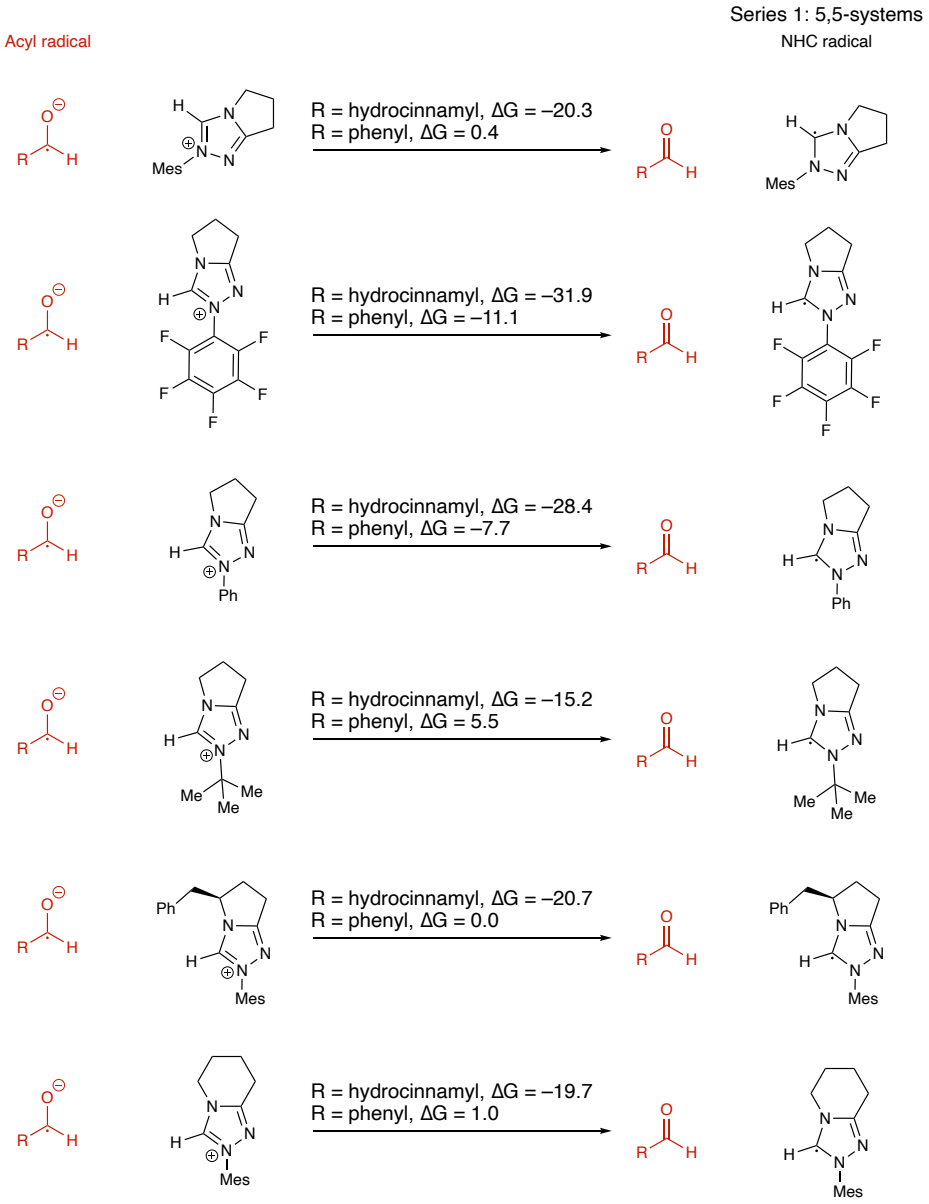

Figure 3-21. Isodesmic reactions for pyrrolotriazoliums.

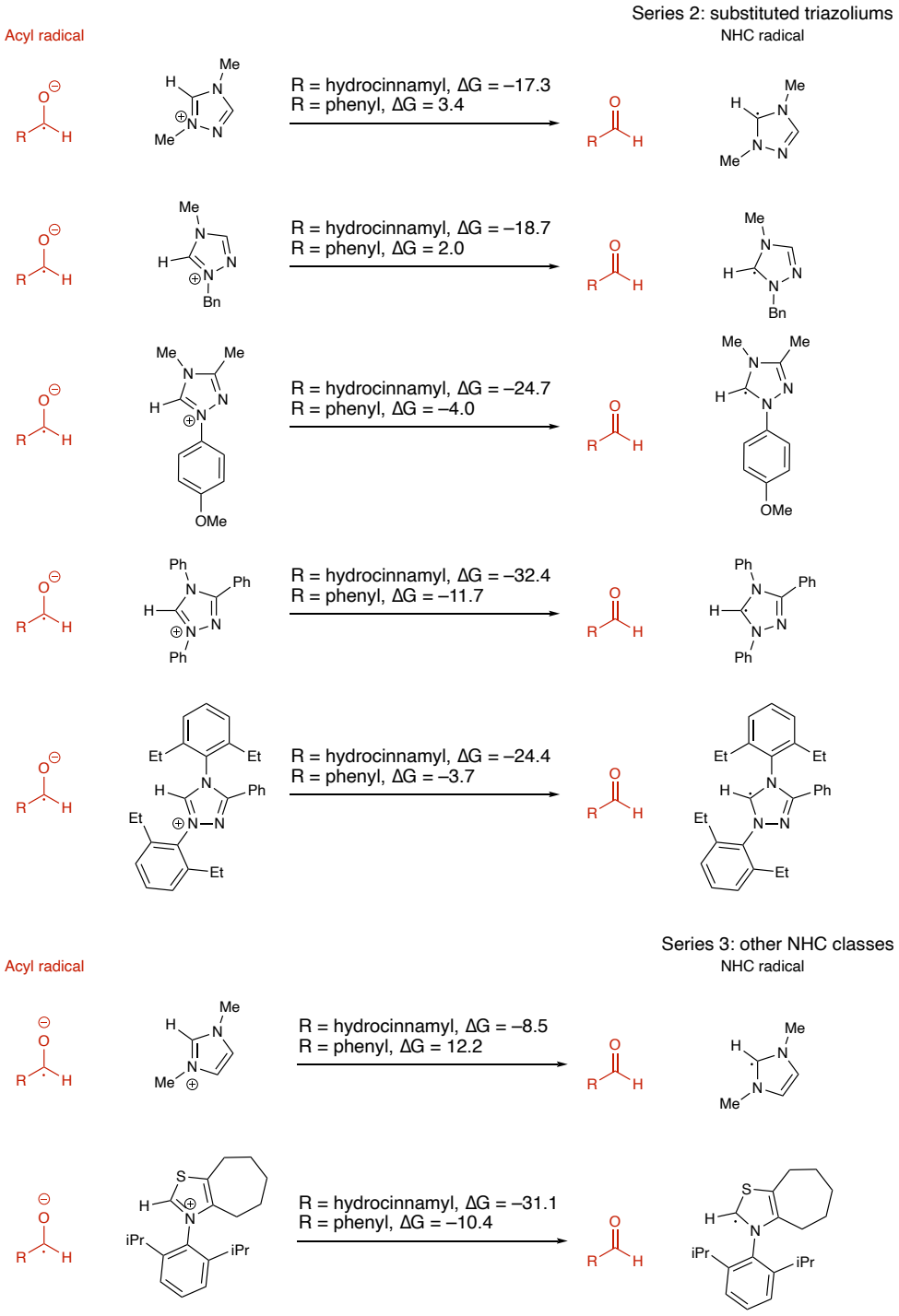

Figure 3-22. Isodesmic reactions using substituted triazoliums and other NHC classes.

3.10.5 Superimposed Figures

Superimposed acyl azolium radicals aligned at O-C1-C2 atoms. The blue and red colored structure corresponds to lowest energy conformation of acyl azolium **III-Az-A** and **III-Az-B**, respectively. Section a) shows aryl acyl azoliums. Sections b) and c) shows aliphatic acyl azoliums.

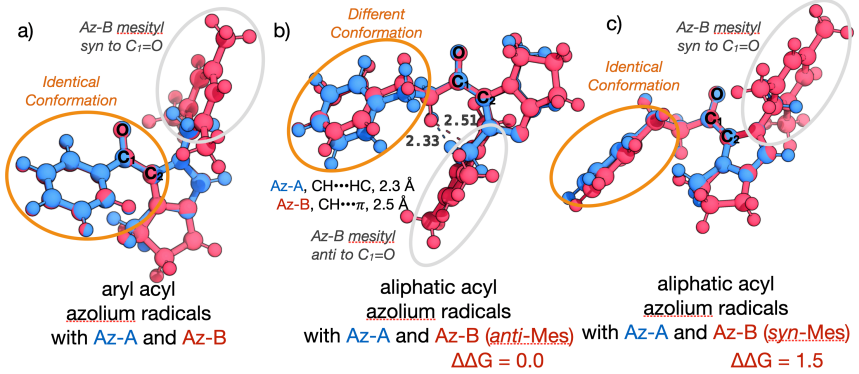

Figure 3-23. Overlayed optimized structures of the acyl azoliums.

In a) **III-Az-A** and **III-Az-B** both adopt a very similar conformation where the aryl acyl group is in the same relative orientation with respect to the NHC. **III-Az-B** mesityl group is *syn* to C_1=O. In b), **III-Az-B** mesityl group is *anti* to C_1=O, and the aliphatic acyl group adopts different conformations between **III-Az-A** and **III-Az-B**. In c) we show the *syn* confromation of the mesityl in aliphatic acyl azolium **III-Az-B** which is 1.5 kcal/mol higher than the *anti*. Note that the aliphatic acyl group of the *syn*-mesityl **III-Az-B** is now very similar to **III-Az-A**.

3.10.6 Mechanistic studies

The complete proposed catalytic cycle and the energies (kcal/mol) for the combined NHC/photoredox-catalyzed construction ofcd aliphatic ketones. The radical partner used to compute from the photocatalytic cycle is benzyl radical. The NHC structures used to compute for the NHC cycle are **III-Az-A** (previous work) and **III-Az-B** (this work).

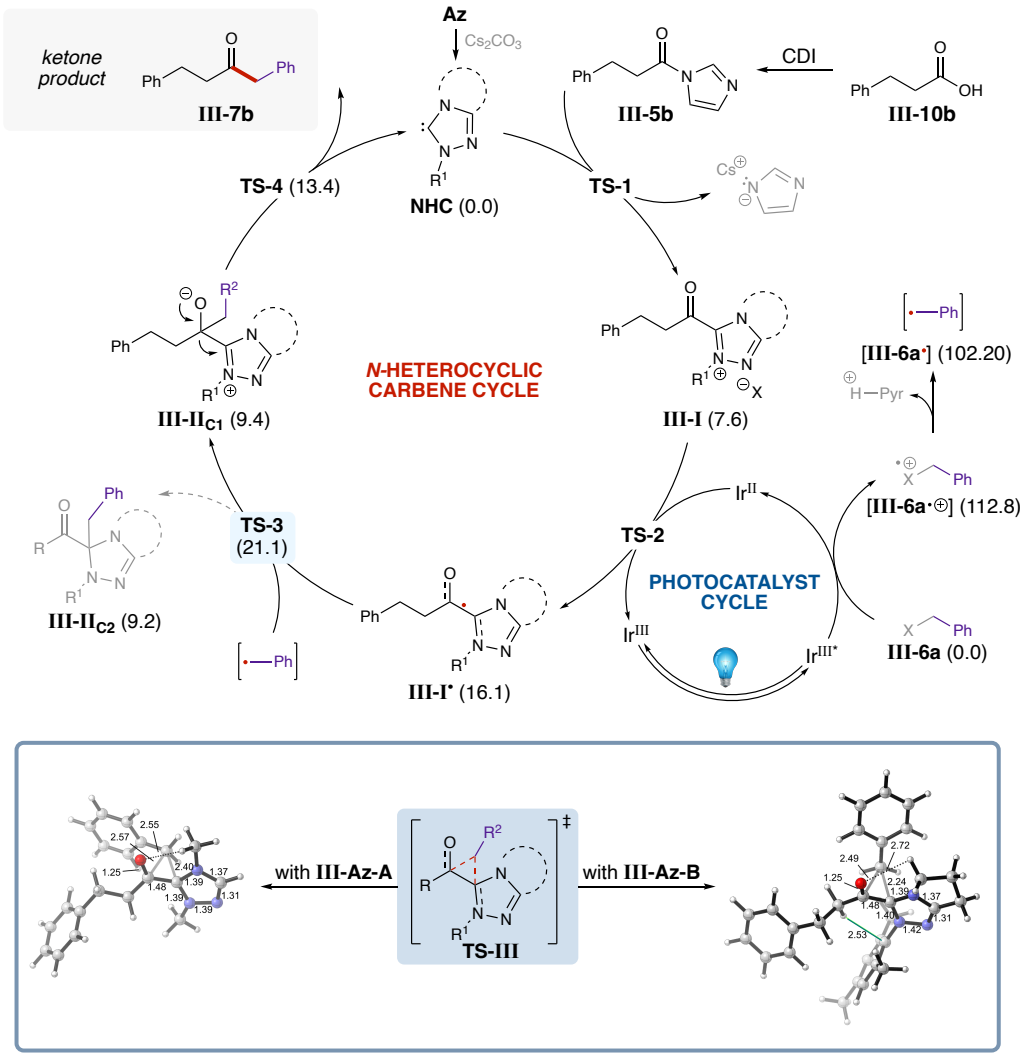

NHC	R	III-I	III-I•	TS-3	III-II$_{C1}$	III-II$_{C2}$	TS-4	III-7b
III-Az-A	hyrdocinnamyl	10.9	18.6	21.0	8.5	5.6	10.6	–16.3
III-Az-B	hyrdocinnamyl	7.6	16.1	21.1	9.4	9.2	13.4	–16.3

Figure 3-24. Proposed mechanism for the combined NHC and photoredox-catalyzed synthesis of ketones from carboxylic acids. The three-membered transition state is shown in the blue box, and the energies of each intermediate derived from the two NHC precursors are shown in the table.

3.10.6.1 Potential Energy Surface

The computed 3D- and 2D-potential energy surfaces (PES) around the three-membered transition structures for the aliphatic acyl azolium radicals **III-I•** of **III-Az-A** and **III-Az-B** with the benzyl radical. The **III-Az-A** PES revealed downhill energy paths leading to both C1- and C2-

coupling products (–1.0 and –0.3 kcal/mol, respectively), suggesting a non-selective reaction wherein considerable **III-II$_{C2}$** is formed. For **III-Az-B**, the PES features a downhill energy path to desired C1 (–1.9 kcal/mol). In contrast, an uphill barrier exists on the path to undesired C2 (0.4 kcal/mol), which translates to a preference of 2.3 kcal/mol for the C1 over C2, in line with our hypothesis that the mesityl group of **III-Az-B** will hinder coupling at the C2 center. These observations suggest a *greater likelihood* for efficient C1-coupling over inefficient C2-coupling using **III-Az-B** as the NHC precursor (**III-II$_{C1}$** and **III-II$_{C2}$**, ΔG = 9.4 and 9.2 kcal/mol, respectively).

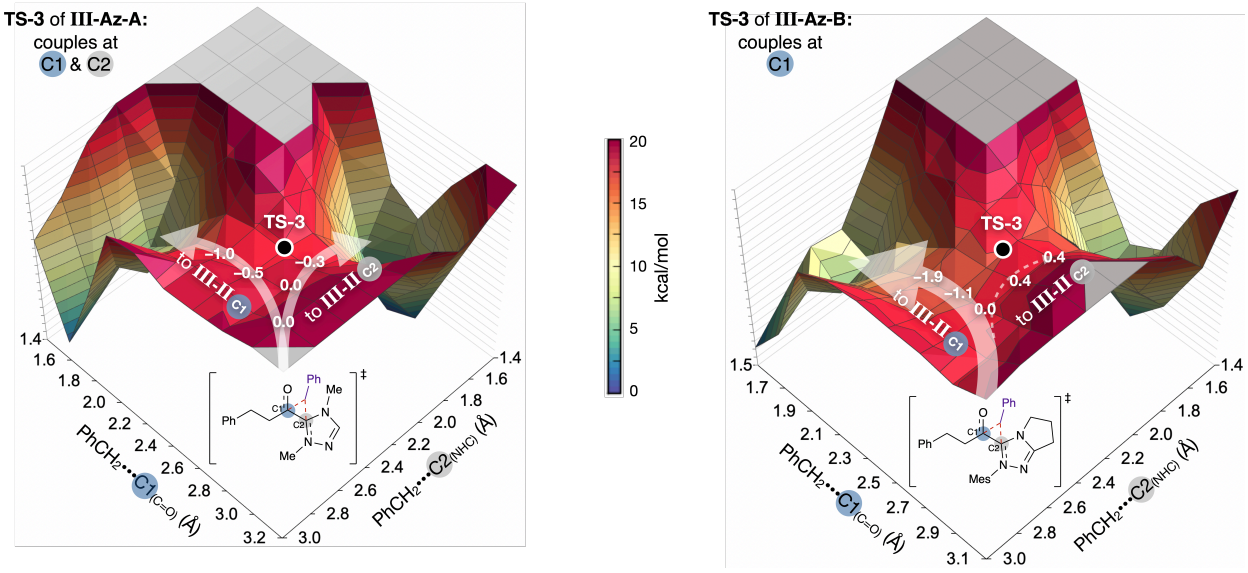

Figure 3-25. Three-dimensional potential energy surfaces with energies (in kcal/mol).

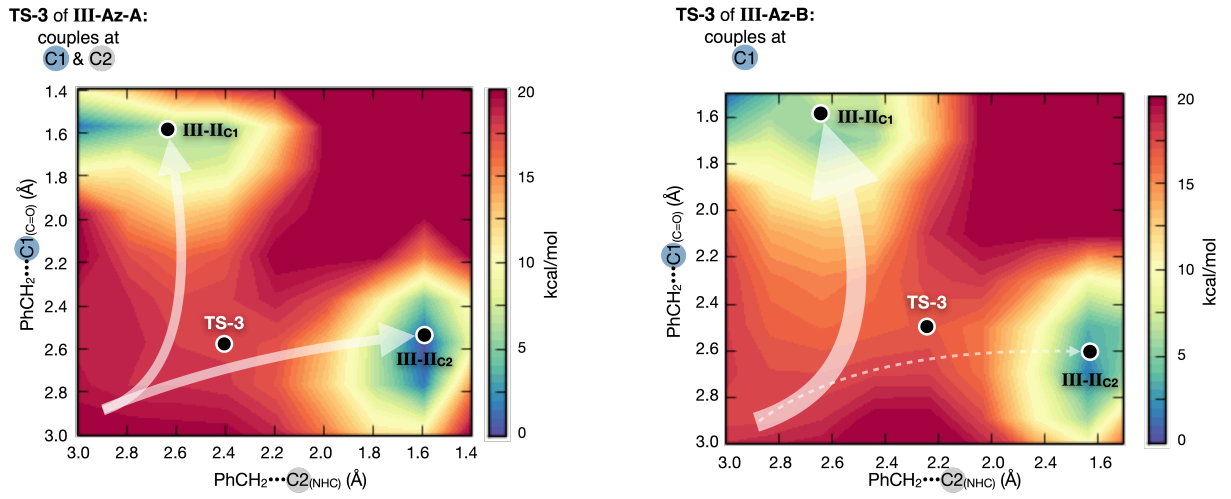

Figure 3-26. Two-dimensional potential energy surfaces.

3.10.7 Computed Structures, Electronic Energies, and Thermal Corrections as well as the Input Parameters

3.10.7.1 Benzyl Hantzsch ester (Bn-HE, ***III-6a****)*

Using Gaussian 16: ES64L-G16RevA.03 25-Dec-2016

==========

pbepbe/6-31g(d)/auto scf=(maxcycle=300,direct,vshift=200,tight,yqc)

density=current scrf=(solvent=ch3cn,smd) opt=(gdiis,maxcycle=250)

freq=noraman

#N Geom=AllCheck Guess=TCheck SCRF=Check GenChk RPBEPBE/6-31G(d)/Auto Freq

---

Pointgroup= C1 Stoichiometry= C18H21NO4 C1[X(C18H21NO4)] #Atoms= 44

Charge = 0 Multiplicity = 1

SCF Energy= -1052.98877496 Predicted Change= -6.857973D-10

==========

Optimization completed. [433]

Item	Max Val.	Criteria	Pass?	RMS Val.	Criteria	Pass?
Force	0.00000	0.00045	[YES]	0.00000	0.00030	[YES]
Displ	0.00063	0.00180	[YES]	0.00063	0.00180	[YES]

Atomic Type	Coordinates (Angstroms) X	Y	Z
C	0.550856	-0.127764	-0.041141
C	0.018267	1.261532	-0.389202
C	0.647654	2.355579	0.161419
C	2.652061	1.028825	0.644385
C	2.068476	-0.094865	0.101162
H	2.310073	2.980235	1.209017
N	1.854990	2.150709	0.821812
C	0.237234	3.800226	0.098923
H	-0.774394	3.901672	-0.310854
H	0.274072	4.242769	1.111844
H	0.942390	4.375435	-0.530358
C	4.090894	1.221728	1.036540
H	4.697123	1.526843	0.163801
H	4.175268	2.017407	1.797117
H	4.528444	0.291732	1.422850
C	-1.175308	1.400270	-1.245329
O	-1.869337	2.408123	-1.422984
O	-1.459844	0.220647	-1.886208
C	2.871850	-1.278157	-0.229024
O	4.101012	-1.392497	-0.158210
O	2.076278	-2.317512	-0.655372
C	-2.646757	0.247986	-2.702603
H	-2.551468	0.984215	-3.518331
H	-2.739529	-0.766755	-3.116210
H	-3.534496	0.494135	-2.096476
C	2.795904	-3.513534	-1.015625
H	2.027587	-4.231061	-1.338589

H	3.503245	-3.317426	-1.838823
H	3.352408	-3.915084	-0.152327
C	-0.088509	-0.685768	1.282614
H	0.421444	-1.641801	1.503153
H	0.150838	0.013173	2.104723
H	0.285267	-0.824375	-0.847988
C	-1.582841	-0.911388	1.212617
C	-2.492613	0.049269	1.699476
C	-2.103446	-2.085216	0.627315
C	-3.879361	-0.151059	1.599414
H	-2.107994	0.962913	2.168209
C	-3.486432	-2.290616	0.525179
H	-1.410095	-2.845865	0.247390
C	-4.381447	-1.321575	1.010243
H	-4.567862	0.607960	1.987595
H	-3.868492	-3.211751	0.070803
H	-5.462523	-1.482255	0.934784

Statistical Thermodynamic Analysis

Temperature= 298.150 Kelvin Pressure= 1.00000 Atm

==========

SCF Energy= -1052.98877496 Predicted Change= -6.857973D-10

Zero-point correction (ZPE)= -1052.6354 0.35329

Internal Energy (U)= -1052.6116 0.37714

Enthalpy (H)= -1052.6106 0.37808

Gibbs Free Energy (G)= -1052.6909 0.29786

Entropy (S)= 0.00026905

Frequencies -- 20.8982 30.0705 47.0096

*3.10.7.2 Bn-HE radical-cation (intermediate [**III-6a**$^{\bullet+}$])*

Using Gaussian 16: ES64L-G16RevA.03 25-Dec-2016

==========

pbepbe/6-31g(d)/auto scf=(maxcycle=300,direct,vshift=200,tight,yqc)

density=current scrf=(solvent=ch3cn,smd) opt=(gdiis,maxcycle=250)

freq=noraman guess=(mix,always)

#N Geom=AllCheck Guess=TCheck SCRF=Check GenChk UPBEPBE/6-31G(d)/Auto Freq

---

Pointgroup= C1 Stoichiometry= C18H21NO4(1+,2) C1[X(C18H21NO4)] #Atoms= 44

Charge = 1 Multiplicity = 2

SCF Energy= -1052.81010814 Predicted Change= -2.345371D-09

==========

Optimization completed. (Found 2 times)

Item	Max Val.	Criteria	Pass?	RMS Val.	Criteria	Pass?
Force	0.00000	0.00045	[YES]	0.00000	0.00030	[YES]
Displ	0.00111	0.00180	[YES]	0.00111	0.00180	[YES]

Atomic Type	Coordinates (Angstroms) X	Y	Z
C	-0.605296	-0.038388	0.178597
C	-0.080378	1.345556	0.355831
C	-0.800503	2.425625	-0.146628
C	-2.774377	0.993286	-0.495828
C	-2.085578	-0.112663	-0.009357

H	-2.581236	2.967209	-1.001924
N	-2.065946	2.167015	-0.616949
C	-0.360307	3.856822	-0.203238
H	0.534695	3.960056	-0.837680
H	-1.161043	4.502268	-0.598508
H	-0.076879	4.212682	0.800603
C	-4.220355	1.072166	-0.879414
H	-4.858148	1.049494	0.021098
H	-4.424716	2.005457	-1.428761
H	-4.510457	0.210083	-1.497441
C	1.244341	1.564814	0.994883
O	1.914580	2.593089	0.918276
O	1.616181	0.472067	1.709808
C	-2.804533	-1.386455	0.254399
O	-4.020921	-1.547736	0.165126
O	-1.944852	-2.363853	0.642209
C	2.915713	0.567869	2.340705
H	2.919811	1.378758	3.087233
H	3.073242	-0.404235	2.827169
H	3.696370	0.756793	1.586883
C	-2.565552	-3.638819	0.944774
H	-1.736129	-4.303924	1.220508
H	-3.271036	-3.531300	1.784160
H	-3.097353	-4.027115	0.061689
C	0.071916	-0.708447	-1.170203
H	-0.473610	-1.656275	-1.298991
H	-0.170266	-0.031899	-2.004974
H	-0.276712	-0.697830	0.995453
C	1.543398	-0.958885	-1.061812
C	2.478747	-0.053387	-1.610672
C	2.020654	-2.124129	-0.417611
C	3.853190	-0.314349	-1.533670
H	2.119884	0.852599	-2.112467
C	3.393157	-2.383410	-0.336508
H	1.301448	-2.829510	0.014764
C	4.313977	-1.478258	-0.893648
H	4.567227	0.388992	-1.974888
H	3.748804	-3.293629	0.157693
H	5.388528	-1.680008	-0.829942

Statistical Thermodynamic Analysis

Temperature= 298.150 Kelvin Pressure= 1.00000 Atm

==========

SCF Energy= -1052.81010814 Predicted Change= -2.345371D-09

Zero-point correction (ZPE)= -1052.4565 0.35350

Internal Energy (U)= -1052.4329 0.37711

Enthalpy (H)= -1052.4320 0.37806

Gibbs Free Energy (G)= -1052.5111 0.29894

Entropy (S)= 0.00026537

Frequencies -- 28.7012 39.0728 43.6617

3.10.7.3 Hantzsch pyridine (HP)

Using Gaussian 16: ES64L-G16RevA.03 25-Dec-2016

==========

pbepbe/6-31g(d)/auto scf=(maxcycle=300,direct,vshift=200,tight,yqc)

density=current scrf=(solvent=ch3cn,smd) opt=(gdiis,maxcycle=250)

freq=noraman

#N Geom=AllCheck Guess=TCheck SCRF=Check GenChk RPBEPBE/6-31G(d)/Auto Freq

---

Pointgroup= C1 Stoichiometry= C11H14NO4(1+) C1[X(C11H14NO4)] #Atoms= 30

Charge = 1 Multiplicity = 1

SCF Energy= -782.238765413 Predicted Change= -1.719735D-08

==========

Optimization completed. [433]

Item	Max Val.	Criteria	Pass?	RMS Val.	Criteria	Pass?
Force	0.00003	0.00045	[YES]	0.00000	0.00030	[YES]
Displ	0.00211	0.00180	[NO]	0.00211	0.00180	[YES]

Atomic Type	Coordinates (Angstroms) X	Y	Z
C	-0.000061	-0.434851	-0.000053
C	1.229355	0.242080	-0.005296
C	1.223360	1.651562	-0.005845
C	-1.223345	1.651633	0.005848
C	-1.229446	0.242148	0.005241
H	0.000052	3.281747	0.000052
N	0.000028	2.252672	0.000015
C	2.413857	2.551702	-0.010264
H	3.008751	2.389749	-0.924429
H	2.114273	3.609931	0.045084
H	3.075539	2.314230	0.838393
C	-2.413729	2.551932	0.010406
H	-3.007930	2.390764	0.925175
H	-2.114010	3.610074	-0.045900
H	-3.076048	2.313909	-0.837579
C	2.525638	-0.515510	-0.019617
O	3.633544	-0.000374	-0.123139
O	2.310203	-1.843678	0.094560
C	-2.525724	-0.515491	0.019519
O	-3.633702	-0.000467	0.122808
O	-2.310173	-1.843661	-0.094412
C	3.508126	-2.662809	0.076783
H	4.162195	-2.401009	0.923400
H	3.149941	-3.696663	0.170234
H	4.051797	-2.524360	-0.870957
C	-3.508037	-2.662880	-0.076666
H	-3.149738	-3.696740	-0.169616
H	-4.052007	-2.524108	0.870854
H	-4.161869	-2.401457	-0.923583
H	-0.000079	-1.526432	-0.000100

Statistical Thermodynamic Analysis

Temperature= 298.150 Kelvin Pressure= 1.00000 Atm

==========

SCF Energy= -782.238765413 Predicted Change= -1.719735D-08

Zero-point correction (ZPE)= -782.0018 0.23692

Internal Energy (U)= -781.9847 0.25405

Enthalpy (H)= -781.9837 0.25500

Gibbs Free Energy (G)= -782.0477 0.19097

Entropy (S)= 0.00021476

Frequencies -- 23.2970 32.5421 76.3780

3.10.7.4 Cs-HE

Using Gaussian 16: ES64L-G16RevA.03 25-Dec-2016

==========

pbepbe/genecp/auto scf=(maxcycle=300,direct,vshift=200,tight,yqc)

density=current scrf=(solvent=ch3cn,smd) opt=(gdiis,maxcycle=250)

freq=noraman 6d 10f

#N Geom=AllCheck Guess=TCheck SCRF=Check GenChk RPBEPBE/GenECP/Auto Freq

---

Pointgroup= C1 Stoichiometry= C11H13CsNO4(1+) C1[X(C11H13CsNO4)] #Atoms= 30

Charge = 1 Multiplicity = 1

SCF Energy= -801.627338546 Predicted Change= -4.060192D-09

==========

Optimization completed on the basis of negligible forces. (Found 2 times)

Item	Max Val.	Criteria	Pass?	RMS Val.	Criteria	Pass?
Force	0.00000	0.00045	[YES]	0.00000	0.00030	[YES]
Displ	0.00278	0.00180	[NO]	0.00278	0.00180	[YES]

Atomic Type	Coordinates (Angstroms) X	Y	Z
C	2.421919	-0.000008	0.000012
C	1.730949	1.219952	-0.013528
C	0.309366	1.177968	0.003622
C	0.309343	-1.177939	-0.003580
C	1.730921	-1.219953	0.013573
N	-0.354321	0.000021	0.000011
C	-0.556454	2.408885	0.036437
H	-0.503496	2.954939	-0.921779
H	-1.600723	2.113923	0.223299
H	-0.226106	3.118105	0.812611
C	-0.556503	-2.408839	-0.036372
H	-0.503951	-2.954574	0.922054
H	-1.600696	-2.113900	-0.223699
H	-0.225879	-3.118324	-0.812179
C	2.482833	2.510678	-0.057192
O	1.996417	3.610270	-0.309984
O	3.802300	2.327022	0.215992
C	2.482781	-2.510692	0.057283
O	1.996386	-3.610225	0.310376
O	3.802189	-2.327112	-0.216226
C	4.607467	3.528309	0.157844
H	4.248602	4.270942	0.888567
H	5.627566	3.205594	0.408116
H	4.579842	3.965785	-0.853367
C	4.607353	-3.528401	-0.158028

H	5.627397	-3.205751	-0.408608
H	4.579962	-3.965672	0.853278
H	4.248303	-4.271175	-0.888516
H	3.513644	-0.000022	0.000005
Cs	-4.281498	0.000011	-0.000028

Statistical Thermodynamic Analysis

Temperature= 298.150 Kelvin Pressure= 1.00000 Atm

==========

SCF Energy= -801.627338546 Predicted Change= -4.060192D-09

Zero-point correction (ZPE)= -801.4030 0.22425

Internal Energy (U)= -801.3838 0.24350

Enthalpy (H)= -801.3828 0.24445

Gibbs Free Energy (G)= -801.4544 0.17286

Entropy (S)= 0.00024011

Frequencies -- 27.8675 29.7462 53.8421

3.10.7.5 Neutral-HE

Using Gaussian 16: ES64L-G16RevA.03 25-Dec-2016

==========

pbepbe/6-31g(d)/auto scf=(maxcycle=300,direct,vshift=200,tight,yqc)

density=current scrf=(solvent=ch3cn,smd) opt=(gdiis,maxcycle=250)

freq=noraman

#N Geom=AllCheck Guess=TCheck SCRF=Check GenChk RPBEPBE/6-31G(d)/Auto Freq

---

Pointgroup= C1 Stoichiometry= C11H13NO4 C1[X(C11H13NO4)] #Atoms= 29

Charge = 0 Multiplicity = 1

SCF Energy= -781.783066738 Predicted Change= -4.691412D-10

==========

Optimization completed. (Found 2 times)

Item	Max Val.	Criteria	Pass?	RMS Val.	Criteria	Pass?
Force	0.00000	0.00045	[YES]	0.00000	0.00030	[YES]
Displ	0.00101	0.00180	[YES]	0.00101	0.00180	[YES]

Atomic Coordinates (Angstroms)

Type	X	Y	Z
C	0.000000	-0.423010	-0.000047
C	1.221538	0.266293	-0.000051
C	1.178128	1.688561	-0.000021
C	-1.178128	1.688560	0.000098
C	-1.221538	0.266293	0.000008
N	-0.000000	2.350921	0.000075
C	2.400069	2.567188	-0.000088
H	3.034849	2.373969	-0.881373
H	2.080286	3.620614	0.000131
H	3.035196	2.373680	0.880879
C	-2.400069	2.567188	0.000246
H	-3.034931	2.373783	0.881433
H	-2.080286	3.620613	0.000276
H	-3.035115	2.373863	-0.880820
C	2.512647	-0.485645	-0.000104
O	3.633226	0.018861	-0.000498
O	2.307716	-1.831017	0.000353

C	-2.512646	-0.485645	-0.000030
O	-3.633225	0.018862	-0.000003
O	-2.307716	-1.831018	-0.000108
C	3.514314	-2.628949	0.000309
H	4.116970	-2.422174	0.899517
H	3.171351	-3.672892	0.000686
H	4.116570	-2.422690	-0.899283
C	-3.514314	-2.628949	-0.000188
H	-3.171351	-3.672892	-0.000194
H	-4.116819	-2.422453	0.899183
H	-4.116721	-2.422412	-0.899617
H	0.000000	-1.514274	-0.000094

Statistical Thermodynamic Analysis

Temperature= 298.150 Kelvin Pressure= 1.00000 Atm

==========

SCF Energy= -781.783066738 Predicted Change= -4.691412D-10

Zero-point correction (ZPE)= -781.5597 0.22331

Internal Energy (U)= -781.5426 0.24042

Enthalpy (H)= -781.5416 0.24136

Gibbs Free Energy (G)= -781.6073 0.17568

Entropy (S)= 0.00022029

Frequencies -- 12.6052 13.8509 45.4035

3.10.7.6 Benzyl Radical

Using Gaussian 16: ES64L-G16RevA.03 25-Dec-2016

==========

pbepbe/6-31g(d)/auto scf=(maxcycle=300,direct,vshift=200,tight,yqc)

density=current scrf=(solvent=ch3cn,smd) opt=(gdiis,maxcycle=250)

freq=noraman

#N Geom=AllCheck Guess=TCheck SCRF=Check GenChk UPBEPBE/6-31G(d)/Auto Freq

---

Pointgroup= C1 Stoichiometry= C7H7(2) C1[X(C7H7)] #Atoms= 14

Charge = 0 Multiplicity = 2

SCF Energy= -270.562485113 Predicted Change= -4.400117D-11

==========

Optimization completed. (Found 2 times)

Item	Max Val.	Criteria	Pass?	RMS Val.	Criteria	Pass?
Force	0.00000	0.00045	[YES]	0.00000	0.00030	[YES]
Displ	0.00001	0.00180	[YES]	0.00001	0.00180	[YES]

Atomic Type	Coordinates (Angstroms) X	Y	Z
C	2.412005	-0.000000	0.000000
H	2.976715	-0.937572	0.000000
H	2.976715	0.937572	-0.000000
C	1.001018	-0.000000	0.000000
C	0.253990	1.225493	-0.000000
C	0.253990	-1.225493	-0.000000
C	-1.139314	1.218706	0.000000
H	0.801976	2.174977	-0.000000
C	-1.139314	-1.218706	0.000000
H	0.801976	-2.174977	-0.000000
C	-1.848993	0.000000	0.000000
H	-1.686853	2.167789	0.000000
H	-1.686853	-2.167788	0.000000

H -2.943956 0.000000 0.000000

Statistical Thermodynamic Analysis

Temperature= 298.150 Kelvin Pressure= 1.00000 Atm

==========

SCF Energy= -270.562485113 Predicted Change= -4.400117D-11

Zero-point correction (ZPE)= -270.4503 0.11208

Internal Energy (U)= -270.4445 0.11793

Enthalpy (H)= -270.4436 0.11887

Gibbs Free Energy (G)= -270.4801 0.08229

Entropy (S)= 0.00012272

Frequencies -- 192.1465 338.1702 377.1921

3.10.7.7 Aliphatic Acyl Imidazole (Hydrocinnamyl Acyl Imidazole)

Using Gaussian 16: ES64L-G16RevA.03 25-Dec-2016

==========

pbepbe/6-31g(d)/auto scf=(maxcycle=300,direct,vshift=200,tight,yqc)

density=current scrf=(solvent=ch3cn,smd) opt=(gdiis,maxcycle=250)

freq=noraman

#N Geom=AllCheck Guess=TCheck SCRF=Check GenChk RPBEPBE/6-31G(d)/Auto Freq

---

Pointgroup= C1 Stoichiometry= C12H12N2O C1[X(C12H12N2O)] #Atoms= 27

Charge = 0 Multiplicity = 1

SCF Energy= -648.467270601 Predicted Change= -3.160547D-09

==========

Optimization completed. (Found 2 times)

Item	Max Val.	Criteria	Pass?	RMS Val.	Criteria	Pass?
Force	0.00002	0.00045	[YES]	0.00000	0.00030	[YES]
Displ	0.00084	0.00180	[YES]	0.00084	0.00180	[YES]

Atomic Type	Coordinates (Angstroms) X	Y	Z
C	1.572423	-0.867909	-0.037692
O	1.740498	-2.079873	-0.092661
N	2.714188	-0.005114	0.002345
C	4.030765	-0.447328	-0.008753
C	2.764324	1.391212	0.059918
H	4.265419	-1.509560	-0.051083
C	4.100424	1.706836	0.080105
H	1.865562	2.002749	0.078867
H	4.552987	2.698372	0.122993
N	4.886728	0.554699	0.037286
C	0.223847	-0.181417	-0.004991
H	0.169438	0.531828	-0.849997
H	0.165524	0.436013	0.912140
C	-0.944350	-1.182327	-0.063494
H	-0.854430	-1.781982	-0.986225
H	-0.860855	-1.882035	0.786172
C	-2.286172	-0.477180	-0.028512
C	-2.887900	-0.013520	-1.216067
C	-2.948043	-0.243765	1.193729
C	-4.115378	0.665313	-1.184317
H	-2.388816	-0.192802	-2.176291
C	-4.176233	0.434193	1.230273
H	-2.495888	-0.603704	2.125990

C	-4.763615	0.892362	0.040351
H	-4.568927	1.013797	-2.118868
H	-4.677317	0.601121	2.190283
H	-5.723653	1.419280	0.066591

Statistical Thermodynamic Analysis

Temperature= 298.150 Kelvin Pressure= 1.00000 Atm

==========

SCF Energy= -648.467270601 Predicted Change= -3.160547D-09

Zero-point correction (ZPE)= -648.2541 0.21309

Internal Energy (U)= -648.2411 0.22615

Enthalpy (H)= -648.2401 0.22710

Gibbs Free Energy (G)= -648.2964 0.17079

Entropy (S)= 0.00018885

Frequencies -- 24.9497 33.7785 51.1490

3.10.7.8 Imidazole

Using Gaussian 16: ES64L-G16RevA.03 25-Dec-2016

==========

pbepbe/6-31g(d)/auto scf=(maxcycle=300,direct,vshift=200,tight,yqc)

density=current scrf=(solvent=ch3cn,smd) opt=(gdiis,maxcycle=250)

freq=noraman

#N Geom=AllCheck Guess=TCheck SCRF=Check GenChk RPBEPBE/6-31G(d)/Auto Freq

---

Pointgroup= C1 Stoichiometry= C3H4N2 C1[X(C3H4N2)] #Atoms= 9

Charge = 0 Multiplicity = 1

SCF Energy= -225.965153602 Predicted Change= -8.884589D-08

==========

Optimization completed. (Found 2 times)

Item	Max Val.	Criteria	Pass?	RMS Val.	Criteria	Pass?
Force	0.00004	0.00045	[YES]	0.00001	0.00030	[YES]
Displ	0.00104	0.00180	[YES]	0.00104	0.00180	[YES]

Atomic Type	Coordinates (Angstroms) X	Y	Z
N	0.213220	-1.226543	-0.000065
C	-0.961882	-0.598936	0.000078
C	1.159865	-0.214064	0.000145
H	-1.944511	-1.069962	0.000050
C	0.548882	1.026871	-0.000183
H	2.228061	-0.436461	-0.000459
H	0.931503	2.045828	0.000710
N	-0.805233	0.758472	0.000090
H	-1.552151	1.453866	-0.000713

Statistical Thermodynamic Analysis
Temperature= 298.150 Kelvin Pressure= 1.00000 Atm

==========

SCF Energy= -225.965153602 Predicted Change= -8.884589D-08
Zero-point correction (ZPE)= -225.8956 0.06949
Internal Energy (U)= -225.8918 0.07331
Enthalpy (H)= -225.8908 0.07426
Gibbs Free Energy (G)= -225.9219 0.04318
Entropy (S)= 0.00010422

Frequencies -- 537.6491 633.5015 669.6671

3.10.7.9 Imidazolium Anion

Using Gaussian 16: ES64L-G16RevA.03 25-Dec-2016

==========

pbepbe/6-31g(d)/auto scf=(maxcycle=300,direct,vshift=200,tight,yqc)

density=current scrf=(solvent=ch3cn,smd) opt=(gdiis,maxcycle=250)

freq=noraman

#N Geom=AllCheck Guess=TCheck SCRF=Check GenChk RPBEPBE/6-31G(d)/Auto Freq

---

Pointgroup= C1 Stoichiometry= C3H3N2(1-) C1[X(C3H3N2)] #Atoms= 8

Charge = -1 Multiplicity = 1

SCF Energy= -225.466352877 Predicted Change= -4.223013D-07

==========

Optimization completed. (Found 2 times)

Item	Max Val.	Criteria	Pass?	RMS Val.	Criteria	Pass?
Force	0.00017	0.00045	[YES]	0.00005	0.00030	[YES]
Displ	0.00130	0.00180	[YES]	0.00130	0.00180	[YES]

Atomic Type	Coordinates (Angstroms) X	Y	Z

N	0.393746	1.157863	0.000287
C	1.109229	0.001777	-0.000126
C	-0.909104	0.697295	-0.000489
H	2.206377	0.003707	-0.001037
C	-0.906489	-0.700304	0.000329
H	-1.757510	1.390724	0.000663
H	-1.751985	-1.397332	-0.001206
N	0.397869	-1.156393	0.000185

Statistical Thermodynamic Analysis

Temperature= 298.150 Kelvin Pressure= 1.00000 Atm

SCF Energy= -225.466352877 Predicted Change= -4.223013D-07

Zero-point correction (ZPE)= -225.4101 0.05624

Internal Energy (U)= -225.4064 0.05986

Enthalpy (H)= -225.4055 0.06080

Gibbs Free Energy (G)= -225.4362 0.03009

Entropy (S)= 0.00010302

Frequencies -- 641.8769 687.7108 724.9630

3.10.7.10 Cs-Imidazolium

Using Gaussian 16: ES64L-G16RevA.03 25-Dec-2016

pbepbe/genecp/auto scf=(maxcycle=300,direct,vshift=200,tight,yqc)

density=current scrf=(solvent=ch3cn,smd) opt=(gdiis,maxcycle=250)

freq=noraman 6d 10f

#N Geom=AllCheck Guess=TCheck SCRF=Check GenChk RPBEPBE/GenECP/Auto Freq

---

Pointgroup= C1 Stoichiometry= C3H3CsN2 C1[X(C3H3CsN2)] #Atoms= 9

Charge = 0 Multiplicity = 1

SCF Energy= -245.318511806 Predicted Change= -3.535592D-07

==========

Optimization completed. (Found 1 times)

Item	Max Val.	Criteria	Pass?	RMS Val.	Criteria	Pass?
Force	0.00026	0.00045	[YES]	0.00006	0.00030	[YES]
Displ	0.00706	0.00180	[NO]	0.00706	0.00180	[NO]

Atomic Type	Coordinates (Angstroms) X	Y	Z
N	1.531401	0.004838	0.000442
C	2.386182	-1.054302	0.000122
C	2.393421	1.086498	0.000222
H	2.021543	-2.088582	0.000222
C	3.710471	0.622069	-0.000308
H	2.015400	2.114398	0.000402
H	4.646821	1.190369	-0.000648
N	3.710272	-0.759691	-0.000168
Cs	-1.751199	0.002585	-0.000038

Statistical Thermodynamic Analysis

Temperature= 298.150 Kelvin Pressure= 1.00000 Atm

==========

SCF Energy= -245.318511806 Predicted Change= -3.535592D-07

Zero-point correction (ZPE)= -245.2618 0.05661

Internal Energy (U)= -245.2557 0.06276

Enthalpy (H)= -245.2548 0.06371

Gibbs Free Energy (G)= -245.2970 0.02144

Entropy (S)= 0.00014177

Frequencies -- 18.3093 44.2638 73.9989

*3.10.7.11 Cs-Dimethyl-Triazolium (**Cs-III-Az-A**)*

Using Gaussian 16: ES64L-G16RevA.03 25-Dec-2016

==========

pbepbe/genecp/auto scf=(maxcycle=300,direct,vshift=200,tight,yqc)

density=current scrf=(solvent=ch3cn,smd) opt=(gdiis,maxcycle=250)

freq=noraman 6d 10f

#N Geom=AllCheck Guess=TCheck SCRF=Check GenChk RPBEPBE/GenECP/Auto Freq

---

Pointgroup= C1 Stoichiometry= C4H7CsN3(1+) C1[X(C4H7CsN3)] #Atoms= 15

Charge = 1 Multiplicity = 1

SCF Energy= -340.313521946 Predicted Change= -7.029789D-08

==========

Optimization completed. (Found 1 times)

Item	Max Val.	Criteria	Pass?	RMS Val.	Criteria	Pass?
Force	0.00002	0.00045	[YES]	0.00000	0.00030	[YES]
Displ	0.01228	0.00180	[NO]	0.01228	0.00180	[NO]

Atomic Coordinates (Angstroms)

Type	X	Y	Z
C	-1.690577	-0.005881	-0.000232
C	-3.870029	0.608598	-0.000561
N	-2.563797	-1.045052	-0.000285
H	-4.741144	1.262397	-0.000706
N	-3.911444	-0.706868	-0.000496
N	-2.570758	1.060870	-0.000409
C	-2.229324	-2.462662	-0.000242
H	-1.135257	-2.559363	0.000298
H	-2.645745	-2.947195	0.897826
H	-2.644843	-2.947069	-0.898801
C	-2.172066	2.467509	-0.000390
H	-3.074634	3.095728	-0.000750
H	-1.576210	2.691136	0.898403
H	-1.575598	2.690979	-0.898813
Cs	2.554316	-0.001721	0.000353

Statistical Thermodynamic Analysis

Temperature= 298.150 Kelvin Pressure= 1.00000 Atm

==========

SCF Energy= -340.313521946 Predicted Change= -7.029789D-08

Zero-point correction (ZPE)= -340.2006 0.11287

Internal Energy (U)= -340.1909 0.12259

Enthalpy (H)= -340.1899 0.12353

Gibbs Free Energy (G)= -340.2427 0.07077

Entropy (S)= 0.00017699

Frequencies -- 10.5461 16.8647 30.1380

*3.10.7.12 Cs-5,5-Mes-triazolium (**Cs-III-Az-B**)*

Using Gaussian 16: ES64L-G16RevA.03 25-Dec-2016

==========

pbepbe/genecp/auto scf=(maxcycle=300,direct,vshift=200,tight,yqc)

density=current scrf=(solvent=ch3cn,smd) opt=(gdiis,maxcycle=250)

freq=noraman 6d 10f

#N Geom=AllCheck Guess=TCheck SCRF=Check GenChk RPBEPBE/GenECP/Auto Freq

---

Pointgroup= C1 Stoichiometry= C14H17CsN3(1+) C1[X(C14H17CsN3)] #Atoms= 35

Charge = 1 Multiplicity = 1

SCF Energy= -726.930594031 Predicted Change= -9.407375D-09

==========

Optimization completed. (Found 1 times)

Item Max Val. Criteria Pass? RMS Val. Criteria Pass?

Force 0.00000 || 0.00045 [YES] 0.00000 || 0.00030 [YES]

Displ 0.00443 || 0.00180 [NO] 0.00443 || 0.00180 [YES]

Atomic Type	Coordinates (Angstroms) X	Y	Z
C	-1.500335	-0.698726	-0.024317
C	-3.558462	0.268508	0.122582
N	-1.485336	0.665076	0.058255
N	-2.743660	1.300353	0.149340
N	-2.854187	-0.913280	0.017385
C	-3.730012	-2.093685	0.016066
H	-3.407406	-2.815463	-0.749353
H	-3.688317	-2.579834	1.006340
C	-5.119959	-1.468492	-0.276165
H	-5.310466	-1.493442	-1.362132
H	-5.927876	-2.021217	0.226106
C	-5.033054	0.013855	0.198960
H	-5.384045	0.127937	1.241238
H	-5.623218	0.700298	-0.428255
C	-0.311146	1.496988	0.035470
C	0.153568	1.989540	-1.203570
C	0.324796	1.815382	1.256083
C	1.303011	2.800189	-1.198578
C	1.470461	2.628932	1.206918
C	1.978995	3.125578	-0.008296
H	1.674815	3.192608	-2.152932
H	1.973301	2.887852	2.146834
C	-0.560593	1.665342	-2.493396
H	-0.562119	0.578492	-2.694291
H	-1.618227	1.982991	-2.459417
H	-0.076444	2.170237	-3.344893
C	3.226408	3.978058	-0.033268
H	4.137647	3.349769	-0.036301
H	3.263736	4.612712	-0.934643
H	3.287796	4.629987	0.855101
C	-0.209068	1.308217	2.574155
H	-1.270336	1.582346	2.712097
H	-0.155295	0.206042	2.638146
H	0.367349	1.727023	3.414905
Cs	2.496249	-2.312391	-0.048896

Statistical Thermodynamic Analysis

Temperature= 298.150 Kelvin Pressure= 1.00000 Atm

==========

SCF Energy= -726.930594031 Predicted Change= -9.407375D-09

Zero-point correction (ZPE)= -726.6506 0.27990

Internal Energy (U)= -726.6315 0.29907

Enthalpy (H)= -726.6305 0.30002

Gibbs Free Energy (G)= -726.7055 0.22509

Entropy (S)= 0.00025131

Frequencies -- 9.4494 14.5851 18.4004

*3.10.7.12 Hydrocinnamyl Acyl Azolium Cation with **III-Az-A (III-I)***

Using Gaussian 16: ES64L-G16RevA.03 25-Dec-2016

==========

pbepbe/6-31g(d)/auto scf=(maxcycle=300,direct,vshift=200,tight,yqc)

density=current scrf=(solvent=ch3cn,smd) opt=(gdiis,maxcycle=250)

freq=noraman

#N Geom=AllCheck Guess=TCheck SCRF=Check GenChk RPBEPBE/6-31G(d)/Auto Freq

---

Pointgroup= C1 Stoichiometry= C13H16N3O(1+) C1[X(C13H16N3O)] #Atoms= 33

Charge = 1 Multiplicity = 1

SCF Energy= -743.448196702 Predicted Change= -6.050572D-09

==========

Optimization completed on the basis of negligible forces. (Found 2 times)

Item	Max Val.	Criteria	Pass?	RMS Val.	Criteria	Pass?
Force	0.00000	0.00045	[YES]	0.00000	0.00030	[YES]
Displ	0.00274	0.00180	[NO]	0.00274	0.00180	[YES]

Atomic Type	Coordinates (Angstroms) X	Y	Z
C	3.479978	-1.254990	-0.108496
C	2.685951	-0.204899	0.396618
C	1.277143	-0.471056	0.885155
C	0.260009	-0.491507	-0.290785
C	3.222967	1.097395	0.413826
C	4.520707	1.346107	-0.059401
C	5.301618	0.292500	-0.559282
C	4.777098	-1.010222	-0.581993
C	-1.113949	-0.918114	0.171121
O	-1.336665	-2.006124	0.698413
C	-2.304286	-0.011234	-0.037731
N	-3.578446	-0.460774	-0.227539
C	-4.369711	0.645837	-0.339865
N	-3.668660	1.759986	-0.208938
N	-2.389605	1.335576	-0.027388
C	-1.344598	2.340630	0.185868
C	-4.047982	-1.851432	-0.316375
H	3.076788	-2.274928	-0.123954
H	1.224709	-1.447563	1.397302
H	0.973946	0.303879	1.611176
H	0.577659	-1.258825	-1.022370
H	0.245407	0.475092	-0.817691
H	2.618368	1.923089	0.808269
H	4.923236	2.364681	-0.033433
H	6.315746	0.484014	-0.926403

H	5.382037	-1.839530	-0.964897
H	-5.442481	0.595187	-0.515862
H	-1.841706	3.234138	0.585353
H	-0.859468	2.577261	-0.773798
H	-0.611674	1.962216	0.910530
H	-5.078675	-1.824006	-0.693187
H	-4.015040	-2.313235	0.679883
H	-3.408227	-2.410074	-1.013123

Statistical Thermodynamic Analysis

Temperature= 298.150 Kelvin Pressure= 1.00000 Atm

==========

SCF Energy= -743.448196702 Predicted Change= -6.050572D-09

Zero-point correction (ZPE)= -743.1782 0.26992

Internal Energy (U)= -743.1619 0.28624

Enthalpy (H)= -743.1610 0.28718

Gibbs Free Energy (G)= -743.2247 0.22344

Entropy (S)= 0.00021378

Frequencies -- 13.9224 29.1879 33.4324

*3.10.7.13 Hydrocinnamyl Acyl Azolium Radical with **III-Az-A** (intermediate **III-I˙**)*

Using Gaussian 16: ES64L-G16RevA.03 25-Dec-2016

==========

pbepbe/6-31g(d)/auto scf=(maxcycle=300,direct,vshift=200,tight,yqc)

density=current scrf=(solvent=ch3cn,smd) opt=(gdiis,maxcycle=250)

freq=noraman guess=(mix,always)

#N Geom=AllCheck Guess=TCheck SCRF=Check GenChk UPBEPBE/6-31G(d)/Auto Freq

---

Pointgroup= C1 Stoichiometry= C13H16N3O(2) C1[X(C13H16N3O)] #Atoms= 33

Charge = 0 Multiplicity = 2

SCF Energy= -743.562650139 Predicted Change= -1.861257D-08

==========

Optimization completed. (Found 1 times)

Item	Max Val.	Criteria	Pass?	RMS Val.	Criteria	Pass?
Force	0.00000	0.00045	[YES]	0.00000	0.00030	[YES]
Displ	0.00654	0.00180	[NO]	0.00654	0.00180	[NO]

Atomic Type	Coordinates (Angstroms) X	Y	Z
C	3.474906	-1.236862	-0.151253
C	2.659689	-0.228092	0.405135
C	1.215747	-0.509913	0.761101
C	0.268415	-0.434891	-0.466883
C	3.216302	1.055396	0.581360
C	4.543962	1.325291	0.214389
C	5.342282	0.311642	-0.338680
C	4.802123	-0.972240	-0.519939
C	-1.137071	-0.924065	-0.124794
O	-1.296003	-2.162278	0.151366
C	-2.260283	-0.033744	-0.106127
N	-3.596641	-0.445019	0.027855
C	-4.375090	0.677107	-0.002484
N	-3.677140	1.783225	-0.128688
N	-2.363507	1.354313	-0.195857

C	-1.321800	2.365849	-0.193997
C	-4.113640	-1.808766	0.096128
H	3.061678	-2.243526	-0.290768
H	1.116424	-1.523955	1.189751
H	0.870292	0.207250	1.528689
H	0.658135	-1.121572	-1.243444
H	0.290980	0.578159	-0.899226
H	2.599793	1.851411	1.017119
H	4.956612	2.329260	0.364783
H	6.379766	0.518980	-0.622894
H	5.418721	-1.772176	-0.945186
H	-5.460589	0.636628	0.072394
H	-1.810531	3.325338	0.027184
H	-0.819046	2.436987	-1.174340
H	-0.574743	2.151691	0.588318
H	-5.209125	-1.742698	0.177461
H	-3.697296	-2.333950	0.966124
H	-3.845293	-2.367513	-0.813813

Statistical Thermodynamic Analysis

Temperature= 298.150 Kelvin Pressure= 1.00000 Atm

==========

SCF Energy= -743.562650139 Predicted Change= -1.861257D-08

Zero-point correction (ZPE)= -743.2954 0.26718

Internal Energy (U)= -743.2787 0.28393

Enthalpy (H)= -743.2777 0.28487

Gibbs Free Energy (G)= -743.3438 0.21878

Entropy (S)= 0.00022166

Frequencies -- 14.9465 21.1525 31.3952

*3.10.7.14 Benzyl Radical and Hydrocinnamyl Acyl Azolium Radical with III-Az-A transition structure (Intermediate **III-TS-3**)*

Using Gaussian 16: ES64L-G16RevA.03 25-Dec-2016

==========

pbepbe/6-31g(d)/auto scf=(maxcycle=300,direct,vshift=200,tight,yqc)

density=current scrf=(solvent=ch3cn,smd)

opt=(gdiis,maxcycle=250,ts,calcfc,noeigentest) freq=noraman

guess=(mix,always)

#N Geom=AllCheck Guess=TCheck SCRF=Check GenChk RPBEPBE/6-31G(d)/Auto Freq

---

Pointgroup= C1 Stoichiometry= C20H23N3O C1[X(C20H23N3O)] #Atoms= 47

Charge = 0 Multiplicity = 1

SCF Energy= -1014.14659399 Predicted Change= -6.726309D-11

==========

Optimization completed. (Found 2 times)

Item	Max Val.	Criteria	Pass?	RMS Val.	Criteria	Pass?
Force	0.00000	0.00045	[YES]	0.00000	0.00030	[YES]
Displ	0.00068	0.00180	[YES]	0.00068	0.00180	[YES]

Atomic Type	Coordinates (Angstroms) X	Y	Z
C	-3.241745	-2.179407	-0.955599

C	-2.790843	-0.875108	-0.662926
C	-1.442023	-0.393998	-1.159793
C	-0.299097	-0.820142	-0.217142
C	-3.616793	-0.045316	0.122389
C	-4.853798	-0.503112	0.602582
C	-5.288387	-1.804293	0.304853
C	-4.476919	-2.642001	-0.477531
C	1.078618	-0.472765	-0.786079
O	1.198733	0.022238	-1.927099
C	2.279683	-0.900452	-0.038305
N	2.390902	-1.715144	1.076328
N	3.556756	-0.933103	-0.596050
C	4.028107	-0.280568	-1.816615
C	1.448516	-1.881527	2.173352
H	-2.615958	-2.837196	-1.571562
H	-1.240734	-0.803317	-2.165199
H	-1.442523	0.705151	-1.258372
H	-0.342117	-1.916916	-0.066280
H	-0.443072	-0.364338	0.778400
H	-3.284833	0.973989	0.354978
H	-5.481592	0.160647	1.207694
H	-6.254986	-2.162212	0.676009
H	-4.809236	-3.657404	-0.721249
H	3.524137	-0.698913	-2.698508
H	5.112021	-0.455924	-1.885319
H	3.831781	0.801170	-1.773327
H	1.995744	-2.377479	2.986697
H	0.592759	-2.508290	1.879883
H	1.086136	-0.898747	2.520325
C	2.003939	1.338300	0.777750
H	2.904972	1.550781	0.190651
C	0.878850	2.209537	0.572807
H	2.201239	1.002682	1.803959
C	0.725955	2.958572	-0.635961
C	-0.164990	2.338178	1.541844
C	-0.387681	3.776847	-0.852936
H	1.508901	2.889514	-1.399576
C	-1.271804	3.163947	1.321208
H	-0.078932	1.785831	2.486420
C	-1.398805	3.890473	0.120456
H	-0.467001	4.341747	-1.789622
H	-2.043474	3.249961	2.095764
H	-2.264879	4.539121	-0.048787
H	5.427471	-1.762692	0.097075

C 4.361638 -1.626594 0.272250
N 3.703739 -2.100108 1.302168

Statistical Thermodynamic Analysis

Temperature= 298.150 Kelvin Pressure= 1.00000 Atm

==========

SCF Energy= -1014.14659399 Predicted Change= -6.726309D-11

Zero-point correction (ZPE)= -1013.7649 0.38162

Internal Energy (U)= -1013.7418 0.40471

Enthalpy (H)= -1013.7409 0.40565

Gibbs Free Energy (G)= -1013.8202 0.32639

Entropy (S)= 0.00026585

Frequencies -- -57.2429 12.1516 19.0047

*3.10.7.15 Benzyl Radical and Hydrocinnamyl Acyl Azolium Radical with **III-Az-A** (intermediate **III-II$_{C1}$**)*

Using Gaussian 16: ES64L-G16RevA.03 25-Dec-2016

==========

pbepbe/6-31g(d)/auto scf=(maxcycle=300,direct,vshift=200,tight,yqc)

density=current scrf=(solvent=ch3cn,smd) opt=(gdiis,maxcycle=250)

freq=noraman

#N Geom=AllCheck Guess=TCheck SCRF=Check GenChk RPBEPBE/6-31G(d)/Auto Freq

---

Pointgroup= C1 Stoichiometry= C20H23N3O C1[X(C20H23N3O)] #Atoms= 47

Charge = 0 Multiplicity = 1

SCF Energy= -1014.17011907 Predicted Change= -1.823276D-09

==========

Optimization completed. (Found 2 times)

Item	Max Val.	Criteria	Pass?	RMS Val.	Criteria	Pass?
Force	0.00000	0.00045	[YES]	0.00000	0.00030	[YES]
Displ	0.00130	0.00180	[YES]	0.00130	0.00180	[YES]

Atomic Type	Coordinates (Angstroms) X	Y	Z
C	-4.162472	-1.549281	0.488280
C	-3.642118	-0.250128	0.298925
C	-2.186878	0.047742	0.587941
C	-1.227100	-0.487175	-0.490930
C	-4.512532	0.746810	-0.187900
C	-5.855562	0.459298	-0.479232
C	-6.356469	-0.837706	-0.287756
C	-5.502835	-1.842126	0.198790
C	0.267568	-0.520457	0.018497
C	0.755317	0.985692	0.230271
N	1.498773	1.418425	1.295070
C	1.668400	2.772807	1.168019
N	1.084790	3.234920	0.083797
N	0.530517	2.113752	-0.490076
C	-0.194351	2.308908	-1.745866
C	2.074360	0.612354	2.383043
H	-3.504064	-2.338100	0.872992

H	-2.053292	1.140430	0.705599
H	-1.867282	-0.430026	1.533766
H	-1.363976	0.047984	-1.447303
H	-1.462420	-1.550460	-0.683178
H	-4.130597	1.764784	-0.335596
H	-6.512551	1.252374	-0.853991
H	-7.404593	-1.064325	-0.511865
H	-5.884780	-2.856892	0.358423
H	2.224020	3.371981	1.886648
H	0.026897	1.489265	-2.441940
H	0.159455	3.258723	-2.168940
H	-1.277729	2.368924	-1.558787
H	1.575516	-0.371008	2.305786
H	1.871276	1.122571	3.336811
H	3.161483	0.527552	2.228828
O	0.376128	-1.241048	1.128055
C	1.151544	-1.075181	-1.202042
H	0.997404	-0.472531	-2.116727
C	2.617340	-1.171321	-0.879106
H	0.730520	-2.080529	-1.388523
C	3.553454	-0.270282	-1.429658
C	3.085271	-2.141980	0.036358
C	4.912691	-0.333690	-1.083673
H	3.210151	0.488042	-2.144621
C	4.442509	-2.206073	0.386597
H	2.360633	-2.829400	0.482118
C	5.362685	-1.302837	-0.171952
H	5.621878	0.372684	-1.530055
H	4.785805	-2.967047	1.097106
H	6.423744	-1.358524	0.095827

Statistical Thermodynamic Analysis

Temperature= 298.150 Kelvin Pressure= 1.00000 Atm

==========

SCF Energy= -1014.17011907 Predicted Change= -1.823276D-09

Zero-point correction (ZPE)= -1013.7856 0.38450

Internal Energy (U)= -1013.7630 0.40710

Enthalpy (H)= -1013.7620 0.40804

Gibbs Free Energy (G)= -1013.8401 0.33000

Entropy (S)= 0.00026174

Frequencies -- 15.6557 27.7609 32.6105

*3.10.7.16 Benzyl Radical and Hydrocinnamyl Acyl Azolium Radical with **III-Az-A** (Intermediate **III-II$_{C2}$**)*

Using Gaussian 16: ES64L-G16RevA.03 25-Dec-2016

==========

pbepbe/6-31g(d)/auto scf=(maxcycle=300,direct,vshift=200,tight,yqc)

density=current scrf=(solvent=ch3cn,smd) opt=(gdiis,maxcycle=250)

freq=noraman

#N Geom=AllCheck Guess=TCheck SCRF=Check GenChk RPBEPBE/6-31G(d)/Auto Freq

---

Pointgroup= C1 Stoichiometry= C20H23N3O C1[X(C20H23N3O)] #Atoms= 47

Charge = 0 Multiplicity = 1

SCF Energy= -1014.17297418 Predicted Change= -8.606276D-10

==========

Optimization completed. (Found 2 times)

Item	Max Val.	Criteria	Pass?	RMS Val.	Criteria	Pass?
Force	0.00000	0.00045	[YES]	0.00000	0.00030	[YES]
Displ	0.00147	0.00180	[YES]	0.00147	0.00180	[YES]

Atomic Type	Coordinates (Angstroms) X	Y	Z
C	-4.475454	0.268272	-1.046777
C	-3.937073	-0.325903	0.114330
C	-3.200987	-1.650952	0.025192
C	-1.770961	-1.523743	-0.533442
C	-4.095195	0.347429	1.342091
C	-4.771352	1.575923	1.410171
C	-5.300894	2.155633	0.246871
C	-5.149473	1.496809	-0.984266
C	-0.771509	-0.950737	0.454923
O	-1.015412	-0.838108	1.655728
C	0.679652	-0.632944	-0.072198
N	1.475526	-1.867148	0.061463
C	2.092330	-2.109781	-1.145745
N	1.743260	-1.300687	-2.103576
N	0.687792	-0.522301	-1.550935
C	0.495325	0.770608	-2.185257
C	1.583394	-2.666223	1.266620
H	-4.369163	-0.244536	-2.010808
H	-3.157360	-2.124936	1.020991
H	-3.761189	-2.332975	-0.639407
H	-1.743429	-0.926890	-1.462995
H	-1.387685	-2.520237	-0.833196
H	-3.676175	-0.097788	2.251080
H	-4.885943	2.080134	2.376332
H	-5.831055	3.112926	0.298708
H	-5.563798	1.937725	-1.897906
H	2.810883	-2.923291	-1.257220
H	0.370270	0.603917	-3.268161
H	1.331475	1.480924	-2.035129
H	-0.432131	1.226313	-1.798683
H	0.653320	-3.226997	1.479720
H	1.815459	-2.039334	2.145364
H	2.402148	-3.389906	1.130371

C	1.247132	0.569889	0.770063
H	1.069795	0.294940	1.824875
C	2.695855	0.956481	0.564191
H	0.595004	1.438703	0.567257
C	3.753841	0.160985	1.057925
C	3.031414	2.167321	-0.080564
C	5.092434	0.542447	0.878421
H	3.531350	-0.759982	1.606105
C	4.367353	2.556300	-0.255458
H	2.228079	2.821403	-0.439757
C	5.406990	1.738838	0.215681
H	5.893150	-0.095498	1.269334
H	4.595395	3.503331	-0.757259
H	6.451930	2.037942	0.079263

Statistical Thermodynamic Analysis

Temperature= 298.150 Kelvin Pressure= 1.00000 Atm

==========

SCF Energy= -1014.17297418 Predicted Change= -8.606276D-10

Zero-point correction (ZPE)= -1013.7891 0.38379

Internal Energy (U)= -1013.7662 0.40675

Enthalpy (H)= -1013.7652 0.40769

Gibbs Free Energy (G)= -1013.8446 0.32828

Entropy (S)= 0.00026636

Frequencies -- 10.5731 14.9950 25.7699

*3.10.7.17 Benzyl Radical and Hydrocinnamyl Acyl Azolium Radical with **III-Az-A** transition structure (**III-TS-4**)*

Using Gaussian 16: ES64L-G16RevA.03 25-Dec-2016

==========

pbepbe/6-31g(d)/auto scf=(maxcycle=300,direct,vshift=200,tight,yqc)

density=current scrf=(solvent=ch3cn,smd)

opt=(gdiis,maxcycle=250,ts,calcfc,noeigentest) freq=noraman

#N Geom=AllCheck Guess=TCheck SCRF=Check GenChk RPBEPBE/6-31G(d)/Auto Freq

---

Pointgroup= C1 Stoichiometry= C20H23N3O C1[X(C20H23N3O)] #Atoms= 47

Charge = 0 Multiplicity = 1

SCF Energy= -1014.16363718 Predicted Change= -4.555326D-11

==========

Optimization completed. (Found 2 times)

Item	Max Val.	Criteria	Pass?	RMS Val.	Criteria	Pass?
Force	0.00000	0.00045	[YES]	0.00000	0.00030	[YES]
Displ	0.00024	0.00180	[YES]	0.00024	0.00180	[YES]

Atomic Type	Coordinates (Angstroms) X	Y	Z
C	-4.244774	-1.673999	0.454649
C	-3.579633	-0.432054	0.365731
C	-2.112782	-0.311183	0.721364

C	-1.180000	-0.813025	-0.395010
C	-4.314162	0.682290	-0.088937
C	-5.666629	0.563271	-0.446341
C	-6.312871	-0.679245	-0.354831
C	-5.595504	-1.798875	0.098285
C	0.298942	-0.926170	0.056428
C	0.773750	1.115000	0.099306
N	1.349941	1.676360	1.212581
C	1.263117	3.045921	1.124835
N	0.661891	3.415460	0.013959
N	0.377896	2.205683	-0.598979
C	-0.291007	2.249318	-1.894769
C	2.037794	0.946754	2.282457
H	-3.693732	-2.552544	0.812649
H	-1.872060	0.743989	0.949704
H	-1.880129	-0.898233	1.628511
H	-1.284818	-0.201019	-1.306570
H	-1.478034	-1.845170	-0.674680
H	-3.817694	1.658355	-0.157769
H	-6.217165	1.444951	-0.793435
H	-7.368873	-0.774658	-0.630358
H	-6.091955	-2.772443	0.180001
H	1.652938	3.724615	1.881657
H	-0.072272	1.322718	-2.442137
H	0.100645	3.110693	-2.455539
H	-1.380138	2.361712	-1.765253
H	1.672886	-0.090686	2.265659
H	1.814607	1.429249	3.245994
H	3.125495	0.967655	2.104487
O	0.518580	-1.395372	1.209164
C	1.235616	-1.346923	-1.122762
H	0.998346	-0.749975	-2.020818
C	2.706727	-1.271534	-0.806543
H	0.951551	-2.396843	-1.342237
C	3.530710	-0.294412	-1.402782
C	3.290869	-2.155580	0.127568
C	4.893975	-0.199759	-1.080844
H	3.096550	0.397419	-2.134833
C	4.652275	-2.062239	0.454200
H	2.662648	-2.914843	0.603216
C	5.460138	-1.083441	-0.148033
H	5.515123	0.564136	-1.562197
H	5.085671	-2.759199	1.180684
H	6.524356	-1.014119	0.103191

Statistical Thermodynamic Analysis

Temperature= 298.150 Kelvin Pressure= 1.00000 Atm

==========

SCF Energy= -1014.16363718 Predicted Change= -4.555326D-11

Zero-point correction (ZPE)= -1013.7802 0.38335

Internal Energy (U)= -1013.7575 0.40609

Enthalpy (H)= -1013.7566 0.40703

Gibbs Free Energy (G)= -1013.8367 0.32688

Entropy (S)= 0.00026882

Frequencies -- -147.3475 9.5521 17.3551

*3.10.7.18 Hydrocinnamyl Acyl Azolium Radical with **III-Az-B** Cation (Intermediate **III-I•**)*

Using Gaussian 16: ES64L-G16RevA.03 25-Dec-2016

==========

pbepbe/6-31g(d)/auto scf=(maxcycle=300,direct,vshift=200,tight,yqc)

density=current scrf=(solvent=ch3cn,smd) opt=(gdiis,maxcycle=250)

freq=noraman

#N Geom=AllCheck Guess=TCheck SCRF=Check GenChk RPBEPBE/6-31G(d)/Auto Freq

---

Pointgroup= C1 Stoichiometry= C23H26N3O(1+) C1[X(C23H26N3O)] #Atoms= 53

Charge = 1 Multiplicity = 1

SCF Energy= -1130.07024547 Predicted Change= -1.564536D-09

==========

Optimization completed. (Found 2 times)

Item	Max Val.	Criteria	Pass?	RMS Val.	Criteria	Pass?
Force	0.00000	0.00045	[YES]	0.00000	0.00030	[YES]
Displ	0.00168	0.00180	[YES]	0.00168	0.00180	[YES]

Atomic Type	Coordinates (Angstroms) X	Y	Z
C	1.613975	-2.526413	0.112530
C	0.647243	-1.330348	0.054409
C	-0.797742	-1.743923	0.131472
C	3.059751	-2.075266	0.042073
C	5.740103	-1.175522	-0.092234
C	3.706087	-1.918301	-1.200505
C	3.779080	-1.774909	1.216262
C	5.108039	-1.329114	1.151933
C	5.034758	-1.472505	-1.269294
O	-1.182220	-2.906303	0.252135
C	-1.882144	-0.697097	0.055873
N	-1.838778	0.661168	0.010389
N	-3.096426	1.216274	-0.034200
C	-3.906723	0.166758	-0.020226
N	-3.200517	-1.003050	0.029058
C	-4.060440	-2.205070	0.065874
C	-5.441059	-1.611912	-0.323483
C	-5.378090	-0.086174	-0.012678
C	-0.695763	1.548040	-0.002003
C	1.454772	3.326154	-0.031242
C	-0.162266	1.930636	-1.251346
C	-0.215774	2.035296	1.232290
C	0.869347	2.926665	1.184627

C	0.921099	2.824365	-1.233171
C	-0.719847	1.404075	-2.550376
C	-0.830934	1.622792	2.546459
C	2.638310	4.262949	-0.046667
H	1.387489	-3.211300	-0.723476
H	1.435638	-3.086488	1.047132
H	0.793016	-0.743872	-0.874324
H	0.849607	-0.618300	0.879002
H	6.778547	-0.830753	-0.144124
H	3.161624	-2.154233	-2.123000
H	3.291737	-1.898173	2.191117
H	5.652296	-1.105473	2.076202
H	5.521649	-1.361304	-2.244488
H	-3.682822	-2.958394	-0.637915
H	-4.030484	-2.615763	1.087749
H	-5.609731	-1.761469	-1.401749
H	-6.251984	-2.109950	0.226722
H	-5.913015	0.529510	-0.751630
H	-5.785576	0.153001	0.986169
H	1.261601	3.323311	2.128196
H	1.354401	3.139967	-2.189373
H	-1.804172	1.596777	-2.637017
H	-0.216721	1.880447	-3.406436
H	-0.575921	0.311032	-2.637587
H	-0.374852	2.184194	3.377018
H	-1.919898	1.807132	2.563047
H	-0.681133	0.545438	2.744863
H	3.587853	3.694801	-0.036177
H	2.642796	4.922691	0.837087
H	2.645169	4.889788	-0.954281

Statistical Thermodynamic Analysis

Temperature= 298.150 Kelvin Pressure= 1.00000 Atm

==========

SCF Energy= -1130.07024547 Predicted Change= -1.564536D-09

Zero-point correction (ZPE)= -1129.6339 0.43625

Internal Energy (U)= -1129.6078 0.46236

Enthalpy (H)= -1129.6069 0.46331

Gibbs Free Energy (G)= -1129.6928 0.37744

Entropy (S)= 0.00028799

Frequencies -- 21.3484 25.0964 27.5922

*3.10.7.19 Hydrocinnamyl Acyl Azolium Radical with **III-Az-B** Radical (Intermediate **III-I•**)*

Using Gaussian 16: ES64L-G16RevA.03 25-Dec-2016

==========

pbepbe/6-31g(d)/auto scf=(maxcycle=300,direct,vshift=200,tight,yqc)

density=current scrf=(solvent=ch3cn,smd) opt=(gdiis,maxcycle=250)

freq=noraman guess=(mix,always)

#N Geom=AllCheck Guess=TCheck SCRF=Check GenChk UPBEPBE/6-31G(d)/Auto Freq

---

Pointgroup= C1 Stoichiometry= C23H26N3O(2) C1[X(C23H26N3O)] #Atoms= 53

Charge = 0 Multiplicity = 2

SCF Energy= -1130.18330607 Predicted Change= -6.235583D-08

==========

Optimization completed. (Found 1 times)

Item Max Val. Criteria Pass? RMS Val. Criteria Pass?

Force 0.00000 || 0.00045 [YES] 0.00000 || 0.00030 [YES]

Displ 0.05949 || 0.00180 [NO] 0.05949 || 0.00180 [NO]

Atomic Type	Coordinates (Angstroms) X	Y	Z
C	-1.649725	-2.307796	-0.320473
C	-0.781314	-1.243411	0.395386
C	0.674435	-1.700407	0.473808
C	-3.124523	-1.969126	-0.295136
C	-5.875016	-1.282833	-0.217169
C	-3.912285	-2.258355	0.839465
C	-3.743278	-1.329785	-1.388868
C	-5.104637	-0.989452	-1.353432
C	-5.272829	-1.919236	0.880660
O	0.953860	-2.902613	0.798114
C	1.742210	-0.804173	0.143170
N	1.792275	0.561354	-0.178978
N	3.089495	0.970447	-0.547692
C	3.803466	-0.126892	-0.418512
N	3.070043	-1.192503	0.021514
C	3.831810	-2.443243	0.088076
C	5.291637	-1.918048	0.029129
C	5.223321	-0.532746	-0.679161
C	0.804773	1.578461	0.009628
C	-1.095419	3.630318	0.345320
C	0.420941	1.954095	1.320489
C	0.280714	2.228201	-1.134911
C	-0.662872	3.250364	-0.939284
C	-0.537078	2.973593	1.457493
C	1.030656	1.306846	2.540052
C	0.711694	1.829832	-2.525686
C	-2.141007	4.706036	0.524418
H	-1.463499	-3.276999	0.174812
H	-1.305523	-2.405166	-1.366780
H	-1.178789	-1.096898	1.420941
H	-0.878733	-0.273048	-0.119966
H	-6.938447	-1.021273	-0.188206
H	-3.450748	-2.761185	1.698388
H	-3.147670	-1.100122	-2.281090
H	-5.565226	-0.497330	-2.217449
H	-5.866495	-2.158151	1.770283
H	3.591804	-2.992175	1.008556

H	3.573460	-3.080399	-0.776644
H	5.673568	-1.788226	1.055410
H	5.953651	-2.622461	-0.496337
H	5.954878	0.190624	-0.286302
H	5.392303	-0.622143	-1.767989
H	-1.077384	3.758397	-1.818752
H	-0.841793	3.274827	2.467421
H	2.134172	1.304797	2.486292
H	0.732246	1.845357	3.454227
H	0.715197	0.252859	2.650139
H	0.153735	2.401825	-3.284772
H	1.790861	2.006453	-2.682854
H	0.538663	0.753616	-2.709174
H	-3.161423	4.277706	0.500990
H	-2.088307	5.459576	-0.279947
H	-2.028118	5.221902	1.493211

Statistical Thermodynamic Analysis

Temperature= 298.150 Kelvin Pressure= 1.00000 Atm

==========

SCF Energy= -1130.18330607 Predicted Change= -6.235583D-08

Zero-point correction (ZPE)= -1129.7493 0.43399

Internal Energy (U)= -1129.7228 0.46043

Enthalpy (H)= -1129.7219 0.46137

Gibbs Free Energy (G)= -1129.8106 0.37268

Entropy (S)= 0.00029747

Frequencies -- 14.8986 18.9027 22.2969

*3.10.7.20 Benzyl Radical and Hydrocinnamyl Acyl Azolium Radical with **III-Az-B** Transition Structure (Intermediate **III-TS-3**)*

Using Gaussian 16: ES64L-G16RevA.03 25-Dec-2016

==========

opt=(modredundant,maxcycle=250,gdiis) pbepbe/6-31g(d)/auto

scrf=(smd,solvent=ch3cn) density=current

scf=(maxcycle=300,direct,vshift=200,tight,yqc)

Modredundant Input: B 3 54 F

Modredundant Input: B 11 54 F

Modredundant Input:

pbepbe/6-31g(d)/auto scf=(maxcycle=300,direct,vshift=200,tight,yqc)

density=current scrf=(solvent=ch3cn,smd)

opt=(nofreeze,gdiis,maxcycle=250,ts,calcfc,noeigentest) freq=noraman

geom=allcheck guess=read

#N Geom=AllCheck Guess=TCheck SCRF=Check GenChk RPBEPBE/6-31G(d)/Auto Freq

---

Pointgroup= C1 Stoichiometry= C30H33N3O C1[X(C30H33N3O)] #Atoms= 67

Charge = 0 Multiplicity = 1

SCF Energy= -1400.76258698 Predicted Change= -5.609635D-10

==========

Optimization completed on the basis of negligible forces. (Found 3 times)

Item	Max Val.	Criteria	Pass?	RMS Val.	Criteria	Pass?
Force	0.00000 ||	0.00045	[YES]	0.00000 ||	0.00030	[YES]
Displ	0.00180 ||	0.00180	[YES]	0.00180 ||	0.00180	[YES]

Atomic Type	Coordinates (Angstroms) X	Y	Z
C	-1.686958	1.555708	-1.384231
C	-0.740462	1.189003	-0.213339
C	0.614817	0.703624	-0.729003
C	-2.963329	2.215558	-0.902325
C	-5.329471	3.445409	0.057601
C	-2.988898	3.591161	-0.590411
C	-4.146095	1.469529	-0.726045
C	-5.319358	2.076110	-0.250648
C	-4.158714	4.201948	-0.114889
O	1.281929	1.421371	-1.504128
C	1.163585	-0.612696	-0.332997
N	0.531309	-1.789326	0.094317
N	1.383377	-2.915858	-0.005165
C	2.456484	-2.432546	-0.583198
N	2.363264	-1.089401	-0.851041
C	3.462956	-0.591718	-1.691495
C	4.527073	-1.701329	-1.488577
C	3.739331	-2.993769	-1.123732
C	-0.859189	-2.044098	0.341428
C	-3.585304	-2.603777	0.790209
C	-1.716372	-2.251031	-0.768683
C	-1.326752	-2.174142	1.670008
C	-2.692785	-2.450698	1.865262
C	-3.073499	-2.516023	-0.518902
C	-1.186625	-2.239591	-2.183158
C	-0.404377	-2.040820	2.857648
C	-5.055584	-2.853952	1.029986
H	-1.931701	0.646826	-1.961897
H	-1.136444	2.236455	-2.057770
H	-0.556426	2.107095	0.376403
H	-1.218014	0.459592	0.460309
H	-6.244589	3.921724	0.426108
H	-2.079543	4.189364	-0.727625

H	-4.144993	0.399322	-0.966455
H	-6.228448	1.477300	-0.124503
H	-4.158023	5.273059	0.116276
H	3.120955	-0.526412	-2.739523
H	3.797137	0.400185	-1.365559
H	5.151719	-1.831110	-2.385264
H	5.184521	-1.421590	-0.648089
H	3.529570	-3.612395	-2.015502
H	4.269380	-3.629152	-0.396601
H	-3.066271	-2.553226	2.891497
H	-3.744899	-2.677895	-1.371332
H	-0.688713	-1.288265	-2.440756
H	-0.439750	-3.041111	-2.330829
H	-2.004025	-2.399741	-2.904923
H	0.549236	-2.570526	2.692560
H	-0.156174	-0.984156	3.065021
H	-0.879592	-2.453926	3.762674
H	-5.629020	-1.908147	0.985377
H	-5.234152	-3.298182	2.023653
H	-5.482146	-3.525416	0.264935
C	1.716173	0.546511	1.502720
H	1.955229	-0.414371	1.975675
C	2.829743	1.443042	1.296223
H	0.775061	0.982609	1.857229
C	4.175503	0.976014	1.380726
C	2.641513	2.810898	0.939676
C	5.259824	1.819599	1.119505
H	4.353761	-0.067455	1.669092
C	3.730158	3.651965	0.681594
H	1.622260	3.209343	0.882835
C	5.047171	3.165548	0.764053
H	6.281511	1.430461	1.202219
H	3.551403	4.700595	0.415929
H	5.896735	3.827664	0.565057

Statistical Thermodynamic Analysis

Temperature= 298.150 Kelvin Pressure= 1.00000 Atm

==========

SCF Energy= -1400.76258698 Predicted Change= -5.609635D-10

Zero-point correction (ZPE)= -1400.2137 0.54884

Internal Energy (U)= -1400.1810 0.58154

Enthalpy (H)= -1400.1800 0.58249

Gibbs Free Energy (G)= -1400.2811 0.48139

Entropy (S)= 0.00033908

Frequencies -- -151.6028 13.4440 17.9378

*3.10.7.21 Benzyl Radical and Hydrocinnamyl Acyl Azolium Radical with **III-Az-B** (Intermediate **III-II$_{C1}$**)*

Using Gaussian 16: ES64L-G16RevA.03 25-Dec-2016

==========

pbepbe/6-31g(d)/auto scf=(maxcycle=300,direct,vshift=200,tight,yqc)

density=current scrf=(solvent=ch3cn,smd) opt=(gdiis,maxcycle=250)

freq=noraman

#N Geom=AllCheck Guess=TCheck SCRF=Check GenChk RPBEPBE/6-31G(d)/Auto Freq

---

Pointgroup= C1 Stoichiometry= C30H33N3O C1[X(C30H33N3O)] #Atoms= 67

Charge = 0 Multiplicity = 1

SCF Energy= -1400.78621291 Predicted Change= -5.006776D-10

==========

Optimization completed on the basis of negligible forces. (Found 2 times)

Item	Max Val.	Criteria	Pass?	RMS Val.	Criteria	Pass?
Force	0.00000	0.00045	[YES]	0.00000	0.00030	[YES]
Displ	0.00242	0.00180	[NO]	0.00242	0.00180	[YES]

Atomic Type	Coordinates (Angstroms) X	Y	Z
C	2.117446	-0.184914	0.906743
C	1.742579	-0.079504	-0.589567
C	0.217345	0.024446	-0.953440
C	3.615920	-0.285397	1.112655
C	6.430257	-0.467031	1.416191
C	4.422820	0.872695	1.104191
C	4.248416	-1.534969	1.277442
C	5.641050	-1.627827	1.427321
C	5.814659	0.785168	1.253814
C	-0.520514	-1.247257	-0.429689
N	-1.767417	-1.441475	0.097025
N	-2.176468	-2.783230	0.063047
C	-1.140454	-3.393130	-0.468148
N	-0.131156	-2.513628	-0.766468
C	0.964003	-3.129122	-1.533384
C	0.366223	-4.514725	-1.902826
C	-0.779770	-4.784576	-0.882789
C	-2.759160	-0.491448	0.535993
C	-4.764565	1.273461	1.372977
C	-3.626515	0.057025	-0.436337
C	-2.875212	-0.207167	1.911546
C	-3.888008	0.687110	2.303694
C	-4.616106	0.948146	0.010354
C	-3.474239	-0.289524	-1.897989
C	-1.949285	-0.828961	2.928430
C	-5.857944	2.213259	1.824387
H	1.626631	-1.071913	1.350813
H	1.733316	0.699662	1.446753
H	2.173391	-0.935779	-1.134866
H	2.213175	0.820233	-1.026321
H	7.516874	-0.536589	1.536818

H	3.949038	1.854444	0.979397
H	3.637725	-2.446486	1.294966
H	6.109799	-2.609656	1.558628
H	6.420781	1.698138	1.248519
H	1.174386	-2.488374	-2.402992
H	1.863829	-3.207300	-0.901366
H	-0.053208	-4.469889	-2.921156
H	1.134676	-5.301447	-1.881596
H	-1.630900	-5.327049	-1.321509
H	-0.423731	-5.361009	-0.009510
H	-3.992577	0.928691	3.368255
H	-5.291425	1.397882	-0.727629
H	-4.151171	0.323596	-2.515110
H	-2.430543	-0.134388	-2.243034
H	-3.718600	-1.353013	-2.080574
H	-0.911517	-0.466052	2.810204
H	-2.276215	-0.583872	3.951858
H	-1.918691	-1.928562	2.829262
H	-5.640031	2.639545	2.817824
H	-6.828500	1.686580	1.896551
H	-5.995920	3.043838	1.110702
O	-0.012013	-0.069163	-2.282506
C	-0.374583	1.332205	-0.288670
H	-0.370810	1.261152	0.814982
C	0.341998	2.594155	-0.717315
H	-1.427802	1.399060	-0.605546
C	0.394447	2.969004	-2.079591
C	0.962884	3.437825	0.227869
C	1.052643	4.141492	-2.478269
H	-0.064786	2.299495	-2.813866
C	1.616854	4.616236	-0.168307
H	0.924776	3.170495	1.291251
C	1.664602	4.973034	-1.524941
H	1.084905	4.411454	-3.540306
H	2.086471	5.257430	0.586370
H	2.171300	5.893050	-1.837012

Statistical Thermodynamic Analysis

Temperature= 298.150 Kelvin Pressure= 1.00000 Atm

==========

SCF Energy= -1400.78621291 Predicted Change= -5.006776D-10

Zero-point correction (ZPE)= -1400.2340 0.55214

Internal Energy (U)= -1400.2017 0.58443

Enthalpy (H)= -1400.2008 0.58538

Gibbs Free Energy (G)= -1400.3014 0.48476

Entropy (S)= 0.00033748

Frequencies -- 13.9712 17.4171 26.3916

*3.10.7.22 Benzyl Radical and Hydrocinnamyl Acyl Azolium Radical with **III-Az-B** (Intermediate **III-II$_{C2}$**)*

Using Gaussian 16: ES64L-G16RevA.03 25-Dec-2016

==========

pbepbe/6-31g(d)/auto scf=(maxcycle=300,direct,vshift=200,tight,yqc)

density=current scrf=(solvent=ch3cn,smd) opt=(gdiis,maxcycle=250)

freq=noraman

#N Geom=AllCheck Guess=TCheck SCRF=Check GenChk RPBEPBE/6-31G(d)/Auto Freq

---

Pointgroup= C1 Stoichiometry= C30H33N3O C1[X(C30H33N3O)] #Atoms= 67

Charge = 0 Multiplicity = 1

SCF Energy= -1400.78614818 Predicted Change= -1.015846D-08

==========

Optimization completed. (Found 1 times)

Item	Max Val.	Criteria	Pass?	RMS Val.	Criteria	Pass?
Force	0.00000	0.00045	[YES]	0.00000	0.00030	[YES]
Displ	0.00671	0.00180	[NO]	0.00671	0.00180	[YES]

Atomic Type	Coordinates (Angstroms) X	Y	Z
C	1.976515	1.162755	-1.445304
C	0.852021	1.037310	-0.399052
C	-0.345936	0.243332	-0.902193
C	3.103661	2.054109	-0.963941
C	5.178919	3.736144	-0.018646
C	4.134161	1.542632	-0.148192
C	3.133119	3.423601	-1.297307
C	4.159801	4.258810	-0.830393
C	5.162563	2.373675	0.321033
O	-0.535373	0.064031	-2.105557
C	-1.330531	-0.389641	0.138788
N	-0.790909	-1.747743	0.655483
N	-1.662798	-2.813603	0.240334
C	-2.649041	-2.233607	-0.375552
N	-2.564124	-0.863807	-0.478283
C	-3.474303	-0.334180	-1.502609
C	-4.581578	-1.417075	-1.498601
C	-3.855290	-2.737627	-1.121227
C	0.608044	-2.101247	0.588636
C	3.360510	-2.844220	0.627638
C	1.187750	-2.752421	-0.541674
C	1.400129	-1.862443	1.745752
C	2.760099	-2.227779	1.736958
C	2.549297	-3.104487	-0.491563
C	0.412706	-3.107279	-1.792244
C	0.821490	-1.255477	3.002462
C	4.826409	-3.212100	0.631189
H	1.548134	1.561878	-2.380441
H	2.361837	0.151890	-1.672375

H	1.231743	0.601424	0.541989
H	0.482101	2.045701	-0.124067
H	5.983358	4.385439	0.343867
H	4.128265	0.478942	0.119866
H	2.342407	3.836862	-1.935515
H	4.165923	5.319407	-1.105592
H	5.955945	1.954894	0.950192
H	-3.857379	0.661259	-1.230572
H	-2.967563	-0.265374	-2.481929
H	-5.329977	-1.171389	-0.725736
H	-5.096931	-1.479196	-2.469588
H	-4.480733	-3.420409	-0.523530
H	-3.526454	-3.291775	-2.019993
H	3.358896	-2.043001	2.637845
H	2.990219	-3.601615	-1.365349
H	1.110713	-3.354350	-2.610350
H	-0.238841	-3.982872	-1.624829
H	-0.236455	-2.284830	-2.131209
H	-0.225293	-1.566703	3.151380
H	1.414926	-1.555208	3.883032
H	0.826026	-0.150184	2.970817
H	5.220038	-3.290904	1.658788
H	5.004726	-4.172651	0.116956
H	5.432408	-2.449556	0.105203
C	-1.629124	0.541886	1.365649
H	-0.683971	0.985432	1.720162
C	-2.665925	1.623313	1.128682
H	-1.989638	-0.132998	2.159863
C	-2.339829	2.867674	0.550169
C	-4.009801	1.392485	1.494348
C	-3.325399	3.841896	0.328726
H	-1.301394	3.084686	0.276738
C	-4.998417	2.363414	1.275072
H	-4.279238	0.436811	1.959408
C	-4.659677	3.592324	0.686689
H	-3.047436	4.802086	-0.119959
H	-6.034180	2.161453	1.569872
H	-5.428440	4.354018	0.517016

Statistical Thermodynamic Analysis

Temperature= 298.150 Kelvin Pressure= 1.00000 Atm

==========

SCF Energy= -1400.78614818 Predicted Change= -1.015846D-08

Zero-point correction (ZPE)= -1400.2348 0.55129

Internal Energy (U)= -1400.2024 0.58372

Enthalpy (H)= -1400.2014 0.58467

Gibbs Free Energy (G)= -1400.3019 0.48422

Entropy (S)= 0.00033689

Frequencies -- 11.8280 17.6194 18.8611

*3.10.7.23 Benzyl Radical and Hydrocinnamyl Acyl Azolium Radical with **III-Az-B** Transition Structure (Intermediate **III-TS-3**)*

Using Gaussian 16: ES64L-G16RevA.03 25-Dec-2016

==========

pbepbe/6-31g(d)/auto scf=(maxcycle=300,direct,vshift=200,tight,yqc)

density=current scrf=(solvent=ch3cn,smd)

opt=(gdiis,maxcycle=250,ts,calcfc,noeigentest) freq=noraman

#N Geom=AllCheck Guess=TCheck SCRF=Check GenChk RPBEPBE/6-31G(d)/Auto Freq

---

Pointgroup= C1 Stoichiometry= C30H33N3O C1[X(C30H33N3O)] #Atoms= 67

Charge = 0 Multiplicity = 1

SCF Energy= -1400.77745763 Predicted Change= -2.293181D-09

==========

Optimization completed on the basis of negligible forces. (Found 2 times)

Item	Max Val.	Criteria	Pass?	RMS Val.	Criteria	Pass?
Force	0.00000	0.00045	[YES]	0.00000	0.00030	[YES]
Displ	0.00217	0.00180	[NO]	0.00217	0.00180	[YES]

Atomic Type	Coordinates (Angstroms) X	Y	Z
C	2.045024	-0.196143	0.841361
C	1.878422	-0.192231	-0.691714
C	0.490649	0.159594	-1.286989
C	3.459350	-0.549096	1.257375
C	6.125527	-1.208238	1.962660
C	4.440940	0.454220	1.398553
C	3.840632	-1.889055	1.476834
C	5.159515	-2.218002	1.825938
C	5.760864	0.130689	1.747553
C	-0.682466	-1.320107	-0.422978
N	-1.961440	-1.403027	0.041514
N	-2.615594	-2.621525	-0.230539
C	-1.685785	-3.290151	-0.877805
N	-0.535072	-2.546197	-1.005561
C	0.501654	-3.220547	-1.801155
C	-0.288230	-4.397394	-2.436082
C	-1.533567	-4.630456	-1.527055
C	-2.724005	-0.378726	0.706009
C	-4.254490	1.595060	1.984163
C	-3.632606	0.383344	-0.063192
C	-2.578739	-0.203117	2.098262
C	-3.355332	0.796104	2.713080
C	-4.384161	1.367314	0.600683
C	-3.798290	0.145283	-1.545617
C	-1.638903	-1.061347	2.910448
C	-5.054465	2.680850	2.665273
H	1.332677	-0.920657	1.277370

H	1.785710	0.798632	1.245999
H	2.193137	-1.165587	-1.106248
H	2.572177	0.558022	-1.122830
H	7.154679	-1.462579	2.238870
H	4.161464	1.502446	1.234315
H	3.089849	-2.683095	1.377570
H	5.432077	-3.265591	1.996763
H	6.505792	0.927048	1.856301
H	0.904139	-2.506655	-2.535757
H	1.312326	-3.563226	-1.135839
H	-0.623011	-4.108291	-3.446051
H	0.334222	-5.299941	-2.527065
H	-2.427917	-4.933955	-2.092944
H	-1.341553	-5.404588	-0.761553
H	-3.257854	0.946376	3.795100
H	-5.091543	1.971211	0.019291
H	-4.460675	0.905764	-1.989769
H	-2.829708	0.176237	-2.077480
H	-4.237654	-0.849286	-1.744702
H	-0.580377	-0.834430	2.686664
H	-1.797086	-0.895711	3.988511
H	-1.787778	-2.135342	2.699827
H	-5.154332	2.491141	3.747204
H	-6.065543	2.770368	2.231923
H	-4.565253	3.666583	2.548029
O	0.317270	-0.064701	-2.521759
C	-0.166188	1.436652	-0.681255
H	-0.230294	1.372245	0.417371
C	0.589747	2.691602	-1.079013
H	-1.195398	1.484154	-1.074790
C	0.698200	3.070406	-2.435435
C	1.205865	3.508593	-0.108444
C	1.397649	4.227424	-2.806377
H	0.238317	2.431372	-3.196746
C	1.905709	4.669221	-0.476528
H	1.126622	3.234929	0.950829
C	2.004215	5.033568	-1.828125
H	1.468921	4.503205	-3.864766
H	2.372532	5.290449	0.296214
H	2.547500	5.939716	-2.118006

Statistical Thermodynamic Analysis

Temperature= 298.150 Kelvin Pressure= 1.00000 Atm

==========

SCF Energy= -1400.77745763 Predicted Change= -2.293181D-09

Zero-point correction (ZPE)= -1400.2268 0.55057

Internal Energy (U)= -1400.1945 0.58295

Enthalpy (H)= -1400.1935 0.58389

Gibbs Free Energy (G)= -1400.2950 0.48238

Entropy (S)= 0.00034045

Frequencies -- -142.7697 14.6396 17.8816

3.10.7.24 1,4-Diphenylbutan-2-one

Using Gaussian 16: ES64L-G16RevA.03 25-Dec-2016

==========

pbepbe/6-31g(d)/auto scf=(maxcycle=300,direct,vshift=200,tight,yqc)

density=current scrf=(solvent=ch3cn,smd) opt=(gdiis,maxcycle=250)

freq=noraman

#N Geom=AllCheck Guess=TCheck SCRF=Check GenChk RPBEPBE/6-31G(d)/Auto Freq

---

Pointgroup= C1 Stoichiometry= C16H16O C1[X(C16H16O)] #Atoms= 33

Charge = 0 Multiplicity = 1

SCF Energy= -693.705462121 Predicted Change= -7.816427D-09

==========

Optimization completed on the basis of negligible forces. (Found 2 times)

Item	Max Val.	Criteria	Pass?	RMS Val.	Criteria	Pass?
Force	0.00000	0.00045	[YES]	0.00000	0.00030	[YES]
Displ	0.00415	0.00180	[NO]	0.00415	0.00180	[YES]

Atomic Type	Coordinates (Angstroms) X	Y	Z
O	0.987310	-0.710784	1.223430
C	0.660749	-0.305945	0.110424
C	1.679759	-0.061249	-1.015552
C	3.115504	0.047790	-0.562775
C	3.763864	1.297709	-0.529592
C	5.093906	1.407976	-0.094792
C	5.796308	0.265073	0.317635
C	5.159635	-0.986563	0.291511
C	3.830744	-1.092794	-0.144057
C	-0.789711	-0.032662	-0.264846
C	-1.805400	-0.496914	0.793423
C	-3.232794	-0.183292	0.392747
C	-3.996853	-1.110012	-0.345715
C	-5.308590	-0.810162	-0.744015
C	-5.881264	0.427254	-0.409284
C	-5.132401	1.359547	0.326719
C	-3.821251	1.054873	0.722908
H	1.551406	-0.913552	-1.714336
H	1.369103	0.835785	-1.581517
H	3.219706	2.193502	-0.852394
H	5.582116	2.388728	-0.081309
H	6.835413	0.347916	0.654583
H	5.701276	-1.884711	0.608591
H	3.341745	-2.073224	-0.168025
H	-0.882990	1.058014	-0.443439
H	-0.992626	-0.501930	-1.247602
H	-1.563754	-0.009047	1.754133

H	-1.687055	-1.584306	0.949206
H	-3.557007	-2.080687	-0.605953
H	-5.886368	-1.547124	-1.313050
H	-6.906473	0.661899	-0.715848
H	-5.572315	2.325701	0.598348
H	-3.243881	1.785526	1.302737

Statistical Thermodynamic Analysis

Temperature= 298.150 Kelvin Pressure= 1.00000 Atm

==========

SCF Energy= -693.705462121 Predicted Change= -7.816427D-09

Zero-point correction (ZPE)= -693.4367 0.26875

Internal Energy (U)= -693.4211 0.28431

Enthalpy (H)= -693.4202 0.28525

Gibbs Free Energy (G)= -693.4839 0.22147

Entropy (S)= 0.00021392

Frequencies -- 12.8246 20.5497 33.6782

3.10.7.25 Radical Stability Model: Benzaldehyde

Using Gaussian 16: ES64L-G16RevA.03 25-Dec-2016

==========

pbepbe/6-31g(d)/auto scf=(maxcycle=300,direct,vshift=200,tight,yqc)

density=current scrf=(solvent=ch3cn,smd) opt=(gdiis,maxcycle=250)

freq=noraman

#N Geom=AllCheck Guess=TCheck SCRF=Check GenChk RPBEPBE/6-31G(d)/Auto Freq

---

Pointgroup= C1 Stoichiometry= C7H6O C1[X(C7H6O)] #Atoms= 14

Charge = 0 Multiplicity = 1

SCF Energy= -345.159845738 Predicted Change= -6.517587D-10

==========

Optimization completed. (Found 2 times)

Item	Max Val.	Criteria	Pass?	RMS Val.	Criteria	Pass?
Force	0.00001	0.00045	[YES]	0.00000	0.00030	[YES]
Displ	0.00005	0.00180	[YES]	0.00005	0.00180	[YES]

Atomic Coordinates (Angstroms)

Type	X	Y	Z
C	1.994380	0.472304	0.000005
O	2.866334	-0.397731	-0.000009
H	2.269908	1.559346	0.000017
C	0.538577	0.210487	0.000003
C	-0.358460	1.298620	-0.000000
C	0.042333	-1.111378	0.000004
C	-1.740113	1.069416	-0.000002
H	0.037295	2.321593	0.000001
C	-1.336350	-1.337918	0.000001
H	0.755101	-1.943166	0.000008
C	-2.227454	-0.247940	-0.000003
H	-2.437725	1.913350	-0.000004
H	-1.724945	-2.361716	0.000002
H	-3.307779	-0.429106	-0.000006

Statistical Thermodynamic Analysis

Temperature= 298.150 Kelvin Pressure= 1.00000 Atm

==========

SCF Energy= -345.159845738 Predicted Change= -6.517587D-10

Zero-point correction (ZPE)= -345.0526 0.10720

Internal Energy (U)= -345.0461 0.11368

Enthalpy (H)= -345.0452 0.11463

Gibbs Free Energy (G)= -345.0833 0.07652

Entropy (S)= 0.00012783

Frequencies -- 118.4465 212.7984 229.7500

3.10.7.26 Radical Stability Model: Benzaldehyde Radical Anion

Using Gaussian 16: ES64L-G16RevA.03 25-Dec-2016

==========

pbepbe/6-31g(d)/auto scf=(maxcycle=300,direct,vshift=200,tight,yqc)

density=current scrf=(solvent=ch3cn,smd) opt=(gdiis,maxcycle=250)

freq=noraman guess=(mix,always)

#N Geom=AllCheck Guess=TCheck SCRF=Check GenChk UPBEPBE/6-31G(d)/Auto Freq

---

Pointgroup= C1 Stoichiometry= C7H6O(1-,2) C1[X(C7H6O)] #Atoms= 14

Charge = -1 Multiplicity = 2

SCF Energy= -345.232059079 Predicted Change= -7.771700D-09

==========

Optimization completed. (Found 2 times)

Item	Max Val.	Criteria	Pass?	RMS Val.	Criteria	Pass?
Force	0.00003	0.00045	[YES]	0.00000	0.00030	[YES]
Displ	0.00046	0.00180	[YES]	0.00046	0.00180	[YES]

Atomic Type	Coordinates (Angstroms) X	Y	Z
C	1.989193	0.478456	0.000018
O	2.912522	-0.402256	0.000009
H	2.263395	1.574620	0.000036
C	0.575074	0.233334	-0.000015
C	-0.386392	1.306482	-0.000018
C	0.039634	-1.108600	-0.000021
C	-1.755726	1.060620	0.000002
H	-0.015866	2.342034	-0.000037
C	-1.332984	-1.340364	0.000001
H	0.754057	-1.941039	-0.000042
C	-2.262404	-0.268450	0.000022
H	-2.455560	1.907017	-0.000003
H	-1.703568	-2.374809	-0.000003
H	-3.341001	-0.458650	0.000050

Statistical Thermodynamic Analysis

Temperature= 298.150 Kelvin Pressure= 1.00000 Atm

==========

SCF Energy= -345.232059079 Predicted Change= -7.771700D-09

Zero-point correction (ZPE)= -345.1283 0.10373

Internal Energy (U)= -345.1216 0.11039

Enthalpy (H)= -345.1207 0.11133

Gibbs Free Energy (G)= -345.1596 0.07240

Entropy (S)= 0.00013058

Frequencies -- 138.7644 194.4067 257.9753

3.10.7.27 Radical Stability Model: ***III-Az-A*** *cation*

Using Gaussian 16: ES64L-G16RevA.03 25-Dec-2016

==========

pbepbe/6-31g(d)/auto scf=(maxcycle=300,direct,vshift=200,tight,yqc)

density=current scrf=(solvent=ch3cn,smd) opt=(gdiis,maxcycle=250)

freq=noraman

#N Geom=AllCheck Guess=TCheck SCRF=Check GenChk RPBEPBE/6-31G(d)/Auto Freq

---

Pointgroup= C1 Stoichiometry= C4H8N3(1+) C1[X(C4H8N3)] #Atoms= 15

Charge = 1 Multiplicity = 1

SCF Energy= -320.962989686 Predicted Change= -3.828699D-08

==========

Optimization completed. (Found 1 times)

Item Max Val. Criteria Pass? RMS Val. Criteria Pass?

Force 0.00002 || 0.00045 [YES] 0.00000 || 0.00030 [YES]

Displ 0.00917 || 0.00180 [NO] 0.00917 || 0.00180 [NO]

Atomic Type	Coordinates (Angstroms) X	Y	Z
C	-0.001787	-0.886699	-0.005945
C	0.604811	1.204567	-0.003593
N	-1.072041	-0.091263	0.003582
H	-0.000760	-1.974676	-0.012084
H	1.252063	2.079364	-0.008239
N	-0.715326	1.229094	0.004067
N	1.082521	-0.083052	-0.011025
C	-2.481610	-0.472737	0.002266
H	-2.542314	-1.568922	0.005646
H	-2.960566	-0.060033	0.902317
H	-2.958556	-0.065502	-0.901420
C	2.488293	-0.507369	0.008520
H	3.090677	0.278695	-0.465987
H	2.810888	-0.653725	1.050428
H	2.584245	-1.445229	-0.554515

Statistical Thermodynamic Analysis

Temperature= 298.150 Kelvin Pressure= 1.00000 Atm

==========

SCF Energy= -320.962989686 Predicted Change= -3.828699D-08

Zero-point correction (ZPE)= -320.8369 0.12602

Internal Energy (U)= -320.8298 0.13314

Enthalpy (H)= -320.8289 0.13408

Gibbs Free Energy (G)= -320.8684 0.09453

Entropy (S)= 0.00013265

Frequencies -- 60.1491 116.5450 179.9420

*3.10.7.28 Radical Stability Model: **III-Az-A** Radical*

Using Gaussian 16: ES64L-G16RevA.03 25-Dec-2016

==========

pbepbe/6-31g(d)/auto scf=(maxcycle=300,direct,vshift=200,tight,yqc)

density=current scrf=(solvent=ch3cn,smd) opt=(gdiis,maxcycle=250)

freq=noraman guess=(mix,always)

#N Geom=AllCheck Guess=TCheck SCRF=Check GenChk UPBEPBE/6-31G(d)/Auto Freq

---

Pointgroup= C1 Stoichiometry= C4H8N3(2) C1[X(C4H8N3)] #Atoms= 15

Charge = 0 Multiplicity = 2

SCF Energy= -321.028771197 Predicted Change= -5.640531D-08

==========

Optimization completed. (Found 1 times)

Item	Max Val.	Criteria	Pass?	RMS Val.	Criteria	Pass?
Force	0.00002	0.00045	[YES]	0.00000	0.00030	[YES]
Displ	0.00376	0.00180	[NO]	0.00376	0.00180	[YES]

Atomic Coordinates (Angstroms)

Type	X	Y	Z
C	0.000764	-0.967030	-0.235778

C	0.591164	1.191282	0.066376
N	-1.109914	-0.078948	-0.277779
H	-0.058045	-1.833594	0.454805
H	1.238117	2.060815	0.186270
N	-0.718581	1.254352	-0.030898
N	1.088859	-0.076933	-0.033855
C	-2.428421	-0.472268	0.178221
H	-2.737079	-1.386934	-0.353816
H	-2.454214	-0.670640	1.271406
H	-3.140287	0.334449	-0.055823
C	2.473374	-0.487434	0.082472
H	3.101304	0.400701	0.247889
H	2.600672	-1.179302	0.936197
H	2.805693	-1.002092	-0.836943

Statistical Thermodynamic Analysis

Temperature= 298.150 Kelvin Pressure= 1.00000 Atm

==========

SCF Energy= -321.028771197 Predicted Change= -5.640531D-08

Zero-point correction (ZPE)= -320.9070 0.12168

Internal Energy (U)= -320.8995 0.12919

Enthalpy (H)= -320.8986 0.13014

Gibbs Free Energy (G)= -320.9392 0.08949

Entropy (S)= 0.00013635

Frequencies -- 96.7277 121.5175 169.3285

3.10.7.28 Radical Stability Model: ***III-Az-B*** *Cation*

Using Gaussian 16: ES64L-G16RevA.03 25-Dec-2016

==========

pbepbe/6-31g(d)/auto scf=(maxcycle=300,direct,vshift=200,tight,yqc)

density=current scrf=(solvent=ch3cn,smd) opt=(gdiis,maxcycle=250)

freq=noraman

#N Geom=AllCheck Guess=TCheck SCRF=Check GenChk RPBEPBE/6-31G(d)/Auto Freq

---

Pointgroup= C1 Stoichiometry= C14H18N3(1+) C1[X(C14H18N3)] #Atoms= 35

Charge = 1 Multiplicity = 1

SCF Energy= -707.578903028 Predicted Change= -1.657186D-10

==========

Optimization completed. (Found 2 times)

Item	Max Val.	Criteria	Pass?	RMS Val.	Criteria	Pass?
Force	0.00000	0.00045	[YES]	0.00000	0.00030	[YES]
Displ	0.00033	0.00180	[YES]	0.00033	0.00180	[YES]

Atomic Type	Coordinates (Angstroms) X	Y	Z
C	1.281959	-0.103588	1.138185
C	2.462436	-0.017269	-0.707122
N	0.481957	-0.042286	0.060487
H	0.957569	-0.151200	2.175211
N	1.207175	0.012863	-1.118538
N	2.536304	-0.085588	0.666042
C	3.919187	-0.154652	1.177159
H	4.037593	0.516235	2.039535
H	4.120931	-1.193342	1.484928

C	4.728552	0.279462	-0.073902
H	4.928459	1.361593	-0.020418
H	5.690896	-0.249568	-0.124489
C	3.830028	-0.023246	-1.311649
H	4.040031	-1.019706	-1.740547
H	3.938323	0.720509	-2.115565
C	-0.961694	-0.014125	0.039653
C	-1.606900	1.241209	0.035253
C	-1.654075	-1.242353	-0.007672
C	-3.011003	1.236753	-0.002525
C	-3.057743	-1.182926	-0.043284
C	-3.752591	0.040582	-0.034209
H	-3.537837	2.198139	-0.011484
H	-3.620958	-2.122585	-0.084936
C	-0.830892	2.535279	0.060579
H	-0.270934	2.656153	1.005980
H	-0.093273	2.583471	-0.760266
H	-1.512701	3.394565	-0.039387
C	-5.262087	0.072125	-0.046310
H	-5.662134	0.141268	0.983140
H	-5.642669	0.947015	-0.600318
H	-5.682002	-0.841062	-0.500079
C	-0.928434	-2.565320	-0.030898
H	-0.179808	-2.604380	-0.842274
H	-0.389277	-2.751549	0.915974
H	-1.640719	-3.392063	-0.180495

Statistical Thermodynamic Analysis

Temperature= 298.150 Kelvin Pressure= 1.00000 Atm

==========

SCF Energy= -707.578903028 Predicted Change= -1.657186D-10

Zero-point correction (ZPE)= -707.2859 0.29298

Internal Energy (U)= -707.2693 0.30954

Enthalpy (H)= -707.2684 0.31048

Gibbs Free Energy (G)= -707.3313 0.24754

Entropy (S)= 0.00021112

Frequencies -- 28.8945 32.9258 49.8949

*3.10.7.29 Radical Stability Model: **III-Az-B** Radical*

Using Gaussian 16: ES64L-G16RevA.03 25-Dec-2016

==========

pbepbe/6-31g(d)/auto scf=(maxcycle=300,direct,vshift=200,tight,yqc)

density=current scrf=(solvent=ch3cn,smd) opt=(gdiis,maxcycle=250)

freq=noraman guess=(mix,always)

#N Geom=AllCheck Guess=TCheck SCRF=Check GenChk UPBEPBE/6-31G(d)/Auto Freq

---

Pointgroup= C1 Stoichiometry= C14H18N3(2) C1[X(C14H18N3)] #Atoms= 35

Charge = 0 Multiplicity = 2

SCF Energy= -707.650433229 Predicted Change= -6.454269D-07

==========

Optimization completed. (Found 1 times)

Item	Max Val.	Criteria	Pass?	RMS Val.	Criteria	Pass?
Force	0.00006	0.00045	[YES]	0.00000	0.00030	[YES]
Displ	0.09594	0.00180	[NO]	0.09594	0.00180	[NO]

Atomic Type	Coordinates (Angstroms) X	Y	Z
C	-1.298494	-0.870919	0.874175
C	-2.479279	0.544509	-0.429318
N	-0.477522	-0.014577	0.096270
H	-1.057424	-1.001748	1.939870
N	-1.236627	0.853450	-0.736571
N	-2.580309	-0.440186	0.507867
C	-3.952266	-0.816592	0.831755
H	-4.066105	-1.913711	0.842406
H	-4.228087	-0.428800	1.831054
C	-4.751951	-0.136229	-0.314375
H	-4.934500	-0.871395	-1.115756
H	-5.726862	0.236527	0.034662
C	-3.842324	1.007577	-0.855066
H	-4.078089	1.976716	-0.377724
H	-3.929508	1.144236	-1.944729
C	0.929866	-0.014133	0.035411
C	1.645496	-1.236739	-0.157152
C	1.637638	1.217454	0.180336
C	3.047537	-1.194555	-0.177158
C	3.040617	1.195795	0.119722
C	3.774334	0.006620	-0.048342
H	3.592125	-2.135561	-0.330770
H	3.581101	2.143824	0.239418
C	0.941156	-2.547611	-0.413166
H	0.300667	-2.861216	0.431384
H	0.271338	-2.476839	-1.290815
H	1.676336	-3.345699	-0.610961
C	5.284964	0.011767	-0.095176
H	5.720755	-0.661612	0.666641
H	5.664819	-0.335162	-1.075290
H	5.689013	1.023531	0.078996
C	0.922576	2.520156	0.452097
H	0.351661	2.877674	-0.423206
H	0.189356	2.412717	1.272652
H	1.645397	3.303105	0.736745

Statistical Thermodynamic Analysis

Temperature= 298.150 Kelvin Pressure= 1.00000 Atm

==========

SCF Energy= -707.650433229 Predicted Change= -6.454269D-07

Zero-point correction (ZPE)= -707.3614 0.28902

Internal Energy (U)= -707.3445 0.30592

Enthalpy (H)= -707.3435 0.30687

Gibbs Free Energy (G)= -707.4070 0.24335

Entropy (S)= 0.00021303

Frequencies -- 37.9889 40.0262 57.0642

3.10.7.30 Radical Stability Model: Perfluorophenyl Dihydropyrrolotriazolium Cation

---

Using Gaussian 16: ES64L-G16RevA.03 25-Dec-2016

==========

pbepbe/6-31g(d)/auto scf=(maxcycle=300,direct,vshift=200,tight,yqc)

density=current scrf=(solvent=ch3cn,smd) opt=(gdiis,maxcycle=250)

freq=noraman

#N Geom=AllCheck Guess=TCheck SCRF=Check GenChk RPBEPBE/6-31G(d)/Auto Freq

---

Pointgroup= C1 Stoichiometry= C11H7F5N3(1+) C1[X(C11H7F5N3)] #Atoms= 26

Charge = 1 Multiplicity = 1

SCF Energy= -1085.48520719 Predicted Change= -1.040908D-08

==========

Optimization completed. (Found 2 times)

Item	Max Val.	Criteria	Pass?	RMS Val.	Criteria	Pass?
Force	0.00002	0.00045	[YES]	0.00000	0.00030	[YES]
Displ	0.00135	0.00180	[YES]	0.00135	0.00180	[YES]

Atomic Type	Coordinates (Angstroms) X	Y	Z
F	0.620019	-2.396992	0.247118
C	1.245896	-1.217161	0.119347
C	2.643480	-1.179121	0.133859
F	3.347162	-2.311197	0.275565
C	3.305753	0.049639	0.012584
F	4.642953	0.089499	0.030242
C	2.574506	1.236482	-0.129892
F	3.214633	2.407564	-0.254746
C	1.176899	1.193621	-0.160133
F	0.492124	2.332921	-0.320531
C	0.502085	-0.033451	-0.029505
N	-0.916461	-0.069001	-0.030265
C	-1.718649	-0.864841	-0.767981
N	-2.965076	-0.533846	-0.420226
C	-2.889198	0.465580	0.527523
C	-4.254602	0.873448	0.975785
C	-5.155648	0.240828	-0.127993
C	-4.350612	-0.939573	-0.732059
N	-1.636133	0.777599	0.797884
H	-1.396130	-1.604885	-1.497138
H	-4.458028	0.442079	1.972557
H	-4.363505	1.965902	1.050265
H	-6.118303	-0.104411	0.274879
H	-5.352693	0.987043	-0.914065
H	-4.473534	-1.057628	-1.817695
H	-4.545591	-1.900206	-0.228604

Statistical Thermodynamic Analysis

Temperature= 298.150 Kelvin Pressure= 1.00000 Atm

==========

SCF Energy= -1085.48520719 Predicted Change= -1.040908D-08

Zero-point correction (ZPE)= -1085.3132 0.17197

Internal Energy (U)= -1085.2974 0.18776

Enthalpy (H)= -1085.2964 0.18871

Gibbs Free Energy (G)= -1085.3568 0.12836

Entropy (S)= 0.00020242

Frequencies -- 45.7289 48.0690 62.0661

3.10.7.31 Perfluorophenyl Dihydropyrrolotriazolium Radical

Using Gaussian 16: ES64L-G16RevA.03 25-Dec-2016

==========

pbepbe/6-31g(d)/auto scf=(maxcycle=300,direct,vshift=200,tight,yqc)

density=current scrf=(solvent=ch3cn,smd) opt=(gdiis,maxcycle=250)

freq=noraman guess=(mix,always)

#N Geom=AllCheck Guess=TCheck SCRF=Check GenChk UPBEPBE/6-31G(d)/Auto Freq

---

Pointgroup= C1 Stoichiometry= C11H7F5N3(2) C1[X(C11H7F5N3)] #Atoms= 26

Charge = 0 Multiplicity = 2

SCF Energy= -1085.57332947 Predicted Change= -1.024848D-08

==========

Optimization completed. (Found 2 times)

Item	Max Val.	Criteria	Pass?	RMS Val.	Criteria	Pass?
Force	0.00001	0.00045	[YES]	0.00000	0.00030	[YES]
Displ	0.00089	0.00180	[YES]	0.00089	0.00180	[YES]

Atomic Coordinates (Angstroms)

Type	X	Y	Z
F	0.660556	-2.425072	0.175907
C	1.256768	-1.211231	0.078915
C	2.650275	-1.178053	0.074457
F	3.343139	-2.333210	0.167899
C	3.337972	0.041970	0.014245
F	4.688132	0.077657	0.049646
C	2.590277	1.225567	-0.067336
F	3.230430	2.410844	-0.168230
C	1.196285	1.196659	-0.099859
F	0.559711	2.376101	-0.274690
C	0.467616	-0.026575	-0.003737
N	-0.913252	-0.074958	-0.011121
C	-1.735377	-1.169314	-0.376648
N	-3.011289	-0.620793	-0.276493
C	-2.917875	0.628992	0.252964
C	-4.277098	1.170992	0.582127
C	-5.209491	0.155487	-0.141806
C	-4.378036	-1.144852	-0.300087
N	-1.676245	1.032515	0.444187
H	-1.452888	-1.809378	-1.216541
H	-4.429159	1.158925	1.677116
H	-4.419582	2.207833	0.238602

H	-6.140950	-0.027192	0.414680
H	-5.475758	0.543614	-1.138781
H	-4.579840	-1.675384	-1.244815
H	-4.521919	-1.850485	0.539522

Statistical Thermodynamic Analysis

Temperature= 298.150 Kelvin Pressure= 1.00000 Atm

==========

SCF Energy= -1085.57332947 Predicted Change= -1.024848D-08

Zero-point correction (ZPE)= -1085.4057 0.16757

Internal Energy (U)= -1085.3891 0.18421

Enthalpy (H)= -1085.3881 0.18515

Gibbs Free Energy (G)= -1085.4509 0.12239

Entropy (S)= 0.0002105

Frequencies -- 39.7013 45.5555 64.3031

3.10.7.32 Phenyl Dihydropyrrolotriazolium Cation

Using Gaussian 16: ES64L-G16RevA.03 25-Dec-2016

==========

pbepbe/6-31g(d)/auto scf=(maxcycle=300,direct,vshift=200,tight,yqc)

density=current scrf=(solvent=ch3cn,smd) opt=(gdiis,maxcycle=250)

freq=noraman

#N Geom=AllCheck Guess=TCheck SCRF=Check GenChk RPBEPBE/6-31G(d)/Auto Freq

---

Pointgroup= C1 Stoichiometry= C11H12N3(1+) C1[X(C11H12N3)] #Atoms= 26

Charge = 1 Multiplicity = 1

SCF Energy= -589.793576417 Predicted Change= -9.138990D-09

==========

Optimization completed. (Found 2 times)

Item	Max Val.	Criteria	Pass?	RMS Val.	Criteria	Pass?
Force	0.00001	0.00045	[YES]	0.00000	0.00030	[YES]
Displ	0.00067	0.00180	[YES]	0.00067	0.00180	[YES]

Atomic Type	Coordinates (Angstroms) X	Y	Z
N	-0.087247	0.071663	0.031757
C	-1.520303	0.027661	0.013880
C	-2.151491	-1.186844	-0.295880
C	-3.550893	-1.230740	-0.319777
C	-4.303220	-0.077541	-0.047583
C	-3.653081	1.127761	0.259473
C	-2.254443	1.189418	0.301093
C	0.709588	1.124345	-0.238050
N	1.964307	0.670701	-0.116077
C	1.895893	-0.660459	0.223721
C	3.264448	-1.232692	0.404072
C	4.157173	-0.138368	-0.257112
C	3.344665	1.183149	-0.210964
N	0.642417	-1.064359	0.323181
H	-1.553756	-2.074005	-0.519740
H	-4.052791	-2.172893	-0.561034
H	-5.396730	-0.118792	-0.070750
H	-4.234150	2.027409	0.484248
H	-1.748540	2.121054	0.571163

H	0.387649	2.124106	-0.518878
H	3.478900	-1.344760	1.482287
H	3.373498	-2.221158	-0.067216
H	5.121390	-0.026584	0.258857
H	4.352842	-0.408695	-1.307048
H	3.455570	1.807173	-1.108933
H	3.549773	1.786964	0.687791

Statistical Thermodynamic Analysis

Temperature= 298.150 Kelvin Pressure= 1.00000 Atm

==========

SCF Energy= -589.793576417 Predicted Change= -9.138990D-09

Zero-point correction (ZPE)= -589.5809 0.21265

Internal Energy (U)= -589.5699 0.22365

Enthalpy (H)= -589.5689 0.22460

Gibbs Free Energy (G)= -589.6188 0.17475

Entropy (S)= 0.00016719

Frequencies -- 30.1210 65.0318 106.3996

3.10.7.33 Phenyl Dihydropyrrolotriazolium Radical

Using Gaussian 16: ES64L-G16RevA.03 25-Dec-2016

==========

pbepbe/6-31g(d)/auto scf=(maxcycle=300,direct,vshift=200,tight,yqc)

density=current scrf=(solvent=ch3cn,smd) opt=(gdiis,maxcycle=250)

freq=noraman guess=(mix,always)

#N Geom=AllCheck Guess=TCheck SCRF=Check GenChk UPBEPBE/6-31G(d)/Auto Freq

---

Pointgroup= C1 Stoichiometry= C11H12N3(2) C1[X(C11H12N3)] #Atoms= 26

Charge = 0 Multiplicity = 2

SCF Energy= -589.877828814 Predicted Change= -4.031291D-09

==========

Optimization completed. (Found 2 times)

Item	Max Val.	Criteria	Pass?	RMS Val.	Criteria	Pass?
Force	0.00001	0.00045	[YES]	0.00000	0.00030	[YES]
Displ	0.00040	0.00180	[YES]	0.00040	0.00180	[YES]

Atomic Coordinates (Angstroms)

Type	X	Y	Z
N	-0.109926	0.067518	0.022195
C	-1.496106	0.016974	0.016228
C	-2.178669	-1.226854	-0.068001
C	-3.574509	-1.253975	-0.091165
C	-4.329248	-0.064661	-0.032481
C	-3.650143	1.164024	0.057832
C	-2.253074	1.220415	0.084671
C	0.704591	1.228020	0.021764
N	1.986983	0.676763	-0.072596
C	1.896553	-0.676118	0.036290
C	3.257938	-1.292551	0.164958
C	4.184880	-0.099608	-0.213097
C	3.352993	1.183533	0.052549
N	0.653898	-1.117915	0.091582
H	-1.598679	-2.151572	-0.119726
H	-4.083755	-2.222209	-0.159596
H	-5.423102	-0.096724	-0.053564

H	-4.217563	2.100151	0.114909
H	-1.745652	2.184717	0.179476
H	0.422909	2.078331	-0.611618
H	3.421880	-1.624678	1.206753
H	3.395937	-2.169015	-0.488013
H	5.122436	-0.099601	0.362900
H	4.440453	-0.154940	-1.284214
H	3.546344	1.983091	-0.681321
H	3.510868	1.592695	1.068469

Statistical Thermodynamic Analysis

Temperature= 298.150 Kelvin Pressure= 1.00000 Atm

==========

SCF Energy= -589.877828814 Predicted Change= -4.031291D-09

Zero-point correction (ZPE)= -589.6689 0.20883

Internal Energy (U)= -589.6575 0.22029

Enthalpy (H)= -589.6565 0.22123

Gibbs Free Energy (G)= -589.7074 0.17037

Entropy (S)= 0.00017059

Frequencies -- 51.9637 68.1840 120.7233

CHAPTER 4: SYNTHESIS OF CYCLOALKANONES BY A TANDEM CARBENE AND PHOTOCATALYZED ANNULATION

Portions of this chapter appear in the following publications:

Bay, A. V.; Farnam, E. J.; Scheidt, K. A. Synthesis of Cyclohexanones by a Tandem Photocatalyzed Annulation *J. Am. Chem. Soc.* **2022**, *144*, 7030–7037.

4.1 The Need for Convergent Syntheses of Privileged Small Molecules

The convergent synthesis of privileged small molecules remains a significant challenge among the organic and medicinal chemistry communities. The vast majority of medicinal chemistry campaigns over the last century have focused on the synthesis of molecules featuring achiral or "flat" chemical architectures.[434] Yet, significant fundamental limitations exist for these classes of molecules: they represent only a small portion of chemical space, may have limited, nonselective interactions with three-dimensional target proteins, and often have low solubility or poor bioavailability due to their ability to engage in π-stacking interactions with one another.[240] The ongoing demand for the discovery and development of efficacious drugs requires the exploration of new chemical space. As a result, there has been a dramatic shift away from flat aromatic compounds towards three-dimensional structures with stereogenic centers in recent years.[435]

4.1.1 Cyclic Ketones in the Pharmaceutical Industry

The synthesis of carbocyclic and heterocyclic scaffolds is of importance in the context of drug discovery.[436-439] In particular, cyclic ketones and derivatives thereof are common motifs in a multitude of bioactive compounds.[440-441] For example, ketamine is a commonly employed anesthetic, and tramadol is an opioid used to treat moderate-to-severe pain (**IV-1** and **IV-3**, respectively, **Figure 4-1**). Ertugliflozin, a substituted oxepane scaffold, is a medication prescribed for the treatment of type 2 diabetes (**IV-4**, **Figure 4-1**). These scaffolds or similar motifs can often be accessed from cycloalkanones, thus highlighting the need for methods that enable the convergent construction of cyclic ketones.[442-444]

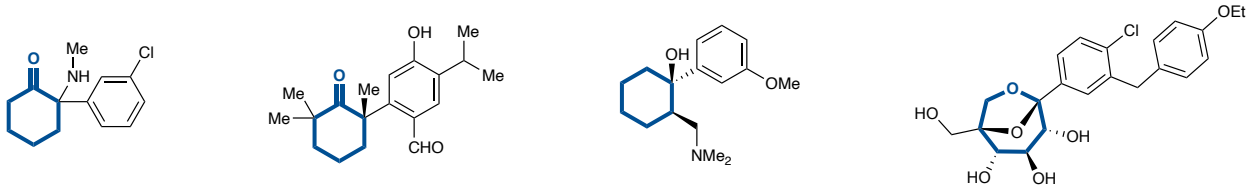

IV-1
ketamine

IV-2
trypanocidal agent

IV-3
tramadol

IV-4
ertugliflozin

Figure 4-1. Bioactive compounds featuring a cyclohexanone motif or a derivative thereof.

4.1.2 Common Synthetic Routes for the Construction of Cyclic Ketones

Cyclohexanones are most frequently synthesized in industry by oxidative or reductive processes (**Scheme 4-1**). For example, reduction of substituted phenols or alkoxybenzenes is known to afford to the corresponding cyclohexanone product.[445-446] Alternatively, oxidative processes have been developed for the synthesis of cyclic ketones, such as the oxidation of cyclohexane derivatives via irradiation of an oxygen-loaded zeolite with visible light.[447] First reported in 1980, the Chapman-Stevens oxidation reaction describes the use of sodium hypochlorite (i.e., bleach) to oxidize alcohols to the corresponding ketone product.[448] These reductive or oxidative processes often require elevated temperatures and strong redox agents or are plagued by over-reduction or over-oxidation, thus limiting their overall utility in the synthesis of complex small molecules.

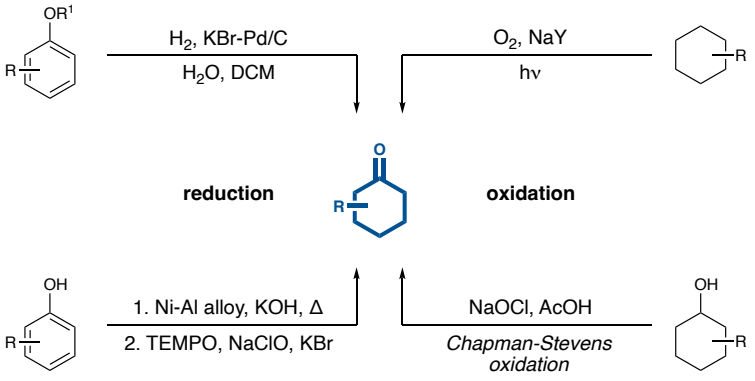

Scheme 4-1. Approaches towards the synthesis of cyclohexanone via oxidation or reduction.

Various cyclization processes can also allow access to substituted cyclic motifs (**Scheme 4-2**). Numerous cycloaddition reactions have been developed to date, such as the Diels-Alder reaction, which often forms six-membered rings via a [4 + 2] reaction.[449-451] Other cyclization processes (e.g., Dieckmann condensation,[452-453] Robinson annulation,[454] etc.) offer alternative routes for accessing cyclic scaffolds. However, the application of these processes in the synthesis of structurally complex cyclohexanones are limited due to electronic requirements, vigorous reaction conditions, or the requirement for functional group interconversions (**Scheme 4-2**).

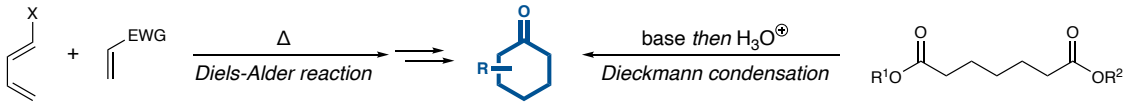

Scheme 4-2. Established approaches to access cyclic motifs via a cyclization process.

4.1.3 Radical Cascade and Radical Relay Mechanisms

The recent renaissance of radical chemistry through the emergence of photocatalysis[210,277-278,455-458] and electrosynthesis[279,281,459-460] has resulted in new approaches for the formation of C–C bonds by enabling non-traditional disconnections. While the versatile reactivity enabled by these radical redox strategies is unquestionable, significant limitations still exist. In particular, the majority of approaches in recent years for the photocatalytic synthesis of ketones concentrate on accessing acyclic products.[288,290,461-462] Early radical chemistry focused on the synthesis of fused ring systems via radical cascade mechanisms. For example, Parker and Fokas developed a tandem radical cyclization strategy for the formal total synthesis of morphine (**Scheme 4-3**).[463] Apart from work focused on the synthesis of fused ring systems via radical cascade mechanisms, the synthesis of carbocyclic or heterocyclic rings via radical C–C bond formation remains underexplored.[455,464-465]

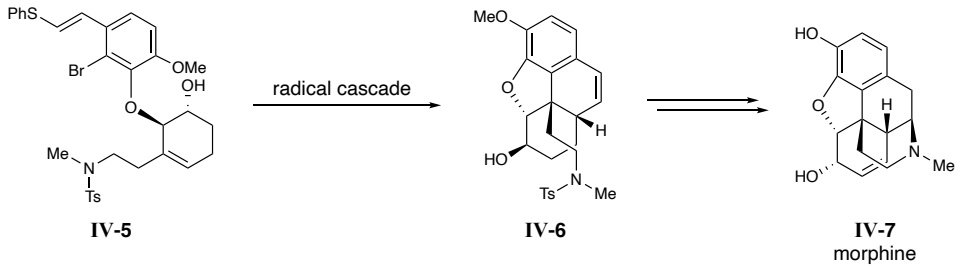

IV-5 **IV-6** **IV-7** morphine

Scheme 4-3. The formal total synthesis of morphine by Parker and Fokas via a radical cascade mechanism.[463]

Structural complexity can be achieved efficiently by the formation of multiple bonds in a one-pot procedure, yet few protocols have been established for the construction of highly functionalized cyclic products. Recent advancements in metal catalysis,[466] photoredox strategies,[288,327,337] and single-electron carbene chemistry[127,149,395-398] have enabled the facile construction of ketones via C–C bond formation, and these reactivity modes have been extended to radical relay processes for the formation of multiple bonds in a single reaction (**Scheme 4-4**).[131,139,157-158,299,464,466-468] While these strategies can afford highly functionalized products, they tend to feature 1,3-bond formation patterns, thus restricting their scope and overall utility. As a result, development of a new methodology for the synthesis of multi-functionalized cyclic scaffolds would allow for the exploration of new chemical space.

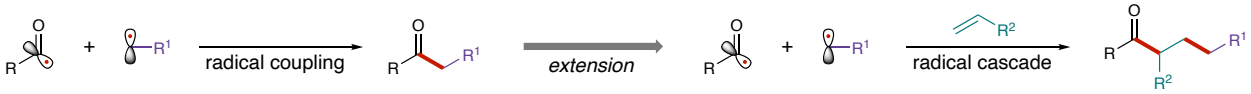

Scheme 4-4. General synthetic schemes of radical coupling and radical cascade reactions for the construction of ketones.

4.1.4 Rise in Benzylic Oxidations

Benzylic C–H bonds are highly prevalent in bioactive compounds (e.g., ~40% of the top 200 small molecule drugs by retail sales in 2020 contain benzylic or benzylic-like C–H bonds),[469]

and their functionalization using single-electron catalysis is of great interest.[153,470-479] Following early reports using superstoichiometric oxidants, such as *o*-iodoxybenzoic acid (IBX), for the oxidation of benzylic groups, photoredox catalysis and electrochemistry have been employed to enable a single-electron oxidation of benzylic C–H bonds.[480] For example, Liu's research group reported a benzylic C–H functionalization process using electrochemistry to perform the single-electron oxidation (**Scheme 4-5**).[481] Additionally, our group developed a combined photoredox and enzymatic approach for C–H benzylic hydroxylations.[482] Radical species featuring benzylic stabilization have been shown to undergo radical-radical coupling with a variety of radical coupling partners in recent years, thus allowing access to an array of functionalized benzylic compounds.

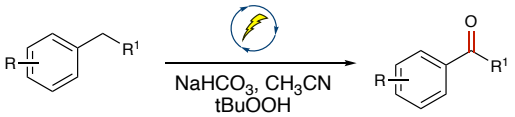

Scheme 4-5. Electrochemical benzylic C–H functionalization strategy developed by Liu and coworkers.[481]

The efficient synthesis of benzylic ketones has also received significant attention, as ketones are highly valuable functional groups that are often the center of reactivity and diversification. Advancements in the construction of these prevalent motifs include the α-arylation of ketones (via transition metal catalysis) and various radical coupling strategies (via acyl/ketyl radicals).[97,149,153,483-495] For example, Studer and coworkers recently developed a benzylic C–H acylation process using combined NHC and photoredox catalysis wherein single-electron oxidation of a benzylic C–H bond affords a radical cation, and subsequent deprotonation by base yields a stabilized benzylic radical (**Scheme 4-6**).[153] However, few strategies exist for the mild α-functionalization of benzylic ketones.

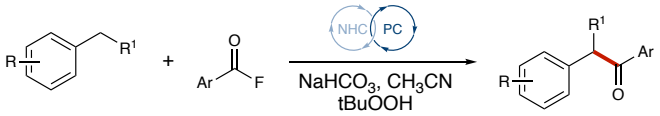

Scheme 4-6. A combined NHC and photoredox-catalyzed method developed by Studer and coworkers for benzylic C–H acylation.[153]

4.2 Hypothesis for the Tandem-catalyzed Synthesis of Cycloalkanones

Given our recent investigations on the synthesis of ketones in combination with the rise in single-electron benzylic oxidations, we envisioned that oxidation of benzylic ketones might be possible. We hypothesized that combined carbene and photoredox catalysis[121,123,496] would allow for the construction of two contiguous C–C bonds via a novel radical α-functionalization of in situ generated benzylic ketones under mild reaction conditions. We thus aimed to develop a tandem carbene and organophotoredox-catalyzed convergent synthesis of α,β-disubstituted cyclohexanones (**Figure 4-2**).

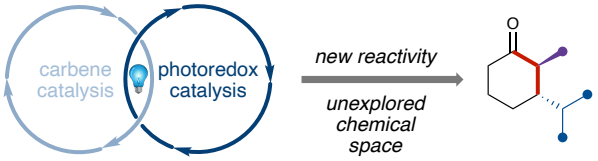

Figure 4-2. Combined carbene and photoredox catalysis for the synthesis of cyclic ketones.

This process would feature consecutive photoredox cycles that facilitate two distinct transformations in one pot for the rapid synthesis of complex cyclic scaffolds. In contrast to established radical relay processes wherein radical addition into an alkene occurs first, the increased stability of benzylic radicals[170] would allow for initial generation of a linear ketone via a light-driven, carbene-catalyzed intermolecular radical-radical coupling. Subsequently, single-electron oxidation of the corresponding enol in a second photoredox cycle would enable intramolecular cyclization to the α,β-disubstituted cyclohexanone product (**Scheme 4-7**).

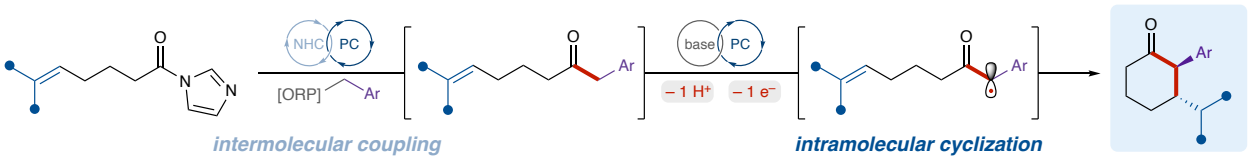

Scheme 4-7. Hypothesized mechanism for the construction of cycloalkanones via a tandem photocatalyzed process.

4.3 Reaction Discovery

A process was envisioned in which an acyl azolium radical (**IV-I•**) derived from δ,ε-unsaturated acyl imidazole **IV-8** and an alkyl radical derived from an oxidatively generated radical precursor (e.g., a Hantzsch ester, **IV-9**) could be accessed using combined carbene and photoredox catalysis. Two mechanistic possibilities exist for the combination of acyl azolium radical **IV-I•** and an oxidatively generated radical (**Figure 4-3**). Radical-radical coupling of **IV-I•** and the alkyl radical could occur to give linear ketone intermediate **IV-10** (produced via pathway 1). Given the recent establishment of single-electron benzylic oxidations, we envisioned that if the alkyl radical is a benzyl radical, then a deprotonation followed by single-electron oxidation would afford α-radical **IV-II•**. Intramolecular cyclization could then occur with the pendant alkene, and a single-electron reduction of the final γ-radical **IV-III•** followed by protonation would yield the corresponding desired **IV-11**. Alternatively, it may be possible for the oxidatively generated radical to initially undergo radical addition into the alkene given the precedence set by over 20 radical relay reactions that have been developed over the past few years;[96] an unstable alkyl radical would be expected to add into the alkene first, in this case producing a more stabilized ε-radical (**IV-I''**, produced via pathway 2). Intramolecular radical-radical coupling would then occur to give the final desired cyclic ketone **IV-11'**.

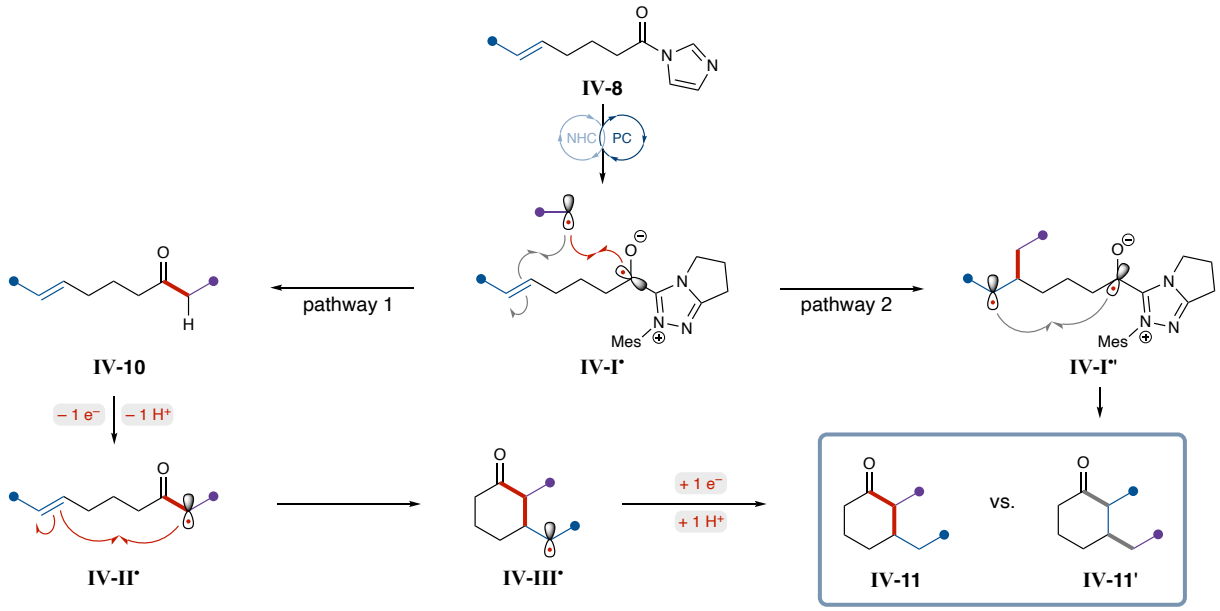

Figure 4-3. Possible mechanistic pathways to access cyclic ketones from **IV-8**.

Initial efforts searching for reactivity involved screening a variety of oxidatively generated radical precursors, including Hantzsch esters (**IV-9**), biscatecholato silicates (**IV-12**), BF_3K salts (**IV-13**), and various trifluoromethyl radical sources (e.g., Langlois reagents, **IV-14**). Reactions were monitored by GCMS, where the fragmentation pattern could be used to identify connectivity. A small peak corresponding to the desired product mass (**IV-11r'** = 230 g/mol) was observed for the reaction between a tert-butyl substituted Hantzsch ester **IV-9r** and acyl imidazole **IV-8a** (**Scheme 4-8**). Analysis of the fragmentation pattern suggested that the product features a 1,3-bond formation pattern with a core α-phenyl cyclohexanone scaffold.

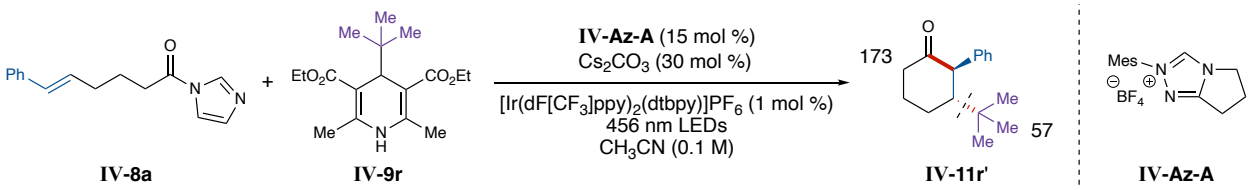

Scheme 4-8. Synthesis of **IV-11r'**, and the corresponding fragmentation pattern observed by GCMS analysis.

The corresponding reaction using 4-chloro-benzyl Hantzsch ester (**IV-9c**) was setup and analyzed. Although a similar fragmentation pattern for the core cyclohexanone motif was expected, analysis of the fragmentation pattern suggested that the cyclohexanone product featured a 1,2-bond formation pattern instead of the 1,3-bond formation pattern that was anticipated based on previous results (vide supra; **Scheme 4-9**). These results suggest that the mechanism may be dependent on the stability of the radical coupling partner. A less stable alkyl radical, such as a tert-butyl radical, may undergo radical addition to a styrenyl alkene to yield the thermodynamically more stable benzylic radical. On the contrary, a more stabilized benzyl radical partner may undergo radical-radical coupling with **IV-I•** to yield a closed-shell linear ketone intermediate (**IV-10**). This intermediate could then undergo cyclization via pathway 2 (**Figure 4-3**).

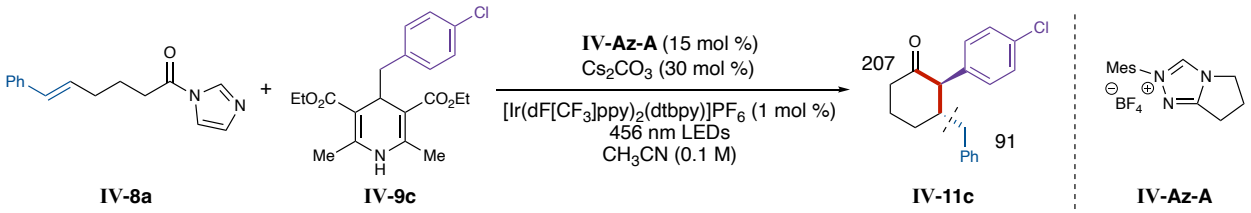

Scheme 4-9. Synthesis of **IV-11c** and the corresponding fragmentation pattern observed by GCMS analysis.

4.3.1 Optimization of Reaction Conditions

Using our previously optimized reaction conditions for the synthesis of aliphatic ketones as a starting point,[97] it was determined that further optimization of the solvent, *N*-heterocyclic carbene (NHC) precursor, and base was unnecessary. The reaction was thus optimized using benzyl Hantzsch **IV-9a** as the oxidatively generated radical precursor. The initial hit reaction conditions provided only trace amounts of the product, only visible by GCMS, and approximately 31% ^{1}H NMR spectroscopic yield of the linear ketone intermediate **IV-10a**, confirming the

feasibility of the first reaction step. Given that this process features two distinct photoredox cycles by the same photocatalyst, choice of photocatalyst unsurprisingly was found to be critical in optimizing for the desired reactivity. Highly oxidizing or highly reducing photocatalysts were not suitable for this process (**Table 4-1**, entries 3-4), as their range of redox potentials were not broad enough to enable the various oxidations and reductions. When organophotocatalyst 3DPAFIPN was employed, significant cyclized product was observed (**Table 4-1**, entry 1), suggesting that the necessary redox potentials fall near its redox range ($E_{1/2}$ PC*/PC$^{\bullet-}$ to $E_{1/2}$ PC/PC$^{\bullet-}$ = +1.09 to –1.59 V vs. SCE).[458] Although this process was optimized with Hantzsch esters,[351-352,497] use of organophotocatalyst 4CzIPN afforded product using benzyl potassium trifluoroborate salts (Bn–BF_3Ks)[413,498] as an alternative oxidatively-generated radical precursor (ORP; **Table 4-1**, entry 5).

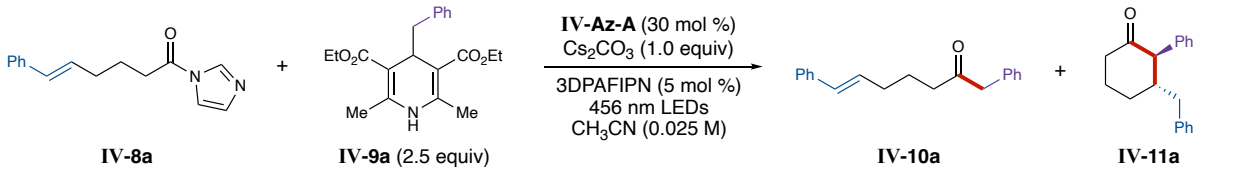

IV-8a **IV-9a** (2.5 equiv) **IV-10a** **IV-11a**

entry	deviation from standard	yield of **IV-10a** (%)[a]	yield of **IV-11a** (%)[a]
1	none	7	55 (52)[b]
2	[Ir(dF[CF_3]ppy)$_2$(dtbpy)]PF_6 instead of 3DPAFIPN	31	0
3	*fac*-Ir(ppy)$_3$ instead of 3DPAFIPN	trace	trace
4	Mes-Acr-Ph instead of 3DPAFIPN	0	0
5	Bn–BF_3K + 4CzIPN instead of Bn–HE + 3DPAFIPN	7	35
6	0.01 M instead of 0.025 M	8	21
7	0.05 M instead of 0.025 M	5	26
8	0.1 M instead of 0.025 M	6	15

Table 4-1. Optimization of the reaction conditions. [a] ^{1}H NMR spectroscopic yield was measured using 1,3,5-trimethoxybenzene as the internal standard. [b] Isolated yield. **IV-Az-A** = 5,5-Mes.

Concentration was also expected to impact reactivity significantly given that this process features both intermolecular and intramolecular processes. The amount of linear ketone increased with increasing concentration, which is in alignment with the linear ketone being formed through an intermolecular radical-radical coupling (**Figure 4-4**). On the contrary, the amount of cyclized

material increased with a decrease in concentration, as an intramolecular process is required to form the cyclized material. A concentration of 0.025 M was found to increase the yield to 45%, while keeping the amount of unreacted linear ketone intermediate to a minimum. Final optimization of the remaining factors, such as stir rate, light intensity, and more, further increased the amount of cyclohexanone product up to 55% ^{1}H NMR spectroscopic yield (entry 1, **Table 4-1**).

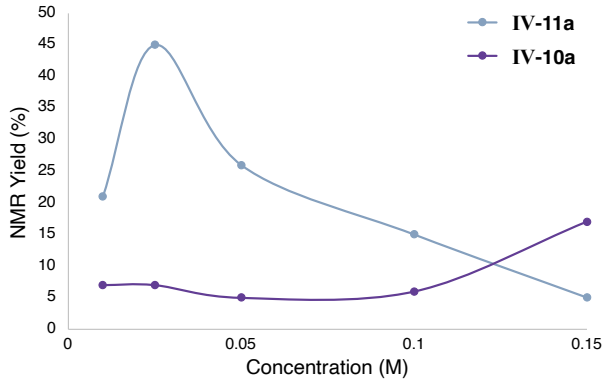

Figure 4-4. ^{1}H NMR spectroscopic yield of the cyclized product (**IV-11a**) and linear intermediate (**IV-10a**) as a function of reaction concentration. ^{1}H NMR spectroscopic yield was measured using 1,3,5-trimethoxybenzene as the internal standard.

Initial attempts at product isolation resulted in a yield that was approximately 20% lower than expected based on the ^{1}H NMR spectroscopic yield. After significant investigation, it was determined that the diminished yield was due to coelution of the product with the Hantzsch pyridine byproduct, which is produced when the Hantzsch ester is oxidized to afford the benzyl radical coupling partner. Unfortunately, Hantzsch pyridine is known to streak on column chromatography, with multiple reports in the literature documenting difficult separations from product (see Chapter 2.6). Over 30 different workup and purification techniques were attempted. It was eventually determined that a highly acidic workup (i.e., washing with concentrated

hydrochloric acid) protonates the Hantzsch pyridine, pulling it into the aqueous layer. When this acidic workup was followed by column chromatography, the product was isolated in 52% yield. Pure isolated product was subjected to the workup conditions to ensure that the final product is not negatively affected by the acidic workup, and over 90% of the product was re-isolated following five vigorous aqueous washes with concentrated hydrochloric acid. The latter data suggests that these workup conditions may be used if separation by column chromatography is not suitable as the sole purification technique.

4.3.2 Examination of Reaction Sensitivity

The optimized reaction was evaluated for its sensitivity to demonstrate the practical nature of this protocol and ensure a high degree of reproducibility with differing reaction setups (**Table 4-2**).[499] Only minor deviations in yield were observed for small changes in concentration, light intensity, and temperature. As expected, it was found that high oxygen levels are detrimental to the reaction efficiency, with a dramatic change in yield (i.e., 0% yield) when air was bubbled through the reaction solution prior to irradiation. Similarly, addition of water decreased the

A

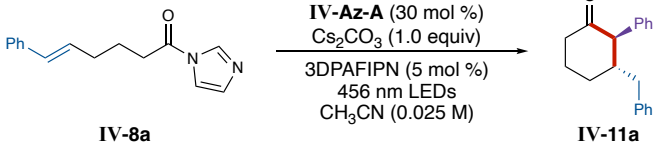

entry	experiment	additive or change in setup
1	high c (–10% V_{rxn})	–10% V_{rxn}
2	low c (+10% V_{rxn})	+10% V_{rxn}
3	high H_2O (H_2O = +1% V_{rxn})	H_2O = +1% V_{rxn} (20 uL)
4	medium O_2	non-degassed solvent
5	high O_2	+ air (10·V_{rxn} = 20 mL)
6	low T	fan placed over reaction
7	high T	reaction heated to 50 °C
8	low intensity (d·4)	d·4 (28 cm from light)
9	high intensity (d/4)	d/4 (1.8 cm from light)
10	control	-

B

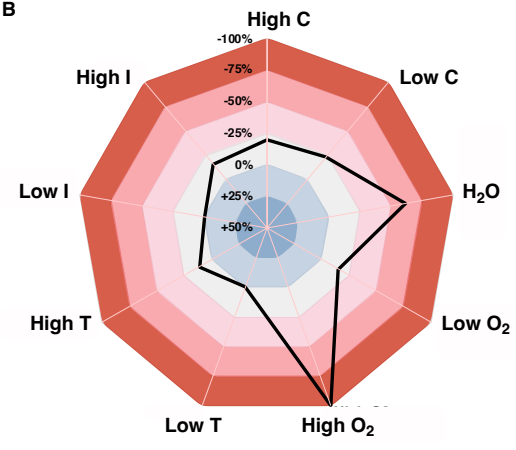

Table 4-2. Reaction sensitivity screen. **A)** Details regarding experimental setup. **B)** Percent changes in yield in comparison to the standard reaction conditions.

reaction efficiency, but normal reactivity was restored using non-degassed acetonitrile without additional drying under inert atmosphere (i.e., low oxygen and low water). The demonstrated overall robustness of this reaction suggests that little-to-no difficulty should be encountered when these reactions are run in other laboratories.

4.4 Substrate Scope of Cycloalkanones

4.4.1 Hantzsch Ester Variation

These reaction conditions were used to synthesize cycloalkanones with a variety of substituted α-aryl substituents (**Table 4-3**). Substituted benzyl radical precursors featuring electron-withdrawing or electron-donating groups were found to be suitable coupling partners and allowed for significant conversion to the corresponding cyclohexanone products (**IV-11b-f**).[500] Many benzylic oxidation strategies are inefficient or completely ineffective with electron-poor arenes, as electron-withdrawing groups increase the oxidation potential of the arene ring significantly. The strategy reported herein, however, tolerates electron-withdrawing groups, with yields up to 66% (**IV-11d**) over two C–C bond-forming steps in our one-pot procedure. This difference in reactivity likely stems from the mechanism of oxidation, wherein deprotonation of the α-position gives the enol, which can be oxidized at lower potentials.

4.4.2 Acyl Imidazole Variation

A diverse array of β-substituted cycloalkanones was accessed using this protocol. Various substituted β-benzyl cyclohexanone products were isolated in moderate-to-good yields (**IV-11g-i,k**, **Table 4-3**). Disubstituted alkenes were also tolerated, with isolation of **IV-11j** in 81% yield. Cyclohexanones featuring heteroaromatic substitution were also constructed using this tandem

cyclization process, with thiophene-substituted **IV-11l** and furan-containing **IV-11m** isolated in moderate-to-good yields. The diversity of products that may be synthesized under these reaction conditions was further showcased by isolation of δ-ester **IV-11n** in high yield, providing a functional group handle for diversification. Isolation of 4-geminal-diester **IV-11o** in excellent yield suggests that highly functionalized cyclohexanones may be synthesized using this method by pre-functionalization of the linear starting material; moreover, the excellent yield obtained for

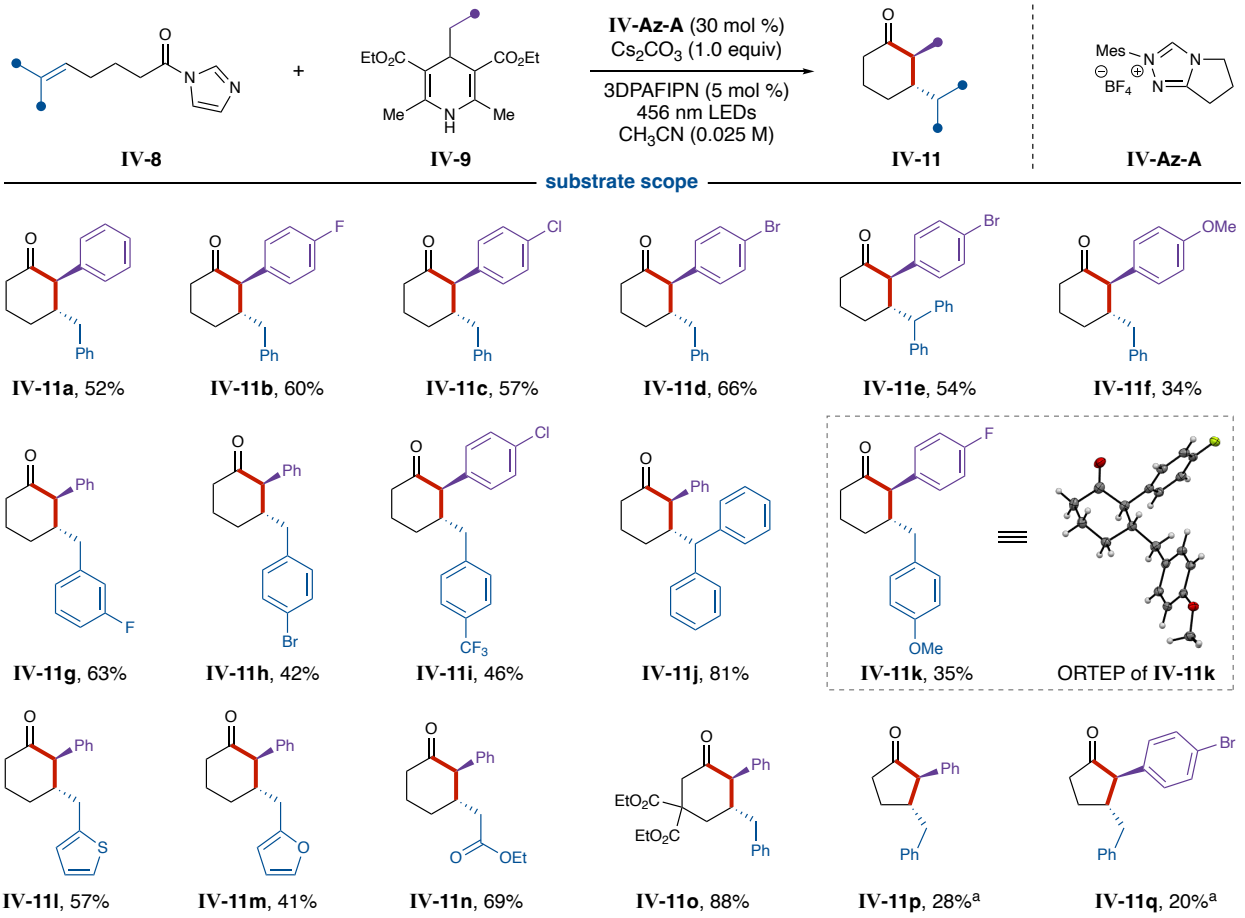

Table 4-3. Substrate scope for the tandem photocatalyzed synthesis of cycloalkanones. Diastereomers were assigned by analogy to X-ray crystal structures of **IV-11k**. [a] Isolated from the corresponding pentenoyl imidazole **IV-8**.

IV-11o demonstrates the potential utility of this method for the construction of key synthetic building blocks. Although these conditions were optimized for the synthesis of cyclohexanone derivatives, isolation of **IV-11p** and **IV-11q** suggests that this process may be employed for the synthesis of cyclopentanones and other cycloalkanones with additional optimization.

4.5 Diversification of Products

Reactions of cyclic ketones have been extensively reported in the literature (e.g., reduction to the corresponding cyclohexane, condensation with an amine, etc.), highlighting their broad versatility as synthetic intermediates.[501-508] As such, the utility of this process in synthesis was demonstrated through a brief series of product diversification reactions (**Figure 4-5**). When **IV-11a** was subjected to modified Beckmann conditions, the corresponding caprolactam **IV-15a** was isolated in 77% yield.[509] Similarly, subjecting **IV-11a** to standard Baeyer-Villiger conditions enabled the corresponding lactone **IV-16a** to be furnished in quantitative yield.[510] A multitude of additional diversification directions can be envisioned for these products given their synthetic utility.

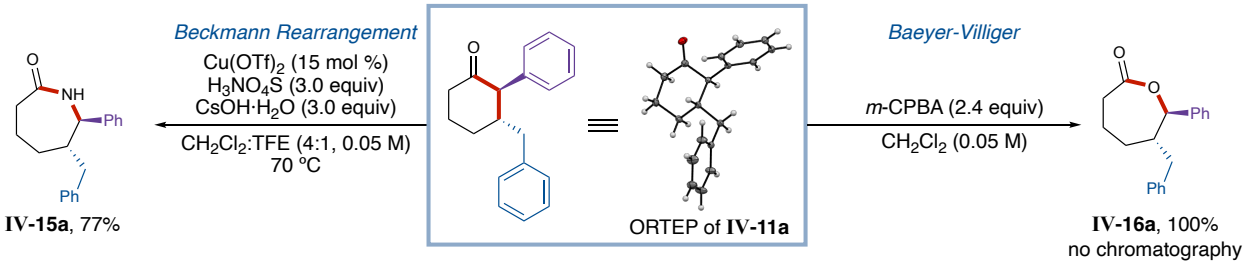

Figure 4-5. Diversification of products to access lactam **IV-15a** and lactone **IV-16a**.

4.6 Mechanism for the Synthesis of Cycloalkanones

4.6.1 Mechanistic Studies

While the mechanism of the carbene-catalyzed radical-radical coupling has been studied,[97,403] key mechanistic experiments were employed to study the reaction mechanism of the benzylic ketone/enol oxidation. Subjecting linear ketone **IV-10a** to the organophotocatalyst and light under basic conditions yielded cyclic **IV-11a** in 90% yield, supporting linear ketone **IV-10a** as an intermediate in this reaction and offering an alternative route to access these products (**Figure 4-6**). Control experiments strongly indicate a photocatalytic transformation, as no reaction occurred in the absence of base, photocatalyst, or light (**Figure 4-6**). Moreover, a TEMPO trapping experiment suggests production of an α-benzylic radical, as the mass of TEMPO-adduct **IV-17a** was observed by high-resolution mass spectrometry (HRMS) and the structure was elucidated by unpurified ^{1}H NMR spectroscopy analysis (**Figure 4-6**).

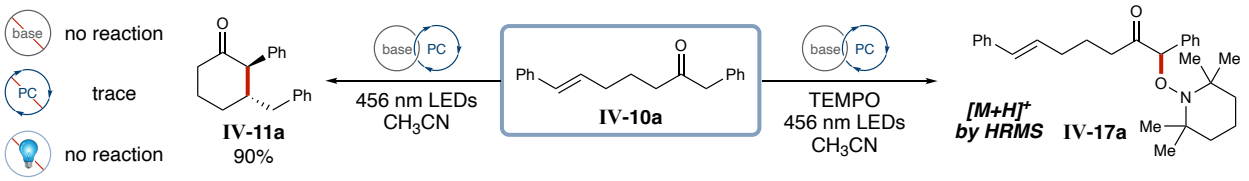

Figure 4-6. Mechanistic studies starting from linear ketone intermediate **IV-10a**. TEMPO = 2,2,6,6-tetramethylpiperidin-1-yl)oxyl radical.

Stern-Volmer fluorescence quenching experiments provide kinetic information regarding the photophysical intermolecular deactivation processes (i.e., photocatalyst quenching) and are frequently employed to study the mechanism of photoredox reactions.[511] Stern-Volmer quenching experiments were used to evaluate the mechanism of this tandem process, and the results reveal that both **IV-10a** and a basic mixture of **IV-10a** with cesium carbonate (**IV-10a-Cs**) quench the

photocatalyst, with the basic mixture being the more prominent quencher (**Figure 4-7**). Together with the requirement of basic reaction conditions as indicated by the control experiments (vide supra), these results suggest that the enol or cesium enolate **IV-10a-Cs** likely undergoes single-electron oxidation by the photocatalyst.

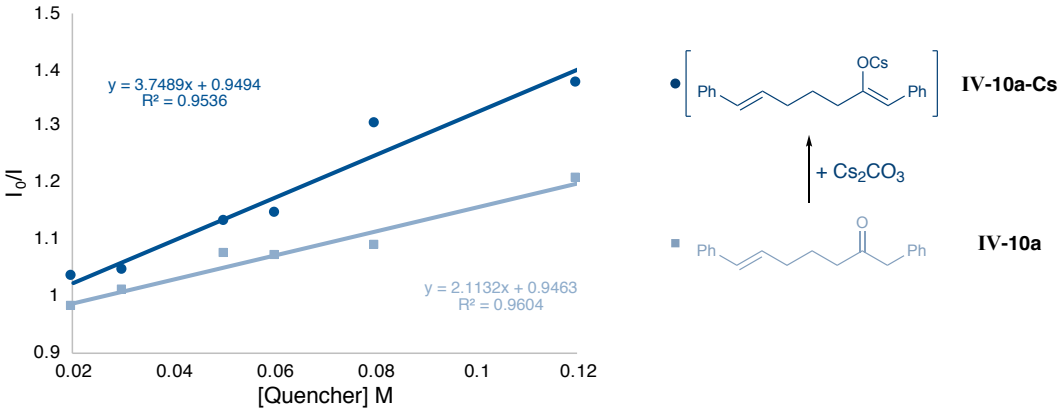

Figure 4-7. Stern-Volmer fluorescence quenching experiment, revealing that **IV-10a-Cs** quenches the photocatalyst to a greater degree than **IV-10a**.

Lastly, the reaction was run under standard reaction conditions in deuterated acetonitrile to shed light on the final step of this reaction. Analysis of the isolated cyclized product revealed significant deuterium incorporation at the ketone α-positions, an expected result given the acidity of these protons. Moreover, approximately 50% deuterium incorporation was identified at the γ-benzylic position (blue highlight, **Scheme 4-10**), suggesting that the mechanism terminates by hydrogen-atom abstraction from the solvent[512] or reduction followed by protonation.[513]

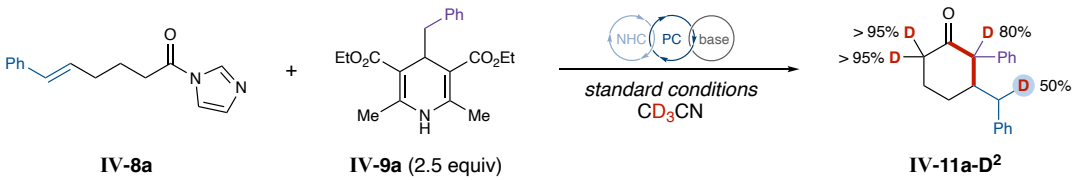

IV-8a **IV-9a** (2.5 equiv) **IV-11a-D²**

Scheme 4-10. Deuterium incorporation experiment to study the final step of the reaction and the fate of γ-benzylic radical **IV-III•**.

4.6.2 Proposed Mechanism for the Tandem Cyclization Process

Using our previous knowledge and the results of these mechanistic experiments, we propose a mechanism featuring two distinct photoredox cycles which operate productively in concert (**Figure 4-8**). Single-electron oxidation of the oxidatively-generated radical precursor **IV-9** yields the corresponding radical cation, which fragments to provide benzylic radical **IV-9•**. Single-electron reduction of acyl azolium **IV-I**, derived in situ from acyl imidazole **IV-8**, affords acyl azolium radical **IV-I•**. Intermolecular radical-radical coupling and loss of the NHC gives linear ketone intermediate **IV-10**. Single-electron oxidation of the corresponding enol or cesium enolate **IV-10-Cs** affords α-benzylic radical **IV-II•**, which engages in an intramolecular cyclization with the alkene. The resulting γ-benzylic radical **IV-III•** may undergo hydrogen atom transfer

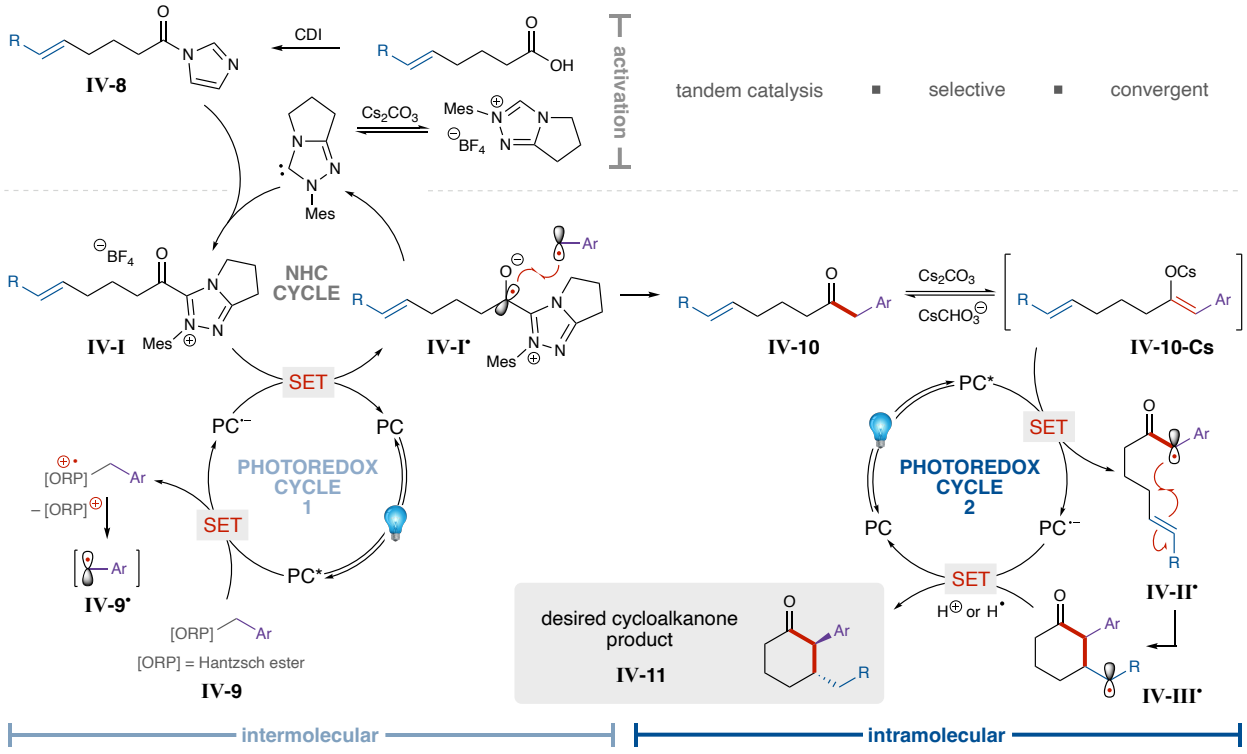

Figure 4-8. Proposed mechanism for the tandem photocatalyzed annulation process.

(HAT) or be reduced by the photocatalyst to the corresponding anion, which deprotonates the solvent or bicarbonate to afford the desired cyclohexanone product **IV-11**.

4.7 Summary of Combined NHC and Photoredox Catalysis

4.7.1 Overview of Results

In summary, a tandem carbene and photoredox-catalyzed strategy for the convergent synthesis of α,β-disubstituted cyclic ketones has been developed. This process enables the construction of two contiguous C–C bonds via a formal [5 + 1] cycloaddition and highlights a novel method for the α-functionalization of ketones under mild reaction conditions. Through the combination of two distinct processes in one pot, this reaction offers a route to synthesize complex cycloalkanone products that can be leveraged to access scaffolds relevant in both the pharmaceutical and materials industries.

4.7.2 Future Directions

The reactivity difference observed using non-benzylic radical coupling partners led to the discovery of a trifluoromethylation cyclization process. Using Langlois reagent as an oxidatively generated trifluoromethyl radical source, a β-trifluoromethyl substituted cyclohexanone was observed by GCMS and unpurified ^{1}H NMR spectroscopy analysis. Control experiments revealed that the reaction works in the absence of **IV-Az-A**, which is in alignment with a different mechanism from the tandem NHC and photoredox-catalyzed annulation described above. Based on the preliminary mechanistic studies, the proposed mechanism is initiated by single-electron oxidation of Langlois reagent (**IV-14**) by the excited photocatalyst to afford trifluoromethyl radical **IV-18**$^{\bullet}$. The unstable alkyl radical undergoes addition to the pendant alkene of acyl imidazole **IV-**

8 to afford ε-radical **IV-19•**, and single-electron reduction of **IV-19•** by the reduced photocatalyst yields anion **IV-19⁻**. Intramolecular cyclization into the acyl imidazole carbonyl yields the final desired cycloalkanone product **IV-20**.

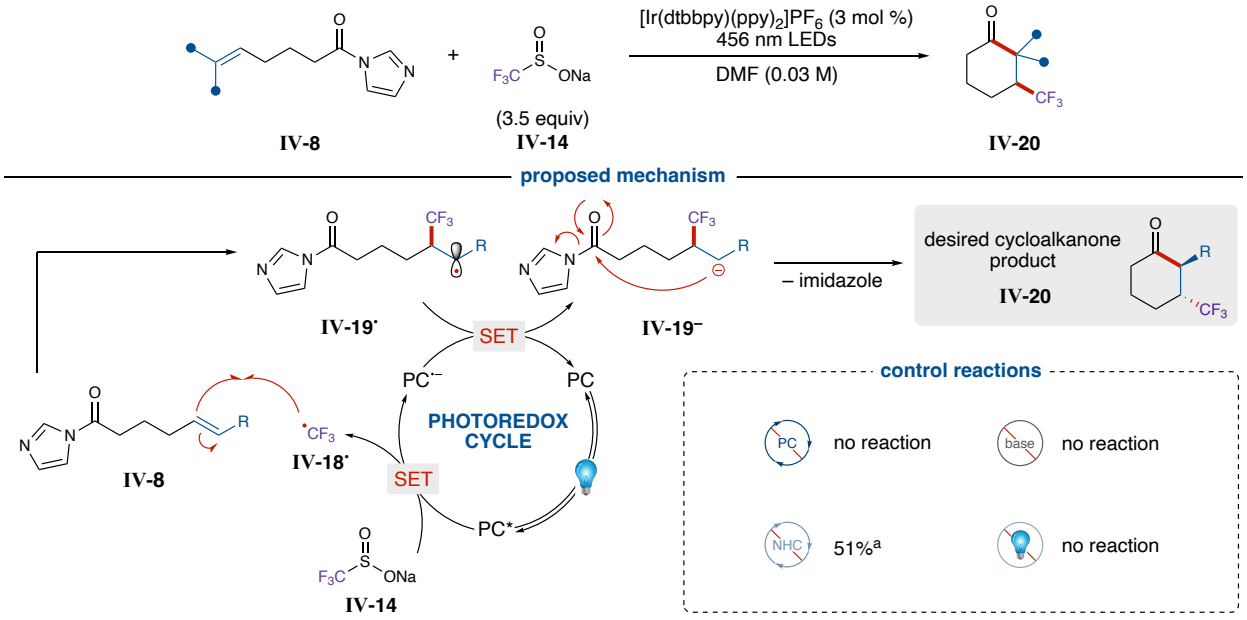

Figure 4-9. Proposed mechanism for the β-trifluoromethylation cyclization process. [a] GCMS yield using 1,3,5-trimethoxybenzene as an internal standard.

Significant optimization of the reaction conditions was required to afford the product in reasonable yield. Over 160 conditions were screened to optimize the solvent, base, photocatalyst, light source, and more. It was found that iridium photocatalyst $[Ir(dtbbpy)(ppy)_2]PF_6$ outperformed organophotocatalyst 3DPAFIPN, the photocatalyst used for the combined NHC and photoredox-catalyzed tandem process (vide supra), and all other photocatalysts screened (entries 1-4, **Table 4-4**). Dimethylformamide (DMF) resulted in a better yield compared to the other screened solvents, including acetonitrile, DCM, and THF (entries 5-7, **Table 4-4**). Similarly, alternative light sources proved less efficient than 456 nm blue LEDs (entries 8-9, **Table 4-4**). Final optimization of the remaining reaction conditions resulted in an efficient reaction that provides the desired product in

72% ^{1}H NMR spectroscopic yield. To date, attempts to isolate the product have resulted in a 46% yield, perhaps due to the high solubility of the product in the high-boiling reaction solvent (**Table 4-4**). Attempts to troubleshoot the isolation of this product can be found in Ada Kwong's thesis in Appendix A2.

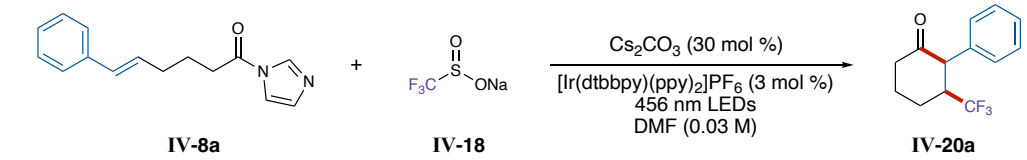

IV-8a + **IV-18** → **IV-20a**

optimization of reaction

entry	deviation from standard	yield **IV-20a** (%)[a]
1	none	53
2	$[Ir(dF[CF_3]ppy)_2(dtbpy)]PF_6$ instead of $[Ir(dtbbpy)(ppy)_2]PF_6$	12
3	3DPAFIPN instead of $[Ir(dtbbpy)(ppy)_2]PF_6$	15
4	Mes-Acr-Ph instead of $[Ir(dtbbpy)(ppy)_2]PF_6$	0
5	CH_3CN instead of DMF	6
6	DCM instead of DMF	4
7	THF instead of DMF	4
8	390 nm light instead of 456 nm light	37
9	427 nm light instead of 456 nm light	40

optimized conditions

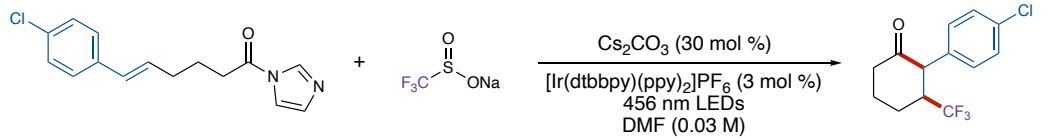

IV-8t + **IV-14** → **IV-20b**, 72%[b] (46%)[c]

Table 4-4. Optimized reaction conditions for the trifluoromethylation cyclization process. [a] GCMS yield using 1,3,5-trimethoxybenzene as an internal standard. [b] ^{1}H NMR spectroscopic yield using 1,3,5-trimethoxybenzene as an internal standard. [c] Isolated yield on a 0.20 mmol reaction scale.

4.8 Experimental Synthesis Protocols and Analyses

4.8.1 General Information

All reactions were carried out under an argon or nitrogen atmosphere in oven-dried glassware with magnetic stirring. All solvents were purified by passing through a bed of activated alumina, dried over 3.0 Å molecular sieves, and then degassed using freeze-pump-thaw method

(3-4 cycles). Purification of reaction products was carried out by flash chromatography on Biotage Isolera 4 or Biotage Dalton 2000 (ELSD-A120) systems with ultra-grade silica cartridges. Analytical thin layer chromatography was performed on EM Reagent 0.25 mm silica gel 60-F plates. Visualization was accomplished with UV light or ceric ammonium molybdate (CAM) stain followed by heating.

^{1}H NMR spectra were recorded on an AVANCE III 500 MHz w/ direct cryoprobe (500 MHz) spectrometer and are reported in ppm using solvent as an internal standard ($CDCl_3$ at 7.26 ppm). Data are reported as (ap = apparent, s = singlet, d = doublet, t = apparent triplet, q = quartet, m = multiplet, b = broad; coupling constant(s) in Hz; integration) Proton-decoupled ^{13}C NMR spectra were recorded on an AVANCE III 500 MHz w/ direct cryoprobe (126 MHz) spectrometer and are reported in ppm using solvent as an internal standard ($CDCl_3$ at 77.16 ppm). Mass spectra were obtained on a WATERS Acquity-H UPLC-MS with a single quad detector (ESI) or an Agilent 7890 gas chromatograph equipped with a 5975C single quadrupole EI-MS. High-resolution mass spectrometry (HRMS) was obtained using an Agilent 6201 MSLC-TOF (ESI) or Bruker IMPACT II (ESI). Fluorescence data was obtained on an Agilent Cary Eclipse Fluorescence Spectrophotometer using Eppendorf UVette 220-1600 nm disposable single sealed cuvettes (height of cuvette was adjusted to obtain clear path). All photocatalytic reactions were carried out using Kessil PhotoReaction PR160L 456 nm lights. $[Ir(dF(CF_3)ppy)_2(dtbpy)]PF_6$ (purchased from Strem Chemicals) and Mes-Acr-Ph (purchased from Sigma Aldrich) were used without purification. *Fac*-$Ir(ppy)_3$ was synthesized according to the literature procedure.[514] 3DPAFIPN and 4CzIPN were prepared according to the literature procedure.[418] *N*-mesityl pyrrolotriazolium (**IV-Az-A**, 5,5-Mes) was prepared based on a known literature procedure.[419]

4.8.2 General Synthetic Procedures and Spectral Data for New Compounds

All oxidatively-generated radical precursors (ORPs; substituted benzyl Hantzsch esters (**IV-9**) and Bn–BF_3K) were synthesized according to the established literature procedure and matched the reported spectral data.[285,371,421,515]

4.8.2.1 General Procedure 1 for the Synthesis of Carboxylic Acids:

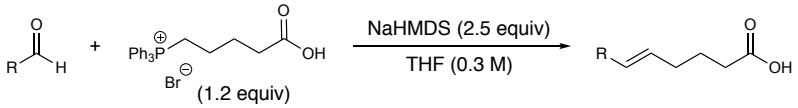

Scheme 4-11. Synthesis of carboxylic acids via a Wittig reaction.

(4-carboxybutyl)triphenyl phosphonium bromide (5.32 g, 12 mmol, 1.2 equiv) was suspended in anhydrous THF (20-40 mL) at 0 °C. NaHMDS (2 M in THF; 12.5 mL, 2.5 equiv) was added dropwise into the suspension and further stirred for 30 minutes. After the respective aldehyde (10 mmol, 1.0 equiv) dissolved in THF was added dropwise to the reaction, the mixture was allowed to warm to room temperature. The reaction was stirred for 12 h or until complete consumption of the aldehyde was observed. The mixture was then quenched by H_2O (20 mL) and acidified to pH = 2 using HCl (1 M). The acidified aqueous layer was extracted with ethyl acetate (3 × 30 mL), and the combined organic layers were washed with brine, dried over anhydrous $MgSO_4$, and filtered. The filtrate was concentrated under reduced pressure and the unpurified oil was purified by flash chromatography on silica gel (CH_2Cl_2(1% AcOH):hexanes column) afforded the product.

4.8.2.2 General Procedure 2 for the Synthesis of Acyl Imidazoles:

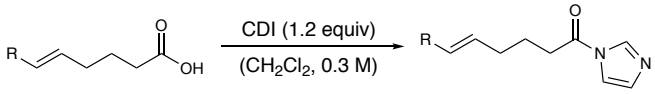

Scheme 4-12. Synthesis of acyl imidazoles from the corresponding carboxylic acid.

The starting acyl imidazoles **IV-8** were prepared based on the method of Lee and Scheidt.[370] The appropriate acid (10 mmol, 1.0 equiv) was dissolved in dichloromethane (0.3 M), and carbonyldiimidazole (CDI, 12 mmol, 1.2 equiv) was added slowly. The resulting solution was stirred for 1-12 h at room temperature. Upon completion, the resulting solution was transferred to a separatory funnel and washed with deionized water (2x25 mL), and the organic layer was dried over $MgSO_4$. Concentration under reduced pressure afforded the acyl imidazole product, which was used in the subsequent reaction (see General Procedure 3) without further purification.

4.8.2.3 General Procedure 3 the Synthesis of Cycloalkanones

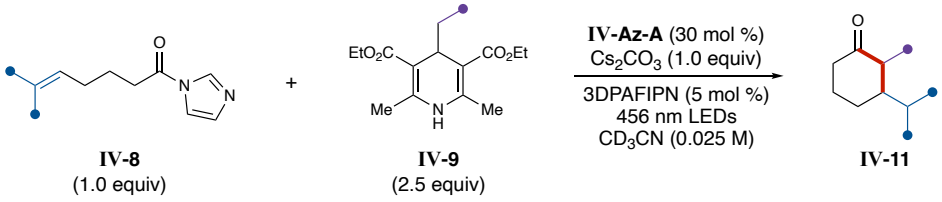

Scheme 4-13. Synthesis of cycloalkanones using combined NHC and photoredox catalysis in a tandem photocatalyzed process.

All reactions were set up inside of a glovebox under N_2 atmosphere. To an oven-dried 20-mL vial containing a stir bar the respective acyl imidazole **IV-8** (0.20 mmol, 1.0 equiv), the respective Hantzsch ester **IV-9** (0.50 mmol, 2.5 equiv), 3DPAFIPN (10 µmol, 0.05 equiv), *N*-mesityl pyrrolotriazolium precursor (**IV-Az-A**; 60 µmol, 0.30 equiv), and cesium carbonate (0.20 mmol, 1.0 equiv) were added. Acetonitrile (0.025 M) was added, the reaction was capped, and the vial was removed from the glovebox. Parafilm was wrapped around the cap to prevent air from

entering, and the vial was stirred and irradiated with 456 nm LEDs. The reactions were monitored by GCMS. When complete consumption of the acyl imidazole was observed (between 16–48 h), the reaction was concentrated under reduced pressure and then purified by column chromatography on silica gel (ethyl acetate/hexanes). If the Hantzsch pyridine byproduct cannot be easily separated by column chromatography, non-acid sensitive products can be dissolved in DCM and washed with concentrated HCl (3 x 15 mL) to remove the Hantzsch pyridine byproduct.

4.8.3 Optimization of Reaction Conditions

The reaction was optimized according to General Procedure 3 for the synthesis of cycloalkanones from acyl imidazoles **IV-8** and the corresponding oxidatively generated radical precursor.

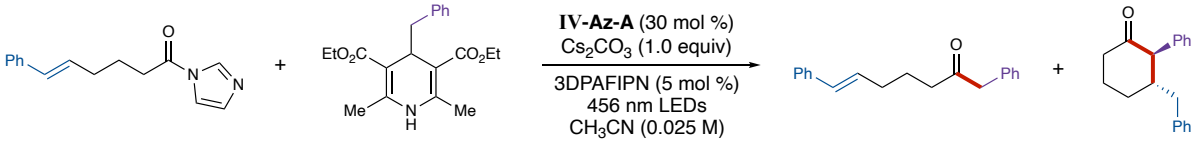

IV-8a **IV-9a** (2.5 equiv) **IV-10a** **IV-11a**

entry	deviation from standard	yield of **IV-10a** (%)[a]	yield of **IV-11a** (%)[a]
1	none	7	55 (52)[b]
2	$[Ir(dF[CF_3]ppy)_2(dtbpy)]PF_6$ instead of 3DPAFIPN	31	0
3	*fac*-$Ir(ppy)_3$ instead of 3DPAFIPN	trace	trace
4	Mes-Acr-Ph instead of 3DPAFIPN	0	0
5	Bn–BF_3K + 4CzIPN instead of Bn–HE + 3DPAFIPN	7	35
6	0.01 M instead of 0.025 M	8	21
7	0.05 M instead of 0.025 M	5	26
8	0.1 M instead of 0.025 M	6	15

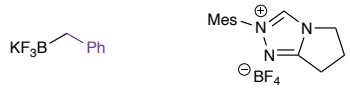

IV-13a Bn–BF_3K **IV-Az-A** (5,5-Mes)

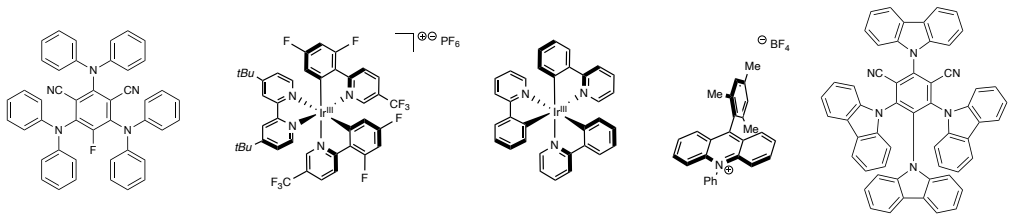

3DPAFIPN $[Ir(dFCF_3ppy)_2(dtbpy)]PF_6$ *fac*-$Ir(ppy)_3$ Ph-Mes-Acr 4CzIPN

Table 4-5. Optimization of the reaction conditions. [a] ^{1}H NMR spectroscopic yield was measured using 1,3,5-trimethoxybenzene as the internal standard. [b] Isolated yield.

4.8.4 Sensitivity Screen

Each reaction was performed on a 0.05 mmol scale and was set up in a glovebox to ensure air-free conditions. A stock solution was made to be used for 11 reactions (10 reaction total with 1 extra reaction to be used if an error is made during setup) containing the acyl imidazole **IV-8a** (132 mg, 0.55 mmol, 1 equiv), benzyl Hantzsch ester **IV-9a** (472 mg, 1.38 mmol, 2.5 equiv), 3DPAFIPN (17.8 mg, 27.5 μmol, 0.05 equiv), and **IV-Az-A** (52.0 mg, 0.165 mmol, 0.3 equiv). Cesium carbonate (16.3 mg, 0.05 mmol, 1.0 equiv) was added to 11 2-dram vials. Under inert atmosphere, dried (over 3.0 Å molecular sieves) and freeze-pump-thawed CH_3CN (11.0 mL) was added to the stock solution vial. After ensuring that all reaction components were dissolved, 1.0 mL of the stock solution was added to each 2-dram vial. See table below to determine additional amount of additional degassed and dried CH_3CN (or non-degassed CH_3CN per the table) that should be added to each vial. The vials were capped, removed from the glovebox, additive was added if detailed below (entries 3 and 5), and the caps were wrapped in parafilm. The vials were stirred at 1000 rpm and were irradiated 7 cm from 456 nm LEDs unless otherwise noted in the table below. After 16 h, the reactions were promptly stopped, solvent was evaporated under reduced pressure, and 2.8 mg of trimethoxybenzene standard was added to each reaction vial (note: reactions were *purposely stopped prior to completion* to accurately measure the impact that each variable has on reactivity and efficiency). $CDCl_3$ (1.0 mL) was added to dissolve the unpurified reaction mixture, which was then filtered through a cotton and celite plug into an NMR tube for ^{1}H NMR spectroscopy analysis.

^{1}H NMR spectroscopic yields were calculated. The deviation from the control reaction was calculated (yield of control – yield of reaction) and *converted into a percentage value* to visualize the impact that each variable has compared to the control reaction (e.g., –100% deviation reflects a –100% change from the control reaction → 0% yield). The radar diagram was plotted using the Excel spreadsheet provided by Glorius et al.[499] as general template (note: the *percent deviation from the control reaction was plotted*).

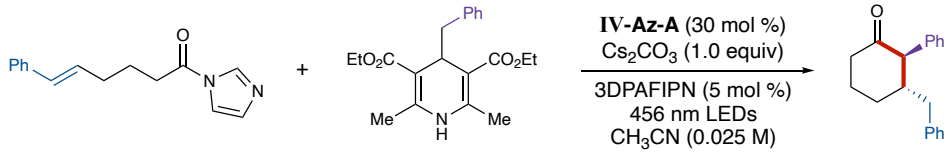

IV-8a **IV-9a** (2.5 equiv) **IV-11a**

entry	experiment	$V_{stock\ solution}$ (mL)	$V_{pure\ CH_3CN}$ (mL)	additive or change in setup	yield **IV-11a** (%)[a]
1	high c (–10% V_{rxn})	1.0	0.8	-	21
2	low c (+10% V_{rxn})	1.0	1.2	-	20
3	high H_2O (H_2O = +1% V_{rxn})	1.0	1.0	+ H_2O (20 uL)	10
4	medium O_2	1.0	1.0[b]	-	22
5	high O_2	1.0	1.0	+ air (10·V_{rxn} = 20 mL)[c]	0
6	low T	1.0	1.0	fan placed over reaction	26
7	high T	1.0	1.0	reaction heated to 50 °C[d]	23
8	low intensity (d·4)	1.0	1.0	28 cm from light	26
9	high intensity (d/4)	1.0	1.0	1.8 cm from light	22
10	control	1.0	1.0	-	26

Table 4-6. Reaction sensitivity screen in the synthesis of **IV-11a**. [a] ^{1}H NMR spectroscopic yield using 1,3,5-trimethoxybenzene as internal standard. [b] Non-degassed CH_3CN. Headspace of reaction is nitrogen atmosphere. [c] A 20-mL syringe was filled with air and bubbled through the reaction solution prior to irradiation. [d] Reaction vial was clamped on a hot plate in front of the light source. A thermocouple was placed into a vial of CH_3CN to measure temperature.

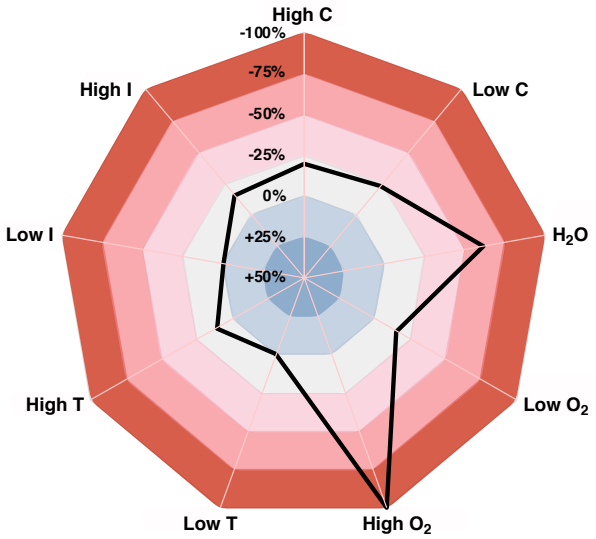

Figure 4-10. Graph showing the reaction sensitivity as a percentage change compared to the standard reaction conditions for small changes to the reaction setup.

4.8.5 Control Experiments

Control experiments were run for the reaction of acyl imidazoles **IV-8** to **IV-11** and linear ketone intermediate **IV-10** to desired cyclized product **IV-11**.

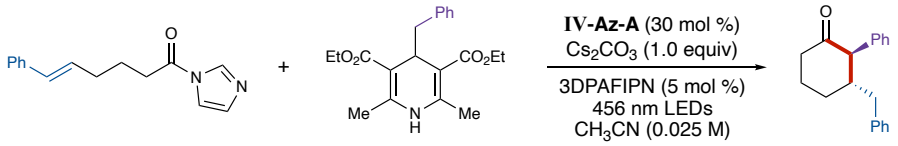

IV-8a **IV-9a** (2.5 equiv) **IV-11a**

entry	deviation from standard	yield **IV-11a** (%)[a]
1	none	55
2	no base	0
3	no 5,5-Mes	trace
4	no base + no azolium	0
5	no photocatalyst	0
6	no light	0

Table 4-7. Control reactions for the synthesis of **IV-11a** from **IV-8a**. [a] ^{1}H NMR spectroscopic yield using 1,3,5-trimethoxybenzene as internal standard.

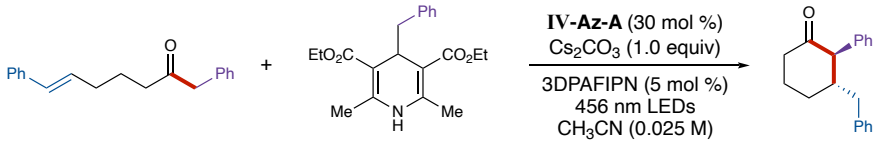

IV-10a | IV-9a (2.5 equiv) | IV-11a

entry	deviation from standard	yield **3a** (%)[a]
1	none	90
2	no base	0
3	no photocatalyst	trace
4	no light	0

Table 4-8. Control reactions for the synthesis of **IV-11a** from **IV-10a**. [a] Isolated yield at a 0.20 mmol scale.

4.8.6 TEMPO-Trapping Experiment

Linear ketone **IV-10a** (4.5 mg, 17 µmol, 1.0 equiv), cesium carbonate (5.5 mg, 17 µmol, 1.0 equiv), 3DPAFIPN (0.6 mg, 0.9 µmol, 0.05 equiv), and TEMPO (5.3 mg, 34 µmol, 2 equiv) were added a 2-dram vial equipped with a stir bar. CH_3CN (680 µL, 0.025 M) was added to the reaction vial. The vial was capped, the cap was wrapped in parafilm, and the reaction was irradiated with 456 nm LEDs for 24 h. Upon completion, the solvent was removed under reduced pressure, 1,3,5-trimethoxybenzene was added as an internal standard, and $CDCl_3$ was added to dissolve all reaction components. The solution was then filtered through a cotton and celite plug into an NMR spectroscopy tube for ^{1}H NMR spectroscopy analysis. A sample of this unpurified mixture was used for HRMS analysis to identify any TEMPO adducts by mass.

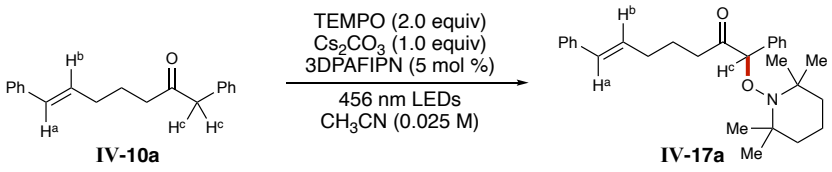

Scheme 4-14. TEMPO-trapping experiment.

Cyclized **IV-11a** was not identified by ^{1}H NMR spectroscopy analysis. Production of **IV-17a** is suggested by the following analysis of the unpurified ^{1}H NMR spectrum:

- A spectrum of clean **IV-10a** has an integration ratio of H^a : H^b : H^c = 1 : 1 : 2.
- The unpurified ^{1}H NMR spectrum of the TEMPO-trapping reaction has a ratio of H^a : H^b : H^c = 1 : 1 : 1.2, suggesting that **IV-17a** was formed in ~40%.

HRMS (ESI): Mass calcd for $C_{28}H_{38}NO_2$ $[M+H]^+$: 420.2902; found 420.2903.

4.8.7 Stern-Volmer Fluorescence Quenching

Stern-Volmer fluorescence quenching experiments were run at room temperature under an inert N_2 atmosphere. The solutions were irradiated at 380 nm and fluorescence was measured from 400-720 nm. A slit width of 5 nm was used. The data summarized in the tables is the fluorescence intensity measured three times for each sample. The data shown in the graphs is the average of three experiments.

Stock solution **SL-1** was made by adding CH_3CN (360 µL) to **IV-10a** (95 mg, 0.36 mmol). Cesium carbonate was weighed into cuvettes according to the table below. The appropriate amount of **SL-1** was added to cuvettes according to the table below. Stock solution **SL-2** was made by adding CH_3CN (10.0 mL) to 3DPAFIPN (1.29 µg, 2.00 µmol). **SL-2** (110 µL) was dispensed into cuvettes according to the table below. Additional CH_3CN was added to each cuvette to bring the total volume up to the amount listed in the table below. Each sample was capped, removed from the glovebox, and measured in triplicate.

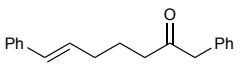

IV-10a

Cs_2CO_3 3DPAFIPN

entry	[Quencher] (M)	Cs_2CO_3 (mg)	V_{SL-1} (µL)	V_{SL-2} (µL)	$V_{pure\ CH_3CN}$ (µL)	V_{total}
A1	0.02	0	20	110	970	1100
A2	0.03	0	30	110	960	1100
A3	0.05	0	50	110	940	1100
A4	0.06	0	60	110	930	1100
A5	0.08	0	80	110	910	1100
A6	0.12	0	120	110	870	1100
B1	0.02	7	20	110	970	1100
B2	0.03	10	30	110	960	1100
B3	0.05	16	50	110	940	1100
B4	0.06	19	60	110	930	1100
B5	0.08	26	80	110	910	1100
B6	0.12	39	120	110	870	1100
base+PC	0.12	39	0	110	1000	1100
PC	-	0	0	110	1000	1100
total	1.08	156	840	N/A	N/A	N/A

Table 4-9. Setup information for the Stern-Volmer fluorescence quenching experiments.

4.8.7.1 Measured Emission Data

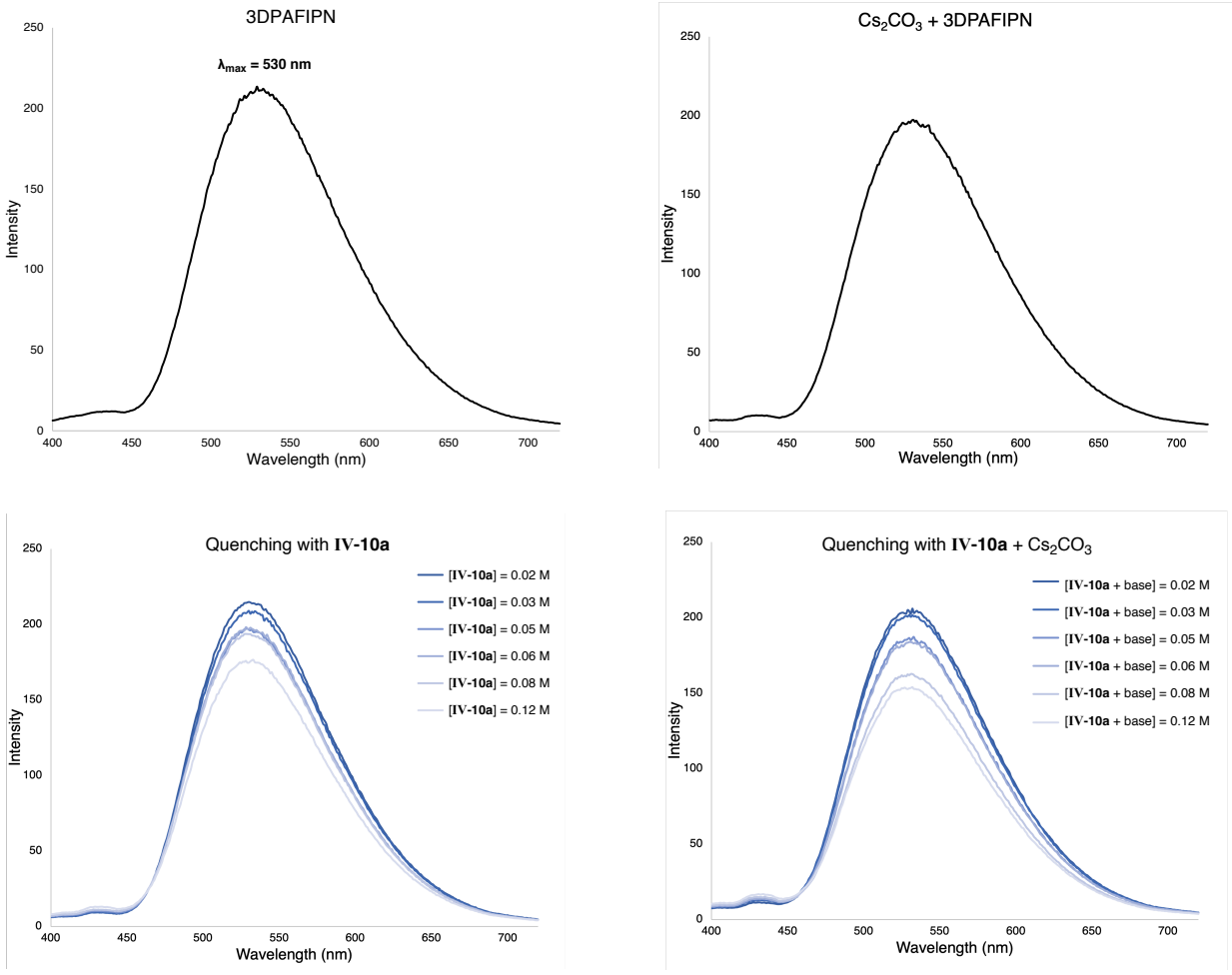

Figure 4-11. Emission and quenching data.

4.8.7.2 Intensity Data

Selected at 530 nm (λ_{max} measured for 3DPAFIPN)

A

[**IV-10a**]	I_{avg}	I_0/I_{avg}
0.02	214.7	0.983
0.03	208.9	1.010
0.05	196.5	1.074
0.06	196.9	1.072
0.08	193.5	1.091
0.12	174.6	1.208

B

[**IV-10a** + Cs_2CO_3]	I_{avg}	I_0/I_{avg}
0.02	204.0	1.035
0.03	201.6	1.047
0.05	186.5	1.132
0.06	183.8	1.148
0.08	161.7	1.305
0.12	153.0	1.379

Table 4-10. Measured intensity data at 530 nm for **A) IV-10a** and **B) IV-10a-Cs**.

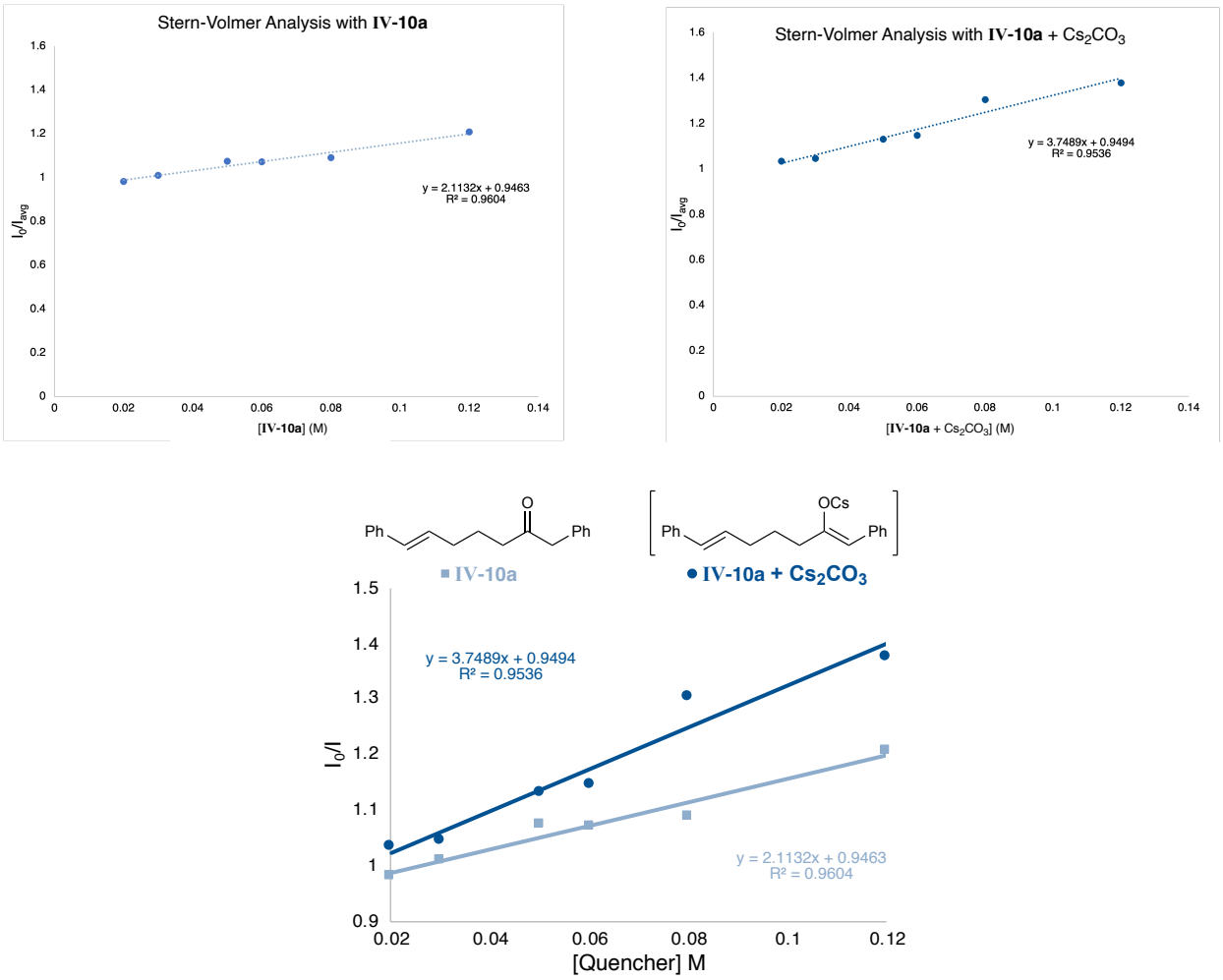

Figure 4-12. Graphs of the Stern-Volmer Fluorescence quenching data.

4.8.8 Deuterium Labeling Studies

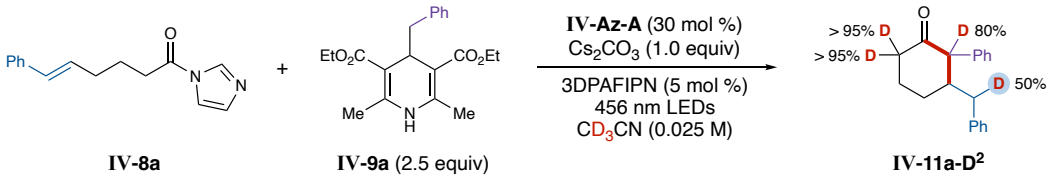

Scheme 4-15. Reaction conditions for the deuterium labeling studies used to study the reaction mechanism.

Acyl imidazole **IV-8a** (24.0 mg, 0.10 mmol, 1.0 equiv), benzyl Hantzsch ester **IV-9a** (85.9 mg, 0.25 mmol, 2.5 equiv), cesium carbonate (32.6 mg, 0.10 mmol, 1.0 equiv), and 3DPAFIPN (3.2 mg, 5.0 µmol, 0.05 equiv) were added a 20-mL vial equipped with a stir bar. CD_3CN (4.0 mL, 0.025 M) was added to the reaction vial. The vial was capped, the cap was wrapped in parafilm, and the reaction was irradiated with 456 nm LEDs for 24 h. Upon completion, 1,3,5-trimethoxybenzene was added as an internal standard, and the solution was filtered through a cotton and celite plug into an NMR spectroscopy tube for ^{1}H NMR spectroscopy analysis. A sample of this unpurified mixture was used for HRMS analysis to identify compounds with deuterium incorporation. The reaction mixture was then purified by column chromatography (0-10% ethyl acetate/hexanes). A sample of the purified product was dissolved in CD_3CN for ^{1}H NMR spectroscopy analysis. A sample of pure **IV-11a-D^2** (obtained from a reaction run in CH_3CN) was dissolved in CD_3CN for ^{1}H NMR spectroscopy analysis and was used for comparison.

4.8.8.1 HMRS Data

HRMS (ESI): Mass calcd for $C_{19}H_{18}\mathbf{D_2}ONa$ $[M+Na]^+$: 289.1538; found 289.1532

HRMS (ESI): Mass calcd for $C_{19}H_{17}\mathbf{D_3}ONa$ $[M+Na]^+$: 290.1601; found 290.1595 – tallest peak

HRMS (ESI): Mass calcd for $C_{19}H_{16}\mathbf{D_4}ONa$ $[M+Na]^+$: 291.1663; found 291.1652

4.8.8.2 [1]H NMR Spectroscopy Data

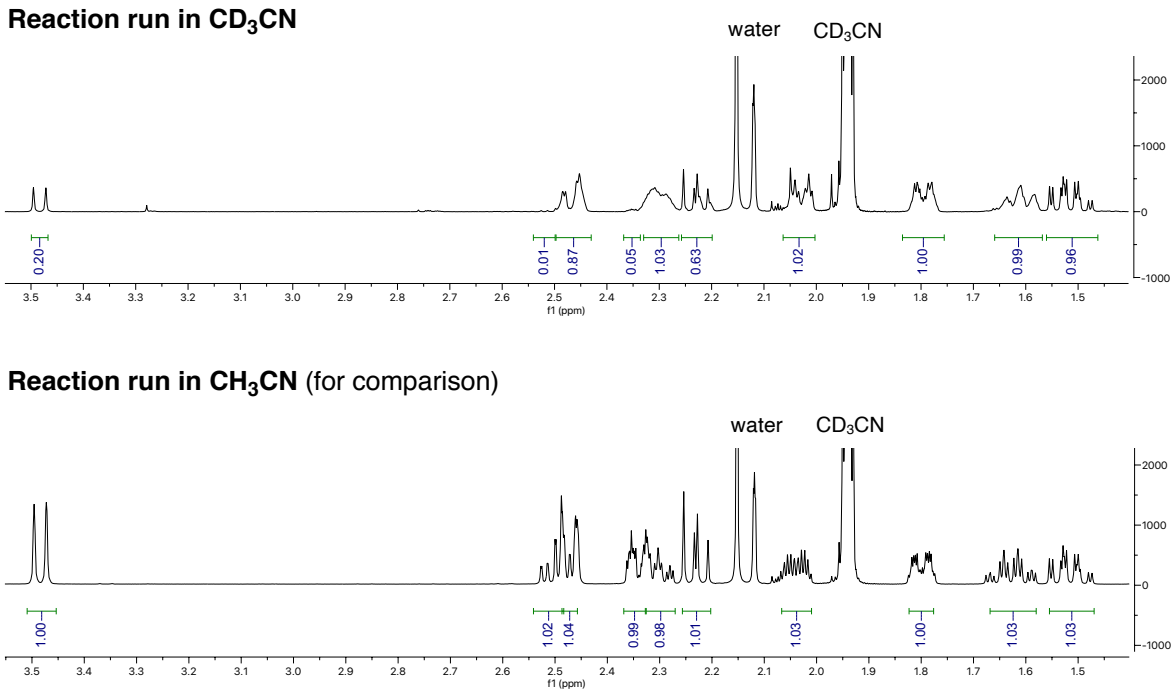

Figure 4-13. [1]H NMR spectroscopy data comparison of the standard reaction for the synthesis of **IV-11a-D[2]** (top) and **IV-11a** (bottom).

4.8.9 Further Exploration of the Reaction Scope: Proof of Concept

The reaction was run with various additional Hantzsch esters to further explore the scope of the reaction with respect to the oxidatively generated radical coupling partner.

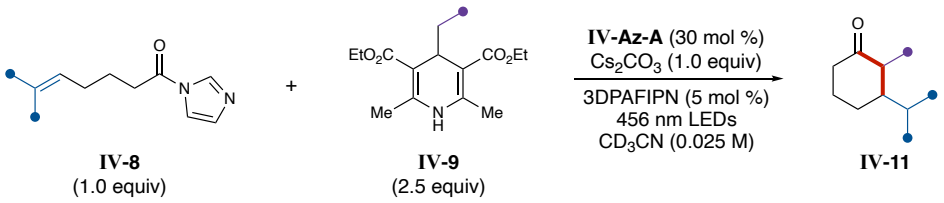

Scheme 4-16. General reaction scheme for the synthesis of **IV-11** from **IV-8**.

4.8.9.1 Products and results:

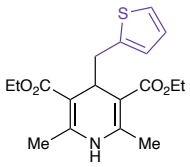

IV-9s

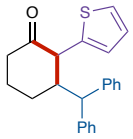

IV-11s

+

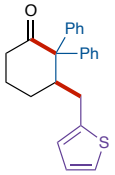

IV-11s'

Mass calcd for $C_{23}H_{22}OS$: 346.1

LRMS: found 346.1

An inseparable mixture of regioisomers was isolated, possibly due to the increased reactivity/decreased stability of the thiophene-derived radical compared to benzylic radicals.

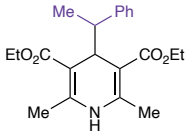

IV-9t

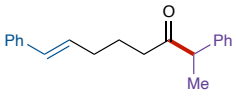

IV-10t

Mass calcd for $C_{20}H_{22}O$: 278.2

LRMS: found 278.2

As expected, only linear ketone was isolated when disubstituted Hantzsch esters were employed, possibly due to the increased steric bulk surrounding the reacting center and the increased stability of the generated α-radical.

4.8.10 Additional Experimental Procedures and Tabulated Data

4.8.10.1 Tabulated Data for Carboxylic Acid Starting Materials

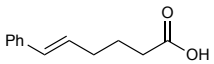

6-phenylhex-5-enoic acid. Prepared according to General Procedure 1 for the synthesis of carboxylic acids using benzaldehyde (1.02 mL, 10 mmol, 1.0 equiv). The crude material was purified by column chromatography (0-40% CH_2Cl_2(1% AcOH):hexanes) to yield the product as a clear and colorless oil (1.69 g, 89%). Analytical data matched the reported data.[516]

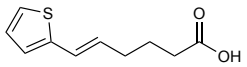

6-(thiophen-2-yl)hex-5-enoic acid. Prepared according to General Procedure 1 for the synthesis of carboxylic acids using thiophene-2-carbaldehyde (0.93 mL, 10 mmol, 1.0 equiv). The crude material was purified by column chromatography (0-80% CH_2Cl_2(1% AcOH):hexanes) to yield the product as a clear oil (1.02 g, 52%). Analytical data for the major isomer of 6-(thiophen-2-yl)hex-5-enoic acid: ^{1}H NMR (500 MHz, $CDCl_3$) δ 7.10 (dt, *J* = 5.2, 1.0 Hz, 1H), 6.94 (dd, *J* = 5.1, 3.5 Hz, 1H), 6.88 (dd, *J* = 3.6, 1.1 Hz, 1H), 6.54 (ddt, *J* = 15.7, 1.7, 0.9 Hz, 1H), 6.02 (dt, *J* = 15.6, 7.0 Hz, 1H), 2.41 (t, *J* = 7.5 Hz, 2H), 2.25 (qd, *J* = 7.2, 1.5 Hz, 2H), 1.81 (q, *J* = 7.4 Hz, 2H). ^{13}C NMR (126 MHz, $CDCl_3$) δ 180.29, 142.77, 129.31, 127.36, 124.72, 124.32, 123.50, 33.44, 32.13, 24.19. Analytical data for the minor isomer: ^{1}H NMR (500 MHz, $CDCl_3$) δ 7.29 – 7.23 (m, 1H), 7.01 (dd, *J* = 5.1, 3.6 Hz, 1H), 6.99 (dd, *J* = 3.7, 1.2 Hz, 1H), 6.58 (dt, *J* = 11.6, 1.9 Hz, 1H), 5.55 (dt, *J* = 11.5, 7.2 Hz, 1H), 2.50 (td, *J* = 7.4, 1.8 Hz, 2H), 2.47 – 2.43 (m, 2H), 1.90 – 1.84 (m, 2H). ^{13}C NMR (126 MHz, $CDCl_3$) δ 180.20, 140.43, 129.37, 127.55, 126.90, 125.29, 122.89, 33.70, 28.57, 24.48. FTIR (diamond, anvil, oil) cm^{-1}: 3104, 3070, 3025, 2933, 1702, 1519. HRMS (ESI): Mass calcd for $C_{10}H_{11}O_2S$ $[M–H]^–$: 195.0485; found 195.0488.

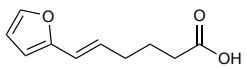

6-(furan-2-yl)hex-5-enoic acid. Prepared according to General Procedure 1 for the synthesis of carboxylic acids using furan-2-carbaldehyde (0.83 mL, 10 mmol, 1.0 equiv). The crude material was purified by column chromatography (0-60% CH_2Cl_2(1% AcOH):hexanes) to yield the product as a clear oil (0.59 g, 33%). Analytical data for the major isomer of 6-(furan-2-yl)hex-5-enoic acid:

^{1}H NMR (500 MHz, Chloroform-*d*) δ 7.37 (d, *J* = 1.8 Hz, 1H), 6.39 (dd, *J* = 3.3, 1.8 Hz, 1H), 6.25 (d, *J* = 3.5 Hz, 1H), 6.22 (dt, *J* = 11.7, 1.5 Hz, 2H), 5.50 (dt, *J* = 11.7, 7.4 Hz, 1H), 2.54 (qd, *J* = 7.4, 1.7 Hz, 2H), 2.43 (t, *J* = 7.5 Hz, 2H), 1.83 (p, *J* = 7.5 Hz, 2H). ^{13}C NMR (126 MHz, $CDCl_3$) δ 180.25, 153.18, 141.59, 129.32, 118.35, 111.19, 109.39, 33.64, 28.49, 24.50. Analytical data for the minor isomer of 6-(furan-2-yl)hex-5-enoate: ^{1}H NMR (500 MHz, Chloroform-*d*) δ 7.31 (d, *J* = 1.8 Hz, 1H), 6.35 (dd, *J* = 3.3, 1.8 Hz, 1H), 6.25 – 6.18 (m, 1H), 6.15 (d, *J* = 3.0 Hz, 1H), 6.11 (dd, *J* = 15.8, 7.0 Hz, 1H), 2.41 (t, *J* = 7.5 Hz, 2H), 2.25 (qd, *J* = 7.2, 1.3 Hz, 2H), 1.81 (p, *J* = 7.4 Hz, 2H). ^{13}C NMR (126 MHz, $CDCl_3$) δ 180.18, 153.03, 141.54, 128.35, 119.71, 111.25, 106.58, 33.41, 32.06, 24.21. FTIR (diamond, anvil, oil) cm^{-1}: 3116, 3024, 2933, 2664, 1703, 1531. HRMS (ESI): Mass calcd for $C_{10}H_{11}O_3$ $[M–H]^–$: 179.0714; found 179.0714.

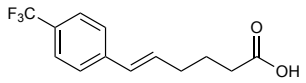

6-(4-(trifluoromethyl)phenyl)hex-5-enoic acid. Prepared according to General Procedure 1 for the synthesis of carboxylic acids using 4-(trifluoromethyl)benzaldehyde (1.37 mL, 10 mmol, 1.0 equiv). The crude material was purified by column chromatography (0-40% CH_2Cl_2(1% AcOH):hexanes) to yield the product as a clear oil (1.56 g, 60%). Analytical data for the major isomer of 6-(thiophen-2-yl)hex-5-enoic 6-(4-(trifluoromethyl)phenyl)hex-5-enoic acid: ^{1}H NMR (500 MHz, $CDCl_3$) δ 7.54 (d, *J* = 8.2 Hz, 2H), 7.42 (d, *J* = 8.1 Hz, 2H), 6.44 (d, *J* = 15.8 Hz, 1H), 6.29 (dt, *J* = 15.8, 6.9 Hz, 1H), 2.42 (t, *J* = 7.4 Hz, 2H), 2.31 (qd, *J* = 7.2, 1.3 Hz, 2H), 1.86 (q, *J* = 7.4 Hz, 2H). ^{13}C NMR (126 MHz, $CDCl_3$) δ 180.07, 132.31, 129.92, 129.05, 128.97 (q, *J* = 32.1 Hz), 126.27, 125.59 (q, *J* = 3.8 Hz), 124.54 (q, *J* = 271.7 Hz), 33.48, 32.39, 24.11. Analytical data for the minor isomer: ^{1}H NMR (500 MHz, $CDCl_3$) δ 7.58 (d, *J* = 8.1 Hz, 2H), 7.36 (d, *J* = 8.0 Hz,

2H), 6.49 (d, *J* = 11.7 Hz, 1H), 5.75 (dt, *J* = 11.6, 7.4 Hz, 1H), 2.40 – 2.33 (m, 4H), 1.83 – 1.76 (m, 2H). ^{13}C NMR (126 MHz, $CDCl_3$) δ 179.95, 141.09, 133.58, 129.01 (q, *J* = 32.3 Hz), 128.96, 126.27, 125.25 (q, *J* = 3.9 Hz), 124.49 (q, *J* = 271.7 Hz), 33.48, 27.89, 24.68.

The data for all other carboxylic acids synthesized via General Procedure 1 matched the reported spectral data.[517-522]

4.8.10.2 Procedure for the synthesis of 3,3-bis(ethoxycarbonyl)-6-phenylhex-5-enoic acid

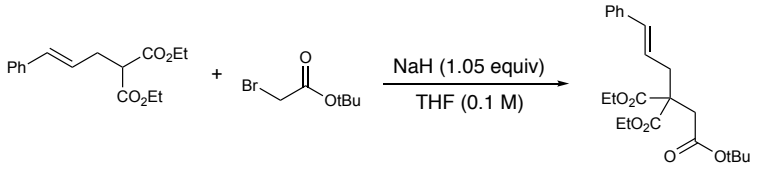

Scheme 4-17. Alkylation of diethyl 2-cinnamylmalonate.

1-(tert-butyl) 2,2-diethyl-5-phenylpent-4-ene-1,2,2-tricarboxylate: diethyl 2-cinnamylmalonate (0.24 g, 0.87 mmol, 1 equiv) was added dropwise to a suspension of NaH (60% dispersion in mineral oil; 22 mg, 0.92 mmol, 1.05 equiv) in THF (9 mL, 0.1 M) at room temperature. The mixture was allowed to stir for 20 minutes, and then tert-butyl-2-bromoacetate (0.15 mL, 1.05 mmol, 1.2 equiv) was added dropwise. The resulting mixture stirred for 10 h and was then quenched with HCl (3 M, 2 mL). The solution was extracted with ethyl acetate (3 x 10 mL), and the combined organic layers were washed with brine and dried over anhydrous $MgSO_4$. The solvent was removed under reduced pressure, and column chromatography (CH_2Cl_2) eluted the product as a clear, colorless oil (270 mg, 80%). Analytical data for 1-(tert-butyl) 2,2-diethyl-5-phenylpent-4-ene-1,2,2-tricarboxylate: ^{1}H NMR (500 MHz, $CDCl_3$) δ 7.32 – 7.27 (m, 4H), 7.24 – 7.18 (m, 1H), 6.45 – 6.40 (m, 1H), 6.09 (dt, J = 15.6, 7.7 Hz, 1H), 4.21 (q, J = 7.1 Hz, 4H), 2.94 –

2.90 (m, 4H), 1.43 (s, 9H), 1.25 (t, J = 7.1 Hz, 6H). ^{13}C NMR (126 MHz, $CDCl_3$) δ 170.20, 169.63, 137.12, 134.50, 128.62, 127.57, 126.36, 124.04, 81.29, 61.71, 55.84, 38.67, 36.98, 28.11, 14.20.

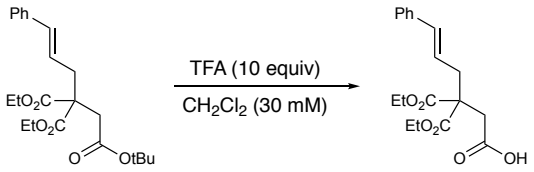

Scheme 4-18. Saponification reaction to yield free carboxylic acid for the synthesis of **IV-11o**.

3,3-bis(ethoxycarbonyl)-6-phenylhex-5-enoic acid: To a flask equipped with a stir bar and 1-(tert-butyl) 2,2-diethyl-5-phenylpent-4-ene-1,2,2-tricarboxylate (240 mg, 0.62 mmol, 1 equiv) dissolved in CH_2Cl_2 (20 mL, 30 mM) was added trifluoroacetic acid (0.47 mL, 6.2 mmol, 10 equiv) at room temperature. The reaction stirred for 10 h, and the solvent was evaporated under reduced pressure. The unpurified reaction mixture was diluted with CH_2Cl_2 (20 mL) and aqueous HCl (0.1 M, 15 mL). The organic layer was separated, and the mixture was further extracted with CH_2Cl_2 (2 x 10 mL). The combined organic extract was then dried over anhydrous $MgSO_4$, filtered, and concentrated under reduced pressure to give the pure named carboxylic acid (200 mg, 97%). ^{1}H NMR (500 MHz, $CDCl_3$) δ 7.34 – 7.26 (m, 4H), 7.25 – 7.20 (m, 1H), 6.50 – 6.42 (m, 1H), 6.06 (dt, *J* = 15.5, 7.7 Hz, 1H), 4.23 (q, *J* = 7.1 Hz, 4H), 3.04 (s, 2H), 2.94 (dd, *J* = 7.6, 1.3 Hz, 2H), 1.26 (t, *J* = 7.1 Hz, 6H). ^{13}C NMR (126 MHz, $CDCl_3$) δ 176.09, 169.96, 136.93, 134.93, 128.66, 127.73, 126.41, 123.52, 62.06, 55.70, 37.30, 37.21, 14.14. HRMS (ESI): Mass calcd for $C_{18}H_{22}O_6$ $[M+Na]^+$: 357.1314; found 357.1314.

*4.8.10.3 Tabulated Data for Cycloalkanones **IV-11***

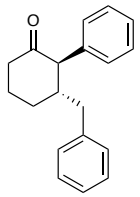

3-benzyl-2-phenylcyclohexan-1-one (**IV-11a**). Prepared according to General Procedure 3 using the respective acyl imidazole (48 mg, 1.0 equiv) and benzyl Hantzsch ester. The reaction mixture was purified by column chromatography (0-10% ethyl acetate/hexanes) to yield the product as a tan solid (27 mg, 52%). Analytical data for **IV-11a**: ^{1}H NMR (500 MHz, $CDCl_3$) δ 7.43 – 7.36 (m, 2H), 7.36 – 7.27 (m, 1H), 7.30 – 7.21 (m, 2H), 7.20 – 7.14 (m, 3H), 7.04 – 6.98 (m, 2H), 3.38 (dd, *J* = 11.4, 1.0 Hz, 1H), 2.60 (dd, *J* = 13.1, 2.8 Hz, 1H), 2.53 (dddd, *J* = 13.7, 4.6, 3.0, 1.6 Hz, 1H), 2.45 (tdd, *J* = 13.6, 6.0, 1.1 Hz, 1H), 2.37 – 2.18 (m, 2H), 2.08 (ddp, *J* = 13.0, 6.9, 3.4 Hz, 1H), 1.95 (dqd, *J* = 13.6, 3.5, 1.6 Hz, 1H), 1.75 – 1.61 (m, 1H), 1.50 (tdd, *J* = 13.1, 11.0, 3.6 Hz, 1H). ^{13}C NMR (126 MHz, $CDCl_3$) δ 210.03, 140.06, 137.43, 129.53, 129.25, 128.67, 128.36, 127.23, 126.20, 63.80, 47.19, 42.14, 41.40, 30.61, 25.75. FTIR (diamond, anvil, solid) cm^{-1}: 3081, 3060, 3024, 2941, 2912, 2860, 1705, 1603, 1584. HRMS (ESI): Mass calcd for $C_{19}H_{20}ONa$ $[M+Na]^+$: 287.1412; found 287.1417.

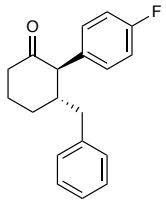

3-benzyl-2-(4-fluorophenyl)cyclohexan-1-one (**IV-11b**). Prepared according to General Procedure 3 using the respective acyl imidazole (48 mg, 1.0 equiv) and 4-fluoro-benzyl Hantzsch

ester. The reaction mixture was purified by column chromatography (0-10% ethyl acetate/hexanes) to yield the product as a yellow-green oil (34 mg, 60%). Analytical data for **IV-11b**: ^{1}H NMR (500 MHz, $CDCl_3$) δ 7.24 (m, 2H), 7.22 – 7.15 (m, 1H), 7.18 – 7.04 (m, 4H), 7.02 – 6.87 (m, 2H), 3.40 – 3.34 (m, 1H), 2.62 – 2.49 (m, 2H), 2.44 (tdd, *J* = 13.6, 13.6, 6.0, 1.1 Hz, 1H), 2.28 – 2.16 (m, 2H), 2.14 – 2.03 (m, 1H), 1.99 – 1.92 (m, 1H), 1.73 – 1.60 (m, 1H), 1.50 (tdd, *J* = 13.6, 13.6, 10.7, 3.6 Hz, 1H). ^{13}C NMR (126 MHz, $CDCl_3$) δ 209.88, 162.03 (d, *J* = 245.1 Hz), 139.83, 133.09 (d, *J* = 3.3 Hz), 130.99 (d, *J* = 7.9 Hz), 129.22, 128.42, 126.29, 115.60 (d, *J* = 21.3 Hz), 63.05, 47.51, 42.12, 41.38, 30.72, 25.80. FTIR (diamond, anvil, oil) cm^{-1}: 3083, 3061, 3026, 2927, 2858, 1712, 1603. HRMS (ESI): Mass calcd for $C_{19}H_{19}FONa$ $[M+Na]^+$: 305.1318; found 305.1321.

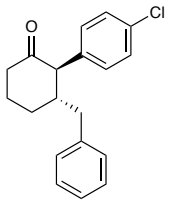

3-benzyl-2-(4-chlorophenyl)cyclohexan-1-one (**IV-11c**). Prepared according to General Procedure 3 using the respective acyl imidazole (48 mg, 1.0 equiv) and 4-chloro-benzyl Hantzsch ester. The reaction mixture was purified by column chromatography (0-10% ethyl acetate/hexanes) to yield the product as a yellow oil (34 mg, 57%). Analytical data for **IV-11c**: ^{1}H NMR (500 MHz, $CDCl_3$) δ 7.40 – 7.32 (m, 2H), 7.27 – 7.13 (m, 3H), 7.13 – 7.04 (m, 2H), 7.03 – 6.96 (m, 2H), 3.36 (d, *J* = 10.9 Hz, 1H), 2.56 (dd, *J* = 9.5, 4.1 Hz, 1H), 2.56 – 2.49 (m, 1H), 2.44 (tdd, *J* = 13.7, 6.1, 1.1 Hz, 1H), 2.28 – 2.21 (m, 1H), 2.25 – 2.16 (m, 1H), 2.14 – 2.03 (m, 1H), 1.96 (ddt, *J* = 13.7, 3.3, 2.0 Hz, 1H), 1.73 – 1.60 (m, 1H), 1.50 (tdd, *J* = 13.5, 10.6, 3.6 Hz, 1H). ^{13}C NMR (126 MHz, $CDCl_3$) δ 209.59, 139.71, 135.94, 133.03, 130.90, 129.23, 128.88, 128.43, 126.32, 63.20, 47.34,

42.10, 41.37, 30.66, 25.77. FTIR (diamond, anvil, oil) cm^{-1}: 3083, 3061, 3027, 2920, 2851, 1712, 1597, 1577. HRMS (ESI): Mass calcd for $C_{19}H_{19}ClONa$ $[M+Na]^+$: 321.1022; found 321.1029.

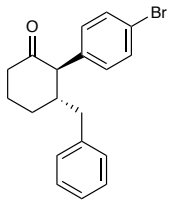

3-benzyl-2-(4-bromophenyl)cyclohexan-1-one (**IV-11d**). Prepared according to General Procedure 3 using the respective acyl imidazole (48 mg, 1.0 equiv) and 4-bromo-benzyl Hantzsch ester. The reaction mixture was purified by column chromatography (0-10% ethyl acetate/hexanes) to yield the product as a light green oil (46 mg, 66%). Analytical data for **IV-11d**: ^{1}H NMR (500 MHz, $CDCl_3$) δ 7.52 (d, *J* = 8.0 Hz, 2H), 7.24 (d, *J* = 7.4 Hz, 2H), 7.21 – 7.15 (m, 1H), 7.04 (d, *J* = 8.0 Hz, 2H), 6.99 (d, *J* = 7.5 Hz, 2H), 3.35 (d, *J* = 10.8 Hz, 1H), 2.62 – 2.49 (m, 2H), 2.43 (td, *J* = 13.6, 6.1 Hz, 1H), 2.29 – 2.16 (m, 2H), 2.09 (ddd, *J* = 13.4, 6.3, 3.2 Hz, 1H), 1.99 – 1.92 (m, 1H), 1.66 (qt, *J* = 13.4, 4.0 Hz, 1H), 1.50 (tdd, *J* = 13.7, 10.4, 3.7 Hz, 1H). ^{13}C NMR (126 MHz, $CDCl_3$) δ 209.44, 139.68, 136.48, 131.81, 131.29, 129.23, 128.43, 126.33, 121.19, 63.27, 47.28, 42.08, 41.37, 30.66, 25.76. FTIR (diamond, anvil, oil) cm^{-1}: 3083, 3061, 3026, 2936, 2862, 1710, 1602, 1592. HRMS (ESI): Mass calcd for $C_{19}H_{19}BrONa$ $[M+Na]^+$: 365.0517; found 365.0517.

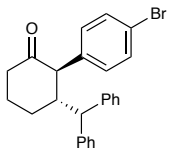

3-benzhydryl-2-(4-bromophenyl)cyclohexan-1-one (**IV-11e**). Prepared according to General Procedure 3 using the respective acyl imidazole (63 mg, 1.0 equiv) and 4-bromo-benzyl Hantzsch

ester. The reaction mixture was purified by column chromatography (0-10% ethyl acetate/hexanes) to yield the product as a white solid (45 mg, 54%). Analytical data for **IV-11e**: Major rotamer: ^{1}H NMR (500 MHz, $CDCl_3$) δ 7.54 – 7.44 (m, 2H), 7.39 – 7.27 (m, 2H), 7.29 – 7.19 (m, 3H), 7.21 – 7.13 (m, 3H), 7.16 – 7.09 (m, 2H), 7.02 – 6.95 (m, 2H), 3.90 (d, *J* = 6.0 Hz, 1H), 3.38 (d, *J* = 9.2 Hz, 1H), 3.12 (tdd, *J* = 9.4, 6.0, 3.2 Hz, 1H), 2.50 (dtd, *J* = 14.1, 5.2, 1.4 Hz, 1H), 2.45 – 2.28 (m, 1H), 2.22 – 2.03 (m, 2H), 1.77 (qdd, *J* = 10.6, 6.5, 2.8 Hz, 1H), 1.68 – 1.58 (m, 1H). ^{13}C NMR (126 MHz, $CDCl_3$) δ 210.49, 142.98, 140.78, 136.68, 131.87, 130.76, 130.16, 128.62, 128.45, 128.12, 126.96, 126.44, 121.14, 60.26, 52.42, 46.27, 41.37, 26.24, 24.48. FTIR (diamond, anvil, solid) cm^{-1}: 3085, 3059, 3026, 2939, 2867, 1706, 1797. HRMS (ESI): Mass calcd for $C_{25}H_{23}BrONa$ $[M+Na]^+$: 441.0830; found 441.0829.

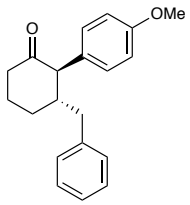

3-benzyl-2-(4-methoxyphenyl)cyclohexan-1-one (**IV-11f**). Prepared according to General Procedure 3 using the respective acyl imidazole (48 mg, 1.0 equiv) and 4-methoxy-benzyl Hantzsch ester. The reaction mixture was purified by column chromatography (0-10% ethyl acetate/hexanes) to yield the product as a white solid (20 mg, 34%). Analytical data for **IV-11f**: ^{1}H NMR (500 MHz, $CDCl_3$) δ 7.26 – 7.18 (m, 2H), 7.21 – 7.14 (m, 1H), 7.11 – 7.05 (m, 2H), 7.04 – 6.98 (m, 2H), 6.97 – 6.89 (m, 2H), 3.82 (s, 3H), 3.35 – 3.29 (m, 1H), 2.62 (d, *J* = 10.1 Hz, 1H), 2.52 (dddd, *J* = 13.6, 4.5, 2.9, 1.6 Hz, 1H), 2.43 (tdd, *J* = 13.6, 6.0, 1.1 Hz, 1H), 2.29 – 2.16 (m, 2H), 2.08 (ddq, *J* = 12.7, 6.4, 3.4 Hz, 1H), 1.95 (ddt, *J* = 13.6, 3.4, 2.1 Hz, 1H), 1.73 – 1.59 (m,

1H), 1.49 (tdd, *J* = 13.2, 10.6, 3.5 Hz, 1H), ^{13}C NMR (126 MHz, $CDCl_3$) δ 210.44, 158.65, 140.15, 130.44, 129.41, 129.27, 128.35, 126.17, 114.14, 62.98, 55.36, 47.38, 42.16, 41.41, 30.70, 25.79. FTIR (diamond, anvil, solid) cm^{-1}: 3060, 3026, 3000, 2920, 2851, 1712, 1653, 1613, 1584. HRMS (ESI): Mass calcd for $C_{20}H_{22}O_2Na$ $[M+Na]^+$: 317.1518; found 317.1520.

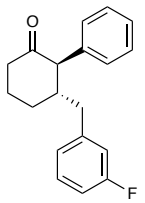

3-(3-fluorobenzyl)-2-phenylcyclohexan-1-one (**IV-11g**). Prepared according to General Procedure 3 using the respective acyl imidazole (52 mg, 1.0 equiv) and benzyl Hantzsch ester. The reaction mixture was purified by column chromatography (0-10% ethyl acetate/hexanes) to yield the product as a yellow-green solid (36 mg, 63%). Analytical data for **IV-11g**: ^{1}H NMR (500 MHz, $CDCl_3$) δ 7.46 – 7.36 (m, 2H), 7.34 – 7.27 (m, 1H), 7.19 (td, *J* = 8.0, 6.1 Hz, 1H), 7.18 – 7.12 (m, 2H), 6.87 (tdd, *J* = 8.5, 2.6, 1.0 Hz, 1H), 6.81 – 6.75 (m, 1H), 6.71 (dt, *J* = 9.9, 2.1 Hz, 1H), 3.36 (dd, *J* = 11.3, 1.0 Hz, 1H), 2.63 – 2.50 (m, 2H), 2.45 (tdd, *J* = 13.6, 6.0, 1.1 Hz, 1H), 2.35 – 2.16 (m, 2H), 2.10 (ddq, *J* = 12.7, 6.5, 3.4 Hz, 1H), 1.94 (dqd, *J* = 13.5, 3.4, 1.6 Hz, 1H), 1.76 – 1.59 (m, 1H), 1.50 (tdd, *J* = 13.2, 10.9, 3.6 Hz, 1H). ^{13}C NMR (126 MHz, Chloroform-*d*) δ 209.71, 162.85 (d, *J* = 245.6 Hz), 142.62 (d, *J* = 7.1 Hz), 137.21, 129.78 (d, *J* = 8.3 Hz), 129.49, 128.74, 127.34, 124.87 (d, *J* = 2.7 Hz), 115.99 (d, *J* = 20.7 Hz), 113.11 (d, *J* = 21.0 Hz), 63.72, 47.04, 42.08, 41.19 (d, *J* = 1.7 Hz), 30.63, 25.68. FTIR (diamond, anvil, solid) cm^{-1}: 2940, 2868, 1710, 1616, 1588. HRMS (ESI): Mass calcd for $C_{19}H_{19}FONa$ $[M+Na]^+$: 305.1318; found 305.1319.

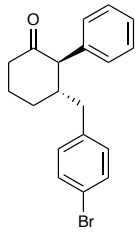

3-(4-bromobenzyl)-2-phenylcyclohexan-1-one (**IV-11h**). Prepared according to General Procedure 3 using the respective acyl imidazole (64 mg, 1.0 equiv) and benzyl Hantzsch ester. The reaction mixture was purified by column chromatography (0-10% ethyl acetate/hexanes) to yield the product as a yellow solid (29 mg, 42%). Analytical data for **IV-11h**: ^{1}H NMR (500 MHz, $CDCl_3$) δ 7.44 – 7.33 (m, 4H), 7.33 – 7.27 (m, 1H), 7.17 – 7.11 (m, 2H), 6.90 – 6.84 (m, 2H), 3.35 (dd, *J* = 11.3, 1.0 Hz, 1H), 2.59 – 2.49 (m, 2H), 2.44 (tdd, *J* = 13.7, 6.1, 1.2 Hz, 1H), 2.31 – 2.16 (m, 2H), 2.14 – 2.03 (m, 1H), 1.92 (dqd, *J* = 13.5, 3.4, 1.6 Hz, 1H), 1.75 – 1.61 (m, 1H), 1.48 (tdd, *J* = 13.1, 10.8, 3.6 Hz, 1H). ^{13}C NMR (126 MHz, $CDCl_3$) δ 209.65, 138.98, 137.24, 131.45, 130.98, 129.50, 128.73, 127.33, 120.03, 63.68, 47.03, 42.06, 40.81, 30.58, 25.67. FTIR (diamond, anvil, solid) cm^{-1}: 3068, 3033, 2952, 2918, 2866, 1701. HRMS (ESI): Mass calcd for $C_{19}H_{19}BrONa$ $[M+Na]^+$: 365.0517; found 365.0516.

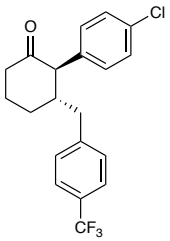

2-(4-chlorophenyl)-3-(4-(trifluoromethyl)benzyl)cyclohexan-1-one (**IV-11i**). Prepared according to General Procedure 3 using the respective acyl imidazole (62 mg, 1.0 equiv) and benzyl Hantzsch ester. The reaction mixture was purified by column chromatography (0-10% ethyl acetate/hexanes)

to yield the product as a yellow-green oil (34 mg, 46%). Analytical data for **IV-11i**: ^{1}H NMR (500 MHz, $CDCl_3$) δ 7.50 (d, *J* = 8.0 Hz, 2H), 7.41 – 7.25 (m, 2H), 7.12 – 7.06 (m, 4H), 3.36 (d, *J* = 11.0 Hz, 1H), 2.61 (dd, *J* = 13.3, 3.0 Hz, 1H), 2.55 (dddd, *J* = 13.7, 4.5, 2.8, 1.7 Hz, 1H), 2.45 (tdd, *J* = 13.8, 6.1, 1.1 Hz, 1H), 2.31 (dd, *J* = 13.2, 9.9 Hz, 1H), 2.28 – 2.18 (m, 1H), 2.11 (ddq, *J* = 12.5, 6.2, 3.3 Hz, 1H), 1.91 (dqd, *J* = 13.2, 3.4, 1.5 Hz, 1H), 1.74 – 1.61 (m, 1H), 1.51 (tdd, *J* = 13.2, 11.1, 3.6 Hz, 1H). ^{13}C NMR (126 MHz, $CDCl_3$) δ 209.05, 143.86, 135.63, 133.21, 130.85, 129.47, 128.97, 128.70 (q, *J* = 32.3 Hz), 125.37 (q, *J* = 3.7 Hz), 124.08 (q, *J* = 271.3 Hz), 63.12, 47.15, 41.99, 41.25, 30.65, 25.65. FTIR (diamond, anvil, oil) cm^{-1}: 3067, 3045, 2937, 2865, 1712, 1618, 1579. HRMS (ESI): Mass calcd for $C_{20}H_{18}ClF_3ONa$ $[M+Na]^+$: 389.0896; found 389.0892.

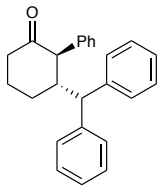

3-benzhydryl-2-phenylcyclohexan-1-one (**IV-11j**). Prepared according to General Procedure 3 using the respective acyl imidazole (63 mg, 1.0 equiv) and benzyl Hantzsch ester. The reaction mixture was purified by column chromatography (0-10% ethyl acetate/hexanes) to yield the product as a light yellow solid (56 mg, 82%). Analytical data for **IV-11j**: ^{1}H NMR (500 MHz, $CDCl_3$) δ 7.36 (dd, *J* = 8.2, 6.8 Hz, 2H), 7.33 – 7.27 (m, 3H), 7.26 – 7.20 (m, 5H), 7.19 – 7.13 (m, 5H), 3.95 (d, *J* = 6.8 Hz, 1H), 3.46 (d, *J* = 8.1 Hz, 1H), 3.25 (tdd, *J* = 8.3, 6.8, 3.5 Hz, 1H), 2.57 – 2.48 (m, 1H), 2.40 – 2.29 (m, 1H), 2.18 – 2.10 (m, 1H), 2.06 (dddd, *J* = 16.6, 10.5, 4.7, 3.0 Hz, 1H), 1.85 – 1.73 (m, 1H), 1.62 (dtd, *J* = 13.3, 8.7, 3.3 Hz, 1H). ^{13}C NMR (126 MHz, $CDCl_3$) δ 211.31, 143.22, 141.29, 137.74, 129.93, 128.81, 128.73, 128.63, 128.43, 128.13, 127.13, 126.81,

126.39, 60.18, 52.41, 45.62, 41.14, 25.60, 24.11. HRMS (ESI): Mass calcd for $C_{25}H_{24}ONa$ $[M+Na]^+$: 363.1725; found 363.1722. Note: the small set of peaks in the ^1H NMR spectrum represent a rotamer.

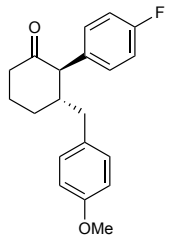

2-(4-fluorophenyl)-3-(4-methoxybenzyl)cyclohexan-1-one (**IV-11k**). Prepared according to General Procedure 3 using the respective acyl imidazole (54 mg, 1.0 equiv) and benzyl Hantzsch ester. The reaction mixture was purified by column chromatography (0-10% ethyl acetate/hexanes) to yield the product as a tan solid (22 mg, 35%). Analytical data for **IV-11k**: ^1H NMR (500 MHz, $CDCl_3$) δ 7.15 – 7.04 (m, 4H), 6.94 – 6.87 (m, 2H), 6.82 – 6.75 (m, 2H), 3.77 (s, 3H), 3.39 – 3.31 (m, 1H), 2.56 – 2.47 (m, 2H), 2.43 (tdd, J = 13.6, 6.0, 1.1 Hz, 1H), 2.23 – 2.13 (m, 2H), 2.09 (ddq, J = 12.7, 6.4, 3.4 Hz, 1H), 2.00 – 1.92 (m, 1H), 1.73 – 1.60 (m, 1H), 1.57 – 1.39 (m, 1H). ^{13}C NMR (126 MHz, $CDCl_3$) δ 210.00, 162.00 (d, J = 245.2 Hz), 158.09, 133.15 (d, J = 3.3 Hz), 131.73, 130.97 (d, J = 7.9 Hz), 130.17, 115.57 (d, J = 21.2 Hz), 113.76, 62.93, 55.36, 47.59, 42.12, 40.37, 30.68, 25.81. FTIR (diamond, anvil, solid) cm^{-1}: 3034, 3005, 2931, 2856, 1710, 1605, 1584. HRMS (ESI): Mass calcd for $C_{20}H_{21}FO_2Na$ $[M+Na]^+$: 335.1424; found 335.1421.

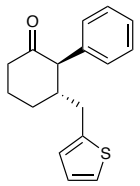

2-phenyl-3-(thiophen-2-ylmethyl)cyclohexan-1-one (**IV-11l**). Prepared according to General Procedure 3 using the respective acyl imidazole (49 mg, 1.0 equiv) and benzyl Hantzsch ester. The reaction mixture was purified by column chromatography (0-10% ethyl acetate/hexanes) to yield the product as a green oil (31 mg, 57%). Analytical data for **IV-11l**: ^{1}H NMR (500 MHz, $CDCl_3$) δ 7.42 – 7.35 (m, 2H), 7.34 – 7.27 (m, 1H), 7.18 – 7.05 (m, 3H), 6.90 (dd, *J* = 5.1, 3.4 Hz, 1H), 6.67 (d, *J* = 3.3 Hz, 1H), 3.39 (d, *J* = 11.8 Hz, 1H), 2.75 (ddd, *J* = 14.8, 3.4, 1.0 Hz, 1H), 2.60 – 2.50 (m, 2H), 2.50 – 2.29 (m, 2H), 2.19 – 2.07 (m, 1H), 2.11 – 2.03 (m, 1H), 1.82 – 1.69 (m, 1H), 1.58 (tdd, *J* = 13.2, 11.2, 3.4 Hz, 1H). ^{13}C NMR (126 MHz, $CDCl_3$) δ 209.85, 141.79, 137.00, 129.55, 128.68, 127.31, 126.88, 125.95, 123.75, 63.07, 46.75, 42.02, 34.92, 30.69, 25.61. FTIR (diamond, anvil, oil) cm^{-1}: 3064, 3029, 2925, 2852, 1710. HRMS (ESI): Mass calcd for $C_{17}H_{18}OSNa$ $[M+Na]^+$: 293.0976; found 293.0974.

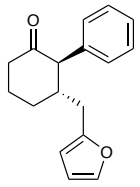

3-(furan-2-ylmethyl)-2-phenylcyclohexan-1-one (**IV-11m**). Prepared according to General Procedure 3 using the respective acyl imidazole (46 mg, 1.0 equiv) and benzyl Hantzsch ester. The reaction mixture was purified by column chromatography (0-10% ethyl acetate/hexanes) to yield the product as a yellow solid (21 mg, 41%). Analytical data for **IV-11m**: ^{1}H NMR (500 MHz,

$CDCl_3$) δ 7.37 (dd, *J* = 8.3, 6.9 Hz, 2H), 7.30 – 7.27 (m, 2H), 7.15 – 7.11 (m, 2H), 6.26 (dd, *J* = 3.1, 1.9 Hz, 1H), 5.92 (d, *J* = 3.1 Hz, 1H), 3.36 (d, *J* = 11.3 Hz, 1H), 2.60 – 2.49 (m, 2H), 2.47 – 2.32 (m, 3H), 2.12 (ddq, *J* = 12.8, 6.4, 3.4 Hz, 1H), 2.02 (dqd, *J* = 13.9, 3.5, 1.6 Hz, 1H), 1.83 – 1.70 (m, 1H), 1.65 – 1.53 (m, 1H). ^{13}C NMR (126 MHz, $CDCl_3$) δ 209.94, 153.60, 141.38, 137.07, 129.57, 128.60, 127.24, 110.24, 107.06, 63.04, 44.53, 42.01, 32.99, 30.95, 25.67. FTIR (diamond, anvil, solid) cm^{-1}: 3410, 3061, 3031, 2957, 2852, 1803, 1711, 1630, 1588. HRMS (ESI): Mass calcd for $C_{17}H_{18}O_2Na$ $[M+Na]^+$: 277.1205; found 277.1205.

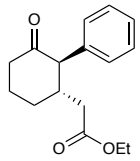

ethyl 2-(3-oxo-2-phenylcyclohexyl)acetate (**IV-11n**). Prepared according to General Procedure 3 using the respective acyl imidazole (47 mg, 1.0 equiv) and benzyl Hantzsch ester. The reaction mixture was purified by column chromatography (0-20% ethyl acetate/hexanes) to yield the product as a light yellow solid (36 mg, 69%). Analytical data for **IV-11n**: ^1H NMR (500 MHz, $CDCl_3$) δ 7.38 – 7.30 (m, 2H), 7.32 – 7.23 (m, 1H), 7.11 – 7.06 (m, 2H), 4.10 – 3.96 (m, 2H), 3.41 (dd, *J* = 12.2, 1.0 Hz, 1H), 2.57 (dddd, *J* = 13.8, 4.5, 2.8, 1.7 Hz, 1H), 2.51 (ddt, *J* = 12.0, 8.4, 3.4 Hz, 1H), 2.50 – 2.41 (m, 1H), 2.22 – 2.00 (m, 4H), 1.91 – 1.78 (m, 1H), 1.72 – 1.60 (m, 1H), 1.19 (t, *J* = 7.1 Hz, 3H). ^{13}C NMR (126 MHz, $CDCl_3$) δ 209.16, 172.29, 136.53, 129.59, 128.62, 127.41, 62.78, 60.51, 42.05, 41.94, 39.62, 31.39, 25.63, 14.31. FTIR (diamond, anvil, solid) cm^{-1}: 3063, 3030, 2927, 2854, 1718. HRMS (ESI): Mass calcd for $C_{16}H_{20}O_3Na$ $[M+Na]^+$: 283.1310; found 283.1309.

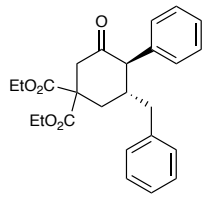

diethyl 3-benzyl-5-oxo-4-phenylcyclohexane-1,1-dicarboxylate (**IV-11o**). Prepared according to General Procedure 3 using the respective acyl imidazole (77 mg, 1.0 equiv) and benzyl Hantzsch ester. The reaction mixture was purified by column chromatography (0-40% ethyl acetate/hexanes) to yield the product as an off-white solid (72 mg, 88%). Analytical data for **IV-11o**: ^{1}H NMR (500 MHz, $CDCl_3$) δ 7.42 – 7.35 (m, 2H), 7.34 – 7.27 (m, 1H), 7.27 – 7.20 (m, 2H), 7.20 – 7.13 (m, 1H), 7.17 – 7.10 (m, 2H), 7.01 – 6.95 (m, 2H), 4.25 – 4.14 (m, 3H), 4.17 – 4.07 (m, 1H), 3.19 (d, J = 11.3 Hz, 1H), 3.16 (dd, J = 15.1, 2.7 Hz, 1H), 2.70 – 2.64 (m, 1H), 2.57 (dd, J = 15.0, 0.9 Hz, 1H), 2.45 (dt, J = 14.1, 2.9 Hz, 1H), 2.36 – 2.21 (m, 2H), 1.96 (dd, J = 14.0, 12.1 Hz, 1H), 1.22 (t, J = 7.1 Hz, 3H), 1.12 (t, J = 7.1 Hz, 3H). ^{13}C NMR (126 MHz, $CDCl_3$) δ 205.20, 170.62, 170.38, 139.04, 137.18, 129.64, 129.05, 128.79, 128.50, 127.44, 126.41, 62.67, 62.05, 62.02, 55.88, 45.60, 41.93, 40.68, 34.96, 14.10. FTIR (diamond, anvil, solid) cm^{-1}: 3062, 3028, 2981, 2927, 2855, 1728, 1603. HRMS (ESI): Mass calcd for $C_{25}H_{28}O_5Na$ $[M+Na]^+$: 431.1835; found 431.1833.

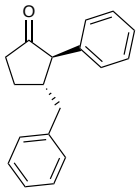

3-benzyl-2-phenylcyclopentan-1-one (**IV-11p**). Prepared according to General Procedure 3 using the respective acyl imidazole (45 mg, 1.0 equiv) and benzyl Hantzsch ester. The reaction mixture was purified by column chromatography (0-10% ethyl acetate/hexanes) to yield the product as a

yellow oil (14 mg, 28%). Analytical data for **IV-11p**: ^{1}H NMR (500 MHz, $CDCl_3$) δ 7.43 – 7.34 (m, 2H), 7.33 – 7.23 (m, 3H), 7.25 – 7.17 (m, 1H), 7.20 – 7.00 (m, 4H), 3.05 – 2.94 (m, 2H), 2.63 – 2.51 (m, 2H), 2.54 – 2.43 (m, 1H), 2.27 (ddd, *J* = 19.0, 11.9, 8.9 Hz, 1H), 2.15 – 2.03 (m, 1H), 1.68 – 1.56 (m, 1H). ^{13}C NMR (126 MHz, $CDCl_3$) δ 217.65, 139.34, 137.51, 129.26, 128.96, 128.93, 128.49, 127.30, 126.39, 62.40, 46.66, 39.94, 38.41, 26.88. FTIR (diamond, anvil, oil) cm^{-1}: 3085, 3061, 3027, 2958, 2923, 2852, 1743, 1601, 1587. HRMS (ESI): Mass calcd for $C_{18}H_{18}ONa$ $[M+Na]^+$: 273.1256; found 273.1254.

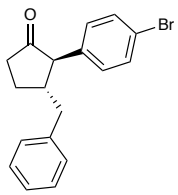

3-benzyl-2-(4-bromophenyl)cyclopentan-1-one (**IV-11q**). Prepared according to General Procedure 3 using the respective acyl imidazole (45 mg, 1.0 equiv) and 4-bromo-benzyl Hantzsch ester. The reaction mixture was purified by column chromatography (0-10% ethyl acetate/hexanes) to yield the product as a white solid (13 mg, 20%). Analytical data for **IV-11q**: ^{1}H NMR (500 MHz, $CDCl_3$) δ 7.54 – 7.46 (m, 2H), 7.31 – 7.26 (m, 2H), 7.24 – 7.17 (m, 1H), 7.20 – 7.06 (m, 2H), 7.05 – 6.98 (m, 2H), 3.01 – 2.90 (m, 2H), 2.59 – 2.41 (m, 3H), 2.25 (ddd, *J* = 19.1, 11.8, 8.8 Hz, 1H), 2.15 – 2.03 (m, 1H), 1.68 – 1.57 (m, 1H). ^{13}C NMR (126 MHz, $CDCl_3$) δ 216.93, 139.00, 136.48, 132.04, 130.64, 129.24, 128.55, 126.51, 121.31, 61.82, 46.55, 39.89, 38.25, 26.86. FTIR (diamond, anvil, solid) cm^{-1}: 3061, 3027, 2957, 2924, 2853, 1742, 1602, 1572. HRMS (ESI): Mass calcd for $C_{18}H_{17}BrONa$ $[M+Na]^+$: 351.0361; found 351.0358.

*4.8.10.4 Procedure for the Synthesis of Linear Ketone **IV-10a***

This procedure can be used for the first two steps of an alternative 3-step protocol to access cyclohexanones if NHC is not readily available.

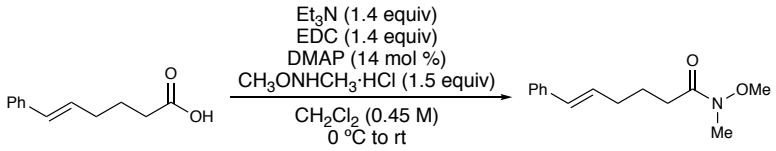

Scheme 4-19. Synthesis of a Weinreb amide from the corresponding carboxylic acid.

To an oven-dried flask equipped with a stir bar at 0 °C was added 6-phenylhex-5-enoic acid (1.00 g, 5.26 mmol, 1.0 equiv) in CH_2Cl_2 (12.0 mL, 0.45 M). *N*,O-dimethyl hydroxylamine hydrochloride (770 mg, 7.89 mmol, 1.5 equiv), triethylamine (745 mg, 7.34 mmol, 1.4 equiv), 4-dimethylaminopyridine (DMAP; 90 mg, 0.74 mmol, 0.14 equiv), and 1-ethyl-3-(-3-dimethylaminopropyl) carbodiimide hydrochloride (EDC; 1.41 g, 7.34 mmol, 1.4 equiv). The reaction mixture was allowed to warm to room temperature and stirred for 24 h under N_2 atmosphere. The unpurified reaction mixture was filtered through a pad of celite. The collected organic layer was washed with aqueous HCl (10 mL, 0.5 M). The aqueous later was extracted with CH_2Cl_2 (3 x 20 mL). The combined organic layers were dried over anhydrous $MgSO_4$, filtered, and concentrated under reduced pressure. *N*-methoxy-*N*-methyl-6-phenylhex-5-enamide was isolated as a clear and colorless oil (1.20 g, 97%) and was used without further purification.

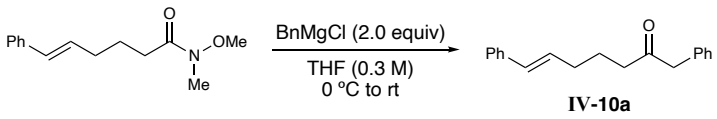

Scheme 4-20. Synthesis of **IV-10a** from the corresponding Weinreb amide.

A stirred solution of unpurified *N*-methoxy-*N*-methyl-6-phenylhex-5-enamide (1.20 g, 5.20 mmol, 1.0 equiv) in THF (14.0 mL, 0.3 M) was cooled to 0 °C. Benzyl magnesium chloride

(2 M in THF; 5.1 mL, 2.0 equiv) was slowly added to the reaction solution, and the resulting mixture was stirred for 20 h at room temperature under N_2 atmosphere. The reaction mixture was cooled, diluted with aqueous HCl (2 M), and extracted with diethyl ether. The organic layer was dried over Na_2SO_4, filtered, and concentrated to yield the crude ketone. Purification by column chromatography (0-20% ethyl acetate/hexanes) afforded **3a'** as a clear and colorless oil (0.44 g, 32% yield). Analytical data for 1,7-diphenylhept-6-en-2-one (**3a'**): ^{1}H NMR (500 MHz, $CDCl_3$) δ 7.28 – 7.21 (m, 7H), 7.18 – 7.13 (m, 3H), 6.28 (dt, *J* = 15.8, 1.5 Hz, 1H), 6.07 (dt, *J* = 15.8, 7.0 Hz, 1H), 3.63 (s, 2H), 2.46 (t, *J* = 7.3 Hz, 2H), 2.12 (qd, *J* = 7.1, 1.4 Hz, 2H), 1.75 – 1.66 (m, 2H). ^{13}C NMR (126 MHz, $CDCl_3$) δ 208.36, 137.66, 134.38, 130.74, 129.94, 129.53, 128.84, 128.62, 128.29, 127.11, 126.08, 50.38, 41.19, 32.34, 23.23. HRMS (ESI): Mass calcd for $C_{19}H_{20}ONa$ $[M+Na]^+$: 287.1412; found 287.1407.

*4.8.10.5 Synthetic Procedure and Tabulated Data for **IV-15a***

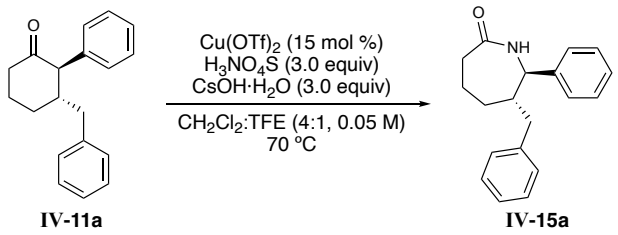

IV-11a **IV-15a**

Scheme 4-21. Synthesis of **IV-15a** from **IV-11a**.

6-benzyl-7-phenylazepan-2-one (**IV-15a**). To a stirred solution of $Cu(OTf)_2$ (5.4 mg, 0.015 mmol, 0.15 equiv) in TFE/CH_2Cl_2 (1:4, 2.0 mL, 0.05 M) was added cyclohexanone **IV-11a** (26 mg, 0.10 mmol, 1.0 equiv), amino hydrogen sulphate (HOSA; 34 mg, 0.30 mmol, 3.0 equiv), and $CsOH·H_2O$ (50 mg, 0.30 mmol, 3.0 equiv) at room temperature. The reaction mixture was maintained at room temperature and stirred overnight. After completion, the mixture was diluted

with CH_2Cl_2 (10 mL) and washed with saturated aqueous Na_2CO_3 (3 × 5 mL). The combined organic layers were washed with brine (5 mL) and dried (anhydrous $MgSO_4$). Column chromatography (0-20% EtOAc/hexane) afforded **IV-15a** as an off-white solid (22 mg, 77%). Analytical data for **IV-15a**: ^{1}H NMR (500 MHz, $CDCl_3$) δ 7.41 (td, *J* = 7.3, 1.6 Hz, 2H), 7.37 – 7.29 (m, 3H), 7.24 (dd, *J* = 8.1, 6.7 Hz, 2H), 7.20 – 7.13 (m, 1H), 7.06 – 7.00 (m, 2H), 5.74 (d, *J* = 4.9 Hz, 1H), 4.25 (dd, *J* = 8.3, 4.9 Hz, 1H), 2.56 (ddd, *J* = 13.7, 10.6, 2.8 Hz, 1H), 2.50 – 2.41 (m, 2H), 2.36 – 2.28 (m, 1H), 2.15 (dd, *J* = 13.5, 10.1 Hz, 1H), 1.99 – 1.80 (m, 2H), 1.65 – 1.54 (m, 1H), 1.49 – 1.38 (m, 1H). ^{13}C NMR (126 MHz, $CDCl_3$) δ 177.57, 140.96, 140.16, 129.45, 129.00, 128.54, 128.26, 126.99, 126.26, 62.22, 44.95, 39.42, 36.67, 33.44, 29.85, 21.14. FTIR (diamond, anvil, solid) cm^{-1}: 3400, 3226, 3084, 3061, 3027, 2928, 2857, 1659, 1602. HRMS (ESI): Mass calcd for $C_{19}H_{21}NONa$ $[M+Na]^+$: 302.1521; found 302.1521.

*4.8.10.6 Synthetic Procedure and Tabulated Data for **IV-16a***

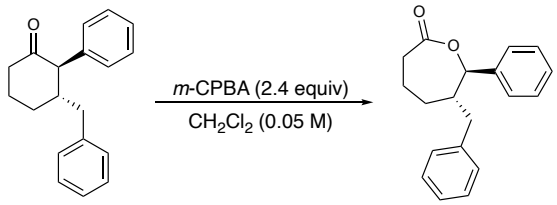

IV-11a **IV-16a**

Scheme 4-22. Synthesis of **IV-16a** from **IV-11a**.

6-benzyl-7-phenyloxepan-2-one (**IV-16a**). To a solution of substituted cyclohexanone **IV-11a** (26 mg, 0.10 mmol, 1.0 equiv) in CH_2Cl_2 (2.0 mL, 0.05 M) at 0 °C was added *m*CPBA (2.4 equiv). After stirring at room temperature overnight, the reaction mixture was quenched with 10% K_2CO_3 solution and a saturated aqueous solution of $Na_2S_2O_3$. The aqueous layer was separated and extracted with CH_2Cl_2. The combined organic layer was dried with anhydrous $MgSO_4$, filtered,

and concentrated under reduced pressure. The named product was isolated as a white solid without additional purification (28 mg, 100% yield). Analytical data for **IV-16a**: ^{1}H NMR (500 MHz, $CDCl_3$) δ 7.45 – 7.35 (m, 4H), 7.35 (ddt, *J* = 7.0, 5.2, 2.9 Hz, 1H), 7.26 – 7.20 (m, 2H), 7.20 – 7.13 (m, 1H), 7.02 – 6.96 (m, 2H), 5.11 (d, *J* = 8.5 Hz, 1H), 2.83 (ddd, *J* = 14.9, 10.8, 4.3 Hz, 1H), 2.69 (ddd, *J* = 14.3, 6.2, 4.1 Hz, 1H), 2.38 (ddt, *J* = 12.1, 8.5, 3.9 Hz, 2H), 2.12 (dd, *J* = 14.3, 12.0 Hz, 1H), 1.99 – 1.85 (m, 1H), 1.75 – 1.62 (m, 1H), 1.49 (dddd, *J* = 13.8, 11.1, 7.7, 2.8 Hz, 1H). ^{13}C NMR (126 MHz, $CDCl_3$) δ 174.70, 139.59, 138.81, 129.00, 128.89, 128.72, 128.55, 127.40, 126.35, 86.07, 45.31, 38.45, 34.16, 31.58, 20.36. FTIR (diamond, anvil, solid) cm^{-1}: 3085, 3062, 3028, 2936, 2863, 1727, 1603. HRMS (ESI): Mass calcd for $C_{19}H_{20}O_2Na$ $[M+Na]^+$: 303.1361; found 303.1362.

4.8.11 X-ray Crystal Structure Data

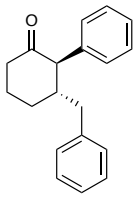

Single crystals of $C_{19}H_{20}O$ **IV-11a** were recrystallized via the slow evaporation of chloroform at 23 °C. A suitable crystal was selected and mounted in inert oil on a XtaLAB Synergy, single source at offset/far, HyPix diffractometer. The crystal was kept at 100.01(10) K during data collection. Using Olex2,[523] the structure was solved with the ShelXT6[524] structure solution program using Intrinsic Phasing and refined with the ShelXL7[525] refinement package using Least Squares minimization. SADABS-2014/5 (Bruker, 2014/5) was used for absorption correction.

Crystal Data for $C_{19}H_{20}O$ **IV-11a** (M =264.35 g/mol): monoclinic, space group I2/a (no. 15), a = 26.0179(5) Å, b = 5.44220(10) Å, c = 21.3303(4) Å, β = 106.364(2)°, V = 2897.91(10) Å^3, Z = 8, T = 100(3) K, μ(MoKα) = 0.073 mm^{-1}, D_{calc} = 1.212 g/cm^3, 70305 reflections measured (3.98° ≤ 2Θ ≤ 67.758°), 5481 unique (R_{int} = 0.0423, R_{sigma} = 0.0204) which were used in all calculations. The final R_1 was 0.0407 (I > 2σ(I)) and wR_1 was 0.1210 (all data). Further information can be found in the CIF file. This crystal structure was deposited in the Cambridge Crystallographic Data Centre and assigned as 2127979.

Refinement Details: No special refinement necessary.

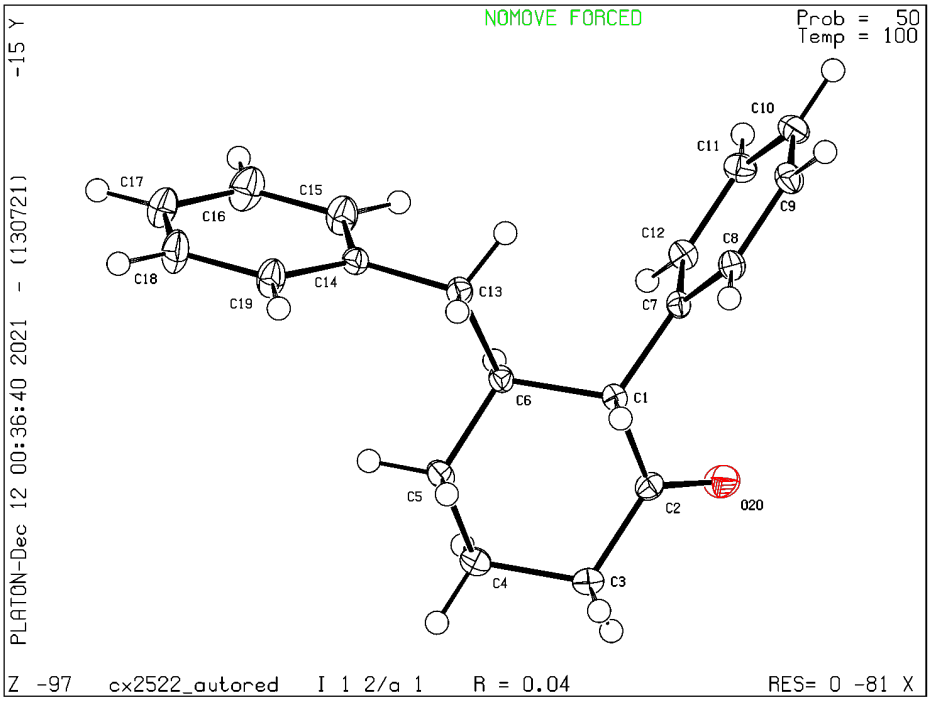

Figure 4-14. Crystal data for **IV-11a**.

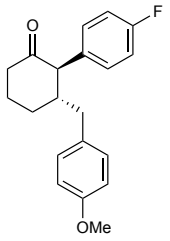

Single crystals of $C_{20}H_{21}FO_2$ **IV-11k** were recrystallized via the slow evaporation of chloroform at 23 °C. A suitable crystal was selected and mounted in inert oil on a XtaLAB Synergy R, DW system, HyPix diffractometer. The crystal was kept at 100.01(10) K during data collection. Using Olex2,[523] the structure was solved with the ShelXT6[524] structure solution program using Intrinsic Phasing and refined with the ShelXL7[525] refinement package using Least Squares minimization. SADABS-2014/5 (Bruker, 2014/5) was used for absorption correction.

Crystal Data for $C_{20}H_{21}FO_2$ (M =312.37 g/mol): orthorhombic, space group P212121 (no. 19), a = 7.54959(12) Å, b = 11.97293(19) Å, c = 17.9915(3) Å, V = 1626.26(4) Å3, Z = 4, T = 100.01(10) K, μ(CuKα) = 0.718 mm^{-1}, D_{calc} = 1.276 g/cm^3, 16112 reflections measured (8.872° ≤ 2Θ ≤ 157.578°), 3372 unique (R_{int} = 0.0305, R_{sigma} = 0.0214) which were used in all calculations. The final R^1 was 0.0299 (I > 2σ(I)) and wR^2 was 0.0791 (all data). Further information can be found in the CIF file. This crystal structure was deposited in the Cambridge Crystallographic Data Centre and assigned as 2127980.

Refinement Details: No special refinement necessary.

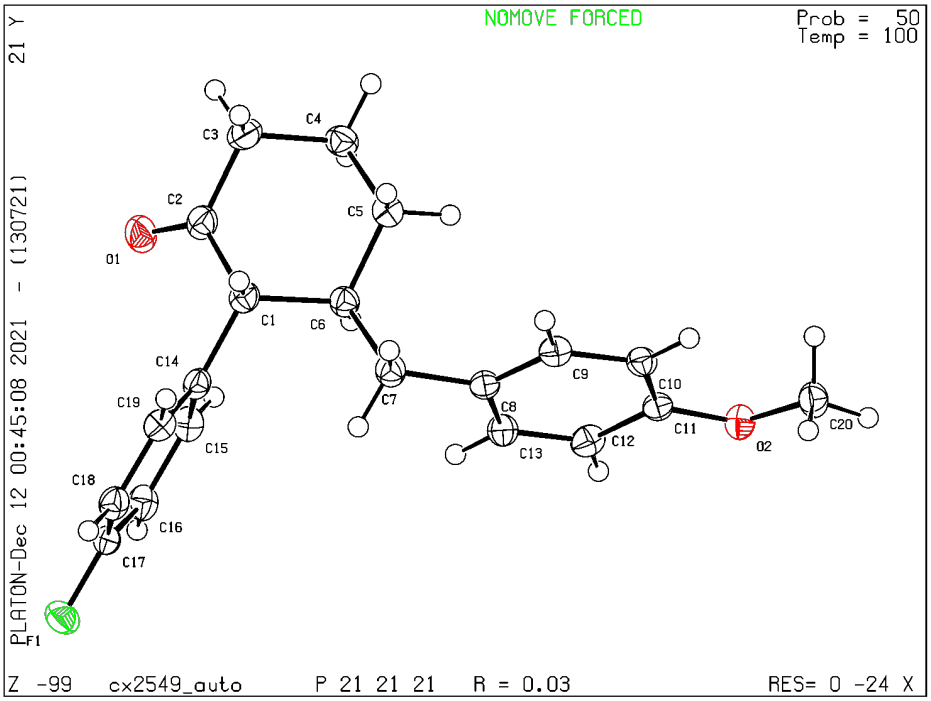

Figure 4-15. Crystal data for **IV-11k**.

CHAPTER 5: PHOTOCATALYZED α-FUNCTIONALIZATION OF CARBONYL COMPOUNDS

5.1 Current Strategies for the α-Functionalization of Carbonyl Compounds

The carbonyl group is a central component of organic synthesis. Carbonyl-containing compounds are versatile synthetic precursors, allowing access to amines, alcohols, alkanes, and a vast array of additional functional groups. Moreover, carbonyl groups are prominent in many bioactive compounds (**Figure 5-1**).[393,526-529] For example, approximately 90% of the top 200 small molecule pharmaceutical compounds by retail sales in 2020 contain a carbonyl group, making ketones, esters, and amides some of the most common functional groups among drugs in the market today.[469]

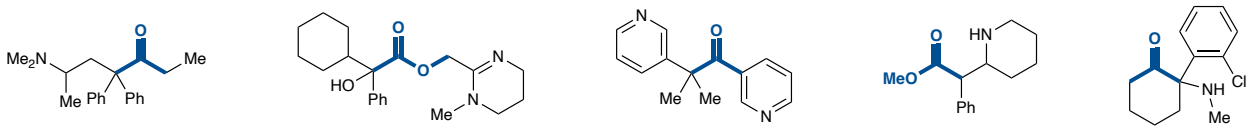

V-1 methadone **V-2** oxyphencyclimine **V-3** metyrapone **V-4** methylphenidate **V-5** esketamine

Figure 5-1. A small selection of carbonyl-containing compounds in the pharmaceutical industry.

The utility of the carbonyl group in organic synthesis is primarily driven by its inherent reactivity. Traditionally, compounds featuring carbonyl groups are electrophilic at the carbonyl carbon and, under the right conditions, are nucleophilic at the α-carbon. Deprotonation at the α-carbon of a carbonyl carbon forms the corresponding nucleophilic enolate, which can engage in various alkylation chemistries (**Figure 5-2**). Analogous to enolates, silyl enol ethers and enamines represent classes of stabilized nucleophiles. Silyl enol ethers are synthesized through enolate addition to a silyl electrophile, and in situ formation of enamines occurs through nucleophilic addition of an amine to a carbonyl group.[530] The recent rise in radical chemistry has also led to the development of α-functionalization strategies using silyl enol ether radicals or enamine-based radical species.

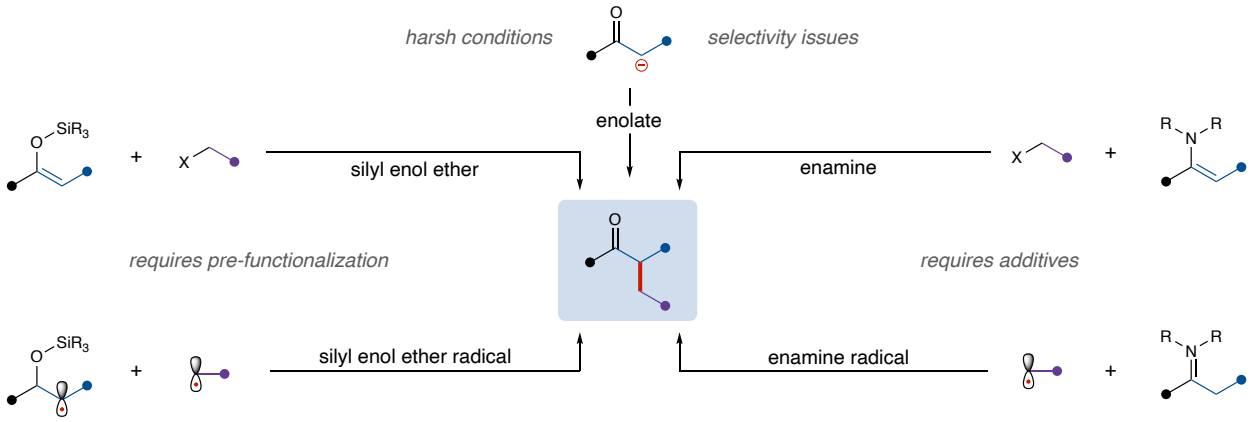

Figure 5-2. Synthetic routes to access α-functionalized carbonyl compounds.

5.1.1 Traditional Enolate Chemistry

Enolates are formed via deprotonation of carbonyl compounds, including ketones, aldehydes, and esters. These nucleophilic species exist in low concentrations when formed using weaker bases, but quantitative conversion from the carbonyl compound (e.g., a ketone) to the corresponding enolate often occurs using strong bases, such as lithium diisopropylamide (LDA). The reactivity of different bases can be harnessed to achieve regioselective deprotonation with unsymmetrical ketones (**Scheme 5-1**).[531] For example, deprotonation of α-methyl cyclohexanone (**V-6**) with a strong base under controlled reaction conditions (e.g., LDA at –78 ºC) occurs at H^a to afford the kinetic enolate, while use of an alkoxide base (i.e., a weaker base) deprotonates H^b to yield the thermodynamically stable, more substituted enolate. These organic anions are employed in various organic processes to enable a broad landscape of reactivity.

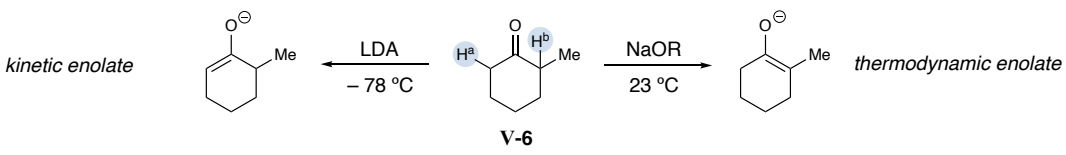

Scheme 5-1. Kinetic versus thermodynamic enolate formation.

Enolates are also known to engage with other carbonyl compounds through nucleophilic addition to the carbonyl carbon. The aldol reaction was first discovered by Alexander Borodin in 1869 and describes the reaction between two carbonyl compounds, commonly a ketone enolate and an aldehyde electrophile (**Scheme 5-2A**). Offering a route to access β-hydroxy carbonyl compounds or α,β-unsaturated ketones (via the aldol condensation), the aldol reaction has been a staple reaction in the field of organic chemistry for centuries. Rainer Ludwig Claisen later reported the nucleophilic addition of esters to another carbonyl compound (often another ester) to yield β-keto esters or β-diketones, a reaction now termed the Claisen condensation reaction (**Scheme 5-2B**). These organic anions are employed in various additional processes to enable access to an array of organic compounds.

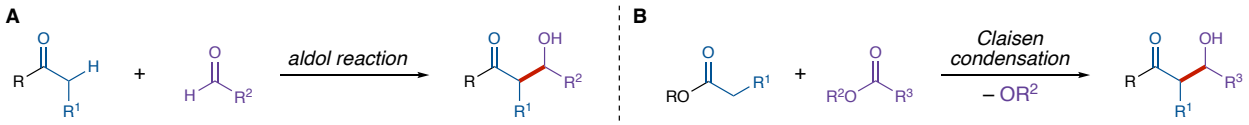

Scheme 5-2. Common enolate reactions, including **A)** the aldol reaction and **B)** the Claisen condensation.

5.1.2 Pre-functionalization to Silyl Enol Ethers

Silyl groups as often used as protecting groups in organic chemistry through the formation of silyl ethers or enol ethers. Silyl enol ethers have increased utility in organic synthesis due to their ability to act as stabilized enolates. These silicon-derived substrates are mildly nucleophilic and often react with carbocations and activated electrophiles, such as an aldehyde in the presence of a Lewis acid. For example, silyl enol ethers are known to engage in alkylation processes, including the Mukaiyama aldol reaction, various Michael reactions, and more.[532-533]

Photochemistry and various redox processes have been applied to chemistry involving silyl enol ethers to expand the scope of this class of compounds significantly. In 1987, Gassman and

Bottorff reported a photoinduced single-electron oxidation of silyl enol ethers ($E_{1/2}$ = +1.29 V vs SCE) to access a radical cation species (**V-7**$^{+\bullet}$) via excitation of 1-cyanonapthalene, which acts as a strong single-electron oxidant ($E_{1/2}$ = +1.84 V vs SCE; **Scheme 5-3A**).[534] The addition of methanol resulted in a light mediated desilylation process to access cyclohexanone (**V-8**) from the corresponding silyl enol ether **(V-7**) using high energy 300 nm light. Similarly, Kochi and Rathore reported the formation of silyl enol ether radical cations less than one decade later (**Scheme 5-3A**).[535] The authors propose formation of an EDA complex between tetranitromethane and silyl enol ethers under thermal or photochemical conditions to afford α-nitro ketones (e.g., **V-9**). Thomson and coworkers developed numerous approaches to the oxidative coupling of ketones using silyl bis-enol ethers (**Scheme 5-3B**).[536] Using electrochemistry, photochemistry, or cerium(IV) ammonium nitrate (CAN; a traditional oxidative metal complex employed for comparison purposes) to oxidize the silyl bis-enol ether, they were able to access a range of 1,4-diketones with modest-to-excellent diastereoselective ratios.

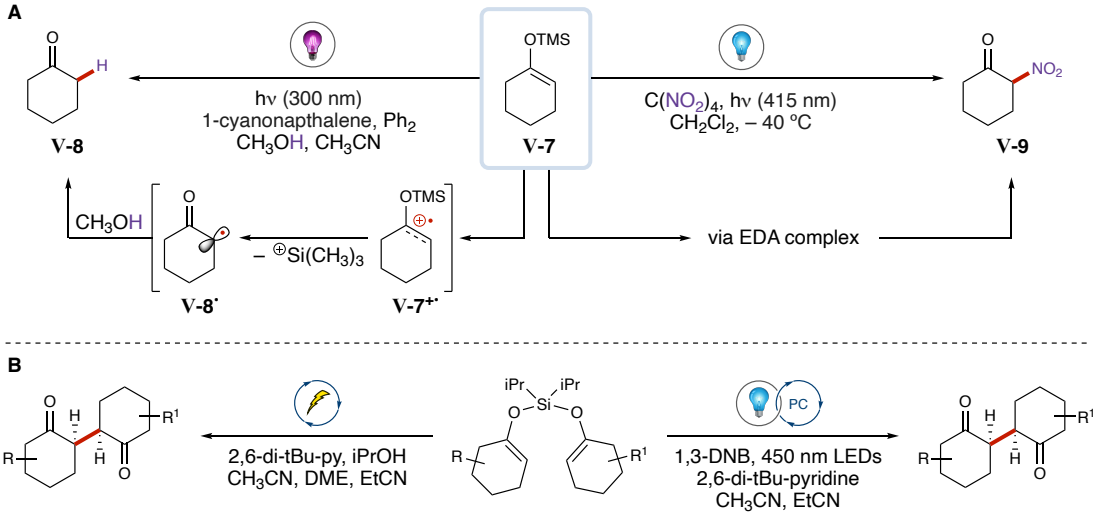

Scheme 5-3. A) Early evidence for silyl enol ether radical cation formation by Gassman (left)[534] and Kochi (right),[535] respectively. **B)** Synthesis of 1,4-diketones by Thomson and coworkers that features a silyl bis-enol ether radical cation intermediate.[536]

While these reports demonstrate the existence of silyl enol ether radical cations, few reports describe the radical-radical coupling of silyl enol ether radicals with reductively generated radicals or the addition of silyl enol ether radicals to alkenes. For example, He and coworkers recently reported a deaminative difluoroalkylation process using difluoroenoxysilanes, but they propose addition of a reductively generated alkyl radical to the α-position of a silyl enol ether (**Scheme 5-4**).[537] Single-electron reduction of a Katritzky salt (**V-10**) affords a reactive radical species, which undergoes regioselective addition to the α-position of the silyl enol ether. The authors suggest that the resulting radical species engages in single-electron transfer with the photocatalyst, and loss of triethylsilane affords the final α-functionalized ketone product. Alternative reports feature similar mechanisms, wherein radical addition to a silyl enol ether leads to product formation.[538]

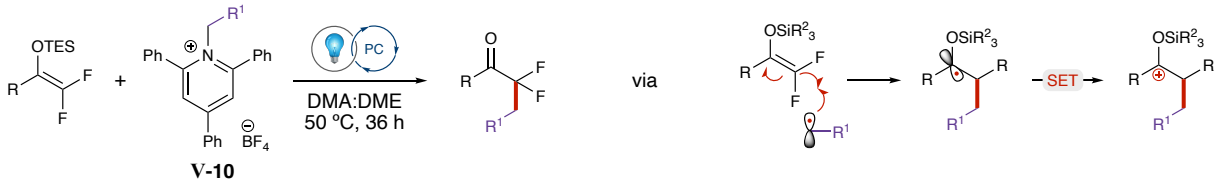

Scheme 5-4. Deaminative difluoroalkylation reaction employing difluoroenoxysilanes reported by He.[537]

5.1.3 In Situ Pre-functionalization via Enamine Catalysis

Inspired by nature's use of the aldolase class of enzymes to catalyze the aldol reactions, chemists began using amines as catalysts for carbonyl-based chemistry. Due to their inherent reactivity, ketones and aldehydes can react with primary or secondary amines to generate the corresponding enamines via dehydration. In 1971, two research groups independently reported an intramolecular enantioselective aldol reaction catalyzed by (*S*)-proline, a reaction now termed the Hajos-Parrish-Eder-Sauer-Wiechert reaction (commonly, the Hajos-Parrish reaction).[539-540] Over two decades later, the groups of Carlos Barbas III, Ian Wilson, and Richard Lerner generated

antibodies that catalyze the intramolecular aldol reaction.[541] Shortly thereafter, a collaboration between the Barbas group and Benjamin List's group led to the development of an intermolecular amino acid-catalyzed asymmetric aldol reaction.[542] For example, the reaction between acetone (**V-11**) and isovaleraldehyde (**V-12**) afforded the desired aldol product (**V-14**) in excellent yield and enantioselectivity using proline (**V-15**) as a catalyst (**Scheme 5-5**). They proposed that the enamine intermediate (**V-13**) raises the highest occupied molecular orbital (HOMO), thus increasing nucleophilicity compared to the corresponding enol ether. Significant work by List and coworkers continued to expand the field of enamine catalysis over the following decades. Today, enamine catalysis has enabled the construction of β-hydroxy ketones, β-amino ketones, β-nitro ketones, α-halogen ketones, and more.[543]

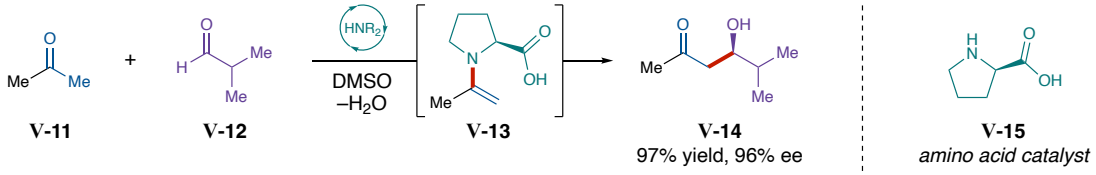

Scheme 5-5. An example of the proline-catalyzed asymmetric aldol reaction developed by List and coworkers.[542]

Combined enamine and photoredox catalysis was first reported by MacMillan in 2008 (see Chapter 2.2.3).[222] This work was later extended to the β-functionalization of ketones using base and catalytic amine and has since led to the development of other processes, including several α-amination and α-hydroxylation reactions.[312] Inspired by these reports, Gianetti and coworkers described a strategy for the α-arylation of cyclic ketones using low energy, green light-mediated photoredox catalysis in early 2022 (**Scheme 5-6**).[544] Mechanistic studies suggest two potential reaction pathways may occur, both of which are initiated by in situ formation of an enamine using superstoichiometric pyrrolidine. In one reaction pathway, subsequent oxidation of the enamine

(E_{ox} = +0.58 V vs SCE) by their newly developed photoreducing acridinium catalyst affords an imine radical cation. Radical-radical coupling with an aryl radical accessed by single-electron reduction of an aryl iodide (E_{red} = –1.9 V vs SCE) yields the final α-aryl ketone product. Alternatively, they state that product may be afforded by a reductive quenching cycle featuring halogen atom abstraction (XAT), wherein an oxidized amine or enamine abstracts the halogen atom from the aryl halide to produce the aryl radical. A subsequent radical chain process furnishes the final α-aryl product.

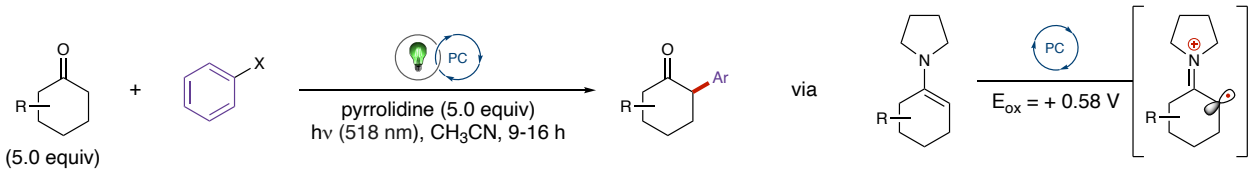

Scheme 5-6. Photoredox-catalyzed α-arylation strategy developed by Gianetti.[544]

5.2 Strategy for the Mild α-Functionalization of Carbonyl Compounds

While numerous approaches for the α-functionalization of carbonyl compounds have been described, each method features limitations which restrict its utility in synthesis. Enamine chemistry requires additives and suffers from various scope limitations, and use of silyl enol ethers requires pre-functionalization of the corresponding carbonyl compound. While well-established, enolate chemistry often involves harsh or strenuous reaction conditions, limiting its overall potential. Moreover, few known procedures feature a versatile α-radical for functionalization of carbonyl compounds. Although enamine catalysis and the use of silyl enol ethers have enabled the development of various methodologies for the functionalization of carbonyl compounds via both two-electron and single-electron pathways, no general and mild method for the α-functionalization of carbonyl compounds currently exists.

We recently expanded our combined NHC and photoredox platform to the synthesis of complex, disubstituted cycloalkanones (see Chapter 4.2-4.8). This process features a radical-radical coupling between an oxidatively generated radical precursor (i.e., a Hantzsch ester, **V-16**) and an acyl azolium radical to form a linear ketone intermediate (**Figure 5-3**). Mechanistic experiments suggest that deprotonation of the linear ketone intermediate forms a cesium enolate or enol in situ, and subsequent single-electron oxidation in a distinct photoredox cycle affords an α-radical. Cyclization into the pendant alkene yields the final ketone product. Inspired by the latter portion of this mechanism, we anticipated that this reactivity may be applied to the development of a broad strategy for the α-functionalization of carbonyl compounds, including esters, ketones, and amides.

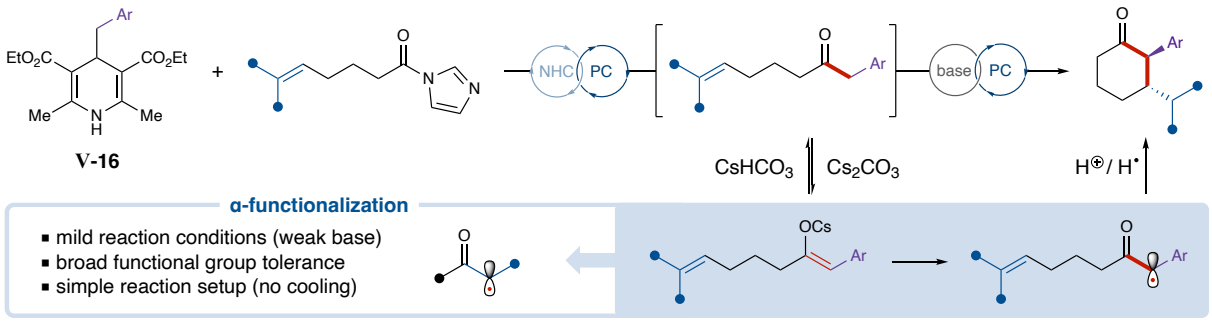

Figure 5-3. Tandem photoredox-catalyzed annulation strategy for the synthesis of cyclohexanones as inspiration for an α-functionalization strategy. ORP = oxidatively generated radical precursor.

We hypothesized that we could develop a mild and broad α-functionalization strategy via single-electron oxidation of an in situ formed enol or enolate. We envisioned a process that features reversible deprotonation of a carbonyl compound by a mild base. A single-electron oxidation of the resulting enol or enolate by a photocatalyst or using electrochemistry would yield a versatile α-radical species capable of undergoing addition to an alkene or engaging with another radical

species via radical cross-coupling (**Figure 5-4**). This process would enable the mild α-functionalization of carbonyl compounds in one-step with readily available starting materials.

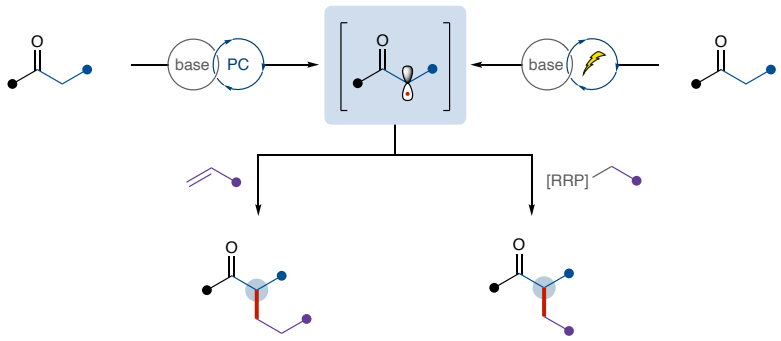

Figure 5-4. Strategy for the mild α-functionalization of carbonyl compounds via photoredox or electrochemical single-electron oxidation of an in situ formed enol or enolate. RRP = reductively generated radical precursor.

5.3 Reaction Discovery

5.3.1 Introduction to Reductively Generated Radical Precursors

A variety of the reaction components were screened to begin testing this hypothesis. In a similar manner to oxidatively generated radical precursors (see Chapter 2.4.2), an array of reductively generated radical precursors have been developed and subsequently employed in radical coupling processes in recent decades. Alkyl halides (**V-17**) represent one of the most atom-economic and readily available radical precursor classes utilized to date. However, their relatively high reduction potentials (e.g., alkyl chloride, E_{red} = –2.70 V vs SCE; alkyl bromide, E_{red} = –2.10 V vs SCE; alkyl iodide, E_{red} = –1.90 V vs SCE) significantly reduce their overall utility as reductively generated radical precursors in synthesis (**Figure 5-5**).[545] In addition to their broad use in reductive aminations, hydrolysis reactions, and more, cyanoarenes (**V-18**) are known to undergo decyanative cross-coupling reactions. Generation of radical coupling partners from cyanoarenes

can occur via single-electron reduction by a photocatalyst (E_{red} = –1.60 V vs SCE for 1,4-dicyanobenzene (**V-18a**); E_{red} = –0.99 V vs SCE for 4-cyanopyridine (**V-18b**)).[546-547]

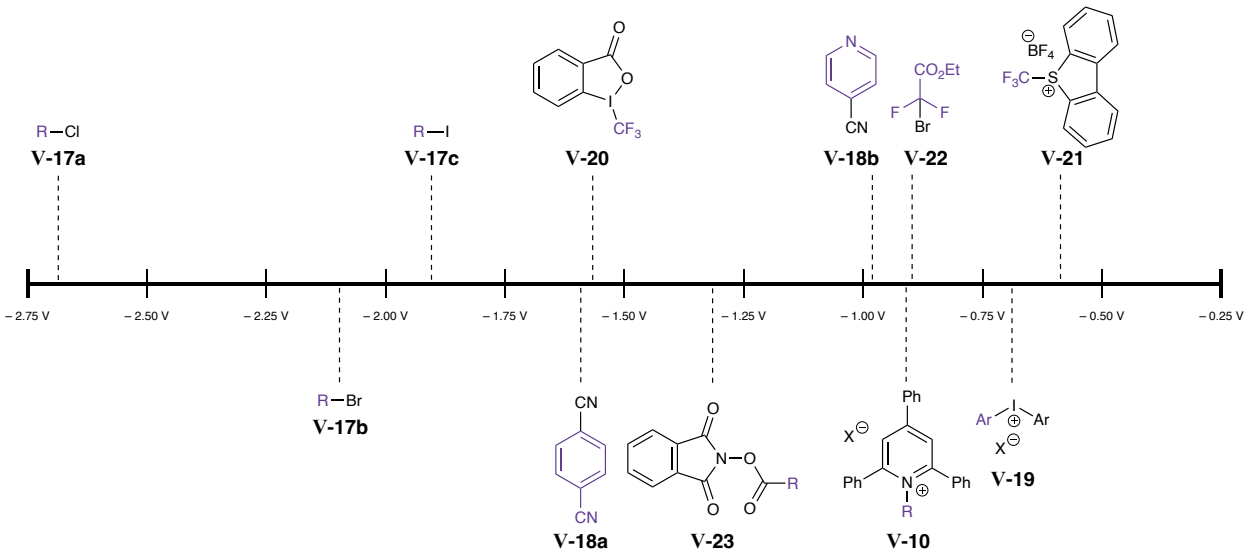

Figure 5-5. Reduction potentials of common reductively generated radical precursors. Potentials reported versus SCE.

A variety of reductively generated radical precursors can also be synthesized for use in radical coupling reactions. For example, hypervalent iodides, such as aryliodonium salts (**V-19**, E_{red} = –0.6 to –0.7 V vs SCE),[548] Togni reagent II (**V-20**, E_{red} = –1.58 V vs SCE),[549] Umemoto's reagent (**V-21**, E_{red} = –0.63 V vs SCE),[550] and various difluoroalkyl radical sources (e.g., $BrCF_2CO_2Et$, **V-22**, E_{red} = –0.89 V vs SCE),[551] can be synthesized or purchased from commercial sources (**Figure 5-5**). Redox-active esters, such as *N*-(acyloxy)phthalimides (**V-23**), have been used in single-electron transfer processes since the early 1990's and have become popular reagents for use as reductively generated radical precursors in recent years due to their low reduction potential (E_{red} = –1.20 to –1.45 V vs SCE)[338] and relative ease of synthesis.[217] Featuring even lower reduction potentials than redox-active esters, Katritzsky salts (**V-10**) can also undergo a single-

electron reduction (E_{red} = –0.90 V vs SCE)[552] to afford versatile alkyl radical coupling partners (**Figure 5-5**).

5.3.2 Initial Broad Reactivity Screens

A series of broad reactivity screens were employed to test for the desired reactivity. An initial reactivity screen investigated the use of various carbonyl compounds, including a benzylic ketone (**V-24a**), ethyl ketone (**V-24b**), and ethyl phenylacetate (**V-25a**). Styrene (**V-26a**) and diphenylethylene (**V-26b**) were tested as reacting partners as well as an array of reductively generated radical precursors (**Figure 5-6**). Six photocatalysts, including highly reducing and highly oxidizing photocatalysts, organophotocatalysts, and metal-derived photocatalysts, were screened for each combination of carbonyl compound and reacting partner.

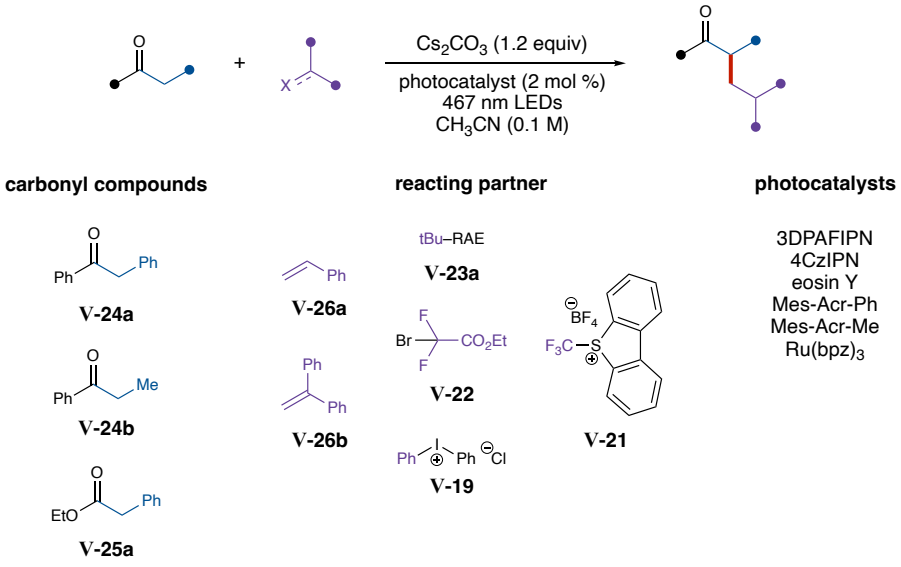

Figure 5-6. Reaction components employed in initial reactivity screens.

The majority of reaction component combinations that were screened did not yield the desired product, but the combination of diphenylethylene (**V-26b**) with ethyl phenylacetate (**V-25a**) afforded desired **V-28a** (**Scheme 5-7A**). Optimization of the reaction concentration enabled

the product to be isolated in 48% yield. Control reactions were performed to obtain preliminary mechanistic insight. The reaction does not proceed in the absence of base, photocatalyst, or light, which suggests a base-promoted and photoredox-catalyzed reaction. The reaction was conducted with styrene (**V-26a**) in place of **V-26b**, but no product was observed (**Scheme 5-7B**). The relative thermodynamic instability of the radical following addition to **V-26a** compared to addition to **V-26b** offers a potential explanation for the lack of reactivity using **V-26a**. Nonetheless, the apparent limited scope for this reaction initiated additional screening of reaction conditions.

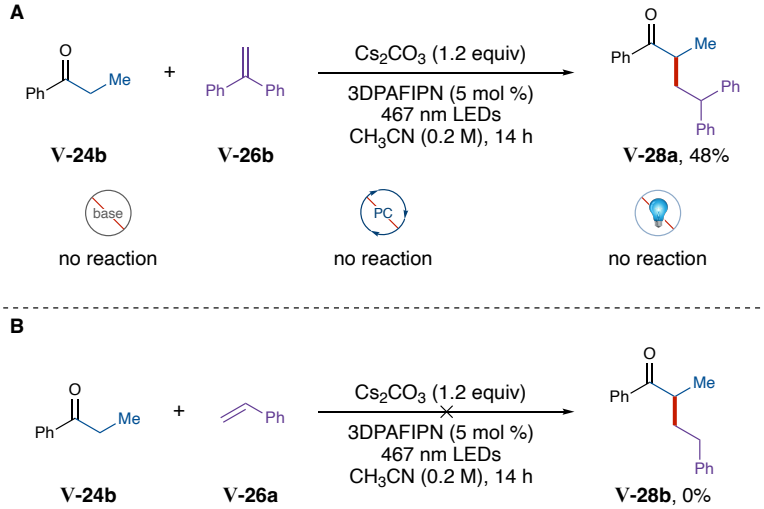

Scheme 5-7. Initial hit reaction for the addition of a ketone (**V-24b**) to alkenes **A) V-26b** and **B) V-26a**, respectively. Reactions were performed at a 0.20 mmol scale.

5.3.2 High-throughput Experimentation for Identification of Reaction Components

Using the initial hit reaction conditions as a guide for reactivity, high-throughput experimentation was employed to explore a broad spectrum of reaction conditions. Two 96-well plates were constructed to investigate the base-promoted photoredox-catalyzed reaction between **V-24b** and styrene (**V-26a**) or tert-butyl redox-active ester (**V-23a**). Reaction screening included three different photocatalysts, eight bases (including both inorganic and organic bases), and four

solvents of differing polarities. Given that acid-promoted enolization is also possible, a variety of Lewis acids were screened for the addition of **V-24b** into **V-26a**. Analysis of the resulting data suggests that basic enolization is more efficient for the α-functionalization of carbonyl compounds, as only one minor hit reaction was identified using Lewis acids (**Figure 5-7**). On the contrary,

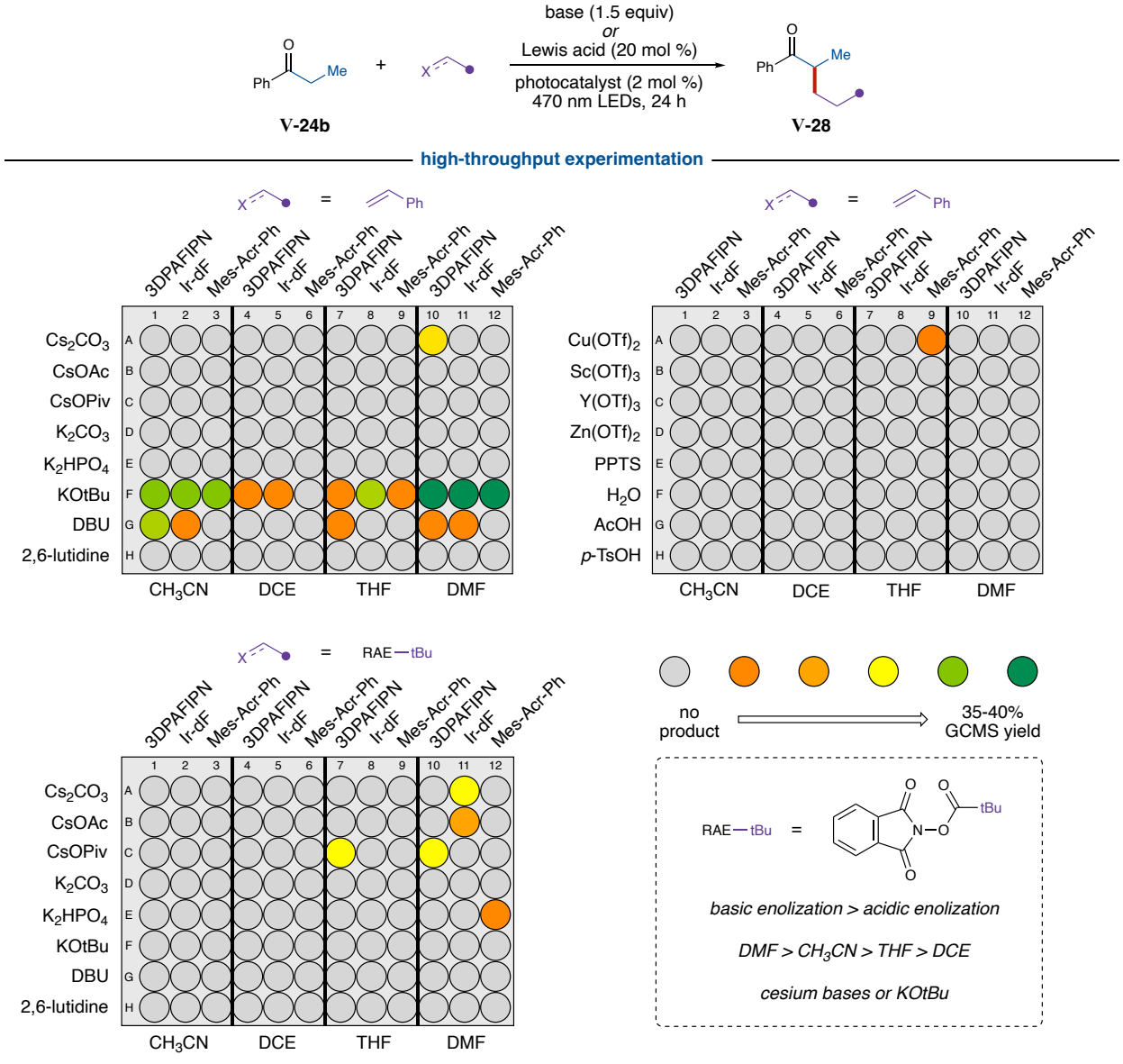

Figure 5-7. High-throughput experimentation results for the reaction of **V-24b** with various reacting partners.

product was observed in numerous reactions under basic reaction conditions. Polar solvents (e.g., dimethylformamide (DMF) and acetonitrile (CH_3CN)) outperformed more nonpolar solvents (e.g., tetrahydrofuran (THF) and dichloroethane (DCE); **Figure 5-7**).

The reaction between ketone **V-24b** and styrene (**V-26a**) using potassium tert-butoxide was found to be efficient in DMF (**Scheme 5-8**). Brief reaction optimization ensued and resulted in an increase in the equivalents of **V-26a** from two to five equivalents. Control reactions were run due to the high basicity of potassium tert-butoxide to ensure that the reaction proceeds via a radical mechanism. No product was observed in the absence of base, indicating that deprotonation at the α-position is required for the reaction. However, the reaction proceeded without photocatalyst and without light, perhaps due to single-electron transfer promoted by the combination of potassium tert-butoxide and DMF (**Scheme 5-8**).[553]

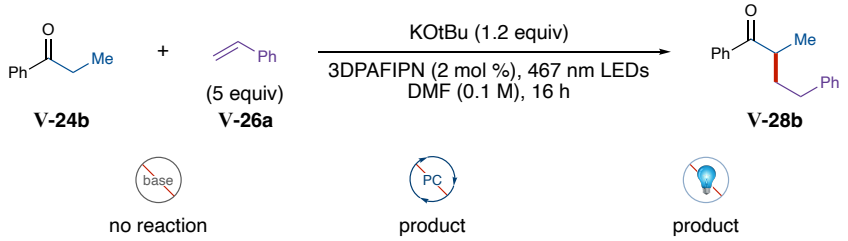

Scheme 5-8. Optimized reaction conditions using potassium tert-butoxide as the base for the α-functionalization of **V-24b**.

Given the initial limited success for the α-functionalization of ketones, screening of reaction conditions proceeded to identify reaction conditions for the photoredox-catalyzed α-functionalization of esters. Benzylic ester **V-25a** was employed in reactivity screens using three 96-well plates (**Figure 5-8**). Conditions exploring base-promoted and acid-promoted enolization were tested, and a variety of photocatalysts, solvents, and reacting partners were screened. Again, basic enolization was found to be more efficient than acid-promoted enolization in promoting the

photoredox-catalyzed α-functionalization process. The results from screening revealed product formation in acetonitrile and THF, with acetonitrile being the optimal solvent for both radical addition into an alkene and radical-radical coupling processes. Moreover, cesium-derived bases, such as cesium carbonate, outperformed all the other bases that were tested (**Figure 5-8**).

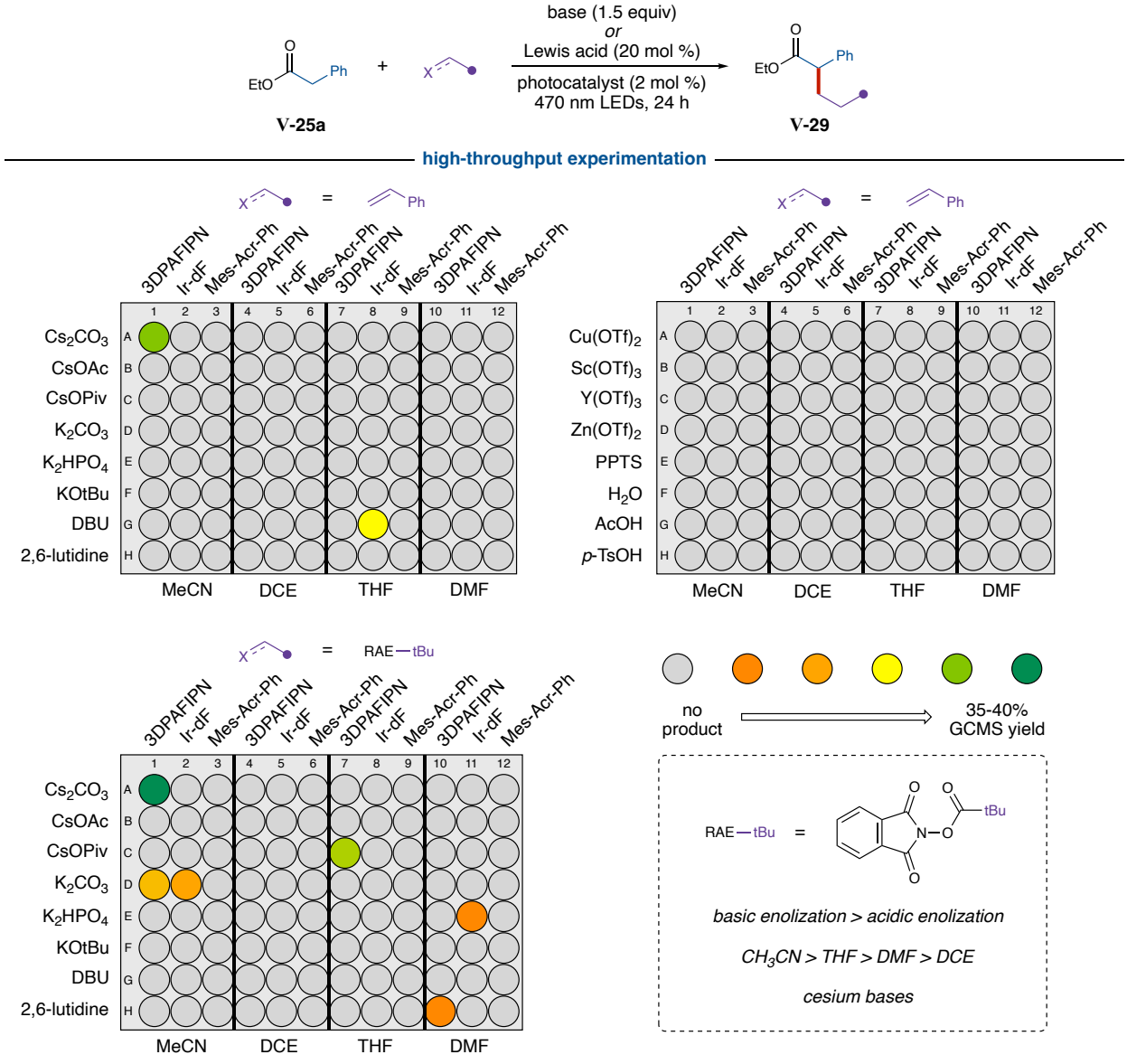

Figure 5-8. High-throughput experimentation for the α-functionalization of esters.

5.4 Optimization of Reaction Conditions

Various reactions were scaled up based on analysis of the high-throughput experimentation results. The reaction between **V-25a** and styrene (**V-26a**) afforded the desired product **V-29a** in 25% isolated yield. Significant optimization was thus required to develop a synthetically useful approach for the α-functionalization of esters. A screen of photocatalysts revealed no increase in yields using highly oxidizing photocatalysts (e.g., acrindium photocatalysts) or other photocatalysts with a broad range of redox potentials (entries 1-3, **Table 5-1**). Other bases and solvents proved ineffective in increasing the yield of **V-29a** (entries 4-8, **Table 5-1**). Use of THF as the reaction solvent did not produce any product, and DMF decreased the yield significantly (entries 8-9, **Table 5-1**). Moreover, increasing the photocatalyst loading led to a decrease in yield, and changes in the reaction concentration did not lead to improvements in the yield (entries 9-15, **Table 5-1**). The optimized reaction conditions thus employ cesium carbonate as the base, organophotocatalyst 3DPAFIPN, and acetonitrile as the solvent (entry 1, **Table 5-1**).

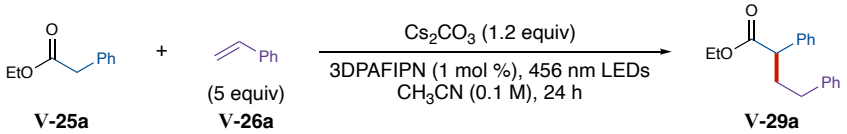

V-25a **V-26a** **V-29a**

entry	deviation from standard	yield[a]
1	none	76
2	Ir-dF instead of 3DPAFIPN	0
3	Mes-Acr-Ph instead of 3DPAFIPN	0
4	4CzIPN instead of 3DPAFIPN	0
5	CsOPiv istead of Cs_2CO_3	0
6	K_2CO_3 instead of Cs_2CO_3	0
7	DBU instead of Cs_2CO_3	0
8	THF instead of CH_3CN	0
9	DMF instead of CH_3CN	22
10	3 mol % 3DPAFIPN instead of 1 mol %	46
11	5 mol % 3DPAFIPN instead of 1 mol %	16
12	0.025 M instead of 0.1 M	3
13	0.05 M instead of 0.1 M	5
14	0.15 M instead of 0.1 M	59
15	0.2 M instead of 0.1 M	25

Table 5-1. Optimization of the reaction conditions for the synthesis of α-functionalized esters. [a] ^{1}H NMR spectroscopic yield using 1,3,5-trimethoxybenzene as the internal standard.

Initial investigation of the ester substrate scope is currently underway using the optimized reaction conditions. Benzyl ester **V-29a** was isolated in high yield (**Table 5-2**). Electron-withdrawing and electron-donating substituents appear to be tolerated on both the ester and alkene components, affording **V-29b-d** in moderate-to-good yields. Isolation of additional products is in progress. A large variety of esters have been synthesized via esterification of the corresponding carboxylic acid, and their use in this reaction will occur shortly.

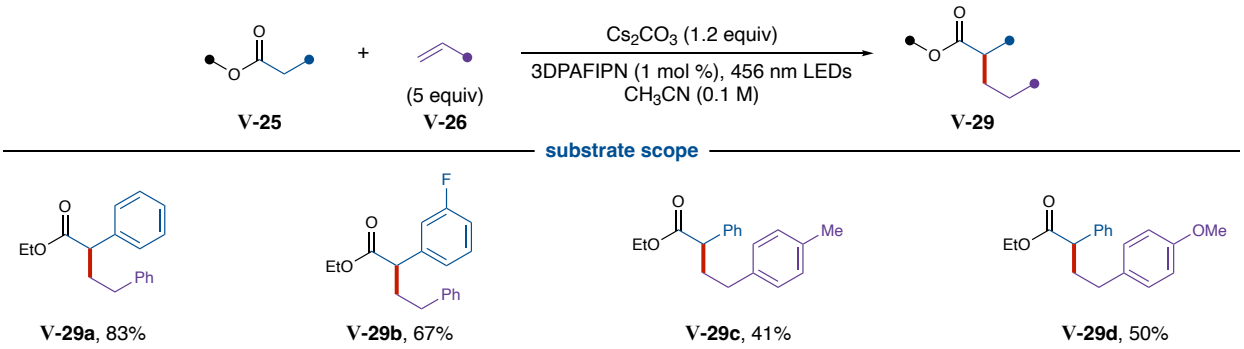

Table 5-2. Initial investigation of the substrate scope. Yields are isolated.

5.5 Mechanism for the α-Functionalization of Carbonyl Compounds

5.5.1 Mechanistic Studies

Various mechanistic studies were conducted to gain insight into the reaction mechanism for the photoredox-catalyzed α-functionalization of esters. The reaction did not proceed in the absence of base, suggesting that deprotonation of the α-position is required for reactivity. Moreover, no reaction occurred in the dark at room temperature or at 40 ºC, which suggests that the reaction is photocatalyzed. Product was observed in 22% ^{1}H NMR spectroscopic yield in the absence of photocatalyst, but the yield was significantly less than that obtained using the standard reaction conditions (i.e., 83% isolated yield). Cyclic voltammetry was also used to probe the reaction mechanism. Interestingly, cyclic voltammetry of **V-25a** revealed no redox events in the

presence and absence of base. Together, this mechanistic data is indicative of a light-driven, photoredox-catalyzed process. However, additional mechanistic experiments are required to further explore the mechanism of this reaction (e.g., PCET, EDA complex formation, etc.).

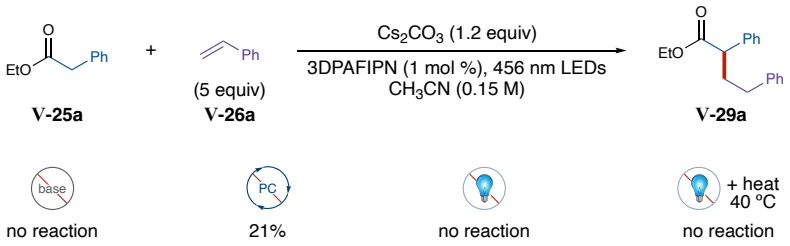

Scheme 5-9. Control reactions for the α-functionalization of **V-25a**.

5.5.2 Proposed Mechanism

Based on the results of the completed mechanistic studies, we propose a mechanism for the α-functionalization of esters that is driven by light. Deprotonation of ester **V-25** by cesium carbonate forms **V-25-Cs**, which likely undergoes single-electron oxidation by the excited organophotocatalyst to yield **V-25˙**. Addition of **V-25˙** into an alkene produces intermediate **V-30**,

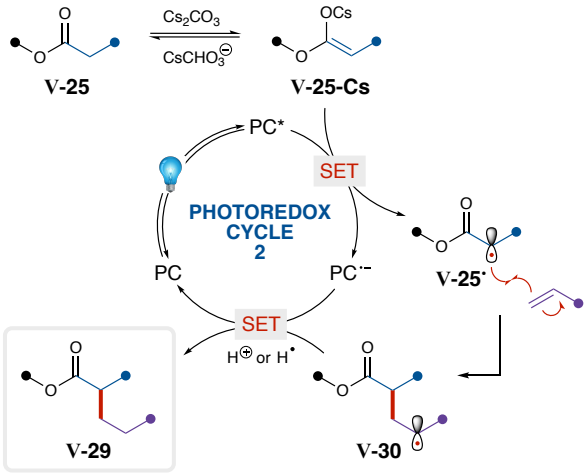

Scheme 5-10. Proposed mechanism for the α-functionalization of esters.

a radical species which can undergo single-electron reduction by the reduced photocatalyst or engage in hydrogen atom transfer to afford the final α-functionalized ester product (**V-29**).

5.6 Future Directions

Additional investigation into the mechanism is necessary to better understand the mechanism by which this reaction proceeds. UV-visible spectrophotometry should be employed to test for formation of an EDA complex between the ester and the alkene component. A shift in the absorption would be expected when the two reagents are combined in solution if an EDA complex is being formed. TEMPO-trapping experiments should also be performed to confirm a radical mechanism, and identification of TEMPO adducts will provide additional insight into the radical species present throughout the course of the reaction. Light/dark studies can be used to study the final step of the reaction to determine whether a radical chain mechanism is occurring or if single-electron reduction by the photocatalyst completes the photoredox cycle and turns over the photocatalyst.

Investigation of radical-radical coupling processes for the α-functionalization of esters and ketones has been initiated. Numerous reductively generated radical precursors were screened for productive radical cross-coupling with the ester α-radical species. It was determined that radical-radical coupling is possible using various reductively generated radical precursors, including Katritzky salts (**V-10a**), aryl iodoniums (**V-19a**), α-bromo esters (**V-22a**), and redox active esters (**V-23b**; **Figure 5-9**, see Chapter 5.7.4 for additional details for the screening of reductively generated radical precursors). Optimization of this radical-radical coupling process should be pursued, and exploration of the substrate scope should follow.

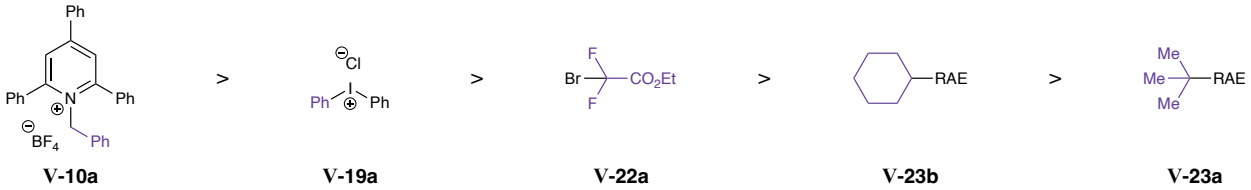

Figure 5-9. Reductively generated radical precursors ranked by reactivity for radical-radical coupling with the ester α-radical species.

Lastly, this α-functionalization platform can be further expanded to afford an array of additional products. The asymmetric functionalization may be achieved using an α-oxo or α-heteroaryl ester in combination with a chiral Lewis acid (**Figure 5-10**). Alternatively, enantioselectivity may be possible using a chiral ester starting material, such as that derived from trans-2-phenylcyclohexanol (**Figure 5-10**).[554-555] Use of α,β-unsaturated ketones and esters may

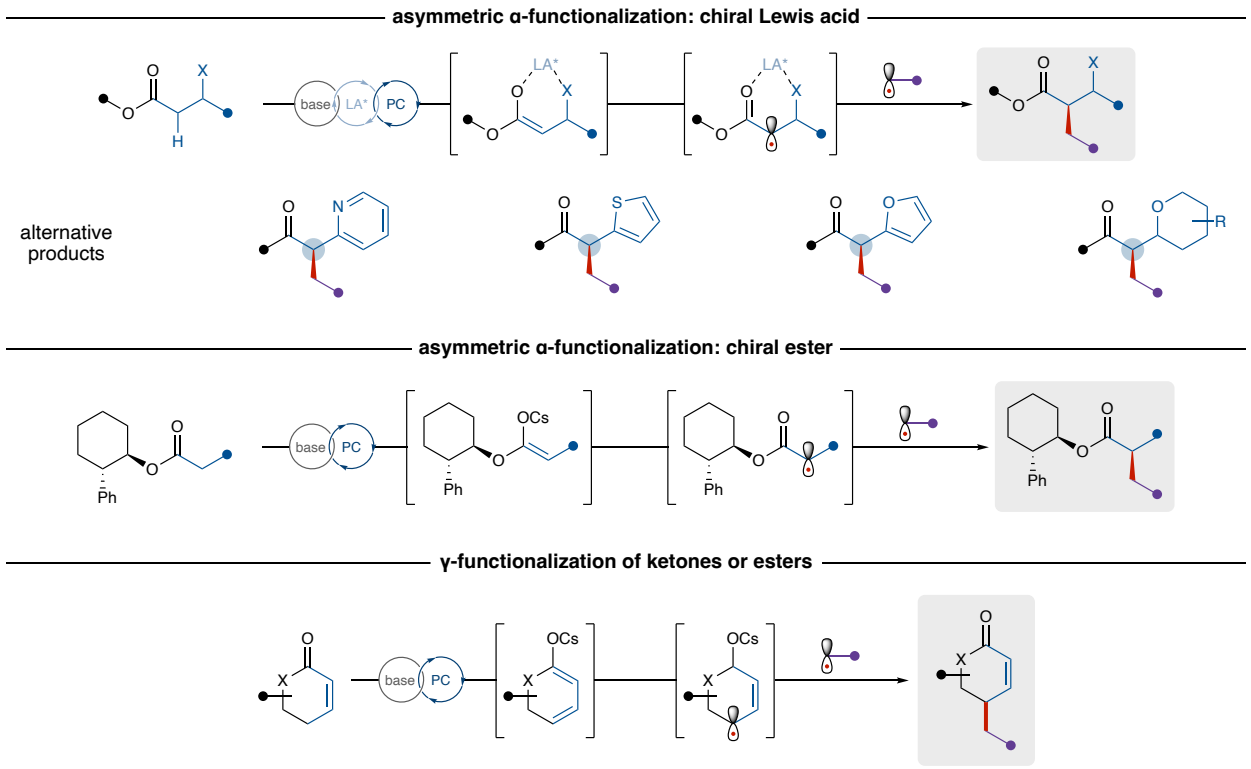

Figure 5-10. Future directions for the α-functionalization of carbonyl compounds using base-promoted, light-driven photoredox catalysis.

allow access to their γ-substituted analogues. Deprotonation at the γ-position would lead to the corresponding cesium dienolate, which may undergo single-electron oxidation by a photocatalyst or via electrochemical means to afford a γ-radical species. Radical-radical coupling or addition into an alkene would yield the final γ-substituted ester or ketone product (**Figure 5-10**).

5.7 Experimental Synthesis Protocols and Analyses

5.7.1 General Information

All reactions were carried out under an argon or nitrogen atmosphere in oven-dried glassware with magnetic stirring. All solvents were degassed using freeze-pump-thaw method (3-4 cycles). Purification of reaction products was carried out by flash chromatography on Biotage Isolera 4 or Biotage Dalton 2000 (ELSD-A120) systems with ultra-grade silica cartridges. Analytical thin layer chromatography was performed on EM Reagent 0.25 mm silica gel 60-F plates. Visualization was accomplished with UV light or ceric ammonium molybdate (CAM) stain followed by heating.

^{1}H NMR spectra were recorded on an AVANCE III 500 MHz w/ direct cryoprobe (500 MHz) spectrometer and are reported in ppm using solvent as an internal standard ($CDCl_3$ at 7.26 ppm). Data are reported as (ap = apparent, s = singlet, d = doublet, t = apparent triplet, q = quartet, m = multiplet, b = broad; coupling constant(s) in Hz; integration) Proton-decoupled ^{13}C NMR spectra were recorded on an AVANCE III 500 MHz w/ direct cryoprobe (126 MHz) spectrometer and are reported in ppm using solvent as an internal standard ($CDCl_3$ at 77.16 ppm). Mass spectra were obtained on a WATERS Acquity-H UPLC-MS with a single quad detector (ESI) or an Agilent 7890 gas chromatograph equipped with a 5975C single quadrupole EI-MS. High-

resolution mass spectrometry (HRMS) was obtained using an Agilent 6201 MSLC-TOF (ESI) or Bruker IMPACT II (ESI). Fluorescence data was obtained on an Agilent Cary Eclipse Fluorescence Spectrophotometer using Eppendorf UVette 220-1600 nm disposable single sealed cuvettes (height of cuvette was adjusted to obtain clear path). All photocatalytic reactions were carried out using Kessil PhotoReaction PR160L 456 nm lights. $[Ir(dF(CF_3)ppy)_2(dtbpy)]PF_6$ (purchased from Strem Chemicals) and Mes-Acr-Ph (purchased from Sigma Aldrich) were used without purification. *Fac*-$Ir(ppy)_3$ was synthesized according to the literature procedure.[514] 3DPAFIPN and 4CzIPN were prepared according to the literature procedure.[418]

5.7.2 General Synthetic Procedures and Spectral Data for New Compounds

5.7.2.1 General Procedure 1 for the Synthesis of Ethyl Esters:

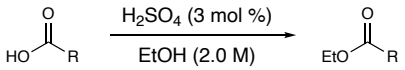

V-31 **V-25**

Scheme 5-11. Synthesis of ethyl esters from the corresponding carboxylic acid.

A solution of carboxylic acid (10.0 mmol, 1.0 equiv) in ethanol (80.0 mmol, 8.0 equiv) with concentrated sulfuric acid (0.30 mmol, 0.03 equiv) was stirred at room temperature overnight. The cooled solution was poured into ice water (30 mL) and was extracted with ethyl acetate (3 x 20 mL). The combined organic layers were washed with brine (1 x 30 mL), dried over anhydrous magnesium sulfate, and concentrated under reduced pressure to give the desired ethyl ester. In most cases, the ester was used without further purification.

5.7.2.3 General Procedure 2 the Synthesis of Substituted Esters

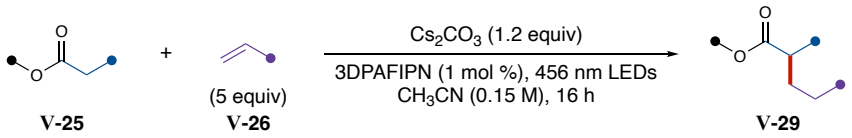

Scheme 5-12. Synthesis of substituted esters using base-promoted photoredox catalysis.

All reactions were set up inside of a glovebox under N_2 atmosphere. The respective ester **V-25** (0.20 mmol, 1.0 equiv), the respective alkene **V-26** (1.00 mmol, 5.0 equiv), 3DPAFIPN (2.00 µmol, 0.01 equiv), and cesium carbonate (0.24 mmol, 1.2 equiv) were added to an oven-dried 2-dram vial containing a stir bar. Acetonitrile (0.15 M) was added, the reaction was capped, and the vial was removed from the glovebox. Parafilm was wrapped around the cap to prevent air from entering, and the vial was stirred and irradiated with 456 nm LEDs. The reactions were monitored by GCMS. When complete consumption of ester **V-25** was observed (between 16–48 h), the reaction was concentrated under reduced pressure and then purified by column chromatography on silica gel (ethyl acetate/hexanes).

5.7.3 Optimization of Reaction Conditions

The reaction was optimized according to General Procedure 2 for the synthesis of substituted esters.

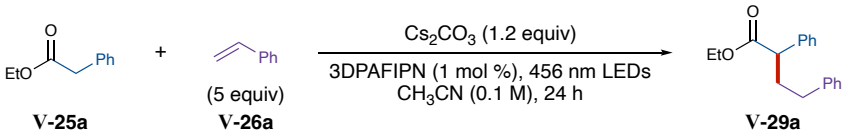

V-25a V-26a V-29a

entry	deviation from standard	yield[a]
1	none	76
2	Ir-dF instead of 3DPAFIPN	0
3	Mes-Acr-Ph instead of 3DPAFIPN	0
4	4CzIPN instead of 3DPAFIPN	0
5	CsOPiv istead of Cs_2CO_3	0
6	K_2CO_3 instead of Cs_2CO_3	0
7	DBU instead of Cs_2CO_3	0
8	THF instead of CH_3CN	0
9	DMF instead of CH_3CN	22
10	3 mol % 3DPAFIPN instead of 1 mol %	46
11	5 mol % 3DPAFIPN instead of 1 mol %	16
12	0.025 M instead of 0.1 M	3
13	0.05 M instead of 0.1 M	5
14	0.15 M instead of 0.1 M	59
15	0.2 M instead of 0.1 M	25

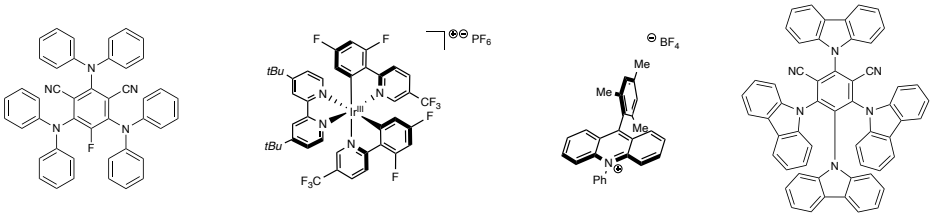

3DPAFIPN [Ir(dFCF3ppy)2(dtbpy)]PF6 (Ir-dF) Mes-Acr-Ph 4CzIPN

Table 5-3. Optimization of the reaction conditions. [a] ^{1}H NMR spectroscopic yield measured using 1,3,5-trimethoxybenzene as the internal standard. Reactions were performed at a 0.1 mmol scale.

5.7.4 Screen of Reductively Generated Radical Precursors

A variety of reductively generated radical precursors were screened in search of a desired radical-radical cross-coupling process.

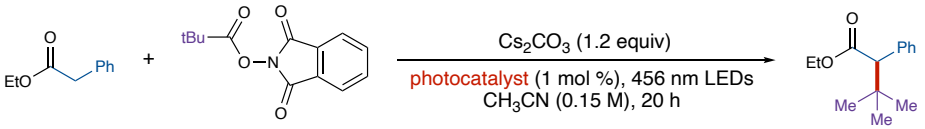

V-25a V-23a (5.0 equiv) V-29e

entry	photocatalyst	product mass by GCMS
1	3DPAFIPN	no
2	fac-Ir(ppy)$_3$	no
3	[Ir(dtbbpy)(ppy)$_2$]PF$_6$	no
4	[Ir(dFCF$_3$ppy)$_2$(dtbpy)]PF$_6$	no

Table 5-4. Photocatalyst screen for radical-radical coupling with redox active ester **V-23a**.

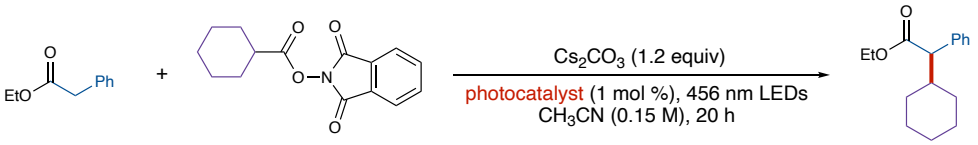

V-25a **V-23b** (5.0 equiv) **V-29f**

entry	photocatalyst	product mass by GCMS
1	3DPAFIPN	yes
2	fac-Ir(ppy)$_3$	yes
3	[Ir(dtbbpy)(ppy)$_2$]PF$_6$	no
4	[Ir(dFCF$_3$ppy)$_2$(dtbpy)]PF$_6$	no

Table 5-5. Photocatalyst screen for radical-radical coupling with redox active ester **V-23b**.

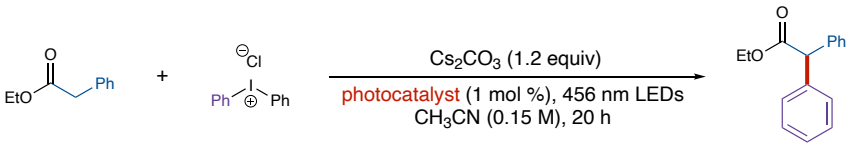

V-25a **V-19a** (5.0 equiv) **V-29g**

entry	photocatalyst	product mass by GCMS
1	3DPAFIPN	yes
2	fac-Ir(ppy)$_3$	yes
3	[Ir(dtbbpy)(ppy)$_2$]PF$_6$	yes
4	[Ir(dFCF$_3$ppy)$_2$(dtbpy)]PF$_6$	yes

Table 5-6. Photocatalyst screen for radical-radical coupling with aryl iodonium **V-19a**.

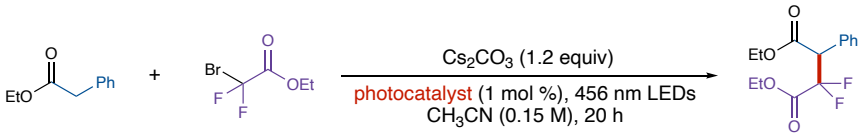

V-25a **V-22a** (5.0 equiv) **V-29h**

entry	photocatalyst	product mass by GCMS
1	3DPAFIPN	yes
2	fac-Ir(ppy)$_3$	yes
3	[Ir(dtbbpy)(ppy)$_2$]PF$_6$	yes
4	[Ir(dFCF$_3$ppy)$_2$(dtbpy)]PF$_6$	yes

Table 5-7. Photocatalyst screen for radical-radical coupling with ester halide **V-22a**.

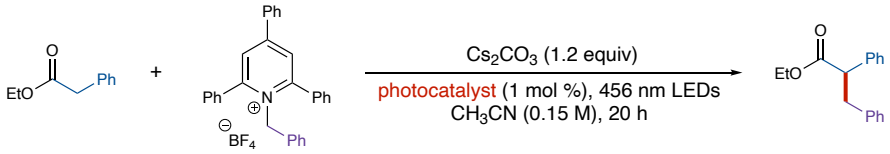

entry	photocatalyst	product mass by GCMS
1	3DPAFIPN	yes
2	fac-Ir(ppy)$_3$	yes
3	[Ir(dtbbpy)(ppy)$_2$]PF$_6$	yes
4	[Ir(dFCF$_3$ppy)$_2$(dtbpy)]PF$_6$	yes

Table 5-8. Photocatalyst screen for radical-radical coupling with Katritzky salt **V-10a**.

5.7.5. Tabulated Data

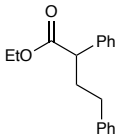

Ethyl 2,4-diphenylbutanoate (**V-29a**). Prepared according to General Procedure 2 for the synthesis of substituted esters. The crude material was purified by column chromatography (0-30% EtOAc:hexanes) to yield **V-29a** as a clear and colorless oil (44 mg, 83%). Analytical data matched the reported data.[556]

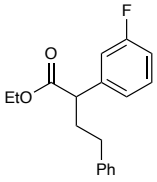

Ethyl 2-(3-fluorophenyl)-4-phenylbutanoate (**V-29b**). Prepared according to General Procedure 2 for the synthesis of substituted esters. The crude material was purified by column chromatography (0-30% EtOAc:hexanes) to yield **V-29b** as a clear and colorless oil (48 mg, 67%). Analytical data matched the reported data. ^{1}H NMR (500 MHz, $CDCl_3$) δ 7.29 (ddt, J = 10.7, 7.9, 3.1 Hz, 3H),

7.23 – 7.15 (m, 1H), 7.17 – 7.12 (m, 2H), 7.15 – 7.01 (m, 2H), 6.96 (tdd, J = 8.4, 2.6, 1.0 Hz, 1H), 4.21 – 4.05 (m, 2H), 3.54 (t, J = 7.7 Hz, 1H), 2.57 (t, J = 7.7 Hz, 2H), 2.39 (dq, J = 13.6, 7.8 Hz, 1H), 2.14 – 2.02 (m, 1H), 1.22 (t, J = 7.1 Hz, 3H). ^{13}C NMR (126 MHz, $CDCl_3$) δ 173.45, 163.02 (dd, J = 487.4, 245.9 Hz), 141.45 (d, J = 7.4 Hz), 141.17, 130.18 (d, J = 8.4 Hz), 128.59, 126.22, 123.92 (d, J = 2.9 Hz), 115.07 (d, J = 21.9 Hz), 114.38 (d, J = 21.0 Hz), 61.11, 50.81, 50.79, 35.04, 33.61, 14.28.

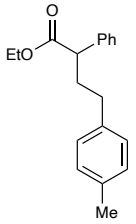

Ethyl 2-phenyl-4-(*p*-tolyl)butanoate (**V-29c**). Prepared according to General Procedure 2 for the synthesis of substituted esters. The crude material was purified by column chromatography (0-30% EtOAc:hexanes) to yield **V-29c** as a clear and colorless oil (29 mg, 41%). Analytical data for **V-29c**: ^{1}H NMR (500 MHz, $CDCl_3$) δ 7.39 – 7.29 (m, 4H), 7.29 – 7.23 (m, 1H), 7.12 – 7.02 (m, 4H), 4.19 – 4.03 (m, 2H), 3.54 (t, J = 7.7 Hz, 1H), 2.53 (t, J = 7.7 Hz, 2H), 2.44 – 2.28 (m, 1H), 2.32 (s, 3H), 2.13 – 2.02 (m, 1H), 1.21 (t, J = 7.1 Hz, 3H). ^{13}C NMR (126 MHz, $CDCl_3$) δ 174.04, 139.12, 138.36, 135.56, 129.20, 128.74, 128.48, 128.14, 127.35, 60.88, 51.08, 35.23, 33.23, 21.16, 14.29.

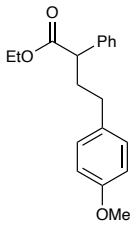

Ethyl 4-(4-methoxyphenyl)-2-phenylbutanoate (**V-29d**). Prepared according to General Procedure 2 for the synthesis of substituted esters. The crude material was purified by column chromatography (0-30% EtOAc:hexanes) to yield **V-29d** as a clear and colorless oil (37 mg, 50%). Analytical data for **V-29d**: ^{1}H NMR (500 MHz, $CDCl_3$) δ 7.31 – 7.20 (m, 3H), 7.21 (d, J = 3.3 Hz, 2H), 7.20 – 7.11 (m, 1H), 6.69 (dt, J = 8.3, 2.4 Hz, 2H), 6.64 (t, J = 2.1 Hz, 1H), 4.14 – 3.98 (m, 2H), 3.73 (s, 3H), 3.49 (t, J = 7.7 Hz, 1H), 2.49 (t, J = 7.7 Hz, 2H), 2.35 (dq, J = 13.5, 7.8 Hz, 1H), 2.04 (ddd, J = 13.1, 8.0, 6.5 Hz, 1H), 1.15 (t, J = 7.1 Hz, 3H). ^{13}C NMR (126 MHz, $CDCl_3$) δ 173.98, 159.72, 143.09, 139.04, 129.49, 128.76, 128.13, 127.39, 121.00, 114.27, 111.43, 60.91, 55.27, 51.05, 34.98, 33.73, 14.29.

REFERENCES

(1) Peleg, M.; Normand, M. D.; Corradini, M. G. The Arrhenius Equation Revisited. *Crit. Rev. Food Sci. Nutr.* **2012**, *52*, 830-851.
(2) Menzinger, M.; Wolfgang, R. The Meaning and Use of the Arrhenius Activation Energy. *Angew. Chem. Int. Ed.* **1969**, *8*, 438-444.
(3) Hynes, J. T. Chemical reaction dynamics in solution. *Annu. Rev. Phys. Chem.* **1985**, *36*, 573-597.
(4) Roduner, E. Understanding catalysis. *Chem. Soc. Rev.* **2014**, *43*, 8226-8239.
(5) Farrauto, R. J.; Dorazio, L.; Bartholomew, C. H. *Introduction to catalysis and industrial catalytic processes*; John Wiley & Sons, 2016.
(6) Lindström, B.; Pettersson, L. J. A Brief History of Catalysis. *CATTECH* **2003**, *7*, 130-138.
(7) Berzelius, J. J. Sur un force jusqu'ici peu remarquée qui est probablement active dans la formation des composes organiques, Section on Vegetable Chemistry. *Jahres-Bericht* **1835**, *14*, 237.
(8) Schlögl, R. Heterogeneous Catalysis. *Angew. Chem. Int. Ed.* **2015**, *54*, 3465-3520.
(9) Cornils, B.; Herrmann, W. A. Concepts in homogeneous catalysis: the industrial view. *J. Catal.* **2003**, *216*, 23-31.
(10) Bell, E. L.; Finnigan, W.; France, S. P.; Green, A. P.; Hayes, M. A.; Hepworth, L. J.; Lovelock, S. L.; Niikura, H.; Osuna, S.; Romero, E.; Ryan, K. S.; Turner, N. J.; Flitsch, S. L. Biocatalysis. *Nat. Rev. Methods Primers* **2021**, *1*, 46.
(11) Cazin, C. *N-Heterocyclic Carbenes in Transition Metal Catalysis and Organocatalysis*; Springer Dordrecht, 2011.
(12) Ranganath, K. V. S.; Onitsuka, S.; Kumar, A. K.; Inanaga, J. Recent progress of N-heterocyclic carbenes in heterogeneous catalysis. *Catal. Sci. Technol.* **2013**, *3*, 2161-2181.
(13) Koy, M.; Bellotti, P.; Das, M.; Glorius, F. N-Heterocyclic carbenes as tunable ligands for catalytic metal surfaces. *Nat. Catal.* **2021**, *4*, 352-363.
(14) Hopkinson, M. N.; Glorius, F. An Overview of NHCs. In *N-Heterocyclic Carbenes in Organocatalysis*; 2018; pp 1-35.
(15) Prier, C. K.; Arnold, F. H. Chemomimetic Biocatalysis: Exploiting the Synthetic Potential of Cofactor-Dependent Enzymes To Create New Catalysts. *J. Am. Chem. Soc.* **2015**, *137*, 13992-14006.
(16) Hopkinson, M. N.; Richter, C.; Schedler, M.; Glorius, F. An overview of N-heterocyclic carbenes. *Nature* **2014**, *510*, 485-496.
(17) Herrmann, W. A.; Köcher, C. N-Heterocyclic Carbenes. *Angew. Chem. Int. Ed.* **1997**, *36*, 2162-2187.
(18) Crabtree, R. H. Abnormal, mesoionic and remote N-heterocyclic carbene complexes. *Coord. Chem. Rev.* **2013**, *257*, 755-766.
(19) Moerdyk, J. P.; Schilter, D.; Bielawski, C. W. N,N′-Diamidocarbenes: Isolable Divalent Carbons with Bona Fide Carbene Reactivity. *Acc. Chem. Res.* **2016**, *49*, 1458-1468.
(20) Jahnke, M. C.; Hahn, F. E. Chapter 1: Introduction to N-Heterocyclic Carbenes: Synthesis and Stereoelectronic Parameters. In *N-Heterocyclic Carbenes: From Laboratory Curiosities to Efficient Synthetic Tools (2)*; The Royal Society of Chemistry: 2017; pp 1-45.

(21) Kuhn, K. M.; Bourg, J.-B.; Chung, C. K.; Virgil, S. C.; Grubbs, R. H. Effects of NHC-Backbone Substitution on Efficiency in Ruthenium-Based Olefin Metathesis. *J. Am. Chem. Soc.* **2009**, *131*, 5313-5320.
(22) Melancon, K. M.; Cundari, T. R. Computational investigations of NHC-backbone configurations for applications in organocatalytic umpolung reactions. *Org. Biomol. Chem.* **2020**, *18*, 7437-7447.
(23) Levens, A.; An, F.; Breugst, M.; Mayr, H.; Lupton, D. W. Influence of the N-Substituents on the Nucleophilicity and Lewis Basicity of N-Heterocyclic Carbenes. *Org. Lett.* **2016**, *18*, 3566-3569.
(24) Janssen-Müller, D.; Schlepphorst, C.; Glorius, F. Privileged chiral N-heterocyclic carbene ligands for asymmetric transition-metal catalysis. *Chem. Soc. Rev.* **2017**, *46*, 4845-4854.
(25) Zhao, C.; Blaszczyk, S. A.; Wang, J. Asymmetric reactions of N-heterocyclic carbene (NHC)-based chiral acyl azoliums and azolium enolates. *Green Synth. Catal.* **2021**, *2*, 198-215.
(26) Benhamou, L.; Chardon, E.; Lavigne, G.; Bellemin-Laponnaz, S.; César, V. Synthetic Routes to N-Heterocyclic Carbene Precursors. *Chem. Rev.* **2011**, *111*, 2705-2733.
(27) Hillier, A. C.; Sommer, W. J.; Yong, B. S.; Petersen, J. L.; Cavallo, L.; Nolan, S. P. A Combined Experimental and Theoretical Study Examining the Binding of N-Heterocyclic Carbenes (NHC) to the Cp*RuCl (Cp* = η5-C5Me5) Moiety: Insight into Stereoelectronic Differences between Unsaturated and Saturated NHC Ligands. *Organometallics* **2003**, *22*, 4322-4326.
(28) Nelson, D. J.; Nolan, S. P. Quantifying and understanding the electronic properties of N-heterocyclic carbenes. *Chem. Soc. Rev.* **2013**, *42*, 6723-6753.
(29) Tolman, C. A. Steric effects of phosphorus ligands in organometallic chemistry and homogeneous catalysis. *Chem. Rev.* **1977**, *77*, 313-348.
(30) Dröge, T.; Glorius, F. The Measure of All Rings—N-Heterocyclic Carbenes. *Angew. Chem. Int. Ed.* **2010**, *49*, 6940-6952.
(31) Chiu, C. C.; Pan, K.; Jordan, F. Modeling an Elementary Step of the Enzyme Pyruvate Oxidase: Oxidation of a Thiamin Diphosphate-Bound Enamine Intermediate by a Flavin Analog. *J. Am. Chem. Soc.* **1995**, *117*, 7027-7028.
(32) Chabrière, E.; Vernède, X.; Guigliarelli, B.; Charon, M.-H.; Hatchikian, E. C.; Fontecilla-Camps, J. C. Crystal Structure of the Free Radical Intermediate of Pyruvate: Ferredoxin Oxidoreductase. *Science* **2001**, *294*, 2559-2563.
(33) Breslow, R. On the Mechanism of Thiamine Action. IV.1 Evidence from Studies on Model Systems. *J. Am. Chem. Soc.* **1958**, *80*, 3719-3726.
(34) Maki, B. E.; Chan, A.; Phillips, E. M.; Scheidt, K. A. Tandem Oxidation of Allylic and Benzylic Alcohols to Esters Catalyzed by N-Heterocyclic Carbenes. *Org. Lett.* **2007**, *9*, 371-374.
(35) Ukai, T.; Tanaka, R.; Dokawa, T. A New Catalyst for Acyloin Condensation. *J. Pharm. Soc. Jpn.* **1943**, *63*, 296-300.
(36) Öfele, K. 1, 3-Dimethyl-4-imidazolinyliden-(2)-pentacarbonylchrom ein neuer Übergangsmetall-carben-komplex. *J. Organomet. Chem.* **1968**, *12*, P42-P43.
(37) Wanzlick, H. W.; Schönherr, H. J. Direct synthesis of a mercury salt-carbene complex. *Angew. Chem. Int. Ed.* **1968**, *7*, 141-142.
(38) Wang, F.; Liu, L.-j.; Wang, W.; Li, S.; Shi, M. Chiral NHC–metal-based asymmetric catalysis. *Coord. Chem. Rev.* **2012**, *256*, 804-853.

(39) Antonova, N. S.; Carbó, J. J.; Poblet, J. M. Quantifying the Donor−Acceptor Properties of Phosphine and N-Heterocyclic Carbene Ligands in Grubbs' Catalysts Using a Modified EDA Procedure Based on Orbital Deletion. *Organometallics* **2009**, *28*, 4283-4287.
(40) Díez-González, S.; Nolan, S. P. Stereoelectronic parameters associated with N-heterocyclic carbene (NHC) ligands: A quest for understanding. *Coord. Chem. Rev.* **2007**, *251*, 874-883.
(41) Jacobsen, H.; Correa, A.; Poater, A.; Costabile, C.; Cavallo, L. Understanding the M(NHC) (NHC=N-heterocyclic carbene) bond. *Coord. Chem. Rev.* **2009**, *253*, 687-703.
(42) Lee, M.-T.; Lee, H. M.; Hu, C.-H. A Theoretical Study of the Heck Reaction: N-Heterocyclic Carbene versus Phosphine Ligands. *Organometallics* **2007**, *26*, 1317-1324.
(43) Scott, N. M.; Clavier, H.; Mahjoor, P.; Stevens, E. D.; Nolan, S. P. Synthetic, Structural, and Thermochemical Studies of N-Heterocyclic Carbene (NHC) and Tertiary Phosphine Ligands in the [(L)2Ni(CO)2] (L = PR3, NHC) System. *Organometallics* **2008**, *27*, 3181-3186.
(44) Crabtree, R. H. NHC ligands versus cyclopentadienyls and phosphines as spectator ligands in organometallic catalysis. *J. Organomet. Chem.* **2005**, *690*, 5451-5457.
(45) Normand, A. T.; Cavell, K. J. Donor-Functionalised N-Heterocyclic Carbene Complexes of Group 9 and 10 Metals in Catalysis: Trends and Directions. *Eur. J. Inorg. Chem.* **2008**, *2008*, 2781-2800.
(46) Matisons, J.; Marciniec, B.; Maciejewski, H.; Pietraszuk, C.; *Advances in Silicon Science*; Springer: 2009.
(47) Marion, N.; Nolan, S. P. N-Heterocyclic carbenes in gold catalysis. *Chem. Soc. Rev.* **2008**, *37*, 1776-1782.
(48) Vougioukalakis, G. C.; Grubbs, R. H. Ruthenium-Based Heterocyclic Carbene-Coordinated Olefin Metathesis Catalysts. *Chem. Rev.* **2010**, *110*, 1746-1787.
(49) Grubbs, R. H. Olefin-Metathesis Catalysts for the Preparation of Molecules and Materials (Nobel Lecture). *Angew. Chem. Int. Ed.* **2006**, *45*, 3760-3765.
(50) Wöhler; Liebig Untersuchungen über das Radikal der Benzoesäure. *Annalen der Pharmacie* **1832**, *3*, 249-282.
(51) Lapworth, A. XCVI.—Reactions involving the addition of hydrogen cyanide to carbon compounds. *J. Chem. Soc., Trans.* **1903**, *83*, 995-1005.
(52) Mizuhara, S.; Tamura, R.; Arata, H. On the Mechanism of Thiamine Action. II. *Proc. Jpn. Acad.* **1951**, *27*, 302-308.
(53) Mizuhara, S.; Handler, P. Mechanism of Thiamine-catalyzed Reactions1. *J. Am. Chem. Soc.* **1954**, *76*, 571-573.
(54) De Sarkar, S.; Grimme, S.; Studer, A. NHC catalyzed oxidations of aldehydes to esters: chemoselective acylation of alcohols in presence of amines. *J. Am. Chem. Soc.* **2010**, *132*, 1190-1191.
(55) Igau, A.; Grutzmacher, H.; Baceiredo, A.; Bertrand, G. Analogous α,α'-bis-carbenoid, triply bonded species: synthesis of a stable λ-3-phosphino carbene-λ-5-phosphaacetylene. *J. Am. Chem. Soc.* **1988**, *110*, 6463-6466.
(56) Arduengo, A. J.; Harlow, R. L.; Kline, M. A stable crystalline carbene. *J. Am. Chem. Soc.* **1991**, *113*, 361-363.
(57) Flanigan, D. M.; Romanov-Michailidis, F.; White, N. A.; Rovis, T. Organocatalytic Reactions Enabled by N-Heterocyclic Carbenes. *Chem. Rev.* **2015**, *115*, 9307-9387.

(58) Stetter, H.; Raemsch, R. Y.; Kuhlmann, H. Über die präparative Nutzung der Thiazoliumsalz-katalysierten Acyloin-und Benzoin-Bildung, I. Herstellung von einfachen Acyloinen und Benzoinen. *Synthesis* **1976**, *1976*, 733-735.
(59) Enders, D.; Kallfass, U. An efficient nucleophilic carbene catalyst for the asymmetric benzoin condensation. *Angew. Chem. Int. Ed.* **2002**, *41*, 1743-1745.
(60) Menon, R. S.; Biju, A. T.; Nair, V. Recent advances in N-heterocyclic carbene (NHC)-catalysed benzoin reactions. *Beilstein J. Org. Chem.* **2016**, *12*, 444-461.
(61) Albanese, D. C. M.; Gaggero, N. An Overview on the N-Heterocyclic Carbene-Catalyzed Aza-Benzoin Condensation Reaction. *Catalysts* **2018**, *8*, 181.
(62) Stetter, H. Catalyzed Addition of Aldehydes to Activated Double Bonds—A New Synthetic Approach. *Angew. Chem. Int. Ed.* **1976**, *15*, 639-647.
(63) Stetter, H.; Schreckenberg, M. A New Method for Addition of Aldehydes to Activated Double Bonds. *Angew. Chem. Int. Ed.* **1973**, *12*, 81-81.
(64) Heravi, M. M.; Zadsirjan, V.; Kafshdarzadeh, K.; Amiri, Z. Recent Advances in Stetter Reaction and Related Chemistry: An update. *Asian J. Org. Chem* **2020**, *9*, 1999-2034.
(65) Trost, B. M.; Shuey, C. D.; DiNinno Jr, F. A stereocontrolled total synthesis of (+-)-hirsutic acid C. *J. Am. Chem. Soc.* **1979**, *101*, 1284-1285.
(66) Ciganek, E. Esters of 2,3-dihydro-3-oxobenzofuran-2-acetic acid and 3,4-dihydro-4-oxo-2H-1-benzopyran-3-acetic acid by intramolecular Stetter reactions. *Synthesis* **1995**, *1995*, 1311-1314.
(67) Enders, D.; Breuer, K.; Runsink, J.; Teles, J. H. The first asymmetric intramolecular Stetter reaction. Preliminary communication. *Helv. Chim. Acta* **1996**, *79*, 1899-1902.
(68) Kerr, M. S.; Read de Alaniz, J.; Rovis, T. A highly enantioselective catalytic intramolecular Stetter reaction. *J. Am. Chem. Soc.* **2002**, *124*, 10298-10299.
(69) Kerr, M. S.; Rovis, T. Effect of the Michael Acceptor in the asymmetric intramolecular Stetter reaction. *Synlett* **2003**, *12*, 1934-1936.
(70) Kerr, M. S.; Rovis, T. Enantioselective synthesis of quaternary stereocenters via a catalytic asymmetric Stetter reaction. *J. Am. Chem. Soc.* **2004**, *126*, 8876-8877.
(71) Nakamura, T.; Hara, O.; Tamura, T.; Makino, K.; Hamada, Y. A facile synthesis of chroman-4-ones and 2, 3-dihydroquinolin-4-ones with quaternary carbon using intramolecular Stetter reaction catalyzed by thiazolium salt. *Synlett* **2005**, *2005*, 155-157.
(72) Moore, J. L.; Kerr, M. S.; Rovis, T. Enantioselective formation of quaternary stereocenters using the catalytic intramolecular Stetter reaction. *Tetrahedron* **2006**, *62*, 11477-11482.
(73) Mattson, A. E.; Bharadwaj, A. R.; Scheidt, K. A. The thiazolium-catalyzed sila-Stetter reaction: Conjugate addition of acylsilanes to unsaturated esters and ketones. *J. Am. Chem. Soc.* **2004**, *126*, 2314-2315.
(74) Mattson, A. E.; Bharadwaj, A. R.; Zuhl, A. M.; Scheidt, K. A. Thiazolium-catalyzed additions of acylsilanes: A general strategy for acyl anion addition reactions. *J. Org. Chem.* **2006**, *71*, 5715-5724.
(75) Mattson, A. E.; Zuhl, A. M.; Reynolds, T. E.; Scheidt, K. A. Direct nucleophilic acylation of nitroalkenes promoted by a fluoride anion/thiourea combination. *J. Am. Chem. Soc.* **2006**, *128*, 4932-4933.
(76) Sheehan, J. C.; Hunneman, D. Homogeneous asymmetric catalysis. *J. Am. Chem. Soc.* **1966**, *88*, 3666-3667.

(77) Tagaki, W.; Tamura, Y.; Yano, Y. Asymmetric benzoin condensation catalyzed by optically active thiazolium salts in micellar two-phase media. *Bull. Chem. Soc. Jpn.* **1980**, *53*, 478-480.
(78) Breslow, R.; Kim, R. The thiazolium catalyzed benzoin condensation with mild base does not involve a "dimer" intermediate. *Tetrahedron Lett.* **1994**, *35*, 699-702.
(79) Enders, D.; Breuer, K.; Raabe, G.; Runsink, J.; Teles, J. H.; Melder, J. P.; Ebel, K.; Brode, S. Preparation, Structure, and Reactivity of 1,3,4-Triphenyl-4,5-dihydro-1H-1,2,4-triazol-5-ylidene, a New Stable Carbene. *Angew. Chem. Int. Ed.* **1995**, *34*, 1021-1023.
(80) Enders, D.; Breuer, K.; Teles, J. H. A novel asymmetric benzoin reaction catalyzed by a chiral triazolium salt. Preliminary communication. *Helv. Chim. Acta* **1996**, *79*, 1217-1221.
(81) Knight, R. L.; Leeper, F. J. Comparison of chiral thiazolium and triazolium salts as asymmetric catalysts for the benzoin condensation. *J. Chem. Soc., Perkin Trans. 1* **1998**, 1891-1894.
(82) Vora, H. U.; Rovis, T. Asymmetric N-Heterocyclic Carbene (NHC) Catalyzed Acyl Anion Reactivity. *Aldrichimica acta* **2011**, *44*, 3-11.
(83) Zhao, M.; Zhang, Y.-T.; Chen, J.; Zhou, L. Enantioselective Reactions Catalyzed by N-Heterocyclic Carbenes. *Asian J. Org. Chem* **2018**, *7*, 54-69.
(84) van der Vlugt, J. I. Cooperative catalysis with first-row late transition metals. *Eur. J. Inorg. Chem.* **2012**, *2012*, 363-375.
(85) Wang, M. H.; Scheidt, K. A. Cooperative Catalysis and Activation with N-Heterocyclic Carbenes. *Angew. Chem. Int. Ed.* **2016**, *55*, 14912-14922.
(86) Cardinal-David, B.; Raup, D. E. A.; Scheidt, K. A. Cooperative N-Heterocyclic Carbene/Lewis Acid Catalysis for Highly Stereoselective Annulation Reactions with Homoenolates. *J. Am. Chem. Soc.* **2010**, *132*, 5345-5347.
(87) Domingo, L. R.; Zaragozá, R. J.; Arnó, M. Understanding the cooperative NHC/LA catalysis for stereoselective annulation reactions with homoenolates. A DFT study. *Org. Biomol. Chem.* **2011**, *9*, 6616-6622.
(88) Domingo, L. R.; Sáez, J. A.; Arnó, M. A DFT study on the NHC catalysed Michael addition of enols to α,β-unsaturated acyl-azoliums. A base catalysed C–C bond-formation step. *Org. Biomol. Chem.* **2014**, *12*, 895-904.
(89) Ikuo, N.; Shinobu, I.; Tomoyoshi, S.; Hiroo, I.; Shunichi, F. Redox Behavior of Active Aldehydes Derived from Thiamin Coenzyme Analogs. *Chem. Lett.* **1997**, *26*, 707-708.
(90) Nakanishi, I.; Itoh, S. Electron transfer properties of active aldehydes derived from thiamin coenzyme analogues. *Chem. Commun.* **1997**, 1927-1928.
(91) Nakanishi, I.; Itoh, S.; Suenobu, T.; Fukuzumi, S. Direct Observation of Radical Intermediates While Investigating the Redox Behavior of Thiamin Coenzyme Models. *Angew. Chem. Int. Ed.* **1998**, *37*, 992-994.
(92) Nakanishi, I.; Itoh, S.; Fukuzumi, S. Electron-Transfer Properties of Active Aldehydes of Thiamin Coenzyme Models, and Mechanism of Formation of the Reactive Intermediates. *Chem. Eur. J.* **1999**, *5*, 2810-2818.
(93) In a recent report by Martin et al., the original redox properties reported by the Fukuzumi group were adjusted significantly. We refer the reader to this recent report for updated values.
(94) Regnier, V.; Romero, E. A.; Molton, F.; Jazzar, R.; Bertrand, G.; Martin, D. What Are the Radical Intermediates in Oxidative N-Heterocyclic Carbene Organocatalysis? *J. Am. Chem. Soc.* **2019**, *141*, 1109-1117.

(95) Delfau, L.; Nichilo, S.; Molton, F.; Broggi, J.; Tomás-Mendivil, E.; Martin, D. Critical Assessment of the Reducing Ability of Breslow-type Derivatives and Implications for Carbene-Catalyzed Radical Reactions. *Angew. Chem. Int. Ed.* **2021**, *60*, 26783-26789.
(96) Bay, A. V.; Scheidt, K. A. Single-electron carbene catalysis in redox processes. *Trends Chem.* **2022**, *4*, 277-290.
(97) Bay, A. V.; Fitzpatrick, K. P.; González-Montiel, G. A.; Farah, A. O.; Cheong, P. H.-Y.; Scheidt, K. A. Light-Driven Carbene Catalysis for the Synthesis of Aliphatic and α-Amino Ketones. *Angew. Chem. Int. Ed.* **2021**, *60*, 17925-17931.
(98) Kakeno, Y.; Kusakabe, M.; Nagao, K.; Ohmiya, H. Direct Synthesis of Dialkyl Ketones from Aliphatic Aldehydes through Radical N-Heterocyclic Carbene Catalysis. *ACS Catal.* **2020**, *10*, 8524-8529.
(99) Maki, B. E.; Scheidt, K. A. N-Heterocyclic Carbene-Catalyzed Oxidation of Unactivated Aldehydes to Esters. *Org. Lett.* **2008**, *10*, 4331-4334.
(100) Guin, J.; De Sarkar, S.; Grimme, S.; Studer, A. Biomimetic Carbene-Catalyzed Oxidations of Aldehydes Using TEMPO. *Angew. Chem. Int. Ed.* **2008**, *47*, 8727-8730.
(101) Finney, E. E.; Ogawa, K. A.; Boydston, A. J. Organocatalyzed anodic oxidation of aldehydes. *J. Am. Chem. Soc.* **2012**, *134*, 12374-12377.
(102) Zhao, J.; Mück-Lichtenfeld, C.; Studer, A. Cooperative N-Heterocyclic Carbene (NHC) and Ruthenium Redox Catalysis: Oxidative Esterification of Aldehydes with Air as the Terminal Oxidant. *Adv. Synth. Catal.* **2013**, *355*, 1098-1106.
(103) Yoshioka, E.; Inoue, M.; Nagoshi, Y.; Kobayashi, A.; Mizobuchi, R.; Kawashima, A.; Kohtani, S.; Miyabe, H. Oxidative Functionalization of Cinnamaldehyde Derivatives: Control of Chemoselectivity by Organophotocatalysis and Dual Organocatalysis. *J. Org. Chem.* **2018**, *83*, 8962-8970.
(104) Green, R. A.; Pletcher, D.; Leach, S. G.; Brown, R. C. D. N-Heterocyclic Carbene-Mediated Microfluidic Oxidative Electrosynthesis of Amides from Aldehydes. *Org. Lett.* **2016**, *18*, 1198-1201.
(105) Du, Y.; Wang, Y.; Li, X.; Shao, Y.; Li, G.; Webster, R. D.; Chi, Y. R. N-heterocyclic carbene organocatalytic reductive β,β-coupling reactions of nitroalkenes via radical intermediates. *Org. Lett.* **2014**, *16*, 5678-5681.
(106) Li, B. S.; Wang, Y.; Proctor, R. S. J.; Zhang, Y.; Webster, R. D.; Yang, S.; Song, B.; Chi, Y. R. Carbene-catalysed reductive coupling of nitrobenzyl bromides and activated ketones or imines via single-electron-transfer process. *Nat. Commun.* **2016**, *7*, 12933.
(107) Wang, Y.; Du, Y.; Huang, X.; Wu, X.; Zhang, Y.; Yang, S.; Chi, Y. R. Carbene-Catalyzed Reductive Coupling of Nitrobenzyl Bromide and Nitroalkene via the Single-Electron-Transfer (SET) Process and Formal 1,4-Addition. *Org. Lett.* **2017**, *19*, 632.
(108) Wang, Y.; Wu, X.; Robin Chi, Y. Synthesis of indanes via carbene-catalyzed single-electron-transfer processes and cascade reactions. *Chem. Commun.* **2017**, *53*, 11952-11955.
(109) Wang, C.; Liu, L. NHC-catalyzed oxindole synthesis via single electron transfer. *Org. Chem. Front.* **2021**, *8*, 1454-1460.
(110) Su, L.; Sun, H.; Liu, J.; Wang, C. Construction of Quaternary Carbon Center via NHC Catalysis Initiated by an Intermolecular Heck-Type Alkyl Radical Addition. *Org. Lett.* **2021**, *23*, 4662-4666.

(111) Nakatsuji, Y.; Kobayashi, Y.; Masuda, S.; Takemoto, Y. Azolium/Hydroquinone Organo-Radical Co-Catalysis: Aerobic C−C-Bond Cleavage in Ketones. *Chem. Eur. J.* **2021**, *27*, 2633-2637.
(112) Liu, Y.; Li, J.-L.; Liu, X.-G.; Wu, J.-Q.; Huang, Z.-S.; Li, Q.; Wang, H. Radical Borylative Cyclization of Isocyanoarenes with N-Heterocyclic Carbene Borane: Synthesis of Borylated Aza-arenes. *Org. Lett.* **2021**, *23*, 1891-1897.
(113) Dong, Z.; Pezzato, C.; Sienkiewicz, A.; Scopelliti, R.; Fadaei-Tirani, F.; Severin, K. SET processes in Lewis acid–base reactions: the tritylation of N-heterocyclic carbenes. *Chem. Sci.* **2020**, *11*, 7615-7618.
(114) White, N. A.; Rovis, T. Enantioselective N·Heterocyclic Carbene-Catalyzed β-Hydroxylation of Enals Using Nitroarenes: An Atom Transfer Reaction That Proceeds via Single Electron Transfer. *J. Am. Chem. Soc.* **2014**, *136*, 14674.
(115) Zhang, Y.; Du, Y.; Huang, Z.; Xu, J.; Wu, X.; Wang, Y.; Wang, M.; Yang, S.; Webster, R. D.; Chi, Y. R. N-Heterocyclic Carbene-Catalyzed Radical Reactions for Highly Enantioselective β-Hydroxylation of Enals. *J. Am. Chem. Soc.* **2015**, *137*, 2416.
(116) Wang, H.; Wang, Y.; Chen, X.; Mou, C.; Yu, S.; Chai, H.; Jin, Z.; Chi, Y. R. Chiral Nitroarenes as Enantioselective Single-Electron-Transfer Oxidants for Carbene-Catalyzed Radical Reactions. *Org. Lett.* **2019**, *21*, 7440-7444.
(117) White, N. A.; Rovis, T. Oxidatively Initiated NHC-Catalyzed Enantioselective Synthesis of 3,4-Disubstituted Cyclopentanones from Enals. *J. Am. Chem. Soc.* **2015**, *137*, 10112.
(118) Chen, X. Y.; Chen, K. Q.; Sun, D. Q.; Ye, S. N-Heterocyclic carbene-catalyzed oxidative [3 + 2] annulation of dioxindoles and enals: cross coupling of homoenolate and enolate. *Chem. Sci.* **2017**, *8*, 1936-1941.
(119) Song, Z.-Y.; Chen, K.-Q.; Chen, X.-Y.; Ye, S. Diastereo- and Enantioselective Synthesis of Spirooxindoles with Contiguous Tetrasubstituted Stereocenters via Catalytic Coupling of Two Tertiary Radicals. *J. Org. Chem.* **2018**, *83*, 2966-2970.
(120) Yang, W.; Hu, W.; Dong, X.; Li, X.; Sun, J. N-Heterocyclic Carbene Catalyzed γ-Dihalomethylenation of Enals by Single-Electron Transfer. *Angew. Chem., Int. Ed.* **2016**, *55*, 15783.
(121) DiRocco, D. A.; Rovis, T. Catalytic asymmetric α-acylation of tertiary amines mediated by a dual catalysis mode: N-heterocyclic carbene and photoredox catalysis. *J. Am. Chem. Soc.* **2012**, *134*, 8094-8097.
(122) In 2012, Rovis and DiRocco developed a dual catalytic process wherein photoredox catalysis was used to generate an iminium ion from an amine. Addition of an NHC-derived acyl anion equivalent to the generated iminium ion afforded α-amino ketones.
(123) Dai, L.; Xia, Z.-H.; Gao, Y.-Y.; Gao, Z.-H.; Ye, S. Visible-Light-Driven N-Heterocyclic Carbene Catalyzed γ- and ϵ-Alkylation with Alkyl Radicals. *Angew. Chem. Int. Ed.* **2019**, *58*, 18124-18130.
(124) Dai, L.; Ye, S. Photo/N-Heterocyclic Carbene Co-catalyzed Ring Opening and γ-Alkylation of Cyclopropane Enal. *Org. Lett.* **2020**.
(125) Dai, L.; Xu, Y.-Y.; Xia, Z.-H.; Ye, S. γ-Difluoroalkylation: Synthesis of γ-Difluoroalkyl-α,β-Unsaturated Esters via Photoredox NHC-Catalyzed Radical Reaction. *Org. Lett.* **2020**, *22*, 8173-8177.

(126) Li, Z.; Huang, M.; Zhang, X.; Chen, J.; Huang, Y. N-Heterocyclic Carbene-Catalyzed Four-Component Reaction: Chemoselective Cradical-Cradical Relay Coupling Involving the Homoenolate Intermediate. *ACS Catal.* **2021**, *11*, 10123-10130.
(127) Ishii, T.; Kakeno, Y.; Nagao, K.; Ohmiya, H. N-Heterocyclic Carbene-Catalyzed Decarboxylative Alkylation of Aldehydes. *J. Am. Chem. Soc.* **2019**, *141*, 3854-3858.
(128) Kim, I.; Im, H.; Lee, H.; Hong, S. N-Heterocyclic carbene-catalyzed deaminative cross-coupling of aldehydes with Katritzky pyridinium salts. *Chem. Sci.* **2020**, *11*, 3192-3197.
(129) Ishii, T.; Nagao, K.; Ohmiya, H. Radical N-heterocyclic carbene catalysis for β-ketocarbonyl synthesis. *Tetrahedron* **2021**, *91*, 132212.
(130) Liu, M.-S.; Shu, W. Catalytic, Metal-Free Amide Synthesis from Aldehydes and Imines Enabled by a Dual-Catalyzed Umpolung Strategy under Redox-Neutral Conditions. *ACS Catal.* **2020**, *10*, 12960-12966.
(131) Ishii, T.; Ota, K.; Nagao, K.; Ohmiya, H. N-Heterocyclic Carbene-Catalyzed Radical Relay Enabling Vicinal Alkylacylation of Alkenes. *J. Am. Chem. Soc.* **2019**, *141*, 14073-14077.
(132) Ota, K.; Nagao, K.; Ohmiya, H. N-Heterocyclic Carbene-Catalyzed Radical Relay Enabling Synthesis of δ-Ketocarbonyls. *Org. Lett.* **2020**, *22*, 3922-3925.
(133) Matsuki, Y.; Ohnishi, N.; Kakeno, Y.; Takemoto, S.; Ishii, T.; Nagao, K.; Ohmiya, H. Aryl radical-mediated N-heterocyclic carbene catalysis. *Nat. Commun.* **2021**, *12*, 3848.
(134) Chen, L.; Jin, S.; Gao, J.; Liu, T.; Shao, Y.; Feng, J.; Wang, K.; Lu, T.; Du, D. N-Heterocyclic Carbene/Magnesium Cocatalyzed Radical Relay Assembly of Aliphatic Keto Nitriles. *Org. Lett.* **2021**, *23*, 394-399.
(135) The authors suggest that magnesium triflate assists in forming an electron donor-acceptor (EDA) complex between the Breslow enolate and the oxime ester.
(136) Gao, Y.; Quan, Y.; Li, Z.; Gao, L.; Zhang, Z.; Zou, X.; Yan, R.; Qu, Y.; Guo, K. Organocatalytic Three-Component 1,2-Cyanoalkylacylation of Alkenes via Radical Relay. *Org. Lett.* **2021**, *23*, 183-189.
(137) Yang, H.-B.; Wan, D.-H. C–C Bond Acylation of Oxime Ethers via NHC Catalysis. *Org. Lett.* **2021**, *23*, 1049-1053.
(138) Zhang, Z.; Zou, X.; Li, Z.; Gao, Y.; Qu, Y.; Quan, Y.; Zhou, Y.; Li, J.; Sun, J.; Guo, K. N-Heterocyclic carbene-catalyzed radical ring-opening acylation of oxime esters with aldehydes. *Org. Chem. Front.* **2021**.
(139) Li, J.-L.; Liu, Y.-Q.; Zou, W.-L.; Zeng, R.; Zhang, X.; Liu, Y.; Han, B.; He, Y.; Leng, H.-J.; Li, Q.-Z. Radical Acylfluoroalkylation of Olefins through N-Heterocyclic Carbene Organocatalysis. *Angew. Chem. Int. Ed.* **2020**, *59*, 1863-1870.
(140) Zhang, B.; Peng, Q.; Guo, D.; Wang, J. NHC-Catalyzed Radical Trifluoromethylation Enabled by Togni Reagent. *Org. Lett.* **2020**, *22*, 443-447.
(141) Yang, H.-B.; Wang, Z.-H.; Li, J.-M.; Wu, C. Modular synthesis of α-aryl β-perfluoroalkyl ketones via N-heterocyclic carbene catalysis. *Chem. Commun.* **2020**, *56*, 3801-3804.
(142) Kusakabe, M.; Nagao, K.; Ohmiya, H. Radical Relay Trichloromethylacylation of Alkenes through N-Heterocyclic Carbene Catalysis. *Org. Lett.* **2021**, *23*, 7242-7247.
(143) Liu, M.-S.; Min, L.; Chen, B.-H.; Shu, W. Dual Catalysis Relay: Coupling of Aldehydes and Alkenes Enabled by Visible-Light and NHC-Catalyzed Cross-Double C–H Functionalizations. *ACS Catal.* **2021**, *11*, 9715-9721.

(144) Liu, W.; Vianna, A.; Zhang, Z.; Huang, S.; Huang, L.; Melaimi, M.; Bertrand, G.; Yan, X. Mesoionic carbene-Breslow intermediates as super electron donors: Application to the metal-free arylacylation of alkenes. *Chem Catalysis* **2021**, *1*, 196-206.
(145) A recent report by Tomás-Mendivil and Martin provides evidence that contradicts the claims made by Yan and coworkers regarding the redox potential of the mesoionic Breslow species.
(146) Mavroskoufis, A.; Rajes, K.; Golz, P.; Agrawal, A.; Ruß, V.; Götze, J. P.; Hopkinson, M. N. N-Heterocyclic Carbene Catalyzed Photoenolization/Diels-Alder Reaction of Acid Fluorides. *Angew. Chem. Int. Ed.* **2020**, *59*, 3190-3194.
(147) Mavroskoufis, A.; Rieck, A.; Hopkinson, M. N. Norrish type II reactions of acyl azolium salts. *Tetrahedron* **2021**, 132497.
(148) Bayly, A. A.; McDonald, B. R.; Mrksich, M.; Scheidt, K. A. High-throughput photocapture approach for reaction discovery. *Proc. Natl. Acad. Sci. U. S. A.* **2020**, *117*, 13261-13266.
(149) Bay, A. V.; Fitzpatrick, K. P.; Betori, R. C.; Scheidt, K. A. Combined Photoredox and Carbene Catalysis for the Synthesis of Ketones from Carboxylic Acids. *Angew. Chem. Int. Ed.* **2020**, *59*, 9143-9148.
(150) Zhu, J. L.; Scheidt, K. A. Photocatalytic acyl azolium-promoted alkoxycarbonylation of trifluoroborates. *Tetrahedron* **2021**, *92*, 132288.
(151) Ren, S.-C.; Lv, W.-X.; Yang, X.; Yan, J.-L.; Xu, J.; Wang, F.-X.; Hao, L.; Chai, H.; Jin, Z.; Chi, Y. R. Carbene-Catalyzed Alkylation of Carboxylic Esters via Direct Photoexcitation of Acyl Azolium Intermediates. *ACS Catal.* **2021**, 2925-2934.
(152) Sato, Y.; Goto, Y.; Nakamura, K.; Miyamoto, Y.; Sumida, Y.; Ohmiya, H. Light-Driven N-Heterocyclic Carbene Catalysis Using Alkylborates. *ACS Catal.* **2021**, 12886-12892.
(153) Meng, Q.-Y.; Lezius, L.; Studer, A. Benzylic C−H acylation by cooperative NHC and photoredox catalysis. *Nat. Commun.* **2021**, *12*, 2068.
(154) Yu, X.; Meng, Q.-Y.; Daniliuc, C. G.; Studer, A. Aroyl Fluorides as Bifunctional Reagents for Dearomatizing Fluoroaroylation of Benzofurans. *J. Am. Chem. Soc.* **2022**, *144*, 7072-7079.
(155) Wang, X.; Zhu, B.; Liu, Y.; Wang, Q. Combined Photoredox and Carbene Catalysis for the Synthesis of α-Amino Ketones from Carboxylic Acids. *ACS Catal.* **2022**, *12*, 2522-2531.
(156) Bay, A. V.; Farnam, E. J.; Scheidt, K. A. Synthesis of Cyclohexanones by a Tandem Photocatalyzed Annulation. *J. Am. Chem. Soc.* **2022**, *144*, 7030-7037.
(157) Meng, Q.-Y.; Döben, N.; Studer, A. Cooperative NHC and Photoredox Catalysis for the Synthesis of β-Trifluoromethylated Alkyl Aryl Ketones. *Angew. Chem. Int. Ed.* **2020**, *59*, 19956-19960.
(158) Wang, P.; Fitzpatrick, K. P.; Scheidt, K. A. Combined Photoredox and Carbene Catalysis for the Synthesis of γ-Aryloxy Ketones. *Adv. Synth. Catal.* **2022**, *364*, 518-524.
(159) Liu, K.; Studer, A. Direct α-Acylation of Alkenes via N-Heterocyclic Carbene, Sulfinate, and Photoredox Cooperative Triple Catalysis. *J. Am. Chem. Soc.* **2021**, *143*, 4903-4909.
(160) Zuo, Z.; Daniliuc, C. G.; Studer, A. Cooperative NHC/Photoredox Catalyzed Ring-Opening of Aryl Cyclopropanes to 1-Aroyloxylated-3-Acylated Alkanes. *Angew. Chem. Int. Ed.* **2021**, *60*, 25252-25257.
(161) Wang, L.; Ma, R.; Sun, J.; Zheng, G.; Zhang, Q. NHC and visible light-mediated photoredox co-catalyzed 1,4-sulfonylacylation of 1,3-enynes for tetrasubstituted allenyl ketones. *Chem. Sci.* **2022**, *13*, 3169-3175.
(162) Lavoisier, L. Traité Élémentaire de Chimie, Cuchet. *Volume 1* **1789**, *1*, 293.

(163) Ihde, A. J. The history of free radicals and Moses Gomberg's contributions. *Pure Appl. Chem.* **1967**, *15*, 1-14.
(164) Gomberg, M. An instance of trivalent carbon: Triphenylmethyl. *J. Am. Chem. Soc.* **1900**, *22*, 757-771.
(165) Zipse, H. Radical Stability–A Theoretical Perspective. In *Radicals in Synthesis I*; Gansäuer, A., Ed.; Springer Berlin Heidelberg: Berlin, Heidelberg, 2006; pp 163-189.
(166) Ratera, I.; Veciana, J. Playing with organic radicals as building blocks for functional molecular materials. *Chem. Soc. Rev.* **2012**, *41*, 303-349.
(167) Griller, D.; Ingold, K. U. Persistent carbon-centered radicals. *Acc. Chem. Res.* **1976**, *9*, 13-19.
(168) Blanksby, S. J.; Ellison, G. B. Bond Dissociation Energies of Organic Molecules. *Acc. Chem. Res.* **2003**, *36*, 255-263.
(169) Studer, A. The Persistent Radical Effect in Organic Synthesis. *Chem. Eur. J.* **2001**, *7*, 1159-1164.
(170) Leifert, D.; Studer, A. The Persistent Radical Effect in Organic Synthesis. *Angew. Chem. Int. Ed.* **2020**, *59*, 74-108.
(171) Tang, B.; Zhao, J.; Xu, J.-F.; Zhang, X. Tuning the stability of organic radicals: from covalent approaches to non-covalent approaches. *Chem. Sci.* **2020**, *11*, 1192-1204.
(172) Lebedev, O.; Kazarnovskii, S. Catalytic oxidation of aliphatic amines with hydrogen peroxide. *Zh. Obshch. Khim* **1960**, *30*, 1631-1635.
(173) Grimme, S.; Schreiner, P. R. Steric Crowding Can Stabilize a Labile Molecule: Solving the Hexaphenylethane Riddle. *Angew. Chem. Int. Ed.* **2011**, *50*, 12639-12642.
(174) Reid, D. Stable π-electron systems and new aromatic structures. *Tetrahedron* **1958**, *3*, 339-352.
(175) Kim, Y.; Lee, E. Stable Organic Radicals Derived from N-Heterocyclic Carbenes. *Chem. Eur. J.* **2018**, *24*, 19110-19121.
(176) Kumar, S.; Ajayakumar, M.; Hundal, G.; Mukhopadhyay, P. Extraordinary stability of naphthalenediimide radical ion and its ultra-electron-deficient precursor: strategic role of the phosphonium group. *J. Am. Chem. Soc.* **2014**, *136*, 12004-12010.
(177) Seifert, S.; Schmidt, D.; Würthner, F. An ambient stable core-substituted perylene bisimide dianion: isolation and single crystal structure analysis. *Chem. Sci.* **2015**, *6*, 1663-1667.
(178) Schmidt, D.; Bialas, D.; Würthner, F. Ambient Stable Zwitterionic Perylene Bisimide-Centered Radical. *Angew. Chem. Int. Ed.* **2015**, *54*, 3611-3614.
(179) Rao, V. P.; Zimmt, M. B.; Turro, N. J. Photoproduction of remarkably stable benzylic radicals in cyclodextrin inclusion complexes. *J. Photochem. Photobiol. A: Chem* **1991**, *60*, 355-360.
(180) Li, J.; Shen, P.; Zhao, Z.; Tang, B. Z. Through-space conjugation: a thriving alternative for optoelectronic materials. *CCS Chemistry* **2019**, 181-196.
(181) Song, Q.; Li, F.; Wang, Z.; Zhang, X. A supramolecular strategy for tuning the energy level of naphthalenediimide: promoted formation of radical anions with extraordinary stability. *Chem. Sci.* **2015**, *6*, 3342-3346.
(182) Sijbesma, R. P.; Beijer, F. H.; Brunsveld, L.; Folmer, B. J.; Hirschberg, J. K.; Lange, R. F.; Lowe, J. K.; Meijer, E. Reversible polymers formed from self-complementary monomers using quadruple hydrogen bonding. *Science* **1997**, *278*, 1601-1604.

(183) Kaim, W. The transition metal coordination chemistry of anion radicals. *Coord. Chem. Rev.* **1987**, *76*, 187-235.
(184) Silaev, M. The competition kinetics of radical-chain addition. *Russ. J. Phys. Chem.* **1999**, *73*, 1050-1054.
(185) Jr., L. G. W. *Organic Chemistry*; 8 ed.; Pearson Education, Inc.: Glenview, IL, 2013.
(186) Morcillo, S. P. Radical-Promoted C−C Bond Cleavage: A Deconstructive Approach for Selective Functionalization. *Angew. Chem. Int. Ed.* **2019**, *58*, 14044-14054.
(187) Gronert, S. An Alternative Interpretation of the C−H Bond Strengths of Alkanes. *J. Org. Chem.* **2006**, *71*, 1209-1219.
(188) Penczek, S. Terminology of kinetics, thermodynamics, and mechanisms of polymerization. *J. Polym. Sci., Part A: Polym. Chem.* **2002**, *40*, 1665-1676.
(189) Yi, H.; Zhang, G.; Wang, H.; Huang, Z.; Wang, J.; Singh, A. K.; Lei, A. Recent Advances in Radical C–H Activation/Radical Cross-Coupling. *Chem. Rev.* **2017**, *117*, 9016-9085.
(190) Wang, S.; Tang, S.; Lei, A. Tuning radical reactivity for selective radical/radical cross-coupling. *Sci. Bull.* **2018**, *63*, 1006-1009.
(191) Bachmann, W. E.; Wiselogle, F. Y. The relative stability of pentaarylethanes. III.1 The reversible dissociation of pentaarylethanes. *J. Org. Chem.* **1936**, *01*, 354-382.
(192) Perkins, M. J. *Free Radicals*. J. K. Kochi, Wiley, 1973.
(193) Fischer, H. The Persistent Radical Effect: A Principle for Selective Radical Reactions and Living Radical Polymerizations. *Chem. Rev.* **2001**, *101*, 3581-3610.
(194) Sowndarya S. V, S.; St. John, P. C.; Paton, R. S. A quantitative metric for organic radical stability and persistence using thermodynamic and kinetic features. *Chem. Sci.* **2021**, *12*, 13158-13166.
(195) Bachmann, W.; Wiselogle, F. The relative stability of pentaarylethanes. III. 1 The reversible dissociation of pentaarylethanes. *J. Org. Chem.* **1936**, *1*, 354-382.
(196) Ciamician, G. The Photochemistry of the Future. *Science* **1912**, *36*, 385-394.
(197) Albini, A.; Fagnoni, M. Green chemistry and photochemistry were born at the same time. *Green Chem.* **2004**, *6*, 1-6.
(198) Rohatgi-Mukherjee, K. *Fundamentals of photochemistry*; New Age International, 1978.
(199) Albini, A.; Fagnoni, M. *Handbook of synthetic photochemistry*; John Wiley & Sons, 2010.
(200) Zhou, Q.-Q.; Zou, Y.-Q.; Lu, L.-Q.; Xiao, W.-J. Visible-Light-Induced Organic Photochemical Reactions through Energy-Transfer Pathways. *Angew. Chem. Int. Ed.* **2019**, *58*, 1586-1604.
(201) Arias-Rotondo, D. M.; McCusker, J. K. The photophysics of photoredox catalysis: a roadmap for catalyst design. *Chem. Soc. Rev.* **2016**, *45*, 5803-5820.
(202) McCusker, J. K. Femtosecond Absorption Spectroscopy of Transition Metal Charge-Transfer Complexes. *Acc. Chem. Res.* **2003**, *36*, 876-887.
(203) Haimerl, J.; Ghosh, I.; König, B.; Vogelsang, J.; Lupton, J. M. Single-molecule photoredox catalysis. *Chem. Sci.* **2019**, *10*, 681-687.
(204) Pitre, S. P.; McTiernan, C. D.; Scaiano, J. C. Understanding the Kinetics and Spectroscopy of Photoredox Catalysis and Transition-Metal-Free Alternatives. *Acc. Chem. Res.* **2016**, *49*, 1320-1330.
(205) Kavarnos, G. J. Fundamental concepts of photoinduced electron transfer. In *Photoinduced electron transfer I*; Springer: 1990; pp 21-58.

(206) Lytle, F. E.; Hercules, D. M. Luminescence of tris(2,2'-bipyridine)ruthenium(II) dichloride. *J. Am. Chem. Soc.* **1969**, *91*, 253-257.
(207) Kalyanasundaram, K. Photophysics, photochemistry and solar energy conversion with tris(bipyridyl)ruthenium(II) and its analogues. *Coord. Chem. Rev.* **1982**, *46*, 159-244.
(208) Wallentin, C.-J.; Nguyen, J. D.; Finkbeiner, P.; Stephenson, C. R. J. Visible Light-Mediated Atom Transfer Radical Addition via Oxidative and Reductive Quenching of Photocatalysts. *J. Am. Chem. Soc.* **2012**, *134*, 8875-8884.
(209) Wiles, R. J.; Molander, G. A. Photoredox-Mediated Net-Neutral Radical/Polar Crossover Reactions. *Isr. J. Chem.* **2020**, *60*, 281-293.
(210) Romero, N. A.; Nicewicz, D. A. Organic Photoredox Catalysis. *Chem. Rev.* **2016**, *116*, 10075-10166.
(211) Hedstrand, D. M.; Kruizinga, W. H.; Kellogg, R. M. Light induced and dye accelerated reductions of phenacyl onium salts by 1, 4-dihydropyridines. *Tetrahedron Lett.* **1978**, *19*, 1255-1258.
(212) Hironaka, K.; Fukuzumi, S.; Tanaka, T. Tris (bipyridyl) ruthenium (II)-photosensitized reaction of 1-benzyl-1, 4-dihydronicotinamide with benzyl bromide. *J. Chem Soc., Perkin Trans. 2* **1984**, 1705-1709.
(213) Pac, C.; Ihama, M.; Yasuda, M.; Miyauchi, Y.; Sakurai, H. Tris (2, 2'-bipyridine) ruthenium (2+)-mediated photoreduction of olefins with 1-benzyl-1, 4-dihydronicotinamide: a mechanistic probe for electron-transfer reactions of NAD (P) H-model compounds. *J. Am. Chem. Soc.* **1981**, *103*, 6495-6497.
(214) Cano-Yelo, H.; Deronzier, A. Photo-oxidation of some carbinols by the Ru (II) polypyridyl complex-aryl diazonium salt system. *Tetrahedron Lett.* **1984**, *25*, 5517-5520.
(215) Cano-Yelo, H.; Deronzier, A. Photocatalysis of the Pschorr reaction by tris-(2,2′-bipyridyl)ruthenium(II) in the phenanthrene series. *J. Chem. Soc., Perkin Trans. 2* **1984**, 1093-1098.
(216) Fukuzumi, S.; Mochizuki, S.; Tanaka, T. Photocatalytic reduction of phenacyl halides by 9,10-dihydro-10-methylacridine: control between the reductive and oxidative quenching pathways of tris(bipyridine)ruthenium complex utilizing an acid catalysis. *J. Phys. Chem.* **1990**, *94*, 722-726.
(217) Okada, K.; Okamoto, K.; Morita, N.; Okubo, K.; Oda, M. Photosensitized decarboxylative Michael addition through N-(acyloxy)phthalimides via an electron-transfer mechanism. *J. Am. Chem. Soc.* **1991**, *113*, 9401-9402.
(218) Okada, K.; Okubo, K.; Morita, N.; Oda, M. Reductive decarboxylation of N-(acyloxy)phthalimides via redox-initiated radical chain mechanism. *Tetrahedron Lett.* **1992**, *33*, 7377-7380.
(219) Keiji, O.; Katsura, O.; Naoto, M.; Masaji, O. Redox-Mediated Decarboxylative Photo-Phenylselenenylation of N-Acyloxyphthalimides. *Chem. Lett.* **1993**, *22*, 2021-2024.
(220) Barton, D. H. R.; Csiba, M. A.; Jaszberenyi, J. C. Ru(bpy)32+-mediated addition of Se-phenyl p-tolueneselenosulfonate to electron rich olefins. *Tetrahedron Lett.* **1994**, *35*, 2869-2872.
(221) Hasegawa, E.; Takizawa, S.; Seida, T.; Yamaguchi, A.; Yamaguchi, N.; Chiba, N.; Takahashi, T.; Ikeda, H.; Akiyama, K. Photoinduced electron-transfer systems consisting of electron-donating pyrenes or anthracenes and benzimidazolines for reductive transformation of carbonyl compounds. *Tetrahedron* **2006**, *62*, 6581-6588.

(222) Nicewicz, D. A.; MacMillan, D. W. C. Merging Photoredox Catalysis with Organocatalysis: The Direct Asymmetric Alkylation of Aldehydes. *Science* **2008**, *322*, 77-80.
(223) Beeson, T. D.; Mastracchio, A.; Hong, J.-B.; Ashton, K.; MacMillan, D. W. Enantioselective organocatalysis using SOMO activation. *Science* **2007**, *316*, 582-585.
(224) Renaud, P.; Schubert, S. Stereoselective Addition of Carbon-Centered Radicals to Chiral Enamines. *Synlett* **1990**, *1990*, 624-626.
(225) Bock, C. R.; Connor, J. A.; Gutierrez, A. R.; Meyer, T. J.; Whitten, D. G.; Sullivan, B. P.; Nagle, J. K. Estimation of excited-state redox potentials by electron-transfer quenching. Application of electron-transfer theory to excited-state redox processes. *J. Am. Chem. Soc.* **1979**, *101*, 4815-4824.
(226) Tanner, D. D.; Singh, H. K. Reduction of α-halo ketones by organotin hydrides. An electron-transfer-hydrogen atom abstraction mechanism. *J. Org. Chem.* **1986**, *51*, 5182-5186.
(227) Ischay, M. A.; Anzovino, M. E.; Du, J.; Yoon, T. P. Efficient Visible Light Photocatalysis of [2+2] Enone Cycloadditions. *J. Am. Chem. Soc.* **2008**, *130*, 12886-12887.
(228) Baik, T.-G.; Luis, A. L.; Wang, L.-C.; Krische, M. J. A Diastereoselective Metal-Catalyzed [2 + 2] Cycloaddition of Bis-enones. *J. Am. Chem. Soc.* **2001**, *123*, 6716-6717.
(229) Wang, L.-C.; Jang, H.-Y.; Roh, Y.; Lynch, V.; Schultz, A. J.; Wang, X.; Krische, M. J. Diastereoselective Cycloreductions and Cycloadditions Catalyzed by Co(dpm)2-Silane (dpm = 2,2,6,6-tetramethylheptane-3,5-dionate): Mechanism and Partitioning of Hydrometallative versus Anion Radical Pathways. *J. Am. Chem. Soc.* **2002**, *124*, 9448-9453.
(230) Yang, J.; Cauble, D. F.; Berro, A. J.; Bauld, N. L.; Krische, M. J. Anion Radical [2 + 2] Cycloaddition as a Mechanistic Probe: Stoichiometry- and Concentration-Dependent Partitioning of Electron-Transfer and Alkylation Pathways in the Reaction of the Gilman Reagent Me2CuLi·LiI with Bis(enones). *J. Org. Chem.* **2004**, *69*, 7979-7984.
(231) Narayanam, J. M. R.; Tucker, J. W.; Stephenson, C. R. J. Electron-Transfer Photoredox Catalysis: Development of a Tin-Free Reductive Dehalogenation Reaction. *J. Am. Chem. Soc.* **2009**, *131*, 8756-8757.
(232) Shaw, M. H.; Twilton, J.; MacMillan, D. W. C. Photoredox Catalysis in Organic Chemistry. *J. Org. Chem.* **2016**, *81*, 6898-6926.
(233) Matsui, J. K.; Lang, S. B.; Heitz, D. R.; Molander, G. A. Photoredox-Mediated Routes to Radicals: The Value of Catalytic Radical Generation in Synthetic Methods Development. *ACS Catal.* **2017**, *7*, 2563-2575.
(234) Chen, K. K. Pharmacology of Methadone and Related Compounds *Ann. N.Y. Acad. Sci.* **1948**, *51*, 83-97.
(235) Boyle, E. A.; Freemanm, P. C.; Mangan, F. R.; Thomson, M. J. Nabumetone (BRL 14777, 4-[6-methoxy-2-naphthyl]-butan-2-one): a new anti-inflammatory agent. *J. Pharm. Pharmacol.* **1982**, *34*, 562-569.
(236) Tanaka, T.; Kawase, M.; Tani, S. α-Hydroxyketones as inhibitors of urease. *Biorg. Med. Chem.* **2004**, *12*, 501-505.
(237) Redelinghuys, P.; Nchinda, A. T.; Chibale, K.; Sturrock, E. D. Novel ketomethylene inhibitors of angiotensin I-converting enzyme (ACE): inhibition and molecular modelling. *Biol. Chem.* **2006**, *387*, 461-466.
(238) Riley, A. B.; Tafreshi, M. J.; Haber, S. L. Prasugrel: A novel antiplatelet agent. *Am. J. Health-Syst. Pharm.* **2008**, *65*, 1019-1028.

(239) Hoyos, P.; Sinisterra, J.-V.; Molinari, F.; Alcántara, A. R.; Domínguez de María, P. Biocatalytic Strategies for the Asymmetric Synthesis of α-Hydroxy Ketones. *Acc. Chem. Res.* **2010**, *43*, 288-299.
(240) Liu, Y.; Han, S.-J.; Liu, W.-B.; Stoltz, B. M. Catalytic Enantioselective Construction of Quaternary Stereocenters: Assembly of Key Building Blocks for the Synthesis of Biologically Active Molecules. *Acc. Chem. Res.* **2015**, *48*, 740-751.
(241) Allen, L. A. T.; Raclea, R.-C.; Natho, P.; Parsons, P. J. Recent advances in the synthesis of α-amino ketones. *Org. Biomol. Chem.* **2021**, *19*, 498-513.
(242) Ertl, P.; Altmann, E.; McKenna, J. M. The Most Common Functional Groups in Bioactive Molecules and How Their Popularity Has Evolved over Time. *J. Med. Chem.* **2020**, *63*, 8408-8418.
(243) Granger, B.; Albu, S. The Haloperidol Story. *Ann. Clin. Psychiatry* **2005**, *17*, 137-140.
(244) Seipel, L.; Breithardt, G. Propafenone — a new antiarrhythmic drug. *Eur. Heart J.* **1980**, *1*, 309-313.
(245) Mawdsley, P. 8 - Fenbufen. *Clin. Rheum. Dis.* **1980**, *6*, 615-632.
(246) Cooper, T. B.; Simpson, G. M.; Haher, E. J.; Bergner, P.-E. E. Butaperazine Pharmacokinetics: Effect of Dosage Regimen on Steady State Blood Levels. *Arch. Gen. Psychiatry* **1975**, *32*, 903-905.
(247) Wadsworth, W. S.; Emmons, W. D. The Utility of Phosphonate Carbanions in Olefin Synthesis. *J. Am. Chem. Soc.* **1961**, *83*, 1733-1738.
(248) Wittig, G.; Schöllkopf, U. Über Triphenyl-phosphin-methylene als olefinbildende Reagenzien I. Mitteil. *Chem. Ber.* **1954**, *87*, 1318-1330.
(249) Milstein, D.; Stille, J. K. A general, selective, and facile method for ketone synthesis from acid chlorides and organotin compounds catalyzed by palladium. *J. Am. Chem. Soc.* **1978**, *100*, 3636-3638.
(250) Richardson, S. K. Aldehydes and ketones. In *General and Synthetic Methods: Volume 14*; Pattenden, G., Ed.; The Royal Society of Chemistry: 1992; pp 26-62.
(251) Dieter, R. K. Reaction of acyl chlorides with organometallic reagents: A banquet table of metals for ketone synthesis. *Tetrahedron* **1999**, *55*, 4177-4236.
(252) Zhou, F.; Li, C.-J. The Barbier–Grignard-type arylation of aldehydes using unactivated aryl iodides in water. *Nat. Commun.* **2014**, *5*, 4254.
(253) Miles, D. H.; Guasch, J.; Toste, F. D. A Nucleophilic Strategy for Enantioselective Intermolecular α-Amination: Access to Enantioenriched α-Arylamino Ketones. *J. Am. Chem. Soc.* **2015**, *137*, 7632-7635.
(254) Zhang, M.; Xie, J.; Zhu, C. A general deoxygenation approach for synthesis of ketones from aromatic carboxylic acids and alkenes. *Nat. Commun.* **2018**, *9*, 3517.
(255) Ruzi, R.; Liu, K.; Zhu, C.; Xie, J. Upgrading ketone synthesis direct from carboxylic acids and organohalides. *Nat. Commun.* **2020**, *11*, 3312.
(256) Grignard, V. Sur quelques nouvelles combinaisons organo-métalliques du magnésium et leurs applications à des synthèses d'alcools et d'hydrocarbures. *C. R. Hebd. Séances. Acad. Sci.* **1900**, *130*, 1322– 1325.
(257) Nahm, S.; Weinreb, S. M. N-methoxy-n-methylamides as effective acylating agents. *Tetrahedron Lett.* **1981**, *22*, 3815-3818.

(258) Alonso, F.; Lorenzo, E.; Yus, M. Direct Easy Synthesis of Ketones from Carboxylic Acids and Chlorinated Compounds. *J. Org. Chem.* **1996**, *61*, 6058-6059.
(259) Knochel, P.; Dohle, W.; Gommermann, N.; Kneisel, F. F.; Kopp, F.; Korn, T.; Sapountzis, I.; Vu, V. A. Highly Functionalized Organomagnesium Reagents Prepared through Halogen–Metal Exchange. *Angew. Chem. Int. Ed.* **2003**, *42*, 4302-4320.
(260) Kagan, H. B. Victor Grignard and Paul Sabatier: Two Showcase Laureates of the Nobel Prize for Chemistry. *Angew. Chem. Int. Ed.* **2012**, *51*, 7376-7382.
(261) Colas, K.; dos Santos, A. C. V. D.; Mendoza, A. i-Pr2NMgCl·LiCl Enables the Synthesis of Ketones by Direct Addition of Grignard Reagents to Carboxylate Anions. *Org. Lett.* **2019**, *21*, 7908-7913.
(262) Rueping, M.; Nachtsheim, B. J. A review of new developments in the Friedel–Crafts alkylation – From green chemistry to asymmetric catalysis. *Beilstein J. Org. Chem.* **2010**, *6*, 6.
(263) Heravi, M. M.; Zadsirjan, V.; Saedi, P.; Momeni, T. Applications of Friedel–Crafts reactions in total synthesis of natural products. *RSC Advances* **2018**, *8*, 40061-40163.
(264) Yin, H.; Zhao, C.; You, H.; Lin, K.; Gong, H. Mild ketone formation via Ni-catalyzed reductive coupling of unactivated alkyl halides with acid anhydrides. *Chem. Commun.* **2012**, *48*, 7034-7036.
(265) Cherney, A. H.; Kadunce, N. T.; Reisman, S. E. Catalytic Asymmetric Reductive Acyl Cross-Coupling: Synthesis of Enantioenriched Acyclic α,α-Disubstituted Ketones. *J. Am. Chem. Soc.* **2013**, *135*, 7442-7445.
(266) Buchspies, J.; Szostak, M. Recent Advances in Acyl Suzuki Cross-Coupling. *Catalysts* **2019**, *9*, 53.
(267) Johnson, J. S. Catalyzed Reactions of Acyl Anion Equivalents. *Angew. Chem. Int. Ed.* **2004**, *43*, 1326-1328.
(268) Bugaut, X.; Glorius, F. Organocatalytic umpolung: N-heterocyclic carbenes and beyond. *Chem. Soc. Rev.* **2012**, *41*, 3511-3522.
(269) Sanz-Marco, A.; Martinez-Erro, S.; Pauze, M.; Gómez-Bengoa, E.; Martín-Matute, B. An umpolung strategy to react catalytic enols with nucleophiles. *Nat. Commun.* **2019**, *10*, 5244.
(270) Enders, D.; Niemeier, O.; Henseler, A. Organocatalysis by N-Heterocyclic Carbenes. *Chem. Rev.* **2007**, *107*, 5606-5655.
(271) Biju, A. T.; Kuhl, N.; Glorius, F. Extending NHC-Catalysis: Coupling Aldehydes with Unconventional Reaction Partners. *Acc. Chem. Res.* **2011**, *44*, 1182-1195.
(272) Nair, V.; Menon, R. S.; Biju, A. T.; Sinu, C. R.; Paul, R. R.; Jose, A.; Sreekumar, V. Employing homoenolates generated by NHC catalysis in carbon–carbon bond-forming reactions: state of the art. *Chem. Soc. Rev.* **2011**, *40*, 5336-5346.
(273) Ryan, S. J.; Candish, L.; Lupton, D. W. Acyl anion free N-heterocyclic carbene organocatalysis. *Chem. Soc. Rev.* **2013**, *42*, 4906-4917.
(274) Mahatthananchai, J.; Bode, J. W. On the Mechanism of N-Heterocyclic Carbene-Catalyzed Reactions Involving Acyl Azoliums. *Acc. Chem. Res.* **2014**, *47*, 696-707.
(275) Chen, X.; Wang, H.; Jin, Z.; Chi, Y. R. N-Heterocyclic Carbene Organocatalysis: Activation Modes and Typical Reactive Intermediates. *Chin. J. Chem* . **2020**, *38*, 1167-1202.
(276) Yoon, T. P.; Ischay, M. A.; Du, J. Visible light photocatalysis as a greener approach to photochemical synthesis. *Nat. Chem.* **2010**, *2*, 527-532.

(277) Xuan, J.; Xiao, W.-J. Visible-Light Photoredox Catalysis. *Angew. Chem. Int. Ed.* **2012**, *51*, 6828-6838.
(278) Prier, C. K.; Rankic, D. A.; MacMillan, D. W. C. Visible Light Photoredox Catalysis with Transition Metal Complexes: Applications in Organic Synthesis. *Chem. Rev.* **2013**, *113*, 5322-5363.
(279) Francke, R.; Little, R. D. Redox catalysis in organic electrosynthesis: basic principles and recent developments. *Chem. Soc. Rev.* **2014**, *43*, 2492-2521.
(280) Skubi, K. L.; Blum, T. R.; Yoon, T. P. Dual Catalysis Strategies in Photochemical Synthesis. *Chem. Rev.* **2016**, *116*, 10035-10074.
(281) Yan, M.; Kawamata, Y.; Baran, P. S. Synthetic Organic Electrochemical Methods Since 2000: On the Verge of a Renaissance. *Chem. Rev.* **2017**, *117*, 13230-13319.
(282) Huang, H.; Yu, C.; Zhang, Y.; Zhang, Y.; Mariano, P. S.; Wang, W. Chemo- and Regioselective Organo-Photoredox Catalyzed Hydroformylation of Styrenes via a Radical Pathway. *J. Am. Chem. Soc.* **2017**, *139*, 9799-9802.
(283) Zhang, S.; Li, L.; Li, J.; Shi, J.; Xu, K.; Gao, W.; Zong, L.; Li, G.; Findlater, M. Electrochemical Arylation of Aldehydes, Ketones, and Alcohols: from Cathodic Reduction to Convergent Paired Electrolysis. *Angew. Chem. Int. Ed.* **2021**, 7275.
(284) Deb, A.; Manna, S.; Modak, A.; Patra, T.; Maity, S.; Maiti, D. Oxidative Trifluoromethylation of Unactivated Olefins: An Efficient and Practical Synthesis of α-Trifluoromethyl-Substituted Ketones. *Angew. Chem. Int. Ed.* **2013**, *52*, 9747-9750.
(285) Chen, W.; Liu, Z.; Tian, J.; Li, J.; Ma, J.; Cheng, X.; Li, G. Building Congested Ketone: Substituted Hantzsch Ester and Nitrile as Alkylation Reagents in Photoredox Catalysis. *J. Am. Chem. Soc.* **2016**, *138*, 12312-12315.
(286) Raviola, C.; Protti, S.; Ravelli, D.; Fagnoni, M. Photogenerated acyl/alkoxycarbonyl/carbamoyl radicals for sustainable synthesis. *Green Chem.* **2019**, *21*, 748-764.
(287) Ni, S.; Padial, N. M.; Kingston, C.; Vantourout, J. C.; Schmitt, D. C.; Edwards, J. T.; Kruszyk, M. M.; Merchant, R. R.; Mykhailiuk, P. K.; Sanchez, B. B.; Yang, S.; Perry, M. A.; Gallego, G. M.; Mousseau, J. J.; Collins, M. R.; Cherney, R. J.; Lebed, P. S.; Chen, J. S.; Qin, T.; Baran, P. S. A Radical Approach to Anionic Chemistry: Synthesis of Ketones, Alcohols, and Amines. *J. Am. Chem. Soc.* **2019**, *141*, 6726-6739.
(288) Chalotra, N.; Sultan, S.; Shah, B. A. Recent Advances in Photoredox Methods for Ketone Synthesis. *Asian J. Org. Chem.* **2020**, *9*, 863-881.
(289) Zuo, Z.; Ahneman, D. T.; Chu, L.; Terrett, J. A.; Doyle, A. G.; MacMillan, D. W. C. Merging photoredox with nickel catalysis: Coupling of α-carboxyl sp3-carbons with aryl halides. *Science* **2014**, *345*, 437-440.
(290) Chu, L.; Lipshultz, J. M.; MacMillan, D. W. C. Merging Photoredox and Nickel Catalysis: The Direct Synthesis of Ketones by the Decarboxylative Arylation of α-Oxo Acids. *Angew. Chem. Int. Ed.* **2015**, *54*, 7929-7933.
(291) Ragsdale, S. W. Pyruvate Ferredoxin Oxidoreductase and Its Radical Intermediate. *Chem. Rev.* **2003**, *103*, 2333.
(292) Kluger, R.; Tittmann, K. Thiamin Diphosphate Catalysis: Enzymic and Nonenzymic Covalent Intermediates. *Chem. Rev.* **2008**, *108*, 1797-1833.

(293) Izquierdo, J.; Hutson, G. E.; Cohen, D. T.; Scheidt, K. A. A Continuum of Progress: Applications of N-Hetereocyclic Carbene Catalysis in Total Synthesis. *Angew. Chem. Int. Ed.* **2012**, *51*, 11686-11698.
(294) De Sarkar, S.; Biswas, A.; Samanta, R. C.; Studer, A. Catalysis with N-heterocyclic carbenes under oxidative conditions. *Chemistry* **2013**, *19*, 4664-4678.
(295) Delidovich, I.; Palkovits, R. Catalytic versus stoichiometric reagents as a key concept for Green Chemistry. *Green Chem.* **2016**, *18*, 590-593.
(296) Nakanishi, I.; Itoh, S.; Suenobu, T.; Inoue, H.; Fukuzumi, S. Redox Behavior of Active Aldehydes Derived from Thiamin Coenzyme Analogs. *Chem. Lett.* **1997**, *26*, 707.
(297) Nakanishi, I.; Itoh, S.; Suenobu, T.; Fukuzumi, S. Direct Observation of Radical Intermediates While Investiganting the Redox Behavior of Thiamin Coenzyme Models. *Angew. Chem. Int. Ed.* **1998**, *37*, 992-994.
(298) Nakanishi, I.; Itoh, S.; Fukuzumi, S. Electron-Transfer Properties of Active Aldehydes of Thiamin Coenzyme Models, and Mechanism of Formation of the Reactive Intermediates. *Chem. Eur. J.* **1999**, *5*, 2810-2818.
(299) Li, J.-L.; Liu, Y.-Q.; Zou, W.-L.; Zeng, R.; Zhang, X.; Liu, Y.; Han, B.; He, Y.; Leng, H.-J.; Li, Q.-Z. Radical Acylfluoroalkylation of Olefins through N-Heterocyclic Carbene Organocatalysis. *Angew. Chem. Int. Ed.* **2019**, *58*, 2-10.
(300) McDonald, B. R.; Scheidt, K. A. Intermolecular Reductive Couplings of Arylidene Malonates via Lewis Acid/Photoredox Cooperative Catalysis. *Org. Lett.* **2018**, *20*, 6877-6881.
(301) Betori, R. C.; McDonald, B. R.; Scheidt, K. A. Reductive annulations of arylidene malonates with unsaturated electrophiles using photoredox/Lewis acid cooperative catalysis. *Chem. Sci.* **2019**, *10*, 3353-3359.
(302) Betori, R. C.; Scheidt, K. A. Reductive Arylation of Arylidene Malonates Using Photoredox Catalysis. *ACS Catal.* **2019**, *9*, 10350-10357.
(303) Jia, Q.; Li, Y.; Lin, Y.; Ren, Q. The Combination of Lewis Acid with N-Heterocyclic Carbene (NHC) Catalysis. *Catalysts* **2019**, *9*, 863.
(304) Cardinal-David, B.; Raup, D. E. A.; Scheidt, K. A. Cooperative N-Heterocyclic Carbene/Lewis Acid Catalysis for Highly Stereoselective Annulation Reactions with Homoenolates. *J. Am. Chem. Soc.* **2010**, *132*, 5345-5347.
(305) Raup, D. E. A.; Cardinal-David, B.; Holte, D.; Scheidt, K. A. Cooperative catalysis by carbenes and Lewis acids in a highly stereoselective route to γ-lactams. *Nat. Chem.* **2010**, *2*, 766-771.
(306) Cohen, D. T.; Scheidt, K. A. Cooperative Lewis acid/N-heterocyclic carbene catalysis. *Chem. Sci.* **2012**, *3*, 53-57.
(307) Mo, J.; Chen, X.; Chi, Y. R. Oxidative γ-Addition of Enals to Trifluoromethyl Ketones: Enantioselectivity Control via Lewis Acid/N-Heterocyclic Carbene Cooperative Catalysis. *J. Am. Chem. Soc.* **2012**, *134*, 8810-8813.
(308) Jin, Z.; Xu, J.; Yang, S.; Song, B.-A.; Chi, Y. R. Enantioselective Sulfonation of Enones with Sulfonyl Imines by Cooperative N-Heterocyclic-Carbene/Thiourea/Tertiary-Amine Multicatalysis. *Angew. Chem. Int. Ed.* **2013**, *52*, 12354-12358.
(309) Tong, Y.-F.; Mao, J.-H.; Wu, S.; Zhao, Y.; Cheng, Y. Changing the Reaction Pathway by NHC/Brønsted Base Cooperative Catalysis: Highly Stereoselective Synthesis of Multifunctional

Benzo[a]fluoren-11-ones from the Dimerization of 2-(Aroylvinyl)arylaldehydes. *J. Org. Chem.* **2014**, *79*, 2075-2081.
(310) Bai, Y.; Xiang, S.; Leow, M. L.; Liu, X. W. Dual-function Pd/NHC catalysis: tandem allylation-isomerization-conjugate addition that allows access to pyrroles, thiophenes and furans. *Chem. Commun.* **2014**, *50*, 6168-6170.
(311) Liu, K.; Hovey, M. T.; Scheidt, K. A. A Cooperative N-Heterocyclic Carbene/Palladium Catalysis System. *Chem. Sci.* **2014**, *5*, 4026-4031.
(312) Terrett, J. A.; Clift, M. D.; Macmillan, D. W. C. Direct β-Alkylation of Aldehydes via Photoredox Organocatalysis. *J. Am. Chem. Soc.* **2014**, *136*, 6858-6861.
(313) Pirnot, M. T.; Rankic, D. A.; Martin, D. B. C.; Macmillan, D. W. C. Photoredox Activation for the Direct -Arylation of Ketones and Aldehydes. *Science* **2013**, *339*, 1593-1596.
(314) Yoon, T. P. Photochemical Stereocontrol Using Tandem Photoredox–Chiral Lewis Acid Catalysis. *Acc. Chem. Res.* **2016**, *49*, 2307-2315.
(315) Rono, L. J.; Yayla, H. G.; Wang, D. Y.; Armstrong, M. F.; Knowles, R. R. Enantioselective Photoredox Catalysis Enabled by Proton-Coupled Electron Transfer: Development of an Asymmetric Aza-Pinacol Cyclization. *J. Am. Chem. Soc.* **2013**, *135*, 17735-17738.
(316) Cheng, W. M.; Shang, R.; Fu, Y. Photoredox/Bronsted Acid Co-Catalysis Enabling Decarboxylative Coupling of Amino Acid and Peptide Redox-Active Esters with N-Heteroarenes. *ACS Catal.* **2017**, *7*, 907-911.
(317) Huo, H.; Shen, X.; Wang, C.; Zhang, L.; Rose, P.; Chen, L. A.; Harms, K.; Marsch, M.; Hilt, G.; Meggers, E. Asymmetric photoredox transition-metal catalysis activated by visible light. *Nature* **2014**, *515*, 100-103.
(318) Lee, K. N.; Ngai, M.-Y. Recent developments in transition-metal photoredox-catalysed reactions of carbonyl derivatives. *Chem. Commun.* **2017**, *53*, 13093-13112.
(319) Gutierrez-Bonet, A.; Tellis, J. C.; Matsui, J. K.; Vara, B. A.; Molander, G. A. 1,4-Dihydropyridines as Alkyl Radical Precursors: Introducing the Aldehyde Feedstock to Nickel/Photoredox Dual Catalysis. *ACS Catal.* **2016**, *6*, 8004-8008.
(320) Vora, H. U.; Wheeler, P.; Rovis, T. Exploiting Acyl and Enol Azolium Intermediates via N-Hetero- cyclic Carbene-Catalyzed Reactions of α-Reducible Aldehydes. *Adv. Synth. Catal.* **2012**, *354*, 1617-1639.
(321) Iqbal, N.; Choi, S.; You, Y.; Cho, E. J. Aerobic oxidation of aldehydes by visible light photocatalysis. *Tetrahedron Lett.* **2013**, *54*, 6222-6225.
(322) Mukherjee, S.; Garza-Sanchez, R. A.; Tlahuext-Aca, A.; Glorius, F. Alkynylation of Csp2 (O)-H Bonds Enabled by Photoredox-Mediated Hydrogen-Atom Transfer. *Angew. Chem. Int. Ed.* **2017**, *56*, 14723-14726.
(323) Zhang, X.; MacMillan, D. W. C. Direct Aldehyde C–H Arylation and Alkylation via the Combination of Nickel, Hydrogen Atom Transfer, and Photoredox Catalysis. *J. Am. Chem. Soc.* **2017**, *139*, 11353-11356.
(324) Liu, J.; Liu, Q.; Yi, H.; Qin, C.; Bai, R.; Qi, X.; Lan, Y.; Lei, A. Visible-Light-Mediated Decarboxylation/Oxidative Amidation of α-Keto Acids with Amines under Mild Reaction Conditions Using O2. *Angew. Chem. Int. Ed.* **2014**, *53*, 502-506.
(325) Chu, L.; Lipshultz, J. M.; MacMillan, D. W. Merging Photoredox and Nickel Catalysis: The Direct Synthesis of Ketones by the Decarboxylative Arylation of α-Oxo Acids. *Angew. Chem. Int. Ed.* **2015**, *54*, 7929-7933.

(326) Zhang, M.; Xi, J.; Ruzi, R.; Li, N.; Wu, Z.; Li, W.; Zhu, C. Domino-Fluorination–Protodefluorination Enables Decarboxylative Cross-Coupling of α-Oxocarboxylic Acids with Styrene via Photoredox Catalysis. *J. Org. Chem.* **2017**, *82*, 9305-9311.
(327) Ngai, M.-Y.; Banerjee, A.; Lei, Z. Acyl Radical Chemistry via Visible-Light Photoredox Catalysis. *Synthesis* **2019**, *51*, 303-333.
(328) Zhou, Q.-Q.; Guo, W.; Ding, W.; Wu, X.; Chen, X.; Lu, L.-Q.; Xiao, W.-J. Decarboxylative Alkynylation and Carbonylative Alkynylation of Carboxylic Acids Enabled by Visible-Light Photoredox Catalysis. *Angew. Chem. Int. Ed.* **2015**, *54*, 11196-11199.
(329) Bergonzini, G.; Cassani, C.; Wallentin, C.-J. Acyl Radicals from Aromatic Carboxylic Acids by Means of Visible-Light Photoredox Catalysis. *Angew. Chem. Int. Ed.* **2015**, *54*, 14066-14069.
(330) Pettersson, F.; Bergonzini, G.; Cassani, C.; Wallentin, C.-J. Redox-Neutral Dual Functionalization of Electron-Deficient Alkenes. *Chem. Eur. J.* **2017**, *23*, 7444-7447.
(331) Zhang, M.; Ruzi, R.; Xi, J.; Li, N.; Wu, Z.; Li, W.; Yu, S.; Zhu, C. Photoredox-Catalyzed Hydroacylation of Olefins Employing Carboxylic Acids and Hydrosilanes. *Org. Lett.* **2017**, *19*, 3430-3433.
(332) Zhang, M.; Li, N.; Tao, X.; Ruzi, R.; Yu, S.; Zhu, C. Selective reduction of carboxylic acids to aldehydes with hydrosilane via photoredox catalysis. *Chem. Commun.* **2017**, *53*, 10228-10231.
(333) Ruzi, R.; Zhang, M.; Ablajan, K.; Zhu, C. Photoredox-Catalyzed Deoxygenative Intramolecular Acylation of Biarylcarboxylic Acids: Access to Fluorenones. *J. Org. Chem.* **2017**, *82*, 12834-12839.
(334) Stache, E. E.; Ertel, A. B.; Rovis, T.; Doyle, A. G. Generation of Phosphoranyl Radicals via Photoredox Catalysis Enables Voltage–Independent Activation of Strong C–O Bonds. *ACS Catal.* **2018**, *8*, 11134-11139.
(335) Martinez Alvarado, J. I.; Ertel, A. B.; Stegner, A.; Stache, E. E.; Doyle, A. G. Direct Use of Carboxylic Acids in the Photocatalytic Hydroacylation of Styrenes To Generate Dialkyl Ketones. *Org. Lett.* **2019**, *21*, 9940-9944.
(336) Wang, J.; Cary, B. P.; Beyer, P. D.; Gellman, S. H.; Weix, D. J. Ketones from Nickel-Catalyzed Decarboxylative, Non-Symmetric Cross-Electrophile Coupling of Carboxylic Acid Esters. *Angew. Chem. Int. Ed.* **2019**, *58*, 12081-12085.
(337) Ni, S.; Padial, N. M.; Kingston, C.; Vantourout, J. C.; Schmitt, D. C.; Edwards, J. T.; Kruszyk, M. M.; Merchant, R. R.; Mykhailiuk, P. K.; Sanchez, B. B.; Yang, S.; Perry, M. A.; Gallego, G. M.; Mousseau, J. J.; Collins, M. R.; Cherney, R. J.; Lebed, P. S.; Chen, J. S.; Qin, T.; Baran, P. S. A Radical Approach to Anionic Chemistry: Synthesis of Ketones, Alcohols, and Amines. *J. Am. Chem. Soc.* **2019**, *141*, 6726-6739.
(338) Crespi, S.; Fagnoni, M. Generation of Alkyl Radicals: From the Tyranny of Tin to the Photon Democracy. *Chem. Rev.* **2020**, *120*, 9790-9833.
(339) Chatgilialoglu, C.; Lalevee, J. Recent applications of the (TMS)3SiH radical-based reagent. *Molecules* **2012**, *17*, 527-555.
(340) Chatgilialoglu, C. Organosilanes as Radical-Based Reducing Agents in Synthesis. *Acc. Chem. Res.* **1992**, *25*, 188-194.
(341) Corce, V.; Chamoreau, L. M.; Derat, E.; Goddard, J. P.; Ollivier, C.; Fensterbank, L. Silicates as Latent Alkyl Radical Precursors: Visible-Light Photocatalytic Oxidation of Hypervalent Bis-Catecholato Silicon Compounds. *Angew. Chem. Int. Ed.* **2015**, *54*, 11414-11418.

(342) Tellis, J. C.; Primer, D. N.; Molander, G. A. Single-electron transmetalation in organoboron cross-coupling by photoredox/nickel dual catalysis. *Science* **2014**, *345*, 433-436.
(343) Frye, C. L. Pentacoordinate Silicon Derivatives. II.1 Salts of Bis(o-arylenedioxy) organosiliconic Acids. *J. Am. Chem. Soc.* **1964**, *86*, 3170-3171.
(344) Yasu, Y.; Koike, T.; Akita, M. Visible Light-Induced Selective Generation of Radicals from Organoborates by Photoredox Catalysis. *Adv. Synth. Catal.* **2012**, *354*, 3414-3420.
(345) Vedejs, E.; Chapman, R. W.; Fields, S. C.; Lin, S.; Schrimpf, M. R. Conversion of Arylboronic Acids into Potassium Aryltrifluoroborates: Convenient Precursors of Arylboron Difluoride Lewis Acids. *J. Org. Chem.* **1995**, *60*, 3020-3027.
(346) Darses, S.; Genêt, J.-P.; Brayer, J.-L.; Demoute, J.-P. Cross-coupling reactions of arenediazonium tetrafluoroborates with potassium aryl- or alkenyltrifluoroborates catalyzed by palladium. *Tetrahedron Lett.* **1997**, *38*, 4393-4396.
(347) Molander, G. A.; Ellis, N. Organotrifluoroborates: Protected Boronic Acids That Expand the Versatility of the Suzuki Coupling Reaction. *Acc. Chem. Res.* **2007**, *40*, 275-286.
(348) Hantzsch, A. Condensationsprodukte aus Aldehydammoniak und ketonartigen Verbindungen. *Ber. Dtsch. Chem. Ges.* **1881**, *14*, 1637-1638.
(349) Sausiņš, A.; Duburs, G. Reactions of 1, 4-dihydropyridines. *Heterocycles* **1988**, *27*, 291-314.
(350) Zhang, D.; Wu, L.-Z.; Zhou, L.; Han, X.; Yang, Q.-Z.; Zhang, L.-P.; Tung, C.-H. Photocatalytic Hydrogen Production from Hantzsch 1,4-Dihydropyridines by Platinum(II) Terpyridyl Complexes in Homogeneous Solution. *J. Am. Chem. Soc.* **2004**, *126*, 3440-3441.
(351) Chen, W.; Liu, Z.; Tian, J.; Li, J.; Ma, J.; Cheng, X.; Li, G. Building Congested Ketone: Substituted Hantzsch Ester and Nitrile as Alkylation Reagents in Photoredox Catalysis. *J. Am. Chem. Soc.* **2016**, *138*, 12312-12315.
(352) Huang, W.; Cheng, X. Hantzsch Esters as Multifunctional Reagents in Visible-Light Photoredox Catalysis. *Synlett* **2017**, *28*, 148-158.
(353) de Assis, F. F.; Huang, X.; Akiyama, M.; Pilli, R. A.; Meggers, E. Visible-Light-Activated Catalytic Enantioselective β-Alkylation of α,β-Unsaturated 2-Acyl Imidazoles Using Hantzsch Esters as Radical Reservoirs. *J. Org. Chem.* **2018**, *83*, 10922-10932.
(354) Krska, S. W.; DiRocco, D. A.; Dreher, S. D.; Shevlin, M. The Evolution of Chemical High-Throughput Experimentation To Address Challenging Problems in Pharmaceutical Synthesis. *Acc. Chem. Res.* **2017**, *50*, 2976-2985.
(355) Isbrandt, E. S.; Sullivan, R. J.; Newman, S. G. High Throughput Strategies for the Discovery and Optimization of Catalytic Reactions. *Angew. Chem. Int. Ed.* **2019**, *58*, 7180-7191.
(356) Mennen, S. M.; Alhambra, C.; Allen, C. L.; Barberis, M.; Berritt, S.; Brandt, T. A.; Campbell, A. D.; Castañón, J.; Cherney, A. H.; Christensen, M.; Damon, D. B.; Eugenio de Diego, J.; García-Cerrada, S.; García-Losada, P.; Haro, R.; Janey, J.; Leitch, D. C.; Li, L.; Liu, F.; Lobben, P. C.; MacMillan, D. W. C.; Magano, J.; McInturff, E.; Monfette, S.; Post, R. J.; Schultz, D.; Sitter, B. J.; Stevens, J. M.; Strambeanu, I. I.; Twilton, J.; Wang, K.; Zajac, M. A. The Evolution of High-Throughput Experimentation in Pharmaceutical Development and Perspectives on the Future. *Org. Process Res. Dev.* **2019**, *23*, 1213-1242.
(357) Crisenza, G. E. M.; Mazzarella, D.; Melchiorre, P. Synthetic Methods Driven by the Photoactivity of Electron Donor–Acceptor Complexes. *J. Am. Chem. Soc.* **2020**, *142*, 5461-5476.

(358) Buzzetti, L.; Prieto, A.; Roy, S. R.; Melchiorre, P. Radical-Based C−C Bond-Forming Processes Enabled by the Photoexcitation of 4-Alkyl-1,4-dihydropyridines. *Angew. Chem. Int. Ed.* **2017**, *56*, 15039-15043.
(359) Lowry, M. S.; Goldsmith, J. I.; Slinker, J. D.; Rohl, R.; Pascal, R. A.; Malliaras, G. G.; Bernhard, S. Single-Layer Electroluminescent Devices and Photoinduced Hydrogen Production from an Ionic Iridium(III) Complex. *Chem. Mater.* **2005**, *17*, 5712-5719.
(360) Tamayo, A. B.; Alleyne, B. D.; Djurovich, P. I.; Lamansky, S.; Tsyba, I.; Ho, N. N.; Bau, R.; Thompson, M. E. Synthesis and Characterization of Facial and Meridional Tris-cyclometalated Iridium(III) Complexes. *J. Am. Chem. Soc.* **2003**, *125*, 7377-7387.
(361) Margrey, K. A.; Nicewicz, D. A. A General Approach to Catalytic Alkene Anti-Markovnikov Hydrofunctionalization Reactions via Acridinium Photoredox Catalysis. *Acc. Chem. Res.* **2016**, *49*, 1997-2006.
(362) Wilger, D. J.; Grandjean, J.-M. M.; Lammert, T. R.; Nicewicz, D. A. The direct anti-Markovnikov addition of mineral acids to styrenes. *Nat. Chem.* **2014**, *6*, 720-726.
(363) v. Meyer, E. LXXXIX. Neue Beiträge zur Kenntnis der dimolekularen Nitrile. *J. Prakt. Chem* **1908**, *78*, 497-534.
(364) Moir, M.; Danon, J. J.; Reekie, T. A.; Kassiou, M. An overview of late-stage functionalization in today's drug discovery. *Expert Opin. Drug Discov.* **2019**, *14*, 1137-1149.
(365) Battershill, A. J.; Scott, L. J. Telmisartan. *Drugs* **2006**, *66*, 51-83.
(366) Moore, J. C.; Pollard, D. J.; Kosjek, B.; Devine, P. N. Advances in the Enzymatic Reduction of Ketones. *Acc. Chem. Res.* **2007**, *40*, 1412-1419.
(367) Wang, C.; Qin, J.; Shen, X.; Riedel, R.; Harms, K.; Meggers, E. Asymmetric Radical–Radical Cross-Coupling through Visible-Light-Activated Iridium Catalysis. *Angew. Chem. Int. Ed.* **2016**, *128*, 695-698.
(368) Liu, Y.; Liu, X.; Li, J.; Zhao, X.; Qiao, B.; Jiang, Z. Catalytic enantioselective radical coupling of activated ketones with N-aryl glycines. *Chem. Sci.* **2018**, *9*, 8094-8098.
(369) Monos, T. M.; Sun, A. C.; McAtee, R. C.; Devery, J. J.; Stephenson, C. R. J. Microwave-Assisted Synthesis of Heteroleptic Ir(III)+ Polypyridyl Complexes. *J. Org. Chem.* **2016**, *81*, 6988-6994.
(370) Lee, A.; Scheidt, K. A. N-Heterocyclic carbene-catalyzed enantioselective annulations: a dual activation strategy for a formal [4+2] addition for dihydrocoumarins. *Chem. Commun.* **2015**, *51*, 3407-3410.
(371) Nakajima, K.; Nojima, S.; Sakata, K.; Nishibayashi, Y. Visible-Light-Mediated Aromatic Substitution Reactions of Cyanoarenes with 4-Alkyl-1,4-dihydropyridines through Double Carbon–Carbon Bond Cleavage. *ChemCatChem* **2016**, *8*, 1028-1032.
(372) Gandolfo, E.; Tang, X.; Raha Roy, S.; Melchiorre, P. Photochemical Asymmetric Nickel-Catalyzed Acyl Cross-Coupling. *Angew. Chem. Int. Ed.* **2019**, *58*, 16854-16858.
(373) Zhao, B.; Lu, X. Cationic Palladium(II)-Catalyzed Addition of Arylboronic Acids to Nitriles. One-Step Synthesis of Benzofurans from Phenoxyacetonitriles. *Org. Lett.* **2006**, *8*, 5987-5990.
(374) Huang, K.; Li, G.; Huang, W.-P.; Yu, D.-G.; Shi, Z.-J. Arylation of α-pivaloxyl ketones with arylboronic reagents viaNi-catalyzed sp3 C–O activation. *Chem. Commun.* **2011**, *47*, 7224-7226.
(375) Wong, Y.-C.; Parthasarathy, K.; Cheng, C.-H. Direct Synthesis of Arylketones by Nickel-Catalyzed Addition of Arylboronic Acids to Nitriles. *Org. Lett.* **2010**, *12*, 1736-1739.

(376) Miao, T.; Wang, G.-W. Synthesis of ketones by palladium-catalysed desulfitative reaction of arylsulfinic acids with nitriles. *Chem. Commun.* **2011**, *47*, 9501-9503.
(377) Bechara, W. S.; Pelletier, G.; Charette, A. B. Chemoselective synthesis of ketones and ketimines by addition of organometallic reagents to secondary amides. *Nat. Chem.* **2012**, *4*, 228-234.
(378) Astarloa, I.; SanMartin, R.; Herrero, M. T.; Domínguez, E. Aqueous α-Arylation of Mono- and Diarylethanone Enolates at Low Catalyst Loading. *Adv. Synth. Catal.* **2018**, *360*, 1711-1718.
(379) Abdel-Motaleb, R. M.; Makhloof, A.-M. A.-S.; Ibrahim, H. M.; Elnagdi, M. H. Studies with azoles and benzoazoles: A novel simple approach for synthesis of 3-functionally substituted 3-acylindoles. *J. Heterocycl. Chem.* **2007**, *44*, 109-114.
(380) Gao, K.; Yorimitsu, H.; Osuka, A. α-Arylation of Ketimines with Aryl Sulfides at a Low Palladium Catalyst Loading. *Angew. Chem. Int. Ed.* **2016**, *55*, 4573-4576.
(381) Zhao, C.; Jia, X.; Wang, X.; Gong, H. Ni-Catalyzed Reductive Coupling of Alkyl Acids with Unactivated Tertiary Alkyl and Glycosyl Halides. *J. Am. Chem. Soc.* **2014**, *136*, 17645-17651.
(382) Chen, X.; Chen, Z.; So, C. M. Exploration of Aryl Phosphates in Palladium-Catalyzed Mono-α-arylation of Aryl and Heteroaryl Ketones. *J. Org. Chem.* **2019**, *84*, 6337-6346.
(383) Wu, X.-F.; Schranck, J.; Neumann, H.; Beller, M. Palladium-Catalyzed Carbonylative Negishi-type Coupling of Aryl Iodides with Benzyl Chlorides. *Chem. Asian J.* **2012**, *7*, 40-44.
(384) Doherty, S.; Knight, J. G.; Smyth, C. H.; Harrington, R. W.; Clegg, W. Biaryl-Like CATPHOS Diphosphines via Double Diels–Alder Cycloaddition between 1,4-Bis(diphenylphosphinoyl)buta-1,3-diyne and Anthracenes: Efficient Ligands for the Palladium-Catalyzed Amination of Aromatic Bromides and α-Arylation of Ketones. *Organometallics* **2008**, *27*, 1679-1682.
(385) Takemiya, A.; Hartwig, J. F. Palladium-Catalyzed Synthesis of Aryl Ketones by Coupling of Aryl Bromides with an Acyl Anion Equivalent. *J. Am. Chem. Soc.* **2006**, *128*, 14800-14801.
(386) Li, Z.; Gevorgyan, V. Double Duty for Cyanogen Bromide in a Cascade Synthesis of Cyanoepoxides. *Angew. Chem. Int. Ed.* **2011**, *50*, 2808-2810.
(387) Ishii, T.; Kakeno, Y.; Nagao, K.; Ohmiya, H. N-Heterocyclic Carbene-Catalyzed Decarboxylative Alkylation of Aldehydes. *J. Am. Chem. Soc.* **2019**, *141*, 3854-3858.
(388) Seebach, D. Methods of reactivity umpolung. *Angew. Chem. Int. Ed.* **1979**, *18*, 239-258.
(389) Díez-González, S.; Correa, A.; Cavallo, L.; Nolan, S. P. (NHC) Copper (I)-Catalyzed [3+ 2] Cycloaddition of Azides and Mono-or Disubstituted Alkynes. *Chem. Eur. J.* **2006**, *12*, 7558-7564.
(390) Ryan, S.; Candish, L.; Lupton, D. W. N-Heterocyclic Carbene (NHC)-Catalyzed All-Carbon [4+ 2] Cycloaddition-Decarboxylation. *Synlett* **2011**, *2011*, 2275-2278.
(391) Ryan, S. J.; Candish, L.; Lupton, D. W. N-heterocyclic carbene-catalyzed (4+ 2) cycloaddition/decarboxylation of silyl dienol ethers with α, β-unsaturated acid fluorides. *J. Am. Chem. Soc.* **2011**, *133*, 4694-4697.
(392) Sarkar, S. D.; Grimme, S.; Studer, A. NHC Catalyzed Oxidations of Aldehydes to Esters: Chemoselective Acylation of Alcohols in Presence of Amines. *J. Am. Chem. Soc.* **2010**, *132*, 1190-1191.
(393) Joseph, H.; Stancliff, S.; Langrod, J. Methadone maintenance treatment (MMT): a review of historical and clinical issues. *Mt. Sinai J. Med.* **2000**, *67*, 347-364.
(394) Wiviott, S. D.; Antman, E. M.; Braunwald, E. Prasugrel. *Circulation* **2010**, *122*, 394-403.

(395) Ishii, T.; Nagao, K.; Ohmiya, H. Recent advances in N-heterocyclic carbene-based radical catalysis. *Chem. Sci.* **2020**, *11*, 5630-5636.
(396) Li, Q.-Z.; Zeng, R.; Han, B.; Li, J.-L. Single-Electron Transfer Reactions Enabled by N-Heterocyclic Carbene Organocatalysis. *Chem. Eur. J.* **2021**, 3238.
(397) Liu, Q.; Chen, X.-Y. Dual N-heterocyclic carbene/photocatalysis: a new strategy for radical processes. *Org. Chem. Front.* **2020**, *7*, 2082-2087.
(398) Mavroskoufis, A.; Jakob, M.; Hopkinson, M. N. Light-Promoted Organocatalysis with N-Heterocyclic Carbenes. *ChemPhotoChem* **2020**, *4*, 5147-5153.
(399) Dai, L.; Ye, S. Recent advances in N-heterocyclic carbene-catalyzed radical reactions. *Chin. Chem. Lett.* **2020**.
(400) Davies, A. V.; Fitzpatrick, K. P.; Betori, R. C.; Scheidt, K. A. Combined Photoredox and Carbene Catalysis for the Synthesis of Ketones from Carboxylic Acids. *Angew. Chem. Int. Ed.* **2020**, *59*, 9143-9148.
(401) Mavroskoufis, A.; Rajes, K.; Golz, P.; Agrawal, A.; Ruß, V.; Götze, J. P.; Hopkinson, M. N. N-Heterocyclic Carbene Catalyzed Photoenolization/Diels–Alder Reaction of Acid Fluorides. *Angew. Chem. Int. Ed.* **2020**, *59*, 3190-3194.
(402) Hopkinson, M. N.; Mavroskoufis, A. Photo-NHC Catalysis: Accessing Ketone Photochemistry with Carboxylic Acid Derivatives. *Synlett* **2021**, *32*, 95-101.
(403) Regnier, V.; Romero, E. A.; Molton, F.; Jazzar, R.; Bertrand, G.; Martin, D. What Are the Radical Intermediates in Oxidative N-Heterocyclic Carbene Organocatalysis? *J. Am. Chem. Soc.* **2019**, *141*, 1109.
(404) Perdew, J. P.; Burke, K.; Ernzerhof, M. Generalized Gradient Approximation Made Simple. *Phys. Rev. Lett.* **1996**, *77*, 3865-3868.
(405) Perdew, J. P.; Burke, K.; Ernzerhof, M. Generalized Gradient Approximation Made Simple. *Phys. Rev. Lett.* **1997**, *78*, 1396-1396.
(406) Hehre, W. J.; Ditchfield, R.; Pople, J. A. Self-Consistent Molecular Orbital Methods. XII. Further Extensions of Gaussian-Type Basis Sets for Use in Molecular Orbital Studies of Organic Molecules. *J. Chem. Phys.* **1972**, *56*, 2257-2261.
(407) Hay, P. J.; Wadt, W. R. Ab initio effective core potentials for molecular calculations. Potentials for the transition metal atoms Sc to Hg. *J. Chem. Phys.* **1985**, *82*, 270-283.
(408) Marenich, A. V.; Cramer, C. J.; Truhlar, D. G. Universal Solvation Model Based on Solute Electron Density and on a Continuum Model of the Solvent Defined by the Bulk Dielectric Constant and Atomic Surface Tensions. *J. Phys. Chem. B* **2009**, *113*, 6378-6396.
(409) Mulliken, R. S.; Ransil, B. J. The Nobel Prize, 1966. In *Life of a Scientist: An Autobiographical Account of the Development of Molecular Orbital Theory*; Ransil, B. J., Ed.; Springer Berlin Heidelberg: Berlin, Heidelberg, 1989; pp 190-192.
(410) Chan, B.; Collins, E.; Raghavachari, K. Applications of isodesmic-type reactions for computational thermochemistry. *WIRES Somput. Mol. Sci.* **2021**, *11*, e1501.
(411) Clavier, H.; Nolan, S. P. Percent buried volume for phosphine and N-heterocyclic carbene ligands: steric properties in organometallic chemistry. *Chem. Commun.* **2010**, *46*, 841-861.
(412) Liu, J.; Liu, X.-P.; Wu, H.; Wei, Y.; Lu, F.-D.; Guo, K.-R.; Cheng, Y.; Xiao, W.-J. Visible-light-induced triple catalysis for a ring-opening cyanation of cyclopropyl ketones. *Chem. Commun.* **2020**, *56*, 11508-11511.

(413) Molander, G. A. Organotrifluoroborates: Another Branch of the Mighty Oak. *J. Org. Chem.* **2015**, *80*, 7837-7848.
(414) Jouffroy, M.; Primer, D. N.; Molander, G. A. Base-Free Photoredox/Nickel Dual-Catalytic Cross-Coupling of Ammonium Alkylsilicates. *J. Am. Chem. Soc.* **2016**, *138*, 475-478.
(415) Uoyama, H.; Goushi, K.; Shizu, K.; Nomura, H.; Adachi, C. Highly efficient organic light-emitting diodes from delayed fluorescence. *Nature* **2012**, *492*, 234-238.
(416) Hörner, A.; Volz, D.; Hagendorn, T.; Fürniss, D.; Greb, L.; Rönicke, F.; Nieger, M.; Schepers, U.; Bräse, S. Switchable fluorescence by click reaction of a novel azidocarbazole dye. *RSC Advances* **2014**, *4*, 11528-11534.
(417) Yu, Y.; Li, N.; Jin, Q.; Ji, Z.; Sun, Z.; Li, G.; Zhang, S.; You, J. Novel fluorescence labeling reagent 4-(carbazole-9-yl)-benzyl chloroformate and its application in the determination of nitrofuran metabolites compounds in foodstuffs by high performance liquid chromatography with fluorescence detection. *Microchem. J.* **2019**, *145*, 9-17.
(418) Luo, J.; Zhang, J. Donor–Acceptor Fluorophores for Visible-Light-Promoted Organic Synthesis: Photoredox/Ni Dual Catalytic C(sp3)–C(sp2) Cross-Coupling. *ACS Catal.* **2016**, *6*, 873-877.
(419) Ling, K. B.; Smith, A. D. α-Aroyloxyaldehydes: scope and limitations as alternatives to α-haloaldehydes for NHC-catalysed redox transformations. *Chem. Commun.* **2011**, *47*, 373-375.
(420) Lévêque, C.; Chenneberg, L.; Corcé, V.; Ollivier, C.; Fensterbank, L. Organic photoredox catalysis for the oxidation of silicates: applications in radical synthesis and dual catalysis. *Chem. Commun.* **2016**, *52*, 9877-9880.
(421) Molander, G. A.; Ito, T. Cross-Coupling Reactions of Potassium Alkyltrifluoroborates with Aryl and 1-Alkenyl Trifluoromethanesulfonates. *Org. Lett.* **2001**, *3*, 393-396.
(422) Samadi, S.; Orellana, A. A New Route to Phenols: Palladium-Catalyzed Cyclization and Oxidation of γ,δ-Unsaturated Ketones. *ChemCatChem* **2016**, *8*, 2472-2475.
(423) Fu, X.-F.; Xiang, Y.; Yu, Z.-X. RhI-Catalyzed Benzo/[7+1] Cycloaddition of Cyclopropyl-Benzocyclobutenes and CO by Merging Thermal and Metal-Catalyzed C–C Bond Cleavages. *Chem. Eur. J.* **2015**, *21*, 4242-4246.
(424) Guo, K.; Zhang, Z.; Li, A.; Li, Y.; Huang, J.; Yang, Z. Photoredox-Catalyzed Isomerization of Highly Substituted Allylic Alcohols by C−H Bond Activation. *Angew. Chem. Int. Ed.* **2020**, *59*, 11660-11668.
(425) Yang, P.-F.; Shu, W. Direct Synthesis of Mono-α-arylated Ketones from Alcohols and Olefins via Ni-Catalyzed Oxidative Cross-Coupling. *Org. Lett.* **2020**, *22*, 6203-6208.
(426) Pennell, M. N.; Unthank, M. G.; Turner, P.; Sheppard, T. D. A General Procedure for the Synthesis of Enones via Gold-Catalyzed Meyer−Schuster Rearrangement of Propargylic Alcohols at Room Temperature. *J. Org. Chem.* **2011**, *76*, 1479-1482.
(427) Kerr, W. J.; Mudd, R. J.; Brown, J. A. Iridium(I) N-Heterocyclic Carbene (NHC)/Phosphine Catalysts for Mild and Chemoselective Hydrogenation Processes. *Chem. Eur. J.* **2016**, *22*, 4738-4742.
(428) Seck, C.; Mbaye, M. D.; Coufourier, S.; Lator, A.; Lohier, J.-F.; Poater, A.; Ward, T. R.; Gaillard, S.; Renaud, J.-L. Alkylation of Ketones Catalyzed by Bifunctional Iron Complexes: From Mechanistic Understanding to Application. *ChemCatChem* **2017**, *9*, 4410-4416.

(429) Talero, A. G.; Martins, B. S.; Burtoloso, A. C. B. Coupling of Sulfoxonium Ylides with Arynes: A Direct Synthesis of Pro-Chiral Aryl Ketosulfoxonium Ylides and Its Application in the Preparation of α-Aryl Ketones. *Org. Lett.* **2018**, *20*, 7206-7211.
(430) Huwig, K.; Schultz, K.; Kazmaier, U. Regio- and Stereoselective Modification of Chiral α-Amino Ketones by Pd-Catalyzed Allylic Alkylation. *Angew. Chem. Int. Ed.* **2015**, *54*, 9120-9123.
(431) Lee, B.; Chirik, P. J. Ketone Synthesis from Benzyldiboronates and Esters: Leveraging α-Boryl Carbanions for Carbon–Carbon Bond Formation. *J. Am. Chem. Soc.* **2020**, *142*, 2429-2437.
(432) Shu, B.; Wang, X.-T.; Shen, Z.-X.; Che, T.; Zhong, M.; Song, J.-L.; Kang, H.-J.; Xie, H.; Zhang, L.; Zhang, S.-S. Iridium-catalyzed arylation of sulfoxonium ylides and arylboronic acids: a straightforward preparation of α-aryl ketones. *Org. Chem. Front.* **2020**, *7*, 1802-1808.
(433) Chashmniam, S.; Tafazzoli, M. Conformation of repaglinide: A solvent dependent structure. *J. Mol. Struct.* **2017**, *1143*, 388-396.
(434) Ritchie, T. J.; Macdonald, S. J. F. The impact of aromatic ring count on compound developability – are too many aromatic rings a liability in drug design? *Drug Discov.* **2009**, *14*, 1011-1020.
(435) Lovering, F.; Bikker, J.; Humblet, C. Escape from Flatland: Increasing Saturation as an Approach to Improving Clinical Success. *J. Med. Chem.* **2009**, *52*, 6752-6756.
(436) Dimitrov, I.; Denny, W. A.; Jose, J. Syntheses of Ketamine and Related Analogues: A Mini Review. *Synthesis* **2018**, *50*, 4201-4215.
(437) Evans, G. R.; Fernández, P. D.; Henshilwood, J. A.; Lloyd, S.; Nicklin, C. Development of Highly Efficient Resolutions of Racemic Tramadol Using Mandelic Acid. *Org. Process Res. Dev.* **2002**, *6*, 729-737.
(438) Abel, S. R. Tramadol: an alternative analgesic to traditional opioids and NSAIDs. *J. Pharmaceut. Care Pain Symptom Contr.* **1995**, *3*, 5-29.
(439) Bowles, P.; Brenek, S. J.; Caron, S.; Do, N. M.; Drexler, M. T.; Duan, S.; Dubé, P.; Hansen, E. C.; Jones, B. P.; Jones, K. N.; Ljubicic, T. A.; Makowski, T. W.; Mustakis, J.; Nelson, J. D.; Olivier, M.; Peng, Z.; Perfect, H. H.; Place, D. W.; Ragan, J. A.; Salisbury, J. J.; Stanchina, C. L.; Vanderplas, B. C.; Webster, M. E.; Weekly, R. M. Commercial Route Research and Development for SGLT2 Inhibitor Candidate Ertugliflozin. *Org. Process Res. Dev.* **2014**, *18*, 66-81.
(440) Martín-Escolano, R.; Guardia, J. J.; Martín-Escolano, J.; Cirauqui, N.; Fernández, A.; Rosales, M. J.; Chahboun, R.; Sánchez-Moreno, M.; Alvarez-Manzaneda, E.; Marín, C. In Vivo Biological Evaluation of a Synthetic Royleanone Derivative as a Promising Fast-Acting Trypanocidal Agent by Inducing Mitochondrial-Dependent Necrosis. *J. Nat. Prod.* **2020**, *83*, 3571-3583.
(441) Kusumoto, N.; Ashitani, T.; Murayama, T.; Ogiyama, K.; Takahashi, K. Antifungal Abietane-Type Diterpenes from the Cones of Taxodium distichum Rich. *J. Chem. Ecol.* **2010**, *36*, 1381-1386.
(442) Morrill, C.; Jensen, C.; Just-Baringo, X.; Grogan, G.; Turner, N. J.; Procter, D. J. Biocatalytic Conversion of Cyclic Ketones Bearing α-Quaternary Stereocenters into Lactones in an Enantioselective Radical Approach to Medium-Sized Carbocycles. *Angew. Chem. Int. Ed.* **2018**, *57*, 3692-3696.
(443) Hadi, T.; Díaz-Rodríguez, A.; Khan, D.; Morrison, J. P.; Kaplan, J. M.; Gallagher, K. T.; Schober, M.; Webb, M. R.; Brown, K. K.; Fuerst, D.; Snajdrova, R.; Roiban, G.-D. Identification

and Implementation of Biocatalytic Transformations in Route Discovery: Synthesis of Chiral 1,3-Substituted Cyclohexanone Building Blocks. *Org. Process Res. Dev.* **2018**, *22*, 871-879.
(444) Monos, T. M.; Jaworski, J. N.; Stephens, J. C.; Jamison, T. F. Continuous-Flow Synthesis of Tramadol from Cyclohexanone. *Synlett* **2020**, *31*, 1888-1893.
(445) Zha, Q.; An, X.; Xu, Z.-J.; Han, W.-B.; Wu, Y. A Low-Cost and Scalable Synthesis of a Cyclohexanone-Related Bifunctional Building Block. *ACS Omega* **2021**, *6*, 30811-30817.
(446) Meng, Q.; Hou, M.; Liu, H.; Song, J.; Han, B. Synthesis of ketones from biomass-derived feedstock. *Nat. Commun.* **2017**, *8*, 14190.
(447) Sun, H.; Blatter, F.; Frei, H. Cyclohexanone from Cyclohexane and O2 in a Zeolite under Visible Light with Complete Selectivity. *J. Am. Chem. Soc.* **1996**, *118*, 6873-6879.
(448) Stevens, R. V.; Chapman, K. T.; Weller, H. N. Convenient and inexpensive procedure for oxidation of secondary alcohols to ketones. *J. Org. Chem.* **1980**, *45*, 2030-2032.
(449) Corey, E. J. Catalytic Enantioselective Diels–Alder Reactions: Methods, Mechanistic Fundamentals, Pathways, and Applications. *Angew. Chem. Int. Ed.* **2002**, *41*, 1650-1667.
(450) Nicolaou, K. C.; Snyder, S. A.; Montagnon, T.; Vassilikogiannakis, G. The Diels–Alder Reaction in Total Synthesis. *Angew. Chem. Int. Ed.* **2002**, *41*, 1668-1698.
(451) Diels, O.; Alder, K. Synthesen in der hydroaromatischen Reihe. *Justus Liebigs Ann. Chem.* **1928**, *460*, 98-122.
(452) Dieckmann, W. Zur Kenntniss der Ringbildung aus Kohlenstoffketten. *Ber. Dtsch. Chem. Ges.* **1894**, *27*, 102-103.
(453) Diec Kmann, W. Ueber cyklische β-Ketoncarbonsäureester. *Justus Liebigs Ann. Chem.* **1901**, *317*, 27-109.
(454) Rapson, W. S.; Robinson, R. 307. Experiments on the synthesis of substances related to the sterols. Part II. A new general method for the synthesis of substituted cyclohexenones. *J. Chem. Soc.* **1935**, 1285-1288.
(455) Wang, C.-S.; Dixneuf, P. H.; Soulé, J.-F. Photoredox Catalysis for Building C–C Bonds from C(sp2)–H Bonds. *Chem. Rev.* **2018**, *118*, 7532-7585.
(456) Narayanam, J. M. R.; Stephenson, C. R. J. Visible light photoredox catalysis: applications in organic synthesis. *Chem. Soc. Rev.* **2011**, *40*, 102-113.
(457) Silvi, M.; Melchiorre, P. Enhancing the potential of enantioselective organocatalysis with light. *Nature* **2018**, *554*, 41-49.
(458) Speckmeier, E.; Fischer, T. G.; Zeitler, K. A Toolbox Approach To Construct Broadly Applicable Metal-Free Catalysts for Photoredox Chemistry: Deliberate Tuning of Redox Potentials and Importance of Halogens in Donor–Acceptor Cyanoarenes. *J. Am. Chem. Soc.* **2018**, *140*, 15353-15365.
(459) Wiebe, A.; Gieshoff, T.; Möhle, S.; Rodrigo, E.; Zirbes, M.; Waldvogel, S. R. Electrifying Organic Synthesis. *Angew. Chem. Int. Ed.* **2018**, *57*, 5594-5619.
(460) Kärkäs, M. D. Electrochemical strategies for C–H functionalization and C–N bond formation. *Chem. Soc. Rev.* **2018**, *47*, 5786-5865.
(461) Amani, J.; Alam, R.; Badir, S.; Molander, G. A. Synergistic Visible-Light Photoredox/Nickel-Catalyzed Synthesis of Aliphatic Ketones via N–C Cleavage of Imides. *Org. Lett.* **2017**, *19*, 2426-2429.
(462) Sagadevan, A.; Charpe, V. P.; Ragupathi, A.; Hwang, K. C. Visible Light Copper Photoredox-Catalyzed Aerobic Oxidative Coupling of Phenols and Terminal Alkynes:

Regioselective Synthesis of Functionalized Ketones via C≡C Triple Bond Cleavage. *J. Am. Chem. Soc.* **2017**, *139*, 2896-2899.
(463) Parker, K. A.; Fokas, D. Convergent synthesis of (+-)-dihydroisocodeine in 11 steps by the tandem radical cyclization strategy. A formal total synthesis of (+-)-morphine. *J. Am. Chem. Soc.* **1992**, *114*, 9688-9689.
(464) Plesniak, M. P.; Huang, H.-M.; Procter, D. J. Radical cascade reactions triggered by single electron transfer. *Nat. Rev. Chem.* **2017**, *1*, 0077.
(465) Tietze, L. F. Domino Reactions in Organic Synthesis. *Chem. Rev.* **1996**, *96*, 115-136.
(466) Péter, Á.; Agasti, S.; Knowles, O.; Pye, E.; Procter, D. J. Recent advances in the chemistry of ketyl radicals. *Chem. Soc. Rev.* **2021**, *50*, 5349-5365.
(467) Zhao, X.; Tu, H.-Y.; Guo, L.; Zhu, S.; Qing, F.-L.; Chu, L. Intermolecular selective carboacylation of alkenes via nickel-catalyzed reductive radical relay. *Nat. Commun.* **2018**, *9*, 3488.
(468) Sato, Y.; Goto, Y.; Nakamura, K.; Miyamoto, Y.; Sumida, Y.; Ohmiya, H. Light-Driven N-Heterocyclic Carbene Catalysis Using Alkylborates. *ACS Catal.* **2021**, *11*, 12886-12892.
(469) McGrath, N. A.; Brichacek, M.; Njardarson, J. T. A Graphical Journey of Innovative Organic Architectures That Have Improved Our Lives. *J. Chem. Educ.* **2010**, *87*, 1348-1349.
(470) Zhang, W.; Wang, F.; McCann, S. D.; Wang, D.; Chen, P.; Stahl, S. S.; Liu, G. Enantioselective cyanation of benzylic C–H bonds via copper-catalyzed radical relay. *Science* **2016**, *353*, 1014-1018.
(471) Guo, S.; AbuSalim, D. I.; Cook, S. P. Aqueous Benzylic C–H Trifluoromethylation for Late-Stage Functionalization. *J. Am. Chem. Soc.* **2018**, *140*, 12378-12382.
(472) Meng, Q.-Y.; Schirmer, T. E.; Berger, A. L.; Donabauer, K.; König, B. Photocarboxylation of Benzylic C–H Bonds. *J. Am. Chem. Soc.* **2019**, *141*, 11393-11397.
(473) Xiao, H.; Liu, Z.; Shen, H.; Zhang, B.; Zhu, L.; Li, C. Copper-Catalyzed Late-Stage Benzylic C(sp3)–H Trifluoromethylation. *Chem* **2019**, *5*, 940-949.
(474) Pandey, G.; Laha, R. Visible-Light-Catalyzed Direct Benzylic C(sp3)–H Amination Reaction by Cross-Dehydrogenative Coupling. *Angew. Chem. Int. Ed.* **2015**, *54*, 14875-14879.
(475) Clark, J. R.; Feng, K.; Sookezian, A.; White, M. C. Manganese-catalysed benzylic C(sp3)–H amination for late-stage functionalization. *Nat. Chem.* **2018**, *10*, 583-591.
(476) Suh, S.-E.; Chen, S.-J.; Mandal, M.; Guzei, I. A.; Cramer, C. J.; Stahl, S. S. Site-Selective Copper-Catalyzed Azidation of Benzylic C–H Bonds. *J. Am. Chem. Soc.* **2020**, *142*, 11388-11393.
(477) Tanwar, L.; Börgel, J.; Ritter, T. Synthesis of Benzylic Alcohols by C–H Oxidation. *J. Am. Chem. Soc.* **2019**, *141*, 17983-17988.
(478) Cheng, X.; Lu, H.; Lu, Z. Enantioselective benzylic C–H arylation via photoredox and nickel dual catalysis. *Nat. Commun.* **2019**, *10*, 3549.
(479) Huang, Z.; Lim, H. N.; Mo, F.; Young, M. C.; Dong, G. Transition metal-catalyzed ketone-directed or mediated C–H functionalization. *Chem. Soc. Rev.* **2015**, *44*, 7764-7786.
(480) Nicolaou, K. C.; Montagnon, T.; Baran, P. S.; Zhong, Y. L. Iodine(V) Reagents in Organic Synthesis. Part 4. o-Iodoxybenzoic Acid as a Chemospecific Tool for Single Electron Transfer-Based Oxidation Processes. *J. Am. Chem. Soc.* **2002**, *124*, 2245-2258.
(481) Marko, J. A.; Durgham, A.; Bretz, S. L.; Liu, W. Electrochemical benzylic oxidation of C–H bonds. *Chem. Commun.* **2019**, *55*, 937-940.

(482) Betori, R. C.; May, C. M.; Scheidt, K. A. Combined Photoredox/Enzymatic C−H Benzylic Hydroxylations. *Angew. Chem. Int. Ed.* **2019**, *58*, 16490-16494.
(483) Hamann, B. C.; Hartwig, J. F. Palladium-Catalyzed Direct α-Arylation of Ketones. Rate Acceleration by Sterically Hindered Chelating Ligands and Reductive Elimination from a Transition Metal Enolate Complex. *J. Am. Chem. Soc.* **1997**, *119*, 12382-12383.
(484) Kawatsura, M.; Hartwig, J. F. Simple, Highly Active Palladium Catalysts for Ketone and Malonate Arylation: Dissecting the Importance of Chelation and Steric Hindrance. *J. Am. Chem. Soc.* **1999**, *121*, 1473-1478.
(485) Palucki, M.; Buchwald, S. L. Palladium-Catalyzed α-Arylation of Ketones. *J. Am. Chem. Soc.* **1997**, *119*, 11108-11109.
(486) Fox, J. M.; Huang, X.; Chieffi, A.; Buchwald, S. L. Highly Active and Selective Catalysts for the Formation of α-Aryl Ketones. *J. Am. Chem. Soc.* **2000**, *122*, 1360-1370.
(487) Ehrentraut, A.; Zapf, A.; Beller, M. Progress in the Palladium-Catalyzed α-Arylation of Ketones with Chloroarenes. *Adv. Synth. Catal.* **2002**, *344*, 209-217.
(488) Ge, S.; Hartwig, J. F. Nickel-Catalyzed Asymmetric α-Arylation and Heteroarylation of Ketones with Chloroarenes: Effect of Halide on Selectivity, Oxidation State, and Room-Temperature Reactions. *J. Am. Chem. Soc.* **2011**, *133*, 16330-16333.
(489) Xu, Y.; Su, T.; Huang, Z.; Dong, G. Practical Direct α-Arylation of Cyclopentanones by Palladium/Enamine Cooperative Catalysis. *Angew. Chem. Int. Ed.* **2016**, *55*, 2559-2563.
(490) Johansson, C. C. C.; Colacot, T. J. Metal-Catalyzed α-Arylation of Carbonyl and Related Molecules: Novel Trends in C–C Bond Formation by C–H Bond Functionalization. *Angew. Chem. Int. Ed.* **2010**, *49*, 676-707.
(491) Escudero-Casao, M.; Licini, G.; Orlandi, M. Enantioselective α-Arylation of Ketones via a Novel Cu(I)–Bis(phosphine) Dioxide Catalytic System. *J. Am. Chem. Soc.* **2021**, *143*, 3289-3294.
(492) Liao, X.; Weng, Z.; Hartwig, J. F. Enantioselective α-Arylation of Ketones with Aryl Triflates Catalyzed by Difluorphos Complexes of Palladium and Nickel. *J. Am. Chem. Soc.* **2008**, *130*, 195-200.
(493) Su, W.; Raders, S.; Verkade, J. G.; Liao, X.; Hartwig, J. F. Pd-Catalyzed α-Arylation of Trimethylsilyl Enol Ethers with Aryl Bromides and Chlorides: A Synergistic Effect of Two Metal Fluorides as Additives. *Angew. Chem. Int. Ed.* **2006**, *45*, 5852-5855.
(494) Kawasaki, T.; Ishida, N.; Murakami, M. Dehydrogenative Coupling of Benzylic and Aldehydic C–H Bonds. *J. Am. Chem. Soc.* **2020**, *142*, 3366-3370.
(495) Griffiths, O. M.; Esteves, H. A.; Chen, Y.; Sowa, K.; May, O. S.; Morse, P.; Blakemore, D. C.; Ley, S. V. Photoredox-Catalyzed Dehydrogenative Csp3–Csp2 Cross-Coupling of Alkylarenes to Aldehydes in Flow. *J. Org. Chem.* **2021**, *86*, 13559-13571.
(496) Wang, C.; Wang, Z.; Yang, J.; Shi, S.-H.; Hui, X.-P. Sequential Visible-Light and N-Heterocyclic Carbene Catalysis: Stereoselective Synthesis of Tetrahydropyrano[2,3-b]indoles. *Org. Lett.* **2020**, *22*, 4440-4443.
(497) Wang, P.-Z.; Chen, J.-R.; Xiao, W.-J. Hantzsch esters: an emerging versatile class of reagents in photoredox catalyzed organic synthesis. *Org. Biomol. Chem.* **2019**, *17*, 6936-6951.
(498) Pucheault, M.; Darses, S.; Genet, J. P. Direct Access to Ketones from Aldehydes via Rhodium-Catalyzed Cross-Coupling Reaction with Potassium Trifluoro(organo)borates. *J. Am. Chem. Soc.* **2004**, *126*, 15356.

(499) Pitzer, L.; Schäfers, F.; Glorius, F. Rapid Assessment of the Reaction-Condition-Based Sensitivity of Chemical Transformations. *Angew. Chem. Int. Ed.* **2019**, *58*, 8572-8576.
(500) Under the optimized reaction conditions, thiophene-substituted Hantzsch ester provided a mixture of disubstituted cyclohexanone products. Use of 1-methyl benzyl-substituted Hantzsch afforded linear ketone as the primary product. Optimization of these additional processes is currently underway.
(501) Renz, M.; Meunier, B. 100 Years of Baeyer–Villiger Oxidations. *Eur. J. Org. Chem.* **1999**, *1999*, 737-750.
(502) Zhong, R.; Wei, Z.; Zhang, W.; Liu, S.; Liu, Q. A Practical and Stereoselective In Situ NHC-Cobalt Catalytic System for Hydrogenation of Ketones and Aldehydes. *Chem* **2019**, *5*, 1552-1566.
(503) Tang, S.-Z.; Bian, H.-L.; Zhan, Z.-S.; Chen, M.-E.; Lv, J.-W.; Xie, S.; Zhang, F.-M. p-Toluenesulfonic acid catalysed fluorination of α-branched ketones for the construction of fluorinated quaternary carbon centres. *Chem. Commun.* **2018**, *54*, 12377-12380.
(504) Cheon, C. H.; Kanno, O.; Toste, F. D. Chiral Brønsted Acid from a Cationic Gold(I) Complex: Catalytic Enantioselective Protonation of Silyl Enol Ethers of Ketones. *J. Am. Chem. Soc.* **2011**, *133*, 13248-13251.
(505) Dal Zotto, C.; Virieux, D.; Campagne, J.-M. FeCl3-catalyzed reduction of ketones and aldehydes to alkane compounds. *Synlett* **2009**, *2009*, 276-278.
(506) Richter, N.; Simon, R. C.; Lechner, H.; Kroutil, W.; Ward, J. M.; Hailes, H. C. ω-Transaminases for the amination of functionalised cyclic ketones. *Org. Biomol. Chem.* **2015**, *13*, 8843-8851.
(507) Ma, Q.; Yuan, H.; Mao, J.; Yao, J.; Li, H. Catalytic oxidation of α-substituted cyclohexanone with steric hindrance to 6-oxohexanoic acid involved during the total synthesis of (+)-biotin. *Appl. Catal. A: Gen.* **2021**, *624*, 118304.
(508) Tripathi, R. P.; Verma, S. S.; Pandey, J.; Agarwal, K. C.; Chaturvedi, V.; Manju, Y. K.; Srivastva, A. K.; Gaikwad, A.; Sinha, S. Search of antitubercular activities in tetrahydroacridines: Synthesis and biological evaluation. *Bioorg. Med. Chem. Lett.* **2006**, *16*, 5144-5147.
(509) Munnuri, S.; Verma, S.; Chandra, D.; Anugu, R. R.; Falck, J. R.; Jat, J. L. Cu (OTf) 2-Catalyzed Beckmann Rearrangement of Ketones Using Hydroxylamine-O-sulfonic Acid (HOSA). *Synthesis* **2019**, *51*, 3709-3714.
(510) Baeyer, A.; Villiger, V. Einwirkung des caro'schen reagens auf ketone. *Ber. Dtsch. Chem. Ges.* **1899**, *32*, 3625-3633.
(511) Gehlen, M. H. The centenary of the Stern-Volmer equation of fluorescence quenching: From the single line plot to the SV quenching map. *J. Photochem. Photobiol. C* **2020**, *42*, 100338.
(512) Capaldo, L.; Ravelli, D. Hydrogen Atom Transfer (HAT): A Versatile Strategy for Substrate Activation in Photocatalyzed Organic Synthesis. *Eur. J. Org. Chem.* **2017**, *2017*, 2056-2071.
(513) Ishiguro, K.; Nakano, T.; Shibata, H.; Sawaki, Y. Redox Reaction of Benzyl Radicals with Aromatic Radical Ions Photogenerated. The Marcus Inverted Region and the Selective Formation of Carbocations or Carbanions. *J. Am. Chem. Soc.* **1996**, *118*, 7255-7264.
(514) Teegardin, K. A.; Weaver, J. D. Preparation of Fac-Tris (2-Phenylpyridinato) Iridium (III). *Organic syntheses; an annual publication of satisfactory methods for the preparation of organic chemicals* **2018**, *95*, 29.
(515) Li, G.; Chen, R.; Wu, L.; Fu, Q.; Zhang, X.; Tang, Z. Alkyl Transfer from C–C Cleavage. *Angew. Chem. Int. Ed.* **2013**, *52*, 8432-8436.

(516) Martin, L. J.; Marzinzik, A. L.; Ley, S. V.; Baxendale, I. R. Safe and Reliable Synthesis of Diazoketones and Quinoxalines in a Continuous Flow Reactor. *Org. Lett.* **2011**, *13*, 320-323.
(517) Guney, T.; Wenderski, T. A.; Boudreau, M. W.; Tan, D. S. Synthesis of Benzannulated Medium-ring Lactams via a Tandem Oxidative Dearomatization-Ring Expansion Reaction. *Chem. Eur. J.* **2018**, *24*, 13150-13157.
(518) Tungen, J. E.; Kristianslund, R.; Vik, A.; Hansen, T. V. Organoselenium Accelerated Bromolactonization Reaction. *J. Org. Chem.* **2019**, *84*, 11373-11381.
(519) Yu, X.-Y.; Chen, J.-R.; Wang, P.-Z.; Yang, M.-N.; Liang, D.; Xiao, W.-J. A Visible-Light-Driven Iminyl Radical-Mediated C−C Single Bond Cleavage/Radical Addition Cascade of Oxime Esters. *Angew. Chem. Int. Ed.* **2018**, *57*, 738-743.
(520) Hamri, S.; Jouha, J.; Oumessaoud, A.; Pujol, M. D.; Khouili, M.; Guillaumet, G. Convenient approach for the synthesis of ONO-LB-457, a potent leukotriene B4 receptor antagonist. *Tetrahedron* **2021**, *77*, 131740.
(521) Coveney, D. J.; Patel, V. F.; Pattenden, G.; Thompson, D. M. Acylcobalt salophen reagents. Precursors to acyl radical intermediates for use in carbon-to-carbon bond-forming reactions to alkenes. *J. Chem. Soc., Perkin Trans. 1* **1990**, 2721-2728.
(522) Wang, Z.; He, Z.; Zhang, L.; Huang, Y. Iridium-Catalyzed Aerobic α,β-Dehydrogenation of γ,δ-Unsaturated Amides and Acids: Activation of Both α- and β-C–H bonds through an Allyl–Iridium Intermediate. *J. Am. Chem. Soc.* **2018**, *140*, 735-740.
(523) Dolomanov, O. V.; Bourhis, L. J.; Gildea, R. J.; Howard, J. A.; Puschmann, H. OLEX2: a complete structure solution, refinement and analysis program. *J. Appl. Crystallogr.* **2009**, *42*, 339-341.
(524) Sheldrick, G. SHELXT - Integrated space-group and crystal-structure determination. *Acta Crystallogr. A* **2015**, *71*, 3-8.
(525) Sheldrick, G. Crystal structure refinement with SHELXL. *Acta Crystallogr. C* **2015**, *71*, 3-8.
(526) Finkelstein, M.; P'An, S. Y.; Niesler, V. N.; Johnson, C. A.; Schneider, J. A. On the pharmacology of oxyphencyclimine hydrochloride. *J. Pharmacol. Exp. Ther.* **1959**, *125*, 330-338.
(527) Jeffcoate, W. J.; Rees, L. H.; Tomlin, S.; Jones, A. E.; Edwards, C. R.; Besser, G. M. Metyrapone in long-term management of Cushing's disease. *Brit. Med. J.* **1977**, *2*, 215-217.
(528) Challman, T. D.; Lipsky, J. J. Methylphenidate: Its Pharmacology and Uses. *Mayo Clin. Proc.* **2000**, *75*, 711-721.
(529) Daly, E. J.; Singh, J. B.; Fedgchin, M.; Cooper, K.; Lim, P.; Shelton, R. C.; Thase, M. E.; Winokur, A.; Van Nueten, L.; Manji, H.; Drevets, W. C. Efficacy and Safety of Intranasal Esketamine Adjunctive to Oral Antidepressant Therapy in Treatment-Resistant Depression: A Randomized Clinical Trial. *JAMA Psychiatry* **2018**, *75*, 139-148.
(530) Brownbridge, P. Silyl Enol Ethers in Synthesis - Part I. *Synthesis* **1983**.
(531) Waddell, D. C.; Thiel, I.; Clark, T. D.; Marcum, S. T.; Mack, J. Making kinetic and thermodynamic enolates via solvent-free high speed ball milling. *Green Chem.* **2010**, *12*, 209-211.
(532) Matsuo, J.-i.; Murakami, M. The Mukaiyama Aldol Reaction: 40 Years of Continuous Development. *Angew. Chem. Int. Ed.* **2013**, *52*, 9109-9118.
(533) Koichi, N.; Kenso, S.; Yukiko, A.; Teruaki, M. The Michael Reaction of Silyl Enol Ethers with α,β-Unsaturated Eetones and Acetals in the Presence of Titanium Tetraalkoxide and Titanium Tetrachloride. *Bull. Chem. Soc. Jpn.* **1976**, *49*, 779-783.

(534) Gassman, P. G.; Bottorff, K. J. Electron transfer induced desilylation of trimethylsilyl enol ethers. *J. Org. Chem.* **1988**, *53*, 1097-1100.
(535) Rathore, R.; Kochi, J. K. α-Nitration of Ketones via Enol Silyl Ethers. Radical Cations as Reactive Intermediates in Thermal and Photochemical Processes. *J. Org. Chem.* **1996**, *61*, 627-639.
(536) Caravana, A. C.; Nagasing, B.; Dhanju, S.; Reynolds, R. G.; Weiss, E. A.; Thomson, R. J. Electrochemical and Photocatalytic Oxidative Coupling of Ketones via Silyl Bis-enol Ethers. *J. Org. Chem.* **2021**, *86*, 6600-6611.
(537) Huang, Y.; Jia, J.; Huang, Q.-P.; Zhao, L.; Wang, P.; Gu, J.; He, C.-Y. Visible light promoted deaminative difluoroalkylation of aliphatic amines with difluoroenoxysilanes. *Chem. Commun.* **2020**, *56*, 14247-14250.
(538) Kong, W.; Yu, C.; An, H.; Song, Q. Photoredox-Catalyzed Decarboxylative Alkylation of Silyl Enol Ethers To Synthesize Functionalized Aryl Alkyl Ketones. *Org. Lett.* **2018**, *20*, 349-352.
(539) Hajos-Parrish-Eder-Sauer-Wiechert Reaction. In *Comprehensive Organic Name Reactions and Reagents*; pp 1305-1309.
(540) List, B.; Hoang, L.; Martin, H. J. New mechanistic studies on the proline-catalyzed aldol reaction. *Proc. Natl. Acad. Sci. U. S. A.* **2004**, *101*, 5839-5842.
(541) Barbas, C. F., 3rd; Heine, A.; Zhong, G.; Hoffmann, T.; Gramatikova, S.; Björnestedt, R.; List, B.; Anderson, J.; Stura, E. A.; Wilson, I. A.; Lerner, R. A. Immune versus natural selection: antibody aldolases with enzymic rates but broader scope. *Science* **1997**, *278*, 2085-2092.
(542) List, B.; Lerner, R. A.; Barbas, C. F. Proline-Catalyzed Direct Asymmetric Aldol Reactions. *J. Am. Chem. Soc.* **2000**, *122*, 2395-2396.
(543) Pihko, P. M.; Majander, I.; Erkkilä, A. Enamine Catalysis. In *Asymmetric Organocatalysis*; List, B., Ed.; Springer Berlin Heidelberg: Berlin, Heidelberg, 2009; pp 145-200.
(544) Hossain, M. M.; Shaikh, A. C.; Moutet, J.; Gianetti, T. L. Photocatalytic α-arylation of cyclic ketones. *Nat. Synth.* **2022**, *1*, 147-157.
(545) Isse, A. A.; Lin, C. Y.; Coote, M. L.; Gennaro, A. Estimation of Standard Reduction Potentials of Halogen Atoms and Alkyl Halides. *J. Phys. Chem. B* **2011**, *115*, 678-684.
(546) Tong, S.; Li, K.; Ouyang, X.; Song, R.; Li, J. Recent advances in the radical-mediated decyanative alkylation of cyano(hetero)arene. *Green Synth. Catal.* **2021**, *2*, 145-155.
(547) Yang, J.; Ma, J.; Yan, K.; Tian, L.; Li, B.; Wen, J. Electrochemical Ammonium Cation-Assisted Hydropyridylation of Ketone-Activated Alkenes: Experimental and Computational Mechanistic Studies. *Adv. Synth. Catal.* **2022**, *364*, 845-854.
(548) Romańczyk, P. P.; Kurek, S. S. Reliable reduction potentials of diaryliodonium cations and aryl radicals in acetonitrile from high-level ab initio computations. *Electrochim. Acta* **2020**, *351*, 136404.
(549) Lübbesmeyer, M.; Leifert, D.; Schäfer, H.; Studer, A. Electrochemical initiation of electron-catalyzed phenanthridine synthesis by trifluoromethylation of isonitriles. *Chem. Commun.* **2018**, *54*, 2240-2243.
(550) Mizuta, S.; Verhoog, S.; Wang, X.; Shibata, N.; Gouverneur, V.; Médebielle, M. Redox chemistry of trifluoromethyl sulfonium salts as CF3 radical sources. *J. Fluorine Chem.* **2013**, *155*, 124-131.
(551) Lemos, A.; Lemaire, C.; Luxen, A. Progress in Difluoroalkylation of Organic Substrates by Visible Light Photoredox Catalysis. *Adv. Synth. Catal.* **2019**, *361*, 1500-1537.

(552) M. Correia, J. T.; A. Fernandes, V.; Matsuo, B. T.; C. Delgado, J. A.; de Souza, W. C.; Paixão, M. W. Photoinduced deaminative strategies: Katritzky salts as alkyl radical precursors. *Chem. Commun.* **2020**, *56*, 503-514.
(553) Barham, J. P.; Coulthard, G.; Emery, K. J.; Doni, E.; Cumine, F.; Nocera, G.; John, M. P.; Berlouis, L. E. A.; McGuire, T.; Tuttle, T.; Murphy, J. A. KOtBu: A Privileged Reagent for Electron Transfer Reactions? *J. Am. Chem. Soc.* **2016**, *138*, 7402-7410.
(554) Buchi, G.; Vogel, D. E. A new method for the preparation of γ,δ-unsaturated ketones via Claisen rearrangement. *J. Org. Chem.* **1985**, *50*, 4664-4665.
(555) Miller, A. K.; Hughes, C. C.; Kennedy-Smith, J. J.; Gradl, S. N.; Trauner, D. Total Synthesis of (−)-Heptemerone B and (−)-Guanacastepene E. *J. Am. Chem. Soc.* **2006**, *128*, 17057-17062.
(556) Jin, S.; Dang, H. T.; Haug, G. C.; Nguyen, V. D.; Arman, H. D.; Larionov, O. V. Deoxygenative α-alkylation and α-arylation of 1,2-dicarbonyls. *Chem. Sci.* **2020**, *11*, 9101-9108.